Title
Detecting, Measuring and Manipulating Copper in Biological Systems

Author
Ackerman, Cheri Marie

Publication Date
2017

Peer reviewed|Thesis/dissertation

Detecting, Measuring and Manipulating Copper in Biological Systems

By

Cheri Marie Ackerman

A dissertation submitted in partial satisfaction of the

requirements for the degree of

Doctor of Philosophy

in

Chemistry

in the

Graduate Division

of the

University of California, Berkeley

Committee in charge:

Professor Christopher J. Chang, Chair
Professor Matthew B. Francis
Professor David E. Wemmer
Professor Andreas Stahl

Summer 2017

Detecting, Measuring and Manipulating Copper in Biological Systems

Cheri Marie Ackerman

Abstract

Detecting, Measuring and Manipulating Copper in Biological Systems

by

Cheri Marie Ackerman

Doctor of Philosophy in Chemistry

University of California, Berkeley

Professor Christopher Chang, Chair

Copper is an essential micronutrient for eukaryotic systems and, thus, an essential mineral in the human diet. As a redox-active metal, copper plays a key role as a catalytic cofactor for a number of enzymes, including those responsible for cellular respiration, neurotransmitter synthesis, extracellular matrix crosslinking, and pigment synthesis. However, the one-electron chemistry that makes copper so valuable within enzymes also makes it potentially toxic to cells, as copper may also generate reactive oxygen species within biological systems. For copper to be loaded into enzymes without causing toxicity, it must be acquired by an organism from the environment and trafficked to the correct tissues, cells, organelles, and proteins. Understanding the complex system of proteins and small molecules that acquire and chaperone copper within vertebrate organisms is a fascinating and challenging puzzle, raising such questions as: Which tissues, cells, and organelles accumulate copper, and which exclude it? Which proteins handle copper during copper trafficking, and which receive copper at its final destination? Is there a role for copper in biological systems beyond enzyme catalysis? What are the functional consequences of copper overload and copper deficiency for an organism? And can copper or copper chelators be used as nutritional supplements to combat disease? Here, we address these questions in the following ways: Chapter 1 provides a review of techniques for mapping the distribution and localization of transition metals within biological systems. Chapter 2 outlines the application of laser ablation ICP-MS and nanoSIMS metal mapping to study the retinal tissue of the zebrafish model of Menkes disease. Chapter 3 explores proteomics methods to find proteins that bind copper transiently, outside enzyme active sites. Finally, Chapter 4 outlines efforts toward genetic tools to study the copper import protein, CTR1.

This work is dedicated to my parents.

Table of Contents

Acknowledgements

One of the fundamental goals of science is to identify patterns of cause and effect. Yet in the ordinary events of daily life, accurately identifying cause and effect and appropriately attributing credit and blame is complex and difficult. Perhaps one of the most common sources of conflict in academia is the distribution of credit for published work, perhaps because very little research is done in a social vacuum. Indeed, very little life happens in a vacuum. Instead, the complexities of the communities around scientists provide rich sources of inspiration and motivation in the daily work of doing science.

This dissertation is a partial summary of the scientific work for which I take credit. However, much of this work was inspired by, performed with, and critiqued by many other people. And since I am not a robot, my ability to get up each morning and care about doing this work has been heavily influenced by the friends and family who have formed my community outside of work. Percolating in my mind over the months of writing this thesis has been a sense of deep wonder and gratitude for the number of people and the scale of the effort that was required for me to reach this point in my life. In the end, I decided to write it all down, if only for my personal reflection. The result is a very long acknowledgements section. But hey, no one reads dissertations anyway, right?

--

None of this work would be possible without the support provided by my advisor, Prof. Christopher Chang. Thank you for providing continual feedback and advice throughout my doctoral work. Your ability to balance your many responsibilities as a professor while continually giving attention to your students is admirable, and your commitment to supporting your students as they continue into their own careers is invaluable. Thank you.

Of course, what would grad school be without the day-to-day grind of actually doing science? To all my labmates, especially the members of 401 Latimer throughout the years, thank you for your camaraderie in the work of learning new things about the world. You have seen me in some of my best and worst moments over the last six years. Thank you for your encouragement, patience, critique, and ideas. My science is better and my life is happier because of you.

Karla, no one can ever hold the place in my heart that you hold – my friend and labmate, from the beginning to the end – I couldn't have asked for a more amazing person to go through grad school with year by year. Your courage, perseverance, and deep love for the people in your life continue to inspire me.

Lakshmi, your guidance and expertise in all things biology have kept me moving in the right direction. So many of the interesting things I've worked on have started from conversations with you, and your encouragement and friendship have strengthened me through many frustrating moments.

Tong, I wouldn't have had any zebrafish this last year without you. Thank you for asking me the right questions about my zebrafish work and caring for me in work and life.

Allegra, my dear friend and partner in all things proteomics, your resilience and faithfulness to yourself are so inspiring. Thank you for working with me as we learned to communicate well, share work and ownership, and navigate the many pitfalls of metalloproteomics. Seeing you remember and maintain your passion for science and your motivation for going to grad school has helped me hold onto mine, and I'm excited to see where your passion and motivation take you!

Marie, watching you give your proposal talk was the first time I had ever seen a woman propose faculty research, and it was the first time I internalized the possibility that I might do that too, someday. You are unapologetically feminine in your excitement for science and strength of mind. I have been so blessed to work alongside you and watch your faculty search process. I hope you achieve everything you're working for in Davis!

Tyler, where to start, haha. From mentoring you that first summer to editing fellowship applications with you to the rollercoaster journey of your qual process, it has been an honor to watch you grow in grad school. Your tenacity and work ethic are enviable. You learn from critique better than most first and second years I've seen (including me). And in these last months of my PhD, you've turned the tables and taken the time to encourage me and help me. Thank you for matching my scathing humor with your equally cynical wit and yet knowing when to offer more gentle encouragement too. I will deeply miss working with you.

Bao, Emily, and Sophia, my amazing undergraduate research students, thank you for all of your work and your excitement for science. Your willingness to work with me while I learned to mentor students in lab has changed my life. Thank you for bringing fresh curiosity and wonder into the lab each day. Much of the work in this thesis was the direct result of experiments we worked on together, and I'm so grateful for each of you.

Thom and Eva, it has been an honor to be in the 2017 graduation cohort with you! You are both amazing scientists, and your ability to weather the storms of grad school and graduation/filing has helped steady me through this process. Thanks for adopting me into your class for a few months!

Mark, what great fun to meet you in grad school after just missing you at Calvin! Thank you for your support and older-brother protection during my grad work. You're so down-to-earth, kind, and caring, and still you're a brilliant synthetic chemist. Thank you for your continued friendship as you've moved beyond the lab into normal life. I'm so happy for you and Melissa! To many excellent skiing, beer-drinking adventures to come!

Brian, thanks for starting the ski trips. You singlehandedly changed Chang Lab culture for the better with a snowboard. And our softball team has never been the same without you and Katie!

Ryan, my running buddy and O-chem guru, thank you for your friendship, encouragement, and willingness to coach me through a reaction or two, even while you were trying to wrap things up in lab and peace out. Your passion for teaching is contagious, and I'm grateful that you shared your experience of looking for liberal arts jobs with me. I've learned so much from you.

Jeff, I wouldn't have gotten off the ground in the Chang Lab without you. Thank you for your advice and honesty about navigating grad school.

Jess, Vivian, and Annie, thank you for your friendship and for walking the road ahead of me in grad school with such grace and perseverance. Talking with you over food and swapping baked goods made me feel at home in the lab from the beginning. I'm so happy for each of you and wish you all the best.

Sarah and Genevieve, thank you for your advice as I joined the lab and now as I move on from here. Your perspective has helped me see my own journey better, and I am grateful for your willingness to share your experiences.

Sheel, thank you for mentoring me during my rotation and for working with me as I got going in the lab. You were an incredible reservoir of knowledge and wisdom in the lab, and you continue to inspire me as you are establishing your own lab now. Thank you!

--

Graduate school has a way of spilling over into normal life with alarming frequency, and I wouldn't have finished graduate school if not for the many people who walked this journey with me without setting foot in the lab.

First and foremost, I want to thank my dad and mom, Daniel and Carla Ackerman, for their unconditional love and support throughout my entire education. From PATH math to OM to AP's to Honors to graduate school, you've never added any pressure to my own desire to achieve, yet you continually support me in pursuit of my dreams. You've seen the pain that shooting so high has brought me, but you've never told me to turn away from it. You've let me walk my own journey, unable to protect me, yet giving me the freedom and love I needed to put one foot in front of the other. You keep me grounded in my humanity. You taught me to live within my limits and keep boundaries on my work, skills that kept me alive during graduate school. You affirm the goodness of my emotions, and you are honest about your own, giving me the most powerful tool I could have asked for to navigate these last six years. You have never been afraid of letting me pursue scientific inquiry and higher education, despite the ongoing cultural struggle between the worldviews of my hometown and the universities where you knew I would study. Instead, you have always encouraged me to pursue science in the presence of the God who blesses us with knowledge. You have encouraged me time and again to enlist my science in His service, and your support means the world to me. Yet you didn't let me escape my education only a scientist. Thank you for teaching me to read, editing my writing, and listening to so much piano practice. You held a vision for my life that went far beyond the

horizons I could perceive as a child, and somehow you have beautifully balanced launching me into that reality while letting me shape and identify that reality on my own. Thank you for moving me across the country and leaving me there. Thank you for every card, every phone call, every prayer, every tear, every visit. You, more than anyone else, know the struggle of the last six years. I couldn't have finished without you. I love you.

Thank you to my amazing siblings, Marcus, Laurel, and Caleb, and now Luke too! Thank you for your encouragement and visits. Thank you for staying connected to me despite the distance. Thank you for being so fiercely your own selves. I don't know of four siblings who are more different in personality and career paths, and I love hearing about the things that excite and motivate each of you. Thank you for sharing your lives with me and caring about the things that happen in my life. You keep my life in perspective. What would I do without you?

To my grandmother, Marylin Zoodsma, thank you for supporting me even as I have been so far from home, and thank you for coming out to California to see my graduation ceremony. Your house was home to me while I spent summers doing research at VAI and Calvin during college, and getting to talk to you about my work then and now is a lot of fun for me. You are one of the people who helped me learn how to talk about my science with people who are curious about science but outside academia. Thank you for being curious and for being willing to listen to me talk about science.

To my Uncle Tom, Professor of Atmospheric Sciences, currently at the University of Washington, thank you for believing in me and giving me a perspective on academia from the other side of the desk. One phone conversation with you during my third year swayed me from walking away from grad school altogether, and I am so thankful for that. Thank you for continuing to check up on me and for cheering for me as things have gotten better.

To my California Family, the community of Christ Church, thank you for being a home for me over the last six years. I thank the pastors and elders for leading the church well through joy and deep sorrow. I thank, especially, Rev. Jonathan St. Clair, for your patience in bearing with me as I grew as a leader. Thank you for your care, encouragement, and instruction. I also thank my fellow deacons for showing me how wide and deep the love of God is for the city of Berkeley. Thank you to the Gourmet Ghetto parish leadership team(s) for being a touchstone of encouragement and for being fellow workers on the ground level. I also thank my various parishes and community groups (ever morphing and multiplying) for your insights, questions, prayers, laughter, tears, and love. I had originally thought that I moved to Berkeley to go to graduate school, but the more I reflect on the last six years, the more I have come to believe that I came here to be part of this church, to serve her, learn from her, and grow as part of her. God is with you, and I have met Him in your midst. Leaving this community is truly my deepest sadness as I say goodbye to Berkeley.

To the "Chem Friends" of the Class of 2016: Dr. Karla Ramos-Torres, Dr. Anna Parker, Dr. Frances Rodriguez-Rivera, Dr. Ioana Aanei, Dr. Tony Rizzuto, Dr. Andrew Attar, Dr. Andrew Neel, Dr. Willie Wolf, Dr. Richard Cooper, Master Scott Belding, and Dr. Pete

Marsden (an honorary member of the Class of 2016 - we love you!). Without you, I would have lived a considerably more boring life. Thank you for making possible our many trips to Tahoe, Yosemite, Sequoia, and the American River. Thank you for teaching me to play volleyball and being patient with me as I continue to learn. Thank you for celebrating our birthdays, qualifying exam passes, engagements, weddings, and moving-on together. Sharing life with each of you has been so sweet.

Joey, words cannot express my gratitude for your companionship and support throughout my graduate work. You have been my closest friend, confidant, and ally. You helped me keep moving when I wanted to quit. You provided perspective when all I could do was scream. Thank you for the intellectual rigor you brought to the lab and each of our projects. You refused to let me see my science as more hopeless than it was, and you refused to let me run headlong after ideas that had not been well examined. Thank you for being a safe space for me as I struggled through experiments and conversations that did not go as I had hoped or planned. Thank you for holding me as I cried, for rejoicing with me in your successes and mine, for laughing with me, for dancing with me (quite literally, much to my surprise), and for exploring northern California with me. My appreciation for food, wine, and classical music has certainly grown from my time spent with you. Thank you for growing with me. I learned so much from you and was so blessed to be side-by-side with you for our time together.

Zach, thank you for pulling me through year six. Who knew burpees could be so fun? They're not. But I'll do them for you. And you'll run the fire trail for me :) Thank you for your big heart and even bigger voice. You have so much passion for life, in and out of lab, and I'm so happy to be counted as your friend. Thank you for holding so much safe space for good conversations and tears. You have been a steady force for emotional health for me this past year. Thanks for singing and loving life with me. Thank you for brainstorming with me about science and letting our NJ's go crazy (even if we end up actually being P's, we'll be ok). I'm super excited for all the brainstorming yet to come. The microbiome is actually the coolest, and I'm so glad you'll be keeping me up to speed on that for the rest of our lives, haha. You're going to be a rockstar PI, and I'm stoked to work with you in the future!

Carolyn Anderson, thank you for many coffee conversations and shared meals throughout my college years and graduate school. The book group you led for Nate, Luke, Alexandra, and me at Calvin has shaped the way I think about science. Your openness about your experience of being a professor at Calvin has helped me see academic life more clearly. Thank you for your mentorship and friendship.

To my undergraduate research mentors, Jeff MacKeigan and Eric Arnoys, thank you for giving me my first look into academic science. You pushed me to be the best scientist I could be. You took my work seriously and gave me the confidence that I needed to get going in graduate school. Thank you for your support.

Alexandra M. Cok, thank you for making me a chemist. Once upon a time, I was pre-med biologist who had never considered that chemistry as a major. Then we found each other,

and we will never be the same. I'm so excited to be living in the same city as you again in just a few months!

Prof. David Koetje, thank you for encouraging me to move beyond introductory biology lab to do academic research. I wouldn't have known that research was a viable summer job without you, and I certainly wouldn't have applied to VAI. That simple encouragement changed my life.

--

Last, but certainly not least, I would like to thank the individuals and organizations that have provided professional, financial, and technical support to me throughout graduate school.

Prof. Bob Bergman, thank you for teaching me Physical Organic Chemistry right out of the gate in graduate school. Your willingness to engage new pedagogical techniques and push each student to be their best made that class one of the best learning experiences I have had. Thank you for asking me to teach with you. Having the opportunity to teach Phys Org was one of the reasons I stayed in graduate school during my third year. Thank you for entrusting pedagogical decisions to your graduate student instructors and providing helpful feedback on those decisions. I learned so much from working with you. Thank you for being a listening ear and wise source of advice for me. Thank you for advocating for graduate student health and excellent faculty mentoring of graduate students in Chemistry. It was an honor for me to serve on the Committee for Faculty Graduate Student Mentorship with you, and I am grateful for your support of that process.

Dr. Christopher Marth, thank you for being my fellow Graduate Student Instructor for Chemistry 115 and Chemistry 200/260. I learned a lot from you, and I'm glad that we taught together.

To the Chemistry Graduate Life Committee, thank you for being an ongoing force for positive change in the chemistry department. Serving with each of you over the years was inspiring and educational. I am hopeful for many more years of healthy work and fun for the Committee!

I would like to thank the Chair of the Chemistry Department, Prof. David Wemmer, and the members of the Committee on Faculty-Graduate Student Mentorship: Prof. Bob Bergman (Chair), Prof. Matt Francis, Prof. Phill Geissler, Prof. Kristie Boering, Lynn Keithlin, Samia Hamed and Stephen Wilson. Our committee had a terrible name and a worse acronym, but I do think we did good work. I deeply appreciate the time and thought you put into improving the Chemistry Department at UC Berkeley.

Carolyn Bertozzi (we'll forget that you're at Stanford now), thank you for your passion for science and advice about how to pursue a scientific question. Your talk at the Beckman Fellows Conference in 2010, along with a talk by Bonnie Bassler, sent me catapulting into

science. And hours of discussing science and academia kept me in science during graduate school.

Matt Francis, thank you for your support throughout my graduate work, but especially in my second and third year. You coached me incredibly well in the months following my qualifying exam, at a time when everything felt like it was crumbling. Thank you for your thoughtfulness and calm presence.

To the guys in the woodshop, especially Mike Brateng, thank you for all of your help installing and moving the LA-ICP-MS system and renovating our beautiful new space in 437 Latimer. My work would not have been possible without that space, and working with you was a really fun and efficient experience. Thank you!

To the administrative staff in the Department of Chemistry and the College of Chemistry, especially Lynn Keithlin and Doris Kaeo, thank you for everything you do to make the Chemistry Department go ‘round. I got paid because of you. We could schedule group meetings because of you. And I always felt respected and heard in the administrative offices, despite the immense amount of work that you all do. Thank you for running the college so well.

I would like to thank the women who run the Cell Culture Facility at UC Berkeley: Ann Fisher, Alison Kililea, and Carissa Tasto. Your dedication and consistency in your work has saved me hours of time during my PhD. Thank you!

I would also like to thank the women of the Zebrafish Facility at UC Berkeley: Mel Boren, Kait Kliman, Jessie McNichols, Sonia Castillo, and Allison Kepple. You keep our fish healthy and well, and our science wouldn’t be possible without you!

Ciaran O’Connor, Julian Wills, Katherine McLachlin, Myron Peskar, Erik Larsen, Leif Summerfield, and Jay Wilkins, thank you for all of your help in getting the LA-ICP-MS system running and adapting it to our application. None of us had any idea how difficult that task would be, and I’m so glad I didn’t have to do it alone. Thank you.

For the financial support that made my PhD possible, I thank the Fannie and John Hertz Foundation. I also thank the staff of the Hertz Foundation for their care for each Hertz Fellow, their dedication to making sure that every payment goes through, and their commitment to building the community of Hertz Fellows. Specifically, I thank Mandy O’Connor for her encouragement and gentleness. I thank Jay and Mary Davis for their hospitality, love of life and wine, and wise advice. Finally, I thank Robbee Kozak for her incredible example of what great leadership is, her willingness to address tough issues, and her unswerving dedication to the wellbeing of the Hertz Foundation and Hertz Fellows. The Foundation has been a huge source of inspiration and support, and I’m excited to participate in the community of fellows as a graduate!

And finally, thank you to my dissertation committee: Profs. Christopher Chang, Matthew Francis, David Wemmer, and Andreas Stahl. Your comments on the science and writing in this work made it a better document. I appreciate your time and feedback. Thank you.

Unless the Lord builds the house,
the builders labor in vain.
Unless the Lord watches over the city,
the guards stand watch in vain.

Psalm 127:1 (NIV)

To him who is able to keep you from stumbling and to present you before his glorious presence without fault and with great joy – to the only God our Savior be glory, majesty, power and authority, through Jesus Christ our Lord, before all ages, now and forevermore! Amen.

Jude 24-25 (NIV)

Chapter 1

Analytical Methods for Imaging Metals in Biology: From Transition Metal Metabolism to Transition Metal Signaling

Introduction

Metal elements represent some of the most fundamental chemical building blocks of life and are required to sustain the growth, development, and sustenance of all living organisms and ecosystems across the planet.[1] Like other major chemical units in biology, metals are distributed in a heterogeneous fashion across biological systems in both a spatial and temporal manner. Depending on their function, select metals are enriched in specific locations within organisms, tissues, and cells, while being depleted in other locations. However, unlike organic biomolecules, metals cannot be synthesized at the location where they are used. Instead, they must be acquired from an organism's environment, carefully trafficked to the correct tissue and cell, and loaded into the correct protein or other biological target.[2-7] Moreover, too much or too little of a given metal nutrient in a given location can be detrimental to the living system.[8-11]

As metals are acquired, they may be part of the labile or static metal pool, or both (Figure 1.1). The labile pool is the collection of metal ions in a cell that are weakly bound and can undergo kinetically appreciable ligand exchange, thereby moving between proteins and small molecules with relative ease. In contrast, the static metal pool is made up of ions that are tightly bound to ligands, usually proteins, and do not dissociate. Typically, the static metal pool is viewed as a thermodynamic sink and the final destination for metals traveling through the labile metal pool.[12] The total metal pool is thus made up of the sum of the labile and static metal pools, and metal homeostasis is maintained by a balance of the acquisition and trafficking pathways with the excretion pathways for metalloproteins or other metal-ligand complexes. Disruption of any of these fundamental processes can lead to complex, multifaceted, and often widespread effects that are detrimental to health and development.[8,13,14] As such, elucidating mechanisms of metal acquisition, mobilization, and/or sequestration is vitally important to understanding the contribution of metals to healthy and disease states within living systems.

In this review, we present an overview of analytical methods for imaging the distributions of metals in biological systems. Specifically, we highlight the power of using multiple complementary analytical techniques, in concert, to map total metal pools and distinguish which subsets of those total pools are static and tightly-bound versus dynamic and weakly-bound. To illustrate this general approach, we focus our attention on the two most abundant redox-active transition metals in living systems, iron and copper. Both iron and copper have been traditionally studied in bioinorganic chemistry as static cofactors that are tightly bound by metallochaperones and buried in protein active sites to protect cells against oxidative stress,[15,16] but they now are emerging as dynamic transition metal signals that can reversibly affect the function of proteins in allosteric regions outside active sites. Applying a suite of analytical techniques to probe the quantity, location, and oxidation state of total and labile transition metal pools can reveal new principles that define the metallobiochemistry of metabolism and signaling.

In this context, available technologies for metal imaging can be divided broadly into two categories. The first category comprises techniques for measuring total metal pools, including laser ablation inductively coupled plasma mass spectrometry (LA-ICP-MS),

secondary ion mass spectrometry (SIMS), X-ray fluorescence microscopy (XFM), X-ray absorbance spectroscopy (XAS), particle-induced X-ray emission (PIXE), and various electron microscopy (EM) methods (Figure 1.1). The second category comprises techniques for measuring labile metal pools using small-molecule and genetically-encodable sensors and indicators (Figure 1.1). We survey the state-of-the-art for metal imaging technologies and conclude by highlighting select case studies to show how multiple complementary methods can be applied to study iron and copper pools over the various timescales that span transition metal metabolism to transition metal signaling.

1. Technologies for Imaging Total Metal Pools

Multiple technologies have been applied to map the relative distribution of elements in biological samples.[17,18] In each of these techniques, the sample is placed in the path of a high-energy beam (e.g., laser, ion, x-ray, or electron) and then moved relative to this source, so that the beam scans across the sample. As with all scanning techniques, tradeoffs are made between analysis time, spatial resolution, extent of sample coverage, and sampling statistics at each location, which govern sensitivities and limits of detection. We point to an elegant recent tutorial review of the tradeoffs of sensitivity, selectivity and spatial resolution for metal imaging in biology.[19]

In this context, we provide a survey of the state-of-the-art for technologies that can be used to image total metal content in biological samples. These technologies can be divided into two categories: (1) methods that measure the mass of the atom using mass spectrometry, and (2) methods that probe the electronic structure of that atom. These categories organize our discussion below, and we highlight considerations for each technique that are specific to copper and iron.

We begin with a few brief comments on sample preparation, a topic that is relevant to all total metal imaging methods. Since metals are not covalently anchored inside of cells, leaching and relocalization of these elements during sample preparation must be approached with caution.[20-27] Best practices for minimal perturbation of metal localization include flash-freezing or freeze-drying samples.[28,29] Additionally, for X-ray-based techniques that provide information about metal oxidation state and binding environments, radiation-induced reduction, as well as oxygen exposure leading to metal oxidation, which is of particular concern for iron and copper, could potentially introduce artifacts and confound interpretation.[30-32]

1.a. Technologies That Probe Atomic Mass

Mass spectrometry-based methods for metal mapping provide direct information about the metal isotope. However, these techniques cannot provide information about the oxidation state or coordination geometry of the metal in the tissue, since the metal is removed from the tissue and ionized during detection.

1.a.i. Laser Ablation Inductively-Coupled Plasma Mass Spectrometry (LA-ICP-MS)

LA-ICP-MS maps the concentration of individual isotopes in samples, most commonly tissue slices, making it a workhorse for imaging metals in biology (Figure 1.2a).[33-37] Quadrupole, sector field,[38] and time-of-flight (TOF)[39] analyzers have all been used for LA-ICP-MS to give single-isotope mass resolution (e.g., ^{56}Fe vs ^{57}Fe, and ^{63}Cu vs ^{65}Cu). This capability has been particularly useful for isotope uptake studies.[40-42] TOF or multicollector sector field mass spectrometers analyze multiple isotopes from exactly the same location and provide the highest precision isotope ratio mapping;[43,44] however, the use of quadrupole mass spectrometers (Q-MS) for isotope ratio mapping is being explored,[42,45,46] since Q-MS is the most common mass analyzer used for ICP-MS.

To achieve the highest signal for LA-ICP-MS metal mapping, the most abundant isotope is typically monitored. For iron and copper, these are ^{56}Fe, with 92% natural abundance, and ^{63}Cu, with 69% natural abundance, respectively. However, polyatomic interferences present a formidable analytical challenge since Q-MS has relatively low mass-resolving power (typically <300 M/ΔM) and cannot discriminate elemental ions from polyatomic ions.[47] For example, $[^{40}Ar^{16}O]^+$ flies at the same mass-to-charge ratio as $[^{56}Fe]^+$, and Q-MS detectors cannot distinguish them. Because the plasma for ICP-MS is based on argon and biological samples contain significant amounts of oxygen, the background signal from $[^{40}Ar^{16}O]^+$ is particularly detrimental to ^{56}Fe imaging. Similar concerns exist for $[^{40}Ar^{23}Na]^+$ interference with $[^{63}Cu]^+$ imaging. Recently, kinetic energy discrimination (KED) using H_2 gas flow was developed to allow ^{56}Fe imaging with Q-MS analyzers.[48] Although the method dramatically decreases overall signal, the ratio of signal:background is improved, and useful images have been obtained.

The raw output of LA-ICP-MS is in units of counts per second, which may be converted to metal concentrations using standards. For biological samples, matrix-matched standards made from soft materials are preferred over glass standards, which are hard and exhibit different ablation properties compared to soft tissue. Standards are typically prepared by adding known amounts of metal to homogenized tissue[49,50] or gelatin[51] and subsequently slicing the standards to the same thickness as the tissue to be analyzed. Additionally, normalization to an internal standard isotope that is evenly distributed in biological tissue (such as ^{13}C or a deposited thin layer of Au) can correct for variations in ablation efficiency across the sample.[52,53] Approaches for quantification of LA-ICP-MS data have been recently reviewed.[54] Although detection limits as low as 0.01 μg g^{-1} have been reported for rare and precious elements (eg. Th, U, and Ag),[55,56] practical detection limits for earth-abundant metals such as copper and iron are in the range of 0.1-2 μg g^{-1} depending on experimental setup;[38,48,50,56-58] this is primarily due to inherent differences in ionizability in the plasma, interferences from the gas background, and environmental contamination of the surfaces used for sample mounting (e.g. glass slides, double-sided tape).

An attractive feature of LA-ICP-MS is the wide variety of samples that can be analyzed. Sample requirements are minimal and include being able to fit inside the sample chamber (standard commercial chambers are approximately 100 cm^2 x 1 cm high) on a flat surface so that the sample surface remains in the focal plane of the beam during imaging. For tissue slices, a thickness of 20 μm or greater is sufficient to provide signal above

background, and a laser power that fully ablates the sample thickness without perturbing the rest of the sample provides the most consistent results.[54,59] Thicker samples can also be used, and depth profiling by ablating through thick samples can provide useful information about changes in elemental concentration in the z-dimension.[60] LA-ICP-MS is a destructive technique, so any other imaging must be done before LA-ICP-MS analysis.

Generally, the dimensions of the laser beam define the lateral spatial resolution of the image, although scan rates that under- or over-sample the ablated area also contribute to spatial resolution.[59] Typical beam diameters used for biological imaging are 5 µm – 150 µm. This range of beam diameters makes LA-ICP-MS quite versatile; large spot sizes provide a rapid and economical way of scanning large tissue sections or a high volume of samples (Figure 1.2c),[61] while small spot sizes allow detailed analysis of a region of interest. Methods have been published for optimizing tradeoffs between spatial resolution and acquisition time.[62] Subcellular imaging of gold and silver nanoparticles and antibodies labeled with precious metals has been achieved,[59,63-65] but subcellular resolution is not yet available for imaging of endogenous metals. Improvements in the limits of detection of LA-ICP-MS may yield instruments capable of quantifying endogenous metals at subcellular resolution.[58,64,66,67]

1.a.ii. Secondary Ion Mass Spectrometry (SIMS)

SIMS maps individual isotopes with higher mass resolution and higher spatial resolution than LA-ICP-MS. Although matrix effects make absolute quantification challenging, the NanoSIMS instrument readily achieves subcellular imaging of endogenous metals and nonmetals.[68-71] As such, NanoSIMS is exceptional for its ability to track isotope uptake, sequestration and mobilization with subcellular resolution.[70]

In SIMS, the sample is affixed to a sample carrier which is pumped into a high-vacuum chamber at ambient temperature (custom-built cryocooled chambers exist, but are not routinely used[72]). A primary ion pulse or reactive primary ion beam delivers charge to the sample, causing secondary ions to be emitted (Figure 1.2b). These secondary ions are focused into a mass spectrometer, and maps of ion counts are generated. Two basic types of SIMS include static SIMS and dynamic SIMS.[69] Static SIMS uses an ion pulse and TOF detector; a full ion spectrum is collected with each pulse, allowing the investigator to view the relative levels of all species at each location.[73] This technique is especially useful for exploratory work and profiling work, but the yield of secondary ions is inherently low in static SIMS, limiting its sensitivity. Dynamic SIMS uses a reactive ion beam with a sector field detector. The reactive ion beam sputters into the sample, embedding ions in the sample surface and dramatically increasing the yield of secondary ions, which improves the sensitivity of the instrument. However, the sector field detector collects only five or seven masses at a time (depending on the model), so the investigator must decide ahead of time which masses to monitor. Although these two techniques can be delineated, instruments designed for static SIMS can be run in dynamic mode, so the distinction is not absolute. In the area of metal imaging, dynamic SIMS provides the sensitivity necessary for high spatial resolution imaging. In particular, the CAMECA

NanoSIMS 50 and 50L dynamic SIMS instruments have set the standard in the field for sensitivity and spatial resolution of SIMS imaging,[68,69] and we focus our discussion on applications with this platform.

Like ICP-MS, SIMS counts the number of ions of a specific mass. The mass resolving power of SIMS is much higher than typical ICP-MS (~3500 M/ΔM at 100% transmission)[74] and can thus discriminate elemental ions from polyatomic interferences, providing a clean readout of each isotope of interest. The sensitivity of SIMS depends on the type of ionizing beam used, and it varies from element to element. Secondary cations are generated by an anionic beam, so elements that readily adopt a positive charge, such as copper and iron, are easiest to map with an anionic primary ion beam (O^- on the NanoSIMS). The converse is true of secondary anions, which are analyzed by a Cs^+ beam on the NanoSIMS instrument. Although carbon, phosphorus and sulfur are much less ionizable in an anionic primary beam, they are orders of magnitude more abundant in a biological sample than iron and copper, so images of these elements can be acquired in anionic mode. The carbon signal is used to normalize for matrix effects at different locations in the sample, and maps of other nonmetals can provide useful information about the elemental composition of areas of high metal concentration (Figure 1.2d).[71] Absolute quantification of SIMS data is challenging because the generation of secondary ions is highly dependent on the matrix in which they are embedded. Although glass and metal standards are most frequently used, in an ideal case, matrix-matched standards for biological samples would provide a more accurate calibration curve. As such, recent studies mapping the distribution of metals in algae[70] and neurons[71] report data in counts-per-second rather than metal concentrations.

SIMS analysis is performed on relatively small biological samples (from single cells to a few cm^2) due to the relatively small sample chamber. Since the lateral spatial resolution of NanoSIMS can routinely approach 100 nm, this technique excels in the analysis of single cells and subcellular metal localization. The samples must be plated on a conductive surface or coated with a thin conductive layer (eg. Au) to diffuse potential buildup of charge from the ion beam. Additionally, the sample must be robust to high vacuum, which means biological samples must be dry. Because SIMS is a surface technique (accessing only the top 100-500 nanometers of the sample), samples as thin as 200 nm can be used.[70] Thicker samples can be scanned at the surface, or depth profiling can be used to probe metal concentration within the sample.

1.b. Technologies That Probe Electronic Structure

A complementary set of technologies is based on measuring energy absorption and emission by the metal of interest. The amount of energy that is absorbed or emitted is characteristic of each element and reflects the energies of the element's orbitals. These techniques cannot provide isotopic information, as they do not interact with the atomic nucleus. However, they do interact with the electronic structure and can provide information about the oxidation state and coordination geometry of the metal in its native environment, since the metal is not removed from the sample during analysis.

1.b.i. X-Ray Fluorescence Microscopy (XFM)

XFM is the most commonly used technique for imaging iron and copper in biological systems. Although it requires the use of a synchrotron facility, many synchrotron facilities around the world have stations dedicated to biological investigation, and improvements in XFM hardware continue to enable new experimental systems to be pursued.[75-78] In XFM, the sample is placed on a sample holder in the path of a high-intensity X-ray beam at ambient pressure and, traditionally, ambient temperature (Figure 1.3a). When an X-ray from the beam collides with an atom in the sample, energy is transferred from the X-ray to the atom. This energy transfer causes an electron from the inner shell of the atom to be ejected, leaving a hole. An outer-shell electron from the atom relaxes to fill the hole. The atom emits an X-ray, which is detected by an energy dispersive detector, allowing for simultaneous, multi-element analysis.[79] The energy of the emitted X-ray is the energy gap between the outer shell and inner shell orbitals involved, and it is characteristic of the atom that emits the X-ray. Because metals have multiple outer shells, multiple X-ray emission energies are possible. However, the most intense X-ray emission from a metal occurs at its K_α line, which is typically used for analysis. K_α denotes emission of an X-ray due to an electron moving into the 1*s* orbital (K shell) from the 2*p* orbital. The K_α lines for iron and copper are 6.404 keV and 8.048 keV, respectively.[80,81] Fortunately, the fluorescence emission lines for the transition metals fall well outside the crowded emission region from lighter, more abundant elements (up to ~4 keV), allowing excellent quantification of iron and copper by XFM in biological samples (Figure 1.3b). With the use of spectral fitting, these elements can be quantified with limits of detection reaching 0.1-1 μg g^{-1}.[80]

Quantification of XFM data can be achieved by calibration with known standards, such as metal thin films[80] or organic standard reference materials, such as bovine liver.[82] The resulting values have units of μg cm^{-2}, which cannot be directly converted to μg g^{-1} unless the thickness and density of the sample is known. By assuming that the sample thickness reflects the slicing thickness during tissue preparation, and by using known tissue densities of similar tissues, these unit conversions have been extrapolated.[83] However, in one comparison between XFM and LA-ICP-MS in brain tissue, a systematic discrepancy in absolute metal quantification was observed, even though both techniques revealed similar metal maps. Values measured for copper using XFM were 60% of the values measured by LA-ICP-MS, whereas XFM values for iron were 150% of the LA-ICP-MS values.[82] Nevertheless, both of these technologies provide excellent metal maps at their respective length scales and offer powerful tools for probing metal biology.

Sample preparation for XFM analysis is quite straightforward, since the only requirement is that the sample be mounted on a substrate that does not absorb or emit X-rays in the energy ranges to be analyzed. Typically, silicon nitride or Ultralene windows are used for cells and small tissue slices (typical tissue thickness is 10-30 μm).[80] However, very large samples can also be analyzed, for example slices of human heart (5 mm thick) sealed inside a polypropylene bag (30 μm thick plastic).[84] Samples are commonly dried or fixed, although the development of cryocooled analysis chambers has permitted the analysis of frozen, unfixed, hydrated samples.[85-87] Some beamlines have an optical setup to image

larger samples, while others are optimized for smaller samples, such as single cells, and provide high spatial resolution images, down to 50 nm (Figure 1.3d).[85,88,89] The Maia detector at the Australian Synchrotron is a notable exception, being designed to accommodate samples as large as 600 x 300 mm^2 (analyzed, for example, at 100 µm resolution), while still achieving <1 µm resolution in other samples.[75,76]

Recent advances in XFM methodology have enabled the analysis of more structurally complex samples, and provided insight into the cellular substructure in which metals are stored. For example, tomographic methods measure metal concentrations in intact 3-dimensional structures.[77,90-93] Additionally, the combination of XFM with ptychography has allowed the unambiguous overlay of subcellular structure with subcellular element distribution, alleviating the longstanding problem of aligning transmitted light microscopy images with XFM images to assign subcellular metal localization.[28]

1.b.ii. X-Ray Absorbance Spectroscopy (XAS)

Like XFM, XAS requires the high-energy X-ray beam of a synchrotron X-ray facility. In XAS, however, the energy that is absorbed by the analyte is measured, rather than the energy that is emitted. Measuring the absorbed energy provides information about the oxidation state of the analyte and, potentially, its coordination geometry and ligands. XAS data can be collected in transmission mode or fluorescence mode. Because copper and iron are quite dilute in a biological sample, they cannot be detected in transmission mode. Thus, we discuss fluorescence-mode XAS here, which achieves detection limits in the low or sub µg g^{-1}.[80,94] The X-ray beam used for XAS has a defined, but variable, energy. During spectrum collection, the energy of the beam starts at a low energy and is increased, by small intervals, to higher and higher energies. When the energy of the beam matches the electron binding energy of a particular atom in the sample, an electron is ejected from the inner shell of the atom, leaving a hole. An outer-shell electron relaxes to fill the hole, emitting an X-ray. Because fluorescence emission is proportional to energy absorption, the number of X-rays that are emitted from the sample can be used as a proxy for the number of photons that were absorbed from the incident beam. Each beam energy stimulates X-ray emission from a specific element (or set of elements); the more X-rays that are emitted when the sample is exposed to a certain beam energy, the more atoms of the corresponding element there are in the sample. An element's largest absorbance occurs at its K-edge.[95] "K" denotes ejection of an electron from the 1*s* orbital (K shell), and the word "edge" is used because a large change in absorbance occurs at this energy, causing an "edge" in the spectrum. The K-edges for iron and copper occur at 7.112 keV and 8.993 keV, respectively.[81] Two types of XAS have been delineated: X-ray absorption near edge structure (XANES), which is also called near-edge X-ray absorption fine structure (NEXAFS) and extended X-ray absorption fine structure (EXAFS). A XANES spectrum starts a few eV before the absorption edge of the element of interest and ends ~150 eV above the absorption edge; XANES provides information about the oxidation state of the atoms of that element. An EXAFS spectrum continues from 150 to 800 eV above the absorption edge and provides information about the coordination environment of the atoms of that element.[96]

The largest limitation to XAS imaging of biological samples has been sample damage due to extensive irradiation during image acquisition. A XANES spectrum for one element typically requires reading the absorption at 100 different beam energies, exposing each location in a sample to 100-times the radiation that it would normally receive during an XFM image.[19] At these radiation doses, sample morphology is altered, and metals may be photoreduced, fundamentally interfering with the purpose of XANES.[30,31] Two experimental approaches have been pursued to overcome this limitation. First, holding the sample at cryogenic temperatures minimizes sample damage.[28,97] Second, exceptionally sensitive detectors have reduced the time necessary to acquire a XANES spectrum,[75] demonstrating a 100-fold reduction in the total radiation used for image acquisition.[76] This method, named φ-XANES, has allowed investigators to map the oxidation state of iron in living, anaesthetized *C. elegans*.

Typically, XAS data are analyzed by comparing the experimental spectrum to a spectrum of a known compound. However, because of the vast number of iron coordination environments present in a biological sample, this method of analysis can be difficult to apply effectively. With φ-XANES data, a new mode of analysis has become available. Principle component analysis was used to identify aggregate modes of iron coordination present in each φ-XANES image.[98] These modes were computationally defined spectra, rather than being derived from the spectrum of a control compound. Each pixel of the image was assigned a color based on its aggregate mode of iron coordination (ie. its spectrum), and a map of coordination modes was generated. By color-coding the image according to the ratio of Fe^{2+}:Fe^{3+} in each computationally-defined coordination mode, an intuitive map of iron oxidation states in *C. elegans* was created (Figure 1.3c).[76] Direct comparison of the maps from wildtype and *ftn-2* worms lacking ferritin reveals a shift to a higher Fe^{2+}:Fe^{3+} ratio throughout the worm, without altering the spatial arrangement of more-oxidizing and less-oxidizing environments within the worm (see section 3.a. for further discussion).

1.b.iii. Micro Particle-Induced X-Ray Emission (μ-PIXE)

Micro-PIXE uses a particle beam to stimulate X-ray emission. Thus, μ-PIXE requires the use of a particle accelerator, making it perhaps the least accessible technique for most metallobiology studies. The main advantage of PIXE is that it is quantitative without the need for standards. The backscattered and transmitted particles from the beam can be analyzed using Rutherford backscattering spectroscopy (RBS) and scanning transmission ion microscopy (STIM) to provide a measurement of the local sample mass. Analyte mass is normalized to sample mass, providing concentrations in units of μg g^{-1}.[99] PIXE operates in a vacuum, so samples must be dried. A sample thickness of 20-30 μm is sufficiently thin to allow STIM measurements of tissue density,[100] and this thickness has been used for imaging fixed[101] and freeze-dried[100,102] biological samples mounted on thin plastic films. Using a beam size of 1-5 μm^2, μ-PIXE achieves limits of detection for iron and copper that are 1-10 μg g^{-1}.[80,102]

1.b.iv. Electron Microscopy (EM)

EM methods for metal analysis use the same principles as XFM and XAS, but the primary beam is an electron beam. These methods can be performed on traditional electron microscopes, but these microscopes must be outfitted with correctly located energy dispersion detectors or energy filters, which may not be available in some EM facilities. Similar to XFM, energy dispersive X-ray spectroscopy (abbreviated EDX, EDS, EDXS, or XEDS) measures the X-rays emitted from the sample due to its interaction with the electron beam.[103] Compared to XFM, the background signal for EDX is quite high. Inelastic electron interactions within the SEM generate a background signal (called *Bremsstrahlung*, which is German for "braking radiation") that greatly diminishes sensitivity for heavy elements. Because of this background radiation, EDS is significantly less sensitive than XFM for iron and copper, providing limits of detection of 0.01 wt% (100 μg g^{-1}) for these elements.[104,105] However, EDX can be used to determine elemental composition of very small subcellular regions that are enriched for iron or copper, such as neuromelanin melanosomes[71] and cataracts.[106] Thus, EDX may provide by far the highest spatial resolution of all metal mapping techniques (~10 nm),[107] but only for subcellular structures in which the local metal concentration exceeds 100 μg g^{-1}.

Unlike EDX, energy loss electron spectroscopy (EELS) can be very sensitive for elements like P, Ca, and Fe,[107] detecting as little as a single iron atom within purified hemoglobin.[108] EELS is a transmission technique that measures the energy lost by electrons as they interact with electrons in the sample. Core losses (50-600 eV) are characteristic of specific elements and can be used to determine elemental composition at a given location in the sample.[18] EELS images can be acquired by two techniques: scanning transmission electron microscopy EELS (STEM-EELS) or energy filtered transmission electron microscopy (EFTEM). STEM-EELS uses a scanning electron beam to record a full EELS spectrum at each location in the sample. Data acquisition is unbiased because a full EEL spectrum is acquired at each location, but a large dose of radiation is also administered to the sample, potentially causing significant sample damage.[109] EFTEM uses a fixed beam to irradiate a large area of the sample and an energy filter to analyze only the electrons that correspond to an energy loss from the element of interest (after background subtraction). EFTEM greatly reduces the radiation dose received by the sample, but only a few energies are analyzed, biasing the analysis toward the elements that are expected to be in the sample. For an excellent comparison of these techniques, see da Cunha *et al.* (2016).[18]

Sample preparation for EELS is nontrivial, following the same process as sample preparation for any transmission electron microscopy (TEM) technique. Electron microscopy is performed in a vacuum, and electrons do not penetrate thick samples. Thus, samples must be fixed (by aldehyde fixation or high-pressure freezing), embedded, and sectioned to very thin slices (50-100 nm). Typically, tissue sections are stained with heavy elements to increase contrast during imaging. However, contrast elements such as osmium and uranium must be avoided for iron analysis because of spectral interferences.[18] EELS imaging has proven particularly powerful for the imaging of ferritin,[110] the principle iron storage protein in mammalian cells (Figure 1.3e).[111] Individual molecules of ferritin can be resolved within a tissue section, and the amount of iron loaded into each ferritin complex can be estimated based on the size of the iron particle that is

visible by EM.[112] Subramaniam and coworkers demonstrated that degenerating neurons of mice have lower ferritin inside their axons, while ferritin instead builds up outside the axon.[113] Previous studies using light microscopy had suggested that neurodegeneration correlated with ferritin accumulation in neuronal axons; only electron microscopy provided the resolution to demonstrate that the increase in ferritin occurred outside of neuronal axons. Additionally, EFTEM tomography has enabled the visualization of 3-dimensional subcellular structure at unprecedented resolution, which can allow ferritin to be visualized within the subcellular context.[114,115] As our understanding of the labile pool grows, EELS is sure to provide valuable information about the role of ferritin in iron sequestration and mobilization.[116,117]

2. Technologies for Imaging Labile Iron and Copper Pools

Analytical methods for assessing labile metal pools[118,119] can complement the suite of techniques for direct imaging of total metal pools. The labile metal pool consists of metal ions that are weakly bound to intracellular ligands, such that these ions can be rapidly removed or sequestered by competing metal chelators in the biological environment. Such metal pools may also undergo ligand exchange with fluorescent probes that respond to metal binding and/or reactivity with a change in fluorescence, enabling metal detection with spatial and temporal resolution. These probes can be reversible sensors or irreversible dosimeters. Desirable properties of an effective fluorescent metal probe include (1) high selectivity for the metal of interest, even in the presence of competing metals, other analytes in the cellular milieu, or local changes in pH, redox, and hydrophilicity/hydrophobicity, (2) a large turn-on increase or ratiometric wavelength shift in fluorescence to provide spatial information, in contrast to probes that turn off (ie. disappear) in the presence of analyte, (3) compatibility with common microscopy laser lines and/or filter sets in terms of excitation/emission wavelengths, (4) visible, red-shifted spectral profiles to minimize sample photodamage and interference from native cellular autofluorescence in blue wavelengths, and (5) predictable localization in a given biological specimen. For redox-active metals such as iron and copper, an additional challenge is to avoid electron- and energy-transfer quenching pathways from transient odd-electron species that can arise from ground or excited states. We will restrict our discussion to probes for labile iron and copper pools that target the Fe(II) and Cu(I) oxidation states, which are dominant within the cell owing to the reducing intracellular environment.

We focus on synthetic small-molecule reagents, which have potential for broad application to many cell, tissue, and organism models as they do not require transfection or other manipulations to be introduced into a specimen. At the same time, however, the complexity of biological systems means that there is no one-size-fits-all probe for all systems, and each chemical reagent has to be tested and validated with proper controls in each biological setting and application. Indeed, potential confounding factors and artifacts can include increases and shifts in fluorescence signals due to accumulation, relocalization, or aggregation of dyes. As such, studies that employ imaging of labile metal pools benefit from biological controls with genetic and/or pharmacological manipulation, as well as complementary direct metal imaging methods. Additionally, the pursuit of

ratiometric indicators with an internal standard and/or control probes that enable disentangling of dye- versus receptor-dependent signal changes, is highly encouraged. Fluorescent indicators fall into one of two basic categories: (1) recognition-based and (2) reaction-based. Recognition-based probes respond to the reversible coordination of a metal to a receptor, whereas reaction-based probes bind a metal to trigger a chemical event that leads to a fluorescence change. Recognition-based detectors are valued for their reversibility but require careful matching of appropriate K_d values in order to avoid stripping and redistributing tightly-bound metal pools. Reaction-based indicators can be valuable for detecting small changes in metal levels when the reaction is catalytic with respect to the metal, allowing the amplification of signal and integration of signal over time. Such indicators do not permanently bind the metal, and thereby avoid perturbing the labile metal pool or undergoing metal-induced fluorescence quenching; however, after the reaction, diffusion of the probe away from the metal leads to a loss of spatial information. Although a wide variety of fluorescent iron and copper probes have been reported in the literature, only a limited subset of these diverse candidates has been satisfactorily characterized in cells, tissues, or animals with comparative images where pharmacological or biological treatments induce metal excess or deficiency, and our discussion focuses on these reagents.

2.a. Fluorescent Probes for Labile Iron

Iron, the body's most abundant transition metal element, presents unique challenges as an analyte, beyond the common challenges of imaging biological metals. This metal readily cycles between Fe^{2+} and Fe^{3+} under biological conditions, and although mounting evidence has suggested that the intracellular labile iron pool[120] consists mainly of Fe^{2+},[121] the redox activity of iron and its ability to adopt high- or low-spin configurations makes iron a potent potential fluorescence quencher by electron and energy transfer. Fe^{2+} is also a weakly-coordinating metal on the Irving-Williams series, so developing effective receptors that can selectively bind this ion over competing Cu^{2+}, Ni^{2+}, and Zn^{2+} in particular, is difficult. During probe characterization, potential complications involving iron solubility[122] or uncontrolled Fenton oxidations must be considered. As such, interest in visualizing Fe^{2+} in living systems is high, but developing selective and sensitive Fe^{2+}-responsive probes remains a significant challenge.

2.a.1. Recognition-Based Iron Sensors

Recognition-based fluorescent sensors for turn-on detection of Fe^{2+} remain elusive, but several turn-off sensors have been employed to observe changes in labile Fe^{2+} levels in cell lysates, live cells, and even model organisms. The two most commonly used sensors, based on a fluorescein scaffold, are the commercially available Calcein and Phen Green SK dyes (Figure 1.5). Neither sensor shows high iron selectivity, as Calcein responds strongly to Cu^{2+}, Co^{2+} and Ni^{2+} (>95% fluorescence decrease for each),[123] and Phen Greek SK responds strongly to Cu^{+} and Cu^{2+} (97% and 70% decrease, respectively).[124] Oxidation state specificity for Fe^{2+} over Fe^{3+} is also modest, as Calcein shows nearly quantitative fluorescence quenching in the presence of Fe^{2+} but 40-50% quenching in the

presence of an equivalent amount of Fe^{3+}. Despite the limited selectivity of Calcein and Phen Greek SK for Fe^{2+}, iron-specific chelators can be used with these probes to identify changes in labile iron pools. Additional Fe^{2+} sensors include the pyridinone-based indicator CP655 (Figure 1.5) that exhibits improved selectivity for Fe^{2+} over other cations, with only Cu^{2+} presenting mild cross-recognition (42% decrease).[125] However, CP655 is not selective for Fe^{2+} over Fe^{3+} and also shows pH sensitivity. Nevertheless, this reagent has been employed to probe labile iron with uniform cellular staining.[126] Finally, RPA, RDA, and PIRO (Figure 1.5) are rhodamine-based fluorescent iron sensors that localize to the mitochondria owing to the positive charge delocalized over the fluorophore structure.[127,128] This set of probes displays decreasing affinity for Fe^{2+} (RPA > RDA > PIRO), enabling visualization of endogenous iron (with RPA and RDA) or exogenous iron (with PIRO) depending on the biological situation. Each of the probes recognizes Cu^{2+} to some extent (RPA: 73% decrease, RDA: 87%, PIRO: 27%), but has good selectivity over other metals. The rhodamine-based iron sensors have identified a rise in mitochondrial labile iron when heme synthesis is blocked, with a control rhodamine 123 dye showing that mitochondrial membrane potential is not disrupted under these conditions.

2.a.2. Reaction-Based Iron Indicators

The growing palette of chemodosimeters for Fe^{2+} detection exploit the potent redox activity of this metal ion. A variety of mechanisms, including N-oxide deoxygenation, TEMPO radical reduction, oxygen-dependent oxidative C-O bond cleavage, and endoperoxide cleavage, have been reported. RhoNox-1 (Figure 1.5) was the first reaction-based Fe^{2+} probe to be used in a cellular system.[129] This rhodamine-based probe relies on the ability of Fe^{2+} to selectively deoxygenate an N-oxide, converting it to a tertiary amine with a concomitant 30-fold fluorescence turn-on response. RhoNox-1 derivatives such as HMRhoNox-M (Figure 1.5), which displays a more stable pH profile and a 60-fold turn-on in fluorescence, has been used to visualize iron uptake via transferrin endocytosis[130] and iron accumulation in ovarian endometriosis.[131] A related rhodamine probe, Rh-T (Figure 1.5), contains a pendant paramagnetic TEMPO group that quenches fluorescence.[132,133] Fe^{2+} reduces the TEMPO radical to a diamagnetic hydroxylamine, resulting in a 2.5-fold fluorescence turn-on with good selectivity for Fe^{2+} over other metal cations, as well as cellular reductants such as ascorbate and NADH. In human fibroblasts, Rh-T responds to the addition of exogenous iron, but its signal does not decrease in response to iron chelation.

Our laboratory published Iron Probe-1 (IP-1, Figure 1.5), a first-generation Fe^{2+} fluorescent indicator inspired by the oxidative reactivity of mononuclear nonheme iron enzymes.[134] In the presence of Fe^{2+} and O_2, IP-1 undergoes a C-O bond-cleavage reaction to release a reduced fluorescein alcohol derivative, resulting in a 6-fold fluorescence turn-on with high selectivity over competing metal ions in the cell. Only free Co^{2+} elicits a response from IP-1 *in vitro*, but more importantly, the probe does not respond to cyanocobalamin (vitamin B_{12}), the biologically relevant form of cobalt in cells. In HepG2/C3A liver cells, IP-1 localizes to the lysosome, where it is able to sense both increases and decrease in iron levels from iron supplementation and chelation, respectively. Additionally, IP-1 was capable of detecting increases in labile iron following

treatment with hepcidin or vitamin C, two natural compounds known to increase labile iron stores.

To improve upon the 3-component reaction of IP-1 and provide a direct reaction-based detector for Fe^{2+}, we recently presented FIP-1 (Figure 1.5), a unique ratiometric fluorescent indicator for this metal ion. FIP-1 is a FRET-based probe that uses an endoperoxide trigger[135] to cleave a linker between 5-aminomethyl coumarin and fluorescein in the presence of Fe^{2+}.[136] This direct and oxygen-independent 2-component reaction proceeds rapidly in the presence of Fe^{2+} and results in a 2-fold FRET change. Moreover, FIP-1 distributes evenly within cells, and can clearly distinguish both increases and decreases in endogenous labile iron pools. Using FIP-1, we demonstrated that cancer cells possess higher levels of labile iron stores compared to noncancerous cells. Finally, we provided the first evidence of elevations in labile iron during the induction of ferroptosis,[136] a form of iron-dependent cell death.[137] A related puromycin-based endoperoxide probe (Trx-Puro, Figure 1.5) reveals that overexpression of ferritin or ferroportin, iron storage and iron export proteins, respectively, decreases labile iron stores in a variety of cancer cell models.[138]

2.b. Fluorescent Probes for Labile Copper

Like iron, copper can cycle between two oxidation states under biological conditions, Cu^{+} and Cu^{2+}, presenting a selectivity challenge for probe design and characterization. Previous reports provide evidence that Cu^{+} is the dominant intracellular copper oxidation state for labile pools,[139,140] although Cu^{+} is prone to disproportionation in water, which requires stabilization by appropriate ligands.[141] Additionally, both oxidation states of copper are capable of quenching fluorescence, making the design of recognition-based probes particularly challenging as charge-transfer processes can generate transient Cu^{+} and Cu^{2+} species. As the field of fluorescent-based Cu^{+} probes has been thoroughly reviewed,[119,142-144] we focus our discussion on probes that have been employed for biological application.

2.b.1. Recognition-Based Copper Sensors

The first sensor for Cu^{+} was introduced by Fahrni and coworkers in 2005.[139] Using a triarylpyrazoline dye and macrocyclic thioether copper-binding motif, CTAP-1 gave a 4.6-fold fluorescent turn-on in the presence of excess Cu^{+}, with no response or interference from other biologically relevant cations (Figure 1.6). In NIH 3T3 fibroblasts, CTAP-1 showed a significant fluorescence increase in cells cultured in high-copper media compared to basal media. Additionally, its signal showed good agreement with the subcellular distribution of total copper observed by XFM. Subsequent careful studies elucidated photophysical properties to improve signal-to-noise responses[145-147] and provide updated CTAP-2 and CTAP-3 versions with improved hydrophilicity (Figure 1.6).[148,149] In particular, CTAP-2, bearing four pendant hydroxyl groups on the thioether macrocycle, was capable of detecting the metallated Atox1 copper metallochaperone on a gel, and CTAP-3, bearing both hydroxyl and sulfonate groups, dissolves directly in water with no nanoparticle formation.

In parallel studies, our laboratory developed the first fluorescent copper sensors with visible excitation and emission profiles, which have enabled the study of copper homeostasis in a broad range of biological models used in our work as well as independent investigations by others. The first-generation BODIPY-based copper sensor, Coppersensor-1 (CS1, Figure 1.6), features a bis(2-((2-(ethylthio)ethyl)thio)ethyl)amine (BETA) receptor[150,151] and shows high selectivity for Cu^+ over all biologically relevant cations, with a 10-fold turn-on in the presence of Cu^+ *in vitro*. Initial studies showed that CS1 can identify copper-loaded HEK 293 cells compared to control cells, and this work was validated by another study[152] that also showed that this first-generation probe has different localization patterns in two other cell lines, M17 and U87MG. It is not surprising, with the complexity of biological systems, that there is not a one-size-fits-all chemical tool for all applications; as such, it is critical to implement both chemical and biological controls when using a given chemical probe for a given biological model. Indeed, with proper controls in place, CS1 has been employed as a pilot screening tool for assessing fluctuations in labile copper pools in bacteria,[153] yeast,[154-156] plant,[157] and mammalian systems.[158] Inspired by work by Nagano on treating fluorescent sensors as electron-transfer cassettes,[159] we developed a next-generation Coppersensor-3 (CS3, Figure 1.6) probe by replacing the fluoro substituents on the BODIPY core with methoxy substituents to improve its brightness (= 0.40 for CS3 vs = 0.13 for CS1) and signal-to-noise response to Cu^+ (75-fold turn-on for CS3 vs 10-fold for CS1).[160] Notably, the more electron-rich BODIPY core also manifests itself in a tighter Cu^+ K_d for CS3 (9×10^{-14} M vs 3×10^{-12} M for CS1). The combination of higher optical brightness, greater turn-on response to Cu^+, and tighter K_d for CS3 has enabled its use for assessing basal pools of labile copper in a variety of cell types, including neurons,[160] tumor cells,[161] mouse fibroblasts,[162] liver cells,[163] and algae.[70] These studies are bolstered by genetic and pharmacological controls as well as independent measures of the total copper pool.

Biological systems are complex mixtures of proteins, nucleic acids, glycans, lipids, and other organic species. Therefore, a balance between the hydrophobicity and hydrophilicity of any probe must be met for the use of a given probe for a given application. Indeed, in the case of copper sensors, similar to CTAP-1, BODIPY-based CS1 and CS3 do not homogeneously stain cells and thus are best suited for use in some biological models but not in others. In an effort to discriminate between dye-dependent fluorescent changes and metal-dependent fluorescent changes, we have introduced the concept of “synthetic mutagenesis” to create matched control probes. A first example is the development of Control Coppersensor-3 (Ctrl-CS3, Figure 1.6), which utilizes the same methoxy BODIPY core as CS3, but where the thioether sulfurs are replaced by isosteric carbons, which is akin to a methionine-to-alanine switch.[70] Thus, Ctl-CS3 cannot bind to copper and does not turn on in the presence of Cu^+. In *Chlamydomonas reinhardtii*, CS3 and Ctl-CS3 were used in pilot screening studies, in conjunction with direct metal imaging techniques, to identify the accumulation of copper in subcellular vesicular compartments, termed cuprosomes; the fluorescence of CS3 increased in the vesicles of experimentally-treated cells compared to control cells, but the fluorescence of Ctl-CS3 did not.[70] Neither probe responded to mutant algae with lipid-trafficking deficiencies, showing that fluorescent changes were not due to changes in the hydrophobicity of subcellular

environments. Our hope is that continued development of control probes to use in conjunction with analyte-responsive probes will help with the interpretation of imaging data using such reagents.

To expand the palette of fluorescent copper probes to more hydrophilic cores with the goal of improving their use in more hydrophobic environments, such as thicker tissue and animal specimens, our laboratory reported a first-generation Copper Rhodol series: CR1 – CR5.[164] The most responsive of these sensors, Copper Rhodol 3 (CR3, Figure 1.6), gave a 13-fold turn-on response to Cu^+. Replacement of the methyl substituent on the receptor-bearing aryl ring with a bulkier, more electron-withdrawing fluoromethyl substituent, gave Copper Fluor 3 (CF3, Figure 1.6) with a 40-fold turn-on response to Cu^+. Partition coefficient measurements demonstrated that CR3 and CF3 were significantly more hydrophilic (log D = 0.96 and 1.15, respectively) than the BODIPY-based CS3 (log D = 3.46). Additionally, both CR3 and CF3 responded to copper selectively in the presence of model liposomes, proteins, glutathione, and cell lysates, whereas control probes based on these scaffolds (Ctl-CR3 and Ctl-CF3, Figure 1.6) did not respond to copper under similar conditions. These new reagents helped to identify an exchangeable pool of copper in developing hippocampal neurons and retinal slices, which regulates normal spontaneous activity in neural circuits.[164]

Replacement of the oxygen atom on the rhodol core with a silicon isostere[165,166] led to the development of Copper Silicon Rhodol-1 (CSR1, Figure 1.6), a highly photostable fluorescent copper sensor that enables imaging of changes in copper pools in the same sample over long periods of time (Figure 1.6).[167] CSR1 retains a selective and sensitive response to Cu^+ (12-fold turn-on) on a hydrophilic probe (log D = 1.15) and was successfully used to monitor changes in labile copper pools in adipocytes, where it stained the cytosol but not lipid droplets. CSR1 discriminated cells pre-treated with copper, chelator or vehicle, and it responded to on-stage addition of the membrane-permeable copper chelator, tris((ethylthio)ethyl)amine (TEMEA). Finally, CSR1 revealed a decrease in labile copper in adipocytes upon stimulation of the beta-adrenergic receptor, concomitant with an increase in lipolysis. Fluorescence from the control probe Ctl-CSR1 (Figure 1.6) remained stable during parallel experiments, demonstrating the copper-specificity of CSR1 fluorescence in adipocytes. With these pilot imaging studies in hand, we went on to demonstrate that copper is an endogenous modulator of lipolysis through a cAMP signaling cascade where copper acts at the level of the cysteine 768 residue to reversibly inhibit the activity of phosphodiesterase PDE3B.[167]

The toolbox of fluorescent copper sensors continues to expand, including sensors with near-IR optical profiles for use in thicker tissue and whole-animal settings, as well as ratiometric and organelle-targeted sensors. For copper sensing in thicker tissue, ACu1 is a 2-photon probe by Cho and coworkers that excites at 750 nm in 2-photon mode (1-photon mode: 365 nm) (Figure 1.6).[168] Localizing to both mitochondria and Golgi, ACu1 has been used to visualize copper in live hippocampal slices from rats. Additionally, Wan and coworkers published a Cy7 Cu^+ sensor using the BETA receptor (structure **3** in Figure 1.6), which was used to visualize copper addition and ascorbate-triggered copper mobilization in MG63 osteosarcoma cells.[169] Our laboratory developed a Cy7 Cu^+ sensor,

Coppersensor 790 acetoxymethyl ester (CS790AM, Figure 1.6), which enables the first fluorescence imaging of labile copper pools in living mice.[170] CS790AM displays a 17-fold turn-on to copper with a highly red-shifted optical profile (λ_{abs} = 760 nm, λ_{em} = 790 nm). When injected into mice, CS790AM revealed both increased copper from copper injection and decreased copper from injection of the copper-specific chelator ATN-224, the FDA-approved choline salt of tetrathiomolybdate. Additionally, CS790AM could discriminate between wildtype mice and Wilson's disease model mice, which lack the copper exporter ATP7B. Compared to wildtype, both the abdomens and isolated livers of ATP7B$^{-/-}$ mice exhibited higher fluorescence signal from CS790AM, indicating an accumulation of copper, which was confirmed by bulk ICP-MS and online LC-MS/AA measurements on digested liver tissue.[170]

To image labile copper pools at the subcellular level, our laboratory reported Mitochondrial Coppersensor-1 (Mito-CS1, Figure 1.6),[171] the first organelle-targetable copper sensor, by appending a triphenylphosphonium tag[172] onto an asymmetric BODIPY scaffold[173] as a cationic, lipophilic tag to localize the probe to the mitochondria based on mitochondrial membrane potential. Mito-CS1, in conjunction with other biochemical assays, revealed that cells prioritize mitochondria for copper homeostasis over other cellular compartments. This reagent enabled observation of expansion and depletion of the mitochondrial copper pool by copper supplementation and chelation. Interestingly, comparative studies in fibroblasts lacking the mitochondrial copper metallochaperones SCO1 and SCO2 and the copper export pump ATP7A showing that total and labile mitochondrial copper pools remain constant even in situations where whole-cell copper pools are altered. Important control experiments with the cationic dye rhodamine 123 demonstrated that mitochondrial membrane potential was not altered due to copper treatment or deletion of SCO1 or SCO2. A related water-soluble derivative of CS1, OBEP-CS1 (Figure 1.6), bears an alkyl pyridinium group to drive it to the mitochondria in live cells but turns off in response to Cu^{+}.[174]

Ratiometric probes are highly valued for their intrinsic internal standard that can correct for variations in dye localization and other experimental imaging conditions. Attachment of the BETA receptor to a naphthyl fluorophore yielded Naphthyl-CS1 (Figure 1.6), which localizes to both mitochondria and the Golgi apparatus in SH-SY5Y cells and was able to sense changes in copper status with copper supplementation.[175] InCCu1, a ratiometric mitochondrial copper sensor developed by New and coworkers (Figure 1.6),[176] can specifically monitor increases in mitochondrial copper upon supplementation. Moreover, InCCu1 was used to suggest that cisplatin interferes with copper transport to the mitochondria upon copper supplementation. Finally, Dns-LLC, a Golgi-targeted peptide-based sensor (Figure 1.6),[177] shows a 12-fold turn-on in the presence of copper with an exceptionally tight binding affinity (12 fM); it responds to increases and decreases in Golgi copper levels following copper supplementation or chelation, respectively.

2.b.2. Reaction-Based Copper Indicators

Reaction-based approaches have proved useful for the development of fluorescent probes that go beyond traditional designs based on lock-and-key recognition.[143,178-181] An elegant bioinspired approach to reaction-based Cu^{+} detection based on oxidative

cleavage of the tetradentate ligand, tris[(2-pyridyl)methyl]amine (TPA), was reported by Taki and Yamamoto in 2010 (Figure 1.7).[182] Upon Cu^+ binding to the probe FluTPA1, oxidative C-O bond cleavage separates the TPA fragment from the fluorophore and releases the fluorescent dye with a 100-fold turn-on. FluTPA1 and its membrane-permeable FluTPA2 analog, based on Tokyo Green,[183] show good selectivity over other metal cations, as well as biological oxidants, including hydrogen peroxide, hypochlorite, and hydroxyl radical. FluTPA2 exhibits a notable fluorescence turn-on in HeLa cells after treatment with copper.[182] The TPA ligand has subsequently been used to cage 2-(2′-hydroxyphenyl) benzothiazole,[184] coumarin,[185] xanthone,[186] resorufin,[187] cyanine-quinone,[188] and imino-coumarin[189] (Figure 1.7), although only the latter three have been applied to cells. Additionally, a mitochondrially-targeted reaction-based Cu^+ probe, RdlTPA-TPP (Figure 1.7), has been developed using the TPA ligand, circumventing the localization problem associated with this probe.[190] We have expanded the scope of oxidative cleavage reactions to detect cobalt[191] and iron.[134] In addition, we have recently utilized the TPA trigger to develop the first bioluminescent probe for Cu^+, Copper Caged Luciferin-1 (CCL-1), which enables the imaging of labile copper levels in cells and living animals.[192] CCL-1 responds selectively to Cu^+ *in vivo* with high signal-to-noise, and the combination of a small-molecule caged substrate and genetically-encoded enzymatic reporter affords a platform for longitudinal imaging of the same living animal over time with cell- and tissue-specific resolution. In conjunction with biochemical and physiological assays, CCL-1 revealed a liver-specific copper deficiency that accompanies the onset of metabolic symptoms of glucose intolerance and weight gain in a diet-induced mouse model of non-alcoholic fatty liver disease (NAFLD).

3. Applying Multiple Analytical Imaging Methods to Study Transition Metals in Biology

The levels, localizations, and redox- and ligand-based speciations of copper and iron in biological systems change over time, as cells, tissues, and organisms grow, age, and respond to their environments. Techniques for visualizing total and/or labile metal pools can enable these changes to be mapped with spatial and temporal resolution and, thus, can aid in gaining insights into the roles of these redox-active metals over the wide range of timescales spanning signaling to metabolism to nutrition and aging. We emphasize the use of a combination of multiple techniques to address these exciting and open questions, as together they can provide a more holistic picture of transition metal dynamics, ranging from localization to oxidation state to bioavailability. Here, we highlight some recent representative examples of studies that combine multiple metal imaging methods to study and understand how copper and iron are sequestered and mobilized in biological systems in physiological and pathological situations.

3.a. Metal Dynamics Over Long Timescales: Transition Metal Nutrition and Aging

Accumulation of iron in tissues as a function of age has been known since the early 1900s,[193,194] but mechanisms by which iron acquisition contributes to senescence and death remain an active area of research. A combination of fluorescent probes and histochemical stains, along with advanced X-ray fluorescence and absorbance imaging

techniques, has produced substantial progress toward addressing these questions. Recently, McColl, Bush, and coworkers examined iron accumulation and ageing in *C. elegans*, specifically focusing on the role of ferritin in iron storage.[195] Using XFM, the investigators observed an accumulation of iron in old worms (12 days) compared to young adult worms (4 days), particularly in the intestinal cells (Figure 1.8a). Control measurements show no change in calcium observed in the same timeframe. Perl's stain showed an age-dependent increase in non-heme iron, revealing iron accumulation specifically in intestinal cell nuclei, dense inclusions in the head, and the germ nuclei of post-reproductive adults. The punctate iron distribution was confirmed by high-resolution XFM in a subsequent study.[26] To determine whether the labile iron pool expanded with increased total iron, the investigators stained live worms with Calcein, which fluoresces less in the presence of labile iron. Indeed, Calcein fluorescence was lower in old worms than young worms, confirming an increase in labile iron with age (Figure 1.8b).[195]

Having demonstrated the expansion of both total and labile iron pools with age, the same researchers examined the role of ferritin, the main iron storage protein,[111] during aging. Size exclusion chromatography experiments revealed that the fraction of iron bound to ferritin decreases as age increases, despite an overall increase in iron levels, suggesting that the Fe^{2+}:Fe^{3+} ratio may increase with age.[195] Relative levels of Fe^{2+} and Fe^{3+} oxidation states in live, hydrated, anaesthetized *C. elegans* were mapped using fluorescence XANES (φ-XANES) microscopy,[195] at a radiation dose demonstrated to preserve sample structure (Figure 1.8c).[76] The iron K-edge position shifts to higher energies with oxidation, so its energy can be used to assess the relative fraction of Fe^{2+} and Fe^{3+} in a sample.[196] Interestingly, young wildtype worms had K-edge positions that corresponded to a mixture of Fe^{2+} and Fe^{3+}, whereas old wildtype worms had K-edge positions that were lower energy and thus shifted toward Fe^{2+}. Taken together, these data suggest that the role of iron in ageing is not simply defined by an overall increase in iron levels but includes a shift from Fe^{3+} to Fe^{2+} *in vivo*, linked to changes in ferritin loading.

3.b. Metal Dynamics Over Medium Timescales: Transition Metal Metabolism

At shorter timescales within the span of minutes to hours, cells actively accumulate, store, mobilize, and efflux copper and iron under specific environmental conditions. Metal imaging experiments with high spatial resolution, using a variety of X-ray, mass spectrometry, and chemical probe methods, have played significant roles in identifying and characterizing intracellular structures for metal storage and mobilization.[26,162,197,198] To provide one representative example, the single-cell eukaryotic model organism *Chlamydomonas reinhardtii* accumulates copper under conditions of environmental zinc deprivation, as demonstrated by bulk ICP-MS measurements.[199] Interestingly, this organism responds to zinc deprivation in a manner associated with intracellular copper deficiency by upregulating copper import machinery and downregulating the synthesis of proteins requiring copper cofactors such as plastocyanin.[70] The mismatch between (1) a measurable accumulation of bulk total copper and (2) a functional response characteristic of low intracellular copper, suggested that the copper pools accumulating inside these cells might be sequestered into compartments where they are not accessible to the cell's copper-sensing machinery. To address this question, pilot imaging studies using the

small-molecule probe CS3 revealed an increase in fluorescent puncta in zinc-deprived cells, suggesting that copper accumulates in distinct subcellular structures under conditions of zinc deprivation (Figure 1.9a).[70] This increase in fluorescence was not observed using the control probe Ctrl-CS3. Further control experiments with copper supplementation or chelation, along with genetic manipulations of copper homeostasis machinery or lipid transport, all confirm that CS3 responds in this model in a copper-dependent fashion. These experiments led to the direct observation of copper and calcium accumulation in electron-dense structures, termed cuprosomes, using NanoSIMS (Figure 1.9b).

Moreover, sequestration of copper in these intracellular cuprosomes is reversible. Upon zinc resupply, fluorescent puncta from CS3 staining started to decrease after 3 hours, and the fluorescence signal became more evenly distributed throughout the cell by 24 hours. NanoSIMS imaging also showed a decrease in copper at sites of copper accumulation following zinc resupply. Further NanoSIMS analysis with isotope labeling showed that, upon restoration of zinc, copper from these compartments is incorporated into newly synthesized plastocyanin preferentially over copper from extracellular media. Additionally, cells moved from low-zinc media to low-copper media had a growth advantage over cells moved from zinc-replete media to low-copper media, suggesting that the copper accumulated during zinc deprivation becomes bioavailable and may provide an evolutionary advantage under conditions of fluctuating nutrient availability. This example adds to the growing literature concerning the identification of new protein machineries that influence the storage and mobilization of copper in intracellular compartments, including CTR1,[200] CTR2,[162,201] ATP7B,[163] metallothionein, and Atox1.[197]

3.c. Metal Dynamics Over Short Timescales: Transition Metal Signaling

In contrast to the wide acceptance of non-redox alkali and alkaline earth metals as mobile metal signals (eg. Na^+, K^+, Ca^{2+}), the localization of redox-active transition metals like copper and iron has been thought to be highly restricted to buried protein active sites and other inaccessible stores in order to protect cells, tissues, and organisms against oxidative stress and damage. However, more recent findings have expanded this traditionally narrow view of metals in biology to a new paradigm of transition metal signaling. As signaling elements, copper and iron can be rapidly mobilized in response to external stimuli in order to convey information. The fast and reversible binding of these elements to proteins and other biological targets outside active sites influences the function of these targets in downstream signaling cascades.

Our laboratory reported a foundational discovery in redox transition metal signaling by identifying fast copper relocalization within a cell, following an external stimulus, as shown using a primary neuronal cell model.[160] A combination of XFM and imaging using the small-molecule fluorescent probe CS3 revealed dynamic mobilization of copper within seconds from neuronal cell bodies to dendritic spines following depolarization of dissociated hippocampal neurons with potassium chloride (Figure 1.10a). XFM control experiments showed that zinc did not relocalize under the same conditions. Further experiments using both imaging methods established that copper mobilization following

membrane depolarization was calcium-dependent, suggesting crosstalk between copper and canonical cell signaling pathways. This work provided direct imaging evidence that complemented older studies on bulk copper release from synaptosomes,[202,203] and explants,[204] as well as the movement of copper-trafficking proteins in neurons.[205-207] Additionally, membrane-impermeable copper chelators disrupt neural function,[164,208] which provides evidence for a functional role for copper in neuronal signaling.[209] Indeed, a more recent study from our laboratory has characterized the functional significance of labile copper in neural circuits within intact tissue using fluorescent sensors for dual two-photon copper and calcium imaging (Figure 1.10b). The data show that copper is an endogenous regulator of spontaneous activity, a fundamental property of all neural circuits, by acting as a type of brake to avoid hyperactivity, via the Ctr1 copper ion channel and NMDA receptor.[164]

The concept of copper as a representative example of a transition metal signal has been expanded beyond the brain by the identification of copper as an essential regulator of lipolysis, the breakdown of fat to control body weight and energy metabolism.[167] Dynamic fluxes of copper in stimulated adipocytes, as imaged by the copper-responsive fluorescent probe CSR1, reversibly inhibit the enzyme PDE3B, a phosphodiesterase responsible for shutting down the lipolysis pathway by breakdown of the second messenger cAMP.[167] Further biochemical studies characterized a key cysteine residue at an allosteric site outside the active site of PDE3B that modulates its copper-dependent function, linking transition metal signaling to a molecular target. These studies directly tie copper to cAMP/PDE, lipolysis, and metabolic processes related to obesity, and parallel studies have linked copper to other disease pathways such as cancer proliferation[210-212] and heart disease.[213-215] Interestingly, many of these disease pathways are interconnected. Indeed, obesity is a risk factor for diseases including diabetes, heart disease, cancer, and liver disease. Thus, these fields are ripe for further imaging studies to directly monitor fluctuations in copper in response to biological stimuli and to elucidate how copper may be used to transmit information at the cellular, tissue, and whole-organism levels.

4. Concluding Remarks

Metals pervade all aspects of the central dogma of biology, as they are required for the synthesis of all DNA and RNA molecules, as well as the proper function of approximately half of all proteins. Because metals can neither be created nor destroyed in biological systems, metal localization is governed by complex acquisition and excretion systems. The ubiquity, necessity, and unique homeostasis of metals drive a desire to study these biomolecules, and the electronic structure and coordination chemistry of metals provide unique chemical signatures that can be harnessed by physical techniques and small molecule probes to map the contributions of metals to the dynamic blueprint of life.

We have reviewed the growing collection of analytical methods to monitor both total and labile metal pools in their native biological contexts. These techniques, when used in concert, can provide complementary information on quantity, location, and oxidation state of a given metal over a wide range of length scales and time regimes, particularly

spanning the shorter timescales of signaling to medium timescales of metabolism to longer timescales of nutrition and aging. A key principle is the open collaboration between chemistry and biology, where disparate communities will continue to work together to evaluate the best available set of chemical imaging tools for a given biological system and question. Multiple independent measurements and controls from both chemical and biological perspectives will push the field forward. Finally, an emerging theme of these investigations, applied to redox-active transition metals such as copper and iron, is the concept of transition metal signaling. In this burgeoning paradigm, these potent and reactive elements are not only viewed as static cofactors buried within protein active sites and other biomolecules to perform structural and catalytic chemistry, but they are also recognized as dynamic signals that can interact with targets outside active sites on faster timescales to affect function. The coming years are sure to illuminate more aspects of this bioinorganic chemistry and metallobiochemistry beyond the active site.

Acknowledgements

We thank the National Institutes of Health (GM 79465) for supporting our work on metal imaging probes. C.M.A. has been supported by a Fannie and John Hertz Foundation Graduate Fellowship as well as by a Chemical Biology Training Grant from the NIH (T32 GM066698). C.J.C. is an Investigator of the Howard Hughes Medical Institute.

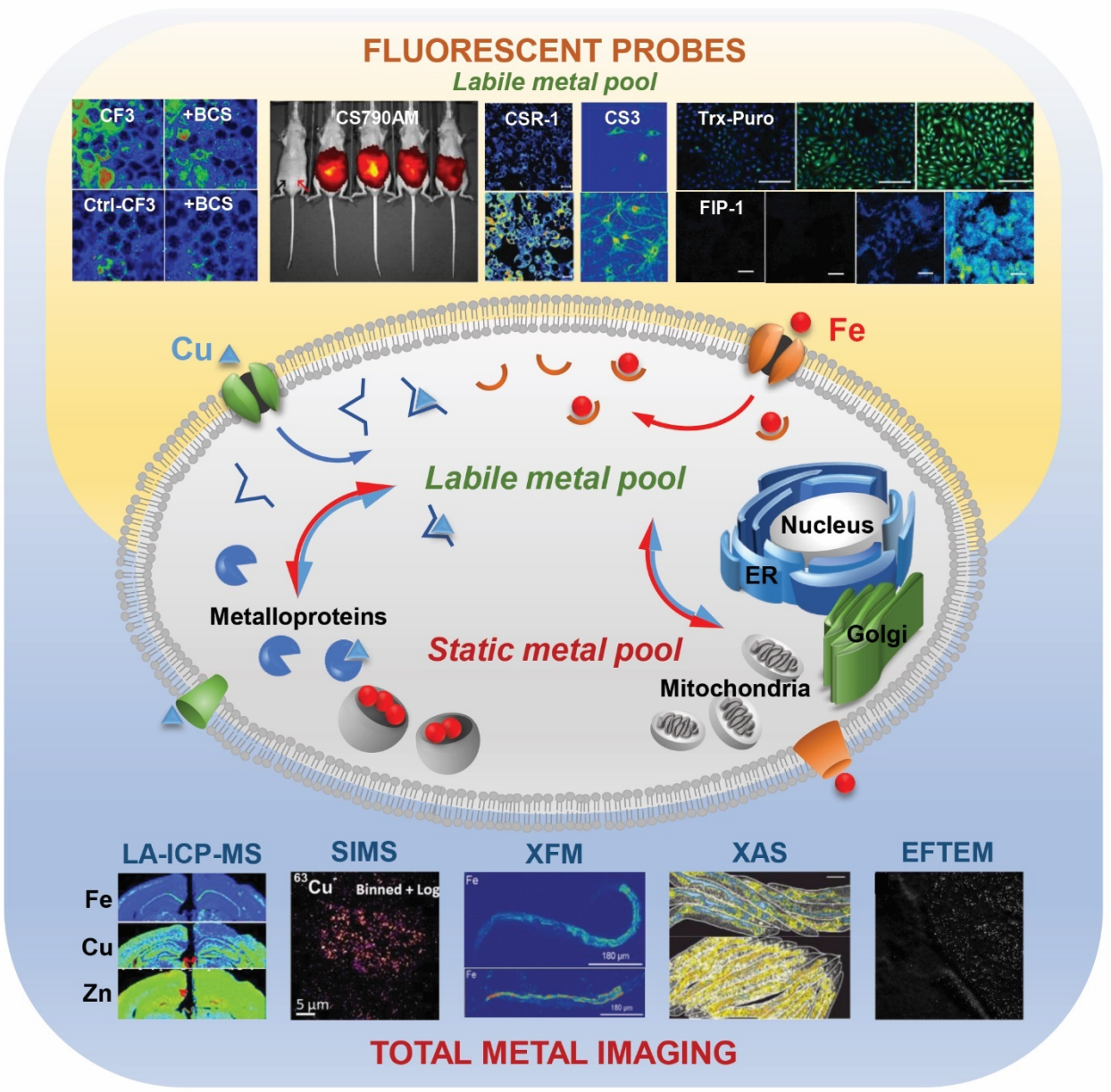

Figure 1.1. The total metal pool comprises the labile and static metal pools. Physical techniques that map the distribution of the total metal pool in cells, tissues and organisms include technologies that measure atomic mass (LA-ICP-MS and SIMS) and technologies that probe electronic structure (eg. XFM, XAS, and EFTEM, among others). Fluorescent sensors map the labile metal pool. Representative data were reproduced from the following publications: CF3/Ctl-CF3 ± BCS: from Dodani, S. C.; Firl, A.; Chan, J.; Nam, C. I.; Aron, A. T.; Onak, C. S.; Ramos-Torres, K. M.; Paek, J.; Webster, C. M.; Feller, M. B.; Chang, C. J. *Proc. Natl. Acad. Sci. U. S. A.* **2014**, *111*, 16280-16285 (ref #164). Copyright 2016 United States National Academy of Sciences. CS790AM: from Hirayama, T.; Van de Bittner, G. C.; Gray, L. W.; Lutsenko, S.; Chang, C. J. *Proc. Natl. Acad. Sci. U. S. A.* **2012**, *109*, 2228-2233 (ref #170). Copyright 2012 United States National

Academy of Sciences. CSR1: from Krishnamoorthy, L.; Cotruvo, J. A.; Chan, J.; Kaluarachchi, H.; Muchenditsi, A.; Pendyala, V. S.; Jia, S.; Aron, A. T.; Ackerman, C. M.; Wal, M. N. V.; Guan, T.; Smaga, L. P.; Farhi, S. L.; New, E. J.; Lutsenko, S.; Chang, C. J. *Nat. Chem. Biol.* **2016**, *12*, 586-592 (ref #167). Copyright 2016 Nature Publishing Group. CS3: from Dodani, S. C.; Domaille, D. W.; Nam, C. I.; Miller, E. W.; Finney, L. A.; Vogt, S.; Chang, C. J. *Proc. Natl. Acad. Sci. U. S. A.* **2011**, *29*, 686-700 (ref #160). Copyright 2016 United States National Academy of Sciences. Trx-Puro: from Spangler, B.; Morgan, C. W.; Fontaine, S. D.; Vander Wal, M. N.; Chang, C. J.; Wells, J. A.; Renslo, A. R. *Nat. Chem. Biol.* **2016**, *12*, 680-685 (ref #138). Copyright 2016 Nature Publishing Group. FIP-1: from Aron, A. T.; Loehr, M. O.; Bogena, J.; Chang, C. J. *J. Am. Chem. Soc.* **2016**, *138*, 14338-14346 (ref #136). Copyright 2016 The American Chemical Society. LA-ICP-MS: from Portbury, S. D.; Hare, D. J.; Sgambelloni, C.; Finkelstein, D. I.; Adlard, P. A. *Metallomics* **2016**, *8*, 193-200 (ref #61) with the permission of The Royal Chemical Society. SIMS: from Biesemeier, A.; Eibl, O.; Eswara, S.; Audinot, J.-N.; Wirtz, T.; Pezzoli, G.; Zucca, F. A.; Zecca, L.; Schraermeyer, U. *J. Neurochem.* **2016**, *138*, 339-353 (ref #71). Copyright 2016 Wiley. XFM and XAS: from James, S. A.; Roberts, B. R.; Hare, D. J.; de Jonge, M. D.; Birchall, I. E.; Jenkins, N. L.; Cherny, R. A.; Bush, A. I.; McColl, G. *Chem. Sci.* **2015**, *6*, 2952-2962 (ref #195) with the permission of The Royal Chemical Society. EFTEM: from Treiber, C. D.; Salzer, M. C.; Riegler, J.; Edelman, N.; Sugar, C.; Breuss, M.; Pichler, P.; Cadiou, H.; Saunders, M.; Lythgoe, M.; Shaw, J.; Keays, D. A. *Nature* **2012**, *484*, 367-370 (ref #110). Copyright 2016 Nature Publishing Group.

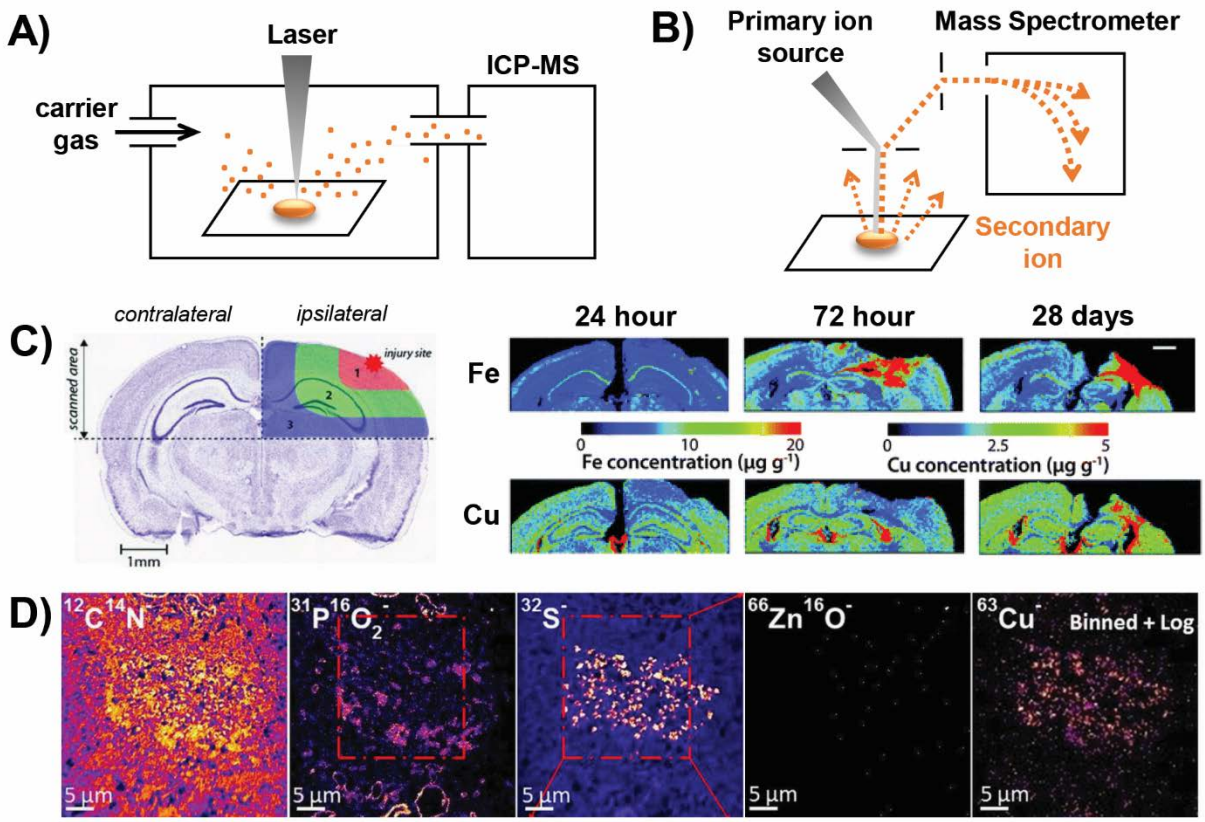

Figure 1.2. Schematic illustration and representative data for technologies that map metals by measuring atomic mass. (A) Schematic illustration of LA-ICP-MS. (B) Schematic illustration of NanoSIMS. (C) LA-ICP-MS was used in a longitudinal study of mouse brain slices. Using the healthy contralateral hemisphere as a control, changes in the metal content of the injured ipsilateral hemisphere were observed at multiple timepoints during the wound-healing process. Reproduced from Portbury, S. D.; Hare, D. J.; Sgambelloni, C.; Finkelstein, D. I.; Adlard, P. A. *Metallomics* **2016**, *8*, 193-200 (ref #61) with the permission of The Royal Chemical Society. (C) Representative data highlighting the use of NanoSIMS for colocalizing metal and non-metal signals at subcellular resolution. PO_2^- marks lipid bodies, while S^- marks neuromelanin. Copper localizes in a pattern that is most similar to S^-, indicating that Cu associates with neuromelanin rather than lipid bodies within neurons. Reproduced from Biesemeier, A.; Eibl, O.; Eswara, S.; Audinot, J.-N.; Wirtz, T.; Pezzoli, G.; Zucca, F. A.; Zecca, L.; Schraermeyer, U. *J. Neurochem.* **2016**, *138*, 339-353 (ref #71). Copyright 2016 Wiley.

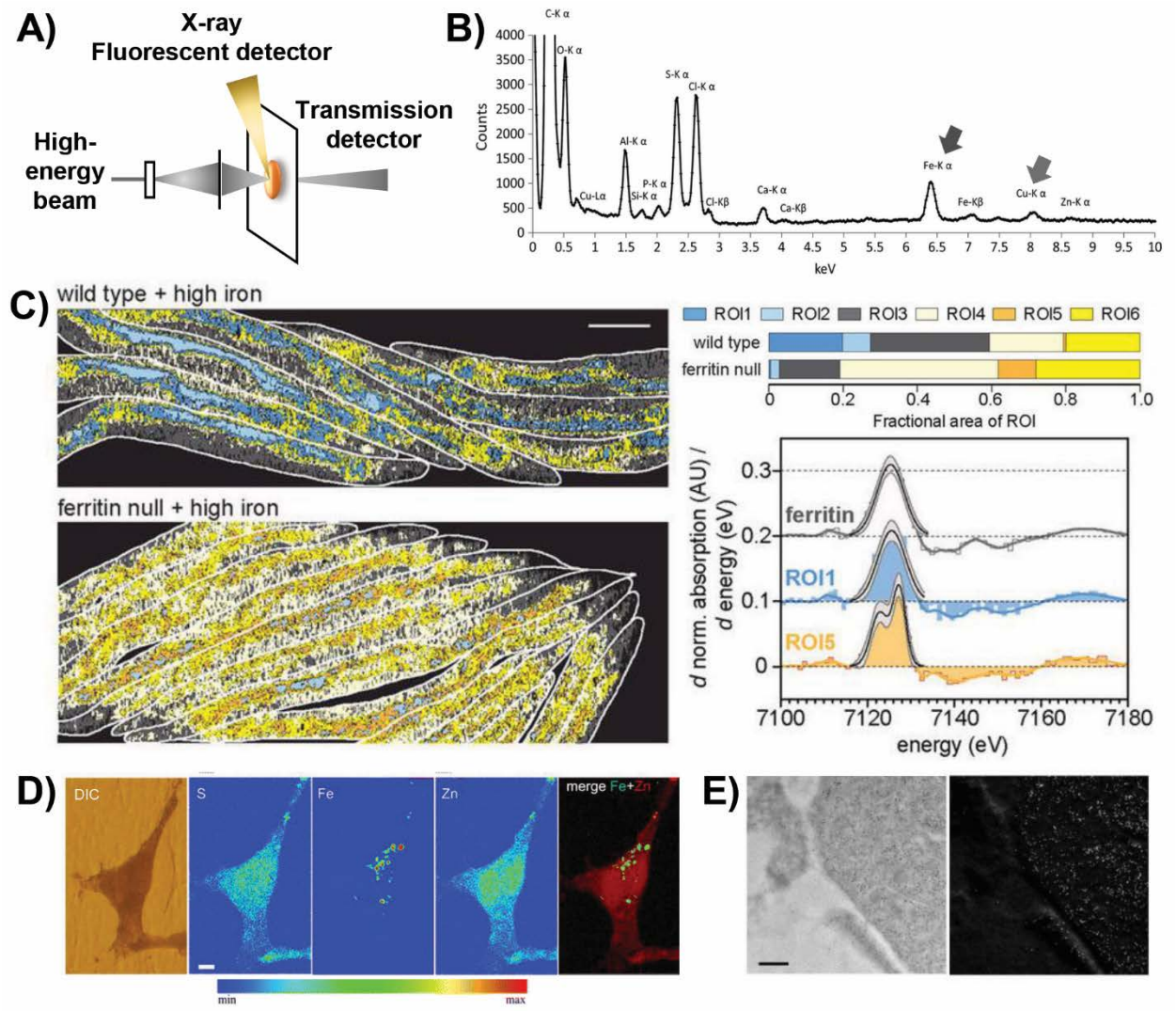

Figure 1.3. Schematic illustration and representative data for technologies that map metals by probing electronic structure. (A) Schematic illustration of the basic setup for technologies that probe the electronic structure of metals. The high-energy beam is composed of X-rays for XFM and XAS; a particle beam is used for μ-PIXE; and an electron beam is used for EDX, STEM-EELS, and EFTEM. (B) An X-ray emission spectrum illustrating the location of the Fe and Cu K_{α}-lines, which are well-defined, lying outside the crowded low-energy region. Reproduced from Biesemeier, A.; Eibl, O.; Eswara, S.; Audinot, J.-N.; Wirtz, T.; Pezzoli, G.; Zucca, F. A.; Zecca, L.; Schraermeyer, U. *J. Neurochem.* **2016**, *138*, 339-353 (ref #71). Copyright 2016 Wiley. (C) φ-XANES maps of wildtype worms and worms lacking the iron storage protein ferritin; computationally-defined ROIs are color coded according to their Fe^{2+}:Fe^{3+} ratio. Cool colors indicate a low Fe^{2+}:Fe^{3+} ratio, similar to ferritin (as shown in the spectral comparisons on the right), while warm colors indicate high Fe^{2+}:Fe^{3+} ratios. Warmer pixels are more prevalent in worms lacking ferritin (percentages are illustrated in the ROI bar graphs on the right). Reproduced from James, S. A.; Hare, D. J.; Jenkins, N. L.; de Jonge, M. D.; Bush, A. I.; McColl, G. *Sci. Rpts.* **2016**, *6*, 20350 (ref #76). Copyright 2016 Nature

Publishing Group. (D) XFM images of iron-treated PC12 rat neural tumor cells overexpressing alpha-synuclein. While sulfur and zinc are relatively homogeneously distributed throughout the cell, iron is confined to subcellular puncta. DIC, differential interference contrast. Reproduced from Ortega, R.; Carmona, A.; Rodeau, S.; Perrin, L.; Dučić, T.; Carboni, E.; Bohic, S.; Cloetens, P.; Lingor, P. *Mol. Neurobiol*. **2016**, *53*, 1925-1934 (ref #89). Copyright 2016 Springer. (E) TEM (left) and EFTEM (right) images of ferritin molecules in macrophages. The dark spots in the TEM image correlate well with the high signal in the EFTEM Fe image, confirming a high iron concentration in these electron-dense puncta. Reproduced from Treiber, C. D.; Salzer, M. C.; Riegler, J.; Edelman, N.; Sugar, C.; Breuss, M.; Pichler, P.; Cadiou, H.; Saunders, M.; Lythgoe, M.; Shaw, J.; Keays, D. A. *Nature* **2012**, *484*, 367-370 (ref #110). Copyright 2016 Nature Publishing Group.

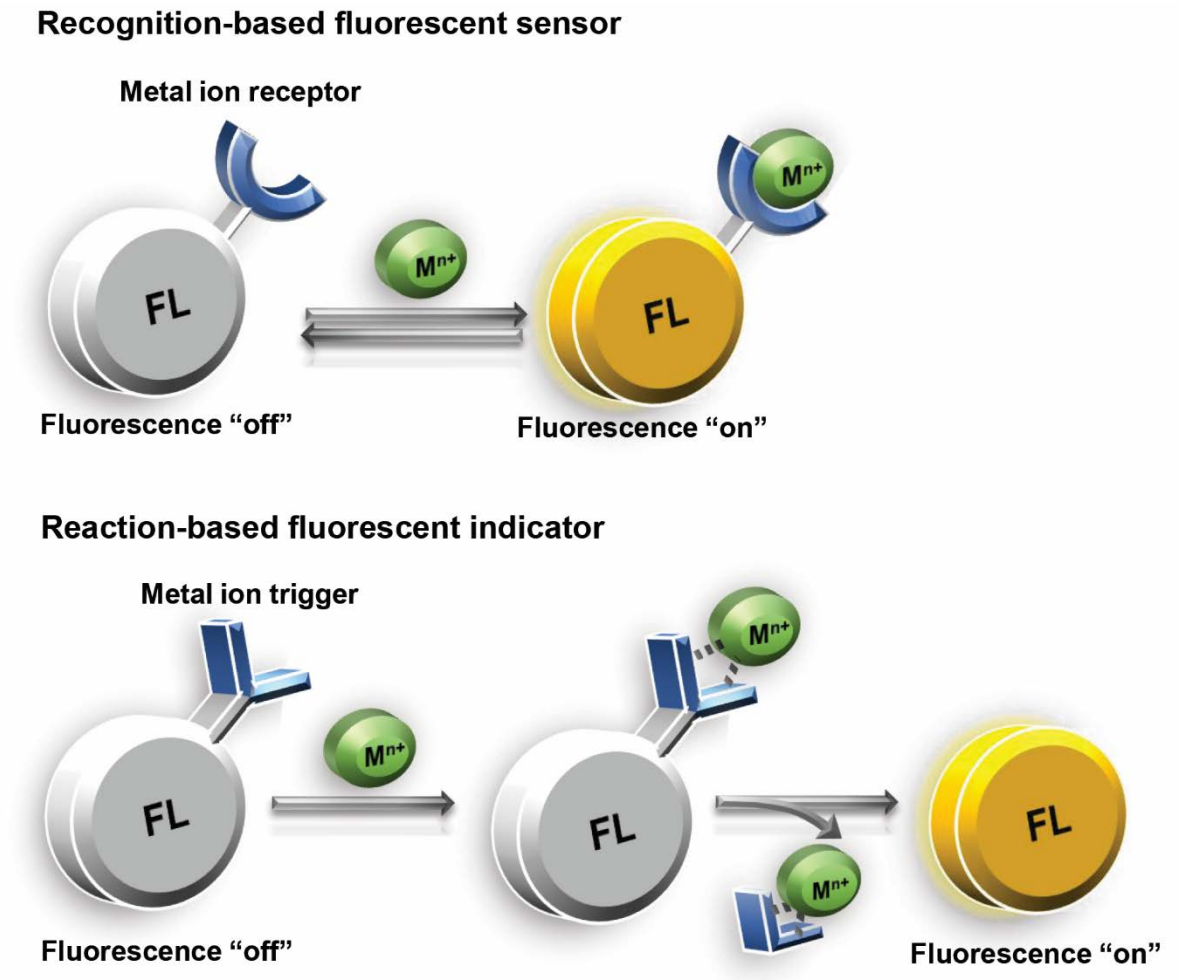

Figure 1.4. Illustration of recognition-based and reaction-based fluorescent sensors for metal ions. (A) Recognition-based turn-on sensors fluoresce when the metal is bound; they are reversible, turning off when the metal is released. (B) Reaction-based indicators fluoresce after a metal-catalyzed irreversible chemical event. The fluorophore does not remain associated with the metal after the reaction takes place.

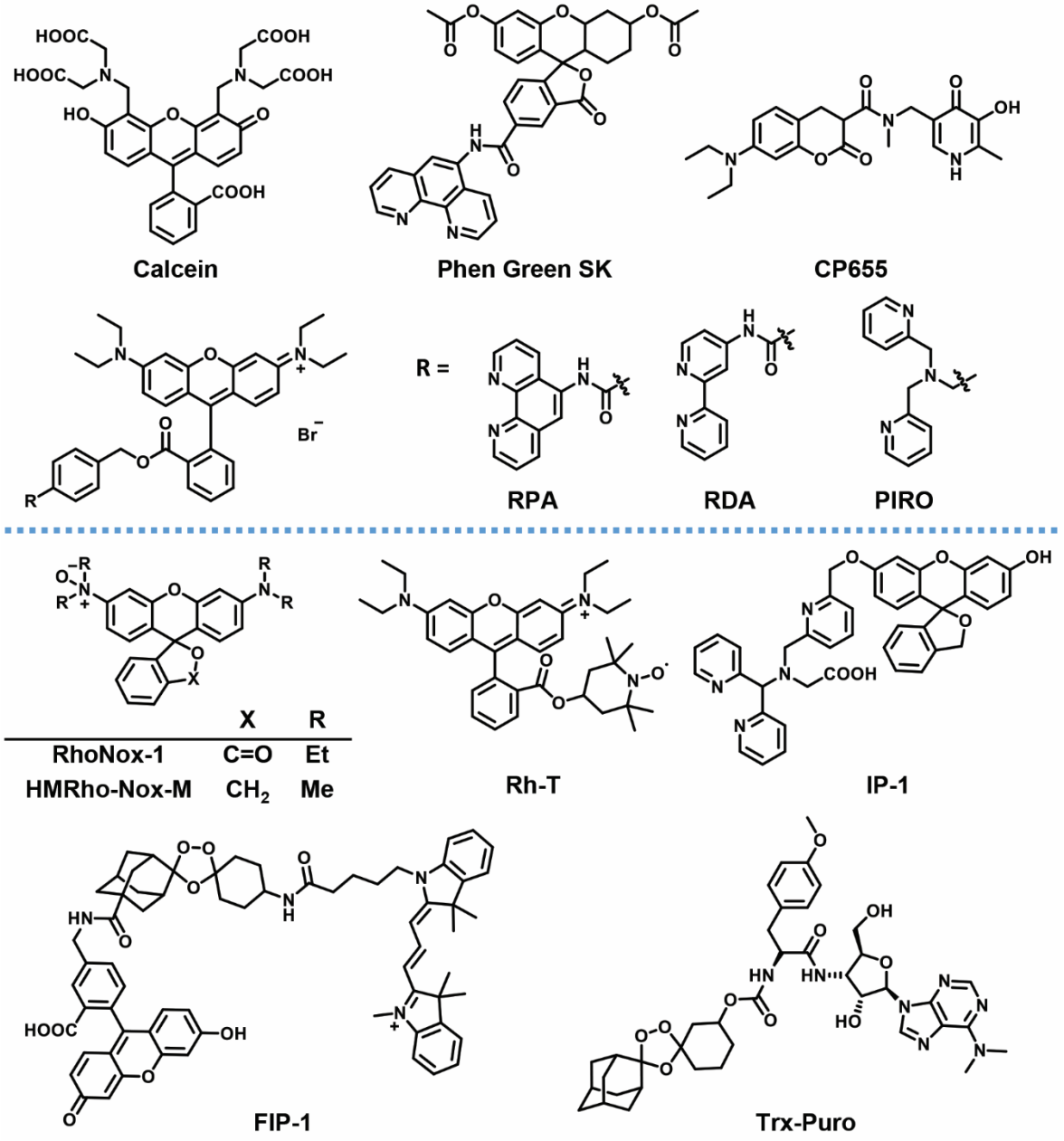

Figure 1.5. Structures of recognition-based (upper section) and reaction-based (lower section) Fe^{2+} probes.

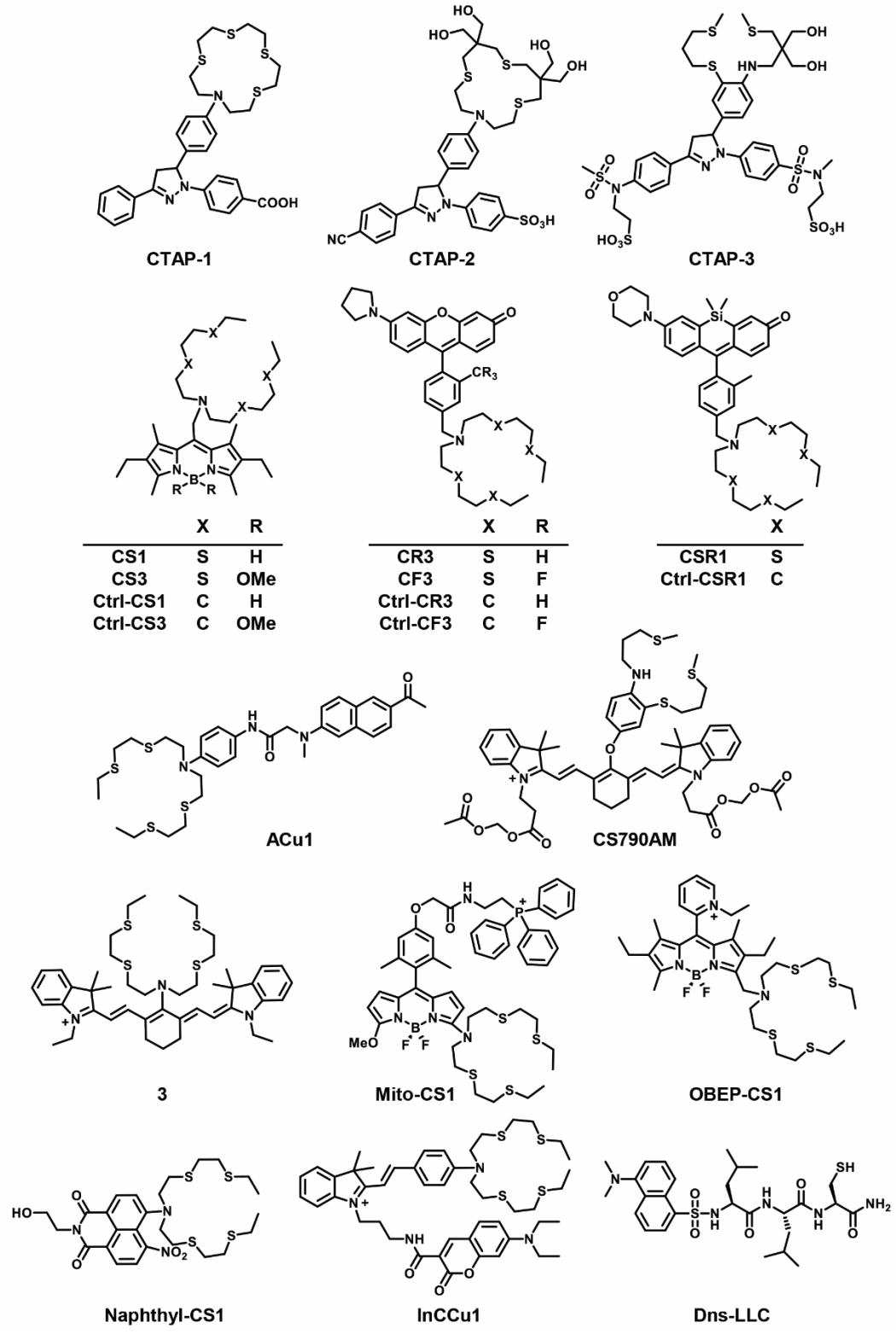

Figure 1.6. Structures of recognition-based Cu^{+} sensors.

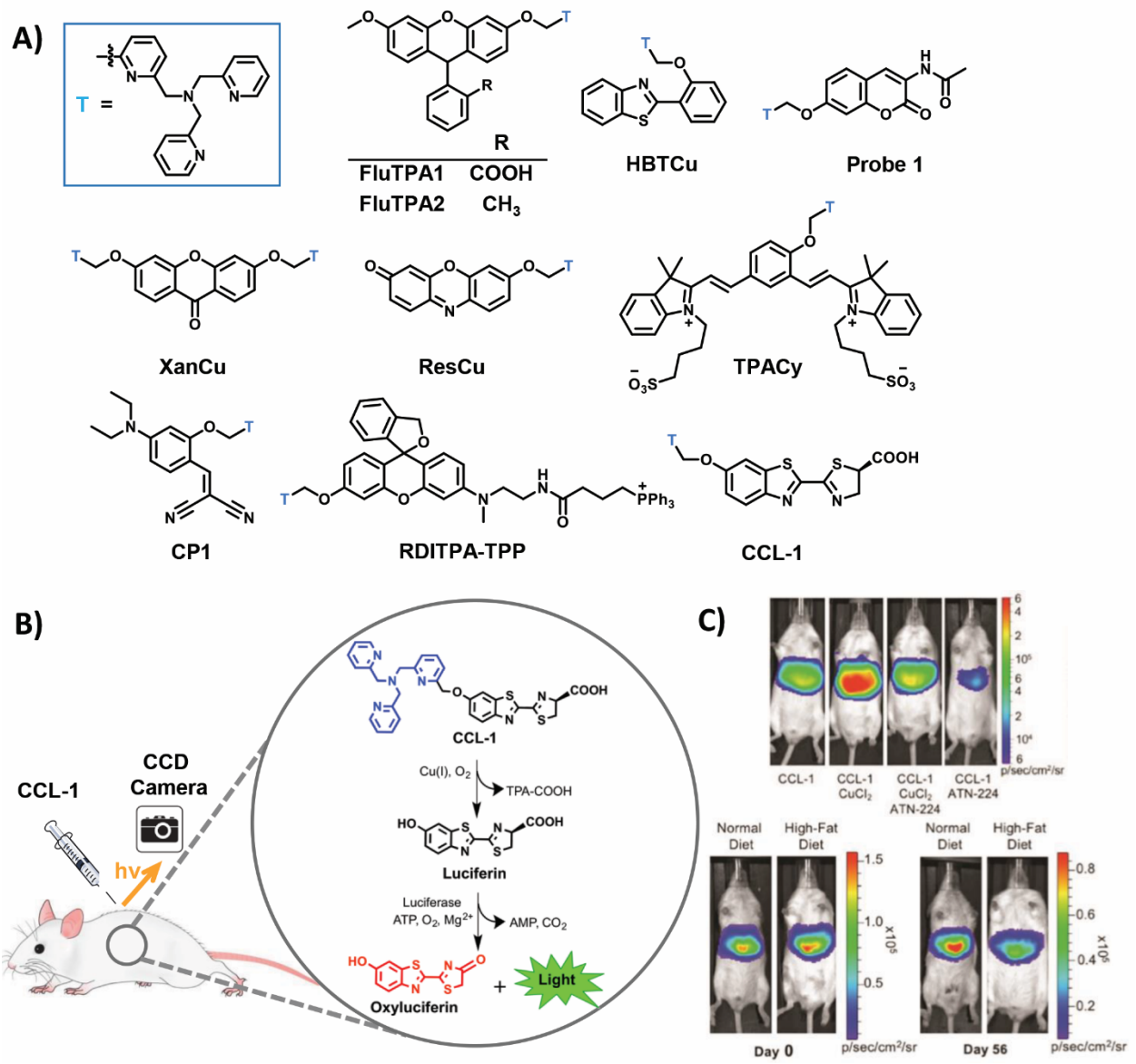

Figure 1.7. Structures and representative data from reaction-based indicators for Cu^{+}. (A) All reaction-based triggers for Cu^{+} are based on the TPA trigger (designated "T", in blue). This trigger has been appended to many small molecule reporters, including fluorescein (FluTPA1), Tokyo Green (FluTPA2), cyanine-quinone (TPACy), an imino-coumarin precursor (CP1), benzothiazole (HBTCu), coumarin (Probe 1), xanthone (XanCu), resorufin (ResCu), rhodol with a mitochondrial tag (RdlTPA-TPP), and, most recently, luciferin (CCL-1). (B) The use and mechanism of action of CCL-1 for imaging Cu^{+} in live animals is illustrated. (C) In mice expressing liver-specific luciferase, CCL-1 signal is observed only in the liver and is dependent on copper levels (top panel); its signal increases in response to copper supplementation with copper chloride and decreases in response to copper chelation with ATN-224, a derivative of tetrathiomolybdate. (C, Bottom panel) After 8 weeks of a high-fat diet, mice have lower CCL-1 liver signal than mice fed a control diet for 8 weeks, even though both groups of mice began the study

with the same CCL-1 liver signal. Reproduced from Heffern, M. C.; Park, H. M.; Au-Yeung, H. Y.; Van de Bittner, G. C.; Ackerman, C. M.; Stahl, A.; Chang, C. J. *Proc. Natl. Acad. Sci. U. S. A.* **2016**, in press, DOI: 10.1073/pnas.1613628113 (ref #192). Copyright 2016 United States Academy of Sciences.

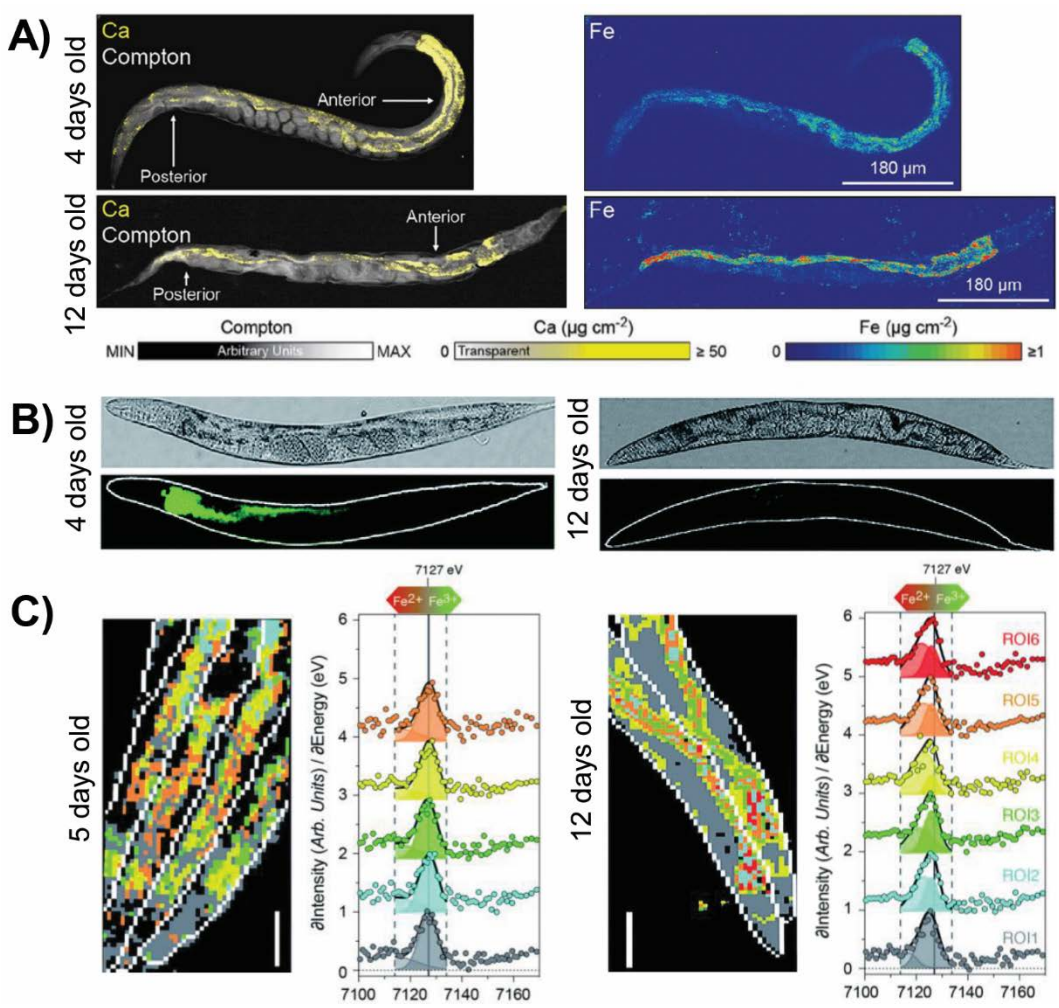

Figure 1.8. Iron accumulates, and the Fe^{2+}:Fe^{3+} ratio increases, in ageing worms. (A) XFM images reveal total iron accumulation, but no change in calcium levels, in old worms compared to young worms. Compton scattering provides anatomical structure. (B) Calcein staining is lower in older worms, indicating an increase in labile iron with ageing. (C) XANES imaging shows a shift to higher Fe^{2+}:Fe^{3+} ratios in older worms, as observed by a shift in the Fe K-edge to lower energies. Reproduced from James, S. A.; Roberts, B. R.; Hare, D. J.; de Jonge, M. D.; Birchall, I. E.; Jenkins, N. L.; Cherny, R. A.; Bush, A. I.; McColl, G. *Chem. Sci.* **2015**, *6*, 2952-2962 (ref #195) with the permission of The Royal Chemical Society.

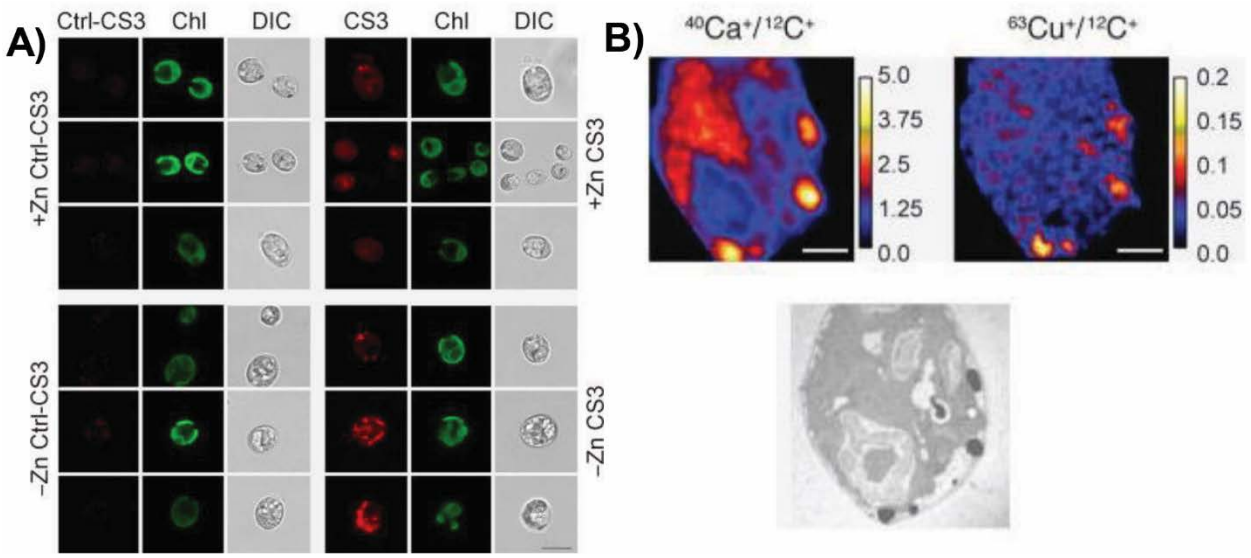

Figure 1.9. The localization of copper changes on the timescale of hours, in order to respond to changes in nutrient availability. (A) In the model organism *C. reinhardtii*, the copper sensor CS3 reveals the accumulation of copper in subcellular structures, termed cuprosomes, under conditions of zinc starvation (- Zn) compared to control (+ Zn). Cuprosomes were not observed by the control sensor Ctl-CS3. Chl: chlorophyll autofluorescence; DIC, differential interference contrast. (B) By NanoSIMS, calcium and copper are observed within electron-dense structures along the cell periphery. NanoSIMS scale bars are metal counts normalized to carbon counts. Reproduced from Hong-Hermesdorf, A. M.; Miethke, M.; Gallaher, S. D.; Kropat, J.; Dodani, S. C.; Chan, J.; Barupala, D.; Domaille, D. W.; Shirasaki, D. I.; Loo, J. A.; Weber, P. K.; Pett-Ridge, J.; Stemmler, T. L.; Chang, C. J.; Merchant, S. S. *Nat. Chem. Biol.* **2014**, *10*, 1034-1042 (ref #70). Copyright 2016 Nature Publishing Group.

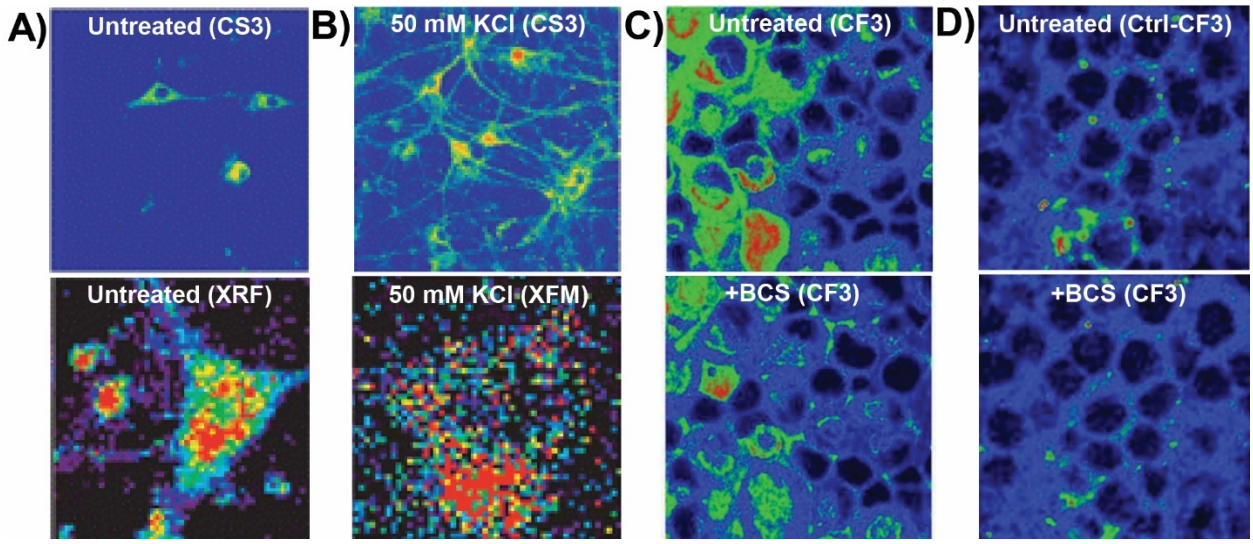

Figure 1.10. Metals undergo dramatic relocalization on short timescales. The copper sensor CS3 was used to visualize the movement of copper in primary hippocampal neurons from (A, upper panel) cell bodies in resting neurons to (B, upper panel) dendritic spines upon neuronal depolarization with potassium chloride. (A lower panel, B lower panel) These results were confirmed by XFM. Reproduced from Dodani, S. C.; Domaille, D. W.; Nam, C. I.; Miller, E. W.; Finney, L. A.; Vogt, S.; Chang, C. J. *Proc. Natl. Acad. Sci. U. S. A.* **2011**, *29*, 686-700 (ref #160). Copyright 2016 United States National Academy of Sciences. (C, upper panel) The copper sensor CF3 revealed a loosely bound copper pool in retinal neurons, which could be rapidly depleted (D, upper panel) upon incubation with an extracellular copper chelator. (C, lower panel) The signal from the matched control probe, Ctl-CF3, was not altered (D, lower panel) by chelator treatment. Reproduced from Dodani, S. C.; Firl, A.; Chan, J.; Nam, C. I.; Aron, A. T.; Onak, C. S.; Ramos-Torres, K. M.; Paek, J.; Webster, C. M.; Feller, M. B.; Chang, C. J. *Proc. Natl. Acad. Sci. U. S. A.* **2014**, *111*, 16280-16285 (ref #164). Copyright 2016 United States National Academy of Sciences. All color schemes scale from cool colors (low signal) to warm colors (high signal) with arbitrary units of fluorescence counts.

References

1 Lippard, S. J. & Berg, J. M. *Principles of Bioinorganic Chemistry*. (University Science Books, 1994).

2 van den Berghe, P. V. E. & Klomp, L. W. J. New developments in the regulation of intestinal copper absorption. *Nutr. Rev.* **67**, 658-672, doi:10.1111/j.1753-4887.2009.00250.x (2009).

3 Lutsenko, S. Copper trafficking to the secretory pathway. *Metallomics* **8**, 840-852, doi:10.1039/c6mt00176a (2016).

4 Printz, B., Lutts, S., Hausman, J.-F. & Sergeant, K. Copper Trafficking in Plants and Its Implication on Cell Wall Dynamics. *Front. Plant Sci.* **7**, 601 (2016).

5 Milto, I. V., Suhodolo, I. V., Prokopieva, V. D. & Klimenteva, T. K. Molecular and cellular bases of iron metabolism in humans. *Biochem. (Mosc.)* **81**, 549-564, doi:10.1134/s0006297916060018 (2016).

6 Kaplan, Jack H. & Maryon, Edward B. How Mammalian Cells Acquire Copper: An Essential but Potentially Toxic Metal. *Biophys. J.* **110**, 7-13, doi:10.1016/j.bpj.2015.11.025 (2016).

7 Festa, R. A. & Thiele, D. J. Copper: An essential metal in biology. *Curr. Biol.* **21**, R877-R883, doi:10.1016/j.cub.2011.09.040 (2011).

8 Gozzelino, R. & Arosio, P. Iron Homeostasis in Health and Disease. *Int. J. Mol. Sci.* **17**, 130 (2016).

9 Poujois, A. *et al.* Bioavailable Trace Metals in Neurological Diseases. *Curr. Treat. Options Neurol.* **18**, 46, doi:10.1007/s11940-016-0426-1 (2016).

10 Wang, P. & Wang, Z.-Y. *Metal ions influx is a double edged sword for the pathogenesis of Alzheimer's disease* (2016).

11 Bashir, K., Rasheed, S., Kobayashi, T., Seki, M. & Nishizawa, N. K. Regulating Subcellular Metal Homeostasis: The Key to Crop Improvement. *Front. Plant Sci.* **7**, 1192 (2016).

12 Banci, L. *et al.* Affinity gradients drive copper to cellular destinations. *Nature* **465**, 645-648, doi:10.1038/nature09018 (2010).

13 Lenartowicz, M. *et al.* Mottled Mice and Non-Mammalian Models of Menkes Disease. *Front. Mol. Neurosci.* **8**, 72 (2015).

14 Wu, X., Leegwater, P. & Fieten, H. Canine Models for Copper Homeostasis Disorders. *Int. J. Mol. Sci.* **17**, 196 (2016).

15 Rubino, J. T. & Franz, K. J. Coordination chemistry of copper proteins: How nature handles a toxic cargo for essential function. *J. Inorg. Biochem.* **107**, 129-143, doi:10.1016/j.jinorgbio.2011.11.024 (2012).

16 Baker, H. M., Anderson, B. F. & Baker, E. N. Dealing with iron: Common structural principles in proteins that transport iron and heme. *Proc. Natl. Acad. Sci. U. S. A.* **100**, 3579-3583, doi:10.1073/pnas.0637295100 (2003).

17 Qin, Z., Caruso, J. A., Lai, B., Matusch, A. & Becker, J. S. Trace metal imaging with high spatial resolution: Applications in biomedicine. *Metallomics* **3**, 28-37, doi:10.1039/c0mt00048e (2011).

18 da Cunha, M. M. L. *et al.* Overview of chemical imaging methods to address biological questions. *Micron* **84**, 23-36, doi:10.1016/j.micron.2016.02.005 (2016).

19 Hare, D. J., New, E. J., de Jonge, M. D. & McColl, G. Imaging metals in biology: balancing sensitivity, selectivity and spatial resolution. *Chem. Soc. Rev.* **44**, 5941-5958, doi:10.1039/c5cs00055f (2015).
20 Al-Ebraheem, A. *et al.* Effect of sample preparation techniques on the concentrations and distributions of elements in biological tissues using μSRXRF: a comparative study. *Physiol. Meas.* **36**, N51-N60, doi:10.1088/0967-3334/36/3/n51 (2015).
21 Missirlis, F., Colvin, R. A., Jin, Q., Lai, B. & Kiedrowski, L. Visualizing Metal Content and Intracellular Distribution in Primary Hippocampal Neurons with Synchrotron X-Ray Fluorescence. *PLoS ONE* **11**, e0159582, doi:10.1371/journal.pone.0159582 (2016).
22 Hare, D. J., Gerlach, M. & Riederer, P. Considerations for measuring iron in post-mortem tissue of Parkinson's disease patients. *J. Neural. Transm.* **119**, 1515-1521, doi:10.1007/s00702-012-0898-4 (2012).
23 Matsuyama, S. *et al.* Elemental mapping of frozen-hydrated cells with cryo-scanning X-ray fluorescence microscopy. *X-Ray Spectrom.* **39**, 260-266, doi:10.1002/xrs.1256 (2010).
24 James, S. A. *et al.* Quantitative comparison of preparation methodologies for x-ray fluorescence microscopy of brain tissue. *Anal. Bioanal. Chem.* **401**, 853-864, doi:10.1007/s00216-011-4978-3 (2011).
25 Hackett, M. J. *et al.* Chemical alterations to murine brain tissue induced by formalin fixation: implications for biospectroscopic imaging and mapping studies of disease pathogenesis. *Analyst* **136**, 2941-2952, doi:10.1039/c0an00269k (2011).
26 Hare, D. J. *et al.* High-resolution complementary chemical imaging of bio-elements in Caenorhabditis elegans. *Metallomics* **8**, 156-160, doi:10.1039/c5mt00288e (2016).
27 Mizuhira, V., Hasegawa, H. & Notoya, M. Fixation and imaging of biological elements: heavy metals, diffusible substances, ions, peptides, and lipids. *Prog. Histochem. Cytochem.* **35**, 67-183 (2000).
28 Deng, J. *et al.* Simultaneous cryo X-ray ptychographic and fluorescence microscopy of green algae. *Proc. Natl. Acad. Sci. U. S. A.* **112**, 2314-2319, doi:10.1073/pnas.1413003112 (2015).
29 Feldmann, J. r., Kindness, A. & Ek, P. Laser ablation of soft tissue using a cryogenically cooled ablation cell. *J. Anal. At. Spectrom.* **17**, 813-818, doi:10.1039/b201960d (2002).
30 George, S. J. *et al.* X-ray photochemistry in iron complexes from Fe(0) to Fe(IV) – Can a bug become a feature? *Inorg. Chim. Acta* **361**, 1157-1165, doi:10.1016/j.ica.2007.10.039 (2008).
31 Yano, J. *et al.* X-ray damage to the Mn4Ca complex in single crystals of photosystem II: A case study for metalloprotein crystallography. *Proc. Natl. Acad. Sci. U. S. A.* **102**, 12047-12052, doi:10.1073/pnas.0505207102 (2005).
32 Bowman, S. E. J., Bridwell-Rabb, J. & Drennan, C. L. Metalloprotein Crystallography: More than a Structure. *Acc. Chem. Res.* **49**, 695-702, doi:10.1021/acs.accounts.5b00538 (2016).

33 Becker, J. S. Imaging of metals in biological tissue by laser ablation inductively coupled plasma mass spectrometry (LA-ICP-MS): state of the art and future developments. *J. Mass. Spectrom.* **48**, 255-268, doi:10.1002/jms.3168 (2013).
34 Becker, J. S., Matusch, A. & Wu, B. Bioimaging mass spectrometry of trace elements – recent advance and applications of LA-ICP-MS: A review. *Anal. Chim. Acta* **835**, 1-18, doi:10.1016/j.aca.2014.04.048 (2014).
35 Sussulini, A., Becker, J. S. & Becker, J. S. Laser ablation ICP-MS: Application in biomedical research. *Mass Spectrom. Rev.*, doi:10.1002/mas.21481 (2015).
36 Konz, I., Fernández, B., Fernández, M. L., Pereiro, R. & Sanz-Medel, A. Laser ablation ICP-MS for quantitative biomedical applications. *Anal. Bioanal. Chem.* **403**, 2113-2125, doi:10.1007/s00216-012-6023-6 (2012).
37 Pozebon, D., Scheffler, G. L., Dressler, V. L. & Nunes, M. A. G. Review of the applications of laser ablation inductively coupled plasma mass spectrometry (LA-ICP-MS) to the analysis of biological samples. *J. Anal. At. Spectrom.* **29**, 2204-2228, doi:10.1039/c4ja00250d (2014).
38 Becker, J. S. *et al.* Bioimaging of metals by laser ablation inductively coupled plasma mass spectrometry (LA-ICP-MS). *Mass Spectrom. Rev.* **29**, 156-175, doi:10.1002/mas.20239 (2009).
39 Kindness, A. Two-Dimensional Mapping of Copper and Zinc in Liver Sections by Laser Ablation-Inductively Coupled Plasma Mass Spectrometry. *Clin. Chem.* **49**, 1916-1923, doi:10.1373/clinchem.2003.022046 (2003).
40 Fosset, C., McGaw, B. A., Reid, M. D. & McArdle, H. J. A non-radioactive method for measuring Cu uptake in HepG2 cells. *J. Inorg. Biochem.* **99**, 1018-1022, doi:10.1016/j.jinorgbio.2005.01.005 (2005).
41 Bondanese, V. P. *et al.* Hypoxia induces copper stable isotope fractionation in hepatocellular carcinoma, in a HIF-independent manner. *Metallomics* **8**, 1177-1184, doi:10.1039/c6mt00102e (2016).
42 Flórez, M. R. *et al.* Isotope ratio mapping by means of laser ablation-single collector-ICP-mass spectrometry: Zn tracer studies in thin sections of Daphnia magna. *J. Anal. At. Spectrom.* **28**, 1005-1015, doi:10.1039/c3ja50087j (2013).
43 Barbaste, M. *et al.* Evaluation of the accuracy of the determination of lead isotope ratios in wine by ICP MS using quadrupole, multicollector magnetic sector and time-of-flight analyzers. *Talanta* **54**, 307-317, doi:10.1016/s0039-9140(00)00651-2 (2001).
44 Vanhaecke, F., Balcaen, L. & Malinovsky, D. Use of single-collector and multi-collector ICP-mass spectrometry for isotopic analysis. *J. Anal. At. Spectrom.* **24**, 863-886, doi:10.1039/b903887f (2009).
45 Urgast, D. S. *et al.* Microanalytical isotope ratio measurements and elemental mapping using laser ablation ICP-MS for tissue thin sections: zinc tracer studies in rats. *Anal. Bioanal. Chem.* **402**, 287-297, doi:10.1007/s00216-011-5461-x (2012).
46 Wehe, C. A. *et al.* Elemental Bioimaging by Means of Fast Scanning Laser Ablation-Inductively Coupled Plasma-Mass Spectrometry. *J. Am. Soc. Mass Spectrom.* **26**, 1274-1282, doi:10.1007/s13361-015-1141-y (2015).
47 *US Geological Survey: High Resolution ICP-MS Laboratory*, <http://crustal.usgs.gov/laboratories/icpms/high_resolution.html> (2013).

48 Lear, J. *et al.* High-Resolution Elemental Bioimaging of Ca, Mn, Fe, Co, Cu, and Zn Employing LA-ICP-MS and Hydrogen Reaction Gas. *Anal. Chem.* **84**, 6707-6714, doi:10.1021/ac301156f (2012).
49 Becker, J. S., Zoriy, M. V., Pickhardt, C., Palomero-Gallagher, N. & Zilles, K. Imaging of Copper, Zinc, and Other Elements in Thin Section of Human Brain Samples (Hippocampus) by Laser Ablation Inductively Coupled Plasma Mass Spectrometry. *Anal. Chem.* **77**, 3208-3216, doi:10.1021/ac040184q (2005).
50 Hare, D. J., Lear, J., Bishop, D., Beavis, A. & Doble, P. A. Protocol for production of matrix-matched brain tissue standards for imaging by laser ablation-inductively coupled plasma-mass spectrometry. *Anal. Methods* **5**, 1915-1921, doi:10.1039/c3ay26248k (2013).
51 Van Malderen, S. J. M. *et al.* Quantitative Determination and Subcellular Imaging of Cu in Single Cells via Laser Ablation-ICP-Mass Spectrometry Using High-Density Microarray Gelatin Standards. *Anal. Chem.* **88**, 5783-5789, doi:10.1021/acs.analchem.6b00334 (2016).
52 Austin, C. *et al.* Factors affecting internal standard selection for quantitative elemental bio-imaging of soft tissues by LA-ICP-MS. *J. Anal. At. Spectrom.* **26**, 1494-1494, doi:10.1039/c0ja00267d (2011).
53 Frick, D. A. & Günther, D. Fundamental studies on the ablation behaviour of carbon in LA-ICP-MS with respect to the suitability as internal standard. *J. Anal. At. Spectrom.* **27**, 1294-1303, doi:10.1039/c2ja30072a (2012).
54 Limbeck, A. *et al.* Recent advances in quantitative LA-ICP-MS analysis: challenges and solutions in the life sciences and environmental chemistry. *Anal. Bioanal. Chem.* **407**, 6593-6617, doi:10.1007/s00216-015-8858-0 (2015).
55 Becker, J. S., Zoriy, M. V., Dehnhardt, M., Pickhardt, C. & Zilles, K. Copper, zinc, phosphorus and sulfur distribution in thin section of rat brain tissues measured by laser ablation inductively coupled plasma mass spectrometry: possibility for small-size tumor analysis. *J. Anal. At. Spectrom.* **20**, 912-917, doi:10.1039/b504978b (2005).
56 Dressler, V. L. *et al.* Biomonitoring of essential and toxic metals in single hair using on-line solution-based calibration in laser ablation inductively coupled plasma mass spectrometry. *Talanta* **82**, 1770-1777, doi:10.1016/j.talanta.2010.07.065 (2010).
57 Phung, A. T. *et al.* Reproducibility of laser ablation–inductively coupled plasma–mass spectrometry (LA–ICP–MS) measurements in mussel shells and comparison with micro-drill sampling and solution ICP–MS. *Talanta* **115**, 6-14, doi:10.1016/j.talanta.2013.04.019 (2013).
58 Bishop, D. P. *et al.* Elemental bio-imaging using laser ablation-triple quadrupole-ICP-MS. *J. Anal. At. Spectrom.* **31**, 197-202, doi:10.1039/c5ja00293a (2016).
59 Mueller, L. *et al.* Trends in single-cell analysis by use of ICP-MS. *Anal. Bioanal. Chem.* **406**, 6963-6977, doi:10.1007/s00216-014-8143-7 (2014).
60 Konz, I. *et al.* Quantitative bioimaging of trace elements in the human lens by LA-ICP-MS. *Anal. Bioanal. Chem.* **406**, 2343-2348, doi:10.1007/s00216-014-7617-y (2014).

61 Portbury, S. D., Hare, D. J., Sgambelloni, C., Finkelstein, D. I. & Adlard, P. A. A time-course analysis of changes in cerebral metal levels following a controlled cortical impact. *Metallomics* **8**, 193-200, doi:10.1039/c5mt00234f (2016).
62 Lear, J., Hare, D., Adlard, P., Finkelstein, D. & Doble, P. Improving acquisition times of elemental bio-imaging for quadrupole-based LA-ICP-MS. *J. Anal. At. Spectrom.* **27**, 159-164, doi:10.1039/c1ja10301f (2012).
63 Drescher, D. *et al.* Quantitative Imaging of Gold and Silver Nanoparticles in Single Eukaryotic Cells by Laser Ablation ICP-MS. *Anal. Chem.* **84**, 9684-9688, doi:10.1021/ac302639c (2012).
64 Wang, H. A. O. *et al.* Fast Chemical Imaging at High Spatial Resolution by Laser Ablation Inductively Coupled Plasma Mass Spectrometry. *Anal. Chem.* **85**, 10107-10116, doi:10.1021/ac400996x (2013).
65 Giesen, C. *et al.* Highly multiplexed imaging of tumor tissues with subcellular resolution by mass cytometry. *Nat. Methods* **11**, 417-422, doi:10.1038/nmeth.2869 (2014).
66 Douglas, D. N., Managh, A. J., Reid, H. J. & Sharp, B. L. High-Speed, Integrated Ablation Cell and Dual Concentric Injector Plasma Torch for Laser Ablation-Inductively Coupled Plasma Mass Spectrometry. *Anal. Chem.* **87**, 11285-11294, doi:10.1021/acs.analchem.5b02466 (2015).
67 Van Malderen, S. J. M., Managh, A. J., Sharp, B. L. & Vanhaecke, F. Recent developments in the design of rapid response cells for laser ablation-inductively coupled plasma-mass spectrometry and their impact on bioimaging applications. *J. Anal. At. Spectrom.* **31**, 423-439, doi:10.1039/c5ja00430f (2016).
68 Herrmann, A. M. *et al.* Nano-scale secondary ion mass spectrometry — A new analytical tool in biogeochemistry and soil ecology: A review article. *Soil Biol. Biochem.* **39**, 1835-1850, doi:10.1016/j.soilbio.2007.03.011 (2007).
69 Boxer, S. G., Kraft, M. L. & Weber, P. K. Advances in Imaging Secondary Ion Mass Spectrometry for Biological Samples. *Annu. Rev. Biophys.* **38**, 53-74, doi:10.1146/annurev.biophys.050708.133634 (2009).
70 Hong-Hermesdorf, A. *et al.* Subcellular metal imaging identifies dynamic sites of Cu accumulation in Chlamydomonas. *Nat. Chem. Biol.* **10**, 1034-1042, doi:10.1038/nchembio.1662 (2014).
71 Biesemeier, A. *et al.* Elemental mapping of Neuromelanin organelles of human Substantia Nigra: correlative ultrastructural and chemical analysis by analytical transmission electron microscopy and nano-secondary ion mass spectrometry. *J. Neurochem.* **138**, 339-353, doi:10.1111/jnc.13648 (2016).
72 Dickinson, M. *et al.* Dynamic SIMS analysis of cryo-prepared biological and geological specimens. *Appl. Surf. Sci.* **252**, 6793-6796, doi:10.1016/j.apsusc.2006.02.236 (2006).
73 Vickerman, J. & Winograd, N. in *Cluster Secondary Ion Mass Spectrometry: Principles and Applications* (ed C. M. Mahoney) 269-312 (John Wiley & Sons, Inc., 2013).
74 CAMECA. NanoSIMS: Introduction to the instrumentation. 1-16 (2016).
75 Ryan, C. G. *et al.* Maia X-ray fluorescence imaging: Capturing detail in complex natural samples. *J. Phys. Conf. Ser.* **499**, 012002 (2014).

76 James, S. A. *et al.* φXANES: In vivo imaging of metal-protein coordination environments. *Sci. Rpts.* **6**, 20350 (2016).
77 Bourassa, D., Gleber, S.-C., Vogt, S., Shin, C. H. & Fahrni, C. J. MicroXRF tomographic visualization of zinc and iron in the zebrafish embryo at the onset of the hatching period. *Metallomics* **8**, 1122-1130, doi:10.1039/c6mt00073h (2016).
78 Chen, S. *et al.* The Bionanoprobe: Synchrotron-Based Hard X-ray Fluorescence Microscopy for 2D/3D Trace Element Mapping. *Micros. Today* **23**, 26-29, doi:10.1017/s1551929515000401 (2015).
79 Fahrni, C. J. Biological applications of X-ray fluorescence microscopy: exploring the subcellular topography and speciation of transition metals. *Curr. Opin. Chem. Biol.* **11**, 121-127, doi:10.1016/j.cbpa.2007.02.039 (2007).
80 Ralle, M. & Lutsenko, S. Quantitative imaging of metals in tissues. *BioMetals* **22**, 197-205, doi:10.1007/s10534-008-9200-5 (2009).
81 Kaye, G. W. C. & Laby, T. H. in *Tables of Physical & Chemical Constants (16th Edition 1995)* (2005).
82 Davies, K. M. *et al.* Comparative Study of Metal Quantification in Neurological Tissue Using Laser Ablation-Inductively Coupled Plasma-Mass Spectrometry Imaging and X-ray Fluorescence Microscopy. *Anal. Chem.* **87**, 6639-6645, doi:10.1021/acs.analchem.5b01454 (2015).
83 Vogt, S. & Ralle, M. Opportunities in multidimensional trace metal imaging: taking copper-associated disease research to the next level. *Anal. Bioanal. Chem.* **405**, 1809-1820, doi:10.1007/s00216-012-6437-1 (2013).
84 House, M. J. *et al.* Mapping iron in human heart tissue with synchrotron x-ray fluorescence microscopy and cardiovascular magnetic resonance. *J. Cardiov. Magn. Reson.* **16**, 80 (2014).
85 Chen, S. *et al.* The Bionanoprobe: hard X-ray fluorescence nanoprobe with cryogenic capabilities. *J. Synchrotron Radiat.* **21**, 66-75, doi:10.1107/s1600577513029676 (2013).
86 Paunesku, T., Vogt, S., Maser, J., Lai, B. & Woloschak, G. X-ray fluorescence microprobe imaging in biology and medicine. *J. Cell. Biochem.* **99**, 1489-1502, doi:10.1002/jcb.21047 (2006).
87 Dučić, T. *et al.* X-ray fluorescence analysis of iron and manganese distribution in primary dopaminergic neurons. *J. Neurochem.* **124**, 250-261, doi:10.1111/jnc.12073 (2013).
88 Martínez-Criado, G. *et al.* ID16B: a hard X-ray nanoprobe beamline at the ESRF for nano-analysis. *J. Synchrotron Radiat.* **23**, 344-352, doi:10.1107/s1600577515019839 (2016).
89 Ortega, R. *et al.* α-Synuclein Over-Expression Induces Increased Iron Accumulation and Redistribution in Iron-Exposed Neurons. *Mol. Neurobiol.* **53**, 1925-1934, doi:10.1007/s12035-015-9146-x (2016).
90 Kim, S. A. *et al.* Localization of Iron in Arabidopsis Seed Requires the Vacuolar Membrane Transporter VIT1. *Science* **314**, 1295-1298, doi:10.1126/science.1132563 (2006).
91 de Jonge, M. D. *et al.* Quantitative 3D elemental microtomography of Cyclotella meneghiniana at 400-nm resolution. *Proc. Natl. Acad. Sci. U. S. A.* **107**, 15676-15680, doi:10.1073/pnas.1001469107 (2010).

92 de Jonge, M. D. & Vogt, S. Hard X-ray fluorescence tomography—an emerging tool for structural visualization. *Curr. Opin. Struct. Biol.* **20**, 606-614, doi:10.1016/j.sbi.2010.09.002 (2010).
93 Bourassa, D. *et al.* 3D imaging of transition metals in the zebrafish embryo by X-ray fluorescence microtomography. *Metallomics* **6**, 1648-1655, doi:10.1039/c4mt00121d (2014).
94 McRae, R., Bagchi, P., Sumalekshmy, S. & Fahrni, C. J. In Situ Imaging of Metals in Cells and Tissues. *Chem. Rev.* **109**, 4780-4827, doi:10.1021/cr900223a (2009).
95 *X-ray Absorption Spectroscopy: Introduction to Experimental Procedures*, <http://www-ssrl.slac.stanford.edu/mes/xafs/xas_intro.html> (
96 Bourassa, M. W. & Miller, L. M. Metal imaging in neurodegenerative diseases. *Metallomics* **4**, 721-738, doi:10.1039/c2mt20052j (2012).
97 Bacquart, T. *et al.* Subcellular Speciation Analysis of Trace Element Oxidation States Using Synchrotron Radiation Micro-X-ray Absorption Near-Edge Structure. *Anal. Chem.* **79**, 7353-7359, doi:10.1021/ac0711135 (2007).
98 Lerotic, M., Jacobsen, C., Schäfer, T. & Vogt, S. Cluster analysis of soft X-ray spectromicroscopy data. *Ultramicroscopy* **100**, 35-57, doi:10.1016/j.ultramic.2004.01.008 (2004).
99 Ortega, R., Deves, G. & Carmona, A. Bio-metals imaging and speciation in cells using proton and synchrotron radiation X-ray microspectroscopy. *J. R. Soc. Interface* **6**, S649-S658, doi:10.1098/rsif.2009.0166.focus (2009).
100 Rajendran, R. *et al.* A novel approach to the identification and quantitative elemental analysis of amyloid deposits—Insights into the pathology of Alzheimer's disease. *Biochem. Biophys. Res. Commun.* **382**, 91-95, doi:10.1016/j.bbrc.2009.02.136 (2009).
101 Lovell, M. A., Robertson, J. D., Teesdale, W. J., Campbell, J. L. & Markesbery, W. R. Copper, iron and zinc in Alzheimer's disease senile plaques. *J. Neurol. Sci.* **158**, 47-52, doi:10.1016/s0022-510x(98)00092-6 (1998).
102 Schnell Ramos, M., Khodja, H., Mary, V. & Thomine, S. Using µPIXE for quantitative mapping of metal concentration in Arabidopsis thaliana seeds. *Front. Plant Sci.* **4**, 168 (2013).
103 Susnea, I. & Weiskirchen, R. Trace metal imaging in diagnostic of hepatic metal disease. *Mass Spectrom. Rev.* **35**, 666-686, doi:10.1002/mas.21454 (2016).
104 Eibl, O., Schultheiss, S., Blitgen-Heinecke, P. & Schraermeyer, U. Quantitative chemical analysis of ocular melanosomes in the TEM. *Micron* **37**, 262-276, doi:10.1016/j.micron.2005.08.006 (2006).
105 Biesemeier, A., Schraermeyer, U. & Eibl, O. Chemical composition of melanosomes, lipofuscin and melanolipofuscin granules of human RPE tissues. *Exp. Eye Res.* **93**, 29-39, doi:10.1016/j.exer.2011.04.004 (2011).
106 Jang, H. J., Kim, J. M. & Choi, C. Y. Elemental analysis of sunflower cataract in Wilson's disease: A study using scanning transmission electron microscopy and energy dispersive spectroscopy. *Exp. Eye Res.* **121**, 58-65, doi:10.1016/j.exer.2014.02.003 (2014).
107 Sousa, A. A. & Leapman, R. D. Development and application of STEM for the biological sciences. *Ultramicroscopy* **123**, 38-49, doi:10.1016/j.ultramic.2012.04.005 (2012).

108 Leapman, R. D. Detecting single atoms of calcium and iron in biological structures by electron energy-loss spectrum-imaging. *J. Microsc.* **210**, 5-15 (2003).
109 Aronova, M. A., Sousa, A. A., Zhang, G. & Leapman, R. D. Limitations of beam damage in electron spectroscopic tomography of embedded cells. *J. Microsc.* **239**, 223-232, doi:10.1111/j.1365-2818.2010.03376.x (2010).
110 Treiber, C. D. *et al.* Clusters of iron-rich cells in the upper beak of pigeons are macrophages not magnetosensitive neurons. *Nature* **484**, 367-370, doi:10.1038/nature11046 (2012).
111 Theil, E. C. Ferritin: Structure, Gene Regulation, and Cellular Function in Animals, Plants, and Microorganisms. *Annu. Rev. Biochem.* **56**, 289-315, doi:10.1146/annurev.bi.56.070187.001445 (1987).
112 Iancu, T. C. Ferritin and hemosiderin in pathological tissues. *Electron Microsc. Rev.* **5**, 209-229 (1992).
113 Zhang, P. *et al.* Electron tomography of degenerating neurons in mice with abnormal regulation of iron metabolism. *J. Struct. Biol.* **150**, 144-153, doi:10.1016/j.jsb.2005.01.007 (2005).
114 Aronova, M. A. & Leapman, R. D. Development of electron energy-loss spectroscopy in the biological sciences. *MRS Bull.* **37**, 53-62, doi:10.1557/mrs.2011.329 (2012).
115 Messaoudi, C. *et al.* Three-Dimensional Chemical Mapping by EFTEM-TomoJ Including Improvement of SNR by PCA and ART Reconstruction of Volume by Noise Suppression. *Microsc. Microanal.* **19**, 1669-1677, doi:10.1017/s1431927613013317 (2013).
116 Salgado, J. C. *et al.* Mathematical modeling of the dynamic storage of iron in ferritin. *BMC Syst. Biol.* **4**, 147 (2010).
117 Kakhlon, O. & Cabantchik, Z. I. The labile iron pool: characterization, measurement, and participation in cellular processes. *Free Radic. Biol. Med.* **33**, 1037-1046 (2002).
118 Qian, X. & Xu, Z. Fluorescence imaging of metal ions implicated in diseases. *Chem. Soc. Rev.* **44**, 4487-4493, doi:10.1039/c4cs00292j (2015).
119 Carter, K. P., Young, A. M. & Palmer, A. E. Fluorescent Sensors for Measuring Metal Ions in Living Systems. *Chem. Rev.* **114**, 4564-4601, doi:10.1021/cr400546e (2014).
120 Jacobs, A. An intracellular transit iron pool. *Ciba Found. Symp.*, 91-106 (1976).
121 Ma, Y., Abbate, V. & Hider, R. C. Iron-sensitive fluorescent probes: monitoring intracellular iron pools. *Metallomics* **7**, 212-222, doi:10.1039/c4mt00214h (2015).
122 Burdette, S. C. Key Considerations for Sensing Fe(II) and Fe(III) in Aqueous Media. *Eur. J. Inorg. Chem.* **2015**, 5728-5729, doi:10.1002/ejic.201500566 (2015).
123 Breuer, W., Epsztejn, S., Millgram, P. & Cabantchik, I. Z. Transport of iron and other transition metals into cells as revealed by a fluorescent probe. *Am. J. Physiol.* **268**, C1354-C1361 (1995).
124 Petrat, F., Rauen, U. & de Groot, H. Determination of the chelatable iron pool of isolated rat hepatocytes by digital fluorescence microscopy using the fluorescent probe, phen green SK. *Hepatology* **29**, 1171-1179, doi:10.1002/hep.510290435 (1999).

125 Ma, Y., de Groot, H., Liu, Z., Hider, Robert C. & Petrat, F. Chelation and determination of labile iron in primary hepatocytes by pyridinone fluorescent probes. *Biochem. J.* **395**, 49-55, doi:10.1042/bj20051496 (2006).
126 Ma, Y., Liu, Z., Hider, R. C. & Petrat, F. Determination of the labile iron pool of human lymphocytes using the fluorescent probe, CP655. *Anal. Chem. Insights* **2**, 61-67 (2007).
127 Petrat, F. *et al.* Selective determination of mitochondrial chelatable iron in viable cells with a new fluorescent sensor. *Biochem. J.* **362**, 137-147 (2002).
128 Rauen, U. *et al.* Assessment of Chelatable Mitochondrial Iron by Using Mitochondrion-Selective Fluorescent Iron Indicators with Different Iron-Binding Affinities. *ChemBioChem* **8**, 341-352, doi:10.1002/cbic.200600311 (2007).
129 Hirayama, T., Okuda, K. & Nagasawa, H. A highly selective turn-on fluorescent probe for iron(ii) to visualize labile iron in living cells. *Chem. Sci.* **4**, 1250-1256, doi:10.1039/c2sc21649c (2013).
130 Niwa, M., Hirayama, T., Okuda, K. & Nagasawa, H. A new class of high-contrast Fe(ii) selective fluorescent probes based on spirocyclized scaffolds for visualization of intracellular labile iron delivered by transferrin. *Org. Biomol. Chem.* **12**, 6590-6597, doi:10.1039/c4ob00935e (2014).
131 Mori, M. *et al.* Ovarian endometriosis-associated stromal cells reveal persistently high affinity for iron. *Redox Biol.* **6**, 578-586, doi:10.1016/j.redox.2015.10.001 (2015).
132 Chen, J.-L. *et al.* High selective determination iron(II) by its enhancement effect on the fluorescence of pyrene-tetramethylpiperidinyl (TEMPO) as a spin fluorescence probe. *Spectrochim. Acta A Mol. Biomol. Spectrosc.* **63**, 438-443, doi:10.1016/j.saa.2005.04.057 (2006).
133 Maiti, S., Aydin, Z., Zhang, Y. & Guo, M. Reaction-based turn-on fluorescent probes with magnetic responses for Fe2+detection in live cells. *Dalton Trans.* **44**, 8942-8949, doi:10.1039/c4dt03792h (2015).
134 Au-Yeung, H. Y., Chan, J., Chantarojsiri, T. & Chang, C. J. Molecular Imaging of Labile Iron(II) Pools in Living Cells with a Turn-On Fluorescent Probe. *J. Am. Chem. Soc.* **135**, 15165-15173, doi:10.1021/ja4072964 (2013).
135 Borstnik, K., Paik, I. H., Shapiro, T. A. & Posner, G. H. Antimalarial chemotherapeutic peroxides: artemisinin, yingzhaosu A and related compounds. *Int. J. Parasitol.* **32**, 1661-1667 (2002).
136 Aron, A. T., Loehr, M. O., Bogena, J. & Chang, C. J. An Endoperoxide Reactivity-Based FRET Probe for Ratiometric Fluorescence Imaging of Labile Iron Pools in Living Cells. *J. Am. Chem. Soc.* **138**, 14338-14346, doi:10.1021/jacs.6b08016 (2016).
137 Bogdan, A. R., Miyazawa, M., Hashimoto, K. & Tsuji, Y. Regulators of Iron Homeostasis: New Players in Metabolism, Cell Death, and Disease. *Trends Biochem. Sci.* **41**, 274-286, doi:10.1016/j.tibs.2015.11.012 (2016).
138 Spangler, B. *et al.* A reactivity-based probe of the intracellular labile ferrous iron pool. *Nat. Chem. Biol.* **12**, 680-685, doi:10.1038/nchembio.2116 (2016).
139 Yang, L. *et al.* Imaging of the intracellular topography of copper with a fluorescent sensor and by synchrotron x-ray fluorescence microscopy. *Proc. Natl. Acad. Sci. U. S. A.* **102**, 11179-11184, doi:10.1073/pnas.0406547102 (2005).

140 Lutsenko, S. Human copper homeostasis: a network of interconnected pathways. *Curr. Opin. Chem. Biol.* **14**, 211-217, doi:10.1016/j.cbpa.2010.01.003 (2010).
141 Paredes, E. & Das, S. R. Optimization of acetonitrile co-solvent and copper stoichiometry for pseudo-ligandless click chemistry with nucleic acids. *Bioorg. Med. Chem. Lett.* **22**, 5313-5316, doi:10.1016/j.bmcl.2012.06.027 (2012).
142 Cotruvo, J. J. A., Aron, A. T., Ramos-Torres, K. M. & Chang, C. J. Synthetic fluorescent probes for studying copper in biological systems. *Chem. Soc. Rev.* **44**, 4400-4414, doi:10.1039/c4cs00346b (2015).
143 Aron, A. T., Ramos-Torres, K. M., Cotruvo, J. A. & Chang, C. J. Recognition- and Reactivity-Based Fluorescent Probes for Studying Transition Metal Signaling in Living Systems. *Acc. Chem. Res.* **48**, 2434-2442, doi:10.1021/acs.accounts.5b00221 (2015).
144 Fahrni, C. J. Synthetic fluorescent probes for monovalent copper. *Curr. Opin. Chem. Biol.* **17**, 656-662, doi:10.1016/j.cbpa.2013.05.019 (2013).
145 Chaudhry, A. F. *et al.* Kinetically Controlled Photoinduced Electron Transfer Switching in Cu(I)-Responsive Fluorescent Probes. *J. Am. Chem. Soc.* **132**, 737-747, doi:10.1021/ja908326z (2010).
146 Verma, M., Chaudhry, A. F., Morgan, M. T. & Fahrni, C. J. Electronically tuned 1,3,5-triarylpyrazolines as Cu(i)-selectivefluorescent probes. *Org. Biomol. Chem.* **8**, 363-370, doi:10.1039/b918311f (2010).
147 Chaudhry, A. F., Mandal, S., Hardcastle, K. I. & Fahrni, C. J. High-contrast Cu(i)-selective fluorescent probes based on synergistic electronic and conformational switching. *Chem. Sci.* **2**, 1016-1024, doi:10.1039/c1sc00024a (2011).
148 Morgan, M. T., Bagchi, P. & Fahrni, C. J. Designed To Dissolve: Suppression of Colloidal Aggregation of Cu(I)-Selective Fluorescent Probes in Aqueous Buffer and In-Gel Detection of a Metallochaperone. *J. Am. Chem. Soc.* **133**, 15906-15909, doi:10.1021/ja207004v (2011).
149 Morgan, M. T., McCallum, A. M. & Fahrni, C. J. Rational design of a water-soluble, lipid-compatible fluorescent probe for Cu(i) with sub-part-per-trillion sensitivity. *Chem. Sci.* **7**, 1468-1473, doi:10.1039/c5sc03643g (2016).
150 Zeng, L., Miller, E. W., Pralle, A., Isacoff, E. Y. & Chang, C. J. A Selective Turn-On Fluorescent Sensor for Imaging Copper in Living Cells. *J. Am. Chem. Soc.* **128**, 10-11, doi:10.1021/ja055064u (2006).
151 Miller, E. W., Zeng, L., Domaille, D. W. & Chang, C. J. Preparation and use of Coppersensor-1, a synthetic fluorophore for live-cell copper imaging. *Nat. Protoc.* **1**, 824-827, doi:10.1038/nprot.2006.140 (2006).
152 Price, K. A. *et al.* The challenges of using a copper fluorescent sensor (CS1) to track intracellular distributions of copper in neuronal and glial cells. *Chem. Sci.* **3**, 2748-2759, doi:10.1039/c2sc20397a (2012).
153 Santo, C. E. *et al.* Bacterial Killing by Dry Metallic Copper Surfaces. *Appl. Environ. Microbiol.* **77**, 794-802, doi:10.1128/aem.01599-10 (2011).
154 Quaranta, D. *et al.* Mechanisms of Contact-Mediated Killing of Yeast Cells on Dry Metallic Copper Surfaces. *Appl. Environ. Microbiol.* **77**, 416-426, doi:10.1128/aem.01704-10 (2011).

155 Beaudoin, J. *et al.* Mfc1 Is a Novel Forespore Membrane Copper Transporter in Meiotic and Sporulating Cells. *J. Biol. Chem.* **286**, 34356-34372, doi:10.1074/jbc.M111.280396 (2011).
156 Cusick, K. D. *et al.* Inhibition of Copper Uptake in Yeast Reveals the Copper Transporter Ctr1p As a Potential Molecular Target of Saxitoxin. *Environ. Sci. Technol.* **46**, 2959-2966, doi:10.1021/es204027m (2012).
157 Bernal, M. *et al.* Transcriptome sequencing identifies SPL7-regulated copper acquisition genes FRO4/FRO5 and the copper dependence of iron homeostasis in Arabidopsis. *Plant Cell* **24**, 738-761 (2012).
158 Achard, Maud E. S. *et al.* Copper redistribution in murine macrophages in response to Salmonella infection. *Biochem. J.* **444**, 51-57, doi:10.1042/bj20112180 (2012).
159 Gabe, Y., Ueno, T., Urano, Y., Kojima, H. & Nagano, T. Tunable design strategy for fluorescence probes based on 4-substituted BODIPY chromophore: improvement of highly sensitive fluorescence probe for nitric oxide. *Anal. Bioanal. Chem.* **386**, 621-626, doi:10.1007/s00216-006-0587-y (2006).
160 Dodani, S. C. *et al.* Calcium-dependent copper redistributions in neuronal cells revealed by a fluorescent copper sensor and X-ray fluorescence microscopy. *Proc. Natl. Acad. Sci. U. S. A.* **108**, 5980-5985, doi:10.1073/pnas.1009932108 (2011).
161 Huang, C. P., Fofana, M., Chan, J., Chang, C. J. & Howell, S. B. Copper transporter 2 regulates intracellular copper and sensitivity to cisplatin. *Metallomics* **6**, 654-661, doi:10.1039/c3mt00331k (2014).
162 Ohrvik, H. *et al.* Ctr2 regulates biogenesis of a cleaved form of mammalian Ctr1 metal transporter lacking the copper- and cisplatin-binding ecto-domain. *Proc. Natl. Acad. Sci. U. S. A.* **110**, E4279-E4288, doi:10.1073/pnas.1311749110 (2013).
163 Polishchuk, Elena V. *et al.* Wilson Disease Protein ATP7B Utilizes Lysosomal Exocytosis to Maintain Copper Homeostasis. *Dev. Cell* **29**, 686-700, doi:10.1016/j.devcel.2014.04.033 (2014).
164 Dodani, S. C. *et al.* Copper is an endogenous modulator of neural circuit spontaneous activity. *Proc. Natl. Acad. Sci. U. S. A.* **111**, 16280-16285, doi:10.1073/pnas.1409796111 (2014).
165 Koide, Y., Urano, Y., Hanaoka, K., Terai, T. & Nagano, T. Evolution of Group 14 Rhodamines as Platforms for Near-Infrared Fluorescence Probes Utilizing Photoinduced Electron Transfer. *ACS Chem. Biol.* **6**, 600-608, doi:10.1021/cb1002416 (2011).
166 Koide, Y., Urano, Y., Hanaoka, K., Terai, T. & Nagano, T. Development of an Si-Rhodamine-Based Far-Red to Near-Infrared Fluorescence Probe Selective for Hypochlorous Acid and Its Applications for Biological Imaging. *J. Am. Chem. Soc.* **133**, 5680-5682, doi:10.1021/ja111470n (2011).
167 Krishnamoorthy, L. *et al.* Copper regulates cyclic-AMP-dependent lipolysis. *Nat. Chem. Biol.* **12**, 586-592, doi:10.1038/nchembio.2098 (2016).
168 Lim, C. S. *et al.* A copper(i)-ion selective two-photon fluorescent probe for in vivo imaging. *Chem. Commun.* **47**, 7146-7148, doi:10.1039/c1cc11568e (2011).

169 Cao, X., Lin, W. & Wan, W. Development of a near-infrared fluorescent probe for imaging of endogenous Cu+ in live cells. *Chem. Commun.* **48**, 6247-6249, doi:10.1039/c2cc32114a (2012).
170 Hirayama, T., Van de Bittner, G. C., Gray, L. W., Lutsenko, S. & Chang, C. J. Near-infrared fluorescent sensor for in vivo copper imaging in a murine Wilson disease model. *Proc. Natl. Acad. Sci. U. S. A.* **109**, 2228-2233, doi:10.1073/pnas.1113729109 (2012).
171 Dodani, S. C., Leary, S. C., Cobine, P. A., Winge, D. R. & Chang, C. J. A Targetable Fluorescent Sensor Reveals That Copper-Deficient SCO1 and SCO2 Patient Cells Prioritize Mitochondrial Copper Homeostasis. *J. Am. Chem. Soc.* **133**, 8606-8616, doi:10.1021/ja2004158 (2011).
172 Smith, R. A. J., Porteous, C. M., Gane, A. M. & Murphy, M. P. Delivery of bioactive molecules to mitochondria in vivo. *Proc. Natl. Acad. Sci. U. S. A.* **100**, 5407-5412, doi:10.1073/pnas.0931245100 (2003).
173 Domaille, D. W., Zeng, L. & Chang, C. J. Visualizing Ascorbate-Triggered Release of Labile Copper within Living Cells using a Ratiometric Fluorescent Sensor. *J. Am. Chem. Soc.* **132**, 1194-1195, doi:10.1021/ja907778b (2010).
174 Giuffrida, M. L., Rizzarelli, E., Tomaselli, G. A., Satriano, C. & Trusso Sfrazzetto, G. A novel fully water-soluble Cu(i) probe for fluorescence live cell imaging. *Chem. Commun.* **50**, 9835-9838, doi:10.1039/c4cc02147a (2014).
175 Satriano, C. *et al.* A ratiometric naphthalimide sensor for live cell imaging of copper(i). *Chem. Commun.* **49**, 5565-5567, doi:10.1039/c3cc42069h (2013).
176 Shen, C. *et al.* A ratiometric fluorescent sensor for the mitochondrial copper pool. *Metallomics* **8**, 915-919, doi:10.1039/c6mt00083e (2016).
177 Jung, K. H., Oh, E.-T., Park, H. J. & Lee, K.-H. Development of new peptide-based receptor of fluorescent probe with femtomolar affinity for Cu+ and detection of Cu+ in Golgi apparatus. *Biosens. Bioelectron.* **85**, 437-444, doi:10.1016/j.bios.2016.04.101 (2016).
178 Chan, J., Dodani, S. C. & Chang, C. J. Reaction-based small-molecule fluorescent probes for chemoselective bioimaging. *Nat. Chem.* **4**, 973-984, doi:10.1038/nchem.1500 (2012).
179 Yang, Y., Zhao, Q., Feng, W. & Li, F. Luminescent Chemodosimeters for Bioimaging. *Chem. Rev.* **113**, 192-270, doi:10.1021/cr2004103 (2013).
180 Kim, S. K. & Sessler, J. L. Ion pair receptors. *Chem. Soc. Rev.* **39**, 3784-3809, doi:10.1039/c002694h (2010).
181 Lee, S., Yuen, K. K. Y., Jolliffe, K. A. & Yoon, J. Fluorescent and colorimetric chemosensors for pyrophosphate. *Chem. Soc. Rev.* **44**, 1749-1762, doi:10.1039/c4cs00353e (2015).
182 Taki, M., Iyoshi, S., Ojida, A., Hamachi, I. & Yamamoto, Y. Development of Highly Sensitive Fluorescent Probes for Detection of Intracellular Copper(I) in Living Systems. *J. Am. Chem. Soc.* **132**, 5938-5939, doi:10.1021/ja100714p (2010).
183 Urano, Y. *et al.* Evolution of Fluorescein as a Platform for Finely Tunable Fluorescence Probes. *J. Am. Chem. Soc.* **127**, 4888-4894, doi:10.1021/ja043919h (2005).

184 Maity, D., Kumar, V. & Govindaraju, T. Reactive Probes for Ratiometric Detection of Co2+and Cu+Based on Excited-State Intramolecular Proton Transfer Mechanism. *Org. Lett.* **14**, 6008-6011, doi:10.1021/ol302904c (2012).
185 Yu, K.-K., Li, K., Hou, J.-T. & Yu, X.-Q. Coumarin–TPA derivative: a reaction-based ratiometric fluorescent probe for Cu(I). *Tetrahedron Lett.* **54**, 5771-5774, doi:10.1016/j.tetlet.2013.08.046 (2013).
186 Maity, D., Sarkar, B., Maiti, S. & Govindaraju, T. A Highly Selective Reaction-Based Two-Photon Probe for Copper(I) in Aqueous Media. *ChemPlusChem* **78**, 785-788, doi:10.1002/cplu.201300089 (2013).
187 Maity, D., Raj, A., Karthigeyan, D., Kundu, T. K. & Govindaraju, T. Reaction-based probes for Co(ii) and Cu(i) with dual output modes: fluorescence live cell imaging. *RSC Adv.* **3**, 16788-16794, doi:10.1039/c3ra41588k (2013).
188 Maity, D., Raj, A., Karthigeyan, D., Kundu, T. K. & Govindaraju, T. A switch-on near-infrared fluorescence-ready probe for Cu(I): live cell imaging. *Supramol. Chem.* **27**, 589-594, doi:10.1080/10610278.2015.1041953 (2015).
189 Hu, Z. *et al.* A TPA-caged precursor of (imino)coumarin for “turn-on” fluorogenic detection of Cu+. *Anal. Chim. Acta* **933**, 189-195, doi:10.1016/j.aca.2016.05.031 (2016).
190 Taki, M., Akaoka, K., Mitsui, K. & Yamamoto, Y. A mitochondria-targeted turn-on fluorescent probe based on a rhodol platform for the detection of copper(i). *Org. Biomol. Chem.* **12**, 4999-5005, doi:10.1039/c4ob00527a (2014).
191 Au-Yeung, H. Y., New, E. J. & Chang, C. J. A selective reaction-based fluorescent probe for detecting cobalt in living cells. *Chem. Commun.* **48**, 5268-5270, doi:10.1039/c2cc31681a (2012).
192 Heffern, M. C. *et al. In vivo bioluminescence imaging reveals copper deficiency in a murine model of nonalcoholic fatty liver disease* (2016).
193 Spatz, H. Über den eisennachweis im gehirn, besonders in zentren des extrapyramidal-motorischen systems. I. Teil. *Zeitschrift für die gesamte Neurologie und Psychiatrie* **77**, 261-390, doi:10.1007/bf02865844 (1922).
194 Hallgren, B. & Sourander, P. The Effect of Age on the Non-Haemin Iron in the Human Brain. *J. Neurochem.* **3**, 41-51, doi:10.1111/j.1471-4159.1958.tb12607.x (1958).
195 James, S. A. *et al.* Direct in vivo imaging of ferrous iron dyshomeostasis in ageing Caenorhabditis elegans. *Chem. Sci.* **6**, 2952-2962, doi:10.1039/c5sc00233h (2015).
196 Berry, A. J., O’Neill, H. S. C., Jayasuriya, K. D., Campbell, S. J. & Foran, G. J. XANES calibrations for the oxidation state of iron in a silicate glass. *Am. Mineral.* **88**, 967-977, doi:10.2138/am-2003-0704 (2003).
197 Miyayama, T., Suzuki, K. T. & Ogra, Y. Copper accumulation and compartmentalization in mouse fibroblast lacking metallothionein and copper chaperone, Atox1. *Toxicol. Appl. Pharmacol.* **237**, 205-213, doi:10.1016/j.taap.2009.03.024 (2009).
198 Ralle, M. *et al.* Wilson Disease at a Single Cell Level: INTRACELLULAR COPPER TRAFFICKING ACTIVATES COMPARTMENT-SPECIFIC RESPONSES IN HEPATOCYTES. *J. Biol. Chem.* **285**, 30875-30883, doi:10.1074/jbc.M110.114447 (2010).

199 Malasarn, D. *et al.* Zinc Deficiency Impacts CO2 Assimilation and Disrupts Copper Homeostasis in Chlamydomonas reinhardtii. *J. Biol. Chem.* **288**, 10672-10683, doi:10.1074/jbc.M113.455105 (2013).
200 Nose, Y., Kim, B.-E. & Thiele, D. J. Ctr1 drives intestinal copper absorption and is essential for growth, iron metabolism, and neonatal cardiac function. *Cell Metab.* **4**, 235-244, doi:10.1016/j.cmet.2006.08.009 (2006).
201 Rees, E. M., Lee, J. & Thiele, D. J. Mobilization of Intracellular Copper Stores by the Ctr2 Vacuolar Copper Transporter. *J. Biol. Chem.* **279**, 54221-54229, doi:10.1074/jbc.M411669200 (2004).
202 Kardos, J., Kovács, I., Hajós, F., Kálmán, M. & Simonyi, M. Nerve endings from rat brain tissue release copper upon depolarization. A possible role in regulating neuronal excitability. *Neurosci. Lett.* **103**, 139-144, doi:10.1016/0304-3940(89)90565-x (1989).
203 Hopt, A. *et al.* Methods for studying synaptosomal copper release. *J. Neurosci. Methods* **128**, 159-172 (2003).
204 Hartter, D. E. & Barnea, A. Evidence for release of copper in the brain: Depolarization-induced release of newly taken-up67copper. *Synapse* **2**, 412-415, doi:10.1002/syn.890020408 (1988).
205 Schlief, M. L., Craig, A. M. & Gitlin, J. D. NMDA Receptor Activation Mediates Copper Homeostasis in Hippocampal Neurons. *J. Neurosci.* **25**, 239-246, doi:10.1523/jneurosci.3699-04.2005 (2005).
206 Schlief, M. L., West, T., Craig, A. M., Holtzman, D. M. & Gitlin, J. D. Role of the Menkes copper-transporting ATPase in NMDA receptor-mediated neuronal toxicity. *Proc. Natl. Acad. Sci. U. S. A.* **103**, 14919-14924, doi:10.1073/pnas.0605390103 (2006).
207 Acevedo, K. M. *et al.* Copper Promotes the Trafficking of the Amyloid Precursor Protein. *J. Biol. Chem.* **286**, 8252-8262, doi:10.1074/jbc.M110.128512 (2010).
208 Gaier, E. D. *et al.* In vivo and in vitro analyses of amygdalar function reveal a role for copper. *J. Neurophysiol.* **111**, 1927-1939, doi:10.1152/jn.00631.2013 (2014).
209 D'Ambrosi, N. & Rossi, L. Copper at synapse: Release, binding and modulation of neurotransmission. *Neurochem. Int.* **90**, 36-45, doi:10.1016/j.neuint.2015.07.006 (2015).
210 Turski, M. L. *et al.* A Novel Role for Copper in Ras/Mitogen-Activated Protein Kinase Signaling. *Mol. Cell Biol.* **32**, 1284-1295, doi:10.1128/mcb.05722-11 (2012).
211 Brady, D. C. *et al.* Copper is required for oncogenic BRAF signalling and tumorigenesis. *Nature* **509**, 492-496, doi:10.1038/nature13180 (2014).
212 Ishida, S., Andreux, P., Poitry-Yamate, C., Auwerx, J. & Hanahan, D. Bioavailable copper modulates oxidative phosphorylation and growth of tumors. *Proc. Natl. Acad. Sci. U. S. A.* **110**, 19507-19512, doi:10.1073/pnas.1318431110 (2013).
213 Kim, B.-E. *et al.* Cardiac Copper Deficiency Activates a Systemic Signaling Mechanism that Communicates with the Copper Acquisition and Storage Organs. *Cell Metab.* **11**, 353-363, doi:10.1016/j.cmet.2010.04.003 (2010).
214 Zheng, L. *et al.* Role of copper in regression of cardiac hypertrophy. *Pharmacol. Ther.* **148**, 66-84, doi:10.1016/j.pharmthera.2014.11.014 (2015).

215 Zhou, Z., Johnson, W. T. & Kang, Y. J. Regression of copper-deficient heart hypertrophy: reduction in the size of hypertrophic cardiomyocytes. *J. Nutr. Biochem.* **20**, 621-628, doi:10.1016/j.jnutbio.2008.06.007 (2009).

Chapter 2

Mapping Copper in the Retina of a Zebrafish Menkes Model using LA-ICP-MS and Nano-SIMS

Introduction

Copper acquisition and trafficking are fundamental functions of eukaryotic organisms[1,2] because cytochrome c oxidase, an enzyme in the mitochondrial electron transport chain, requires a copper cofactor.[3] Like any element, copper cannot be created within a biological system, so it must be obtained from the environment and trafficked to the correct tissues, cells, organelles, and proteins within an organism. Dysregulation of copper trafficking can lead to mislocalization of copper within an organism, causing toxicity and even death.[4-6] Understanding the proteins responsible for transporting copper across cellular membranes provides a molecular handle to understand diseases associated with copper mislocalization and potential targets for therapy.[7-10]

ATP7A is the copper export protein ubiquitously expressed across mammalian tissues.[11] On a cellular level, ATP7A is responsible for exporting copper from the cell as well as loading copper into copper-containing enzymes during Golgi processing.[12] On a tissue level, ATP7A is required to mobilize copper from intestinal cells into the blood stream.[13] Loss of ATP7A has been linked to accumulation of copper in the kidneys and intestines and severe copper deficiency in the other tissues of the body.[14]

In humans, mutations in the ATP7A protein are associated with a spectrum of diseases that span a wide range of severities.[15] Distal motor neuropathy (DMN) is the least severe, manifesting in young-adulthood with the death of motor neurons, leading to progressive muscle weakness.[16] Occipital horn syndrome (OHS) typically appears in teenagers, with patients showing mild cognitive defects, failure of the autonomic nervous system, poor formation of connective tissue leading to lax skin and joints, as well as characteristic horns on the occipital bone at the base of the skull.[17] Menkes disease is the most severe disease associated with ATP7A mutations, with symptoms typically manifesting within months of birth.[15] Patients often have brain atrophy and seizures, poor formation of connective tissue, and coarse, light-colored hair; Menkes disease is typically lethal during childhood. Neurological symptoms are common to all of these diseases, regardless of severity, leading to the hypothesis that the central nervous system is particularly sensitive to defects in copper metabolism.[18,19] However, studying the neurological effects of copper deficiency in these diseases and their models can be complicated because neurological effects may be masked by other pathologies such as poor motor function.

The *Calamity*^{gw71} allele in zebrafish contains an I1061S point mutation in ATP7A that causes impaired copper export.[20] Interestingly, *Cal*^{gw71} embryos are morphologically indistinguishable from their wildtype siblings but are sensitive to copper deprivation. The application of low levels of the copper chelator neocuproine impairs pigmentation in *Cal*^{gw71} embryos at concentrations that have no effect on their wildtype siblings,[20] suggesting that *Cal*^{gw71} fish contain lower levels of copper than their wildtype siblings. We reasoned that if *Cal*^{gw71} fish had lower copper levels than their wildtype siblings, the *Cal*^{gw71} fish could provide an excellent model system for studying the effect of copper deficiency on neurobiology without the complications of gross morphological or functional defects typically associated with Menkes models.[21] The copper content of *Cal*^{gw71} fish, however, had not been published, and we were specifically interested to know if neural

tissue within these fish was copper deficient. Zebrafish embryos are prohibitively small to subject to traditional dissection and elemental analysis methods. Thus, we turned to metal imaging methods to quantify the amount and location of copper within *Cal*^{gw71} embryos.[22] Here, we use laser ablation inductively coupled plasma mass spectrometry (LA-ICP-MS) and nano-secondary ion mass spectrometry (nanoSIMS) to show that the neuroretina of wildtype zebrafish embryos contain copper puncta which are copper-deficient in *Cal*^{gw71} embryos. Additionally, we provide electron microscopy and confocal microscopy evidence that these copper puncta represent the contents of the megamitochondria of photoreceptors, achieving the first measurement of mitochondrial copper content within the context of complex tissue.

Results

To assess whether *Cal*^{gw71} embryos have altered copper levels relative to their wildtype siblings, I analyzed tissue slices of *Cal*^{gw71} and WT embryos by LA-ICP-MS. In this technique, each tissue slice is ablated by a laser beam rastering across its surface, and the metal concentration of the ablated material at each location is measured by ICP-MS, rendering a 2-dimensional metal map of the tissue.[22] At 6 days post-fertilization (dpf), embryos were embedded in mounting media and flash frozen in dry ice/isopentane to avoid the redistribution of metals that can occur during tissue fixation.[23,24] Frozen samples were sliced, mounted on glass slides and air dried. LA-ICP-MS was performed using a 6 µm diameter spot, which was sufficient to resolve distinct tissues within the zebrafish embryo and achieved the highest resolution images of endogenous metals acquired by laser ablation techniques to our knowledge. LA-ICP-MS revealed tissue-specific enrichment of copper in the liver and heart of wildtype embryos, as well as neural tissue, relative to the rest of the body (Figure 2.1). However, in *Cal*^{gw71} embryos, copper accumulated in the kidneys and was largely excluded from the neural tissue (Figure 2.1). Matrix-matched standards[25] allowed quantification of these images, revealing significant differences in copper levels in the kidney, liver, and neural tissue of the two genotypes (Figure 2.2).

Interested in the differences in neural tissue copper levels between the two genotypes, I focused on the stark difference in copper content in the outer retina of *Cal*^{gw71} vs wildtype fish. In wildtype fish, a bright ring of copper was observed along the outer edge of the retina, and this ring was absent in *Cal*^{gw71} retinas (Figure 2.1, arrowheads). The retina is a highly structured tissue, consisting of multiple concentric cell layers that radiate from the lens.[26,27] Each cell layer has a distinct function, so I reasoned that I might be able to identify the function of the retinal copper rings by identifying the retinal cell layer that contained them. However, retinal cell layers in zebrafish embryos are ~5-30 µm wide each, making them difficult to distinguish with a 6 µm diameter ablation spot. Thus, I turned to the CAMECA NanoSIMS, a high-resolution ion mapping instrument that has achieved 100-200 nm spatial resolution metal maps of biological tissue.[28,29] In collaboration with Peter Weber and Jenniffer Pett-Ridge at the Lawrence Livermore National Lab, we mapped the localization of copper and phosphorous relative to carbon in wildtype and *Cal*^{gw71} embryos (Figure 2.3). Surprisingly, rather than revealing continuous rings of copper around the edge of the retina, nanoSIMS images resolved

distinct copper puncta. Using the phosphorous signal to identify cellular nuclei which distinguish retinal cell layers, the copper puncta were assigned to the outer nuclear layer, the retinal layer containing the photoreceptors (Figure 2.3). Additionally, matrix-matched standards enabled quantification of the copper content of these puncta (Figure 2.4). To our knowledge, this is the first use of matrix-matched standards in nanoSIMS to quantify metal concentrations in biological samples.

Photoreceptor cells are highly complex neural cells responsible for sensing photons and generating the initial electrochemical signals that propagate through the neuroretina and are transmitted to the brain via the optic nerve.[26,27] Photoreceptor cells are the most energy-demanding cells of the retina. In the dark, energy is devoted to maintaining ion gradients in the steady state; in the light, even more energy is required to mediate the turnover of each rhodopsin molecule that interacts with a photon.[30-32] To provide the large quantity of ATP required for these processes, photoreceptors contain a large mass of mitochondria. In most mammals studied, many long, thin mitochondria are arranged in parallel within the inner segment of the photoreceptor cell.[33,34] However, in other animals, including zebrafish[35-38] and some tree shrews,[39,40] large, bulky mitochondria with diameters exceeding 2 µm have been observed in the inner segments of photoreceptors. The unusual size of these mitochondria places them in a morphological class known as megamitochondria.[41] Interestingly, megamitochondria are typically observed under conditions of cell stress.[42-44] However, some megamitochondria have been observed in healthy cells,[45,46] and the megamitochondria of photoreceptors appear to belong in this category. The role of megamitochondria in photoreceptors is unclear. Some groups have argued that megamitochondria provide the high ATP levels necessary for photoreceptor health.[37] Others maintain that the main driver of megamitochondrial morphology is optical: the refractive index of megamitochondria is much higher than that of the rest of the retina, perhaps revealing a role for megamitochondria in collecting and focusing light.[47,48] Regardless of the underlying role of megamitochondria, we hypothesized that these mitochondria contain cytochrome c oxidase, a cupro-protein which serves as the terminus of the electron transport chain. We wondered if the copper puncta we observed in the photoreceptors might be coming from copper contained in megamitochondria. Indeed, electron micrographs revealed a localization pattern of megamitochondria relative to nuclei that matched the pattern of copper puncta relative to phosphorous that we observed in nanoSIMS images (Figure 2.5).

Next, we attempted to test colocalization of megamitochondria from electron micrographs and copper puncta from nanoSIMS images of the same region. However, these efforts were frustrated by relocalization of copper in tissues that had been embedded in resin for electron microscopy. Rather than being located in puncta in the outer nuclear layer, copper had accumulated in the retinal pigmented epithelium (data not shown). To circumvent the possibility of metal relocalization and identify mitochondria without using formaldehyde fixation or embedding, I generated zebrafish embryos expressing Actin:TOM20-mCherry, an mCherry construct localized to the mitochondria and expressed under the actin promoter.[49,50] Indeed, megamitochondria labeled with mCherry colocalized with copper puncta from nanoSIMS images of the same region (Figure 2.6). Interestingly, the mapping of fluorescent mitochondria to copper puncta was not

completely 1:1, likely for two reasons: 1) fluorescently labeled fish were actin:TOM20-mCherry mosaics; therefore, some cells did not express actin:TOM20-mCherry, and some megamitochondria were unlabeled; and 2) nanoSIMS analysis only represents a 100-nm slice of tissue, while confocal microscopy optical slices are 1-2 µm, making it likely that some megamitochondria observed by confocal microscopy were outside the slice analyzed by nanoSIMS.

Having demonstrated that copper puncta observed in nanoSIMS images originate from megamitochondrial copper, we were curious what the functional consequences of lower copper in *Cal*^{gw71} embryos might be. Photoreceptors with damaged or missing megamitochondria degrade due to the inability to produce sufficient ATP to support rhodopsin turnover.[51] Initial electron microscopy experiments have revealed no gross morphological defects in photoreceptor or megamitochondrial architecture between wildtype and *Cal*^{gw71} embryos (Figure 2.7). However, it is possible that the *Cal*^{gw71} megamitochondria are able to produce sufficient ATP under the basal light/dark cycles typically used for raising zebrafish but may be unable to meet ATP demand under conditions of light stress typically used for assessing megamitochondrial function.[52] Experiments are underway to determine whether *Cal*^{gw71} megamitochondria produce ATP at the same rate as wildtype megamitochondria in response to increased photon flux.

Discussion and Future Directions

The retina is a complex tissue composed of multiple neural and glial cell layers that work together to perceive light, one of the most valuable sensory inputs in daily human life.[26] Vision impairment due to eye disease affects over 30 million adults in the United States, with over 2 million cases due to macular degeneration,[53] the degeneration of the central portion of the retina. Retinal degeneration is currently considered to be an incurable disease,[54] and improvements in our understanding of the mechanisms and processes that govern retinal health may lead to better therapies and cures to these widespread illnesses.

Over a half century of research has shed light on the importance of copper in retinal health. Studies of Menkes[55,56] and Wilson's diseases,[57,58] copper metabolism disorders caused by mutations in the copper exporters ATP7A and ATP7B, respectively, have found significant optical pathologies including disrupted retinal signaling and loss of sight.[59,60] Additionally, alterations in copper metabolism have been associated with age-related macular degeneration.[61,62] More recently, the importance of peptidylglycine α-amidating monooxygenase (PAM), a copper-containing monoamine oxidase, in photoreceptor ciliogenesis has been identified,[63,64] and copper has been found to be required for spontaneous firing in the retina.[65] Here, we show that copper accumulates in the megamitochondria of photoreceptors, and that disruption of the ATP7A transporter disrupts copper trafficking to these organelles. As the retina is neural tissue, located behind the blood-brain barrier, these results suggest that ATP7A plays a role in the mobilization of copper to the brain. Additionally, these results support the use of the *Cal*^{gw71} zebrafish as a model of neural copper deprivation in fish that are otherwise morphologically healthy.

Additionally, these studies highlight the use of metal imaging for identifying new roles for copper in tissues by identifying areas of copper enrichment. Rapid profiling methods such as LA-ICP-MS are powerful because of their ability to scan many tissue slices over a short period of time, providing metal signatures for specific tissues and genotypes and identifying differences between them. After using LA-ICP-MS to identify specific regions of interest, techniques such as nanoSIMS may be used to obtain higher resolution images of copper distribution, identifying the specific cellular and subcellular context in which the copper is located. Using matrix-matched standards, both LA-ICP-MS and nanoSIMS can be quantitative, providing numerical readouts of metal content in tissues without dissection or digestion and facilitating the quantification of copper concentrations in structures that are otherwise too small to analyze, such as a single mitochondrion. Additionally, nanoSIMS may be combined with other microscopy techniques that do not require sample fixation in order to generate colocalization images using fluorescent markers.

As techniques for imaging metals in biological tissue continue to improve and the statistical methods applied to metal image analysis become more sophisticated,[66,67] the power of metal imaging to identify biologically relevant differences between genotypes will become increasingly valuable. The application of high-resolution metal imaging to highly structured tissues may resolve unappreciated roles of metals in cellular subtypes within tissues, roles that were previously invisible because bulk or low-resolution imaging techniques average across many cells within a tissue. We expect that these techniques will be particularly powerful in complex tissues such as the brain, and our laboratory continues to pursue studies in this area.

Materials and Methods

Materials

All chemicals were purchased from Sigma Aldrich, unless otherwise noted.

Zebrafish Husbandry

All zebrafish housing, care, and experiments were conducted according to the lab Animal Use Protocol, approved by the UC Berkeley Animal Care and Use Committee. Zebrafish were housed in the UC Berkeley Zebrafish Facility and kept at 28.5 °C on a 14 hour light/10 hour dark cycle. Embryos were produced by natural crosses and staged by hours post fertilization (hpf) or days post fertilization (dpf). To tightly control metal content in growing embryos, embryos were raised in E3 medium made from doubly-distilled (18 MΩ) water. Wildtype zebrafish were from the AB strain. Transgenic *Calamity*^{gw71} (*Cal*^{gw71}) fish were a gift from Prof. Jonathan Gitlin; genotyping of the *Cal*^{gw71} line was conducted as described previously.[20]

Sample Preparation for LA-ICP-MS and nanoSIMS

Zebrafish embryos were raised in E3 medium to 6 dpf. Embryos were euthanized in ice water and immediately embedded in Optimal Cutting Temperature (OCT) mounting media (Tissue Tek) in cryomolds (Tissue Tek). The embedded embryos were immediately frozen in a dry ice/isopentane bath and stored at -80 °C until sectioning. For 4-18 hours before sectioning, the embedded embryos were equilibrated to -20 °C. The embryos were sectioned into 20 µm slices using a Cryostat (Leica CM1950) and placed directly onto Superfrost PLUS slides (Thermo Fisher). For nanoSIMS analysis, before mounting slices on the slides, the slides were trimmed to 1.5 inches long using a diamond knife so that the slides could fit inside the nanoSIMS sample carrier. To avoid touching the surface of the trimmed slides during sample mounting, the slides were taped at the edges to standard-length slides using removable tape (Scotch). The slices were air-dried and stored at room temperature until analysis.

To test the effect of fixation on metal imaging, some samples were fixed before mounting. In this case, 6 dpf embryos were euthanized in ice water and immediately submerged in 4% paraformaldehyde (PFA, Thermo Fisher, 28906) in phosphate buffered saline (PBS) overnight at 4 °C. The next day, embryos were washed three times in PBS, transferred to a solution of 30% sucrose in PBS for cryoprotection, and allowed to equilibrate until the embryos had sunk to the bottom of the tube (typically overnight). The fixed, cryoprotected embryos were mounted in OCT and processed as outlined above. Fixation perturbed metal localization and was not used in subsequent sample preparation (Figure 2.8).

Laser Ablation Inductively Coupled Plasma Mass Spectrometry

Samples were prepared as outlined above. Laser ablation was performed on an NWR213 laser with a TV2 sample chamber (ESI, Bozeman, MT) using the following parameters:

Spot size: 6 µm; Fluence: 2.3 J cm^{-2}; Stage speed: 15 µm s^{-1}; Firing rate: 20 Hz; He flow: 800 mL min^{-1}; Pattern spacing: 6 µm. Using these parameters, the tissue was fully ablated but the glass slide remained undamaged. The ablated material was introduced by helium gas flow into an iCAP-Qc ICP-MS (Thermo Fisher) and analyzed for ^{63}Cu or ^{66}Zn content using a 0.4 sec dwell time in standard acquisition mode. The resulting mass spectrometry traces and laser log files were processed in Igor Pro using the Iolite application. The Trace Elements data reduction scheme was used in Semi-quantitative mode using ^{63}Cu or ^{66}Zn as the reference trace and a custom matrix-matched standard to convert mass spectrometer counts to metal concentration. Quantitative metal maps were exported in csv format and imported into ImageJ for quantification of regions of interest.

Nano Secondary Ion Mass Spectrometry

Samples were prepared as outlined above. Preparation of samples mounted on TEM grids is outlined below (see Electron Microscopy). Samples were dried for at least 24 hours before use in order to prevent sample distortion in the nanoSIMS vacuum chamber. To create a conductive surface, the samples were coated with 15-20 nm of gold using a Hummer sputter coater (Technics). During the initial optimization of sample preparation methods, carbon coating (12-15 nm, EMS 150T ES by EMS Quorum) was also tested. In our hands, both carbon and gold coating yielded excellent SIMS images (Figure 2.8). Due to the ease and consistency of gold coating in our facility, gold coating was used for all subsequent sample preparation.

The Cameca NanoSIMS 50 (Gennevilliers, France) at Lawrence Livermore National Lab was used to image the intracellular distribution of P, Ca, Cu, and Fe. All samples were first imaged by transmitted light using an SMZ800 stereo microscope (Nikon) for slide mapping and a compound microscope mounted on an encoded X-Y stage (Leitz) for high magnification images. Fluorescence microscopy was performed as described below (see Confocal Microscopy). Areas identified by transmitted light or fluorescence microscopy were relocated and analyzed in the NanoSIMS 50. The analysis areas were sputtered to a depth of ~60 nm before analysis with a focused 100 to 120 pA negative oxygen ion primary beam, which was scanned over 2500 μm^2 rasters with 512 x 512 pixels to generate secondary ions. The secondary ion mass spectrometer was tuned for ~3000 and $^{12}C^+$, $^{31}P^+$, $^{40}Ca^+$, $^{56}Fe^+$, and $^{63}Cu^+$ were detected simultaneously by electron multipliers in pulse counting mode. The correct metal ion peaks were identified using NBS610 glass (National Institute of Standards and Technology, USA). Each analysis area was scanned 30 to 50 times with 500 ns/pixel dwell times to collect serial secondary ion images for quantification.

The NanoSIMS ion image data were processed using custom software (LIMAGE, L.R. Nittler, Carnegie Institute of Washington, USA). The ion images were corrected for detector dead time and image shifts between scans, and then used to produce ion ratio images. For defined regions of interest, ion ratios were calculated for $^{31}P^+/^{12}C^+$, $^{40}Ca^+/^{12}C^+$, $^{56}Fe^+/^{12}C^+$ and $^{63}Cu^+/^{12}C^+$ by averaging the replicate scans. These data were quantified using matrix-matched standards (see below).

Preparation of Matrix-Matched Standards for Quantitative Metal Maps

This protocol was adapted from published methods.[25,68] Salmon muscle (30 mL of packed tissue) was digested by adding 10 mL of protease solution (0.25% trypsin, 10 mM EDTA, 0.1X PBS) and 48 µL of Collagenase P (100 mg mL^{-1} in HBSS) in a 50 mL plastic conical tube. The solution was mixed with a plastic spatula (to minimize metal contamination) and incubated at 28° C for 4 hours with periodic mixing. The tissue was stored at 4°C overnight. The next day, the tissue was warmed to 28 °C for an additional 6 hours of digestion and homogenized in a Dounce homogenizer using 10 passes until the tissue was gooey and smooth. The tissue was separated into 500 µL aliquots in 1.5 mL Sarstedt tubes and frozen at -20 °C until metal addition. A solution of $CuCl_2$, $ZnCl_2$, Fe(citrate), $CaCl_2$, $MgCl_2$, and KCl (10,000 ppm each) was prepared in water. Dilutions of 5000, 1000, 500, 100, 50, and 10 ppm were made in water. Each dilution was mixed 1:10 with an aliquot of tissue (50 µL metal mixture per 500 µL tissue) and mixed with a hand-held mechanical homogenizer. To remove bubbles, the standards were centrifuged at 16,000 x g at room temperature for 2 hours. Any resulting supernatant was removed, and the vials were frozen in a dry ice/isopentane bath and stored at -80 °C until sectioning. Before sectioning, the standards were cut in half vertically. One half was sectioned into 20 µm slices using a Cryostat (Leica CM1950) and placed directly onto Superfrost PLUS slides (Thermo Fisher), air-dried, and stored at room temperature until analysis. The other half was divided into three parts for liquid ICP-MS analysis. The samples for liquid analysis were weighed in 1.5 mL tubes (Sarstedt) and combined 1:1 (w/v) with concentrated nitric acid (BDH Aristar Ultra). After overnight incubation at room temperature, samples were diluted into 2% HNO3 (prepared from concentrated acid in milliQ water) and doped with a gallium internal standard (Inorganic Ventures, 20 ppb final concentration). The metal content was determined by measuring ^{63}Cu and ^{66}Zn using a Thermo Fisher iCAP-Qc ICP-MS in Kinetic Energy Discrimination (KED) mode with the He flow set to 4.426 mL min^{-1}. Measurements were normalized to a standard curve of known metal concentrations doped with 20 ppb Ga. The standard curve was diluted from CMS-5 standard (Al, Cs, Co, Fe, Mg, Ni, Rb, Na, Zn, Ca, Cr, Cu, Li, Mn, K, Ag, and Sr in 2% nitric acid) with molybdenum, phosphorous and sulfur added (Inorganic Ventures). The calibration curves for LA-ICP-MS and nanoSIMS are shown in Figure 2.9.

Electron Microscopy

At 6 dpf, zebrafish embryos were euthanized in ice water and submerged in 0.1 M phosphate buffer containing 2% glutaraldehyde (Electron Microscopy Sciences, 16020). A fresh razor blade was used to remove the tail of each embryo in order to improve permeabilization with the fixative. Zebrafish were fixed for 1 hour at room temperature on a rotator and then left in fixative at 4 °C up to two weeks until embedding. To each tube containing zebrafish embryos in 1 mL of 2% glutaraldehyde in 0.1 M phosphate buffer was added 4 drops (~50 µL) of 4% OsO_4 (Electron Microscopy Sciences) in water. The tubes were placed on a rocker for 15 minutes at room temperature. Osmium-containing fixative was removed, and the samples were washed three times with 0.1 M sodium cacodylate buffer (pH 7.4) for 5 minutes per wash. Sodium cacodylate buffer was removed, and embryos were dehydrated through a series of acetone:water washes (30%,

50%, 70%, 90%, 95% and 3x 100% acetone), 10 minutes per wash, at room temperature with rotation. Fresh resin was prepared: for 50 mL of resin, 23.5 g Eponate 12™ Resin (Ted Pella), 12.5 g dodecenylsuccinic anhydride (Ted Pella), and 14 g methyl-5-norbornene-2,3-dicarboxylic anhydride (Ted Pella) were combined and stirred thoroughly. Dehydrated embryos were infused with resin through a series of acetone:resin washes (3:1 acetone:resin, 1:1 acetone:resin, 1:3 acetone:resin), 20 minutes per wash at room temperature with rotation. The embryos were then treated with resin 2x 30 minutes and left in a fresh resin wash overnight at room temperature with rotation. The next day, benzyldimethylamine (BDMA, Ted Pella) accelerant was added to extra pre-mixed resin solution (0.75 mL BDMA per 50 mL resin) and stirred thoroughly for at least ten minutes. Bubbles were removed under vacuum for 15 minutes. Embryos were removed from tubes containing resin and placed in fresh 1.5 mL tubes. Resin containing accelerate was added to each tube containing samples, and the samples were careful stirred into suspension using a wooden toothpick. Samples were infused with accelerant by three washes with resin containing accelerant, at least 2 hours per wash, up to 12 hours total. Samples were mounted in resin containing accelerant in flat rubber molds (Pelco 10535) and hardened in a 60 °C oven (Fisher Isotemp Oven 100 Series Model) for at least 48 hours.

Blocks containing samples were trimmed manually using a fresh razor blade rinsed with 95% ethanol. Trimmed blocks were faced using a glass knife (cut on a KnifeMaker II, LKB Bromma, 2178) and sectioned using a 3.0 ultra diamond knife (Diatome, MS 16745) on an UltraCut microtome (Reichert-Jung). Samples prepared for nanoSIMS were sliced to 200 nm, mounted on molybdenum grids coated with formvar (Ted Pella, 01808M) and used for nanoSIMS without staining. Samples prepared for electron microscopy were sliced to 70-100 nm and mounted on copper grids coated with formvar (Ted Pella, 01700-F). Grids were stained in a Pelco Grid Staining System with 2% aqueous uranyl acetate (Ted Pella) for 7 minutes, followed by six washes with distilled water. Grids were immediately stained for 5 minutes with Reynolds lead citrate composed of 1.76 g sodium citrate, dihydrate (Fisher Scientific), 1.33 g lead nitrate (Fisher Scientific), and 8 mL 1N NaOH in 30 mL distilled water. Stained grids were washed six times with distilled water. Grids were dried and stored at room temperature in the dark until imaging. Electron microscopy was performed on a Tecnai 120 KV (FEI by Thermo Scientific) in the UC Berkeley Electron Microscopy Facility.

Cloning

pSCAC-69-pActin:TOM20-mCherry was assembled by inserting the actin promoter and a gBlock coding for TOM20-iRFP into the pSCAC-69 backbone and subsequently replacing iRFP with mCherry due to a mismatch in laser lines on the stereoscope used for sorting zebrafish. pSCAC-69 was a gift from Seok-Yong Choi (Addgene plasmid # 31241)[69] and was amplified using the following primers: (FWD: cgttgagtataggtaatgactaggccGCCCCTTATTTGTGCTTGAT, REV: taggcctatttaggtgacactatagCCATGTCTGGACTTCTGAGG; T_m: 59 °C). The actin promoter was amplified from pMTB2-NLS-BirA-2A-mCherry_Ras, a gift from Tatjana Sauka-Spengler (Addgene plasmid # 80067)[70] using the following primers: (FWD: ATAAGGGGCggcctagtcattacctatactcaacg, REV: CATGGctatagtgtcacctaaataggccta; T_m:

56 °C). The resulting vector and promoter PCR products were assembled by Gibson Assembly (NEB) to create the pSCAC-69-pActin plasmid. TOM20-iRFP was inserted into pSCAC-69-pActin by amplification of the plasmid backbone using the following primers (FWD: AGCTCGAATTAATTCATCGA, REV: GGCTATAGTGTCACCTAAATAGG; T_m: 57 °C) and Gibson Assembly of the backbone and a gBlock coding for TOM20-iRFP. To exchange iRFP for mCherry, the pSCAC-69-pActin:TOM20 vector was amplified using the following primers (FWD: AGAACCGCTGTTAGGATCT, REV: TAAAGCTCGAATTAATTCATCGA, T_m: 58 °C) and mCherry was amplified from pcDNA3.1(+)-ePDZb-mCherry using the following primers (FWD: AAACGACGGTCAGATCCTAACAGCGGTTCTATGGTGAGCAAGGGC, REV: TGGATCATCATCGATGAATTAATTCGAGCTTTACTTGTACAGCTCGTCCAT, T_m: 58 °C). The resulting vector and insert PCR products were assembled by Gibson Assembly (NEB) to create the final pSCAC-69-pActin:TOM20-mCherry construct.

The TOM20-iRFP gBlock was ordered from Integrated DNA Technologies (IDT). Overlap regions for the Gibson Assembly are highlighted in gray.

TGGATCATCATCGATGAATTAATTCGAGCTTTAACTCTCCAACGCCGTGATGCGCGTGGCAATT
CTTTCTGCAAGCCGCTTACAGATGGCCCGGAGCTCAAAGCGGATAAATCGCGGCAAATAGTGAT
GGCAAACTACCAGTCCCCAGAGCTTGCCTCCGACGACCAATGAGACAGCCAAAGTCGCGCGGAC
ACCCATATCCTTCAAAAACTGGAGATGACAGGGGCTCATGCTCCGAAGAAAGCAGCCTGACATA
TCAAGGTCCCTGCCCGTCAACGGTGACAGACGTGGCTCCAGTGGAACCGGCTGGTATGTTACGT
CTACGAGAACTCTGACTCTCTGGCGAACGTACAATTGACGTGCCATCTGAGGTACAGTGCTACT
AGGGTATCGATTACCGAAATAGCTTTCAAGACCTGGCACGTGACACTCAGAAAAGACCAAACCG
TGCCCCTGCTCATCGAATCTATATACCATTACCCTGTCGTACCCCGTACACTGTTGGAACAACA
ACACTGTGTCGTCACAGAGCGCTCGCAAAGAGCCAGCAGTTCTAATGCGTTCAAGTGCAGGTGC
CAAAGTGCCGGAAAGATCGATAGAGGGACCGGCACGTTCCAATTCTATAATCAACCCCCCCTCG
GGTGGTCGATGCATCAATCCGCAATACTCGGTGGACGGGTTACCTATTCTACACCTTACGGCGA
CCGGCATCCCTTCAGCCGTAGGATCCAAATGGGGGAGTATCTTAATAAGAAGGTCTCCGTCTAT
TTCAGCGAGTGGTACGCCCAAGACTGAACCAAGATTGAGAAACTCGGCTGCGTTGGCGCTCGCT
TGAATTACTCTATGGTCATGCTCACTTACAACCAGCAATGCTCCGTGAGGCTGGATAGAACCTG
CGAGATGAATTTCTTCGTGCTCGCAGTTTGAATGACTAGCGGTCCCGAAAGCGGGGCTTCCAGA
AGCGTGGCCGGCGACAGAACCGCTGTTAGGATCTGACCGTCGTTTACGGTCAAAATATATACAG
TACCCTATGAACAGAGCCCCACAGACGCCAGCGGCAATAGCAGAGTTCCGGCCCACCATGGcta
tagtgtcacctaaataggcctagga

For a more thorough explanation of cloning protocols used in the laboratory, see Chapter 4. For DNA used for injections, DNA was purified using the Zyppy Miniprep Kit (Zymo) to remove endotoxin.

Generation of Tg(Actin:mito-mCherry) Zebrafish Embryos

Zebrafish embryos at the 1- or 2-cell stage were injected with 1 nL of injection solution containing 25 ng μL^{-1} TolII RNA and 25 ng μL^{-1} pSCAC-69-pActin:TOM20-mCherry in water containing phenol red. Embryos were raised in E3 media and monitored daily for

toxicity, but no toxicity was observed. At 6 dpf, embryos were prepared for nanoSIMS (see Sample Preparation, above).

Fluorescence Microscopy

Air-dried slices of zebrafish embryo retinas containing fluorescently labeled mitochondria were imaged using a Zeiss LSM 710 confocal microscope with a 20x air objective. The slides were placed up-side-down to decrease the distance between the objective and the sample, since the glass slide was too thick for focusing with a 20x objective. Samples were scanned with 543 nm excitation, and emitted light was collected between 578-696 nm. Transmitted light was collected to visualize slice morphology. ZEN 2010 software was used to calculate the optimal scan rate and pixel dimensions for each region.

Acknowledgements

We thank Peter Weber, Jennifer Pett-Ridge, and Christina Ramon for helping with sample preparation, analyzing samples by nanoSIMS, and discussing results. Your curiosity and enthusiasm made this project so much fun. Thank you for helping me frame and reframe this project as the data proved surprising again and again. This project would not have been possible without you. Thank you!

We thank Bao Thai for assistance with cloning and for sectioning So. Many. Zebrafish. Your frozen hands contributed to some truly beautiful data. Thank you!

We thank Tong Xiao for the TolII RNA and for many helpful discussions. We thank Emily Zhang and Tong Xiao for maintaining and genotyping the *Cal*^{gw71} zebrafish colony. We thank Prof. Jonathan Gitlin for the *Cal*^{gw71} zebrafish line. We thank Reena Zalpuri and the UC Berkeley Electron Microscope facility for instruction and assistance in preparing and imaging samples by electron microscopy. We thank Mel Boren, Kate Kliman and the staff at the UC Berkeley Zebrafish Facility for housing and feeding our zebrafish lines.

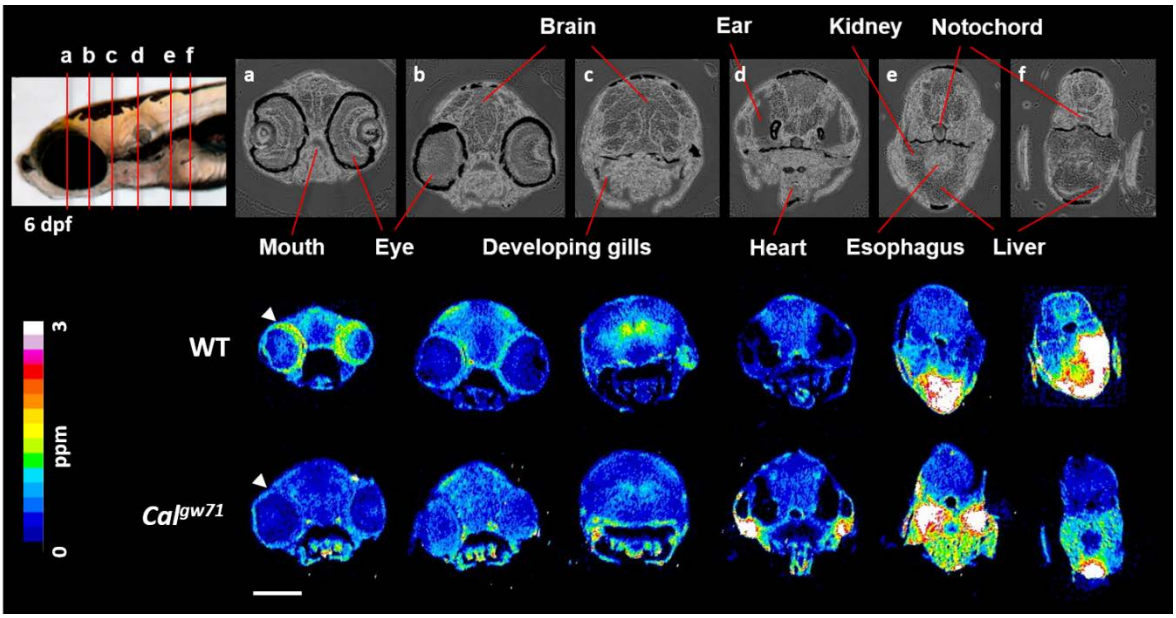

Figure 2.1 LA-ICP-MS images of wildtype and *Calamity*^{gw71} embryos (6 dpf) that were flash frozen, sliced to 20 µm and air dried. Transmitted light images (a-f) provide anatomical orientation. Arrowheads indicate the ring of copper observed around the outer edge of the retina of wildtype fish which is absent in *Cal*^{gw71} embryos. Scale bar: 200 µm.

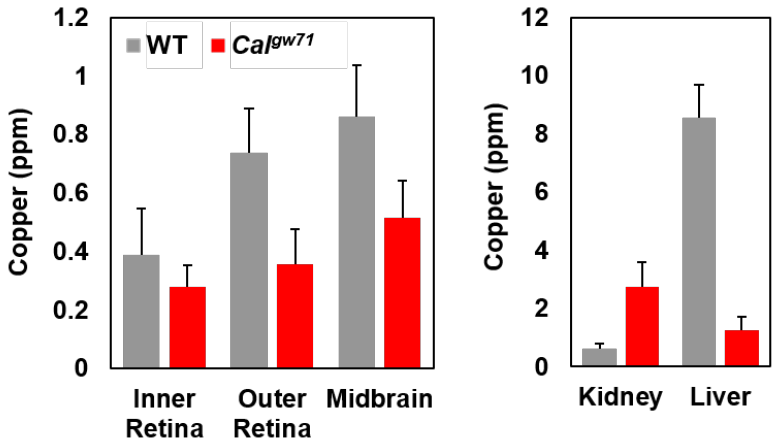

Figure 2.2 Quantification of LA-ICP-MS images of wildtype and *Cal*^{gw71} embryos; n = 3 for each genotype.

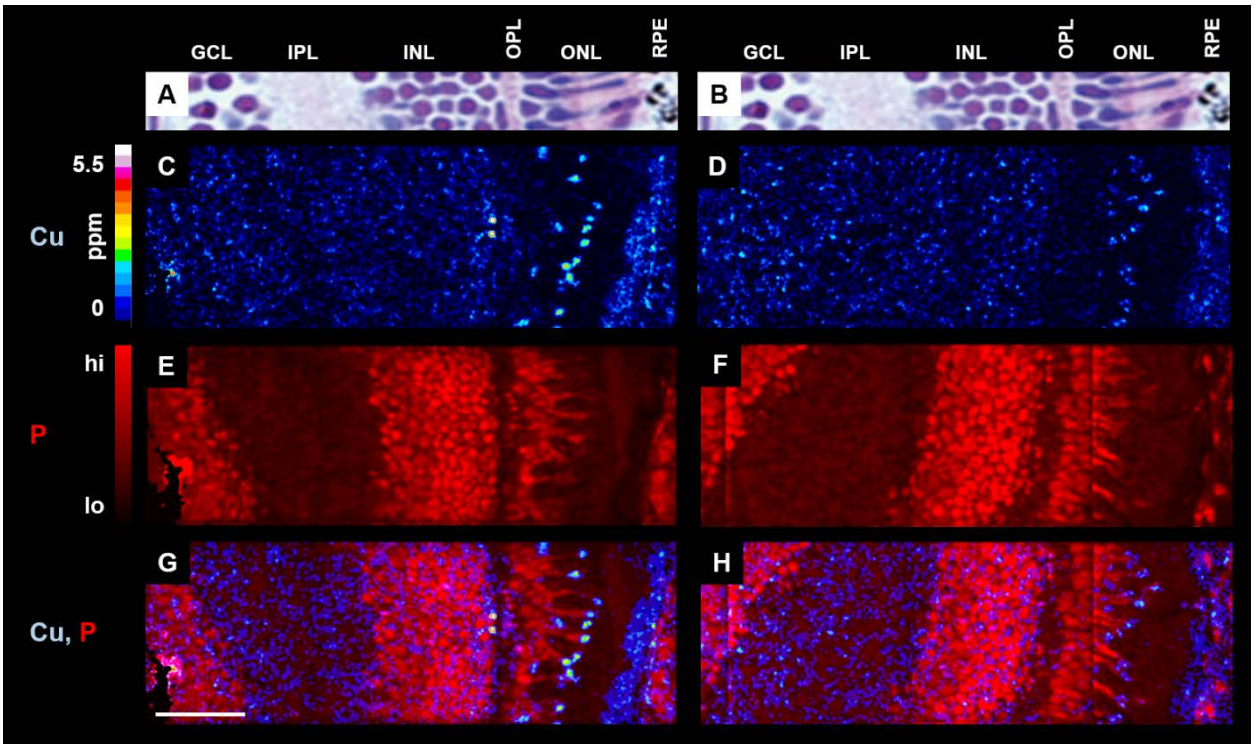

Figure 2.3 In the zebrafish embryo retina, copper is enriched in puncta in the outer nuclear layer (ONL); *Cal*^{gw71} embryos (D, F, and H) contain less copper in this region than WT embryos (C, E, and G). Representative nuclear staining provides anatomical orientation (A and B). NanoSIMS images include copper (C and D), phosphorous (E and F) and an overlay of copper and phosphorous signals (G and H). GCL = Ganglion cell layer; IPL = Inner plexiform layer; INL = Inner nuclear layer; OPL = Outer plexiform layer; ONL = Outer nuclear layer; RPE = Retinal pigmented epithelium. Scale bar 25 µm.

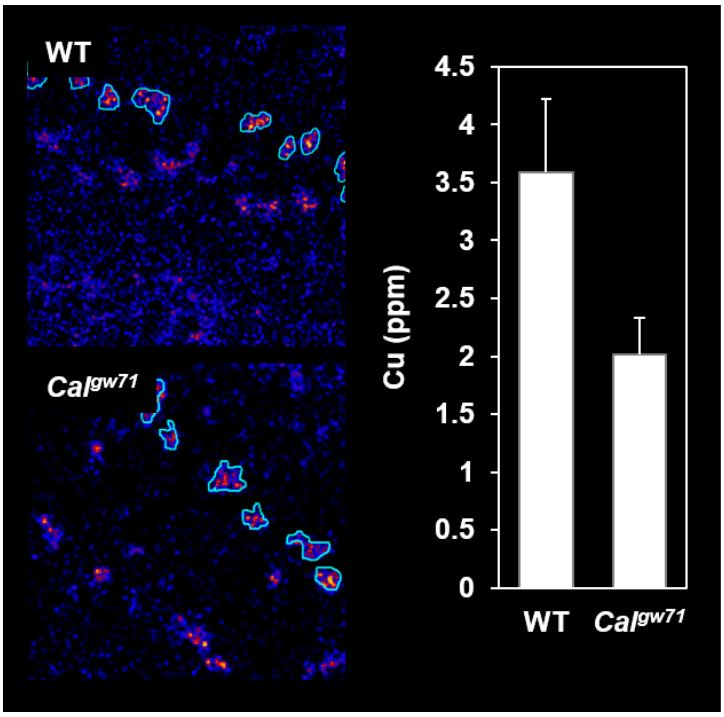

Figure 2.4 Quantification of nanoSIMS images of wildtype and *Cal*^{gw71} embryos; n = 15 puncta per genotype.

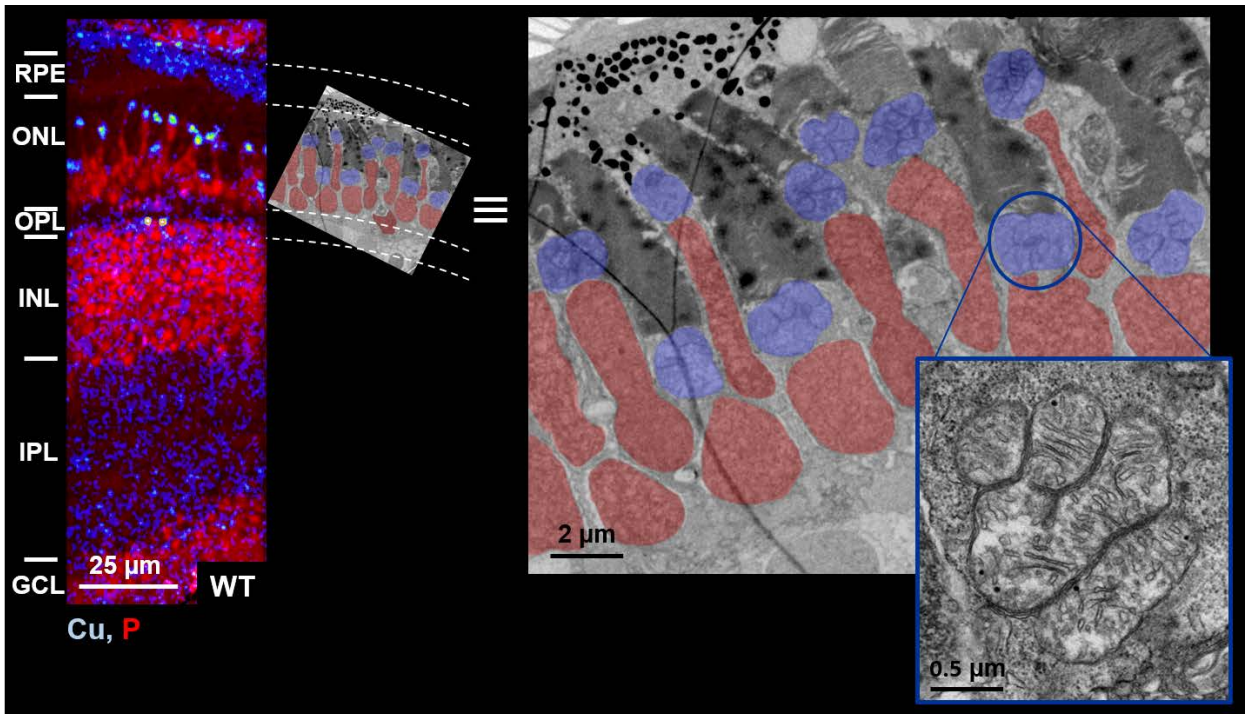

Figure 2.5 Megamitochondria are located between nuclei and receptors in the outer nuclear layer, matching the pattern of copper puncta observed in the nanoSIMS images. NanoSIMS copper and phosphorous overlay (left) and electron micrograph (right) with false color for nuclei (red) and megamitochondria (blue). A copy of the electron micrograph is scaled and rotated to align with the nanoSIMS image. Inset: zoomed image of one megamitochondrion in gray scale. Scale bars are labeled. GCL = Ganglion cell layer; IPL = Inner plexiform layer; INL = Inner nuclear layer; OPL = Outer plexiform layer; ONL = Outer nuclear layer; RPE = Retinal pigmented epithelium.

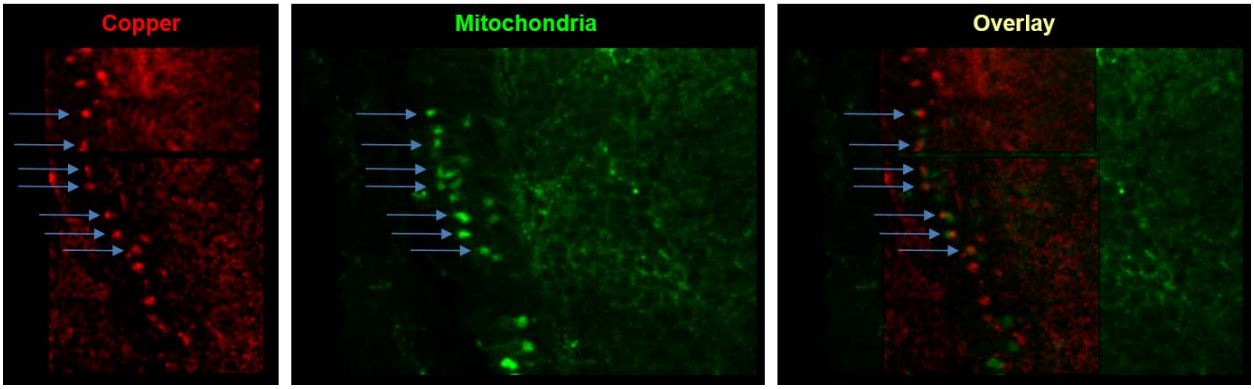

Figure 2.6 The copper puncta observed by nanoSIMS (left, red) and the fluorescent signal from megamitochondria labeled with TOM20-mCherry (center, green) overlap in some mitochondria (right, overlay). Arrows indicate puncta with colocalization in the final image.

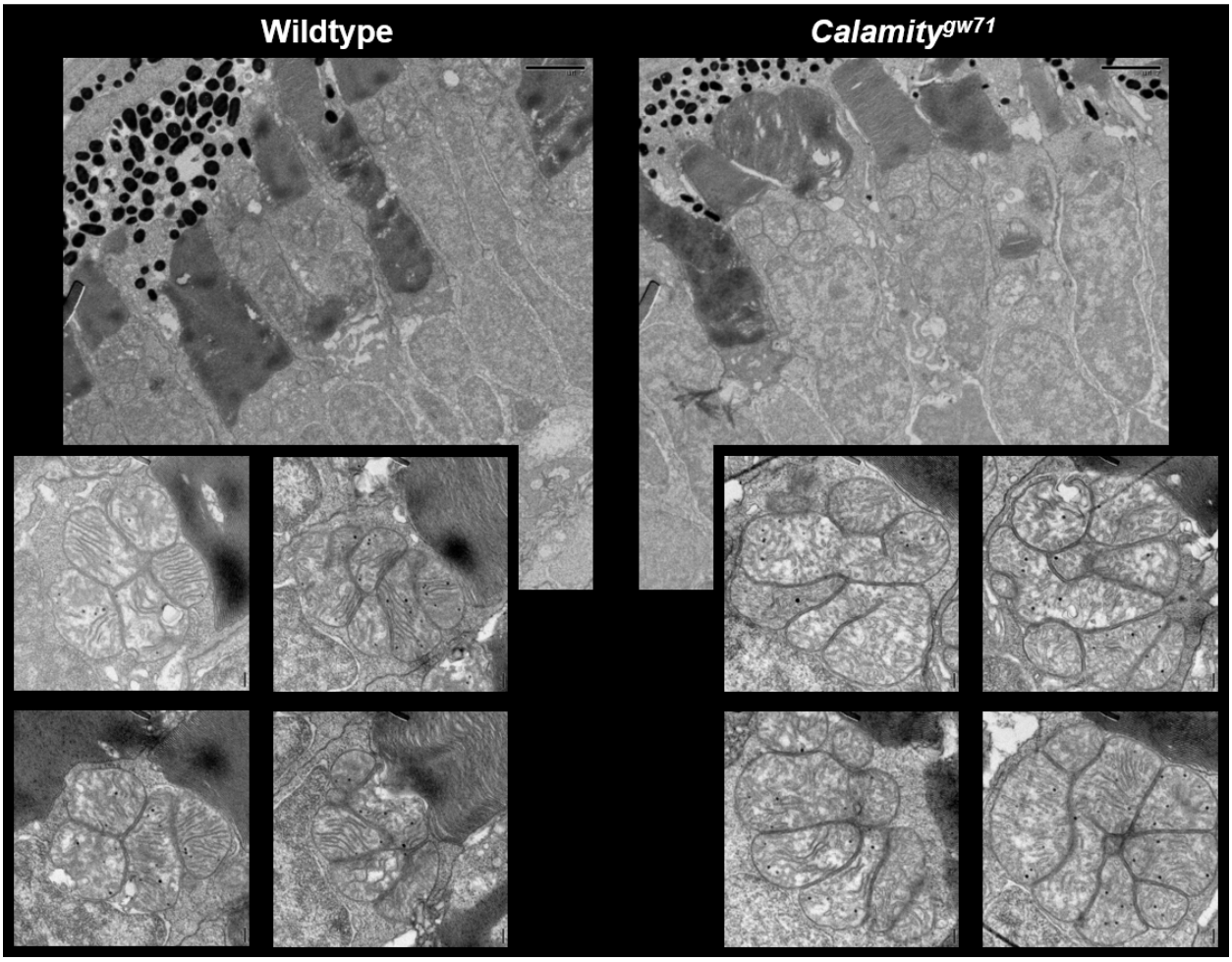

Figure 2.7 Electron micrographs of wildtype and *Cal*^{gw71} embryos reveal no significant morphological differences in receptor architecture (top) or megamitochondria (bottom, inset).

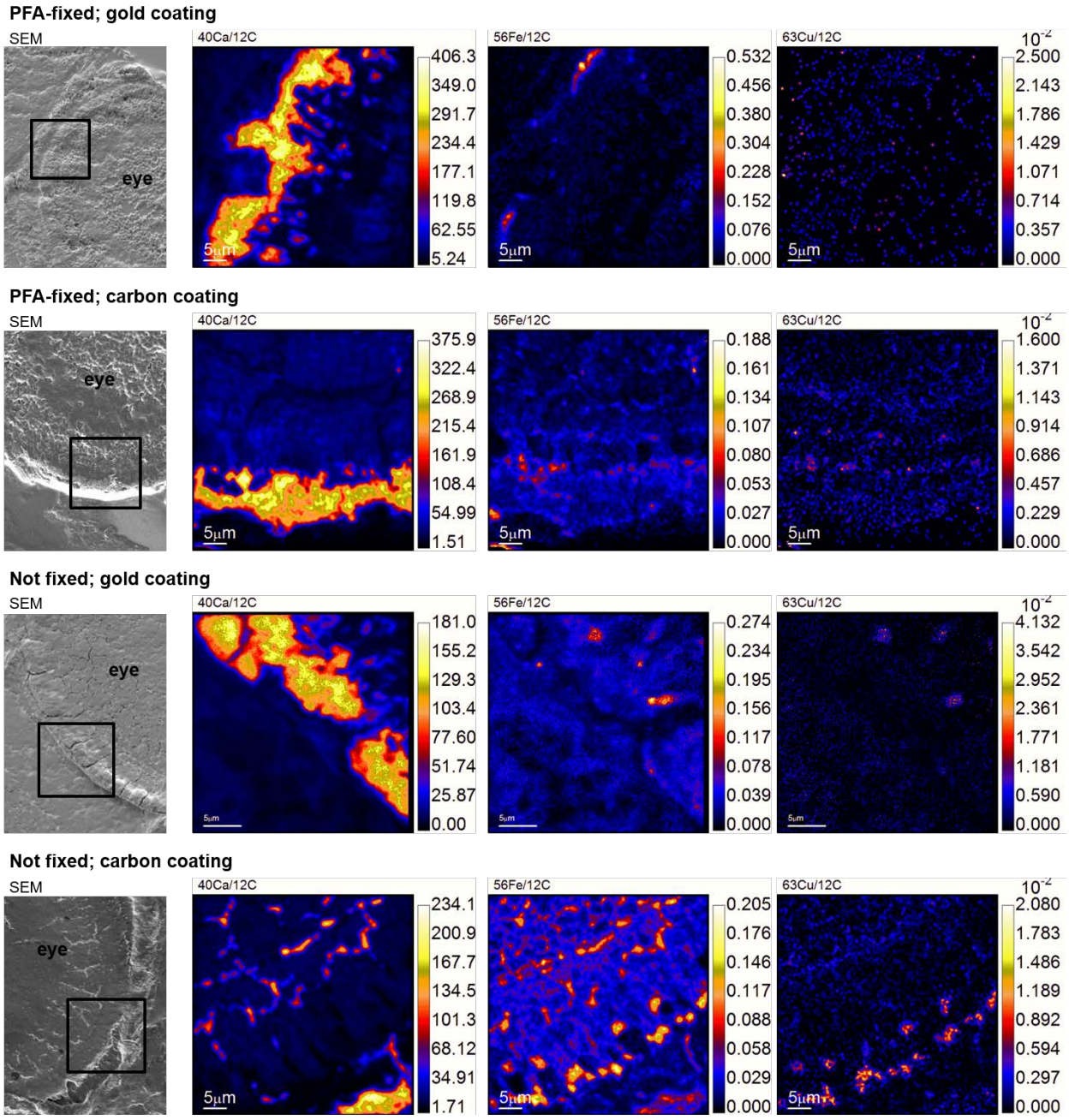

Figure 2.8 PFA fixation abolishes signal from copper puncta. Four zebrafish embryos were fixed or not fixed, as indicated, and coated with the indicated conductive substrate. SEM images (far left) confirmed retention of morphology through the coating process. Calcium signal (center left) may increase with fixation (top two rows vs bottom two rows). Both iron and copper signals (center right and far right, respectively) decrease with fixation. Copper puncta are not visible in fixed samples (far right, top two rows). Scale bars are element counts per carbon counts, scaled automatically by the LIMAGE software.

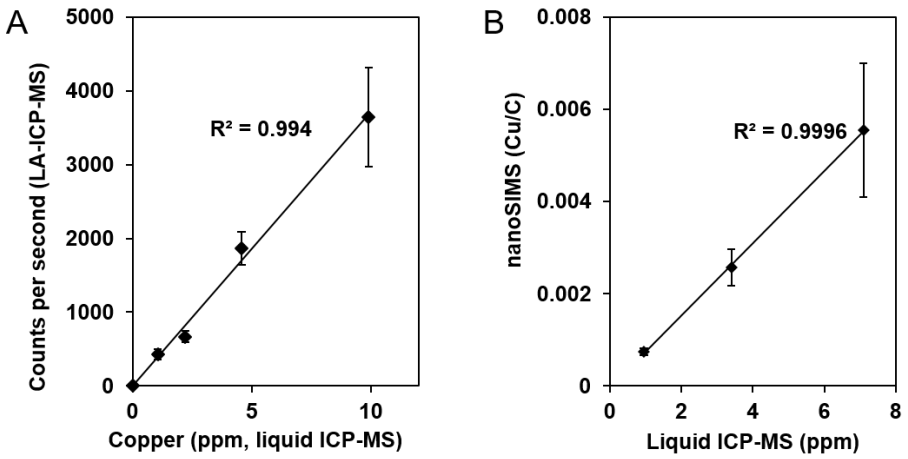

Figure 2.9 Standard curves for copper generated by A) LA-ICP-MS and B) nanoSIMS analysis of matrix-matched standards plotted against copper concentrations determined by liquid ICP-MS.

References

1 Lutsenko, S. Copper trafficking to the secretory pathway. *Metallomics* **8**, 840-852, doi:10.1039/c6mt00176a (2016).

2 Öhrvik, H. & Thiele, D. J. How copper traverses cellular membranes through the mammalian copper transporter 1, Ctr1. *Annals of the New York Academy of Sciences* **1314**, 32-41, doi:10.1111/nyas.12371 (2014).

3 Hamza, I. & Gitlin, J. D. Copper chaperones for cytochrome c oxidase and human disease. *Journal of bioenergetics and biomembranes* **34**, 381-388 (2002).

4 Prasad, A. N. & Ojha, R. Menkes disease: what a multidisciplinary approach can do. *Journal of Multidisciplinary Healthcare* **9**, 371-385, doi:10.2147/jmdh.s93454 (2016).

5 Lutsenko, S. Modifying factors and phenotypic diversity in Wilson's disease. *Annals of the New York Academy of Sciences* **1315**, 56-63, doi:10.1111/nyas.12420 (2014).

6 Lee, J., Prohaska, J. R. & Thiele, D. J. Essential role for mammalian copper transporter Ctr1 in copper homeostasis and embryonic development. *Proceedings of the National Academy of Sciences* **98**, 6842-6847, doi:10.1073/pnas.111058698 (2001).

7 Hedera, P. Update on the clinical management of Wilson's disease. *The Application of Clinical Genetics* **10**, 9-19, doi:10.2147/tacg.s79121 (2017).

8 Davies, K. M., Mercer, J. F. B., Chen, N. & Double, K. L. Copper dyshomoeostasis in Parkinson's disease: implications for pathogenesis and indications for novel therapeutics. *Clinical Science* **130**, 565-574, doi:10.1042/cs20150153 (2016).

9 Hordyjewska, A., Popiołek, Ł. & Kocot, J. The many “faces” of copper in medicine and treatment. *BioMetals* **27**, 611-621, doi:10.1007/s10534-014-9736-5 (2014).

10 Kaler, S. G. Translational research investigations on ATP7A: an important human copper ATPase. *Annals of the New York Academy of Sciences* **1314**, 64-68, doi:10.1111/nyas.12422 (2014).

11 Linz, R. & Lutsenko, S. Copper-transporting ATPases ATP7A and ATP7B: cousins, not twins. *Journal of bioenergetics and biomembranes* **39**, 403-407, doi:10.1007/s10863-007-9101-2 (2007).

12 Lutsenko, S., LeShane, E. S. & Shinde, U. Biochemical basis of regulation of human copper-transporting ATPases. *Archives of Biochemistry and Biophysics* **463**, 134-148, doi:10.1016/j.abb.2007.04.013 (2007).

13 Gupta, A. & Lutsenko, S. Human copper transporters: mechanism, role in human diseases and therapeutic potential. *Future Medicinal Chemistry* **1**, 1125-1142, doi:10.4155/fmc.09.84 (2009).

14 Yoshimura, N., Kida, K., Usutani, S. & Nishimura, M. Histochemical localization of copper in various organs of brindled mice after copper therapy. *Pathology International* **45**, 10-18, doi:10.1111/j.1440-1827.1995.tb03374.x (1995).

15 Kaler, S. G. ATP7A-related copper transport diseases—emerging concepts and future trends. *Nature Reviews Neurology* **7**, 15-29, doi:10.1038/nrneurol.2010.180 (2011).

16 Kaler, S. G. in *GeneReviews(R)* (eds R. A. Pagon *et al.*) (1993).

17 Tumer, Z. An overview and update of ATP7A mutations leading to Menkes disease and occipital horn syndrome. *Human mutation* **34**, 417-429, doi:10.1002/humu.22266 (2013).
18 Chang, C. J. Bioinorganic Life and Neural Activity: Toward a Chemistry of Consciousness? *Accounts of Chemical Research* **50**, 535-538, doi:10.1021/acs.accounts.6b00531 (2017).
19 Ahuja, A., Dev, K., Tanwar, R. S., Selwal, K. K. & Tyagi, P. K. Copper mediated neurological disorder: Visions into amyotrophic lateral sclerosis, Alzheimer and Menkes disease. *Journal of Trace Elements in Medicine and Biology* **29**, 11-23, doi:10.1016/j.jtemb.2014.05.003 (2015).
20 Madsen, E. C. & Gitlin, J. D. Zebrafish Mutants calamity and catastrophe Define Critical Pathways of Gene–Nutrient Interactions in Developmental Copper Metabolism. *PLoS Genetics* **4**, e1000261, doi:10.1371/journal.pgen.1000261 (2008).
21 Lenartowicz, M. *et al.* Mottled Mice and Non-Mammalian Models of Menkes Disease. *Frontiers in Molecular Neuroscience* **8**, doi:10.3389/fnmol.2015.00072 (2015).
22 Ackerman, C. M., Lee, S. & Chang, C. J. Analytical Methods for Imaging Metals in Biology: From Transition Metal Metabolism to Transition Metal Signaling. *Analytical Chemistry* **89**, 22-41, doi:10.1021/acs.analchem.6b04631 (2017).
23 Hackett, M. J. *et al.* Chemical alterations to murine brain tissue induced by formalin fixation: implications for biospectroscopic imaging and mapping studies of disease pathogenesis. *The Analyst* **136**, 2941, doi:10.1039/c0an00269k (2011).
24 Hare, D. J., Gerlach, M. & Riederer, P. Considerations for measuring iron in post-mortem tissue of Parkinson's disease patients. *Journal of Neural Transmission* **119**, 1515-1521, doi:10.1007/s00702-012-0898-4 (2012).
25 Hare, D. J., Lear, J., Bishop, D., Beavis, A. & Doble, P. A. Protocol for production of matrix-matched brain tissue standards for imaging by laser ablation-inductively coupled plasma-mass spectrometry. *Analytical Methods* **5**, 1915, doi:10.1039/c3ay26248k (2013).
26 Grossniklaus, H. E., Geisert, E. E. & Nickerson, J. M. Introduction to the Retina. **134**, 383-396, doi:10.1016/bs.pmbts.2015.06.001 (2015).
27 Stenkamp, D. L. Development of the Vertebrate Eye and Retina. **134**, 397-414, doi:10.1016/bs.pmbts.2015.06.006 (2015).
28 Herrmann, A. M. *et al.* Nano-scale secondary ion mass spectrometry — A new analytical tool in biogeochemistry and soil ecology: A review article. *Soil Biology and Biochemistry* **39**, 1835-1850, doi:10.1016/j.soilbio.2007.03.011 (2007).
29 Hong-Hermesdorf, A. *et al.* Subcellular metal imaging identifies dynamic sites of Cu accumulation in Chlamydomonas. *Nature Chemical Biology* **10**, 1034-1042, doi:10.1038/nchembio.1662 (2014).
30 Yu, D.-Y. & Cringle, S. J. Oxygen Distribution and Consumption within the Retina in Vascularised and Avascular Retinas and in Animal Models of Retinal Disease. *Progress in Retinal and Eye Research* **20**, 175-208, doi:10.1016/s1350-9462(00)00027-6 (2001).

31 Linton, J. D. *et al.* Flow of energy in the outer retina in darkness and in light. *Proceedings of the National Academy of Sciences* **107**, 8599-8604, doi:10.1073/pnas.1002471107 (2010).
32 Kooragayala, K. *et al.* Quantification of Oxygen Consumption in Retina Ex Vivo Demonstrates Limited Reserve Capacity of Photoreceptor Mitochondria. *Investigative Opthalmology & Visual Science* **56**, 8428, doi:10.1167/iovs.15-17901 (2015).
33 Stone, J., van Driel, D., Valter, K., Rees, S. & Provis, J. The locations of mitochondria in mammalian photoreceptors: Relation to retinal vasculature. *Brain Research* **1189**, 58-69, doi:10.1016/j.brainres.2007.10.083 (2008).
34 Hoang, Q. V., Linsenmeier, R. A., Chung, C. K. & Curcio, C. A. Photoreceptor inner segments in monkey and human retina: mitochondrial density, optics, and regional variation. *Vis Neurosci* **19**, 395-407 (2002).
35 Tarboush, R., Novales Flamarique, I., Chapman, G. B. & Connaughton, V. P. Variability in mitochondria of zebrafish photoreceptor ellipsoids. *Visual Neuroscience* **31**, 11-23, doi:10.1017/s095252381300059x (2014).
36 Kim, J. *et al.* The Presence of Megamitochondria in the Ellipsoid of Photoreceptor Inner Segment of the Zebrafish Retina. *Anatomia, Histologia, Embryologia: Journal of Veterinary Medicine Series C* **34**, 339-342, doi:10.1111/j.1439-0264.2005.00612.x (2005).
37 Masuda, T., Wada, Y. & Kawamura, S. ES1 is a mitochondrial enlarging factor contributing to form mega-mitochondria in zebrafish cones. *Scientific Reports* **6**, doi:10.1038/srep22360 (2016).
38 Tarboush, R., Chapman, G. B. & Connaughton, V. P. Ultrastructure of the distal retina of the adult zebrafish, Danio rerio. *Tissue and Cell* **44**, 264-279, doi:10.1016/j.tice.2012.04.004 (2012).
39 Knabe, W. & Kuhn, H. J. Morphogenesis of megamitochondria in the retinal cone inner segments of Tupaia belangeri (Scandentia). *Cell and tissue research* **285**, 1-9 (1996).
40 Lluch, S., López-Fuster, M. J. & Ventura, J. Cornea, retina, and lens morphology in five Soricidae species (Soricomorpha: Mammalia). *Anatomical Science International* **84**, 312-322, doi:10.1007/s12565-009-0042-1 (2009).
41 Wakabayashi, T. Megamitochondria formation - physiology and pathology. *Journal of cellular and molecular medicine* **6**, 497-538 (2002).
42 Hoppel, C. L., Tandler, B., Fujioka, H. & Riva, A. Dynamic organization of mitochondria in human heart and in myocardial disease. *The International Journal of Biochemistry & Cell Biology* **41**, 1949-1956, doi:10.1016/j.biocel.2009.05.004 (2009).
43 Caldwell, S. H. *et al.* NASH and cryptogenic cirrhosis: a histological analysis. *Annals of hepatology* **8**, 346-352 (2009).
44 Zsengellér, Z. K. *et al.* Methylmalonic acidemia: A megamitochondrial disorder affecting the kidney. *Pediatric Nephrology* **29**, 2139-2146, doi:10.1007/s00467-014-2847-y (2014).
45 Tandler, B., Nagato, T. & Phillips, C. J. Megamitochondria in the serous acinar cells of the submandibular gland of the neotropical fruit bat, Artibeus obscurus. *The Anatomical record* **248**, 13-17 (1997).

46 Spicer, S. S., Parmley, R. T., Boyd, L. & Schulte, B. A. Giant mitochondria distinct from enlarged mitochondria in secretory and ciliated cells of gerbil trachea and bronchioles. *American Journal of Anatomy* **188**, 269-281, doi:10.1002/aja.1001880306 (1990).
47 Knabe, W., Skatchkov, S. & Kuhn, H. J. "Lens mitochondria" in the retinal cones of the tree-shrew Tupaia belangeri. *Vision research* **37**, 267-271 (1997).
48 Lluch, S., López-Fuster, M. J. & Ventura, J. Giant mitochondria in the retina cone inner segments of shrews of genusSorex(Insectivora, Soricidae). *The Anatomical Record Part A: Discoveries in Molecular, Cellular, and Evolutionary Biology* **272A**, 484-490, doi:10.1002/ar.a.10066 (2003).
49 Kanaji, S., Iwahashi, J., Kida, Y., Sakaguchi, M. & Mihara, K. Characterization of the Signal That Directs Tom20 to the Mitochondrial Outer Membrane. *The Journal of Cell Biology* **151**, 277-288, doi:10.1083/jcb.151.2.277 (2000).
50 Noble, S., Godoy, R., Affaticati, P. & Ekker, M. Transgenic Zebrafish Expressing mCherry in the Mitochondria of Dopaminergic Neurons. *Zebrafish* **12**, 349-356, doi:10.1089/zeb.2015.1085 (2015).
51 Desplan, C. *et al.* Impaired Mitochondrial Energy Production Causes Light-Induced Photoreceptor Degeneration Independent of Oxidative Stress. *PLOS Biology* **13**, e1002197, doi:10.1371/journal.pbio.1002197 (2015).
52 Kawase, R. *et al.* EP300 Protects from Light-Induced Retinopathy in Zebrafish. *Frontiers in Pharmacology* **7**, doi:10.3389/fphar.2016.00126 (2016).
53 National Eye Institute. *Prevalence of Adult Vision Impairment and Age-Related Eye Diseases in America*, <https://nei.nih.gov/eyedata/adultvision_usa> (2017).
54 American Macular Degeneration Foundation. *What is Macular Degeneration?*, <https://www.macular.org/what-macular-degeneration> (2017).
55 Seelenfreund, M. H., Gartner, S. & Vinger, P. F. The ocular pathology of Menkes' disease. (Kinky hair disease). *Archives of ophthalmology* **80**, 718-720 (1968).
56 Ferreira, R. Menkes disease New ocular and electroretinographic findings. *Ophthalmology* **105**, 1076-1078, doi:10.1016/s0161-6420(98)96010-9 (1998).
57 Dingle, J. & Havener, W. H. Ophthalmoscopic changes in a patient with Wilson's disease during long-term penicillamine therapy. *Annals of ophthalmology* **10**, 1227-1230 (1978).
58 Satishchandra, P. & Ravishankar Naik, K. Visual pathway abnormalities Wilson's disease: an electrophysiological study using electroretinography and visual evoked potentials. *Journal of the neurological sciences* **176**, 13-20 (2000).
59 Waggoner, D. J., Bartnikas, T. B. & Gitlin, J. D. The Role of Copper in Neurodegenerative Disease. *Neurobiology of Disease* **6**, 221-230, doi:10.1006/nbdi.1999.0250 (1999).
60 Krajacic, P. *et al.* Retinal Localization and Copper-Dependent Relocalization of the Wilson and Menkes Disease Proteins. *Investigative Opthalmology & Visual Science* **47**, 3129, doi:10.1167/iovs.05-1601 (2006).
61 Erie, J. C., Good, J. A., Butz, J. A. & Pulido, J. S. Reduced Zinc and Copper in the Retinal Pigment Epithelium and Choroid in Age-related Macular Degeneration. *American Journal of Ophthalmology* **147**, 276-282.e271, doi:10.1016/j.ajo.2008.08.014 (2009).

62 Newsome, D. A. *et al.* Macular degeneration and elevated serum ceruloplasmin. *Investigative ophthalmology & visual science* **27**, 1675-1680 (1986).
63 Kumar, D. *et al.* Early eukaryotic origins for cilia-associated bioactive peptide-amidating activity. *Journal of Cell Science* **129**, 943-956, doi:10.1242/jcs.177410 (2016).
64 Bachmann-Gagescu, R. *et al.* The ciliopathy gene cc2d2a controls zebrafish photoreceptor outer segment development through a role in Rab8-dependent vesicle trafficking. *Human Molecular Genetics* **20**, 4041-4055, doi:10.1093/hmg/ddr332 (2011).
65 Dodani, S. C. *et al.* Copper is an endogenous modulator of neural circuit spontaneous activity. *Proceedings of the National Academy of Sciences* **111**, 16280-16285, doi:10.1073/pnas.1409796111 (2014).
66 James, C. J. & Hesse, C. W. Independent component analysis for biomedical signals. *Physiological measurement* **26**, R15-39 (2005).
67 James, S. A. *et al.* φXANES: In vivo imaging of metal-protein coordination environments. *Scientific Reports* **6**, doi:10.1038/srep20350 (2016).
68 Becker, J. S., Zoriy, M. V., Pickhardt, C., Palomero-Gallagher, N. & Zilles, K. Imaging of Copper, Zinc, and Other Elements in Thin Section of Human Brain Samples (Hippocampus) by Laser Ablation Inductively Coupled Plasma Mass Spectrometry. *Analytical Chemistry* **77**, 3208-3216, doi:10.1021/ac040184q (2005).
69 Jung Kim, M., Ho Kang, K., Kim, C.-H. & Choi, S.-Y. Real-time imaging of mitochondria in transgenic zebrafish expressing mitochondrially targeted GFP. *BioTechniques* **45**, 331-334, doi:10.2144/000112909 (2008).
70 Trinh, L. A. *et al.* Biotagging of Specific Cell Populations in Zebrafish Reveals Gene Regulatory Logic Encoded in the Nuclear Transcriptome. *Cell Reports* **19**, 425-440, doi:10.1016/j.celrep.2017.03.045 (2017).

Chapter 3

In Search of Copper Proteins: Proteomics Methods for Discovering Proteins that Bind and Respond to Copper

Introduction

Copper is an essential cofactor for many enzymes in biological systems, including those responsible for respiration, neurotransmitter synthesis, detoxification of reactive oxygen species, extracellular matrix crosslinking, and pigment synthesis.[1-3] The coordination environments and mechanisms of copper-binding enzymes have been well-studied and yield many insights into how nature harnesses this redox-active metal to accomplish one-electron chemistry under biological conditions.[4] Recently, a new role for copper in biology has emerged. Not only can copper serve as an active-site cofactor in enzymes, but copper can also interact with enzymes outside of active sites as an allosteric regulator of enzyme function. Chang *et al*. demonstrated that copper regulates the function of PDE3B, a phosphodiesterase critical for lipid metabolism,[5] and Thiele and Counter *et al*. discovered a role for copper in the regulation of MAPK signaling, a kinase pathway implicated in cancer proliferation.[6,7] The effect of copper on PDE3B and MAPK is due to a direct binding interaction between copper and the protein, which occurs outside the protein active sites, establishing a role for copper in allosteric regulation.[8] These examples suggest that copper may play additional, undiscovered roles in regulating cellular proteins and led us to look for new copper-binding proteins in biological systems.

Activity-Based Profiling to Discover Copper-Responsive Kinases

In order to narrow our search for proteins regulated by copper, we focused on kinases. Cellular kinases play a key role in transmitting cellular signals by transferring phosphoryl groups from adenosine triphosphate (ATP) to target proteins, lipids, and small molecules.[9] One active kinase may phosphorylate a large number of targets; thus, kinase pathways can amplify signals hundreds of fold as each kinase activates many downstream target kinases. Small molecules that interact with kinases in signaling pathways can have a large impact on cellular function and fate, and many such small molecules have been approved for pharmaceutical use.[10,11] Understanding the molecules and ions that interact with kinases to regulate their function can lead to a better understanding of cellular signaling as well as new therapeutics.

In search of kinases regulated by copper binding, we profiled kinase activity in mouse embryonic fibroblast (MEF) cells derived from mice lacking the copper import protein CTR1 compared to MEFs from their wildtype siblings.[12,13] $CTR1^{-/-}$ MEFs contain 60% less copper than wildtype MEFs (Figure 3.1A) and represent an established cellular model of impaired copper import and copper deprivation.[7,14-17] In order to activate cellular kinase cascades, I stimulated serum-starved cells with epidermal growth factor (EGF) before kinase activity profiling. Epidermal growth factor receptor (EGFR) is upstream of multiple kinase cascades, including PI3K/AKT and MEK/ERK.[18,19] I used ERK phosphorylation to confirm functional EGF stimulation in these cell lines. In agreement with literature precedent, ERK phosphorylation was higher in wildtype cells than in knockout cells because its kinase (MEK1/2) is more active in the presence of copper (Figure 3.1B).[7] Higher pERK levels were observed in wildtype cells than knockout cells under basal conditions and in response to multiple stimuli (Figure 3.2), indicating that copper's effect on ERK phosphorylation does not depend on EGF stimulation. Additionally, this effect is

MEK1/2 specific, as pAKT, another downstream target of EGF signaling, is not altered in CTR1$^{-/-}$ MEFs compared to wildtype cells (Figure 3.3).

Next, I harvested EGF-stimulated CTR1$^{-/-}$ or wildtype MEFs for multiplexed inhibitor bead (MIB) kinase activity profiling.[20,21] In the MIB strategy, kinases are pulled out of a cellular lysate based on their ability to bind kinase inhibitors (Scheme 3.1 and Table 3.1). Only active kinases are able to bind to the beads, while inactive kinases and other cellular components are washed away. Bound kinases are eluted from the beads by boiling and analyzed by mass spectrometry. A comparison of ion counts from wildtype and knockout cells yields a semi-quantitative readout of the abundance of each kinase pulled down from a sample. In collaboration with the Shokat Lab at UCSF, we identified 18 kinases that were enriched in an activity-dependent MIB pulldown from CTR1$^{-/-}$ MEFs compared to wildtype MEFs and 19 kinases that were depleted (Tables 3.2 and 3.3). Gratifyingly, casein kinase 1 isoform gamma 3 (CK1γ3) showed a decrease in activity in CTR1$^{-/-}$ MEFs relative to matched controls. CK1γ3 protein levels are dependent on the presence of active Cu/Zn SOD (SOD1),[22] and SOD1 activity is diminished in CTR1$^{-/-}$ MEFs compared to wildtype controls.[13] Thus, literature precedent suggests that CK1γ3 levels would be lower in CTR1$^{-/-}$ MEFs, and this prediction was confirmed in our kinase profiling experiments. Encouraged by these results, we pursued the study of other kinases identified in our screen.

To identify which kinases could be good candidates for further follow-up, I sought to control for protein expression differences between the two cell lines. The abundance of a kinase on the MIB profiling beads is an integrated readout of the kinase's cellular abundance and enzyme activity. I hypothesized that CTR1$^{-/-}$ MEFs may compensate for lower copper by altering the expression of some proteins, and these proteins may represent false positives in our screen, since their abundance in the pulldown would have changed based on protein expression rather than activity. To control for this, I performed quantitative RT-PCR (qPCR) and RNA sequencing (RNA-seq) on mRNA from CTR1$^{-/-}$ and wildtype MEFs (Tables 3.2 and 3.3). By plotting the relative expression of each gene measured against the change in its kinase activity, I identified kinases whose altered activity could not be explained by a change in expression alone (Figure 3.4). I identified two kinases whose activity had increased without an increase in expression (Rps6ka4/MSK2 and Fer), three kinases with a small increase in expression relative to the increase in their activity (CDK18, TAOK3, and MAP4K2), two kinases whose activity decreased despite overexpression (EGFR and EphB3), and seven kinases whose activity decreased without any change in expression (CDK4, CDKL5, CK1γ3, BMPR2, TAOK1, TAOK2, and AURKB) (Figure 3.4). I decided to focus on kinases with increased activity in the knockout cells because I reasoned that an increase in activity would provide higher signal-to-noise for enzyme assays, perhaps making these hits easier to study. Although MSK2 displayed the highest increase in kinase activity without any change in protein expression, I chose not to pursue this kinase because it is directly downstream of MEK1/2, a kinase whose copper-dependent activity is well known.[7,23] Instead, I focused my efforts on Fer kinase because its activity in CTR1$^{-/-}$ MEFs was double its activity in wildtype MEFs, without any change in expression.

Feline sarcoma related (Fer) kinase is a non-receptor protein tyrosine kinase that plays roles in fibroblast migration, cell cycle progression, and cancer metastasis.[24] Upon activation by growth factors or oxidative stress, Fer is phosphorylated, and cytosolic Fer associates with cadherins[25,26] and integrins[27] at the cell membrane, regulating focal adhesions and adherens junctions. Activated Fer phosphorylates cortactin,[28] a protein involved in stabilizing actin filaments, and phospho-cortactin may be used as a readout of Fer activity in cells. Indeed, phosphorylation of cortactin was higher in $CTR1^{-/-}$ MEFs relative to control MEFs (Figure 3.5A). This difference depended on serum starvation, as cells that had not been serum starved before stimulation did not show this difference (Figure 3.5B). If Fer activity is indeed modulated by copper levels, I reasoned that raising copper levels in $CTR1^{-/-}$ MEFs should rescue cortactin phosphorylation. However, the addition of copper did not modulate the phosphorylation of cortactin in MEFs (Figure 3.6), and the transient overexpression of human CTR1 yielded inconsistent results, perhaps due to the difficulty of transfecting MEFs (data not shown). Additionally, phosphotyrosine blots of immunoprecipitated Fer showed that Fer phosphorylation is higher in $CTR1^{-/-}$ MEFs than in $CTR1^{+/+}$ MEFs (Figure 3.7A) but is not significantly modulated by changes in copper levels (Figure 3.7B). Because Fer is both phosphorylated by other kinases, such as Src,[29] and autophosphorylated, it is difficult to determine whether a change in Fer phosphorylation should be attributed to a difference in Fer activity or a difference in some other upstream kinase.

Curious to know whether some other component of Fer signaling was significantly altered between these two cell types, I assessed the levels of E-cadherin and β-catenin, two proteins involved in adherens junctions,[25] in $CTR1^{-/-}$ and wildtype MEFs. E-cadherin is nearly undetectable in wildtype cells but is robustly expressed in knockout cells, while β-catenin shows more similar expression between the two cell lines but is still more highly expressed in knockout cells (Figure 3.8A). Indeed, E-cadherin showed 50-fold higher expression in $CTR1^{-/-}$ MEFs by RNA-seq; however, β-catenin was downregulated 2-fold. The expression of these proteins was unaltered by changes in copper levels (Figure 3.8A). Additionally, I found that signaling induced by oxidative stress was more robust in $CTR1^{-/-}$ MEFs than wildtype MEFs based on phosphotyrosine levels in total lysates from these cell lines. However, phosphotyrosine levels were not responsive to copper chelation or copper addition (Figure 3.8B). Taken together, these data suggest that Fer activity is higher in knockout cells compared to wildtype controls but that this difference is likely due to an effect upstream of Fer, perhaps impacting membrane composition and overall signaling in $CTR1^{-/-}$ MEFs.

Upon finding that $CTR1^{-/-}$ and wildtype MEFs responded significantly differently to oxidative stress, I became concerned about the role of EGF/EGFR in these experiments. EGFR is known to be redox-sensitive,[30,31] and I considered the possibility that the differences I had seen in H_2O_2-induced phosphotyrosine levels between these two cell lines could be due to differences in EGFR activity. I had originally used EGF/EGFR to activate downstream kinases for MIB profiling. Subsequently, kinase activity profiling showed that EGFR activity was significantly lower in $CTR1^{-/-}$ MEFs than wildtype MEFs despite overexpression of EGFR transcripts, as measured by qPCR. Indeed, preliminary experiments showed that EGFR levels were higher in $CTR1^{-/-}$ MEFs compared to

wildtype, but EGFR phosphorylation at Tyr1068 was lower in CTR1$^{-/-}$ MEFs when normalized to total EGFR levels (Figure 3.9). These results suggested that differences in EGFR signaling may have confounded downstream signaling, and led me to reevaluate our profiling results.

Examining Expression Changes in Cells Lacking CTR1

Given the global differences we observed in EGFR activation, phosphotyrosine levels, and membrane protein expression between CTR1$^{-/-}$ and wildtype MEFs, I reasoned that I would not be able to deconvolute the effects of copper on kinase activity from genetic compensation, altered redox-sensitivity, or altered EGFR activity in the knockout cells. Instead, I refocused my work on the expression changes I had observed between these two cell lines. I wondered if these expression changes were directly dependent on differences in copper levels. To test this, I supplemented CTR1$^{-/-}$ MEFs with 5 μM copper for 16 hours to rescue copper levels. I also depleted wildtype MEFs of copper for 24-48 hours using two copper chelators. Bathocuproine disulfonate (BCS) is a cell-impermeable chelator that sequesters Cu(I) outside of cells, gradually depleting the cell of copper over time. Most cell types are very tolerant of high BCS concentrations (up to 500 μM). ATN-224 (bis-choline tetrathiomolybdate) is a cell-permeable copper chelator that is used at much lower doses (100 nM - 10 μM) due to its high potency. Copper depletion with BCS decreased copper levels to 30% of wildtype, while ATN-224 decreased copper to 10% of wildtype levels over 48 hours (Figure 3.10). Copper supplemented or depleted cells were harvested, along with their untreated controls, and qPCR was used to determine changes in expression. I focused on genes with the largest changes observed between CTR1$^{-/-}$ and wildtype MEFs. However, copper supplementation could not rescue and copper depletion could not reproduce the expression changes observed between CTR1$^{-/-}$ and wildtype MEFs (Figure 3.11).

Having found that the changes in kinase activity and gene expression we had observed between CTR1$^{-/-}$ and wildtype MEFs were not due to changes in copper levels, I next asked whether these changes were CTR1-dependent. CTR1$^{-/-}$ MEFs and wildtype MEFs were transiently transfected with a plasmid encoding human CTR1 with an N-terminal Myc tag (Myc-hCTR1),[32] but overexpression of Myc-hCTR1 did not alter the expression of the genes of interest, even though copper levels in cells expressing Myc-CTR1 were double those of cells transfected with vector control (Figure 3.12). I wondered if these rescue experiments might have been impeded by poor transfection efficiency and sought to perform these experiments in a cell line more amenable to transient transfection. I turned to HEK293T cells that had been genetically modified using CRISPR/Cas9 to eliminate CTR1 expression.[33] Like CTR1$^{-/-}$ MEFs, CTR1$^{-/-}$ HEK293T cells contain 60-70% less copper than wildtype cells (Figure 3.13A). Additionally, both wildtype and CTR1$^{-/-}$ HEK293T cells could be transiently transfected with a plasmid encoding Myc-hCTR1, and this transfection increased steady-state copper levels significantly (Figure 3.13B). However, CTR1$^{-/-}$ HEK293T cells did not have the same changes in expression observed in the CTR1$^{-/-}$ MEFs (Figure 3.13C). Additionally, E-cadherin protein levels did not differ between wildtype and knockout HEK293T cells and were not altered by Myc-hCTR1 overexpression (Figure 3.13D).

Since the differences between CTR1$^{-/-}$ and wildtype MEFs could not be rescued or reproduced by changes in copper or transient changes in CTR1 expression, I hypothesized that CTR1$^{-/-}$ and wildtype MEFs had followed different, irreversible developmental trajectories. Mouse embryonic fibroblasts are immortalized from primary mouse cells; CTR1$^{-/-}$ MEFs and wildtype MEFs were immortalized from mouse embryos lacking or containing a functional CTR1 gene, respectively. If copper levels or CTR1 expression influences development, differentiation, or immortalization, this could alter gene expression in these cells in a way that could not be rescued simply by adding copper or CTR1 to the knockout cells at a later time. Indeed, RNA sequencing of CTR1$^{-/-}$ and wildtype MEFs showed that genes involved in developmental processes were overrepresented (2.4- to 4.1-fold enrichment) in the collection of genes that were differentially expressed between the two cell lines (Figure 3.14).

Interestingly, one of the kinases identified in our screen, bone morphogenetic protein receptor 2 (BMPR2), is a receptor implicated in the differentiation of adipose tissue[34,35] and pulmonary hypertension,[36] two areas of physiology connected to copper homeostasis.[37-39] BMPR2 is not known to be involved in EGFR signaling, so we wondered how this kinase came to be activated in these cells. I found that both BMPR2 ligands (BMP2 and BMP7)[40,41] are upregulated over 100-fold in CTR1$^{-/-}$ MEFs relative to controls, as measured by RNA sequencing. Additionally, genes downstream of BMPR2 (ID1, ID2, and ID3)[42] are upregulated 5-8x in CTR1$^{-/-}$ MEFs relative to controls, as measured by qPCR. ID1, ID2, and ID3 negatively regulate basic helix-loop-helix transcription factors and influence differentiation pathways, among other functions.[43] These data suggest that CTR1$^{-/-}$ MEFs may have followed a significantly different differentiation trajectory from CTR1$^{+/+}$ MEFs before immortalization, and could explain why the differences between these cell lines cannot be readily reversed. Indeed, in our hands, even MEK1/2 activity could not be rescued by copper supplementation in CTR1-/- MEFs (Figure 3.15), and copper levels did not modulate MEK1/2 activity in a variety of other cell lines, including DM440, DM738 and A375 melanoma cells, HeLa cervical cancer cells, and differentiated 3T3L1 adipocytes (data not shown). Together, these results indicate a likely role for copper in embryonic development, beyond the necessity of copper for mitochondrial function, and suggest that the role of copper in differentiation may be an area of fruitful research.[44]

Reactive Cysteine Profiling of Copper-Binding Proteins

Motivated to discover proteins whose activity is directly responsive to copper binding, we refocused our efforts on a new screen that could more directly assess the interaction of copper with proteins. To accomplish this, we turned to reactivity-based protein profiling. Recently, the Weerapana group used cysteine reactivity profiling to discover new zinc-binding proteins.[45] Both zinc and copper commonly bind to cysteine residues in cells,[46] and we sought to adapt cysteine profiling technology to the discovery of copper-binding proteins. In this experiment, outlined in Scheme 3.2, the copper content of a complex cellular proteome is modulated by the addition of copper or a copper chelator. Lysates are then labeled with the cysteine-reactive small molecule iodoacetamide-alkyne (IA-

alkyne). Relative to control lysates, copper-treated lysates should have fewer reactive cysteines because some cysteine reactivity will be blocked by copper binding; however, we expect that chelator-treated lysates will have more reactive cysteines because copper has been removed from some cysteines. After labeling, click chemistry is used to append a fluorophore or biotin tag to the label for subsequent visualization by gel electrophoresis or quantitation by mass spectrometry.[47]

Proof-of-concept experiments performed in collaboration with other members of the laboratory demonstrated that the cysteine reactivity of Atox1, a copper chaperone protein known to bind copper through a CXXC motif,[48,49] could be modulated *in vitro* and *in vivo* by copper addition and chelation (data not shown). Encouraged by these results, we pursued copper-dependent cysteine reactivity profiling of HEK293T cells treated with 200 μM $CuCl_2$ for 1 hour, in collaboration with the Cravatt lab at the Scripps Research Institute. Following copper supplementation, cells were lysed and labeled with IA-alkyne. The control and copper-treated lysates were clicked to isobarically labeled TEV-biotin tags, combined and subjected to on-bead trypsinization. Captured peptides were released from the beads by TEV protease cleavage and analyzed by mass spectrometry.[50] The ratio of light- to heavy-labeled peptides was used as a readout of labeling in the control sample relative to the copper-treated sample. Proteins with ratios greater than 3 were designated as significant hits and considered for further study (Table 3.4; see Appendix 2 for the full list of results).

Reassuringly, among the significant hits was the known copper chaperone, Atox1, with a ratio of 12.4 for its CXXC motif cysteines (Cys12 and Cys15), indicating that Cys12/Cys15 labeling was 12 times higher in the control sample than in the sample that had been treated with copper. Atox1 also contains a third cysteine, Cys41, that does not bind copper. Cys41 was labeled with a ratio of 0.93, suggesting that the change in reactivity of Cys12 and Cys15 upon copper addition was specific to these copper-binding cysteines and did not involve a change in Atox1 protein levels. With this positive control high on our list of significant hits, we proceeded to examine other significant hits, in search of novel copper-binding proteins.

When selecting protein hits for further study, we focused on proteins with well-established function and activity assays that would allow us to readily assess the effect of copper on the protein. Among those proteins with ratios greater than 3 was a transcription factor known for its role in cellular proliferation, immune function, and oncogenesis: STAT3.[51] Upon activation through interleukin-6 (IL-6) signaling, STAT3 is phosphorylated at Tyr705 and translocates to the nucleus where it induces the expression of a variety of genes, including Cyclin D1.[52] Cysteine profiling identified Cys712 and Cys718 as potential copper-binding cysteines on STAT3, with a ratio of 3.85. Interestingly, alkylation of these cysteines prevents phosphorylation of STAT3 at Tyr705 and downstream gene activation.[53] I hypothesized that copper binding at these cysteines may have a similar effect. To test this, I pre-treated HEK293T cells with copper for an hour, stimulated them with IL-6, and probed for STAT3 phosphorylation by Western blot. Indeed, treatment of cells with copper prevented phosphorylation of Tyr705 as effectively as the STAT3 small-molecule inhibitor Stattic[54] (Figure 3.16A). The effect was dose-dependent (Figure 3.16B)

and could also be observed by monitoring STAT3 translocation to the nucleus (Figure 3.16C).

Because of STAT3's importance in oncogenesis and cancer proliferation, I tested a variety of cancer cell lines to see if copper's effect on STAT3 activation is consistent across many types of cancer. Interestingly, colon, bone, and breast cancers show copper-mediated STAT3 inhibition, while lung and cervical cancer do not (Figure 3.17). This was not due to changes in total STAT3 levels.

To determine the molecular interaction between copper and STAT3 responsible for the copper dependence of STAT3 activation, I overexpressed wildtype STAT3 and various cysteine-to-serine mutants of STAT3 in HEK293T cells. Following overexpression, the cells were incubated with copper for an hour and then stimulated with IL-6 in the presence of copper. Like endogenous STAT3, overexpressed STAT3 could be activated with IL-6 treatment, and copper blocked STAT3 activation (Figure 3.18A). Mutants of cysteines that had not been labeled or had an insignificant ratio change in the cysteine profiling experiment showed the same copper-dependence as wildtype STAT3 (Figure 3.18B and C). Unexpectedly, mutations of cysteine 712 and 718, as well as the double C712/718S mutant, also retained copper-dependent STAT3 inhibition (Figure 3.18C). From these results, I concluded that the inhibition of STAT3 activation by copper occurs upstream of STAT3 and likely does not involve a direct molecular interaction between copper and the STAT3 cysteines labeled in our cysteine profiling experiments. In light of these data, I chose to investigate a different hit from our copper-dependent reactive cysteine profiling results.

Another well-known protein among the significant hits found by copper-dependent reactive cysteine profiling was Keap1. Keap1 is an adapter protein that binds to Nrf2 and targets Nrf2 to the E3 ubiquitin ligase Cul3 for ubiquitination and degradation under normal conditions.[55] However, in response to oxidative stress, Keap1 dissociates from Cul3, allowing Nrf2 protein to accumulate, translocate to the nucleus, and act as a transcription factor for a variety of stress-response genes, including heme oxygenase 1 (HO1). Interestingly, a number of cysteines on Keap1 have been found to be required for these processes.[56] Cys273 and Cys288 are required for Nrf2 degradation, and neither C273S nor C288S Keap1 can cause Nrf2 degradation under basal conditions. Cys151 is required for Nrf2 stabilization, and C151S mutants fail to stabilize Nrf2 even under conditions of oxidative stress; thus, Cys151 is proposed to be the residue through which Keap1 senses oxidative stress.[56] Copper-dependent reactive cysteine profiling revealed a change in the reactivity of Cys288, with a ratio of 3.51, upon copper treatment, while Cys273 and Cys151 were not labeled. I hypothesized that copper could bind to Cys288, preventing Keap1 from binding Nrf2, and causing an increase in the expression of HO1. Indeed, qPCR experiments revealed an increase in HO1 expression upon copper treatment that was time- and dose- dependent, requiring only 1 μM copper for a measurable response (Figure 3.19A and B). This effect is specific to copper and is not induced by treatment with zinc, iron, or hydrogen peroxide (Figure 3.19C). Additionally, the effect of copper on Keap1 does not seem to be due to general oxidative stress, since

HO1 expression can be induced by copper in the presence of an excess of the cell-permeable reductant N-acetylcysteine (Figure 3.19C).

Our studies of STAT3 and Keap1 were cut short, however, by a concerning result we obtained from metabolomic profiling of HEK293T cells treated with 200 μM $CuCl_2$ compared to untreated cells (data not shown). We originally pursued metabolic profiling of copper-treated cells because we reasoned that changes in metabolic flux could give us clues about which proteins on our copper-dependent cysteine reactivity profiling hit list might respond to copper. However, the most striking result of the metabolomic study was a large increase in the oxidized-to-reduced glutathione ratio (GSSG:GSH), indicating that cells treated with 200 μM copper experience oxidative stress (data not shown). This is especially concerning because cysteines are redox-sensitive residues which can form disulfide bonds under oxidizing conditions, as well as undergo a variety of oxidative modifications such as S-sulfenylation, S-nitrosation, and S-glutathionylation, among others.[57] A change in cysteine reactivity due to disulfide formation or oxidative modification would appear as a false positive in the copper-dependent reactive cysteine profiling experiment. While the effect of copper on Keap1 could be observed with the addition of very low doses of copper and did not appear to involve the induction of oxidative stress (Figure 3.19A and C), the effect of copper on STAT3 could only be observed at much higher concentrations and could be due to oxidative stress (Figure 3.16B). Indeed, STAT3 transcriptional activity is known to be sensitive to cellular redox events.[58] Concerned that many of the hits on the copper-dependent cysteine profiling list could be attributed to oxidative cysteine modifications, we took a step back to reevaluate other experimental designs that could find native copper-binding proteins.

Discussion and Future Directions

While many copper-containing enzymes, as well as the proteins responsible for copper trafficking, are well-established, the recent discoveries that MAPK1/2[7,23] and PDE3B[37] are allosterically modulated by copper binding hints at the existence of a yet-unknown population of cellular proteins that respond to intracellular copper concentrations. The search for proteins whose activity is modulated by copper has only begun. In this work, we profiled a genetic model of copper deficiency, $CTR1^{-/-}$ MEFs, as well as a pharmacological model of copper excess, HEK293T cells treated with exogenous copper. We used MIB kinase activity profiling to search for kinases with copper-dependent activity, and reactive cysteine profiling to search for proteins with copper-dependent cysteine reactivity. While both profiling techniques may possess the capability of discovering proteins that bind and respond to copper, limitations of the model systems confounded the results of these screens. RNA-seq revealed that $CTR1^{-/-}$ and $CTR1^{+/+}$ MEFs likely diverged developmentally, causing significant differences in gene expression that could not be reversed by the addition of copper or CTR1 to the knockout cell line and could not be deconvoluted from potential copper-specific differences between the two cell lines. Copper addition to HEK293T cells caused oxidative stress, which could cause cysteine modifications that would not be distinguishable from copper-cysteine binding. The risk of inducing oxidative stress could be avoided by treating cells or lysates with copper chelators or by treating lysates with Cu(I) in an anaerobic environment. Ongoing

studies in our laboratory include cysteine profiling of lysates treated with copper chelators or Cu(I).

RNA sequencing of CTR1$^{-/-}$ and CTR1$^{+/+}$ MEFs raised compelling questions about the role of copper in development and differentiation. It is well known that the CTR1$^{-/-}$ mutation is embryonic lethal in mice,[13,59] and this lethality has been attributed to the high demand for mitochondrial copper during development.[60,61] Indeed, cellular copper load influences mitochondrial physiology and metabolic flux,[62-64] suggesting that cellular copper levels may be relevant to the study of metabolic reprogramming, for example in the context of cancer stem cell differentiation and tumor growth.[65] Recent studies, however, suggest that copper may play roles in differentiation that go beyond its role in mitochondrial health and function. Cellular differentiation leads to changes in redox state and copper homeostasis,[66-69] and lysyl oxidase, an enzyme containing a copper cofactor, is required for correct cellular differentiation.[70] Here, RNA-seq and Western blots show that CTR1$^{-/-}$ cells express E-cadherin at levels that far exceed E-cadherin expression levels in CTR1$^{+/+}$ cells. E-cadherin governs the epithelial cell fate, and E-cadherin downregulation is required for the epithelial-to-mesenchymal transition (EMT), a process of de-differentiation that is essential for cancer progression and metastasis.[71] Our data suggest that the presence of CTR1 or copper may influence regulatory events that govern the expression of E-cadherin, suggesting that cellular copper status or the presence or absence of CTR1 may influence the differentiation of the epithelium and the ability of cells to undergo EMT.

Additionally, specific questions about the proteins identified in these screens remain. The ability of copper to influence Nrf2 transcriptional activity has been recently suggested,[72] but the molecular mechanism has not yet been elucidated. Here, we suggest that copper binds Keap1 at Cys288, disrupting the Keap1-Nrf2 interaction and leading to the induction of downstream genes. Further studies could assess whether copper binds purified Keap1 protein in a manner that is dependent on Cys288, and whether a copper-Keap1 interaction prevents the association of Keap1 and Nrf2 *in vitro*.

As our understanding of copper's role in biology grows, the appreciation of copper's ability to modulate protein function will likely increase. Chemical biology plays an important role in the development of chemical tools to dissect the roles of ions and molecules in biological systems. Ions are particularly difficult to study because they do not participate in covalent bonding and cannot be labeled by traditional methods. Additionally, copper is a particularly challenging analyte because of its ability to perform redox chemistry by cycling between Cu(I) and Cu(II) in biological systems. However, it is exactly this powerful redox chemistry that makes copper an essential micronutrient for all known eukaryotic systems and a worthwhile subject of study. With the knowledge gained through these studies, we will continue pursuing technologies that can identify new copper-binding proteins within the context of the complex cellular milieu.

Materials and Methods

Materials

All chemicals were purchased from Sigma Aldrich, unless otherwise noted. Antibody suppliers and part numbers are provided in Table 3.5.

Cell Culture

CTR1$^{-/-}$ (knockout) mouse embryonic fibroblasts (MEFs) and matched CTR1$^{+/+}$ (wildtype) controls were a gift from Prof. Denis Thiele.[13] MEFs were maintained in Dulbecco's Modified Eagle Medium (DMEM, Gibco by Life Technologies), 10% fetal bovine serum (FBS, Seradigm), 1% non-essential amino acids (NEAA, Gibco by Life Technologies), 1% sodium pyruvate (Gibco by Life Technologies), 50 µM beta-mercaptoethanol (BME, Fisher). HEK293T lines lacking CTR1 and their matched controls were a gift from Prof. Steven Howell; the CTR1 KO2 line was used in these studies.[33] HEK293Ts were maintained in DMEM, 10% FBS, 1% NEAA. A549, NCI H2228, HeLa, SW 620, HCT 116, SAOS 2 and U-2 OS cells were maintained in DMEM with 10% FBS. MCF7 cells were maintained in DMEM, 10% FBS, 1% NEAA, and 1% sodium pyruvate. For all cell lines, serum starvation was performed in DMEM. All cell culture and cell treatments were performed under standard sterile conditions, and cells were kept at 37 °C under a 5% CO_2 atmosphere for growth and incubations.

Cloning

Myc-hCTR1 was constructed by Gibson Assembly of PCR products. PCR amplification reactions were performed using the Phusion High-Fidelity DNA Polymerase kit (New England Biolabs, NEB). For each plasmid constructed, two PCR reactions were performed, one to amplify the vector and one to amplify the insert, and the products were combined by Gibson Assembly (see below). Primers for PCR reactions were designed to contain a priming region and an overlap region. The length of the priming region was determined using the NEB T_m Calculator online tool (http://tmcalculator.neb.com/) such that the annealing temperature (T_m) was between 56 °C and 62 °C. The overlap region was designed to create 20-30 base pair overlap regions on the 5' and 3' ends of each vector and insert pair used for Gibson Assembly in order to ensure successful assembly reactions. The vector PCR reaction contained a final concentration of 1X Phusion HF buffer, 3% DMSO, 200 µM dNTPs, 0.5 µM forward primer (TCCAGTGTGGTGGAATTCT), 0.5 µM reverse primer (TGGACTAGTGGATCCGAG), 0.2 ng/µL pcDNA3.1(+) (Invitrogen), and 1X Phusion polymerase (0.5 µL/50 µL reaction). The reaction was thermal cycled using the following program: 98 °C for 30 seconds, followed by 25 cycles of 98 °C for 10 seconds, 59 °C for 30 seconds, and 72 °C for 4 minutes. The product was extended at 72 °C for 5 minutes, and the reaction was stored at 4 °C until further use. The insert PCR reaction contained a final concentration of 1X Phusion HF buffer, 200 µM dNTPs, 0.5 µM forward primer (ATGGAACAAAAACTCATCTCAGAAGAGGATCTGGATCATTCCCACCATATGG), 0.5 µM reverse primer (TCAATGGCAATGCTCTGT), 0.2 ng/µL template DNA, a gift from

Prof. Steven Howell, and 1X Phusion polymerase (0.5 µL/50 µL reaction). Insert PCR reactions were thermal cycled using the following program: 98 °C for 30 seconds, followed by 25 cycles of 98 °C for 10 seconds, 60 °C for 30 seconds, and 72 °C for 1 minute. The product was extended at 72 °C for 5 minutes, and the reaction was stored at 4 °C until further use.

Gibson reactions were performed using the Gibson Assembly Master Mix kit (NEB). The insert fragment (0.07 pmol) and vector (0.01 pmol) (calculated using the NEBioCalculator tool (http://nebiocalculator.neb.com/)) were added to 10 µL of the 2X Gibson Assembly Master Mix, and sterile water was added to bring the reaction to a final volume of 20 µL. The assembly reaction was held at 50 °C for an hour in a thermal cycler and stored at 4 °C until further use. The reaction product (2 µL) was added to NEB 5α competent cells (50 µL) in 1.5 mL sterile tubes on ice with gentle mixing using the pipet tip but without pipetting up and down, and NEB 5α cells were transformed according to the protocol below.

DNA coding for STAT3 in the pcDNA3 vector was a gift from Jim Darnell (STAT3-pcDNA3 Addgene plasmid #8706).[73] Site-directed mutagenesis (SDM) was performed using the Q5 Site-Directed Mutagenesis Kit (New England Biolabs, NEB) according to the manufacturer's instructions. Briefly, SDM primers were designed using the NEBaseChanger tool (http://nebasechanger.neb.com/), and primers are listed in Table 3.6. Q5 reactions containing a final concentration of 1x Q5 mix, 0.5 µM forward primer, 0.5 µM reverse primer, and 1.25 ng/µL STAT3-pcDNA3 template were thermal cycled on a T100 Thermal Cycler (Bio-Rad) using the following program: 95 °C for 30 seconds, followed by 25 cycles of 98 °C or 10 seconds, 59 °C for 15 seconds, and 72 °C for 4 minutes. The products were extended at 72 °C for 2 minutes, and the reaction was stored at 4 °C until further use. The KLD reaction was run for 5 minutes at room temperature, and 1.6 µL of the reaction was added into 16 µL of NEB 5α competent cells in 1.5 mL sterile tubes on ice with gentle mixing using the pipet tip (no pipetting up and down). The cells were transformed according to the protocol below.

STAT3-C718S-pcDNA3 was subjected to a second round of site-directed mutagenesis to introduce the C712S mutation and create the double mutant.

Bacterial Transformations and Isolation of DNA for Transfections

Cells were incubated on ice for 30 minutes, heat shocked in a 42 °C water bath for 30 seconds, and recovered on ice for 2 minutes. SOC medium (300 µL, NEB) was added to each tube, and the cells were incubated at 37 °C with shaking for 1 hour. Cells (20 µL) were spread on plates of LB-Agar (EMD Millipore) containing Ampicillin or Carbenicillin (100 µg/mL) and incubated at 37 °C overnight. Colonies were picked into 5 mL of LB medium (Fisher Scientific) containing 100 µg/mL Ampicillin or Carbenicillin and grown overnight at 37 °C with vigorous agitation. DNA was harvested using the Qiagen Miniprep Kit, according to the manufacturer's instructions, including all recommended steps. Samples were submitted to Qintara Biosciences for sequencing, and sequencing alignments were analyzed using Benchling. All constructs were amplified in 100 mL LB

cultures (100 µg/mL Ampicillin or Carbenicillin), and DNA for mammalian cell transfection was harvested using the Qiagen Maxiprep Kit, according to the manufacturer's instructions, including all recommended steps. DNA was resuspended in 250 µL of Tris-EDTA (TE) buffer to yield final concentrations of 500-1300 ng/µL.

Cell Treatments and Transfections

The following conditions were used for cell treatments unless otherwise indicated. For treatments with copper, cells were serum starved for 16-20 hours to lower basal copper levels, and copper ($CuCl_2$) was added to the serum-free media at the indicated concentrations and times. For treatments with epidermal growth factor (EGF) or interleukin-6 (IL-6, PeproTech), cells were serum starved for 16-20 hours to induce quiescence, as serum contains growth factors, cytokines, and other small molecules that can stimulate cellular signaling. For treatments with copper chelators, cells were maintained in serum-containing media to achieve the largest change in copper by maintaining cellular copper at normal levels until chelation. For transfection experiments, cells were plated to be 70% confluent at the time of transfection; $3.5*10^5$ cells were added to each well of a 12-well plate the day before transfection. MEF cells were transfected with Lipofectamine 2000 (Thermo Fisher), according to the manufacturer's protocol, using 100 µL Optimem, 4 µL transfection reagent, and 1 µg DNA per well in a 12-well plate. HEK293T cells were transfected with TransIT-LT1 reagent (Mirus Bio) according to the manufacturer's protocol, using 100 µL Optimem, 2 µL transfection reagent, and 1 µg DNA per well in a 12-well plate.

Inductively Coupled Plasma Mass Spectrometry

Cells were plated in 6-well plastic dishes (Corning) to be 90% confluent the day before harvesting and serum-starved overnight (12-20 hours). For long copper treatments, copper was added to the serum-free media when the media was changed. For short copper treatments, copper was added to the serum-free media in each well at the indicated time before harvesting. To harvest cells, media was decanted, and cells were placed on ice. Cells were washed three times with ice-cold HEPES (20 mM, pH 7.5), and trace-metals grade nitric acid (215 µL, BD Aristar Ultra) was added to each well. Care was taken to ensure that nitric acid spread over the bottom of the entire well. Parafilm M (Bemis) was used to seal the edges of the plate lid, and the plates were left on a shaker overnight at room temperature. The next day, concentrated samples (150 µL) were diluted into 2% nitric acid made with milliQ water and trace-metals grade nitric acid (2 mL/sample), and Ga was added as an internal standard (40 µL of a 1 ppm stock, Inorganic Ventures). The samples were analyzed on an iCAP-Qc ICP-MS equipped with a CETAC ASX-520 autosampler (Thermo Fisher) and concentrations were calculated based on a standard curve diluted from the CMS-5 standard (Al, Cs, Co, Fe, Mg, Ni, Rb, Na, Zn, Ca, Cr, Cu, Li, Mn, K, Ag, and Sr in 2% nitric acid) with molybdenum, phosphorous and sulfur added (Inorganic Ventures).

Western blots

Cells were plated in 6-well plastic dishes (Corning) to be 90% confluent the day before harvesting and serum-starved overnight (12-20 hours). Cell treatments were added to the serum-free media in each well at the indicated time points. To harvest cells, media was decanted, and cells were placed on ice. Cells were washed three times with ice-cold PBS, and lysis buffer (200 µL/well, 50 mM Tris-HCl, pH 7.4, 150 mM NaCl, 0.5% sodium deoxycholate, 0.1% SDS, with 1% NP-40 or Triton X-100 (Boston BioProducts) with phosphatase inhibitors (PhosSTOP, Roche) and protease inhibitors (Complete ULTRA, without EDTA, Roche)) was added to each well. Lysates were scraped off of each well and pipetted into 1.5 mL tubes (Axygen). Lysates were clarified by centrifugation (16,100 x *g*, 10 min, 4 °C), and the supernatant was transferred to a fresh 1.5 mL tube. Protein was quantified by BCA assay (Pierce). For gel electrophoresis, samples were prepared by diluting the lysates into PBS to the concentration of the most dilute sample (15 µL final volume, typically 500-1500 µg/mL) and 7 µL of sample buffer (4:1 4x LDS Sample Buffer:beta-mercaptoethanol, Life Technologies and Fisher, respectively) was added to each sample and mixed by pipetting and inversion. Samples (18 µL) were loaded onto precast gels (NuPAGE 4-12% Bis-Tris, 1.5 mm, 15 wells, unless otherwise noted, Life Technologies) and run at 140V for 1-2 hours. Proteins were transferred to a PVDF membrane (Bio-Rad or Millipore) using the 1.5 mm transfer program (1.3 A, 25V, 10 min) on the Transblot Turbo Transfer system (Bio-Rad). For proteins above 100 kDa, the transfer program was run twice to ensure efficient transfer. Membranes were blocked in 5% low-fat, dry milk (Carnation) in Tris-buffered saline with 0.05% Tween-20 (TBST, Santa Cruz) with rocking for 1 hour at room temperature or overnight at 4 °C. Primary antibody was applied in 5% milk TBST with rocking for 1 hour at room temperature or overnight at 4 °C. Membranes were washed twice for 5 seconds and twice for 5 minutes in TBST. Secondary antibody was applied in TBST for 1 hour at room temperature with rocking. All secondary antibodies were HRP conjugates except for the secondary antibody used for actin blotting; a fluorescent secondary antibody was used for actin blots. Although the antibody for E-cadherin was fluorescently conjugated, we found that using a secondary antibody significantly amplified signal, and all images of E-cadherin were obtained after application of a secondary HRP antibody. Membranes were washed twice for 5 seconds and twice for 5 minutes in TBST. Membranes probed with HRP-conjugated antibodies were visualized using Western Lightning Plus ECL or Western Lightning ULTRA ECL (Perkin Elmer). Membranes probed with fluorescent antibodies were visualized by illumination. All images were collected on a ChemiDoc MP (Bio-Rad). A list of antibodies used in this work may be found in Table 3.5.

Multiplexed Inhibitor Bead Profiling

CTR1$^{-/-}$ or CTR1$^{+/+}$ MEFs were plated to be 90% confluent and were serum starved overnight (20 hours). Cells were stimulated for 22-24 minutes at 37 °C with 200 ng/mL EGF. Media was decanted, and the plates were placed on ice. Each plate of cells was washed 3x with ice-cold PBS, scraped into PBS, and pelleted 2500 x g in PBS. Each pellet contained the cells from twelve 15-cm plates; plates were harvested in 3 batches of 4 plates/batch. The supernatant was removed, and the pellet was snap frozen in liquid nitrogen and stored at -80 °C until analysis. Lysis buffer (1.5 mL of 50 mM HEPES, pH 7.5, 150 mM NaCl, 0.5% Triton X-100, 1 mM EDTA, 1 mM EGTA, 10 mM NaF, 2.5 mM

NaVO4, Roche protease inhibitors, and Roche PhosSTOP phosphatase inhibitors) was added to each frozen cell pellet, and the pellets were allowed to thaw on ice for 20 minutes. Thawed pellets were resuspended in the lysis buffer, transferred to 2 mL plastic tubes and incubated on ice for 10 minutes to allow for complete lysis. The tubes were sonicated for 10 seconds in a water bath sonicator, and the lysates were clarified by centrifugation (10 min, full speed, 4 °C). The supernatant was transferred to a new tube, and protein concentration was determined by BCA Assay (Pierce).

To prepare the pre-cleaning and kinase binding columns, disposable columns (Bio-Rad, 731-1550) were decapped (if the cap does not snap cleanly, discard the column, as this will disrupt the column flow) and rinsed with milliQ water. For each sample, a pre-clearing column was packed with EAH Sepharose 4B (100 µL) and ECH Sepharose 4B (400 µL) using a clipped pipet tip. The columns were flushed with one column volume of high salt buffer (50 mM HEPES, pH 7.5, 1 M NaCl, 0.5% Triton X-100, 1 mM EDTA, 1 mM EGTA), lightly capped without applying pressure to the column, and stored at 4 °C until use (up to a few hours). For each sample, the kinase binding column was packed with inhibitor-bound beads (Table 3.1) such that the most specific inhibitors were on the top of the column and more promiscuous inhibitors were on the bottom of the column to catch any remaining kinases. The columns were flushed with 5 column volumes of high salt buffer, lightly capped without applying pressure to the column, and stored at 4 °C until use (up to a few hours). Three 4x10 tube racks were clamped to between two metal ring stands such that the racks formed three “stories” of racks. The top story held the pre-clearing columns; the middle story held the kinase binding columns, capped with 26 G needles (⅝ inch, Bio-Rad 305115); the bottom story held 15 mL tubes. In this arrangement, the lysate could be loaded onto the pre-clearing column, and the flow-through from this column would gently drip into the kinase binding column, which drained into the collection tubes. The racks of columns were set up in a cold room to maintain the temperature constantly at 4 °C.

Lysates were brought to the concentration of the least concentrated sample in high salt buffer with extra salt added (5M NaCl, Ambion AM9759) to a final concentration of 1 M NaCl, and 20-40 mg of each lysate in 10 mL buffer were loaded onto each pre-clearing column. After the sample had completely loaded onto the column, the tubes collecting the flow through were capped and moved to -80 °C, and the pre-clearing columns were discarded. The kinase binding columns were flushed with 10 mL of high salt buffer and 10 mL of low salt buffer, and the flow-through was collected in a plastic pan and discarded. For elution, 1 mL of low salt buffer containing 0.1% SDS was added to each column, and the column outlets were capped securely. Pre-heated elution buffer (95 °C, 500 µL) was added to each column, and the columns were vortexed to resuspend the beads. The kinases were eluted by boiling in a bead bath for 5 minutes, and the eluent was drained into a 2 mL plastic tube (low-bind tubes are not necessary). The elution was repeated with an additional 500 µL of elution buffer with a 10-minute boiling step. All remaining liquid was removed by blowing air through the column with a 25 mL Stripette, and any eluent caught in the tube cap was also transferred to the 2 mL tube. Columns were discarded, and samples were stored at -80 °C (no flash freezing necessary).

Samples were processed for mass spectrometry and data was analyzed by the Shokat Lab, according to published methods.[21]

Quantitative Reverse Transcription Polymerase Chain Reaction (qRT-PCR or qPCR)

Cells were treated or transfected as indicated; single samples were made from cell volumes ranging from a 10-cm dish to one well of a 12-well plate. Media was decanted, and the plates were placed on ice. Plates were washed 3x with ice-cold PBS, and 350 µL of Buffer RLT (without reductant) was added to each well. Cells were scraped and collected in RNase-free 1.5 mL tubes (Axygen, sterile), and RNA was harvested using the Qiagen RNeasy Minikit, according to the manufacturer's protocol. All work with RNA was performed in an area sterilized with 70% ethanol and wiped clean with RNase-ZAP. Fresh, sterile, filter tips (Eppendorf) were used to prevent sample contamination. All recommended steps were performed, including DNase digestion. Typically, purified RNA was achieved at 300-800 ng/µL. cDNA was synthesized from 1 µg of RNA using the iScript Reverse Transcription Supermix for RT-qPCR (Bio-Rad), according to the manufacturer's protocol. The resulting cDNA was diluted by adding 80 µL of RNase/DNase free water to yield cDNA; this concentration was designated to be 10^0. Ten-fold dilutions were made (10^{-1}, 10^{-2}, and 10^{-3}), and these dilutions were used to assess the linearity of each primer pair for the genes of interest. qRT-PCR reactions were performed using cDNA concentrations in the linear range for each primer pair. All gene expression was normalized to the expression of RPLP0. qRT-PCR was performed using iQ SYBR Green Supermix (Bio-Rad), according to the manufacturer's instructions. PCR plates (black shell/white well, Bio-Rad) were sealed with a clear adhesive cover (Bio-Rad), spun briefly to collect all reagents at the bottom of the tube, and cycled on a CFX96 Real-Time System thermal cycler (Bio-Rad). Thermal cycling steps were: 95 °C for 3 min and 40 cycles of 95 °C for 12 seconds followed by 61 °C for 1 minute with a plate read at the end of each cycle. A melt curve (65 to 95 °C at 0.5 °C intervals every 5 seconds) was performed at the end of each qRT-PCR experiment to assess the presence of a single PCR product. Primers used for qRT-PCR are provided in Table 3.6 and were ordered from Integrated DNA Technologies. When available, primers were selected from the Primer Bank (https://pga.mgh.harvard.edu/primerbank/index.html). For genes with no verified primers in the Primer Bank, primers were designed using the Primer3 tool (http://bioinfo.ut.ee/primer3-0.4.0/) with the cDNA sequence available on Ensembl.org as the input. Primers bridging introns were preferred, if possible. Resulting primers were blasted against the mouse genome using NCBI PrimerBlast (https://www.ncbi.nlm.nih.gov/tools/primer-blast/), and only primers that specifically targeted the gene of interest were used.

RNA Sequencing

Cells were plated on 10-cm dishes such that each dish contained 10^7 cells on the day of harvest. RNA was prepared using the same method described for qRT-PCR experiments. RNA quality was assessed using a BioAnalyzer (Agilent), and all samples had RIN scores of 9.8 or higher. RNA was submitted to the New York Genome Center for library preparation and sequencing. RNA sequencing libraries were prepared using the KAPA

Total Stranded RNA-Seq Kit with RiboErase HMR (KAPA Biosystems) in accordance with the manufacturer's instructions. Briefly, 500 ng of total RNA was depleted of ribosomal RNA using hybridization of complementary DNA oligonucleotides and treatment with RNase H and DNase to remove duplexed rRNA. Depleted RNA was fragmented by divalent cations under elevated temperature. The fragmented RNA underwent first strand synthesis using reverse transcriptase and random primers. Second strand synthesis created the cDNA fragments using DNA polymerase I and RNaseH. cDNA was then adenylated and ligated to Illumina sequencing adapters followed by enrichment using 9 cycles by PCR. Final libraries were evaluated by PicoGreen (Life Technologies) and Fragment Analyzer (Advanced Analytics). Sequencing was performed on the HiSeq 2500 instrument with 2x125bp read length using v4 SBS chemistry according to the Illumina protocol, as described in Bentley et al, 2008 (PMID: 18987734). RNA sequence reads were aligned to the mouse genome reference mm10 using STAR aligner (v2.4.0c) (PMID: 23104886). Genes annotated in Gencode vM5 were quantified using featureCounts (v1.4.3) (PMID: 24227677). Normalization and differential expression were performed using the Bioconductor package DESeq2 (doi:10.1101/002832). Picard (http://broadinstitute.github.io/picard/) and RSeQC (PMID: 22743226) were used to collect and evaluate QC metrics. See Appendix 1 for a list of genes up-regulated or down-regulated 6-fold or greater.

Immunoprecipitation

Cells were plated in 10-cm dishes to be 80% confluent the day before the experiment and were serum starved overnight (16-20 hours). Cells were treated with vehicle, EGF (50 ng/mL) or H2O2 (2 mM, which is 2 µL of 30% H_2O_2 into 10 mL media) for 30 minutes at 37 °C. Media was decanted, and cells were placed on ice. Cells were washed 3x with ice-cold PBS. Lysis buffer (400 µL/dish, 50 mM Tris-HCl, pH 7.4, 150 mM NaCl, 0.5% sodium deoxycholate, 0.1% SDS, with 1% NP-40 or Triton X-100 (Boston BioProducts) with phosphatase inhibitors (PhosSTOP, Roche); note: if 6-cm dishes were used, 200 µL of lysis buffer was used) was added to each dish, and cells were scraped into 1.5 mL tubes (Axygen). Lysates were clarified by centrifugation at 16,100 x *g* for 10 minutes at 4 °C, and supernatants were transferred to fresh 1.5 mL tubes. Protein concentration was determined by BCA assay (Pierce), and all lysates were diluted to 1 mg/mL in lysis buffer. Lysates were not precleared because, in our hands, preclearing did not have an effect on the results (data not shown). Antibody (1 µL, anti-Fer (EP1824Y) Abcam) was added to the lysate (200 µg) and incubated at 4 °C overnight with rotation. The next morning, Protein A/G agarose beads (20 µL of a 50% slurry per sample, Pierce) were washed 3x with lysis buffer by centrifugation and resuspension, and a 50% slurry of washed beads in lysis buffer was prepared and chilled to 4 °C. To each sample, 20 µL of this slurry was added, and the samples were incubated at 4 °C with rotation for 3-4 hours. Beads were collected in the bottom of the tube by centrifugation, and the supernatant was removed and stored on ice for further analysis. Beads were washed by centrifugation and resuspension in 5 changes of 300-500 µL lysis buffer, and as much supernatant as possible was removed. 30 µL of sample buffer (4:1 NuPAGE 4x LDS Sample Buffer:beta-mercaptoethanol, Life Technologies and Fisher, respectively) was added to each tube. Samples were flicked to mix and briefly spun on a bench-top centrifuge. Samples were

then boiled in a sand bath for 3 minutes to elute bound proteins. To remove beads, the samples were spun at 16,100 x *g* for 10 minutes at room temperature (to avoid precipitating the LDS), and 15 µL of the supernatant was loaded onto a gel for electrophoresis. Western blotting for Fer and phosphotyrosine were performed as described above.

Reactive Cysteine Profiling

HEK293T cells were plated in 10-cm dishes to be 90% confluent on the day of the experiment. One 10-cm dish was used per sample. Experiments were conducted in quadruplicate. Cells were treated with 200 µM $CuCl_2$ or vehicle for 1 hour. Media was aspirated, and the plates were placed on ice. Cells were scraped into a minimum volume of PBS and spun down at 1000 x *g* for 5 min at 4 °C. Cells were washed twice with PBS by resuspension and centrifugation. The resulting cell pellet was resuspended in 300 µL of PBS and sonicated on ice (50% duty cycle, 0.5 seconds on, 0.5 seconds off, 4 pulses/round, 4 rounds). Lysis was confirmed by visual inspection. Lysates were clarified by centrifugation at 16,100 x *g* for 10 minutes at 4 °C, and the supernatant was transferred to a new tube. Protein concentration was determined by Bradford Assay (Pierce), and samples were brought to 1 mg/mL in PBS. To a sample volume of 500 µL, 5 µL of iodoacetamide alkyne was added (10 mM in DMSO, aliquots stored at -80 °C), and the samples were thoroughly mixed and incubated on a rotator for 1 hour at room temperature. Isotopically light (for control samples) or heavy (for copper-treated samples) N_3-TEV-biotin tag (9.5 uL/sample, 5 mM in DMSO, synthesized according to published methods,[50] aliquots stored at -80 °C) was added to each sample and mixed by inversion. A click chemistry master mix was prepared by combining 10 µL tris-(2-carboxyethyl)phosphine (TCEP, freshly prepared, 13 mg/mL in water), 30 µL tris(benzyltriazolylmethyl)amine (TBTA, 1.7 mM in 1:4 tBuOH:DMSO, aliquots stored at -20 °C), and 10 µL copper sulfate (50 mM in water, aliquots stored at -20 °C) per sample. The master mix (50 µL/sample) was added to each sample, and samples were vortexed immediately to ensure sufficient mixing. Samples were incubated on a rotator for 1 hour at room temperature.

The click reaction was stopped by adding 1 mL of -80 °C MeOH to each sample, and the precipitated proteins were collected by centrifugation (16,100 x *g*, 5 min, 4 °C). The supernatant was aspirated, and the pellets were washed with 0.5 mL cold MeOH. Samples were sonicated (50% duty cycle, 0.5 seconds on, 0.5 seconds off, 5 pulses) to resuspend the pellet. One control sample was added to each copper-treated sample, and the combined samples were spun down (16,100 x *g*, 5 min, 4 °C). The supernatant was aspirated. Cold MeOH (1 mL) was added to each sample. The samples were resuspended by sonicated (50% duty cycle, 0.5 seconds on, 0.5 seconds off, 5 pulses) and centrifuged (16,100 x *g*, 5 min 4 °C). The supernatant was aspirated, and 400 µL of urea (6 M in PBS, 1.8 g/5 mL final volume, freshly prepared) was added. The samples were sonicated (50% duty cycle, 0.5 seconds on, 0.5 seconds off, 5 pulses) to solubilize the protein. DTT (20 µL/sample, 30 mg/mL in water, freshly prepared, Fisher) was added to each sample to a final concentration of 10 mM. If the protein was not fully dissolved at this stage, the samples were sonicated until fully dissolved. Samples were incubated in a

65 °C water bath for 15 minutes. Iodoacetamide (20 µL/sample, 400 mM, 74 mg/mL in water, freshly prepared) was added to a final concentration of 20 mM, and the samples were incubated at 37 °C for 30 minutes with shaking. The reaction was quenched with DTT (40 µL/sample), and the volume was brought to 1.2 mL by adding 720 µL PBS. Trypsinization was initiated by adding $CaCl_2$ (12 µL/sample, 100 mM in water, 1 mM final) and 1 vial of reconstituted trypsin (Promega Sequencing Grade, 20 µg trypsin dissolved in 40 µL provided Trypsin buffer). Samples were incubated overnight at 37 °C on a shaker.

The next day, SDS (139 µL/sample, 10% in water) was added to each sample to a final concentration of 1%. The samples were flicked to resuspend the pellet and incubated at 65 °C for 5 minutes to dissolve the pellet. If the pellet did not dissolve, further heating at 65 °C in 5-minute intervals, as well as sonication, was used to fully dissolve the pellet. Streptavidin beads (Pierce, 100 µL of 50% slurry/sample) were transferred to a 1.5 mL tube and washed 3x with PBS by spinning the beads down with quick-pulse centrifugation, aspirating the supernatant, and resuspending the beads in PBS. The washed streptavidin beads were resuspended in PBS to create a 50% slurry. Each sample was transferred to a 15-mL conical tube, and 5.6 mL PBS and 100 µL washed 50% streptavidin bead slurry was added to each conical. Samples were incubated at room temperature for 3 hours and spun down at 1080 x *g* for 5 minutes. Leaving ~500 µL extra PBS in the bottom of the tube (to avoid disturbing the pellet), the supernatant was aspirated. The beads were washed 3x by resuspension in 10 mL PBS and 3x by resuspension in 10 mL milliQ water. On the last wash, the sample was aspirated to a final volume of 1 mL. Each sample was transferred to a 1.5 mL tube, with care taken to fully resuspend the sample such that all beads were transferred. The beads were collected by quick-pulse centrifugation, and the supernatant was aspirated, leaving 20-50 µL of supernatant so that the beads were not disturbed. The beads were washed once in 150 µL of TEV buffer by resuspension and centrifugation, with 20-50 µL of supernatant left in the tube to avoid disturbing the beads. The remaining liquid was removed by aspiration through an 18 G needle (BD Biosciences). TEV buffer (150 µL/sample) and 5 µL of TEV protease (Thermo Fisher) were added to each sample, and samples were incubated on a rotator at 30 °C for 24 hours.

The next day, the samples were spun down at 3000 x *g* for 15 seconds. The beads were resuspended by pipetting with a clipped p200 tip and transferred to a Micro Bio-Spin column (Bio-Rad, filter column only; no resin). The columns were spun at 3000 x *g* for 15 seconds. PBS (150 µL) was added to the remaining beads left in the 1.5 mL tubes, and the same tips used to transfer the beads were used to wash as many beads off the tube walls as possible and add them to the Micro Bio-Spin columns. The columns were spun at 3000 x *g* for 15 seconds. The resulting flow-through (~300 µL) was acidified by the addition of formic acid (15 µL) and vortexed briefly. The samples were stored at -20 °C until mass spectrometry analysis.

Mass spectrometry and data analysis was performed by the Cravatt lab according to published methods.[47] Only cysteines labeled in at least two of the four replicates were included in the list of significant hits. Hits with ratios above 20 are set to a ratio of 20, as very high ratios cease to be quantitative.

Immunofluorescence

HEK293T cells were plated on 4-well chamber slides ($1.2*10^5$ cells/well, Lab-Tek II Chambered Coverglass with Cover, #1.5, Borosilicate Glass, Thermo Fisher) 2 days before immunofluorescence. The day before immunofluorescence, the cells were serum-starved overnight (12-18 h). Cells were treated with 0, 50, or 100 µM $CuCl_2$ for 1 hour and then IL-6 (50 ng/mL, PeproTech) was added to the well for 45 minutes. Media was aspirated and slides were placed on ice. Cells were washed 3x with ice-cold PBS and fixed at room temperature for 15 minutes with 4% PFA (Thermo Scientific, #28906) in PBS. Fixed cells were washed once with room temperature PBS and methanol-permeabilized in 100% ice-cold MeOH at -20 °C for 10 minutes. MeOH was aspirated without allowing the cells to dry out, and cells were washed once with room-temperature PBS. The cells were blocked in blocking buffer (3% donkey serum (Jackson Labs) and 0.5% Triton X-100 in PBS) for 1 hour with rocking. Primary antibody (Mouse anti-STAT3 (124H6), Cell Signaling Technologies, 1:1500 in blocking buffer) was applied for 1 hour with rocking, after which the cells were washed 3x 5 min with PBS. Secondary antibody (Donkey anti-mouse AlexaFluor647, Life Technologies, 1:100 in blocking buffer) was applied for 1 hour with rocking, and the cells were washed twice with PBS. Hoechst stain (1:2000 dilution in PBS, from a 10 mg/mL stock, Life Technologies) was applied for 5 minutes with rocking and the cells were washed 3x 5 min with PBS before imaging. Imaging was performed on the same day as treatment and staining.

Acknowledgements

We thank Prof. Denis Thiele and Prof. Steve Howell for their generous gifts of CTR1 knockout cell lines. We thank Ann Fisher, Carissa Tasto, and Alison Kililea in the UC Berkeley Cell Culture Facility for maintaining the cell lines used in these experiments. We thank Dr. John Gordan, Dr. Rebecca Levin, and Prof. Kevan Shokat for helpful advice and experimental work for the MIB kinase profiling experiments. We thank Dr. Liron Bar-Peled, Dr. Keriann Backus and Prof. Ben Cravatt for helpful advice and experimental work for the reactive cysteine profiling experiments. We thank Prof. Eranthie Weerapana for reagents and helpful advice for the reactive cysteine profiling experiments.

In vitro studies of Atox1 for reactive cysteine profiling was a rotation project completed by Tyler Detomasi under the mentorship of Dr. Joseph Cotruvo and Allegra Aron. *In vivo* studies of Atox1 for reactive cysteine profiling was a Master's Thesis project completed by Celine Constantin under the mentorship of CMA. Metabolomics profiling was performed by Allegra Aron in collaboration with Carl Ward and Prof. Dan Nomura.

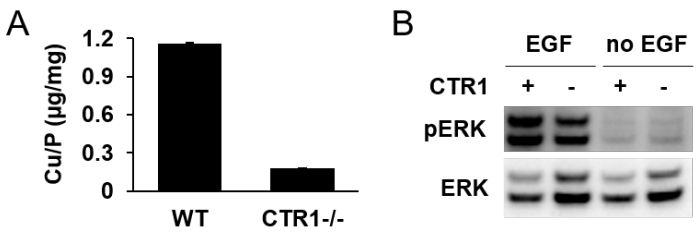

Figure 3.1 Characterization of CTR1$^{-/-}$ and CTR1$^{+/+}$ MEF cells. A) Copper content of wildtype and CTR1$^{-/-}$ MEF cells normalized to cellular phosphorous levels, measured by ICP-MS. B) Western blots of phospho-ERK (pERK) and total ERK in wildtype and CTR1$^{-/-}$ MEF cells stimulated with 200 ng/mL EGF or vehicle for 15 minutes.

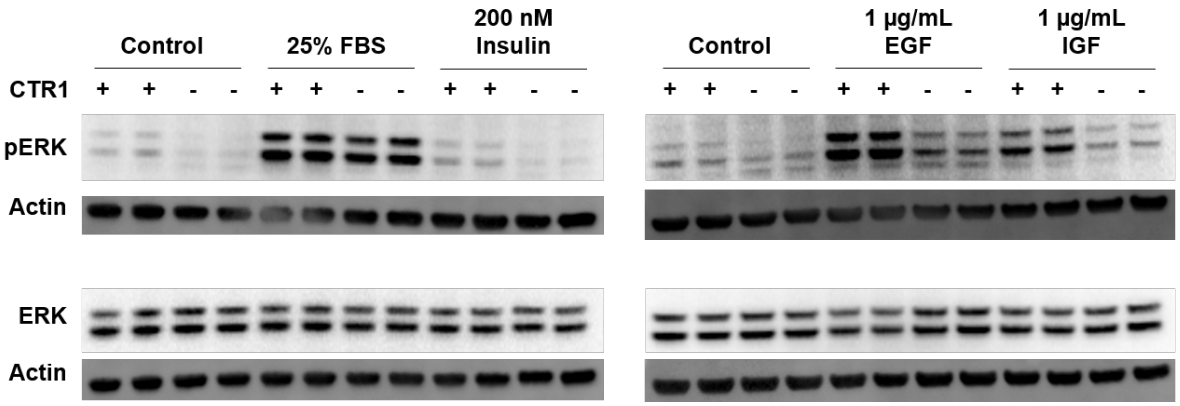

Figure 3.2 ERK phosphorylation is lower in CTR1$^{-/-}$ MEFs than wildtype cells, regardless of stimulation. Western blots of wildtype or knockout MEFs stimulated for 18 minutes with the indicated stimulus. Because the anti-pERK antibody interferes with the anti-ERK antibody, pERK and ERK were probed on different membranes. Actin is shown as a loading control for each membrane.

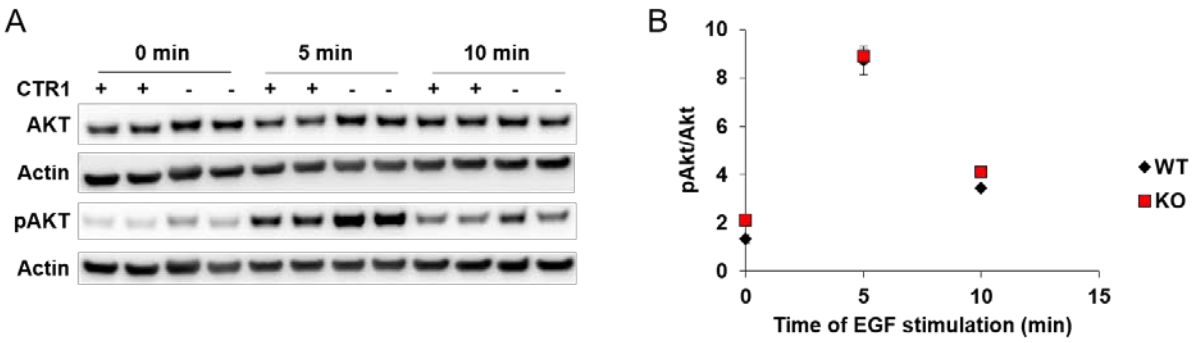

Figure 3.3 Phosphorylation of AKT is not altered in CTR1$^{-/-}$ MEFs. A) Western blots of phospho-AKT (pAKT) and total AKT with actin loading controls. B) Quantification of the ratio of pAKT band intensity to AKT band intensity, normalized to actin.

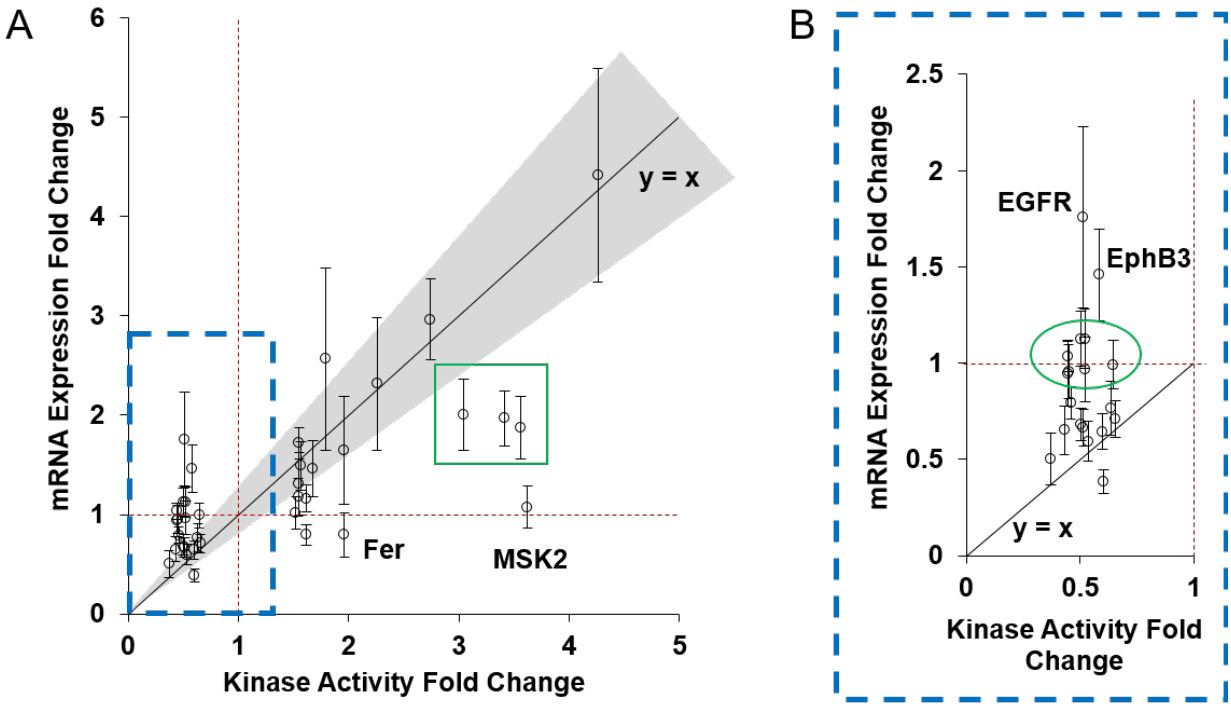

Figure 3.4 Comparison of the kinase activity and gene expression for each kinase identified by MIB profiling. A) Scatter plot of the mRNA expression of each kinase compared to its activity. mRNA expression was determined by qRT-PCR. Each circle represents a kinase. The gray triangle highlights the area around the y=x line where activity change may be explained by a change in expression. Red dotted lines mark y = 1 (no change in expression) and x = 1 (no change in activity). Fer and MSK2 are marked. Map4K2, TAOK3, and CDK18 are indicated by the green box. B) Magnification of the area highlighted in blue in (A). EGFR and EphB3 are marked. The green circle highlights CDK4, CDKL5, CK1γ3, BMPR2, TAOK1, TAOK2 and AURKB.

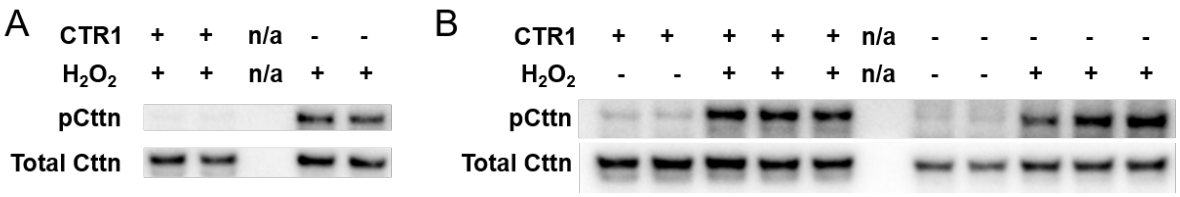

Figure 3.5 Phosphorylation of cortactin is altered in serum-starved CTR1$^{-/-}$ MEFs compared to wildtype controls, but not in cells kept in serum-containing media. A) Western blots of serum-starved wildtype and CTR1$^{-/-}$ MEFs stimulated with hydrogen peroxide (2 mM, 30 min). B) Western blots of wildtype and CTR1$^{-/-}$ MEFs that had not been serum starved but were subsequently stimulated with hydrogen peroxide (2 mM, 30 min). In each blot, the middle lane, labeled with n/a, contains the protein ladder. pCttn: phospho-cortactin; Cttn: cortactin.

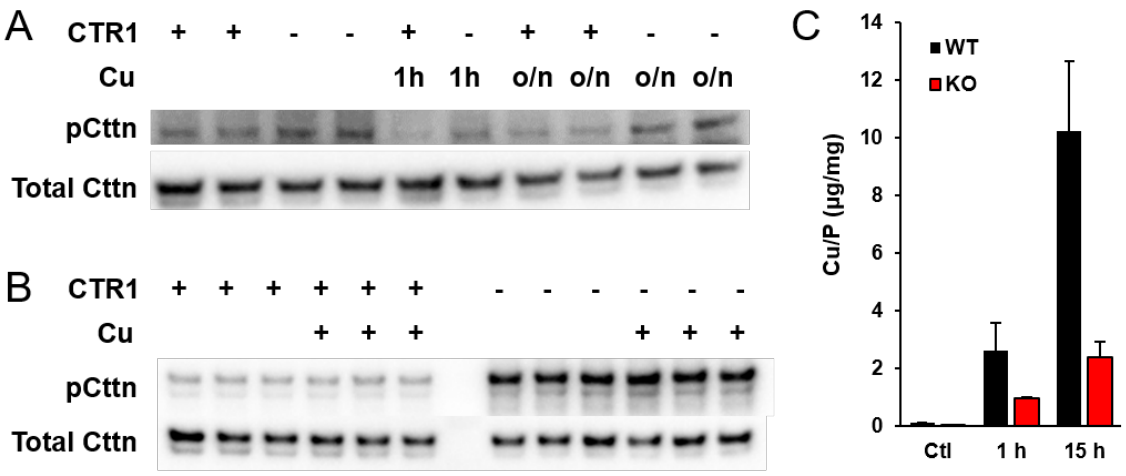

Figure 3.6 Manipulation of copper levels does not alter the levels of phospho-cortactin (pCttn) in $CTR1^{-/-}$ or $CTR1^{+/+}$ MEFs. A) Western blots of unstimulated MEFs supplemented with copper (5 µM $CuCl_2$) for the indicated times (o/n: overnight). B) Western blots of MEFs supplemented with copper (5 µM $CuCl_2$) overnight and stimulated with hydrogen peroxide. C) Copper concentrations in MEFs following copper addition (5 µM $CuCl_2$) assessed by ICP-MS and normalized to cellular phosphorous levels. pCttn: phospho-cortactin; Cttn: cortactin; WT: wildtype, $CTR1^{+/+}$; KO: knockout, $CTR1^{-/-}$.

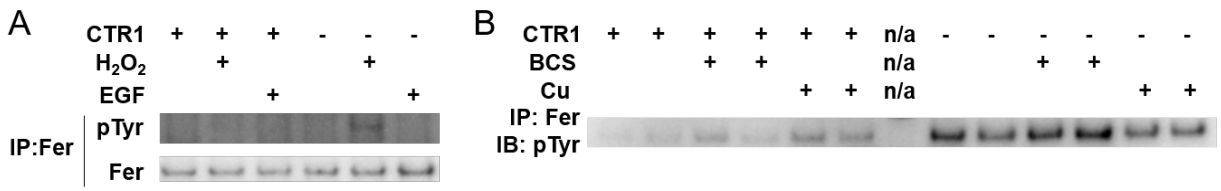

Figure 3.7 Manipulation of copper levels does not alter the levels of phospho-Fer in CTR1$^{-/-}$ or wildtype MEFs. A) Western blots of phosphotyrosine and Fer performed on anti-Fer immunoprecipitations from lysates generated from serum-starved CTR1$^{-/-}$ or wildtype MEFs stimulated for 30 minutes with EGF (50 ng/mL) or H_2O_2 (2 mM). B) Western blot against phosphotyrosine performed on anti-Fer immunoprecipitations from lysates generated from CTR1$^{-/-}$ or wildtype MEFs that had been pretreated with the cell-impermeable copper chelator bathocuproine disulfonate (BCS, 500 µM) or $CuCl_2$ (5 µM) overnight in serum free media and stimulated with H_2O_2 (2 mM) for 30 minutes.

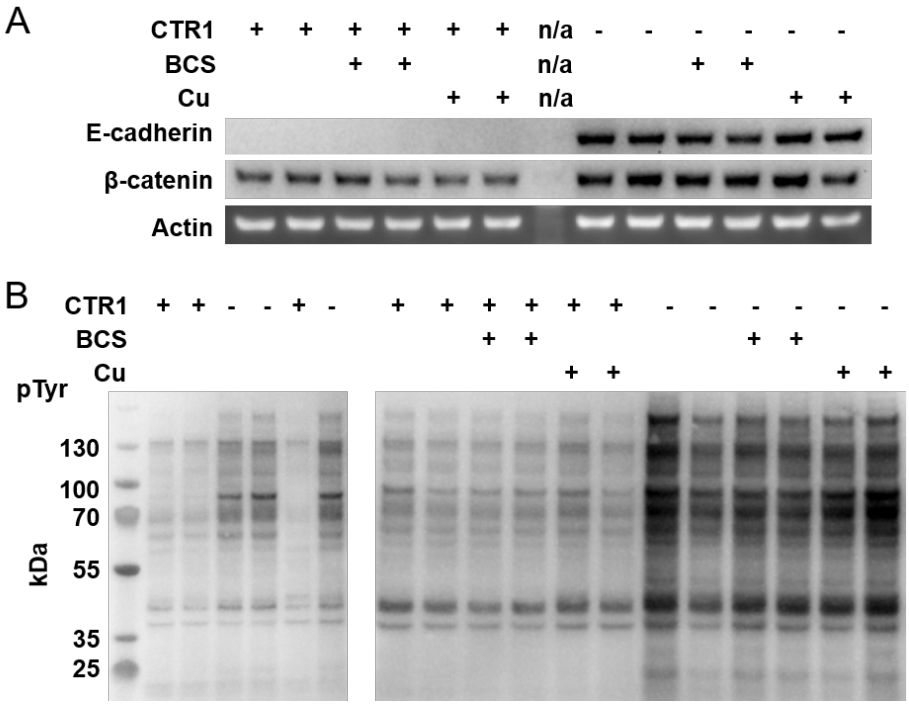

Figure 3.8 Components of Fer signaling are altered in CTR1$^{-/-}$ MEFs compared to wildtype MEFs but do not respond to changes in copper levels. A) Western blots of CTR1$^{-/-}$ and wildtype MEFs treated with the cell-impermeable copper chelator bathocuproine disulfonate (BCS, 500 µM) or $CuCl_2$ (5 µM) overnight in serum-free media, probed for E-cadherin and β-catenin. Actin is shown as a loading control. B) Western blots of total phosphotyrosine levels in CTR1$^{-/-}$ and wildtype MEFs treated with vehicle, BCS (500 µM) or $CuCl_2$ (5 µM) overnight in serum-free media and stimulated with H_2O_2 (2 mM, 30 minutes).

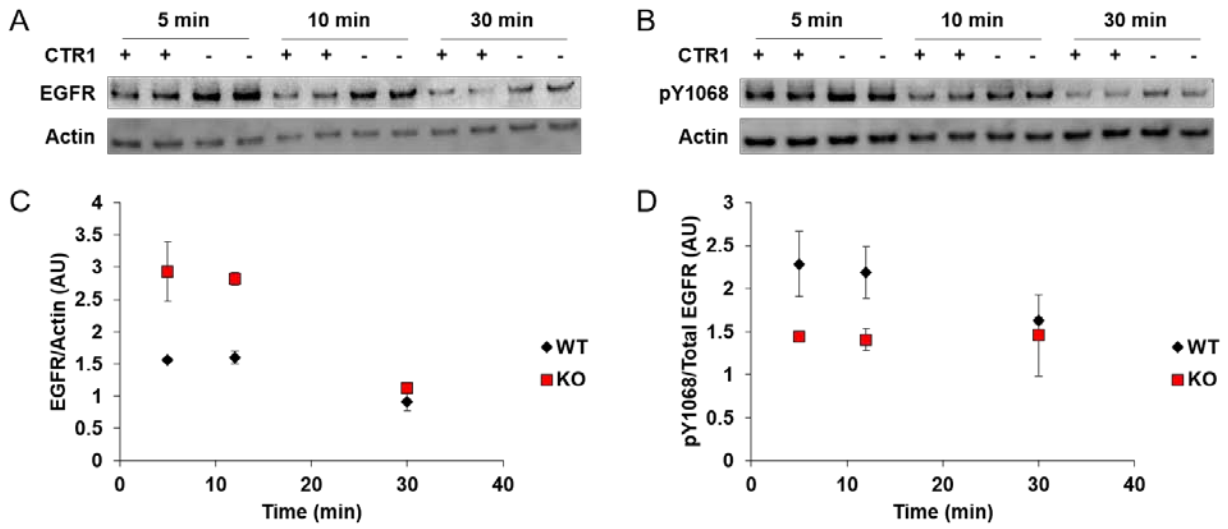

Figure 3.9 EGFR activity is lower in CTR1$^{-/-}$ MEFs compared to wildtype MEFs, despite overexpression of EGFR in CTR1$^{-/-}$ MEFs. A) Western blots of serum-starved MEFs stimulated with 100 ng/mL EGF for the indicated times. B) Western blots of the same lysates shown in A. EGFR and pY1068-EGFR blots were performed separately to eliminate the possibility of interference between the two antibodies. Actin serves as a loading control. C) Quantification of total EGFR normalized to actin. D) Quantification of pY1068 normalized to total EGFR. Both are normalized to the actin levels on the respective blots. The graphs in (C) and (D) display the averages and standard deviations from biological duplicates, each done in technical duplicate. pY1068 = phosphotyrosine 1068 of EGFR; WT: wildtype, CTR1$^{+/+}$; KO: knockout, CTR1$^{-/-}$.

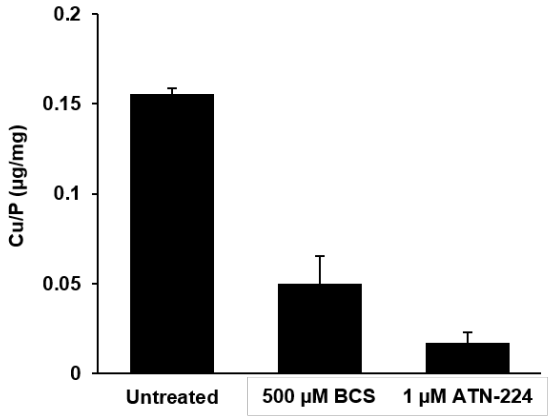

Figure 3.10 Copper chelators decrease cellular copper content of wildtype MEFs. Cells were treated with the indicated chelator for 48 hours before being harvested and analyzed by ICP-MS. Copper content is normalized to cellular phosphorous content.

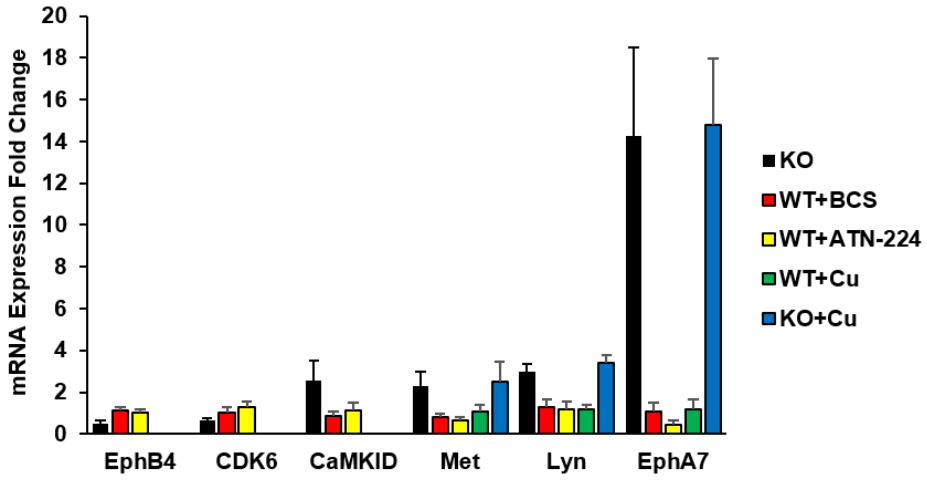

Figure 3.11 Copper chelation does not cause and copper addition does not rescue changes in gene expression observed between CTR1$^{-/-}$ MEFs and wildtype controls. Two genes expressed at lower levels in CTR1$^{-/-}$ MEFs (EphB4 and CDK6) and four genes expressed at higher levels in CTR1$^{-/-}$ MEFs (CaMKID, Met, Lyn, and EphA7) are shown. All bars represent mRNA expression relative to wildtype control, normalized to RPLP0. A ratio of 1 represents no change relative to wildtype. BCS (500 µM) and ATN-224 (1 µM) were applied for 48 hours before mRNA was harvested. Copper (5 µM $CuCl_2$) was applied 24 hours before mRNA was harvested. WT: wildtype, CTR1$^{+/+}$; KO: knockout, CTR1$^{-/-}$.

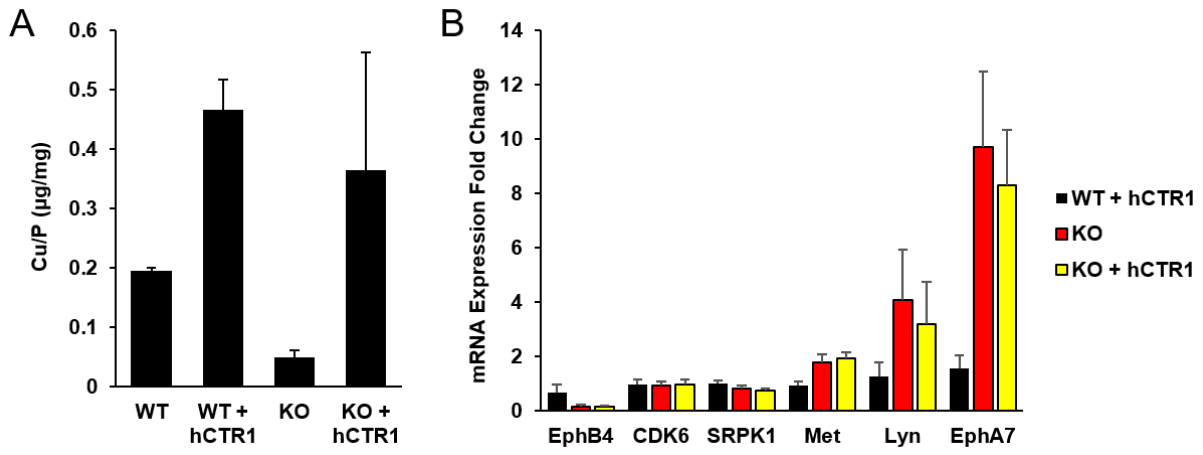

Figure 3.12 Transfection of CTR1$^{-/-}$ MEFs and wildtype MEFs with Myc-hCTR1 raises copper levels but does not alter expression of target genes. A) Copper content of wildtype and CTR1$^{-/-}$ MEFs transfected with vector control or Myc-hCTR1, normalized to cellular phosphorous levels, assessed by ICP-MS. B) Expression of select target genes in wildtype and CTR1$^{-/-}$ MEFs transfected with vector control or Myc-hCTR1, assessed by qPCR and normalized to RPLP0 expression. WT: wildtype, CTR1$^{+/+}$; KO: knockout, CTR1$^{-/-}$.

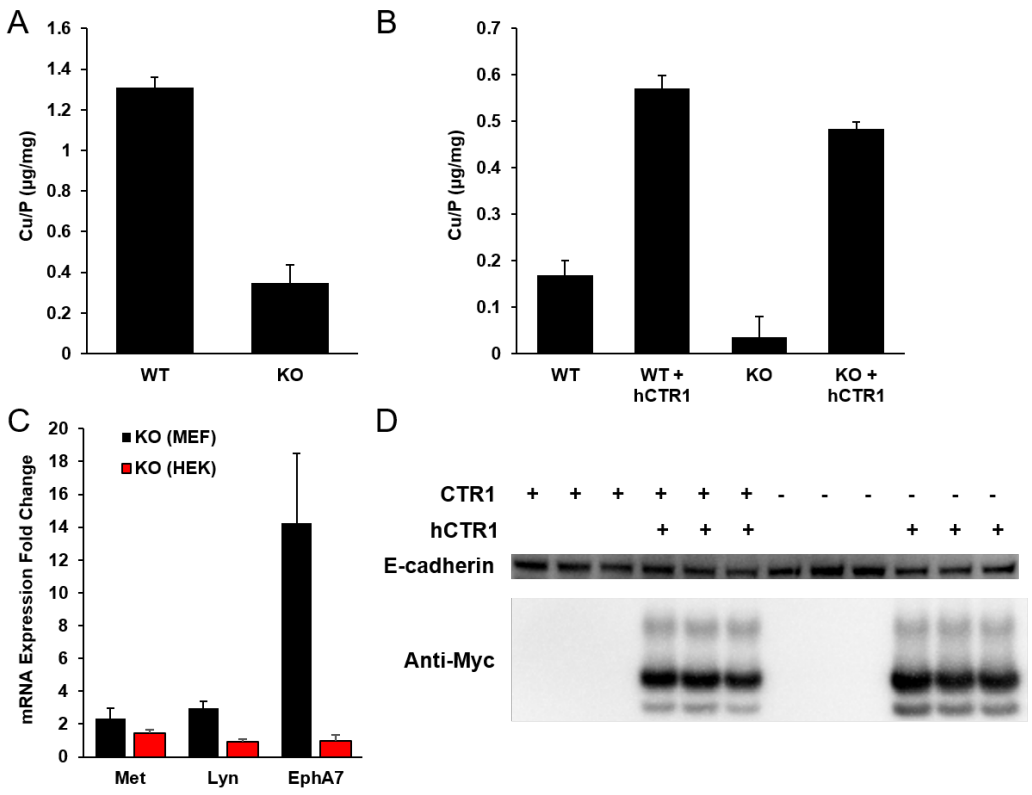

Figure 3.13 CTR1$^{-/-}$ HEK293T cells have lower copper levels than wildtype HEK293T cells, which can be rescued by transfection with Myc-hCTR1; however, CTR1$^{-/-}$ HEK293T cells do not display the changes in target gene expression or E-cadherin protein levels observed in CTR1$^{-/-}$ MEFs. A) Copper levels in CTR1$^{-/-}$ HEK293T cells and wildtype controls normalized to phosphorous, assessed by ICP-MS. B) Copper levels in CTR1$^{-/-}$ HEK293T cells and wildtype controls transfected with vector control or Myc-hCTR1, normalized to cellular phosphorous levels, assessed by ICP-MS. C) Expression of three genes with higher expression in CTR1$^{-/-}$ MEFs relative to wildtype MEFs. qRT-PCR shows no changes in the expression of these genes in CTR1$^{-/-}$ HEK293T cells relative to wildtype HEK293T cells. D) Western blots of E-cadherin levels and Myc-hCTR1 expression in CTR1$^{-/-}$ HEK293T cells and wildtype HEK293T cells transfected with vector control or Myc-hCTR1. WT: wildtype, CTR1$^{+/+}$; KO: knockout, CTR1$^{-/-}$.

A

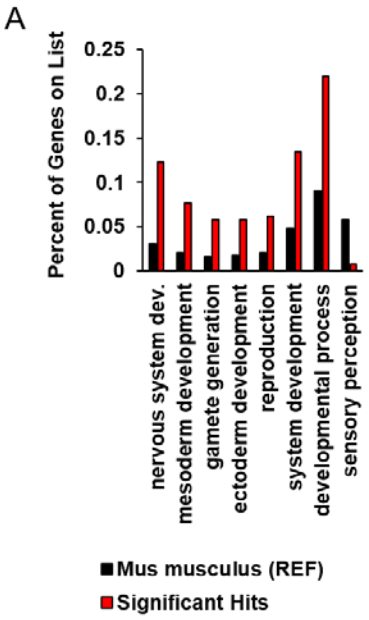

B

Analysis Type:	PANTHER Overrepresentation Test (release 20170413)					
Annotation Version and Release Date:	PANTHER version 11.1 Released 2016-10-24					
Analyzed List:	Client Text Box Input (Mus musculus) (Up&Down6)					
Reference List:	Mus musculus (all genes in database)					
Bonferroni correction:	TRUE					
Bonferroni count:	241					
PANTHER GO-Slim Biological Process	Mus musculus - REFLIST (22322)	Client Text Box Input (260)	Client Text Box Input (expected)	Client Text Box Input (over/under)	Client Text Box Input (fold Enrichment)	Client Text Box Input (P-value)
sensory perception of sound (GO:0007605)	69	6	0.8	+	7.47	4.36E-02
nervous system development (GO:0007399)	668	32	7.78	+	4.11	5.07E-09
mesoderm development (GO:0007498)	456	20	5.31	+	3.77	1.38E-04
gamete generation (GO:0007276)	362	15	4.22	+	3.56	7.00E-03
ectoderm development (GO:0007398)	396	15	4.61	+	3.25	1.90E-02
reproduction (GO:0000003)	462	16	5.38	+	2.97	3.07E-02
system development (GO:0048731)	1084	35	12.63	+	2.77	1.48E-05
developmental process (GO:0032502)	2027	57	23.61	+	2.41	8.89E-08
Unclassified (UNCLASSIFIED)	9053	77	105.45	-	0.73	0.00E+00
sensory perception (GO:0007600)	1283	2	14.94	-	< 0.2	7.09E-03

Figure 3.14 Genes involved in development are differentially regulated in CTR1$^{-/-}$ MEF cells compared to the *Mus musculus* reference genome. A) Select biological processes overrepresented in the list of differentially regulated genes from RNA sequencing of CTR1$^{-/-}$ MEFs. B) Analysis parameters used to calculate overrepresentation using the PANTHER tool. The analyzed list was a combined gene list of upregulated (>6-fold increase) and downregulated (>6-fold decrease) transcripts; see Appendix 1. The full list of overrepresented biological processes with p-values are listed.

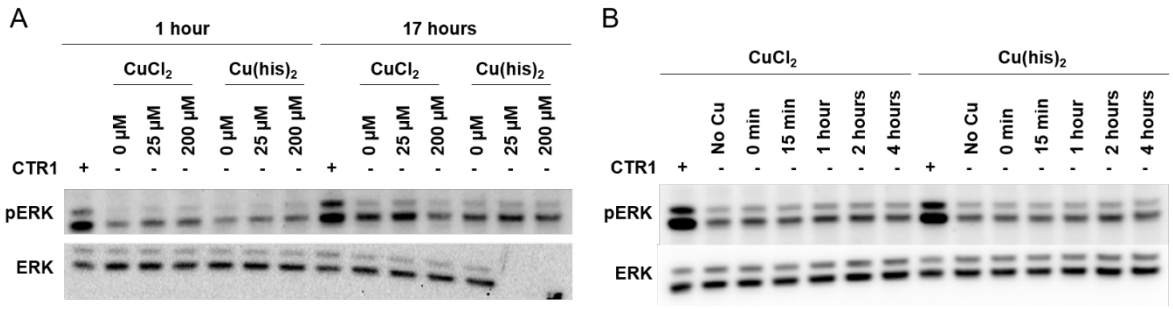

Figure 3.15 pERK1/2 levels are not altered by changes in copper levels in CTR1$^{-/-}$ MEFs. A) Western blots of MEFs of the indicated genotype treated with copper (II) chloride or a copper (II) histidine complex at the indicated concentrations and times in serum-free media and stimulated with EGF (200 ng/mL, 20 min). The total ERK blot deformed in the right corner, and samples were lost. B) Same as A. Copper dose was 200 µM.

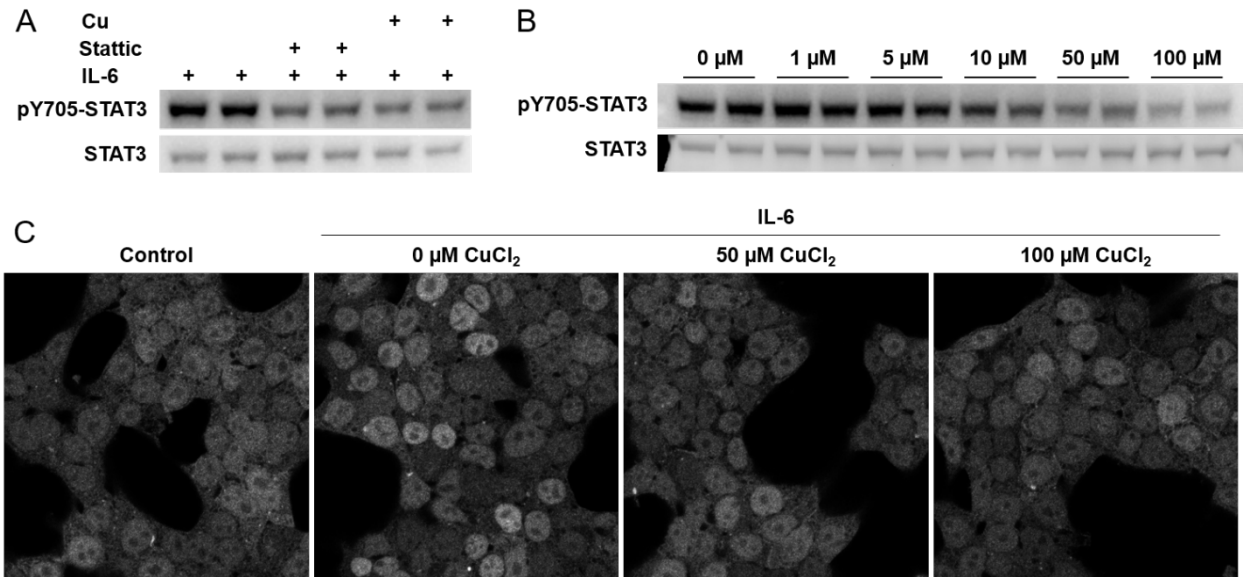

Figure 3.16 STAT3 activation is altered by cellular copper load. A) Western blot of HEK293T cells stimulated by IL-6 (50 ng/mL, 30 min) following treatment with vehicle, $CuCl_2$ (50 μM, 1 hour) or the STAT3 small-molecule inhibitor Stattic (20 μM, 1 hour). B) Western blot of HEK293T cells that were pre-treated for 1 hour with the indicated amount of $CuCl_2$ and stimulated with IL-6 (50 ng/mL, 30 min). C) Immunofluorescence of HEK293T cells pre-treated with the indicated concentration of copper, stimulated with IL-6 (50 ng/mL, 30 min), fixed, and stained for STAT3. pY705-STAT3: phosphotyrosine 705 on STAT3.

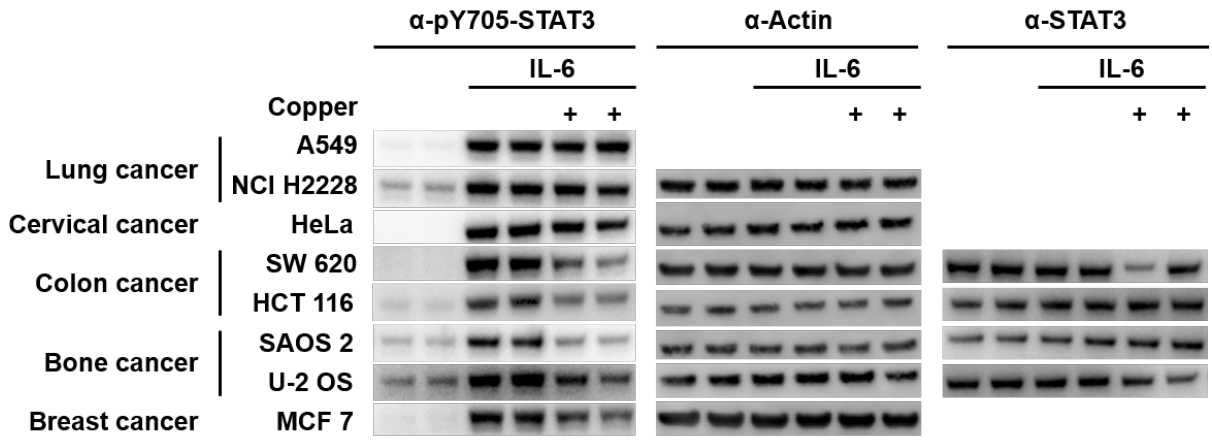

Figure 3.17 STAT3 activation is copper-dependent in some cancer cell lines, but not all. Western blots of lysates from the indicated cell lines pre-treated with 100 μM $CuCl_2$ for 1 hour and stimulated with IL-6 (10 ng/mL, 30 min). Actin and total STAT3 blots are provided for a subset of cell lines. pY705-STAT3: phosphotyrosine 705 on STAT3.

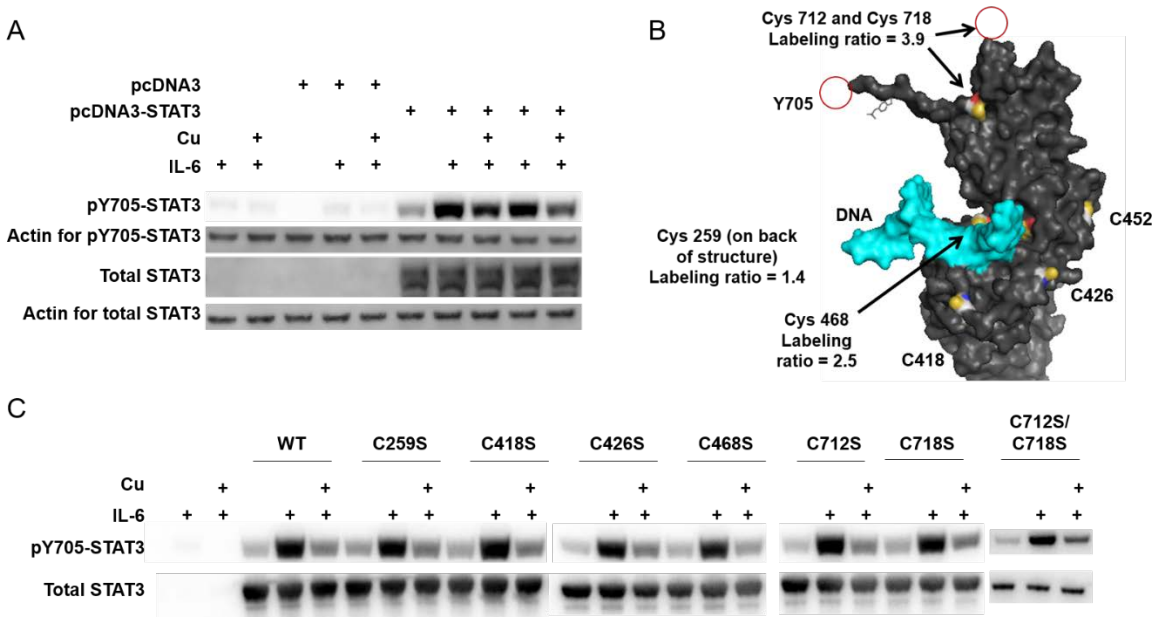

Figure 3.18 Activation of overexpressed STAT3 is dependent on copper levels, but not on surface-exposed STAT3 cysteines. A) Western blots of HEK293T cells transfected with wildtype STAT3 or vector control, pretreated with vehicle or 100 µM $CuCl_2$ for 1 hour and stimulated with IL-6 (50 ng/mL, 30 min). B) Graphical rendering of the locations of surface-exposed cysteines on STAT3. PDB: 1BG1. C) Western blots of HEK293T cells transfected with the indicated STAT3 mutants, pretreated with vehicle of 100 µM $CuCl_2$ for 1 hour and stimulated with IL-6 (50 ng/mL, 30 min). pY705-STAT3: phosphotyrosine 705 on STAT3.

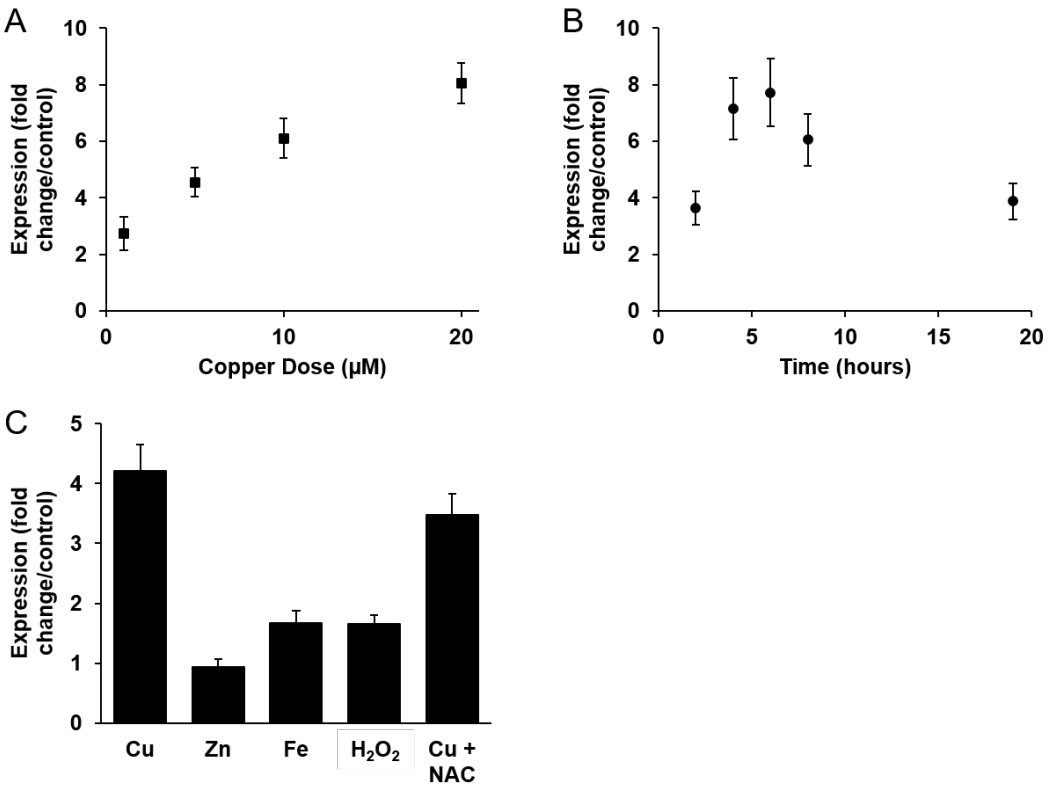

Figure 3.19 Expression of heme oxygenase 1 (HO1), a downstream target of Nrf2/Keap1, may be induced by copper treatment in a time- and dose-dependent manner, as well as in the presence of reductant. A) qPCR of HO1 from HEK293T cells treated with indicated concentration of copper for 7 hours. B) qPCR of HO1 from HEK293T cells treated with 10 μM $CuCl_2$ for the indicated time. C) qPCR of HO1 from HEK293T cells treated with 10 μM $CuCl_2$, 10 μM $ZnCl_2$, 10 μM ferrous ammonium sulfate, 100 μM H_2O_2, or 10 μM $CuCl_2$ + 50 μM N-acetyl cysteine for 3 hours.

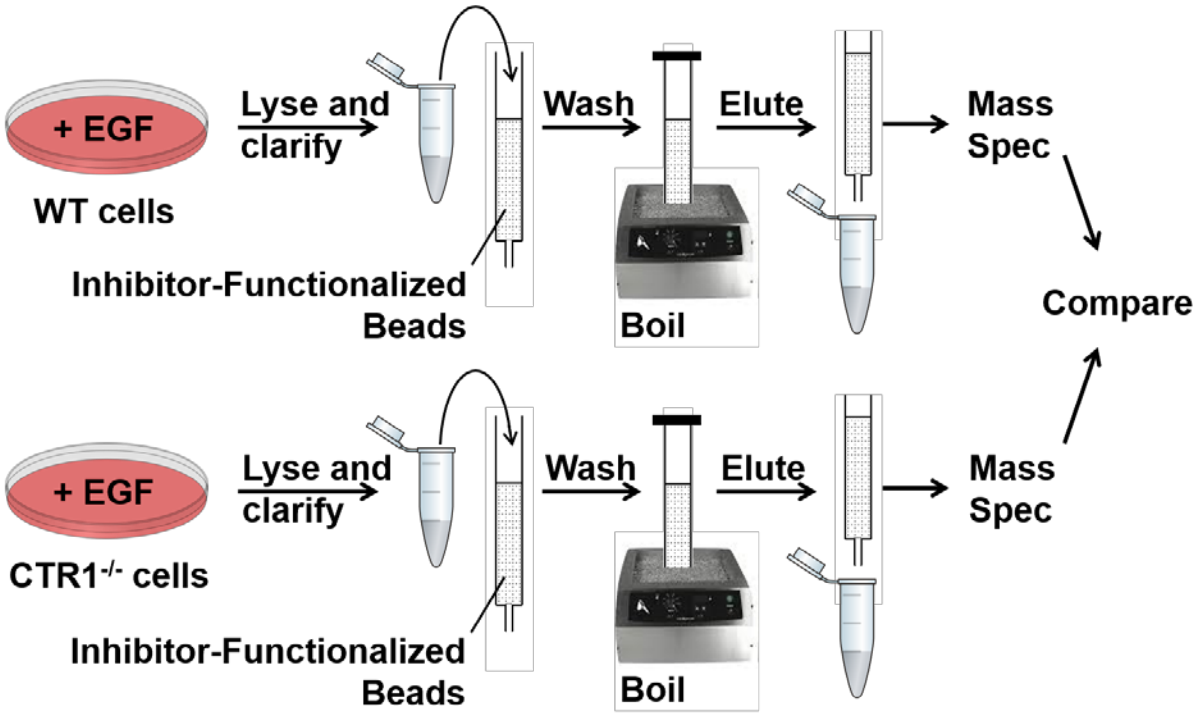

Scheme 3.1 Kinase activity profiling experimental scheme.

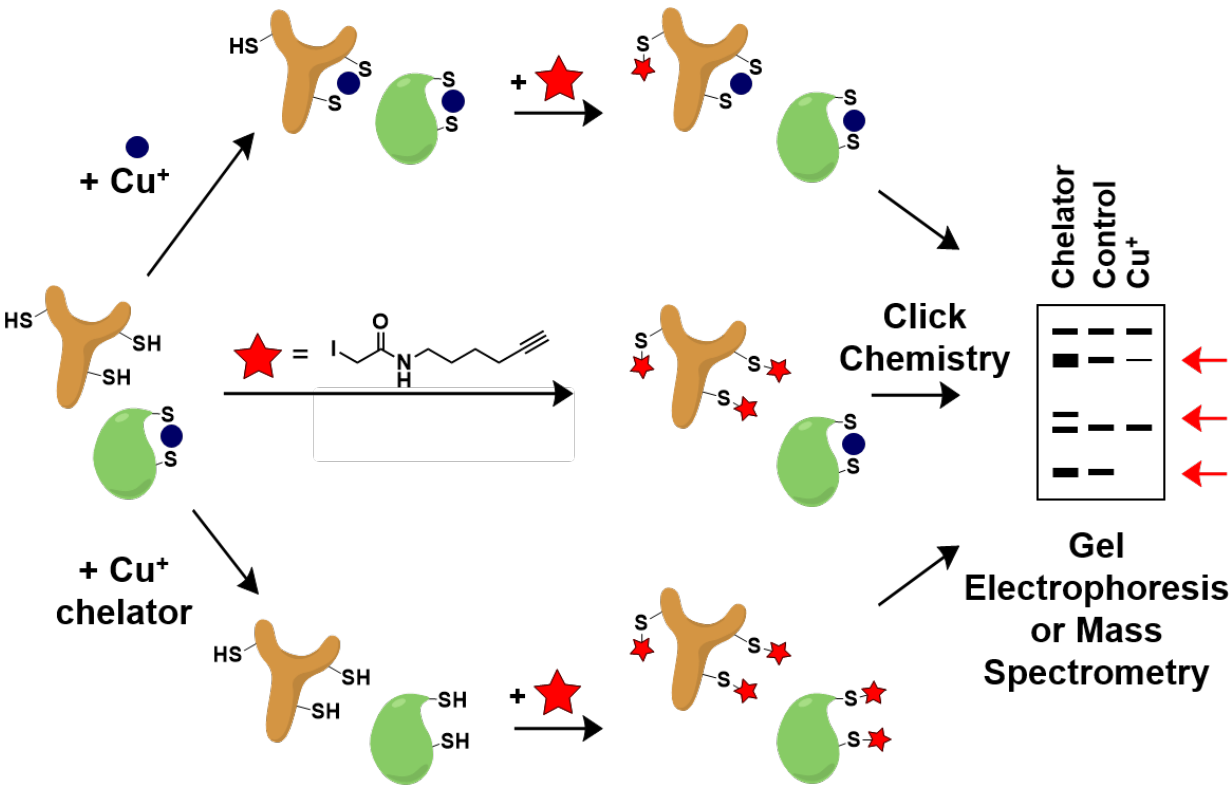

Scheme 3.2 Reactive cysteine profiling experimental scheme.

Inhibitors	Volume (µL)	Primary Targets
JG4	200	Hinge binder, promiscuous
VI16832	100	Hydrophobic, promiscuous
Staurosporine	75	Planar aromatic, promiscuous
Hydroxyl-PP2	100	SRC family
Purvalanol B	100	Cyclin-dependent kinases
GDC-0068	50	AKT
Dasatinib	100	SRC family
Sorafenib	50	BRAF
Crizotinib	50	MET
Lapatinib	50	EGFR, RIPK2
SB 202190	50	p38, non-canonical MAPKs
Maleimide X	50	Protein Kinase C

Table 3.1 Kinase inhibitors used in MIB profiling, in the order of addition to the bead column. Volume column displays the volume of a 50% bead slurry added to the column.

Acronym	Activity	RNA-seq	qPCR
EphA7	4.26	7.46	4.42
Rps6Ka4	3.62	1.33	1.08
CDK18	3.56	2.04	1.87
TAOK3	3.41	1.35	1.97
Map4K2	3.04	2.01	2.01
Met	2.74	2.71	2.97
Lyn	2.26	2.27	2.32
Fer	1.96	0.8	0.80
RpsKa1	1.96	1.48	1.65
CamK1d	1.79	2.16	2.57
STK3	1.67	1.09	1.46
MapK9	1.62	1.09	1.16
ACVR1	1.62	0.62	0.79
IRAK4	1.57	0.97	1.49
Map3K2	1.55	1.25	1.31
MapK3	1.55	1.25	1.72
Map2K1	1.54	1.01	1.18
MapK1	1.52	0.98	1.02

Table 3.2 Kinases with more mass counts in the CTR1$^{-/-}$ MIB eluent than the wildtype MIB eluent. The values in the “Activity” column denote the fold change in kinase activity between the knockout and wildtype cells (eg. EphA7 was pulled down 4.3x more from knockout cells than wildtype cells, suggesting a 4.3x increase in activity in knockout cells compared to wildtype). The values in the “RNA-seq” and “qPCR” columns denote the fold change in gene expression between the knockout and wildtype cells as assessed by these two methods (eg. EphA7 transcripts are 7.4x more abundant in knockout cells than wildtype cells as assessed by RNA sequencing and 4.4x more abundant as assessed by quantitative RT-PCR).

Acronym	Activity	RNA-seq	qPCR
PKN2	0.65	0.66	0.71
AURKB	0.65	0.92	0.99
RIPK2	0.63	0.77	0.76
CDK17	0.60	0.41	0.39
DDR2	0.60	0.68	0.64
EphB3	0.58	0.81	1.46
SPRK1	0.53	0.66	0.59
TAOK2	0.52	0.97	0.97
TAOK1	0.52	1.00	1.13
STK16	0.51	0.72	0.66
EGFR	0.51	1.13	1.76
BMPR2	0.50	0.91	1.13
PKCe	0.50	0.66	0.68
CK1γ2	0.46	0.71	0.79
CK1γ3	0.45	0.98	0.95
CDK4	0.45	0.80	1.04
CDKL5	0.45	0.90	0.94
CDK6	0.43	0.77	0.65
EphB4	0.37	0.44	0.50

Table 3.3 Kinases with fewer mass counts in the CTR1$^{-/-}$ MIB eluent than the wildtype MIB eluent. See Table 3.2 legend for details.

UniProt ID	Labeled Cys	Protein	Ratio	Std Dev	Rep No
Q6FI81	C249	CIAPIN1	20	NA	3
P53384	C25	NUBP1	20	NA	2
P53384	C235	NUBP1	20	NA	2
P53384	C277	NUBP1	20	NA	2
P07339	C117	CTSD	20	NA	2
Q6PJ69	C112	TRIM65	20	NA	2
Q7RTV0	C40	PHF5A	20	NA	2
Q9Y3E2	C18	BOLA1	18.0	3.54	4
Q9Y3E2	C20	BOLA1	18.0	3.54	4
P23921	C787	RRM1	16.6	5.93	4
P23921	C790	RRM1	16.6	5.93	4
P23921	C779	RRM1	16.0	7.01	4
O95793	C574	STAU1	12.8	5.29	3
O00244	C12	ATOX1	12.4	5.06	4
O00244	C15	ATOX1	12.4	5.06	4
Q13572	C391	ITPK1	11.5	4.13	2
Q13572	C403	ITPK1	11.5	4.13	2
Q3KQU3	C361	MAP7D1	9.85	7.19	3
P00441	C147	SOD1	8.96	5.30	4
Q9UJY4	C343	GGA2	8.9	3.31	2
Q3KQU3	C373	MAP7D1	6.02	2.14	3
Q9Y5Y2	C54	NUBP2	4.93	1.02	3
Q15005	C17	SPCS2	4.65	1.47	2
Q15005	C26	SPCS2	4.65	1.47	2
P54136	C32	RARS	4.37	0.60	3
P54136	C34	RARS	4.37	0.60	3
Q9UBB4	C354	ATXN10	4.29	1.30	2
Q9UBB4	C356	ATXN10	4.29	1.30	2
P85037	C254	FOXK1	4.09	0.69	2
Q96SK2	C158	TMEM209	3.97	1.46	2
P40763	C712	STAT3	3.85	1.03	3
P40763	C718	STAT3	3.85	1.03	3
Q53EZ4	C159	CEP55	3.79	0.54	2

Q9Y5Y2	C196	NUBP2	3.71	0.42	2
Q9Y5Y2	C199	NUBP2	3.71	0.42	2
Q9Y5Y2	C202	NUBP2	3.71	0.42	2
Q9H7E9	C42	C8orf33	3.54	7.23	3
Q9H7E9	C44	C8orf33	3.54	7.23	3
Q9H7E9	C50	C8orf33	3.54	7.23	3
Q9C0C2	C631	TNKS1BP1	3.51	8.25	2
Q14145	C288	KEAP1	3.51	0.02	2
Q147X3	C74	NAA30	3.51	0.47	2
Q15365	C201	PCBP1	3.46	0.52	4
P17509	C72	HOXB6	3.45	0.01	2
Q6FI81	C285	CIAPIN1	3.44	0.02	2
Q6FI81	C288	CIAPIN1	3.44	0.02	2
Q15365	C194	PCBP1	3.41	0.66	4
O14654	C658	IRS4	3.36	0.84	2
Q9UHQ1	C172	NARF	3.34	8.33	2
O95685	C26	PPP1R3D	3.28	0.44	2
P51610	C1139	HCFC1	3.13	1.17	3
P42166	C341	TMPO	3.13	0.30	2
Q9BRA2	C43	TXNDC17	3.12	1.41	4
P29401	C133	TKT	3.08	0.35	2
H3BVE0	C63	Uncharacterized	3	0.61	2
P60174	C124	TPI1	3	1.02	2
Q9H3K6	C31	BOLA2B	3	0.61	2

Table 3.4 Significant hits from copper-dependent reactive cysteine profiling with copper addition. The columns provide the UniProt ID (uniprot.org), number of the cysteine labeled, name of the protein containing that cysteine, ratio of labeling (control sample)/(copper addition sample), standard deviation of ratios from the replicates in which this cysteine was labeled, and number of replicates in which this cysteine was labeled.

Antibody	Supplier	Part No	Dilution	Use
p44/42 MAPK (ERK1/2) (137F5)	Cell Signaling	4695S	1:1000	WB
P-p44/42 MAPK (T202/Y204) (D13.14.4E)	Cell Signaling	4370P	1:1000	WB
β-actin (AC-15)	Santa Cruz	sc-69879	1:1000	WB
AKT pan (11E7)	Cell Signaling	4685S	1:1000	WB
pAKT (S473) (D9E)	Cell Signaling	4060S	1:1000	WB
Cortactin (p80/85) (4F11)	Millipore	05-180	1:1000	WB
pCortactin pY421	Millipore	AB3852	1:1000	WB
Phosphotyrosine (4G10)	Millipore	05-321	1:1000	WB
Fer (EP1842Y)	Abcam	ab52479	1:1000	WB
Fer (EP1842Y)	Abcam	ab52479	1:200	IP
E-cadherin (24E10)	Cell Signaling	3195S	1:1000	WB
Beta-catenin (6B3)	Cell Signaling	9582S	1:1000	WB
EGFR (1005)	Santa Cruz	sc-03	1:1000	WB
Phospho-EGFR (Tyr1068)	Cell Signaling	2234S	1:1000	WB
Myc (c-myc)	Life Technologies	132500	1:1000	WB
STAT3 (124H6)	Cell Signaling	9139S	1:1000	WB
STAT3 (124H6)	Cell Signaling	9139S	1:1500	IF
Phospho-STAT3 (Y705) (D3A7)	Cell Signaling	9145S	1:1000	WB
Goat anti-mouse HRP (secondary Ab)	Santa Cruz	sc-2005	1:2000	WB
Goat anti-rabbit HRP (secondary Ab)	Santa Cruz	sc-2007	1:5000	WB
Anti-mouse AlexaFluor-647 (secondary Ab)	Life Technologies	A31571	1:100	IF
Anti-mouse AlexaFluor-647 (secondary Ab)	Life Technologies	A31571	1:1000	WB

Table 3.5 Antibodies and conditions used for Western blots (WB), immunoprecipitation (IP) and immunofluorescence (IF).

Name	Sequence	Tm	Target/Purpose	Source	Pdt Size
mEphB4-F	GGAAACGGCGGATCTGAAATG	59.9	EPHB4_MOUSE	PrimerBank	124
mEphB4-R	TGGACGCTTCATGTCGCAC	61			
mBMPR2-F	TTGGGATAGGTGAGAGTCGAAT	58.4	BMPR2_MOUSE	PrimerBank	115
mBMPR2-R	TGTTTCACAAGATTGATGTCCCC	59.2			
mEGFR-F	GCCATCTGGGCCAAAGATACC	61.1	EGFR_MOUSE	PrimerBank	101
mEGFR-R	GTCTTCGCATGAATAGGCCAAT	59.1			
mEphA7-F	TGACCCTGAAACCTATGAGGAC	59.2	EPHA7_MOUSE	PrimerBank	104
mEphA7-R	ATTCTCCTGCACCAATCACAC	58.6			
mCDK6-F	GGCGTACCCACAGAAACCATA	60	CDK6_MOUSE	PrimerBank	187
mCDK6-R	AGGTAAGGGCCATCTGAAAACT	59.4			
mCDKL5-F	TGCAGACACAAGGAAACACAT	58.4	CDKL5_MOUSE	PrimerBank	108
mCDKL5-R	GCGAAGCATTTTAAGCTCTCGTA	59.7			
mCDK4-F	ATGGCTGCCACTCGATATGAA	59.6	CDK4_MOUSE	PrimerBank	129
mCDK4-R	TCCTCCATTAGGAACTCTCACAC	59.2			
mPKCe-F	GGGGTGTCATAGGAAAACAGG	58.3	KPCE_MOUSE	PrimerBank	146
mPKCe-R	GACGCTGAACCGTTGGGAG	61			
mSTK16-F	TGACAATAAGCGTTACCTCTTCG	58.8	STK16_MOUSE	PrimerBank	100
mSTK16-R	CAGGGCGTAGAAGTGTCCATC	60.5			
mTAOK1-F	AGCTGAATGAAAACCAGAGCAC	59.4	TAOK1_MOUSE	PrimerBank	158
mTAOK1-R	TCTTCTTTTGAAGCGACGACAT	58.6			
mTAOK2-F	AGGAAGTGCGGTTCTTACAGA	59	TAOK2_MOUSE	PrimerBank	109
mTAOK2-R	GAGCCCAGGCAATACTCCAT	59.5			
mSRPK1-F	AGGCCCGAAAGAAAAGGACC	60.3	SRPK1_MOUSE	PrimerBank	106
mSRPK1-R	TGCTCTGGGATGTCGCTCT	60.7			
mEphB3-F	CATGGACACGAAATGGGTGAC	59.5	EPHB3_MOUSE	PrimerBank	103
mEphB3-R	GCGGATAGGATTCATGGCTTCA	60.6			
mCDK18-F	TTGAGGAGTCGTTGGCTGAG	59.7	CDK18_MOUSE	PrimerBank	123
mCDK18-R	GGTTCTGCCGTTGTTGATACT	58.6			
mTAOK3-F	TTGCATGAAATTGGACATGGGA	58.8	TAOK3_MOUSE	PrimerBank	178
mTAOK3-R	CGATGGTGTTAGGATGCTTCAG	59.1			
mMap4K2-F	CTTCGAGCTGCTACAGCGT	60.2	M4K2_MOUSE	PrimerBank	109
mMap4K2-R	TGGGTCTAGCTTGACGATCTTC	59.6			
mLyn-F	ATCCAACGTCCAATAAACAGCA	58.6	LYN_MOUSE	PrimerBank	111
mLyn-R	ATAAGGCCACCACAATGTCAC	58.6			
mFer-F	ATTTGGGAGTGACCTGAAGAACT	59.6	FER_MOUSE	PrimerBank	225
mFer-R	TGCTGAATCATCAGTAGCCAAG	58.5			
mRps6ka1-F	CCATCACACACCACGTCAAG	59.1	KS6A1_MOUSE	PrimerBank	109
mRps6ka1-R	TTGCGTACCAGGAAGACTTTG	58.5			

mCam1kd-F	TTCGCAGTGAAGTGCATCCC	61	KCC1D_MOUSE	PrimerBank	80
mCam1kd-R	TTTCTAAGCACGGCAATCTCG	59			
mSTK3-F	CGGGGTCCGTTTCAGACATAA	60	STK3_MOUSE	PrimerBank	224
mSTK3-R	GCGTTTTGCCATTGTATCTGTT	58.4			
mMapk9-F	TCAGTGGGTTGCATCATGGG	60.3	MK09_MOUSE	PrimerBank	108
mMapk9-R	GGATGGTGTTCCTAGCTGTTCA	60			
mRps6ka4-F	GGTGAGCGTGGAGAACTTCG	61	KS6A4_MOUSE	PrimerBank	235
mRps6ka4-R	GAAGGCGTAGTGCAGTGTGA	60.3			
mACVR1-F	GTGGAAGATTACAAGCCACCA	58.2	ACVR1_MOUSE	PrimerBank	125
mACVR1-R	GGGTCTGAGAACCATCTGTTAGG	60.1			
mIRAK4-F	CATACGCAACCTTAATGTGGGG	59.6	IRAK4_MOUSE	PrimerBank	125
mIRAK4-R	GGAACTGATTGTATCTGTCGTCG	59.2			
mMap3k2-F	TTCAATCATGCAAGATTTGGCTG	58.5	M3K2_MOUSE	PrimerBank	227
mMap3k2-R	AGTGTAGATCCATAGACTGCCC	58.8			
mMapK3-F	TCCGCCATGAGAATGTTATAGGC	60.6	MK03_MOUSE	PrimerBank	248
mMapK3-R	GGTGGTGTTGATAAGCAGATTGG	59.9			
mMap2K1-F	AAGGTGGGGGAACTGAAGGAT	60.8	M2K1_MOUSE	PrimerBank	149
mMap2K1-R	CGGATTGCGGGTTTGATCTC	59.3			
mMapK1-F	CAGGTGTTCGACGTAGGGC	60.5	MK01_MOUSE	PrimerBank	139
mMapK1-R	TCTGGTGCTCAAAAGGACTGA	59.2			
mDDR2-F	ATCACAGCCTCAAGTCAGTGG	60	DDR2_MOUSE	PrimerBank	116
mDDR2-R	TTCAGGTCATCGGGTTGCAC	60.6			
mCDK17-F	TTTAAGAGGAGACTGTCCCTCAC	59.2	CDK17_MOUSE	PrimerBank	110
mCDK17-R	TCGTTGTCCTTGCTACTGCTC	60.3			
mRIPK2-F	ATCCCGTACCACAAGCTCG	59.5	RIPK2_MOUSE	PrimerBank	118
mRIPK2-R	GGATGTGTAGGTGCTTCACTG	58.7			
mAURKB-F	CAGAAGGAGAACGCCTACCC	59.8	AURKB_MOUSE	PrimerBank	117
mAURKB-R	GAGAGCAAGCGCAGATGTC	59			
mPKN2-F	TGTCCAATGATGTTTGTGCTGT	59	PKN2_MOUSE	PrimerBank	120
mPKN2-R	GTGACCTGTCTAGTTCCAGTGTA	59.2			
mMap4k3-F	GCAAAGCCATCCCACGTTC	59.8	M4K3_MOUSE	PrimerBank	106
mMap4k3-R	GCTCACCATTTAGCTGGAAGG	59			
mCsn1g2-F	AGGAGTACATCGACCCTGAGA	59.4	KC1G2_MOUSE	PrimerBank	112
mCsn1g2-R	CTCTGCTCTTTGCCCAAGTG	59.1			
mCsn1g3-F	TGGGACCGAGTTTGGAGGATT	61.1	KC1G3_MOUSE	PrimerBank	165
mCsn1g3-R	CTGGCCGTCCTATTAAGAAGTTC	58.9			
mMet-F	GTGAACATGAAGTATCAGCTCCC	59.1	MET_MOUSE	PrimerBank	100
mMet-R	TGTAGTTTGTGGCTCCGAGAT	59.1			
mRPLP0-F	AGATTCGGGATATGCTGTTGGC	60.8	RPLP0_MOUSE	PrimerBank	109
mRPLP0-R	TCGGGTCCTAGACCAGTGTTC	60.9			

mID1-F	CCTAGCTGTTCGCTGAAGGC	61.1	ID1_MOUSE	PrimerBank	141
mID1-R	GTAGAGCAGGACGTTCACCT	59.1			
mID2-F	ATGAAAGCCTTCAGTCCGGTG	60.6	ID2_MOUSE	PrimerBank	107
mID2-R	AGCAGACTCATCGGGTCGT	60.7			
mID3-F	CTGTCGGAACGTAGCCTGG	60.2	ID3_MOUSE	PrimerBank	90
mID3-R	GTGGTTCATGTCGTCCAAGAG	58.9			
hHO-1-F	AAGACTGCGTTCCTGCTCAAC	61.1	HMOX1_HUMAN	PrimerBank	247
hHO-2-R	AAAGCCCTACAGCAACTGTCG	60.9			
C259S REV	GAGGGCCTCCGATGCACG	59	STAT3 mutation	NEB	
C259S FWD	CCAACATCAGCCTGGACCGTCTG	59	STAT3 mutation	NEB	
C418S REV	CTAAGGGTCAGGTGCTTGAACTCTGC	59	STAT3 mutation	NEB	
C418S FWD	GGAGCAGAGAAGTGGGAATGGAGG	59	STAT3 mutation	NEB	
C426S REV	GCCTCCATTCCCACATCTCTGCT	59	STAT3 mutation	NEB	
C426S FWD	CGTGCCAATAGTGATGCCTCCTTG	59	STAT3 mutation	NEB	
C428S REV	CCACAACTGGCAAGGAGTGGGT	59	STAT3 mutation	NEB	
C468S FWD	TGATCTCCAACATCAGTCAGATGCCAAATG	59	STAT3 mutation	NEB	
C712S REV	GTCTTCAGGTACGGGGCAGCAC	59	STAT3 mutation	NEB	
C718S REV	TGTCACACAGATGAACTTGGTCTTCAGG	59	STAT3 mutation	NEB	
C712S FWD	CAAGTTCATCAGTGTGACACCAACGAC	59	STAT3 mutation	NEB	
C718S FWD	CCAACGACCAGCAGCAATACCATTG	59	STAT3 mutation	NEB	

Table 3.6 Primers used for qRT-PCR and cloning. Name indicates the primer name; “m” is for mouse targets; “h” is for human targets. T_m is the annealing temperature used for that primer. Target/Purpose indicates the gene name of the target for qPCR primers and the purpose of the primers used for cloning. Source indicates how the primers were found or created. NEB is the NEBaseChanger online tool (http://nebasechanger.neb.com/). Pdt size applies only to qPCR primers and indicates the size of the amplified fragment.

References

1 Nevitt, T., Öhrvik, H. & Thiele, D. J. Charting the travels of copper in eukaryotes from yeast to mammals. *Biochimica et Biophysica Acta (BBA) - Molecular Cell Research* **1823**, 1580-1593, doi:10.1016/j.bbamcr.2012.02.011 (2012).

2 Besold, A. N., Culbertson, E. M. & Culotta, V. C. The Yin and Yang of copper during infection. *JBIC Journal of Biological Inorganic Chemistry* **21**, 137-144, doi:10.1007/s00775-016-1335-1 (2016).

3 Lutsenko, S., Bhattacharjee, A. & Hubbard, A. L. Copper handling machinery of the brain. *Metallomics* **2**, 596, doi:10.1039/c0mt00006j (2010).

4 Rubino, J. T. & Franz, K. J. Coordination chemistry of copper proteins: How nature handles a toxic cargo for essential function. *Journal of Inorganic Biochemistry* **107**, 129-143, doi:10.1016/j.jinorgbio.2011.11.024 (2012).

5 Krishnamoorthy, L. *et al.* Copper regulates cyclic-AMP-dependent lipolysis. *Nature Chemical Biology* **12**, 586-592, doi:10.1038/nchembio.2098 (2016).

6 Turski, M. L. *et al.* A Novel Role for Copper in Ras/Mitogen-Activated Protein Kinase Signaling. *Molecular and Cellular Biology* **32**, 1284-1295, doi:10.1128/mcb.05722-11 (2012).

7 Brady, D. C. *et al.* Copper is required for oncogenic BRAF signalling and tumorigenesis. *Nature* **509**, 492-496, doi:10.1038/nature13180 (2014).

8 Chang, C. J. Searching for harmony in transition-metal signaling. *Nature Chemical Biology* **11**, 744-747, doi:10.1038/nchembio.1913 (2015).

9 Lehninger, A. L., Nelson, D. L. & Cox, M. M. *Lehninger principles of biochemistry*. 5th edn, (W.H. Freeman, 2008).

10 Wu, P., Nielsen, T. E. & Clausen, M. H. Small-molecule kinase inhibitors: an analysis of FDA-approved drugs. *Drug Discovery Today* **21**, 5-10, doi:10.1016/j.drudis.2015.07.008 (2016).

11 Zhang, J. *et al.* Effects of 31 FDA approved small-molecule kinase inhibitors on isolated rat liver mitochondria. *Archives of Toxicology*, doi:10.1007/s00204-016-1918-1 (2016).

12 Lee, J., Prohaska, J. R. & Thiele, D. J. Essential role for mammalian copper transporter Ctr1 in copper homeostasis and embryonic development. *Proceedings of the National Academy of Sciences* **98**, 6842-6847, doi:10.1073/pnas.111058698 (2001).

13 Lee, J., Petris, M. J. & Thiele, D. J. Characterization of Mouse Embryonic Cells Deficient in the Ctr1 High Affinity Copper Transporter. *Journal of Biological Chemistry* **277**, 40253-40259, doi:10.1074/jbc.M208002200 (2002).

14 Haas, K. L., Putterman, A. B., White, D. R., Thiele, D. J. & Franz, K. J. Model Peptides Provide New Insights into the Role of Histidine Residues as Potential Ligands in Human Cellular Copper Acquisition via Ctr1. *Journal of the American Chemical Society* **133**, 4427-4437, doi:10.1021/ja108890c (2011).

15 Ivy, K. D. & Kaplan, J. H. A Re-Evaluation of the Role of hCTR1, the Human High-Affinity Copper Transporter, in Platinum-Drug Entry into Human Cells. *Molecular Pharmacology* **83**, 1237-1246, doi:10.1124/mol.113.085068 (2013).

16 Ramos, D. *et al.* Mechanism of Copper Uptake from Blood Plasma Ceruloplasmin by Mammalian Cells. *Plos One* **11**, e0149516, doi:10.1371/journal.pone.0149516 (2016).
17 Bertinato, J., Cheung, L., Hoque, R. & Plouffe, L. J. Ctr1 transports silver into mammalian cells. *Journal of Trace Elements in Medicine and Biology* **24**, 178-184, doi:10.1016/j.jtemb.2010.01.009 (2010).
18 Ceresa, B. P. & Peterson, J. L. Cell and Molecular Biology of Epidermal Growth Factor Receptor. *International Review of Cell and Molecular Biology* **313**, 145-178, doi:10.1016/b978-0-12-800177-6.00005-0 (2014).
19 Guo, G. *et al.* Ligand-Independent EGFR Signaling. *Cancer Research* **75**, 3436-3441, doi:10.1158/0008-5472.can-15-0989 (2015).
20 Duncan, James S. *et al.* Dynamic Reprogramming of the Kinome in Response to Targeted MEK Inhibition in Triple-Negative Breast Cancer. *Cell* **149**, 307-321, doi:10.1016/j.cell.2012.02.053 (2012).
21 Sos, Martin L. *et al.* Oncogene Mimicry as a Mechanism of Primary Resistance to BRAF Inhibitors. *Cell Reports* **8**, 1037-1048, doi:10.1016/j.celrep.2014.07.010 (2014).
22 Reddi, Amit R. & Culotta, Valeria C. SOD1 Integrates Signals from Oxygen and Glucose to Repress Respiration. *Cell* **152**, 224-235, doi:10.1016/j.cell.2012.11.046 (2013).
23 Turski, M. L. *et al.* A Novel Role for Copper in Ras/Mitogen-Activated Protein Kinase Signaling. *Mol. Cell Biol.* **32**, 1284-1295, doi:10.1128/mcb.05722-11 (2012).
24 Greer, P. Closing in on the biological functions of fps/fes and fer. *Nature Reviews Molecular Cell Biology* **3**, 278-289, doi:10.1038/nrm783 (2002).
25 Piedra, J. *et al.* p120 Catenin-Associated Fer and Fyn Tyrosine Kinases Regulate -Catenin Tyr-142 Phosphorylation and -Catenin- -Catenin Interaction. *Molecular and Cellular Biology* **23**, 2287-2297, doi:10.1128/mcb.23.7.2287-2297.2003 (2003).
26 Xu, G. *et al.* Continuous association of cadherin with -catenin requires the non-receptor tyrosine-kinase Fer. *Journal of Cell Science* **117**, 3207-3219, doi:10.1242/jcs.01174 (2004).
27 Sangrar, W., Gao, Y., Scott, M., Truesdell, P. & Greer, P. A. Fer-Mediated Cortactin Phosphorylation Is Associated with Efficient Fibroblast Migration and Is Dependent on Reactive Oxygen Species Generation during Integrin-Mediated Cell Adhesion. *Molecular and Cellular Biology* **27**, 6140-6152, doi:10.1128/mcb.01744-06 (2007).
28 Craig, A. W. B., Zirngibl, R., Williams, K., Cole, L. A. & Greer, P. A. Mice Devoid of Fer Protein-Tyrosine Kinase Activity Are Viable and Fertile but Display Reduced Cortactin Phosphorylation. *Molecular and Cellular Biology* **21**, 603-613, doi:10.1128/mcb.21.2.603-613.2001 (2001).
29 Oneyama, C. *et al.* Fer tyrosine kinase oligomer mediates and amplifies Src-induced tumor progression. *Oncogene* **35**, 501-512, doi:10.1038/onc.2015.110 (2015).

30 Truong, T. H. & Carroll, K. S. Redox Regulation of Epidermal Growth Factor Receptor Signaling through Cysteine Oxidation. *Biochemistry* **51**, 9954-9965, doi:10.1021/bi301441e (2012).
31 Heppner, D. E. & van der Vliet, A. Redox-dependent regulation of epidermal growth factor receptor signaling. *Redox Biology* **8**, 24-27, doi:10.1016/j.redox.2015.12.002 (2016).
32 Tsai, C.-Y., Larson, C. A., Safaei, R. & Howell, S. B. Molecular modulation of the copper and cisplatin transport function of CTR1 and its interaction with IRS-4. *Biochemical Pharmacology* **90**, 379-387, doi:10.1016/j.bcp.2014.06.019 (2014).
33 Tsai, C.-Y., Liebig, J. K., Tsigelny, I. F. & Howell, S. B. The copper transporter 1 (CTR1) is required to maintain the stability of copper transporter 2 (CTR2). *Metallomics* **7**, 1477-1487, doi:10.1039/c5mt00131e (2015).
34 Wang, S.-S. *et al.* Gdf6 induces commitment of pluripotent mesenchymal C3H10T1/2 cells to the adipocyte lineage. *FEBS Journal* **280**, 2644-2651, doi:10.1111/febs.12256 (2013).
35 Calbet, J. *et al.* Genetic and Evolutionary Analyses of the Human Bone Morphogenetic Protein Receptor 2 (BMPR2) in the Pathophysiology of Obesity. *PLoS ONE* **6**, e16155, doi:10.1371/journal.pone.0016155 (2011).
36 Cai, J., Pardali, E., Sánchez-Duffhues, G. & ten Dijke, P. BMP signaling in vascular diseases. *FEBS Letters* **586**, 1993-2002, doi:10.1016/j.febslet.2012.04.030 (2012).
37 Krishnamoorthy, L. *et al.* Copper regulates cyclic-AMP-dependent lipolysis. *Nat. Chem. Biol.* **12**, 586-592, doi:10.1038/nchembio.2098 (2016).
38 Zimnicka, A. M. *et al.* Upregulated Copper Transporters in Hypoxia-Induced Pulmonary Hypertension. *PLoS ONE* **9**, e90544, doi:10.1371/journal.pone.0090544 (2014).
39 Bogaard, H. J. *et al.* Copper Dependence of Angioproliferation in Pulmonary Arterial Hypertension in Rats and Humans. *American Journal of Respiratory Cell and Molecular Biology* **46**, 582-591, doi:10.1165/rcmb.2011-0296OC (2012).
40 Lavery, K., Swain, P., Falb, D. & Alaoui-Ismaili, M. H. BMP-2/4 and BMP-6/7 Differentially Utilize Cell Surface Receptors to Induce Osteoblastic Differentiation of Human Bone Marrow-derived Mesenchymal Stem Cells. *Journal of Biological Chemistry* **283**, 20948-20958, doi:10.1074/jbc.M800850200 (2008).
41 David, L., Feige, J.-J. & Bailly, S. Emerging role of bone morphogenetic proteins in angiogenesis. *Cytokine & Growth Factor Reviews* **20**, 203-212, doi:10.1016/j.cytogfr.2009.05.001 (2009).
42 ten Dijke, P., Korchynskyi, O., Valdimarsdottir, G. & Goumans, M.-J. Controlling cell fate by bone morphogenetic protein receptors. *Molecular and Cellular Endocrinology* **211**, 105-113, doi:10.1016/j.mce.2003.09.016 (2003).
43 Miyazono, K. & Miyazawa, K. Id: A Target of BMP Signaling. *Science Signaling* **2002**, pe40, doi:10.1126/stke.2002.151.pe40 (2002).
44 Haremaki, T., Fraser, S. T., Kuo, Y. M., Baron, M. H. & Weinstein, D. C. Vertebrate Ctr1 coordinates morphogenesis and progenitor cell fate and regulates embryonic stem cell differentiation. *Proceedings of the National Academy of Sciences* **104**, 12029-12034, doi:10.1073/pnas.0701413104 (2007).

45 Pace, N. J. & Weerapana, E. A Competitive Chemical-Proteomic Platform To Identify Zinc-Binding Cysteines. *ACS Chemical Biology* **9**, 258-265, doi:10.1021/cb400622q (2014).
46 Lippard, S. J. & Berg, J. M. *Principles of Bioinorganic Chemistry*. (University Science Books, 1994).
47 Weerapana, E. *et al.* Quantitative reactivity profiling predicts functional cysteines in proteomes. *Nature* **468**, 790-795, doi:10.1038/nature09472 (2010).
48 Strausak, D. *et al.* Kinetic Analysis of the Interaction of the Copper Chaperone Atox1 with the Metal Binding Sites of the Menkes Protein. *Journal of Biological Chemistry* **278**, 20821-20827, doi:10.1074/jbc.M212437200 (2003).
49 Badarau, A. & Dennison, C. Copper Trafficking Mechanism of CXXC-Containing Domains: Insight from the pH-Dependence of Their Cu(I) Affinities. *Journal of the American Chemical Society* **133**, 2983-2988, doi:10.1021/ja1091547 (2011).
50 Weerapana, E., Speers, A. E. & Cravatt, B. F. Tandem orthogonal proteolysis-activity-based protein profiling (TOP-ABPP)—a general method for mapping sites of probe modification in proteomes. *Nature Protocols* **2**, 1414-1425, doi:10.1038/nprot.2007.194 (2007).
51 Jackson, C., Ruzevick, J., Amin, A. G. & Lim, M. Potential Role for STAT3 Inhibitors in Glioblastoma. *Neurosurgery Clinics of North America* **23**, 379-389, doi:10.1016/j.nec.2012.04.002 (2012).
52 Banerjee, K. & Resat, H. Constitutive activation of STAT3 in breast cancer cells: A review. *International Journal of Cancer* **138**, 2570-2578, doi:10.1002/ijc.29923 (2016).
53 Lebedeva, I. V., Yu, X., He, L., Cao, P. & Yu, Q. Eriocalyxin B Inhibits STAT3 Signaling by Covalently Targeting STAT3 and Blocking Phosphorylation and Activation of STAT3. *Plos One* **10**, e0128406, doi:10.1371/journal.pone.0128406 (2015).
54 Schust, J., Sperl, B., Hollis, A., Mayer, T. U. & Berg, T. Stattic: A Small-Molecule Inhibitor of STAT3 Activation and Dimerization. *Chemistry & Biology* **13**, 1235-1242, doi:10.1016/j.chembiol.2006.09.018 (2006).
55 Zhang, D. D., Lo, S. C., Cross, J. V., Templeton, D. J. & Hannink, M. Keap1 Is a Redox-Regulated Substrate Adaptor Protein for a Cul3-Dependent Ubiquitin Ligase Complex. *Molecular and Cellular Biology* **24**, 10941-10953, doi:10.1128/mcb.24.24.10941-10953.2004 (2004).
56 Zhang, D. D. & Hannink, M. Distinct Cysteine Residues in Keap1 Are Required for Keap1-Dependent Ubiquitination of Nrf2 and for Stabilization of Nrf2 by Chemopreventive Agents and Oxidative Stress. *Molecular and Cellular Biology* **23**, 8137-8151, doi:10.1128/mcb.23.22.8137-8151.2003 (2003).
57 Yang, J., Carroll, K. S. & Liebler, D. C. The Expanding Landscape of the Thiol Redox Proteome. *Molecular & Cellular Proteomics* **15**, 1-11, doi:10.1074/mcp.O115.056051 (2016).
58 Sobotta, M. C. *et al.* Peroxiredoxin-2 and STAT3 form a redox relay for H2O2 signaling. *Nature Chemical Biology* **11**, 64-70, doi:10.1038/nchembio.1695 (2014).
59 Kuo, Y. M., Zhou, B., Cosco, D. & Gitschier, J. The copper transporter CTR1 provides an essential function in mammalian embryonic development.

Proceedings of the National Academy of Sciences **98**, 6836-6841, doi:10.1073/pnas.111057298 (2001).

60 Takahashi, Y. *et al.* Mammalian Copper Chaperone Cox17p Has an Essential Role in Activation of Cytochrome c Oxidase and Embryonic Development. *Molecular and Cellular Biology* **22**, 7614-7621, doi:10.1128/mcb.22.21.7614-7621.2002 (2002).

61 Wee, N. K. Y., Weinstein, D. C., Fraser, S. T. & Assinder, S. J. The mammalian copper transporters CTR1 and CTR2 and their roles in development and disease. *The International Journal of Biochemistry & Cell Biology* **45**, 960-963, doi:10.1016/j.biocel.2013.01.018 (2013).

62 Bustos, R. I. *et al.* Copper deficiency alters cell bioenergetics and induces mitochondrial fusion through up-regulation of MFN2 and OPA1 in erythropoietic cells. *Biochemical and Biophysical Research Communications* **437**, 426-432, doi:10.1016/j.bbrc.2013.06.095 (2013).

63 Ruiz, L. M. *et al.* Non-cytotoxic copper overload boosts mitochondrial energy metabolism to modulate cell proliferation and differentiation in the human erythroleukemic cell line K562. *Mitochondrion* **29**, 18-30, doi:10.1016/j.mito.2016.04.005 (2016).

64 Ishida, S., Andreux, P., Poitry-Yamate, C., Auwerx, J. & Hanahan, D. Bioavailable copper modulates oxidative phosphorylation and growth of tumors. *Proceedings of the National Academy of Sciences* **110**, 19507-19512, doi:10.1073/pnas.1318431110 (2013).

65 Shen, Y.-A., Wang, C.-Y., Hsieh, Y.-T., Chen, Y.-J. & Wei, Y.-H. Metabolic reprogramming orchestrates cancer stem cell properties in nasopharyngeal carcinoma. *Cell Cycle* **14**, 86-98, doi:10.4161/15384101.2014.974419 (2014).

66 Hatori, Y. *et al.* Neuronal differentiation is associated with a redox-regulated increase of copper flow to the secretory pathway. *Nature Communications* **7**, 10640, doi:10.1038/ncomms10640 (2016).

67 Ogra, Y. *et al.* Changes in intracellular copper concentration and copper-regulating gene expression after PC12 differentiation into neurons. *Scientific Reports* **6**, doi:10.1038/srep33007 (2016).

68 Hatori, Y. & Lutsenko, S. The Role of Copper Chaperone Atox1 in Coupling Redox Homeostasis to Intracellular Copper Distribution. *Antioxidants* **5**, 25, doi:10.3390/antiox5030025 (2016).

69 Freestone, D. *et al.* Copper and lactational hormones influence the CTR1 copper transporter in PMC42-LA mammary epithelial cell culture models. *The Journal of Nutritional Biochemistry* **25**, 377-387, doi:10.1016/j.jnutbio.2013.11.011 (2014).

70 Sharma-Bhandari, A., Park, S.-H., Kim, J.-Y., Oh, J. & Kim, Y. Lysyl oxidase modulates the osteoblast differentiation of primary mouse calvaria cells. *International Journal of Molecular Medicine* **36**, 1664-1670, doi:10.3892/ijmm.2015.2384 (2015).

71 Serrano-Gomez, S. J., Maziveyi, M. & Alahari, S. K. Regulation of epithelial-mesenchymal transition through epigenetic and post-translational modifications. *Molecular Cancer* **15**, doi:10.1186/s12943-016-0502-x (2016).

72 Fujie, T. *et al.* Copper diethyldithiocarbamate as an activator of Nrf2 in cultured vascular endothelial cells. *JBIC Journal of Biological Inorganic Chemistry* **21**, 263-273, doi:10.1007/s00775-016-1337-z (2016).
73 Zhong, Z., Wen, Z. & Darnell, J. E. Stat3 and Stat4: members of the family of signal transducers and activators of transcription. *Proceedings of the National Academy of Sciences* **91**, 4806-4810, doi:10.1073/pnas.91.11.4806 (1994).

Chapter 4

New Genetic Tools for Studying Copper Import

Introduction

Copper is an essential micronutrient in eukaryotic systems, required for diverse processes including cellular respiration and maintenance of the extracellular matrix.[1-3] Like all elements, copper cannot be created or destroyed within a biological system; thus, copper homeostasis depends on the orderly import and export of copper across cell layers and tissues for regulated distribution of copper throughout the body.[4,5] Copper transporter 1 (CTR1) is the only known mammalian high-affinity copper import protein.[6-8] It is responsible for the import of ~70% of total copper uptake in mammalian cells,[9] and the deletion of this transporter is lethal in mice.[10,11] Human CTR1 (hCTR1) is relatively small, comprising 190 amino acids that form 3 transmembrane domains; in order to form a pore, hCTR1 has been shown to trimerize in the plasma membrane.[12,13] The extracellular N-terminus of hCTR1 is rich in histidine and methionine residues, which are thought to coordinate copper in the extracellular space and facilitate copper uptake.[14-16] The C-terminus, in the intracellular space, is involved in regulating hCTR1 localization and copper uptake.[17-19]

Interestingly, CTR1 is not known to possess an “off” or “closed” state. Instead, under conditions of high copper, CTR1 internalizes, shutting the cell off to the import of additional copper.[20-22] Mutants of CTR1 that are unable to internalize mediate unregulated copper uptake, leading to cell death.[17] In mammalian cells, CTR1 internalization has been shown to be clathrin-dependent.[23] Internalized CTR1 has been observed in endosomal compartments, from which it may be recycled back to the plasma membrane.[23] Despite these advances, the regulation of CTR1 function and localization, as well as the cellular processes directly downstream of copper import, are not yet fully understood. To address such questions, we sought to develop genetically encoded tools to study CTR1.

The fusion of a protein of interest with genetically encoded biochemical tools facilitates a wide variety of *in situ* biochemical experiments. Fluorescent protein fusions[24] have been used to visualize protein localization[25] and measure protein movement in real time.[26] Optically responsive proteins may be used to induce a conformational change or control the assembly or disassembly of a protein complex, conferring precise spatiotemporal control over downstream biological functions in response to light.[27-32] Proteins of interest have also been fused to enzymes that promiscuously label other proteins in their vicinity for proximity labeling of binding partners that interact transiently or with low affinity *in situ*.[33,34] Each of these technologies enables the investigation of a protein within its native cellular context. However, such technologies have yet to be applied to the study of hCTR1 because the fusion of small proteins to the N- or C-terminus of hCTR1 causes loss of copper import or unregulated copper import, respectively.[17,35]

Here, we present functional hCTR1 constructs, each containing an insertion of circularly permuted enhanced green fluorescent protein (cpEGFP), which localize to the plasma membrane and internalize upon exposure to copper. Additionally, we demonstrate that other proteins with spatially proximate N- and C-termini may be inserted into hCTR1 without disrupting its function, including the optically-responsive *Avena sativa* LOV2 domain and APEX2, a peroxidase that may be used for proximity labeling. Although the

insertion of LOV2 did not confer optical sensitivity to hCTR1, we show that APEX2 retains its function within the hCTR1 protein and may be used to discover hCTR1 binding partners.

Functional CTR1-cpEGFP

To test whether circularly permuted proteins may be inserted into hCTR1 without disrupting CTR1 function or localization, I selected seven sites within hCTR1 to insert cpEGFP (27 kDa).[36,37] These included three sites in the N-terminal ectodomain (insertions immediately following Gly36, Ser59 or Leu61), three sites in the intracellular loop (insertions immediately following Ser92, Ser100, or Ile115), and a fusion of cpEGFP to the C-terminus (His190). The Myc epitope tag, which does not disrupt hCTR1 function,[38] was appended to the N-terminus to facilitate protein identification with the anti-Myc antibody, since CTR1 antibodies are notoriously scarce.[39] The location of the insertions relative to the hCTR1 architecture is illustrated in Figure 4.1A.

Constructs with an insertion of cpEGFP following Gly36, Ser59, Leu61 and Ser92 failed to express robustly (Figure 4.1B). The remaining three constructs, with insertions following Ser100, Ile115 or His190, expressed robustly, and are named Myc-hCTR1-100cpEGFP, Myc-hCTR1-115cpEGFP, and Myc-CTR1-190cpEGFP, respectively. HEK293T cells and mouse embryonic fibroblasts (MEFs) transiently transfected with wildtype Myc-hCTR1, Myc-hCTR1-100cpEGFP, or Myc-hCTR1-115cpEGFP had elevated levels of intracellular copper under basal conditions relative to cells transfected with vector alone, indicating that these constructs retain the function of high-affinity copper transport (Figure 4.1C and D). Interestingly, overexpression of Myc-hCTR1-190cpEGFP did not lead to an increase in basal intracellular copper levels (Figure 4.1C and D).

To assess the localization of each construct relative to that of wildtype Myc-hCTR1, HEK293T cells transiently transfected with each construct were fixed and probed with an α-Myc antibody. Immunofluorescence images showed each construct localized primarily to the plasma membrane, with some signal visible at other organelle membranes, perhaps due to mislocalization from overexpression (Figure 4.2A). Cell-surface biotinylation[21,40] robustly labeled both wildtype Myc-hCTR1 and Myc-hCTR1-100cpEGFP, establishing the presence of these proteins at the cell membrane under resting conditions (Figure 4.2B). Upon addition of copper, biotinylation of Myc-hCTR1 and Myc-hCTR1-100cpEGFP decreased, indicating a lower level of these proteins at the cell surface. This was not due to overall changes in membrane architecture, as biotinylation of the Na^+/K^+-ATPase remained constant. The response was also specific to CTR1 among copper transporters, as plasma membrane levels of the copper export protein ATP7A increased in response to copper treatment (Figure 4.2B).[41] Interestingly, incubating cells with the copper chelator bathocuproine disulfonate (BCS) led to higher Myc-hCTR1 at the plasma membrane but did not change Myc-hCTR1-100cpEGFP plasma membrane levels (Figure 4.2B). While the properties of Myc-hCTR1 and Myc-hCTR1-100cpEGFP are similar, these results demonstrate that the machinery that

delivers CTR1 to the cell membrane under copper deprivation is not able to act on Myc-hCTR1-100cpEGFP.

The functional consequence of CTR1 internalization is the cell's ability to regulate copper uptake, while lack of internalization leads to unregulated copper acquisition. To assess whether our constructs could internalize to prevent copper overload, HEK293T cells overexpressing each construct were treated with 10 μM $CuCl_2$ for 30, 60 and 90 minutes, and cellular copper uptake was assessed by ICP-MS. Copper levels in cells expressing wildtype Myc-hCTR1, Myc-hCTR1-100cpEGFP or Myc-CTR1-115cpEGFP increased sharply over the first thirty minutes, but the rate of copper uptake slowed over the subsequent hour, suggesting that these CTR1 constructs were able to internalize in response to excess copper (Figure 4.2C). These data agree with published CTR1 internalization times of around 30 minutes.[21] In contrast to the functional constructs, the C-terminal fusion of cpEGFP to CTR1 (Myc-CTR1-190cpEGFP) caused unregulated copper uptake (Figure 4.2C), suggesting that this construct does not internalize in response to excess copper, as expected based on literature precedent.[17]

Efforts Toward an Optically-Responsive CTR1

Encouraged by the discovery of functional CTR1-cpEGFP constructs, we sought to insert optically responsive proteins into CTR1 with the goal of creating a copper import protein whose function could be modulated by light. From the extensive array of optically responsive proteins presented in the literature, I selected the light-oxygen-voltage (LOV) domain from *Avena sativa* (AsLOV2) because it is small (16 kDa) and its N- and C-termini are spatially close together, making it amendable to insertion within a protein of interest.[42] Upon illumination with blue light (λ_{max}: 450 nm), the C-terminal alpha helix (Jα helix) of AsLOV2 unfolds, causing a large conformational change.[43-45] For some applications, the light-induced conformational change may directly alter the conformation or steric accessibility of the protein of interest.[46] In other cases, the unfolding of the Jα helix is used to uncage a non-native peptide sequence that recruits a co-expressed fusion protein consisting of the peptide's binding partner and a protein that alters the function of the protein of interest.[32] Very little is known about how the conformation of CTR1 influences its ability to transport copper. Thus, I selected a system that could induce a conformational change and recruit a secondary protein to CTR1 upon illumination: the tunable, light-controlled interacting protein tags (TULIPs) technology.[28]

In the TULIPs system, the AsLOV2 Jα helix is capped with the pep sequence –ADTWV–COOH, an epitope recognized by the Erbin PDZ domain.[28] In the dark, the Jα helix is folded and docked against the side of the LOV domain, sequestering the pep sequence. Upon illumination, the J-alpha helix unfolds, and the pep sequence is exposed, recruiting the PDZ domain. To adapt this system to CTR1, AsLOV2, with or without the pep sequence, was inserted into CTR1 immediately following Ser100 (Myc-CTR1-100AsLOV2pep and Myc-CTR1-100AsLOV2) or Ile115 (Myc-CTR1-115AsLOV2pep and Myc-CTR1-115AsLOV2). The PDZ domain was fused to Atox1, a copper chaperone protein known to interact with the intracellular domain of CTR1 and facilitate copper uptake.[19,47,48] Additionally, a PDZ-mCherry construct was used to test whether

recruitment of steric bulk would be sufficient to alter CTR1 function.[28] Both circularly permuted native PDZ (cpPDZ, K_d(ARVCF C-terminal peptide) = 25 μM)[49] and enhanced PDZ (ePDZb, K_d(ARVCF C-terminal peptide) = 50 nM)[50] fusions to mCherry were assembled, as the ideal binding affinity for this application was unknown.

HEK293T cells transiently expressing Myc-hCTR1-100AsLOV2 or Myc-hCTR1-115AsLOV2 transported copper at elevated levels compared to cells transfected with vector, albeit at somewhat reduced levels compared to wildtype Myc-hCTR1 (Figure 4.3). Interestingly, the inclusion of the pep sequence on the AsLOV2 Jα helix increased copper transport, and copper transport was further increased by the co-expression of any ePDZ construct with an AsLOV2pep construct (Figure 4.4). However, copper uptake by these constructs was not responsive to light exposure (Figure 4.4). These results suggested that within the context of the hCTR1 intracellular loop, AsLOV2pep may not sufficiently sequester the pep sequence to prevent interaction with binding partners; however, initial efforts to move the pep sequence further into the Jα helix for better caging were unsuccessful (data not shown). Our data also suggested that the pep-PDZ system could be interacting with native cellular components involved in hCTR1 function, since the addition of the pep sequence to Myc-hCTR1-AsLOV2 constructs was sufficient to alter copper transport. To test this hypothesis, the pep sequence alone was cloned into hCTR1, and copper uptake was measured with or without co-expression of ePDZb-mCherry. Once again, the insertion of pep increased copper transport, and co-expression of ePDZb-mCherry increased copper transport, even for wildtype Myc-hCTR1 (Figure 4.5). While the possibility that native cellular PDZ domains may be involved in the function of CTR1 was intriguing, we had hoped to develop hCTR1 constructs that were responsive to light. Since the pep and PDZ components seemed to interfere with this, I turned to a different AsLOV2-based protein recruitment strategy: improved light-induced dimer (iLID).[30]

The iLID system employs the same basic strategy as the TULIPs system, but uses the SsrA peptide and its binding partner, SspB.[30] In the iLID protein, the SsrA peptide sequence is appended to the AsLOV2 Jα helix such that SsrA will be caged in the dark and uncaged following illumination.[51] Three variants of SspB have been created: SspB-Milli, SspB-Micro, and SspB-Nano, displaying millimolar, micromolar, and nanomolar binding affinities toward SsrA, respectively.[52] Each SspB construct was fused to the C-terminus of the tagRFPt fluorophore to verify expression *in vivo*.[53] We tested all three SspB variants, since the binding affinity that would be optimal in the CTR1 system was unknown. iLID was inserted into Myc-hCTR1 immediately following Ser100 to create Myc-hCTR1-100iLID. Myc-hCTR1 or Myc-hCTR1-100iLID was overexpressed in HEK293T cells with or without each SspB construct, and copper uptake after 60 minutes of copper exposure was assessed under dark and light conditions. Myc-hCTR1-100iLID behaved similarly to wildtype Myc-hCTR1, and only the RFPt-SspB-Micro construct altered Myc-hCTR1-100iLID copper uptake (Figure 4.6). However, light exposure did not alter copper uptake in a manner that was specific to the presence of iLID (Figure 4.6). A general decrease in copper uptake overall may be due to light toxicity observed in these experiments.

Through our efforts to generate an optically responsive copper importer, we found that the light-sensitive AsLOV2 domain, as well as its iLID variant, could be inserted into hCTR1 while maintaining the construct's ability to transport copper and internalize in response to copper. Additionally, co-expression of proteins that can bind to AsLOV2 or iLID typically led to an increase in copper import. However, as I sought to improve our constructs, I found that the lack of information concerning the intracellular and membrane-bound binding partners of CTR1 made rational protein engineering difficult. Thus, we turned our attention toward generating a construct that could elucidate the proteins that natively bind CTR1 in the presence or absence of copper.

CTR1-APEX2 Constructs for the Discovery of CTR1 Binding Partners

Determining the native binding partners of proteins within the cellular context is fraught with challenges. Traditional coimmunoprecipitation methods can only identify high-affinity interactions which are stable through many washes. Alternatively, coimmunoprecipitations after application of a cross-linking reagent can stabilize interactions to sample processing but can lead to false positives.[54] Additionally, coimmunoprecipitation of integral membrane proteins,[55] such as CTR1, is particularly challenging because the detergents necessary to remove the integral membrane protein from the membrane can disrupt protein-protein interactions. Immunoprecipitation of Myc-hCTR1 following crosslinking has been previously performed, revealing an interaction between Myc-hCTR1 and insulin receptor substrate 4 (IRS-4).[40] However, no other interactions were reported in this study. We hypothesized that multiple proteins interact with CTR1 transiently following exposure to copper and during the CTR1 internalization process, and we set out to create a tool that could identify these proteins.

Recently, proximity labeling techniques have been developed to identify protein-protein interactions *in situ*.[33] In these techniques, the protein of interest is fused to an enzyme that promiscuously labels nearby proteins with a protein or small molecule tag which can later be identified by mass spectrometry. Any protein carrying the modification is presumed to have been associated with the protein of interest at some time during the labeling process. However, proximity labeling systems often involve the use of bulky labeling enzymes, which cannot be inserted into small proteins such as CTR1. One exception to this norm is APEX2,[56] a small (27 kDa) ascorbate peroxidase with N- and C-termini that are close together, facilitating its insertion into protein loops. In the presence of biotin phenol and hydrogen peroxide, APEX2 generates biotin-phenoxyl radicals which rapidly react with nearby molecules, appending biotin residues to proteins in the vicinity of APEX2. The activation of APEX2 is rapid (within seconds), and the lifetime of the biotin-phenoxyl radical is also short (<1 ms), leading to quick, localized labeling. Biotinylated proteins are readily identified by mass spectrometry following streptavidin bead pulldown. Recently, APEX2 was applied to map the localization and binding partners of G-protein coupled receptors (GPCRs),[57,58] membrane-bound receptors which participate in rapid signaling events and relocalize upon activation. I reasoned that the ability of APEX2 to resolve GPCR signaling events made it an excellent candidate for studying the proteins that associate with CTR1 during copper transport and internalization.

We inserted APEX2 into Myc-hCTR1 immediately following Ser100, Ile115, and His190 to create Myc-hCTR1-100APEX2, Myc-hCTR1-115APEX2, and Myc-hCTR1-190APEX2, respectively. Because we are interested to find proteins that bind to hCTR1 in a copper-transport-dependent manner, we also generated mutants of these constructs that are missing one or two key methionine residues (M150L, M154L, or the double mutant M150/154L) and are unable to transport copper.[22] These mutations were introduced into the wildtype Myc-hCTR1 background to yield Myc-hCTR1(M150L), Myc-hCTR1(M154L), and Myc-hCTR1(M150/154L), and the mutations were introduced into Myc-hCTR1-100APEX2 to yield Myc-hCTR1(M150L)-100APEX2, Myc-hCTR1(M154)-100APEX2, and Myc-hCTR1(M150/154L)-100APEX2.

HEK293T cells transfected with hCTR1 constructs containing APEX2 robustly express these proteins (Figure 4.7A). Additionally, copper uptake by Myc-hCTR1, Myc-hCTR1-100APEX2 and Myc-hCTR1-115APEX2 were similar, while Myc-hCTR1-190APEX2 showed unregulated copper import, similar to Myc-hCTR1-190cpEGFP and as expected based on literature precedent (Figure 4.7B).[17] However, copper uptake was impeded by single or double mutations of M150 or M154 (Figure 4.7B).

Curious to see whether proximity labeling could identify different CTR1 interactors in response to copper treatment or methionine mutation, I performed initial proximity labeling experiments using streptavidin-HRP blots as a readout. HEK293T cells transiently transfected with each construct were pre-treated with biotin phenol for 30 minutes. Copper was added to the media for 5, 10 or 30 minutes during the biotin phenol treatment. APEX2 was activated by the addition of hydrogen peroxide for 30 seconds, and cells were harvested immediately. Whole cell lysates blotted with streptavidin-HRP showed robust signal in cells expressing constructs containing APEX2, while the background signal in cells expressing wildtype Myc-hCTR1 was very low (Figure 4.7C). While the labeling pattern did not change significantly in response to copper addition or methionine mutation, it is possible that this is due to background labeling of bystander proteins that masks the true signal. In mass spectrometry experiments, these proteins can be identified and removed from the analysis by comparing labeling before and after a stimulation such as copper addition. In cases where the protein relocalizes (thus potentially changing the bystander proteins), mass spectrometry results may be normalized to the proteins labeled by cell-compartment-specific APEX2 constructs, as recently demonstrated by the Krogan lab.[57]

Before proceeding with mass spectrometry experiments, we wanted to verify that differences in internalization were responsible for the changes in copper uptake we had observed between Myc-hCTR1-190APEX2 and the other constructs. CTR1 internalization is known to be dependent on clathrin-dependent endocytosis, which may be inhibited using the dynein inhibitor Dynasore. HEK293T cells transiently transfected with each construct were pre-treated with Dynasore for 2 hours, and copper was added to the media in each well for an additional hour. While Dynasore treatment increased copper uptake in cells transfected with Myc-hCTR1, Myc-hCTR1-100APEX2 and Myc-hCTR1-115APEX2, it did not further increase copper uptake by Myc-hCTR1-190APEX2 (Figure 4.8). Meanwhile, Dynasore had very little effect on Myc-hCTR1(M150/154L),

which cannot transport copper (Figure 4.8). These results suggest that Myc-hCTR1-190APEX2 is already unable to internalize in response to copper treatment, such that inhibition of endocytosis is not able to further increase copper uptake by cells expressing this construct. Together, these results suggest that proximity labeling using Myc-hCTR1-190APEX2 may generate a different labeled proteome from the proteome labeled by other constructs. With these results in hand, we are pursuing mass spectrometry experiments to identify proteins that interact with hCTR1 in response to copper treatment.

Discussion and Future Directions

Understanding copper uptake is essential for understanding human health, as this transition metal is an essential micronutrient for humans. Relatively little is known about the dynamics and binding partners of hCTR1 *in situ* because genetically encoded tools cannot be fused to the N- or C-terminus of this protein without disrupting its function. In this study, we establish, for the first time, that small proteins may be inserted into the hCTR1 intracellular loop without disrupting hCTR1 function. These include cpEGFP, the optically responsive AsLOV2 domain, and the proximity labeling enzyme APEX2. While we used cpEGFP as a proof of concept to screen potential insertion sites, Myc-hCTR1-cpEGFP constructs may be applied to biophysical experiments examining the localization and movement of hCTR1 within live cells. Our efforts to generate an optically responsive hCTR1 by fusion with AsLOV2 and its derivatives were met with difficulty when we discovered that conformational change alone was not sufficient to alter hCTR1 copper transport and co-expression of binding partners such as ePDZb or RFPt-SspB-micro could alter copper transport independent of illumination. As we sought to improve our potential optically responsive hCTR1, we found that lack of information concerning the intracellular binding partners of hCTR1 made rational engineering difficult. Thus, we turned to the application of the proximity labeling enzyme APEX2 in this system.

We have demonstrated that hCTR1 bearing an internal APEX2 domain is functional for copper transport. Additionally, APEX2 inserted into hCTR1 may be activated with biotin phenol and hydrogen peroxide to effect the biotinylation of multiple proteins, as observed by streptavidin blots. Our current efforts include the generation of monoclonal cell lines stably expressing these Myc-hCTR1-APEX2 constructs for use in proteomics experiments. We expect that selecting stable lines that express these constructs at lower levels than levels typically seen in transiently transfected cells may improve the localization of the constructs and decrease background labeling. Additionally, monoclonal populations improve proteomics data by decreasing variability within and between samples. Once these lines have been generated and characterized, we plan to proceed with proximity labeling mass spectrometry experiments.

Materials and Methods

Materials

All chemicals were purchased from Sigma Aldrich, unless otherwise noted. Antibody suppliers and part numbers are provided in Table 4.1. Primers and gBlocks were ordered from Integrated DNA Technologies (IDT). All DNA constructs were created in the pcDNA3.1(+) mammalian expression vector (Invitrogen by Thermo Fisher). Plasmids for TULIPs constructs (AsLOV2, cpPDZ, and ePDZb) were gifts from Michael Glotzer (Addgene plasmids #34971, 34983, and 34980).[28]

Cell Culture

Mouse embryonic fibroblasts (MEFs) were a gift from Prof. Denis Thiele[9] and were maintained in Dulbecco's Modified Eagle Medium (DMEM, Gibco by Life Technologies), 10% fetal bovine serum (FBS, Seradigm), 1% non-essential amino acids (NEAA, Gibco by Life Technologies), 1% sodium pyruvate (Gibco by Life Technologies), 50 µM beta-mercaptoethanol (BME, Fisher). HEK293T lines lacking CTR1 and their matched controls were a gift from Prof. Steven Howell; the CTR1 KO2 line was used in these studies.[59] HEK293T cells were maintained in DMEM, 10% FBS, 1% NEAA. For all cell lines, serum starvation was performed in DMEM. All cell culture and cell treatments were performed under standard sterile conditions, and cells were kept at 37 °C under a 5% CO_2 atmosphere for growth and incubations.

DNA Amplification by Polymerase Chain Reaction

Polymerase chain reaction (PCR) amplification reactions were performed using the Phusion High-Fidelity DNA Polymerase kit (New England Biolabs, NEB). For each plasmid constructed, two PCR reactions were performed, one to amplify the vector and one to amplify the insert, and the products were combined by Gibson Assembly (see Gibson Assembly below). Primers for PCR reactions were designed to contain a priming region and an overlap region. The length of the priming region was determined using the NEB T_m Calculator online tool (http://tmcalculator.neb.com/) such that the annealing temperature (T_m) was between 56 °C and 62 °C. The overlap region was designed to create 20-30 base pair overlap regions on the 5' and 3' ends of each vector and insert pair used for Gibson Assembly in order to ensure successful assembly reactions. The PCR reactions performed in this work with the primer names and sequences, template plasmids, and annealing temperatures are tabulated in Table 4.2. The general procedure for vector PCR was as follows: PCR reactions contained a final concentration of 1X Phusion HF buffer, 3% DMSO, 200 µM dNTPs, 0.5 µM forward primer, 0.5 µM reverse primer, 0.2 ng/µL template DNA, and 1X Phusion polymerase (0.5 µL/50 µL reaction). Vector PCR reactions were thermal cycled using the following program: 98 °C for 30 seconds, followed by 25 cycles of 98 °C for 10 seconds, the calculated T_m for 30 seconds, and 72 °C for 4 minutes. The products were extended at 72 °C for 5 minutes, and the reaction was stored at 4 °C until further use. The general procedure for insert PCR was as follows: PCR reactions contained a final concentration of 1X Phusion HF buffer, 200

μM dNTPs, 0.5 μM forward primer, 0.5 μM reverse primer, 0.2 ng/μL template DNA, and 1X Phusion polymerase (0.5 μL/50 μL reaction). Insert PCR reactions were thermal cycled using the following program: 98 °C for 30 seconds, followed by 25 cycles of 98 °C for 10 seconds, calculated T_m for 30 seconds, and 72 °C for 1-2 minutes (30 seconds/kb). The products were extended at 72 °C for 5 minutes, and the reaction was stored at 4 °C until further use.

Gibson Assembly

Gibson reactions were performed using the Gibson Assembly Master Mix kit (NEB). A list of Gibson Assembly reactions performed in this work may be found in Table 4.3. In some cases, the insert used in a Gibson Assembly reaction was a purchased gBlock (IDT); these sequences are tabulated in Table 4.4. The insert fragment (0.07 pmol) and vector (0.01 pmol) (calculated using the NEBioCalculator tool (http://nebiocalculator.neb.com/)) were added to 10 μL of the 2X Gibson Assembly Master Mix, and sterile water was added to bring the reaction to a final volume of 20 μL. The assembly reaction was held at 50 °C for an hour in a thermal cycler and stored at 4 °C until further use. The reaction product (2 μL) was added to NEB 5α competent cells (50 μL) in 1.5 mL sterile tubes on ice with gentle mixing using the pipet tip but without pipetting up and down, and NEB 5α cells were transformed according to the protocol below.

Site-Directed Mutagenesis

Site-directed mutagenesis (SDM) was performed using the Q5 Site-Directed Mutagenesis Kit (NEB) according to the manufacturer's instructions. Briefly, SDM primers were designed using the NEBaseChanger tool (http://nebasechanger.neb.com/), and primers are listed in Table 4.2. Q5 reactions containing a final concentration of 1x Q5 mix, 0.5 μM forward primer, 0.5 μM reverse primer, and 0.2 ng/μL template DNA were thermal cycled on a T100 Thermal Cycler (Bio-Rad) using the following program: 95 °C for 30 seconds, followed by 25 cycles of 98 °C for 10 seconds, calculated T_m for 15 seconds, and 72 °C for 4 minutes. The products were extended at 72 °C for 2 minutes, and the reaction was stored at 4 °C until further use. The KLD reaction was run for 5 minutes at room temperature, and 5 μL of the reaction was added into 50 μL of NEB 5α competent cells in 1.5 mL sterile tubes on ice with gentle mixing using the pipet tip but without pipetting up and down, and NEB 5α cells were transformed according to the protocol below.

Bacterial Transformation, DNA Harvesting, and Sequence Analysis

The mixture of cells with DNA was incubated on ice for 30 minutes, heat shocked in a 42 °C water bath for 30 seconds, and recovered on ice for 2 minutes. SOC medium (950 μL, NEB) was added to each tube, and the cells were incubated at 37 °C with shaking for 1 hour. Cells (80 μL) were spread on plates of LB-Agar (EMD Millipore) containing Ampicillin or Carbenicillin (100 μg/mL) and incubated at 37 °C overnight. Colonies were picked into 5 mL of LB medium (Fisher Scientific) containing 100 μg/mL Ampicillin or Carbenicillin and grown overnight at 37 °C with vigorous agitation. DNA was harvested using the Qiagen Miniprep Kit, according to the manufacturer's instructions, including all

recommended steps. Samples were submitted to Qintara Biosciences for sequencing, and sequencing alignments were analyzed using Benchling. A table of the amino acid sequences of the proteins used in this work may be found in Table 4.5.

Transfections and Cell Treatments

For transfection experiments, cells were plated to be 70% confluent at the time of transfection; $3.5*10^5$ cells were added to each well of a 12-well plate or $8.75*10^5$ cells were added to each well of a 6-well plate the day before transfection. MEF cells were transfected with Lipofectamine 2000 (Thermo Fisher), according to the manufacturer's protocol, using 100 µL Optimem, 4 µL transfection reagent, and 1 µg DNA per well in a 12-well plate. HEK293T cells were transfected with TransIT-LT1 reagent (Mirus Bio) according to the manufacturer's protocol, using 100 µL Optimem, 2 µL transfection reagent, and 1 µg DNA per well in a 12-well plate.

The following conditions were used for cell treatments unless otherwise indicated. Cells grown under basal conditions were kept in serum-containing media until harvesting. For treatments with copper, cells were serum starved for 16-20 hours to lower basal copper levels, and copper ($CuCl_2$) was added to the serum-free media at the indicated concentrations and times. For treatments with copper chelators, cells were maintained in serum-containing media to achieve the largest change in copper by maintaining cellular copper at normal levels until chelation. For plates incubated in the dark, lights in the tissue culture room and biosafety hood were turned off as copper was added, and after copper addition, plates were covered in aluminum foil to prevent exposure to light when the cell incubator door was opened. For plates incubated in the light, cells were pre-illuminated for 5 minutes under full-intensity 465 nm full blue LED light by an Adafruit Neopixel NeoMatrix 8x8 LED array set up inside the incubator (37 °C), with a 2-cm gap between the light array and the top of the tissue culture plate. After pre-illumination, copper was added to the wells, and cells were put back under the same light for the indicated time. For treatments with Dynasore, cells were kept in serum-containing media until Dynsaore treatment, as Dynasore treatment after serum starvation caused significant toxicity; this included experiments where copper was added. Dynasore (80 µM final concentration in 1% DMSO) was applied in serum-free media for 3 hours, and copper was added directly to each well 1 hour before harvesting the cells (2 hours after Dynasore treatment).

Western blots

Cells were plated in 12-well plastic dishes (Corning) to be 70% confluent at the time of transfection, which was two days before harvesting, and maintained in serum-containing media until harvest. To harvest cells, media was decanted, and cells were placed on ice. Cells were washed three times with ice-cold PBS, and lysis buffer (200 µL/well, 50 mM Tris-HCl, pH 7.4, 150 mM NaCl, 0.5% sodium deoxycholate, 0.1% SDS, with 1% NP-40 or Triton X-100 (Boston BioProducts) with protease inhibitors (Complete ULTRA, without EDTA, Roche)) was added to each well. Lysates were scraped off of each well and pipetted into 1.5 mL tubes (Axygen). Lysates were clarified by centrifugation (16,100 x *g*, 10 min, 4 °C), and the supernatant was transferred to a fresh 1.5 mL tube. Protein was

quantified by BCA assay (Pierce). For gel electrophoresis, samples were prepared by diluting the lysates into PBS to the concentration of the most dilute sample (30 µL final volume) and 15 µL of sample buffer (4:1 4x LDS Sample Buffer:beta-mercaptoethanol, Life Technologies and Fisher, respectively) was added to each sample and mixed by pipetting and inversion. Samples (15 µL) were loaded onto precast gels (NuPAGE 4-12% Bis-Tris, 1.5 mm, 15 wells, unless otherwise noted, Life Technologies) and run at 140V for 1-2 hours. Proteins were transferred to a PVDF membrane (Bio-Rad) using the 1.5 mm transfer program (1.3 A, 25V, 10 min) on the Transblot Turbo Transfer system (Bio-Rad). For proteins above 100 kDa, the transfer program was run twice to ensure efficient transfer. Membranes were blocked in 5% low-fat, dry milk (Carnation) in Tris-buffered saline with 0.05% Tween-20 (TBST, Santa Cruz) with rocking for 1 hour at room temperature or overnight at 4 °C. Primary antibody was applied in 5% milk TBST with rocking for 1 hour at room temperature or overnight at 4 °C. Membranes were washed twice for 5 seconds and twice for 5 minutes in TBST. Secondary antibody was applied in TBST for 1 hour at room temperature with rocking. Membranes were washed twice for 5 seconds and twice for 5 minutes in TBST. Membranes probed with HRP-conjugated antibodies were visualized using Western Lightning Plus ECL or Western Lightning ULTRA ECL (Perkin Elmer). Membranes probed with fluorescent antibodies were visualized by illumination. All images were collected on a ChemiDoc MP (Bio-Rad). A list of antibodies used in this work may be found in Table 4.1.

Inductively Coupled Plasma Mass Spectrometry

Cells were plated in 12-well plastic dishes (Corning) to be 70% confluent at the time of transfection, which was two days before harvesting cells for ICP-MS. Cells were transfected and treated according to the conditions above (see Transfections and Cell Treatments) unless stated otherwise in the text. To harvest cells, media was decanted, and cells were placed on ice. Cells were washed three times with ice-cold HEPES (20 mM, pH 7.5), and trace-metals grade nitric acid (100 µL, BD Aristar Ultra) was added to each well. Care was taken to ensure that nitric acid spread over the bottom of the entire well. Parafilm M (Bemis) was used to seal the edges of the plate lid, and the plates were left on a shaker overnight at room temperature. The next day, concentrated samples (40 µL) were diluted into 180 µL of 2% nitric acid made with milliQ water and trace-metals grade nitric acid. The samples were analyzed on an iCAP-Qc ICP-MS (Thermo Fisher) in KED mode by manual sampling, and concentrations were calculated based on a standard curve diluted from the CMS-5 standard (Al, Cs, Co, Fe, Mg, Ni, Rb, Na, Zn, Ca, Cr, Cu, Li, Mn, K, Ag, and Sr in 2% nitric acid) with molybdenum, phosphorous and sulfur added (Inorganic Ventures).

Immunofluorescence

HEK293T cells were plated on 4-well chamber slides ($1.2*10^5$ cells/well, Lab-Tek II Chambered Coverglass with Cover, #1.5, Borosilicate Glass, Thermo Fisher) 2 days before immunofluorescence. The day before immunofluorescence, cells were serum-starved overnight (12-18 h). Media was aspirated and slides were placed on ice. Cells were washed 3x with ice-cold PBS and fixed at room temperature for 15 minutes with 4%

PFA (Thermo Scientific, #28906) in PBS. Fixed cells were washed three times with room temperature PBS and blocked in blocking buffer (3% donkey serum (Jackson Labs) and 0.5% Triton X-100 in PBS) for 1 hour with rocking. Primary antibody (Mouse anti-Myc (c-myc), Life Technologies #132500, 1:500 in blocking buffer) was applied for 1 hour with rocking, after which the cells were washed 3x 5 min with PBS. Secondary antibody (Donkey anti-mouse AlexaFluor647, Life Technologies, 1:100 in blocking buffer) was applied for 1 hour with rocking, and the cells were washed twice with PBS before imaging. Imaging was performed on the same day as staining.

Cell-Surface Biotinylation

This protocol was adapted from published methods.[21] Specifically, HEK293T cells were plated in 6-well plastic dishes (Corning) to be 70% confluent for transfection two days before the biotinylation experiment. The day before the biotyinylation experiment, the cells were serum-starved overnight (12-20 hours). One well was used per sample, and each condition was run in duplicate (2 wells per condition). Cells treated with chelator were exposed to 200 µM BCS in serum free media (DMEM) overnight. On the day of the experiment, cycloheximide in DMSO was mixed thoroughly with serum-free media and an equal volume of cycloheximide-containing media was added to the existing volume of each well such that the final concentration of cycloheximide was 100 µg mL^{-1}. Cells were incubated in media containing cycloheximide for at least 30 minutes at 37 °C. $CuCl_2$ (20 µM) was then added to the wells designated for copper treatment for 30 minutes. At the completion of cell treatments, the media was decanted and cells were placed on ice. Each well was washed three times with 0.5 mL ice-cold PBS with 0.1 mM $CaCl_2$ and 1 mM $MgCl_2$ on ice. To initiate the biotinylating reaction, cells were treated with 0.77 mg mL^{-1} EZ-link Sulfo-NHS-SS-Biotin (Thermo Fisher) in an ice-cold solution of 10 mM triethanolamine, 2 mM $CaCl_2$, 150 mM NaCl, pH 7.5 for 30 minutes at 4 °C. At the end of labeling, the supernatant was aspirated. To quench the reaction, cells were rinsed once with ice-cold quenching buffer (1x PBS with 0.1 mM $CaCl_2$, 1 mM $MgCl_2$ and 100 mM glycine) and incubated with a fresh wash of quenching buffer for 20 minutes at 4 °C. The quenching process was repeated once more for a total of 40 minutes of quenching. Cells were transferred to 1.5 mL tubes (Axygen) by gently pipetting the cells off the plates and into each tube using P1000 pipette tips. Cells were collected by centrifugation at 500 x *g* for 5 minutes at 4 °C. The supernatant was aspirated, and lysis buffer (200 µL, ice-cold PBS containing 1% Triton X-100, 150 mM NaCl, 5 mM EDTA and 50 mM Tris, pH 7.5) was added to each tube. Cells were lysed by incubation at 4 °C for 1 hour on a rotator. Lysates were clarified by centrifugation at 10,000 x *g* for 10 minutes, and the supernatant was transferred to new tubes by pipetting or decanting. Protein concentrations were determined using the Bradford Reagent (Pierce). Lysates were diluted to the same protein concentration using ice-cold lysis buffer. Diluted cell lysates (100 µL) were applied to a resin-free Micro Bio-Spin 6 column (Bio-Rad). Streptavidin beads (20 µL of 50% bead suspension per sample, Pierce) were washed 3x with lysis buffer to equilibrate them, and the beads were resuspended in lysis buffer to create a 50% suspension. Beads (20 µL of a 50% suspension in lysis buffer) were added to each spin column. The columns were capped and placed on a rotator at 4 °C overnight. The next day, beads were collected by centrifugation at 500 x *g* for 5 minutes, and the flow-through was discarded. The beads

were washed on the column three times with 500 µL ice-cold lysis buffer, two times with 500 µL ice-cold salt wash buffer (0.1% Triton X-100, 500 mM NaCl, 5 mM EDTA, 50 mM Tris, pH 7.5), and one time with 500 µL ice-cold no-salt wash buffer (10 mM Tris, pH 7.5). Beads were dried by centrifugation at 10,000 x *g* for 5 minutes. To elute the protein off the beads, 2X SDS-Page buffer (50 µL, 1:1 4x NuPAGE Sample Buffer:PBS containing 150 mM DDT) was added to each sample, and samples were incubated at room temperature for 10 minutes. The eluent was collected by centrifugation at 10,000 x *g* for 1 minute. Eluted samples were subjected to analysis by Western blot.

APEX2 Proximity Labeling for Western Blot

HEK293T cells were plated in 12-well plastic dishes (Corning) to be 70% confluent and transfected with the indicated constructs two days before APEX2 labeling and harvesting. On the day of the experiment, serum-containing media was removed and cells were placed in serum-free media containing 500 µM biotinyl tyramide (Cedarlane) for 30 minutes. For 30-minute copper treatments, $CuCl_2$ (10 µM) was added immediately. For shorter copper treatments, copper was added to the media in the wells at the indicated time before harvest. At 30 seconds before harvest, an equal volume of room temperature serum-free media containing 2 mM H_2O_2 was added to each well, such that the total H_2O_2 concentration in the wells was 1 mM. Media was decanted, and cells were immediately placed on ice. Cells were washed three times with quenching buffer (1x PBS containing 1 mM $CaCl_2$, 10 mM sodium ascorbate, 1 mM sodium azide, 1 mM Trolox). Lysis buffer (100 µL/well, 50 mM Tris-HCl, pH 7.4, 150 mM NaCl, 0.5% sodium deoxycholate, 0.1% SDS, with 1% Triton X-100 (Boston BioProducts) with protease inhibitors (Complete ULTRA, without EDTA, Roche) containing 10 mM sodium ascorbate, 1 mM sodium azide, 1 mM Trolox, and 1 mM DTT) was added to each well, and cells were scraped into 1.5 mL tubes (Axygen). Cells were incubated on ice for 10-20 minutes to lyse. Lysates were clarified by centrifugation at 16,100 x *g* for 10 minutes at 4 °C. Protein was quantified using Detergent Compatible Bradford Reagent (Pierce), and lysates were diluted to 1 mg/mL protein concentration in lysis buffer. To each sample (15 µL) was added sample buffer (7 µL of 4:1 4x LDS Sample Buffer:beta-mercaptoethanol, Life Technologies and Fisher, respectively), and the solution was mixed by pipetting and inversion. Samples (18 µL) were loaded onto precast gels (NuPAGE 4-12% Bis-Tris, 1.5 mm, 15 wells, unless otherwise noted, Life Technologies). Protein ladder (5 µL, PageRuler Plus Prestained Protein Ladder, 10 to 250 kDa, Thermo Fisher) was loaded to estimate molecular weight, and gels were run at 140V for 1-2 hours. Proteins were transferred to a PVDF membrane (Bio-Rad) using the 1.5 mm transfer program (1.3 A, 25V, 10 min) on the Transblot Turbo Transfer system (Bio-Rad). Membranes were blocked in 5% low-fat, dry milk (Carnation) in Tris-buffered saline with 0.05% Tween-20 (TBST, Santa Cruz) with rocking for 1 hour at room temperature or overnight at 4 °C. Membranes were washed twice for 5 seconds and twice for 5 minutes in TBST to remove potential biotin contamination from milk. Streptavidin-HRP (Jackson Labs, 016-030-084, 1:10,000) was applied in TBST with rocking for 1 hour at room temperature or overnight at 4 °C. Membranes were washed twice for 5 seconds and twice for 5 minutes in TBST and visualized using Western Lightning Plus ECL (Perkin Elmer). Images were collected on a ChemiDoc MP (Bio-Rad).

Acknowledgements

We thank Prof. Denis Thiele and Prof. Steve Howell for their generous gifts of CTR1 knockout cell lines. We thank Ann Fisher, Carissa Tasto, and Alison Kililea in the UC Berkeley Cell Culture Facility for maintaining the cell lines used in these experiments.

The work presented here was conducted in close collaboration with Bao Thai, an undergraduate student in the Chang Lab who worked with me for three years on everything from cryosectioning zebrafish embryos to cloning to running ICP-MS samples. Truly, this project would not have happened without you. Thank you!

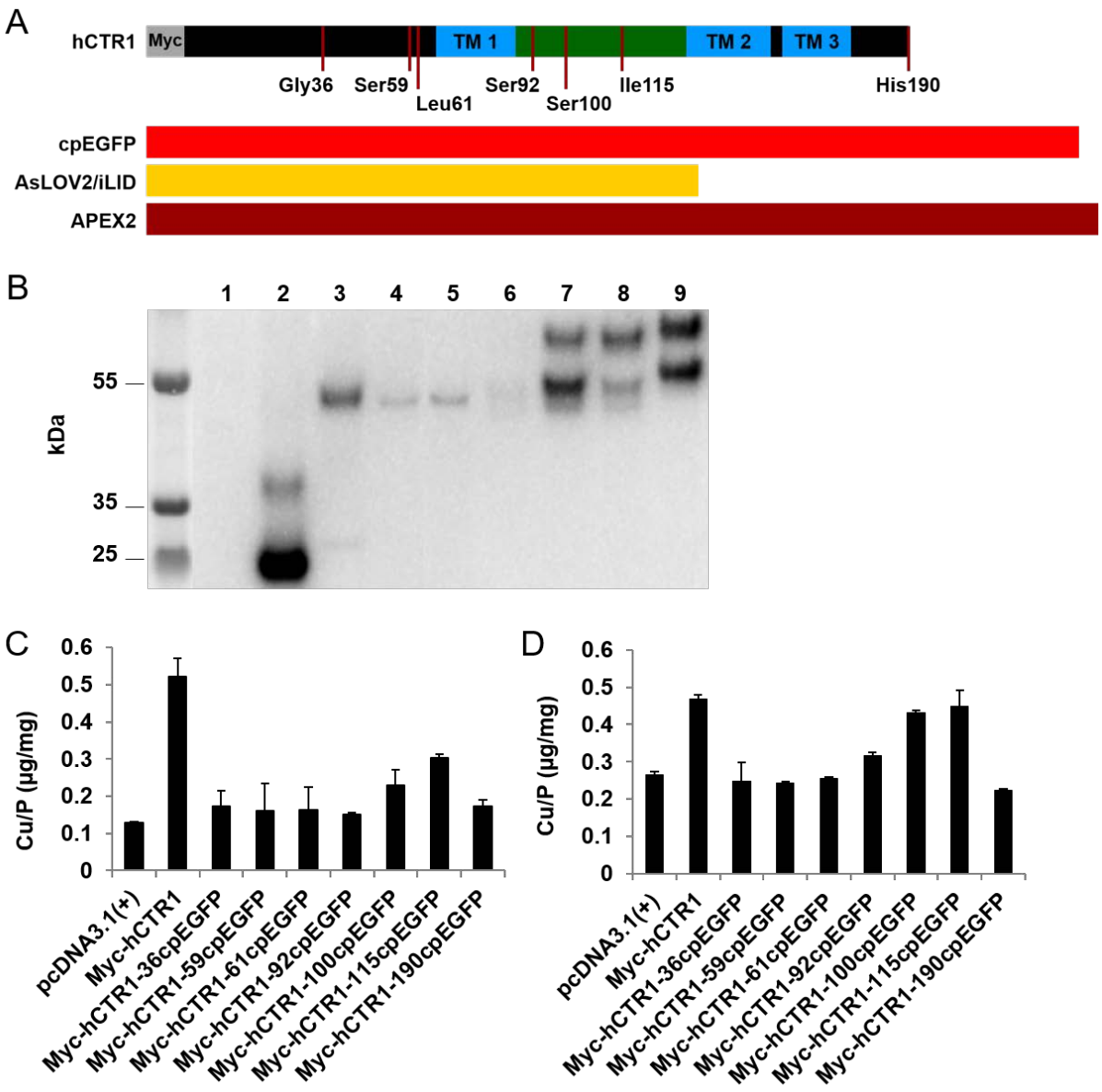

Figure 4.1 Circularly permuted EGFP (cpEGFP) may be inserted into hCTR1 while maintaining hCTR1's ability to transport copper. A) Cartoon of hCTR1 with insertion locations marked. The N-terminal Myc tag is shown in gray. Three transmembrane domains (TM1-3) are in blue. The intracellular loop is green. Below CTR1, the proteins inserted into hCTR1 in this work are drawn to scale based on length of amino acid (aa) sequence. hCTR1: 190 aa. cpEGFP: 245 aa. AsLOV2/iLID: 145 aa. APEX2: 250 aa. A 9-aa linker was appended to both ends of each insert to increase structural flexibility between CTR1 and the insert (not shown). B) Western blot of HEK293T cells transfected with pcDNA3.1(+), Myc-hCTR1, Myc-hCTR1-36cpEGFP, Myc-hCTR1-59cpEGFP, Myc-hCTR1-61cpEGFP, Myc-hCTR1-92cpEGFP, Myc-hCTR1-100cpEGFP, Myc-hCTR1-115cpEGFP and Myc-hCTR1-190cpEGFP (lanes 1-9, respectively) and probed for the Myc epitope. C) Copper uptake under basal growth conditions of HEK293T cells

transfected with the indicated constructs, measured by ICP-MS and normalized to cellular phosphorous. D) Copper uptake under basal growth conditions of MEF cells transfected with the indicated constructs, measured by ICP-MS and normalized to cellular phosphorous.

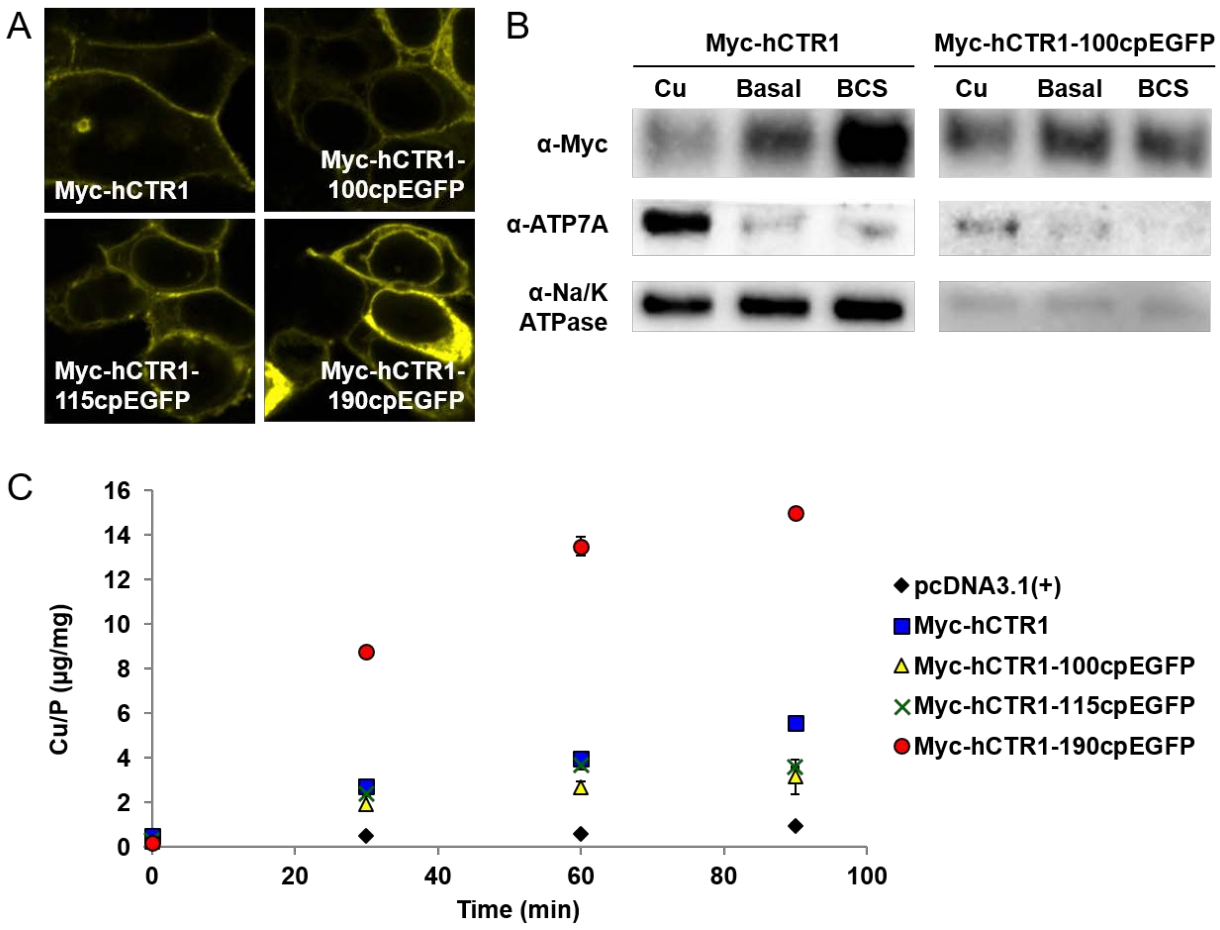

Figure 4.2 cpEGFP may be inserted into hCTR1 while maintaining hCTR1 internalization. A) Immunofluorescence of HEK293T cells transfected with the indicated constructs and probed for the Myc epitope. B) Cell-surface biotinylation of HEK293T cells transfected with the indicated constructs and grown under basal conditions or with the addition of 20 µM $CuCl_2$ for 30 minutes or 200 µM BCS for 20 to 24 hours. Membranes were probed for the Myc epitope, as well as Na^+/K^+-ATPase α1 and ATP7A for controls. C) Time-course of copper uptake in HEK293T cells transfected with the indicated constructs and treated with 10 µM $CuCl_2$ for the indicated times, measured by ICP-MS and normalized to cellular phosphorous.

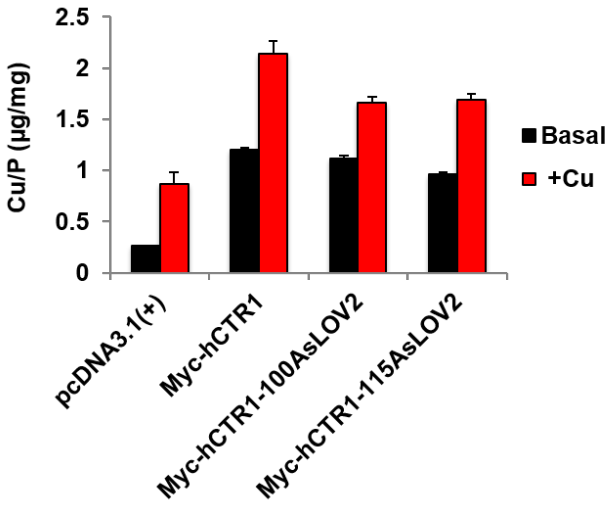

Figure 4.3 AsLOV2 may be inserted into hCTR1 while preserving hCTR1 function. Copper uptake in HEK293T cells transfected with the indicated constructs and grown under basal conditions or treated with 10 µM $CuCl_2$ for 60 minutes, measured by ICP-MS and normalized to cellular phosphorous.

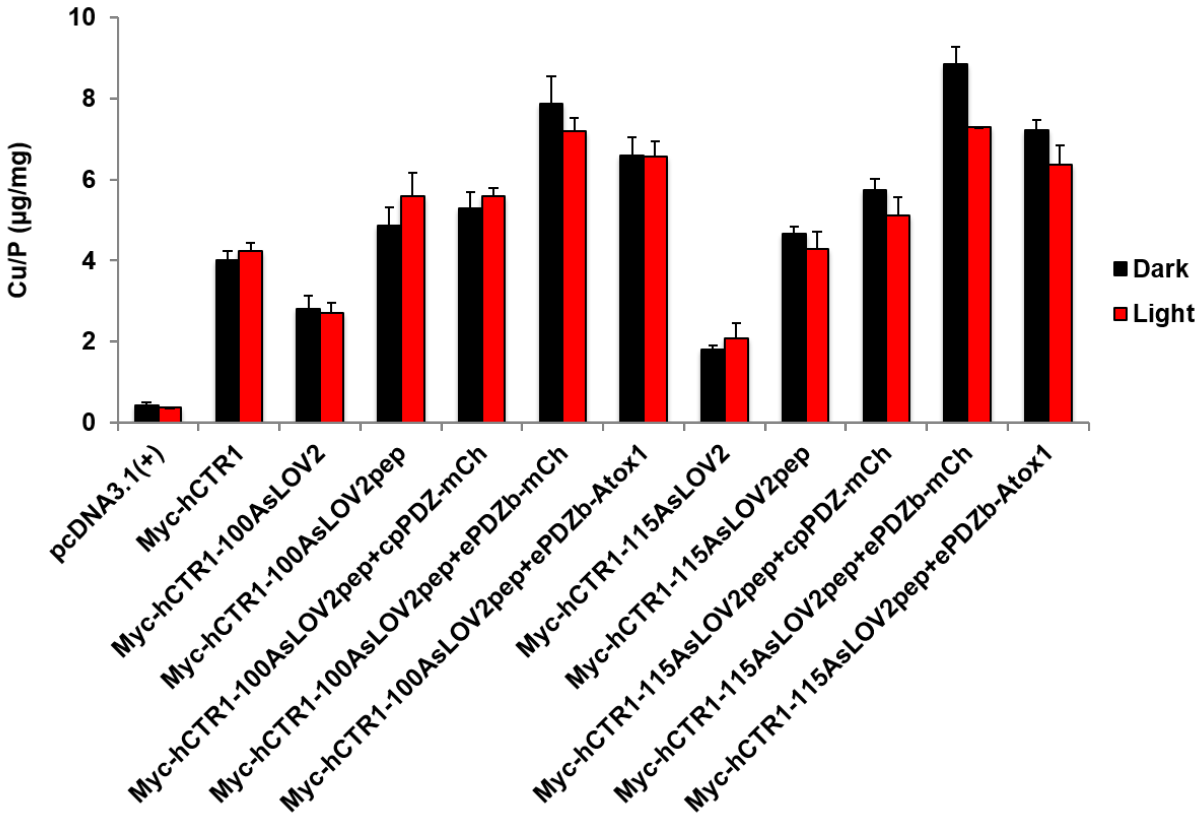

Figure 4.4 The presence of pep or PDZ, but not light, alters copper uptake by Myc-hCTR1-AsLOV2 constructs. Copper uptake in HEK293T cells lacking endogenous CTR1, transfected with the indicated constructs and treated with 10 µM $CuCl_2$ for 60 minutes in the dark or illuminated by 465 nm full blue light, measured by ICP-MS and normalized to cellular phosphorous.

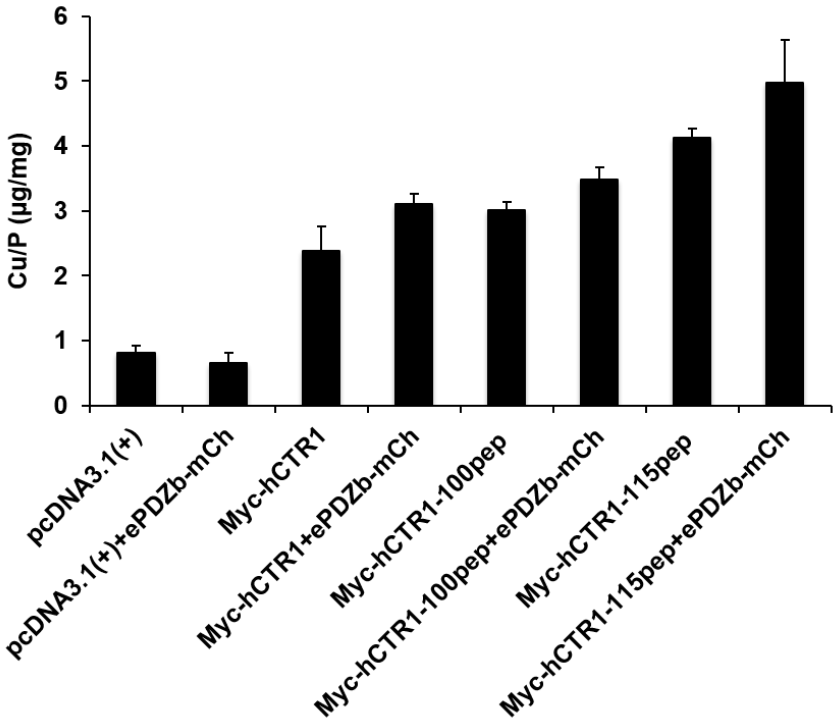

Figure 4.5 The insertion of pep or coexpression of PDZ increases copper uptake by Myc-hCTR1. Copper uptake in HEK293T cells transfected with the indicated constructs and treated with 10 µM $CuCl_2$ for 60 minutes, measured by ICP-MS and normalized to cellular phosphorous.

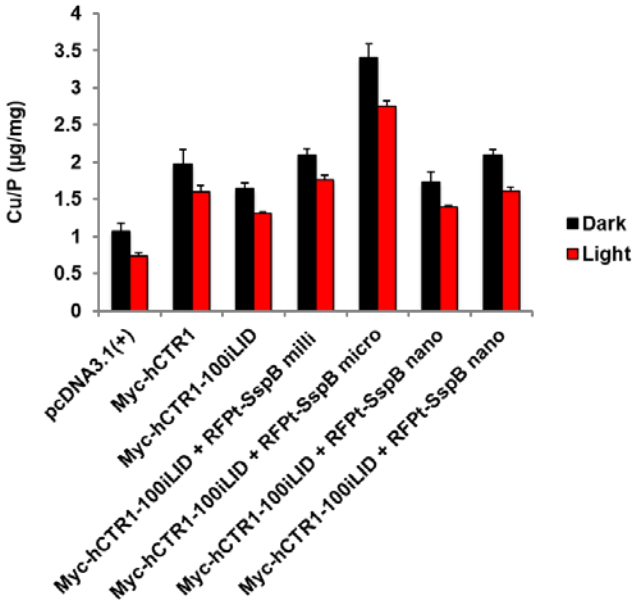

Figure 4.6 Insertion of iLID into hCTR1 does not alter hCTR1 copper uptake, but hCTR1-iLID responds to SspB-micro and not light or other SspB binding partners. Copper uptake in HEK293T cells transfected with the indicated constructs and grown under basal conditions or treated with 10 µM $CuCl_2$ for 60 minutes in the dark or illuminated with 465 nm full blue light, measured by ICP-MS and normalized to cellular phosphorous.

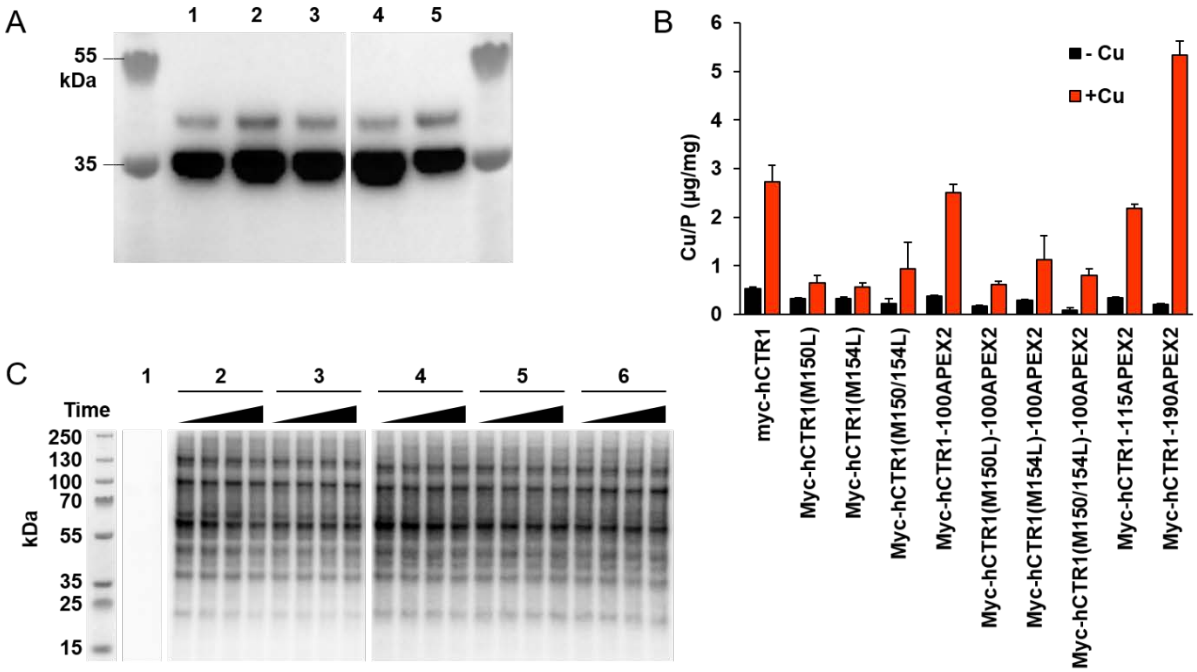

Figure 4.7 The functions of hCTR1 and APEX2 are maintained when APEX2 is inserted into the hCTR1 intracellular loop, and point mutations in hCTR1 disrupt copper transport but not APEX2 function. A) Western blot of HEK293T cells transfected with Myc-hCTR1-100APEX2, Myc-hCTR1(M150L)-100APEX2, Myc-hCTR1(M154L)-100APEX2, Myc-hCTR1-115APEX2, and Myc-hCTR1-190APEX2 (lanes 1-5, respectively) and probed for the Myc epitope. B) Copper uptake in HEK293T cells transfected with the indicated constructs and treated with 10 µM $CuCl_2$ in serum-free media for 30 minutes. C) Whole cell lysates from HEK293T cells transfected with Myc-hCTR1, Myc-hCTR1-100APEX2, Myc-hCTR1(M150L)-100APEX2, Myc-hCTR1(M150/154L)-100APEX2, Myc-hCTR1-115APEX2, or Myc-hCTR1-190APEX2 (sections 1-7, respectively) and treated with biotin phenol (500 µM, 30 min), 10 µM $CuCl_2$ for increasing amounts of time (0, 5, 10, or 30 minutes), and H_2O_2 (1 mM, 30 seconds) to activate APEX2, probed for biotinylation using streptavidin-HRP.

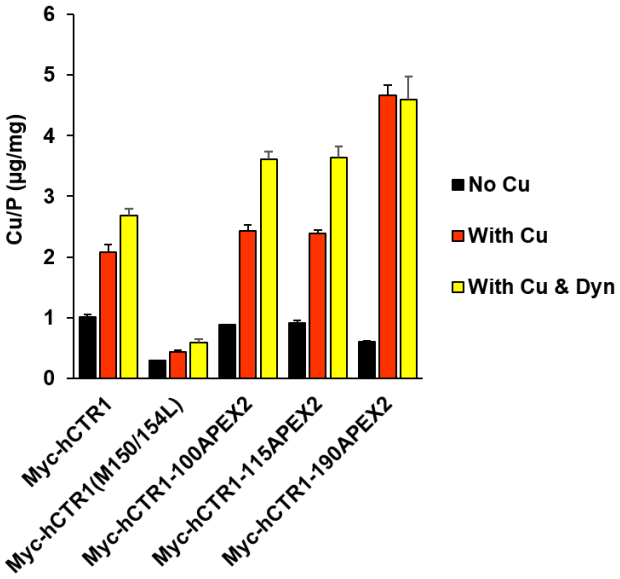

Figure 4.8 Inhibition of dynein-mediated endocytosis increases copper uptake from constructs that are normally able to internalize. Copper uptake by HEK293T cells transfected with the indicated constructs and treated with Dynasore (Dyn, 80 µM) for 2 hours before copper addition (10 µM $CuCl_2$) for 1 hour, for a total of 3 hours of Dynasore treatment.

Antibody	Supplier	Part No	Dilution	Use
Myc (c-myc)	Life Technologies	132500	1:1000	WB
Myc (c-myc)	Life Technologies	132500	1:500	IF
ATP7A	Hycult Biotech	HP8040	1:1000	WB
Na/K-ATPase alpha-1	Abcam	ab7671	1:1000	WB
Goat anti-mouse HRP (secondary Ab)	Santa Cruz	sc-2005	1:2000	WB
Anti-mouse AlexaFluor-647 (secondary Ab)	Life Technologies	A31571	1:100	IF
Anti-mouse AlexaFluor-647 (secondary Ab)	Life Technologies	A31571	1:1000	WB

Table 4.1 Antibodies and conditions used for Western blots (WB) and immunofluorescence (IF).

PCR Rxn No	Name of primer	Sequence	T_m	Template DNA
1	Myc-hCTR1 insert forward	ATGGAACAAAAACTCATCTCAGAAGAGGATC TGGATCATTCCCACCATATGG	60	hCTR1
	Myc-hCTR1 insert reverse	TCAATGGCAATGCTCTGT		
2	pcDNA3.1(+) vector forward	TCCAGTGTGGTGGAATTCT	59	pcDNA3.1(+)
	pcDNA3.1(+) vector reverse	TGGACTAGTGGATCCGAG		
3	Insert L1-cpEGFP-forward	GGTTCTGCTGGTTCGGCTGCCTCTGGTAGCC ACAACGTCTATATCAT	60	cpEGFP
	Insert L2-cpEGFP-reverse	ACCAGAGGCACCAGAGGCAGCAGAACCGTT AAAGTTGTACTCCAGCTTAT		
4	Vector D37-forward	GGTTCTGCTGCCTCTGGTGCCTCTGGTGACA GCAGCATGATGATGAT	60	pcDNA3.1(+)-Myc-hCTR1
	Vector G36-reverse	ACCAGAGGCAGCCGAACCAGCAGAACCTCC TCCACCATGGGAG		
5	Vector G60-forward	GGTTCTGCTGCCTCTGGTGCCTCTGGTGGTT TGGTGATCAATACAGCT	60	pcDNA3.1(+)-Myc-hCTR1
	Vector S59 -reverse	ACCAGAGGCAGCCGAACCAGCAGAACCGGA AAACAGTAGTTCCACATTCTT		
6	Vector V62-forward	GGTTCTGCTGCCTCTGGTGCCTCTGGTGTGA TCAATACAGCTGGAGAA	60	pcDNA3.1(+)-Myc-hCTR1
	Vector L61 -reverse	ACCAGAGGCAGCCGAACCAGCAGAACCCAA ACCGGAAAACAGTAGTTC		
7	Vector L93 -forward	GGTTCTGCTGCCTCTGGTGCCTCTGGTCTGC TGCGTAAGTCACAAGT	60	pcDNA3.1(+)-Myc-hCTR1
	Vector S92 -reverse	ACCAGAGGCAGCCGAACCAGCAGAACCGCT CTCTCGGGCTATCTTG		
8	Vector I101-forward	GGTTCTGCTGCCTCTGGTGCCTCTGGTATTC GCTACAATTCCATGC	60	pcDNA3.1(+)-Myc-hCTR1
	Vector S100-reverse	ACCAGAGGCAGCCGAACCAGCAGAACCGCT GACTTGTGACTTACGCA		
9	Vector L116-forward	GGTTCTGCTGCCTCTGGTGCCTCTGGTCTTA TGGAGACACACAAAACTGT	60	pcDNA3.1(+)-Myc-hCTR1
	Vector I115-reverse	ACCAGAGGCAGCCGAACCAGCAGAACCGAT GGTTCCATTTGGTCCT		
10	Vector STOP-forward	GGTTCTGCTGCCTCTGGTGCCTCTGGTTGAT CCAGTGTGGTGGAATTCTG	60	pcDNA3.1(+)-Myc-hCTR1
	Vector H190-reverse	ACCAGAGGCAGCCGAACCAGCAGAACCATG GCAATGCTCTGTGATA		
11	Insert linker1+LOV-forward	GGTTCTGCTGGTTCGGCTGCCTCTGGTTTGG CTACTACACTTGAACG	57	pDS257
	Insert linker 2+LOV-reverse	ACCAGAGGCACCAGAGGCAGCAGAACCATC AATCTCTTCTGCAGTTTT		

12	Insert linker1+LOV-forward	GGTTCTGCTGGTTCGGCTGCCTCTGGTTTGGCTACTACACTTGAACG	57	pDS257
	Insert linker 2+LOVpep-reverse	ACCAGAGGCACCAGAGGCAGCAGAACCCACCCAGGTATCCACC		
13	Insert cpPDZmCh-forward	ATGCCAGAACTTGGATTTAG	58	pDS282
	Insert cpPDZmCh-reverse	TTACTTGTACAGCTCGTCCAT		
14	Vector pcDNA3.1-PDZmCh-forward	ACCGGCGGCATGGACGAGCTGTACAAGTAATCCAGTGTGGTGGAATTCTG	63	pcDNA3.1(+)
	Vector	ACCTGATATGCTAAATCCAAGTTCTGGCATTGGACTAGTGGATCCGAGC		
15	Insert ePDZbmCh-forward	ATGCCAGAACTTGGATTTAG	58	pDS220
	Insert ePDZbmCh-reverse	TTACTTGTACAGCTCGTCCAT		
16	Vector pcDNA3.1-ePDZbmCh-forward	ACCGGCGGCATGGACGAGCTGTACAAGTAATCCAGTGTGGTGGAATTCTG	63	pcDNA3.1(+)
	Vector pcDNA3.1-ePDZbmCh-reverse	ACCTGATATGCTAAATCCAAGTTCTGGCATTGGACTAGTGGATCCGAGC		
17	Insert ePDZb-forward	ATGCCAGAACTTGGATTTAG	58	pcDNA3.1(+)-ePDZb-mCherry
	Insert ePDZb-reverse	GGTACGGTAGTTAATCGAGATTG		
18	Vector ePDZb-Atox1-forward	TCTAGCCCAATCTCGATTAACTACCGTACCTCTAGACTCGAGCTCAAGC	58	Atox1
	Vector ePDZb-Atox1-reverse	TGATATGCTAAATCCAAGTTCTG		
19	C56hCTR1pep-Q5F (removes AsLOV2 except for pep)	AAAGCGGTGGATACCTGGG	59	pcDNA3.1(+)-Myc-(1-100)hCTR1-AsLOV2pep-(101-190)hCTR1 or pcDNA3.1(+)-Myc-(1-115)hCTR1-AsLOV2pep-(116-190)hCTR1
	C56hCTR1pep-Q5R (removes AsLOV2 except for pep)	ACCAGAGGCAGCCGAACC		
20	Vector iLID-forward	GGTTCTGCTGCCTCTGG	58	pcDNA3.1(+)-Myc-(1-100)hCTR1-AsLOV2-(101-190)hCTR1
	Vector iLID-reverse	CCAGAACTTTTTACCACTCTTT		
21	Vector-SspB-micro-forward	TCCAGTGTGGTGGAATTC	58	pcDNA3.1(+)
	Vector-SspB-reverse	GGACTAGTGGATCCGAGCT		
22	Vector APEX2-forward	GCAGATGCGGGTTCTGCTGCCTCTGG	58	pcDNA3.1(+)-Myc-(1-100)hCTR1-AsLOV2-(101-190)hCTR1
	Vector 100APEX2-reverse	acctgaagctgcagaacccgcggagccGCTGACTTGTGACTTACGCA		

23	Vector APEX2-forward	GCAGATGCGGGTTCTGCTGCCTCTGG	58	pcDNA3.1(+)-Myc-(1-115)hCTR1-AsLOV2-(116-190)hCTR1
	Vector 115APEX2-reverse	acctgaagctgcagaacccgcggagccGATGGTTCCATTTGGTCCT		
24	Vector APEX2-C-term-forward	GCAGATGCGggttctgctgcctctggtgccTGATCCAGTGTGGTGGAAT	58	pcDNA3.1(+)-Myc-hCTR1
	Vector APEX2-C-term-reverse	CATacctgaagctgcagaacccgcggagccATGGCAATGCTCTGTGATATC		
25	SspB micro-to-milli A58V forward	GTCTGCAAGTgtgACCGGCAACC	67	pcDNA3.1(+)-TagRFPt-SspB-micro
	SspB micro-to-milli A58V reverse	AGATTCAGCACGATCTGACCG		
26	SspB micro-to-nano Q73R forward	GTTCAACGCCagaTTTAAGGGCGTG	57	pcDNA3.1(+)-TagRFPt-SspB-micro
	SspB micro-to-nano Q73R reverse	TGGATAAAATCATTTGTCAGTTG		
27	hCTR1(M150L) forward	CTACTTCCTCctgCTCATCTTCATG	60	pcDNA3.1(+)-Myc-hCTR1 or pcDNA3.(+)-Myc-hCTR1-APEX2 plasmids
	hCTR1(M150L) reverse	CTTATGACCACCTGGATG		
28	hCTR1(M154L) forward	GCTCATCTTCctgACCTACAACG	60	pcDNA3.1(+)-Myc-hCTR1 or pcDNA3.(+)-Myc-hCTR1-APEX2 plasmids
	hCTR1(M154L) reverse	ATGAGGAAGTAGCTTATGAC		

Table 4.2 PCR reactions performed in these studies. The PCR reaction number is the identifier used in the Gibson Assmebly table (Table 4.3). T_m is the annealing temperature used for the reaction. PCR reactions 19 and 25-28 list reactions to perform site-directed mutagenesis at the indicated locations; these reactions were performed on each of the plasmids listed in the Template DNA column to introduce these mutations into the constructs.

Name of Plasmid Constructed	Vector PCR Rxn Number	Insert PCR Rxn Number
pcDNA3.1(+)-Myc-hCTR1	2	1
pcDNA3.1(+)-Myc-(1-36)hCTR1-cpEGFP-(37-190)hCTR1	4	3
pcDNA3.1(+)-Myc-(1-59)hCTR1-cpEGFP-(60-190)hCTR1	5	3
pcDNA3.1(+)-Myc-(1-61)hCTR1-cpEGFP-(62-190)hCTR1	6	3
pcDNA3.1(+)-Myc-(1-92)hCTR1-cpEGFP-(93-190)hCTR1	7	3
pcDNA3.1(+)-Myc-(1-100)hCTR1-cpEGFP-(101-190)hCTR1	8	3
pcDNA3.1(+)-Myc-(1-115)hCTR1-cpEGFP-(116-190)hCTR1	9	3
pcDNA3.1(+)-Myc-(1-190)hCTR1-cpEGFP	10	3
pcDNA3.1(+)-Myc-(1-100)hCTR1-AsLOV2-(101-190)hCTR1	8	11
pcDNA3.1(+)-Myc-(1-100)hCTR1-AsLOV2pep-(101-190)hCTR1	8	12
pcDNA3.1(+)-Myc-(1-115)hCTR1-AsLOV2-(116-190)hCTR1	9	11
pcDNA3.1(+)-Myc-(1-115)hCTR1-AsLOV2pep-(116-190)hCTR1	9	12
pcDNA3.1(+)-cpPDZ-mCherry	14	13
pcDNA3.1(+)-ePDZb-mCherry	16	15
pcDNA3.1(+)-ePDZb-Atox1	18	17
pcDNA3.1(+)-Myc-(1-100)hCTR1-iLID-(101-190)hCTR1	20	iLID gBlock
pcDNA3.1(+)-TagRFPt-SspB-micro	21	SspB gBlock
pcDNA3.1(+)-Myc-(1-100)hCTR1-APEX2-(101-190)hCTR1	22	APEX2 gBlock
pcDNA3.1(+)-Myc-(1-115)hCTR1-APEX2-(116-190)hCTR1	23	APEX2 gBlock
pcDNA3.1(+)-Myc-(1-190)hCTR1-APEX2	24	APEX2 gBlock
pcDNA3.1(+)-Myc-(1-115)hCTR1-APEX2-(116-190)hCTR1	23	APEX2 gBlock
pcDNA3.1(+)-Myc-(1-190)hCTR1-APEX2	24	APEX2 gBlock

Table 4.3 Gibson assembly reactions performed to create the final constructs used in these studies. Vector and insert PCR reaction numbers reference the numbers assigned in Table 4.2.

Table 4.4 gBlocks ordered for this work. Overlap sequences are highlighted in gray.

iLID gBlock (to convert AsLOV2 into iLID)**:**

AATTATACAAAGAGTGGTAAAAAGTTCTGGAACGTCTTTCATCTGCAACCAATGCGCGACTACA
AGGGTGACGTGCAGTACTTTATTGGGGTACAACTCGATGGAACGGAGCGATTGCACGGAGCAGC
AGAAAGAGAGGCTGTTTGTTTGATAAAGAAGACTGCGTTCGGAATAGAGGCAGCAAATGATGAA
AACTACTTTGGTTCTGCTGCCTCTGGTGCCTCTGG

SspB gBlock (TagRFPt-SspB-Milli to go into pcDNA3.1(+)):

CTTGGTACCGAGCTCGGATCCACTAGTCCAATGGTGTCTAAGGGCGAAGAGCTGATTAAGGAGA
ACATGCACATGAAGCTGTACATGGAGGGCACCGTGAACAACCACCACTTCAAGTGCACATCCGA
GGGCGAAGGCAAGCCCTACGAGGGCACCCAGACCATGAGAATCAAGGTGGTCGAGGGCGGCCCT
CTCCCCTTCGCCTTCGACATCCTGGCTACCAGCTTCATGTACGGCAGCAGAACCTTCATCAACC
ACACCCAGGGCATCCCCGACTTCTTTAAGCAGTCCTTCCCTGAGGGCTTCACATGGGAGAGAGT
CACCACATACGAAGACGGGGGCGTGCTGACCGCTACCCAGGACACCAGCCTCCAGGACGGCTGC
CTCATCTACAACGTCAAGATCAGAGGGGTGAACTTCCCATCCAACGGCCCTGTGATGCAGAAGA
AAACACTCGGCTGGGAGGCCAACACCGAGATGCTGTACCCCGCTGACGGCGGCCTGGAAGGCAG
AACCGACATGGCCCTGAAGCTCGTGGGCGGGGGCCACCTGATCTGCAACTTCAAGACCACATAC
AGATCCAAGAAACCCGCTAAGAACCTCAAGATGCCCGGCGTCTACTATGTGGACCACAGACTGG
AAAGAATCAAGGAGGCCGACAAAGAGACCTACGTCGAGCAGCACGAGGTGGCTGTGGCCAGATA
CTGCGACCTCCCTAGCAAACTGGGGCACAAACTTAATGGCATGGACGAGCTGTACAAGtccgga
ctcagatctcgagctcaagcttcgaacGAATTCggcattgatctgagcggcctgaccctgcagG
AATTCAGCTCCCCGAAACGCCCTAAGCTGCTGCGTGAATATTACGATTGGCTGGTTGATAACAG
CTTTACCCCATATCTGGTGGTGGATGCCACATACCTGGGCGTGAACGTGCCCGTGGAGTATGTG
AAAGACGGTCAGATCGTGCTGAATCTGTCTGCAAGTGCGACCGGCAACCTGCAACTGACAAATG
ATTTTATCCAGTTCAACGCCCAGTTTAAGGGCGTGTCTCGTGAACTGTATATCCCGATGGGTGC
CGCTCTGGCCATTTACGCTCGCGAGAACGGCGATGGTGTGATGTTCGAACCAGAAGAAATCTAT
GACGAGCTGAATATTGGTTAATCCAGTGTGGTGGAATTCTGCAGATATCCA

APEX2 gBlock (to insert APEX2 into hCTR1):

ggctccgcgggttctgcagcttcaggtATGGGTAAAAGCTATCCGACTGTTTCCGCCGACTATC
AAGATGCAGTGGAAAAGGCTAAGAAGAAGTTGCGGGGGTTTATAGCGGAGAAACGCTGCGCTCC
GCTTATGCTCCGCCTTGCTTTCCACAGCGCGGGTACTTTCGACAAGGGAACCAAGACGGGTGGC
CCGTTCGGAACAATAAAACATCCTGCCGAGCTGGCCCACAGTGCTAATAACGGGCTGGACATCG
CTGTACGGCTGTTGGAACCATTGAAAGCCGAGTTCCCAATACTGAGCTACGCCGACTTTTATCA
ACTCGCGGGGGTGGTCGCGGTTGAGGTAACTGGTGGCCCTAAAGTACCTTTCCACCCGGGGCGG
GAGGATAAACCTGAACCCCCTCCGGAAGGTAGGCTGCCAGACCCAACAAAAGGATCAGATCATC
TCCGCGACGTTTTCGGGAAGGCGATGGGCTTGACCGACCAGGACATAGTTGCTCTTTCCGGAGG
ACATACTATAGGTGCCGCCCATAAGGAAAGGTCAGGGTTTGAAGGCCCGTGGACTAGCAATCCA
CTTATTTTCGACAACTCCTATTTTACGGAATTGCTCAGCGGGGAAAAAGAAGGACTGCTTCAGC
TGCCATCCGATAAAGCTTTGCTTAGCGACCCCGTCTTTAGACCGCTTGTAGACAAGTACGCTGC
CGACGAGGACGCGTTCTTCGCTGATTACGCGGAAGCCCATCAGAAACTCTCTGAACTTGGCTTT
GCAGATGCGggttctgctgcctctggtgcc

Table 4.5 Descriptions and amino acid sequences of proteins used in this work. Insertions are underlined. Linkers are double underlined. The Myc tag is underlined with a thick line. Point mutations are indicated by bold font.

Full name: Myc-hCTR1
Abbreviation in the text: Myc-hCTR1
Description: Human CTR1 with an N-terminal Myc tag
MEQKLISEEDLDHSHHMGMSYMDSNSTMQPSHHHPTTSASHSHGGGDSSMMMMPMTFYFGFKNV
ELLFSGLVINTAGEMAGAFVAVFLLAMFYEGLKIARESLLRKSQVSIRYNSMPVPGPNGTILME
THKTVGQQMLSFPHLLQTVLHIIQVVISYFLMLIFMTYNGYLCIAVAAGAGTGYFLFSWKKAVV
VDITEHCH*

cpEGFP Insertions:

Full name: Myc-(1-36)hCTR1-cpEGFP-(37-190)hCTR1
Abbreviation in the text: Myc-hCTR1-36cpEGFP
Description: Human CTR1 with an N-terminal Myc tag and an extracellular circularly-permutated, enhanced GFP in between G36 and D37
MEQKLISEEDLDHSHHMGMSYMDSNSTMQPSHHHPTTSASHSHGGGGSAGSAASGSHNVYIMAD
KQRNGIKANFKIRHNIEDGGVQLAYHYQQNTPIGDGPVLLPDNHYLSTQSKLSKDPNEKRDHMV
LLEFVTAAGITLGMDELYKGGTGGSMVSKGEELFTGVVPILVELDGDVNGHKFSVSGEGEGDAT
YGKLTLKFICTTGKLPVPWPTLVTTLTYGVQCFSRYPDHMKQHDFFKSAMPEGYIQERTIFFKD
DGNYKTRAEVKFEGDTLVNRIELKGIDFKEDGNILGHKLEYNFNGSAASGASGDSSMMMMPMTF
YFGFKNVELLFSGLVINTAGEMAGAFVAVFLLAMFYEGLKIARESLLRKSQVSIRYNSMPVPGP
NGTILMETHKTVGQQMLSFPHLLQTVLHIIQVVISYFLMLIFMTYNGYLCIAVAAGAGTGYFLF
SWKKAVVVDITEHCH*

Full name: Myc-(1-59)hCTR1-cpEGFP-(60-190)hCTR1
Abbreviation in the text: Myc-hCTR1-59cpEGFP
Description: Human CTR1 with an N-terminal Myc tag and an extracellular circularly-permutated, enhanced GFP in between S59 and G60
MEQKLISEEDLDHSHHMGMSYMDSNSTMQPSHHHPTTSASHSHGGGDSSMMMMPMTFYFGFKNV
ELLFSGSAGSAASGSHNVYIMADKQRNGIKANFKIRHNIEDGGVQLAYHYQQNTPIGDGPVLLP
DNHYLSTQSKLSKDPNEKRDHMVLLEFVTAAGITLGMDELYKGGTGGSMVSKGEELFTGVVPIL
VELDGDVNGHKFSVSGEGEGDATYGKLTLKFICTTGKLPVPWPTLVTTLTYGVQCFSRYPDHMK
QHDFFKSAMPEGYIQERTIFFKDDGNYKTRAEVKFEGDTLVNRIELKGIDFKEDGNILGHKLEY
NFNGSAASGASGGLVINTAGEMAGAFVAVFLLAMFYEGLKIARESLLRKSQVSIRYNSMPVPGP
NGTILMETHKTVGQQMLSFPHLLQTVLHIIQVVISYFLMLIFMTYNGYLCIAVAAGAGTGYFLF
SWKKAVVVDITEHCH*

Full name: Myc-(1-61)hCTR1-cpEGFP-(62-190)hCTR1
Abbreviation in the text: Myc-hCTR1-61cpEGFP
Description: Human CTR1 with an N-terminal Myc tag and an extracellular circularly-permutated, enhanced GFP in between L61 and V62
MEQKLISEEDLDHSHHMGMSYMDSNSTMQPSHHHPTTSASHSHGGGDSSMMMMPMTFYFGFKNV
ELLFSGLGSAGSAASGSHNVYIMADKQRNGIKANFKIRHNIEDGGVQLAYHYQQNTPIGDGPVL
LPDNHYLSTQSKLSKDPNEKRDHMVLLEFVTAAGITLGMDELYKGGTGGSMVSKGEELFTGVVP
ILVELDGDVNGHKFSVSGEGEGDATYGKLTLKFICTTGKLPVPWPTLVTTLTYGVQCFSRYPDH
MKQHDFFKSAMPEGYIQERTIFFKDDGNYKTRAEVKFEGDTLVNRIELKGIDFKEDGNILGHKL
EYNFNGSAASGASGVINTAGEMAGAFVAVFLLAMFYEGLKIARESLLRKSQVSIRYNSMPVPGP
NGTILMETHKTVGQQMLSFPHLLQTVLHIIQVVISYFLMLIFMTYNGYLCIAVAAGAGTGYFLF
SWKKAVVVDITEHCH*

Full name: Myc-(1-92)hCTR1-cpEGFP-(93-190)hCTR1
Abbreviation in the text: Myc-hCTR1-92cpEGFP
Description: Human CTR1 with an N-terminal Myc tag and an intracellular circularly-permutated, enhanced GFP in between S92 and L93
MEQKLISEEDLDHSHHMGMSYMDSNSTMQPSHHHPTTSASHSHGGGDSSMMMMPMTFYFGFKNV
ELLFSGLVINTAGEMAGAFVAVFLLAMFYEGLKIARESGSAGSAASGSHNVYIMADKQRNGIKA
NFKIRHNIEDGGVQLAYHYQQNTPIGDGPVLLPDNHYLSTQSKLSKDPNEKRDHMVLLEFVTAA
GITLGMDELYKGGTGGSMVSKGEELFTGVVPILVELDGDVNGHKFSVSGEGEGDATYGKLTLKF
ICTTGKLPVPWPTLVTTLTYGVQCFSRYPDHMKQHDFFKSAMPEGYIQERTIFFKDDGNYKTRA
EVKFEGDTLVNRIELKGIDFKEDGNILGHKLEYNFNGSAASGASGLLRKSQVSIRYNSMPVPGP
NGTILMETHKTVGQQMLSFPHLLQTVLHIIQVVISYFLMLIFMTYNGYLCIAVAAGAGTGYFLF
SWKKAVVVDITEHCH*

Full name: Myc-(1-100)hCTR1-cpEGFP-(101-190)hCTR1
Abbreviation in the text: Myc-hCTR1-100cpEGFP
Description: Human CTR1 with an N-terminal Myc tag and an intracellular circularly-permutated, enhanced GFP in between S100 and I101
MEQKLISEEDLDHSHHMGMSYMDSNSTMQPSHHHPTTSASHSHGGGDSSMMMMPMTFYFGFKNV
ELLFSGLVINTAGEMAGAFVAVFLLAMFYEGLKIARESLLRKSQVSGSAGSAASGSHNVYIMAD
KQRNGIKANFKIRHNIEDGGVQLAYHYQQNTPIGDGPVLLPDNHYLSTQSKLSKDPNEKRDHMV
LLEFVTAAGITLGMDELYKGGTGGSMVSKGEELFTGVVPILVELDGDVNGHKFSVSGEGEGDAT
YGKLTLKFICTTGKLPVPWPTLVTTLTYGVQCFSRYPDHMKQHDFFKSAMPEGYIQERTIFFKD
DGNYKTRAEVKFEGDTLVNRIELKGIDFKEDGNILGHKLEYNFNGSAASGASGIRYNSMPVPGP
NGTILMETHKTVGQQMLSFPHLLQTVLHIIQVVISYFLMLIFMTYNGYLCIAVAAGAGTGYFLF
SWKKAVVVDITEHCH*

Full name: Myc-(1-115)hCTR1-cpEGFP-(116-190)hCTR1
Abbreviation in the text: Myc-hCTR1-115cpEGFP
Description: Human CTR1 with an N-terminal Myc tag and an intracellular circularly-permutated, enhanced GFP in between I115 and L116
MEQKLISEEDLDHSHHMGMSYMDSNSTMQPSHHHPTTSASHSHGGGDSSMMMMPMTFYFGFKNV
ELLFSGLVINTAGEMAGAFVAVFLLAMFYEGLKIARESLLRKSQVSIRYNSMPVPGPNGTIGSA
GSAASGSHNVYIMADKQRNGIKANFKIRHNIEDGGVQLAYHYQQNTPIGDGPVLLPDNHYLSTQ
SKLSKDPNEKRDHMVLLEFVTAAGITLGMDELYKGGTGGSMVSKGEELFTGVVPILVELDGDVN
GHKFSVSGEGEGDATYGKLTLKFICTTGKLPVPWPTLVTTLTYGVQCFSRYPDHMKQHDFFKSA
MPEGYIQERTIFFKDDGNYKTRAEVKFEGDTLVNRIELKGIDFKEDGNILGHKLEYNFNGSAAS
GASGLMETHKTVGQQMLSFPHLLQTVLHIIQVVISYFLMLIFMTYNGYLCIAVAAGAGTGYFLF
SWKKAVVVDITEHCH*

Full name: Myc-(1-190)hCTR1-cpEGFP
Abbreviation in the text: Myc-hCTR1-190cpEGFP
Description: Human CTR1 with an N-terminal Myc tag and an intracellular C-terminal circularly-permutated, enhanced GFP
MEQKLISEEDLDHSHHMGMSYMDSNSTMQPSHHHPTTSASHSHGGGDSSMMMMPMTFYFGFKNV
ELLFSGLVINTAGEMAGAFVAVFLLAMFYEGLKIARESLLRKSQVSIRYNSMPVPGPNGTILME
THKTVGQQMLSFPHLLQTVLHIIQVVISYFLMLIFMTYNGYLCIAVAAGAGTGYFLFSWKKAVV
VDITEHCHGSAGSAASGSHNVYIMADKQRNGIKANFKIRHNIEDGGVQLAYHYQQNTPIGDGPV
LLPDNHYLSTQSKLSKDPNEKRDHMVLLEFVTAAGITLGMDELYKGGTGGSMVSKGEELFTGVV
PILVELDGDVNGHKFSVSGEGEGDATYGKLTLKFICTTGKLPVPWPTLVTTLTYGVQCFSRYPD
HMKQHDFFKSAMPEGYIQERTIFFKDDGNYKTRAEVKFEGDTLVNRIELKGIDFKEDGNILGHK
LEYNFNGSAASGASG*

AsLOV2 Insertions:

Full name: Myc-(1-100)hCTR1-AsLOV2-(101-190)hCTR1
Abbreviation in the text: Myc-hCTR1-100AsLOV2
Description: Human CTR1 with an N-terminal Myc tag and an intracellular AsLOV2 domain in between S100 and I101
MEQKLISEEDLDHSHHMGMSYMDSNSTMQPSHHHPTTSASHSHGGGDSSMMMMPMTFYFGFKNV
ELLFSGLVINTAGEMAGAFVAVFLLAMFYEGLKIARESLLRKSQVSGSAGSAASGLATTLERIE
KNFVITDPRLPDNPIIFASDSFLQLTEYSREEILGRNCRFLQGPETDRATVRKIRDAIDNQTEV
TVQLINYTKSGKKFWNLFHLQPMRDQKGDVQYFIGVQLDGTEHVRDAAEREAVMLIKKTAEEID
GSAASGASGIRYNSMPVPGPNGTILMETHKTVGQQMLSFPHLLQTVLHIIQVVISYFLMLIFMT
YNGYLCIAVAAGAGTGYFLFSWKKAVVVDITEHCH*

Full name: Myc-(1-100)hCTR1-AsLOV2pep-(101-190)hCTR1
Abbreviation in the text: Myc-hCTR1-100AsLOV2pep
Description: Human CTR1 with an N-terminal Myc tag and an intracellular AsLOV2 domain with the pep sequence in between S100 and I101
MEQKLISEEDLDHSHHMGMSYMDSNSTMQPSHHHPTTSASHSHGGGDSSMMMMPMTFYFGFKNV
ELLFSGLVINTAGEMAGAFVAVFLLAMFYEGLKIARESLLRKSQVSGSAGSAASGLATTLERIE
KNFVITDPRLPDNPIIFASDSFLQLTEYSREEILGRNCRFLQGPETDRATVRKIRDAIDNQTEV
TVQLINYTKSGKKFWNLFHLQPMRDQKGDVQYFIGVQLDGTEHVRDAAEREAVMLIKKTAEEID
KAVDTWVGSAASGASGIRYNSMPVPGPNGTILMETHKTVGQQMLSFPHLLQTVLHIIQVVISYF
LMLIFMTYNGYLCIAVAAGAGTGYFLFSWKKAVVVDITEHCH*

Full name: Myc-(1-115)hCTR1-AsLOV2-(116-190)hCTR1
Abbreviation in the text: Myc-hCTR1-115AsLOV2
Description: Human CTR1 with an N-terminal Myc tag and an intracellular AsLOV2 domain in between I115 and L116
MEQKLISEEDLDHSHHMGMSYMDSNSTMQPSHHHPTTSASHSHGGGDSSMMMMPMTFYFGFKNV
ELLFSGLVINTAGEMAGAFVAVFLLAMFYEGLKIARESLLRKSQVSIRYNSMPVPGPNGTIGSA
GSAASGLATTLERIEKNFVITDPRLPDNPIIFASDSFLQLTEYSREEILGRNCRFLQGPETDRA
TVRKIRDAIDNQTEVTVQLINYTKSGKKFWNLFHLQPMRDQKGDVQYFIGVQLDGTEHVRDAAE
REAVMLIKKTAEEIDGSAASGASGLMETHKTVGQQMLSFPHLLQTVLHIIQVVISYFLMLIFMT
YNGYLCIAVAAGAGTGYFLFSWKKAVVVDITEHCH*

Full name: Myc-(1-115)hCTR1-AsLOV2pep-(116-190)hCTR1
Abbreviation in the text: Myc-hCTR1-115AsLOV2pep
Description: Human CTR1 with an N-terminal Myc tag and an intracellular AsLOV2 domain with the pep sequence in between I115 and L116
MEQKLISEEDLDHSHHMGMSYMDSNSTMQPSHHHPTTSASHSHGGGDSSMMMMPMTFYFGFKNV
ELLFSGLVINTAGEMAGAFVAVFLLAMFYEGLKIARESLLRKSQVSIRYNSMPVPGPNGTIGSA
GSAASGLATTLERIEKNFVITDPRLPDNPIIFASDSFLQLTEYSREEILGRNCRFLQGPETDRA
TVRKIRDAIDNQTEVTVQLINYTKSGKKFWNLFHLQPMRDQKGDVQYFIGVQLDGTEHVRDAAE
REAVMLIKKTAEEIDKAVDTWVGSAASGASGLMETHKTVGQQMLSFPHLLQTVLHIIQVVISYF
LMLIFMTYNGYLCIAVAAGAGTGYFLFSWKKAVVVDITEHCH*

Full name: Myc-(1-100)hCTR1-pep-(101-190)hCTR1
Abbreviation in the text: Myc-hCTR1-100pep
Description: Human CTR1 with an N-terminal Myc tag and an intracellular pep sequence in between S100 and I101
MEQKLISEEDLDHSHHMGMSYMDSNSTMQPSHHHPTTSASHSHGGGDSSMMMMPMTFYFGFKNV
ELLFSGLVINTAGEMAGAFVAVFLLAMFYEGLKIARESLLRKSQVSGSAGSAASGKAVDTWVGS
AASGASGIRYNSMPVPGPNGTILMETHKTVGQQMLSFPHLLQTVLHIIQVVISYFLMLIFMTYN
GYLCIAVAAGAGTGYFLFSWKKAVVVDITEHCH*

Full name: Myc-(1-115)hCTR1-pep-(116-190)hCTR1
Abbreviation in the text: Myc-hCTR1-115pep
Description: Human CTR1 with an N-terminal Myc tag and an intracellular pep sequence in between I115 and L116
MEQKLISEEDLDHSHHMGMSYMDSNSTMQPSHHHPTTSASHSHGGGDSSMMMMPMTFYFGFKNV
ELLFSGLVINTAGEMAGAFVAVFLLAMFYEGLKIARESLLRKSQVSIRYNSMPVPGPNGTIGSA
GSAASGKAVDTWVGSAASGASGLMETHKTVGQQMLSFPHLLQTVLHIIQVVISYFLMLIFMTYN
GYLCIAVAAGAGTGYFLFSWKKAVVVDITEHCH*

iLID Insertion:

Full name: Myc-(1-100)hCTR1-iLID-(101-190)hCTR1
Abbreviation in the text: Myc-hCTR1-100iLID
Description: Human CTR1 with an N-terminal Myc tag and an intracellular iLID in between S100 and I101
MEQKLISEEDLDHSHHMGMSYMDSNSTMQPSHHHPTTSASHSHGGGDSSMMMMPMTFYFGFKNV
ELLFSGLVINTAGEMAGAFVAVFLLAMFYEGLKIARESLLRKSQVSGSAGSAASGLATTLERIE
KNFVITDPRLPDNPIIFASDSFLQLTEYSREEILGRNCRFLQGPETDRATVRKIRDAIDNQTEV
TVQLINYTKSGKKFWNVFHLQPMRDYKGDVQYFIGVQLDGTERLHGAAEREAVCLIKKTAFGIE
AANDENYFGSAASGASGIRYNSMPVPGPNGTILMETHKTVGQQMLSFPHLLQTVLHIIQVVISY
FLMLIFMTYNGYLCIAVAAGAGTGYFLFSWKKAVVVDITEHCH*

APEX2 Insertions:

Full name: Myc-(1-100)hCTR1-APEX2-(101-190)hCTR1
Abbreviation in the text: Myc-hCTR1-100APEX2
Description: Human CTR1 with an N-terminal Myc tag and an intracellular APEX2 in between S100 and I101
MEQKLISEEDLDHSHHMGMSYMDSNSTMQPSHHHPTTSASHSHGGGDSSMMMMPMTFYFGFKNV
ELLFSGLVINTAGEMAGAFVAVFLLAMFYEGLKIARESLLRKSQVSGSAGSAASGMGKSYPTVS
ADYQDAVEKAKKKLRGFIAEKRCAPLMLRLAFHSAGTFDKGTKTGGPFGTIKHPAELAHSANNG
LDIAVRLLEPLKAEFPILSYADFYQLAGVVAVEVTGGPKVPFHPGREDKPEPPPEGRLPDPTKG
SDHLRDVFGKAMGLTDQDIVALSGGHTIGAAHKERSGFEGPWTSNPLIFDNSYFTELLSGEKEG
LLQLPSDKALLSDPVFRPLVDKYAADEDAFFADYAEAHQKLSELGFADAGSAASGASGIRYNSM
PVPGPNGTILMETHKTVGQQMLSFPHLLQTVLHIIQVVISYFLMLIFMTYNGYLCIAVAAGAGT
GYFLFSWKKAVVVDITEHCH*

Full name: Myc-(1-115)hCTR1-APEX2-(116-190)hCTR1
Abbreviation in the text: Myc-hCTR1-115APEX2
Description: Human CTR1 with an N-terminal Myc tag and an intracellular APEX2 in between I115 and L116
MEQKLISEEDLDHSHHMGMSYMDSNSTMQPSHHHPTTSASHSHGGGDSSMMMMPMTFYFGFKNV
ELLFSGLVINTAGEMAGAFVAVFLLAMFYEGLKIARESLLRKSQVSIRYNSMPVPGPNGTIGSA
GSAASGMGKSYPTVSADYQDAVEKAKKKLRGFIAEKRCAPLMLRLAFHSAGTFDKGTKTGGPFG
TIKHPAELAHSANNGLDIAVRLLEPLKAEFPILSYADFYQLAGVVAVEVTGGPKVPFHPGREDK
PEPPPEGRLPDPTKGSDHLRDVFGKAMGLTDQDIVALSGGHTIGAAHKERSGFEGPWTSNPLIF
DNSYFTELLSGEKEGLLQLPSDKALLSDPVFRPLVDKYAADEDAFFADYAEAHQKLSELGFADA
GSAASGASGLMETHKTVGQQMLSFPHLLQTVLHIIQVVISYFLMLIFMTYNGYLCIAVAAGAGT
GYFLFSWKKAVVVDITEHCH*

Co-Expressed Constructs (PDZ, SspB):

Full name: cpPDZ-mCherry
Abbreviation in the text: cpPDZ-mCh
Description: Circularly-permutated PDZ with a C-terminal mCherry
MPELGFSISGGVGGRGNPFRPDDDGIFVTRVQPEGPASKLLQPGDKIIQANGYSFINIEHGQAV
SLLKTFQNTVELIIVREVGNGAKQEIRVRVEKDSRLELKLRILQSTVPRARDPPVATMVSKGEE
DNMAIIKEFMRFKVHMEGSVNGHEFEIEGEGEGRPYEGTQTAKLKVTKGGPLPFAWDILSPQFM
YGSKAYVKHPADIPDYLKLSFPEGFKWERVMNFEDGGVVTVTQDSSLQDGEFIYKVKLRGTNFP
SDGPVMQKKTMGWEASSERMYPEDGALKGEIKQRLKLKDGGHYDAEVKTTYKAKKPVQLPGAYN
VNIKLDITSHNEDYTIVEQYERAEGRHSTGGMDELYK*

Full name: ePDZb-mCherry
Abbreviation in the text: ePDZb-mCh
Description: Engineered PDZ (fused with fibronectin type III) with a C-terminal mCherry
MPELGFSISGGVGGRGNPFRPDDDGIFVTRVQPEGPASKLLQPGDKIIQANGYSFINIEHGQAV
SLLKTFQNTVELIIVREVGNGAKQEIRVRVEKDGGSGGVSSVPTNLEVVAATPTSLLISWDAYY
DSHVSYYRITYGETGGNSPVQEFTVPGSKSTATISGLKPGVDYTITVYAHYNYHYYSSPISINY
RTSRLELKLRILQSTVPRARDPPVATMVSKGEEDNMAIIKEFMRFKVHMEGSVNGHEFEIEGEG
EGRPYEGTQTAKLKVTKGGPLPFAWDILSPQFMYGSKAYVKHPADIPDYLKLSFPEGFKWERVM
NFEDGGVVTVTQDSSLQDGEFIYKVKLRGTNFPSDGPVMQKKTMGWEASSERMYPEDGALKGEI
KQRLKLKDGGHYDAEVKTTYKAKKPVQLPGAYNVNIKLDITSHNEDYTIVEQYERAEGRHSTGG
MDELYK*

Full name: ePDZb-Atox1
Abbreviation in the text: ePDZb-Atox1
Description: Engineered PDZ (fused with fibronectin type III) with a C-terminal Atox1
MPELGFSISGGVGGRGNPFRPDDDGIFVTRVQPEGPASKLLQPGDKIIQANGYSFINIEHGQAV
SLLKTFQNTVELIIVREVGNGAKQEIRVRVEKDGGSGGVSSVPTNLEVVAATPTSLLISWDAYY
DSHVSYYRITYGETGGNSPVQEFTVPGSKSTATISGLKPGVDYTITVYAHYNYHYYSSPISINY
RTSRLELKLRILQSTVPRARDPPVATMPKHEFSVDMTCGGCAEAVSRVLNKLGGVKYDIDLPNK
KVCIESEHSMDTLLATLKKTGKTVSYLGLE*

Full name: TagRFPt-SspB-Nano
Abbreviation in the text: RFPt-SspB-Nano
Description: Wild-type SspB with an N-terminal monomeric red fluorescent protein TagRFPt
MVSKGEELIKENMHMKLYMEGTVNNHHFKCTSEGEGKPYEGTQTMRIKVVEGGPLPFAFDILAT
SFMYGSRTFINHTQGIPDFFKQSFPEGFTWERVTTYEDGGVLTATQDTSLQDGCLIYNVKIRGV
NFPSNGPVMQKKTLGWEANTEMLYPADGGLEGRTDMALKLVGGGHLICNFKTTYRSKKPAKNLK
MPGVYYVDHRLERIKEADKETYVEQHEVAVARYCDLPSKLGHKLNGMDELYKSGLRSRAQASNE
FGIDLSGLTLQEFSSPKRPKLLREYYDWLVDNSFTPYLVVDATYLGVNVPVEYVKDGQIVLNLS
ASATGNLQLTNDFIQFNARFKGVSRELYIPMGAALAIYARENGDGVMFEPEEIYDELNIG*

Full name: TagRFPt-SspB-Micro
Abbreviation in the text: RFPt-SspB-Micro
Description: SspB with an R73Q mutation and an N-terminal monomeric red fluorescent protein TagRFPt
MVSKGEELIKENMHMKLYMEGTVNNHHFKCTSEGEGKPYEGTQTMRIKVVEGGPLPFAFDILAT
SFMYGSRTFINHTQGIPDFFKQSFPEGFTWERVTTYEDGGVLTATQDTSLQDGCLIYNVKIRGV
NFPSNGPVMQKKTLGWEANTEMLYPADGGLEGRTDMALKLVGGGHLICNFKTTYRSKKPAKNLK
MPGVYYVDHRLERIKEADKETYVEQHEVAVARYCDLPSKLGHKLNGMDELYKSGLRSRAQASNE
FGIDLSGLTLQEFSSPKRPKLLREYYDWLVDNSFTPYLVVDATYLGVNVPVEYVKDGQIVLNLS
ASATGNLQLTNDFIQFNA**Q**FKGVSRELYIPMGAALAIYARENGDGVMFEPEEIYDELNIG*

Full name: TagRFPt-SspB-Milli
Abbreviation in the text: RFPt-SspB-Milli
Description: SspB with R73Q and A58V mutations and an N-terminal monomeric red fluorescent protein TagRFP-t
MVSKGEELIKENMHMKLYMEGTVNNHHFKCTSEGEGKPYEGTQTMRIKVVEGGPLPFAFDILAT
SFMYGSRTFINHTQGIPDFFKQSFPEGFTWERVTTYEDGGVLTATQDTSLQDGCLIYNVKIRGV
NFPSNGPVMQKKTLGWEANTEMLYPADGGLEGRTDMALKLVGGGHLICNFKTTYRSKKPAKNLK
MPGVYYVDHRLERIKEADKETYVEQHEVAVARYCDLPSKLGHKLNGMDELYKSGLRSRAQASNE
FGIDLSGLTLQEFSSPKRPKLLREYYDWLVDNSFTPYLVVDATYLGVNVPVEYVKDGQIVLNLS
AS**V**TGNLQLTNDFIQFNA**Q**FKGVSRELYIPMGAALAIYARENGDGVMFEPEEIYDELNIG*

Point Mutations in hCTR1 and hCTR1-APEX2 constructs:

Full name: Myc-hCTR1(M150L)
Abbreviation in the text: Myc-hCTR1(M150L)
Description: Human CTR1 with an N-terminal Myc tag and a point mutation converting Met150 to Leucine
MEQKLISEEDLDHSHHMGMSYMDSNSTMQPSHHHPTTSASHSHGGGDSSMMMMPMTFYFGFKNV
ELLFSGLVINTAGEMAGAFVAVFLLAMFYEGLKIARESLLRKSQVSIRYNSMPVPGPNGTILME
THKTVGQQMLSFPHLLQTVLHIIQVVISYFL**L**LIFMTYNGYLCIAVAAGAGTGYFLFSWKKAVV
VDITEHCH*

Full name: Myc-hCTR1(M150/154L)
Abbreviation in the text: Myc-hCTR1(M150/154L)
Description: Human CTR1 with an N-terminal Myc tag and two point mutations converting Met150 and Met154 to Leucines
MEQKLISEEDLDHSHHMGMSYMDSNSTMQPSHHHPTTSASHSHGGGDSSMMMMPMTFYFGFKNV
ELLFSGLVINTAGEMAGAFVAVFLLAMFYEGLKIARESLLRKSQVSIRYNSMPVPGPNGTILME
THKTVGQQMLSFPHLLQTVLHIIQVVISYFL**L**LIF**L**TYNGYLCIAVAAGAGTGYFLFSWKKAVV
VDITEHCH*

Full name: Myc-(1-100)hCTR1-APEX2-(101-190)hCTR1(M150L)
Abbreviation in the text: Myc-hCTR1(M150L)-100APEX2
Description: Human CTR1 with an N-terminal Myc tag, an intracellular APEX2 in between S100 and I101, and a point mutation converting Met150 to Leucine
MEQKLISEEDLDHSHHMGMSYMDSNSTMQPSHHHPTTSASHSHGGGDSSMMMMPMTFYFGFKNV
ELLFSGLVINTAGEMAGAFVAVFLLAMFYEGLKIARESLLRKSQVSGSAGSAASGMGKSYPTVS
ADYQDAVEKAKKKLRGFIAEKRCAPLMLRLAFHSAGTFDKGTKTGGPFGTIKHPAELAHSANNG
LDIAVRLLEPLKAEFPILSYADFYQLAGVVAVEVTGGPKVPFHPGREDKPEPPPEGRLPDPTKG
SDHLRDVFGKAMGLTDQDIVALSGGHTIGAAHKERSGFEGPWTSNPLIFDNSYFTELLSGEKEG
LLQLPSDKALLSDPVFRPLVDKYAADEDAFFADYAEAHQKLSELGFADAGSAASGASGIRYNSM
PVPGPNGTILMETHKTVGQQMLSFPHLLQTVLHIIQVVISYFL**L**LIFMTYNGYLCIAVAAGAGT
GYFLFSWKKAVVVDITEHCH*

Full name: Myc-(1-100)hCTR1-APEX2-(101-190)hCTR1(M150/154L)
Abbreviation in the text: Myc-hCTR1(M150/154L)-100APEX2
Description: Human CTR1 with an N-terminal Myc tag, an intracellular APEX2 in between S100 and I101, and two point mutations converting Met150 and Met154 to Leucines
MEQKLISEEDLDHSHHMGMSYMDSNSTMQPSHHHPTTSASHSHGGGDSSMMMMPMTFYFGFKNV
ELLFSGLVINTAGEMAGAFVAVFLLAMFYEGLKIARESLLRKSQVSGSAGSAASGMGKSYPTVS
ADYQDAVEKAKKKLRGFIAEKRCAPLMLRLAFHSAGTFDKGTKTGGPFGTIKHPAELAHSANNG
LDIAVRLLEPLKAEFPILSYADFYQLAGVVAVEVTGGPKVPFHPGREDKPEPPPEGRLPDPTKG
SDHLRDVFGKAMGLTDQDIVALSGGHTIGAAHKERSGFEGPWTSNPLIFDNSYFTELLSGEKEG
LLQLPSDKALLSDPVFRPLVDKYAADEDAFFADYAEAHQKLSELGFADAGSAASGASGIRYNSM
PVPGPNGTILMETHKTVGQQMLSFPHLLQTVLHIIQVVISYFL**L**LIF**L**TYNGYLCIAVAAGAGT
GYFLFSWKKAVVVDITEHCH*

Full name: Myc-(1-115)hCTR1-APEX2-(116-190)hCTR1(M150L)
Abbreviation in the text: Myc-hCTR1(M150L)-115APEX2
Description: Human CTR1 with an N-terminal Myc tag, an intracellular APEX2 in between I115 and L116, and a point mutation converting Met150 to Leucine
MEQKLISEEDLDHSHHMGMSYMDSNSTMQPSHHHPTTSASHSHGGGDSSMMMMPMTFYFGFKNV
ELLFSGLVINTAGEMAGAFVAVFLLAMFYEGLKIARESLLRKSQVSIRYNSMPVPGPNGTIGSA
GSAASGMGKSYPTVSADYQDAVEKAKKKLRGFIAEKRCAPLMLRLAFHSAGTFDKGTKTGGPFG
TIKHPAELAHSANNGLDIAVRLLEPLKAEFPILSYADFYQLAGVVAVEVTGGPKVPFHPGREDK
PEPPPEGRLPDPTKGSDHLRDVFGKAMGLTDQDIVALSGGHTIGAAHKERSGFEGPWTSNPLIF
DNSYFTELLSGEKEGLLQLPSDKALLSDPVFRPLVDKYAADEDAFFADYAEAHQKLSELGFADA
GSAASGASGLMETHKTVGQQMLSFPHLLQTVLHIIQVVISYFL**L**LIFMTYNGYLCIAVAAGAGT
GYFLFSWKKAVVVDITEHCH*

Full name: Myc-(1-115)hCTR1-APEX2-(116-190)hCTR1(M150/154L)
Abbreviation in the text: Myc-hCTR1(M150/154L)-115APEX2
Description: Human CTR1 with an N-terminal Myc tag, an intracellular APEX2 in between I115 and L116, and two point mutations converting Met150 and Met154 to Leucines
MEQKLISEEDLDHSHHMGMSYMDSNSTMQPSHHHPTTSASHSHGGGDSSMMMMPMTFYFGFKNV
ELLFSGLVINTAGEMAGAFVAVFLLAMFYEGLKIARESLLRKSQVSIRYNSMPVPGPNGTIGSA
GSAASGMGKSYPTVSADYQDAVEKAKKKLRGFIAEKRCAPLMLRLAFHSAGTFDKGTKTGGPFG
TIKHPAELAHSANNGLDIAVRLLEPLKAEFPILSYADFYQLAGVVAVEVTGGPKVPFHPGREDK
PEPPPEGRLPDPTKGSDHLRDVFGKAMGLTDQDIVALSGGHTIGAAHKERSGFEGPWTSNPLIF
DNSYFTELLSGEKEGLLQLPSDKALLSDPVFRPLVDKYAADEDAFFADYAEAHQKLSELGFADA
GSAASGASGLMETHKTVGQQMLSFPHLLQTVLHIIQVVISYFL**L**LIF**L**TYNGYLCIAVAAGAGT
GYFLFSWKKAVVVDITEHCH*

References

1 Nevitt, T., Öhrvik, H. & Thiele, D. J. Charting the travels of copper in eukaryotes from yeast to mammals. *Biochimica et Biophysica Acta (BBA) - Molecular Cell Research* **1823**, 1580-1593, doi:10.1016/j.bbamcr.2012.02.011 (2012).

2 Finney, J., Moon, H.-J., Ronnebaum, T., Lantz, M. & Mure, M. Human copper-dependent amine oxidases. *Archives of Biochemistry and Biophysics* **546**, 19-32, doi:10.1016/j.abb.2013.12.022 (2014).

3 Horn, D. & Barrientos, A. Mitochondrial copper metabolism and delivery to cytochrome c oxidase. *IUBMB Life* **60**, 421-429, doi:10.1002/iub.50 (2008).

4 Kim, B.-E., Nevitt, T. & Thiele, D. J. Mechanisms for copper acquisition, distribution and regulation. *Nature Chemical Biology* **4**, 176-185, doi:10.1038/nchembio.72 (2008).

5 Lutsenko, S. Copper trafficking to the secretory pathway. *Metallomics* **8**, 840-852, doi:10.1039/c6mt00176a (2016).

6 Zhou, B. & Gitschier, J. hCTR1: a human gene for copper uptake identified by complementation in yeast. *Proceedings of the National Academy of Sciences of the United States of America* **94**, 7481-7486 (1997).

7 Lee, J., Prohaska, J. R., Dagenais, S. L., Glover, T. W. & Thiele, D. J. Isolation of a murine copper transporter gene, tissue specific expression and functional complementation of a yeast copper transport mutant. *Gene* **254**, 87-96, doi:10.1016/s0378-1119(00)00287-0 (2000).

8 Lin, C., Zhang, Z., Wang, T., Chen, C. & James Kang, Y. Copper uptake by DMT1: a compensatory mechanism for CTR1 deficiency in human umbilical vein endothelial cells. *Metallomics* **7**, 1285-1289, doi:10.1039/c5mt00097a (2015).

9 Lee, J., Petris, M. J. & Thiele, D. J. Characterization of Mouse Embryonic Cells Deficient in the Ctr1 High Affinity Copper Transporter. *Journal of Biological Chemistry* **277**, 40253-40259, doi:10.1074/jbc.M208002200 (2002).

10 Kuo, Y. M., Zhou, B., Cosco, D. & Gitschier, J. The copper transporter CTR1 provides an essential function in mammalian embryonic development. *Proceedings of the National Academy of Sciences* **98**, 6836-6841, doi:10.1073/pnas.111057298 (2001).

11 Lee, J., Prohaska, J. R. & Thiele, D. J. Essential role for mammalian copper transporter Ctr1 in copper homeostasis and embryonic development. *Proceedings of the National Academy of Sciences* **98**, 6842-6847, doi:10.1073/pnas.111058698 (2001).

12 Aller, S. G. & Unger, V. M. Projection structure of the human copper transporter CTR1 at 6-A resolution reveals a compact trimer with a novel channel-like architecture. *Proceedings of the National Academy of Sciences* **103**, 3627-3632, doi:10.1073/pnas.0509929103 (2006).

13 De Feo, C. J., Aller, S. G., Siluvai, G. S., Blackburn, N. J. & Unger, V. M. Three-dimensional structure of the human copper transporter hCTR1. *Proceedings of the National Academy of Sciences* **106**, 4237-4242, doi:10.1073/pnas.0810286106 (2009).

14 Pushie, M. J., Shaw, K., Franz, K. J., Shearer, J. & Haas, K. L. Model Peptide Studies Reveal a Mixed Histidine-Methionine Cu(I) Binding Site at the N-Terminus of Human Copper Transporter 1. *Inorganic Chemistry* **54**, 8544-8551, doi:10.1021/acs.inorgchem.5b01162 (2015).
15 Haas, K. L., Putterman, A. B., White, D. R., Thiele, D. J. & Franz, K. J. Model Peptides Provide New Insights into the Role of Histidine Residues as Potential Ligands in Human Cellular Copper Acquisition via Ctr1. *Journal of the American Chemical Society* **133**, 4427-4437, doi:10.1021/ja108890c (2011).
16 Öhrvik, H., Logeman, B., Turk, B., Reinheckel, T. & Thiele, D. J. Cathepsin Protease Controls Copper and Cisplatin Accumulation via Cleavage of the Ctr1 Metal-binding Ectodomain. *Journal of Biological Chemistry* **291**, 13905-13916, doi:10.1074/jbc.M116.731281 (2016).
17 Wu, X., Sinani, D., Kim, H. & Lee, J. Copper Transport Activity of Yeast Ctr1 Is Down-regulated via Its C Terminus in Response to Excess Copper. *Journal of Biological Chemistry* **284**, 4112-4122, doi:10.1074/jbc.M807909200 (2009).
18 Maryon, E. B., Molloy, S. A., Ivy, K., Yu, H. & Kaplan, J. H. Rate and Regulation of Copper Transport by Human Copper Transporter 1 (hCTR1). *Journal of Biological Chemistry* **288**, 18035-18046, doi:10.1074/jbc.M112.442426 (2013).
19 Kahra, D., Kovermann, M. & Wittung-Stafshede, P. The C-Terminus of Human Copper Importer Ctr1 Acts as a Binding Site and Transfers Copper to Atox1. *Biophysical Journal* **110**, 95-102, doi:10.1016/j.bpj.2015.11.016 (2016).
20 Petris, M. J., Smith, K., Lee, J. & Thiele, D. J. Copper-stimulated Endocytosis and Degradation of the Human Copper Transporter, hCtr1. *Journal of Biological Chemistry* **278**, 9639-9646, doi:10.1074/jbc.M209455200 (2003).
21 Molloy, S. A. & Kaplan, J. H. Copper-dependent Recycling of hCTR1, the Human High Affinity Copper Transporter. *Journal of Biological Chemistry* **284**, 29704-29713, doi:10.1074/jbc.M109.000166 (2009).
22 Guo, Y., Smith, K., Lee, J., Thiele, D. J. & Petris, M. J. Identification of Methionine-rich Clusters That Regulate Copper-stimulated Endocytosis of the Human Ctr1 Copper Transporter. *Journal of Biological Chemistry* **279**, 17428-17433, doi:10.1074/jbc.M401493200 (2004).
23 Clifford, R. J., Maryon, E. B. & Kaplan, J. H. Dynamic internalization and recycling of a metal ion transporter: Cu homeostasis and CTR1, the human Cu+ uptake system. *Journal of Cell Science* **129**, 1711-1721, doi:10.1242/jcs.173351 (2016).
24 Cubitt, A. B. *et al.* Understanding, improving and using green fluorescent proteins. *Trends in biochemical sciences* **20**, 448-455 (1995).
25 Collings, D. A. Subcellular Localization of Transiently Expressed Fluorescent Fusion Proteins. **1069**, 227-258, doi:10.1007/978-1-62703-613-9_16 (2013).
26 De Los Santos, C., Chang, C.-W., Mycek, M.-A. & Cardullo, R. A. FRAP, FLIM, and FRET: Detection and analysis of cellular dynamics on a molecular scale using fluorescence microscopy. *Molecular Reproduction and Development* **82**, 587-604, doi:10.1002/mrd.22501 (2015).
27 Toettcher, J. E., Gong, D., Lim, W. A. & Weiner, O. D. Light Control of Plasma Membrane Recruitment Using the Phy–PIF System. **497**, 409-423, doi:10.1016/b978-0-12-385075-1.00017-2 (2011).

28 Strickland, D. *et al.* TULIPs: tunable, light-controlled interacting protein tags for cell biology. *Nature Methods* **9**, 379-384, doi:10.1038/nmeth.1904 (2012).
29 Bugaj, L. J. *et al.* Regulation of endogenous transmembrane receptors through optogenetic Cry2 clustering. *Nature Communications* **6**, 6898, doi:10.1038/ncomms7898 (2015).
30 Guntas, G. *et al.* Engineering an improved light-induced dimer (iLID) for controlling the localization and activity of signaling proteins. *Proceedings of the National Academy of Sciences* **112**, 112-117, doi:10.1073/pnas.1417910112 (2015).
31 Zhang, K. & Cui, B. Optogenetic control of intracellular signaling pathways. *Trends in Biotechnology* **33**, 92-100, doi:10.1016/j.tibtech.2014.11.007 (2015).
32 Hallett, R. A., Zimmerman, S. P., Yumerefendi, H., Bear, J. E. & Kuhlman, B. Correlating in Vitro and in Vivo Activities of Light-Inducible Dimers: A Cellular Optogenetics Guide. *ACS Synthetic Biology* **5**, 53-64, doi:10.1021/acssynbio.5b00119 (2016).
33 Chen, C.-L. & Perrimon, N. Proximity-dependent labeling methods for proteomic profiling in living cells. *Wiley Interdisciplinary Reviews: Developmental Biology* **6**, e272, doi:10.1002/wdev.272 (2017).
34 Zhuang, M., Guan, S., Wang, H., Burlingame, Alma L. & Wells, James A. Substrates of IAP Ubiquitin Ligases Identified with a Designed Orthogonal E3 Ligase, the NEDDylator. *Molecular Cell* **49**, 273-282, doi:10.1016/j.molcel.2012.10.022 (2013).
35 Puig, S., Lee, J., Lau, M. & Thiele, D. J. Biochemical and Genetic Analyses of Yeast and Human High Affinity Copper Transporters Suggest a Conserved Mechanism for Copper Uptake. *Journal of Biological Chemistry* **277**, 26021-26030, doi:10.1074/jbc.M202547200 (2002).
36 Zhang, G., Gurtu, V. & Kain, S. R. An Enhanced Green Fluorescent Protein Allows Sensitive Detection of Gene Transfer in Mammalian Cells. *Biochemical and Biophysical Research Communications* **227**, 707-711, doi:10.1006/bbrc.1996.1573 (1996).
37 Topell, S. & Glockshuber, R. Circular Permutation of the Green Fluorescent Protein. **183**, 031-048, doi:10.1385/1-59259-280-5:031 (2002).
38 Lee, J., Peña, M. M. O., Nose, Y. & Thiele, D. J. Biochemical Characterization of the Human Copper Transporter Ctr1. *Journal of Biological Chemistry* **277**, 4380-4387, doi:10.1074/jbc.M104728200 (2002).
39 Quail, J. F., Tsai, C.-Y. & Howell, S. B. Characterization of a monoclonal antibody capable of reliably quantifying expression of Human Copper Transporter 1 (hCTR1). *Journal of Trace Elements in Medicine and Biology* **28**, 151-159, doi:10.1016/j.jtemb.2013.12.003 (2014).
40 Tsai, C.-Y., Larson, C. A., Safaei, R. & Howell, S. B. Molecular modulation of the copper and cisplatin transport function of CTR1 and its interaction with IRS-4. *Biochemical Pharmacology* **90**, 379-387, doi:10.1016/j.bcp.2014.06.019 (2014).
41 Pase, L., Voskoboinik, I., Greenough, M. & Camakaris, J. Copper stimulates trafficking of a distinct pool of the Menkes copper ATPase (ATP7A) to the plasma membrane and diverts it into a rapid recycling pool. *Biochemical Journal* **378**, 1031-1037, doi:10.1042/bj20031181 (2004).

42 Pudasaini, A., El-Arab, K. K. & Zoltowski, B. D. LOV-based optogenetic devices: light-driven modules to impart photoregulated control of cellular signaling. *Frontiers in Molecular Biosciences* **2**, doi:10.3389/fmolb.2015.00018 (2015).
43 Halavaty, A. S. & Moffat, K. N- and C-Terminal Flanking Regions Modulate Light-Induced Signal Transduction in the LOV2 Domain of the Blue Light Sensor Phototropin 1 from Avena sativa. *Biochemistry* **46**, 14001-14009, doi:10.1021/bi701543e (2007).
44 Zayner, J. P., Antoniou, C. & Sosnick, T. R. The Amino-Terminal Helix Modulates Light-Activated Conformational Changes in AsLOV2. *Journal of Molecular Biology* **419**, 61-74, doi:10.1016/j.jmb.2012.02.037 (2012).
45 Harper, S. M. Structural Basis of a Phototropin Light Switch. *Science* **301**, 1541-1544, doi:10.1126/science.1086810 (2003).
46 Wu, Y. I. *et al.* A genetically encoded photoactivatable Rac controls the motility of living cells. *Nature* **461**, 104-108, doi:10.1038/nature08241 (2009).
47 Hatori, Y. & Lutsenko, S. The Role of Copper Chaperone Atox1 in Coupling Redox Homeostasis to Intracellular Copper Distribution. *Antioxidants* **5**, 25, doi:10.3390/antiox5030025 (2016).
48 Levy, A. R., Nissim, M., Mendelman, N., Chill, J. & Ruthstein, S. Ctr1 Intracellular Loop Is Involved in the Copper Transfer Mechanism to the Atox1 Metallochaperone. *The Journal of Physical Chemistry B* **120**, 12334-12345, doi:10.1021/acs.jpcb.6b10222 (2016).
49 Huang, J., Koide, A., Makabe, K. & Koide, S. Design of protein function leaps by directed domain interface evolution. *Proceedings of the National Academy of Sciences* **105**, 6578-6583, doi:10.1073/pnas.0801097105 (2008).
50 Huang, J., Makabe, K., Biancalana, M., Koide, A. & Koide, S. Structural Basis for Exquisite Specificity of Affinity Clamps, Synthetic Binding Proteins Generated through Directed Domain-interface Evolution. *Journal of Molecular Biology* **392**, 1221-1231, doi:10.1016/j.jmb.2009.07.067 (2009).
51 Lungu, Oana I. *et al.* Designing Photoswitchable Peptides Using the AsLOV2 Domain. *Chemistry & Biology* **19**, 507-517, doi:10.1016/j.chembiol.2012.02.006 (2012).
52 Zimmerman, S. P. *et al.* Tuning the Binding Affinities and Reversion Kinetics of a Light Inducible Dimer Allows Control of Transmembrane Protein Localization. *Biochemistry* **55**, 5264-5271, doi:10.1021/acs.biochem.6b00529 (2016).
53 Shaner, N. C. *et al.* Improving the photostability of bright monomeric orange and red fluorescent proteins. *Nature Methods* **5**, 545-551, doi:10.1038/nmeth.1209 (2008).
54 Chan, J. S., Teo, Z., Sng, M. K. & Tan, N. S. Probing for protein-protein interactions during cell migration: limitations and challenges. *Histology and histopathology* **29**, 965-976, doi:10.14670/HH-29.965 (2014).
55 Avila, J. R., Lee, J. S. & Toriia, K. U. Co-Immunoprecipitation of Membrane-Bound Receptors. *The Arabidopsis Book* **13**, e0180, doi:10.1199/tab.0180 (2015).
56 Hung, V. *et al.* Spatially resolved proteomic mapping in living cells with the engineered peroxidase APEX2. *Nature Protocols* **11**, 456-475, doi:10.1038/nprot.2016.018 (2016).

57 Lobingier, B. T. *et al.* An Approach to Spatiotemporally Resolve Protein Interaction Networks in Living Cells. *Cell* **169**, 350-360.e312, doi:10.1016/j.cell.2017.03.022 (2017).
58 Paek, J. *et al.* Multidimensional Tracking of GPCR Signaling via Peroxidase-Catalyzed Proximity Labeling. *Cell* **169**, 338-349.e311, doi:10.1016/j.cell.2017.03.028 (2017).
59 Tsai, C.-Y., Liebig, J. K., Tsigelny, I. F. & Howell, S. B. The copper transporter 1 (CTR1) is required to maintain the stability of copper transporter 2 (CTR2). *Metallomics* **7**, 1477-1487, doi:10.1039/c5mt00131e (2015).

Appendix I

RNA Sequencing Data from $CTR1^{-/-}$ and $CTR1^{+/+}$ Mouse Embryonic Fibroblasts

The following pages list the genes downregulated (log_2(FoldChange) = log2FC < -6.0) and upregulated (log2FC > 6.0) in $CTR1^{-/-}$ MEFs relative to $CTR1^{+/+}$ mouse embryonic fibroblasts (MEFs), from the RNA sequencing experiment described in Chapter 3.

GeneID	baseMean	log2FC	padj	Gene_name
ENSMUSG00000069045.8	5711.7	-12.29	1.14E-168	Ddx3y
ENSMUSG00000049047.8	1675.9	-10.71	9.79E-115	Armcx3
ENSMUSG00000060969.8	1653.7	-10.69	3.08E-114	Irx1
ENSMUSG00000063632.6	3928.8	-10.44	9.37E-102	Sox11
ENSMUSG00000036103.8	2717.7	-10.13	2.15E-198	Colec12
ENSMUSG00000037060.2	3665.7	-10.02	1.60E-132	Prkcdbp
ENSMUSG00000029377.4	920.7	-9.93	4.79E-93	Ereg
ENSMUSG00000031198.4	4731.4	-9.89	1.77E-140	Fundc2
ENSMUSG00000047712.7	730.2	-9.63	1.88E-85	Ust
ENSMUSG00000033436.10	4216.3	-9.43	9.24E-286	Armcx2
ENSMUSG00000020473.10	11993.8	-9.34	1.15E-57	Aebp1
ENSMUSG00000029661.13	24051.8	-9.27	0	Col1a2
ENSMUSG00000025666.13	549.3	-9.26	2.19E-76	Tmem47
ENSMUSG00000025104.10	3492.8	-9.08	7.82E-88	Hdgfrp3
ENSMUSG00000034463.3	2316.3	-9.08	3.92E-103	Scara3
ENSMUSG00000074682.4	458.7	-9.03	3.20E-71	Zcchc3
ENSMUSG00000039095.8	2020.4	-8.95	3.46E-192	En2
ENSMUSG00000010751.11	2801.6	-8.91	2.33E-281	Tnfrsf22
ENSMUSG00000036745.12	5778.2	-8.84	0	Ttll7
ENSMUSG00000056673.11	2004.1	-8.75	6.69E-51	Kdm5d
ENSMUSG00000050248.11	1995.7	-8.53	2.15E-85	Evc2
ENSMUSG00000029913.11	1201.1	-8.45	9.40E-138	Prdm5
ENSMUSG00000027859.7	473.2	-8.35	6.66E-78	Ngf
ENSMUSG00000025534.14	2265.0	-8.34	5.64E-59	Gusb
ENSMUSG00000031673.5	1321.3	-8.32	1.32E-68	Cdh11
ENSMUSG00000037375.13	304.3	-8.18	9.40E-58	Hhat
ENSMUSG00000001555.7	6488.2	-8.01	0	Fkbp10
ENSMUSG00000016262.11	5714.2	-7.94	0	Sertad4
ENSMUSG00000057074.6	1630.4	-7.92	2.41E-83	Ces1g
ENSMUSG00000069049.8	2965.6	-7.92	2.64E-36	Eif2s3y
ENSMUSG00000004044.9	40563.0	-7.86	0	Ptrf
ENSMUSG00000030272.12	1656.3	-7.77	2.97E-54	Camk1
ENSMUSG00000068457.11	2111.7	-7.72	1.61E-34	Uty
ENSMUSG00000035045.14	788.1	-7.72	1.96E-48	Zc3h12b
ENSMUSG00000005950.11	876.3	-7.67	2.77E-144	P2rx5
ENSMUSG00000074516.5	1106.3	-7.66	1.24E-203	Gm10709
ENSMUSG00000036368.7	554.2	-7.63	3.77E-83	Rmdn2
ENSMUSG00000068758.7	156.0	-7.59	1.03E-43	Il3ra
ENSMUSG00000020695.11	4330.3	-7.49	2.22E-253	Mrc2
ENSMUSG00000097431.1	388.5	-7.46	3.20E-36	Gm26782
ENSMUSG00000025232.7	3367.9	-7.45	0	Hexa
ENSMUSG00000008206.12	366.1	-7.39	3.40E-79	Cers4

ENSMUSG00000031196.10	346.2	-7.38	3.99E-64	F8
ENSMUSG00000030826.14	1073.3	-7.24	2.86E-196	Bcat2
ENSMUSG00000020176.14	3068.4	-7.12	6.98E-77	Grb10
ENSMUSG00000037001.10	652.8	-7.02	9.63E-29	Zfp39
ENSMUSG00000028701.4	550.9	-6.98	3.05E-33	Lurap1
ENSMUSG00000031841.15	616.7	-6.96	2.84E-28	Cdh13
ENSMUSG00000031565.14	6550.8	-6.95	0	Fgfr1
ENSMUSG00000053475.5	96.1	-6.92	8.78E-34	Tnfaip6
ENSMUSG00000037784.11	4146.2	-6.83	6.15E-292	Dzip1l
ENSMUSG00000067928.6	1128.4	-6.82	5.74E-182	Zfp760
ENSMUSG00000021186.8	454.1	-6.75	7.95E-31	Fbln5
ENSMUSG00000090523.2	727.9	-6.75	2.08E-25	Gypc
ENSMUSG00000097348.5	76.1	-6.59	1.90E-29	Rmst
ENSMUSG00000021118.7	198.0	-6.59	4.05E-62	Plek2
ENSMUSG00000099876.1	74.0	-6.55	5.32E-29	Gm29650
ENSMUSG00000050394.11	70.2	-6.47	4.66E-28	Armcx6
ENSMUSG00000028464.13	8470.7	-6.45	0	Tpm2
ENSMUSG00000085154.4	85.2	-6.45	4.60E-30	C130046K22Rik
ENSMUSG00000016200.10	132.9	-6.45	1.31E-35	Syt14
ENSMUSG00000067212.8	688.6	-6.44	2.25E-25	H2-T23
ENSMUSG00000050908.9	838.2	-6.42	1.69E-39	Tvp23a
ENSMUSG00000046768.10	640.0	-6.42	8.30E-107	Rhoj
ENSMUSG00000022575.4	357.6	-6.37	9.64E-29	Gsdmd
ENSMUSG00000038070.12	2062.1	-6.36	4.64E-225	Cntln
ENSMUSG00000047996.13	1218.0	-6.34	2.31E-276	Prrg1
ENSMUSG00000025498.11	345.6	-6.32	9.10E-53	Irf7
ENSMUSG00000089812.2	123.6	-6.30	3.29E-32	Gm15867
ENSMUSG00000026433.10	102.0	-6.29	2.00E-28	Rab29
ENSMUSG00000060550.12	119.1	-6.29	7.44E-33	H2-Q7
ENSMUSG00000067818.6	385.5	-6.26	9.53E-59	Myl9
ENSMUSG00000049916.9	177.6	-6.25	6.73E-37	2610318N02Rik
ENSMUSG00000104623.1	715.0	-6.24	3.25E-156	RP24-352B14.1
ENSMUSG00000031767.10	59.3	-6.23	2.94E-25	Nudt7
ENSMUSG00000018698.12	151.4	-6.16	1.80E-38	Lhx1
ENSMUSG00000034040.13	55.1	-6.12	4.15E-24	Wbscr17
ENSMUSG00000023191.6	770.4	-6.07	5.27E-31	P3h3
ENSMUSG00000062743.6	120.7	-6.02	7.96E-36	Zfp677
ENSMUSG00000041143.13	628.8	-6.01	4.95E-107	Tmco4
ENSMUSG00000031340.8	599.3	-6.00	2.57E-27	Gabre
ENSMUSG00000036469.13	50.0	6.01	6.99E-23	March1
ENSMUSG00000034324.13	51.6	6.01	5.82E-23	Tmem132c
ENSMUSG00000094378.4	50.8	6.03	4.68E-23	Gm15097

ENSMUSG00000064194.7	90.3	6.03	7.66E-25	Zfp936
ENSMUSG00000019936.7	53.1	6.04	3.17E-23	Epyc
ENSMUSG00000034127.11	1516.5	6.06	1.58E-19	Tspan8
ENSMUSG00000032053.7	51.9	6.07	1.87E-23	Pou2af1
ENSMUSG00000021613.8	53.3	6.07	1.89E-23	Hapln1
ENSMUSG00000030220.10	6031.8	6.07	0	Arhgdib
ENSMUSG00000031342.14	103.3	6.09	8.00E-30	Gpm6b
ENSMUSG00000034634.7	57.5	6.10	6.87E-24	Ly6d
ENSMUSG00000042477.7	53.1	6.10	8.35E-24	Tfap2e
ENSMUSG00000010592.8	53.7	6.11	6.79E-24	Dazl
ENSMUSG00000027790.11	679.1	6.13	9.33E-21	Sis
ENSMUSG00000028565.15	4598.6	6.14	0	Nfia
ENSMUSG00000024500.15	596.9	6.15	5.48E-113	Ppp2r2b
ENSMUSG00000002190.10	836.4	6.15	5.37E-134	Clgn
ENSMUSG00000036553.13	2030.7	6.16	0	Sh3tc1
ENSMUSG00000029490.3	56.2	6.18	1.21E-24	Mfsd7a
ENSMUSG00000018986.9	230.9	6.18	4.30E-60	Slfn3
ENSMUSG00000067860.8	79.3	6.20	1.90E-29	Zic3
ENSMUSG00000032092.4	89.4	6.21	4.70E-28	Mpzl2
ENSMUSG00000029636.10	57.4	6.21	5.30E-25	Wasf3
ENSMUSG00000021728.7	395.4	6.21	2.29E-68	Emb
ENSMUSG00000068151.7	91.5	6.22	4.84E-28	A230006K03Rik
ENSMUSG00000027965.12	91.9	6.22	4.70E-28	Olfm3
ENSMUSG00000087620.4	104.6	6.22	2.30E-33	5330434G04Rik
ENSMUSG00000028369.12	95.9	6.24	7.56E-28	Svep1
ENSMUSG00000031618.10	505.7	6.24	1.13E-96	Nr3c2
ENSMUSG00000074011.3	60.0	6.24	2.09E-25	Gm7682
ENSMUSG00000039611.2	300.3	6.25	4.27E-27	Tmem246
ENSMUSG00000054863.8	84.0	6.25	8.84E-30	Fam19a5
ENSMUSG00000020154.9	325.8	6.26	4.97E-70	Ptprb
ENSMUSG00000030560.13	111.9	6.28	2.36E-27	Ctsc
ENSMUSG00000060314.9	258.4	6.28	2.01E-60	Zfp941
ENSMUSG00000078234.6	237.1	6.28	1.46E-44	Klhdc7a
ENSMUSG00000032702.13	4538.9	6.29	0	Kank1
ENSMUSG00000021732.11	95.0	6.29	8.89E-29	Fgf10
ENSMUSG00000029032.9	235.3	6.29	7.67E-49	Arhgef16
ENSMUSG00000026833.15	923.0	6.29	9.57E-167	Olfm1
ENSMUSG00000022076.9	157.6	6.31	2.82E-42	Klhl1
ENSMUSG00000046916.8	318.2	6.31	1.45E-27	Myct1
ENSMUSG00000049001.4	619.0	6.32	2.16E-39	Ndnf
ENSMUSG00000020098.6	62.2	6.33	2.56E-26	Pcbd1
ENSMUSG00000027971.13	432.4	6.35	2.50E-23	Ndst4
ENSMUSG00000034810.7	93.4	6.38	2.80E-31	Scn7a

ENSMUSG00000037910.2	66.6	6.43	1.89E-27	1700018B24Rik
ENSMUSG00000024678.6	610.9	6.45	2.82E-25	Ms4a4d
ENSMUSG00000041134.12	92.5	6.45	3.94E-33	Cyyr1
ENSMUSG00000026249.7	306.6	6.47	2.89E-27	Serpine2
ENSMUSG00000063488.5	68.7	6.47	5.45E-28	Zkscan7
ENSMUSG00000074971.4	106.8	6.48	2.94E-31	Fibin
ENSMUSG00000054942.10	1612.6	6.48	1.55E-215	Fam73a
ENSMUSG00000032179.7	70.2	6.48	4.33E-28	Bmp5
ENSMUSG00000036095.10	71.3	6.48	4.12E-28	Dgkb
ENSMUSG00000030162.11	115.5	6.51	5.53E-31	Olr1
ENSMUSG00000097694.4	617.6	6.52	1.16E-28	G730013B05Rik
ENSMUSG00000015599.8	1321.0	6.52	7.81E-268	Ttbk1
ENSMUSG00000057836.9	219.6	6.53	2.93E-46	Xlr3a
ENSMUSG00000096225.5	117.6	6.53	1.30E-31	Lhx8
ENSMUSG00000085282.5	113.2	6.54	3.20E-32	Gm15663
ENSMUSG00000054850.3	254.6	6.54	8.97E-50	6330419J24Rik
ENSMUSG00000028005.10	118.9	6.55	6.35E-32	Gucy1b3
ENSMUSG00000044647.13	143.7	6.56	2.47E-36	Csrnp3
ENSMUSG00000090744.4	98.7	6.58	5.47E-35	Gm6871
ENSMUSG00000031410.11	165.5	6.60	2.02E-35	Nxf7
ENSMUSG00000033152.10	199.6	6.60	8.51E-46	Podxl2
ENSMUSG00000029695.10	286.0	6.62	4.10E-48	Aass
ENSMUSG00000042258.10	77.1	6.62	8.83E-30	Isl1
ENSMUSG00000026405.11	163.6	6.64	1.23E-36	C4bp
ENSMUSG00000055421.5	3727.7	6.64	6.75E-223	Pcdh9
ENSMUSG00000042985.7	1838.9	6.66	1.42E-55	Upk3b
ENSMUSG00000034981.9	875.1	6.66	8.31E-52	Parm1
ENSMUSG00000036295.4	304.7	6.67	2.61E-53	Lrrn3
ENSMUSG00000019892.9	79.7	6.67	2.08E-30	Lrriq1
ENSMUSG00000062309.7	264.8	6.68	2.44E-27	Rpp25
ENSMUSG00000040811.12	766.3	6.69	1.06E-92	Eml2
ENSMUSG00000021950.12	8336.7	6.70	0	Anxa8
ENSMUSG00000036782.10	80.8	6.70	7.66E-31	Klhl13
ENSMUSG00000033453.7	138.3	6.71	3.58E-43	Adamts15
ENSMUSG00000021747.11	697.9	6.71	4.08E-25	4930452B06Rik
ENSMUSG00000022876.14	116.7	6.71	4.82E-36	Samsn1
ENSMUSG00000011148.10	1212.0	6.72	8.66E-174	Adssl1
ENSMUSG00000055745.4	83.0	6.74	2.48E-31	Ldoc1l
ENSMUSG00000021457.11	688.1	6.76	2.99E-96	Syk
ENSMUSG00000032940.13	593.0	6.76	3.40E-36	Rbm11
ENSMUSG00000036446.4	89.5	6.77	8.72E-32	Lum
ENSMUSG00000059857.12	86.6	6.78	7.96E-32	Ntng1
ENSMUSG00000005251.11	575.1	6.79	4.33E-29	Ripk4

ENSMUSG00000040264.10	340.7	6.80	3.32E-28	Gbp2b
ENSMUSG00000027792.8	478.3	6.85	1.24E-32	Bche
ENSMUSG00000031189.9	1430.4	6.85	1.70E-25	Aff2
ENSMUSG00000003051.10	407.2	6.86	2.55E-62	Elf3
ENSMUSG00000032062.1	294.5	6.86	7.65E-70	2310030G06Rik
ENSMUSG00000049436.4	566.5	6.86	5.35E-33	Upk1b
ENSMUSG00000019929.12	3634.7	6.87	6.46E-63	Dcn
ENSMUSG00000062345.7	91.5	6.88	3.88E-33	Serpinb2
ENSMUSG00000048424.12	385.4	6.89	1.42E-28	Ranbp3l
ENSMUSG00000024030.6	492.3	6.90	6.49E-28	Abcg1
ENSMUSG00000084128.7	523.9	6.91	1.48E-35	Esrp2
ENSMUSG00000074887.3	94.0	6.92	1.04E-33	EU599041
ENSMUSG00000039431.13	321.9	6.94	1.01E-54	Mtmr7
ENSMUSG00000021509.5	879.6	6.97	1.13E-28	Slc25a48
ENSMUSG00000035566.6	198.3	6.97	6.74E-43	Pcdh17
ENSMUSG00000038296.11	265.4	6.97	1.23E-51	Galnt18
ENSMUSG00000030513.11	356.1	6.97	1.06E-87	Pcsk6
ENSMUSG00000086748.1	97.5	6.97	2.06E-34	Gm13261
ENSMUSG00000058624.9	101.1	6.98	1.84E-34	Gda
ENSMUSG00000031379.10	930.8	6.98	1.82E-27	Pir
ENSMUSG00000035403.8	705.2	6.99	4.87E-107	Crb2
ENSMUSG00000031803.7	2246.4	7.00	3.34E-57	B3gnt3
ENSMUSG00000064115.10	1057.0	7.00	6.25E-34	Cadm2
ENSMUSG00000041193.12	101.0	7.00	8.47E-35	Pla2g5
ENSMUSG00000056025.9	1496.3	7.03	2.63E-171	Clca3a1
ENSMUSG00000047686.9	108.8	7.08	6.98E-36	Zcchc5
ENSMUSG00000027358.6	105.6	7.08	5.90E-36	Bmp2
ENSMUSG00000086807.4	106.2	7.09	4.33E-36	C330013F16Rik
ENSMUSG00000008999.7	150.1	7.12	3.86E-43	Bmp7
ENSMUSG00000040543.13	834.7	7.13	3.91E-111	Pitpnm3
ENSMUSG00000050808.10	111.1	7.15	5.91E-37	Muc15
ENSMUSG00000040569.10	485.1	7.17	1.88E-31	Slc26a7
ENSMUSG00000030587.4	2094.7	7.18	0	2200002D01Rik
ENSMUSG00000086646.4	205.2	7.18	8.76E-50	5133400J02Rik
ENSMUSG00000022311.12	116.8	7.18	2.24E-37	Csmd3
ENSMUSG00000020340.13	693.0	7.19	1.86E-122	Cyfip2
ENSMUSG00000097101.2	147.3	7.19	5.15E-40	1810034E14Rik
ENSMUSG00000031209.11	182.3	7.21	1.08E-41	Heph
ENSMUSG00000048337.3	1239.1	7.21	6.67E-31	Npy4r
ENSMUSG00000068327.4	468.4	7.21	4.30E-88	Tlx2
ENSMUSG00000052821.3	119.1	7.23	4.12E-38	Cysltr1
ENSMUSG00000031553.12	156.4	7.24	1.44E-46	Adam3
ENSMUSG00000032315.5	1158.3	7.24	7.47E-30	Cyp1a1

ENSMUSG00000030064.13	1426.9	7.26	6.66E-284	Frmd4b
ENSMUSG00000030222.10	121.9	7.28	8.45E-39	Rerg
ENSMUSG00000025328.6	4475.3	7.31	0	Padi3
ENSMUSG00000049387.6	242.5	7.31	8.15E-50	Cox7b2
ENSMUSG00000054889.6	3125.9	7.35	0	Dsp
ENSMUSG00000097216.3	128.5	7.35	6.21E-40	4932441J04Rik
ENSMUSG00000052371.5	129.3	7.36	4.17E-40	Hoxd3os1
ENSMUSG00000091071.2	129.1	7.37	4.18E-40	1700030C10Rik
ENSMUSG00000020679.8	459.4	7.37	2.17E-38	Hnf1b
ENSMUSG00000053411.13	3933.7	7.43	5.63E-300	Cbx7
ENSMUSG00000075316.8	255.2	7.44	3.41E-53	Scn9a
ENSMUSG00000061469.2	136.9	7.44	2.45E-41	Gm12569
ENSMUSG00000032359.11	344.5	7.46	6.49E-68	Ctsh
ENSMUSG00000054342.7	767.2	7.47	1.17E-119	Kcnn4
ENSMUSG00000024261.5	141.2	7.48	6.10E-42	Syt4
ENSMUSG00000016494.6	9137.5	7.49	0	Cd34
ENSMUSG00000035131.11	3572.9	7.50	2.40E-31	Brinp3
ENSMUSG00000025128.7	143.9	7.50	3.09E-42	Bhlhe22
ENSMUSG00000034533.9	153.7	7.57	2.39E-43	Scn10a
ENSMUSG00000050071.8	330.9	7.57	2.53E-63	Bex1
ENSMUSG00000025161.13	2224.8	7.58	1.12E-295	Slc16a3
ENSMUSG00000036098.12	6713.3	7.59	0	Myrf
ENSMUSG00000067001.8	156.6	7.60	7.79E-44	Serpinb7
ENSMUSG00000020467.12	8046.2	7.62	1.27E-32	Efemp1
ENSMUSG00000029838.8	351.6	7.75	9.56E-64	Ptn
ENSMUSG00000053279.6	4467.2	7.78	3.00E-34	Aldh1a1
ENSMUSG00000050663.7	175.4	7.79	6.75E-47	Trhde
ENSMUSG00000056004.13	519.1	7.79	2.93E-105	9330182L06Rik
ENSMUSG00000055717.10	176.2	7.79	5.44E-47	Slain1
ENSMUSG00000039349.5	187.3	7.87	2.15E-48	C130074G19Rik
ENSMUSG00000063297.6	188.6	7.88	1.55E-48	Luzp2
ENSMUSG00000073177.5	2994.7	7.94	0	Gm773
ENSMUSG00000025927.10	201.8	7.96	5.64E-50	Tfap2b
ENSMUSG00000026620.8	570.7	7.99	6.58E-104	Mark1
ENSMUSG00000022788.13	809.6	7.99	3.63E-56	Fgd4
ENSMUSG00000006360.8	1214.4	8.00	4.27E-56	Crip1
ENSMUSG00000025504.9	7877.7	8.03	0	Eps8l2
ENSMUSG00000078452.7	574.3	8.04	2.13E-111	Raet1d
ENSMUSG00000048138.9	218.9	8.08	4.76E-52	Dmrt2
ENSMUSG00000105940.1	229.8	8.13	4.82E-53	RP23-458G12.1
ENSMUSG00000050505.7	1186.3	8.14	3.86E-45	Pcdh20
ENSMUSG00000043773.4	232.3	8.16	1.38E-53	1700048O20Rik
ENSMUSG00000042377.8	244.6	8.23	6.87E-55	Fam83g

ENSMUSG00000032948.10	258.1	8.27	1.22E-55	Lipi
ENSMUSG00000042717.4	261.6	8.29	6.72E-56	Ppp1r3a
ENSMUSG00000032911.5	979.7	8.30	4.42E-134	Cspg4
ENSMUSG00000019851.7	2918.6	8.32	1.48E-69	Perp
ENSMUSG00000022762.14	274.9	8.35	5.04E-57	Ncam2
ENSMUSG00000006519.10	1900.3	8.35	1.78E-80	Cyba
ENSMUSG00000045629.7	2705.7	8.42	0	Sh3tc2
ENSMUSG00000029375.6	319.0	8.51	3.88E-60	Cxcl15
ENSMUSG00000016087.10	302.3	8.51	2.62E-60	Fli1
ENSMUSG00000025329.3	453.4	8.51	7.25E-78	Padi1
ENSMUSG00000029322.9	4101.0	8.52	0	Plac8
ENSMUSG00000042386.7	10566.6	8.53	5.92E-45	Tex13
ENSMUSG00000031075.14	5750.7	8.55	0	Ano1
ENSMUSG00000036019.8	1330.6	8.61	2.16E-55	Tmtc2
ENSMUSG00000037157.8	1033.8	8.62	1.78E-56	Il22ra1
ENSMUSG00000051022.7	327.6	8.62	1.67E-62	Hs3st1
ENSMUSG00000035395.8	3160.7	8.63	2.00E-237	Pet2
ENSMUSG00000031517.7	343.1	8.63	1.07E-62	Gpm6a
ENSMUSG00000019768.13	339.5	8.65	3.76E-63	Esr1
ENSMUSG00000031451.5	6201.3	8.66	2.80E-92	Gas6
ENSMUSG00000033910.10	372.4	8.67	2.14E-63	Gucy1a3
ENSMUSG00000019888.12	350.4	8.68	9.90E-64	Mgat4c
ENSMUSG00000037440.7	687.2	8.72	9.66E-103	Vnn1
ENSMUSG00000027375.11	368.1	8.77	1.52E-65	Mal
ENSMUSG00000025375.12	409.0	8.90	1.77E-68	Aatk
ENSMUSG00000031216.10	408.9	8.91	1.62E-68	Stard8
ENSMUSG00000074968.8	3153.0	9.12	3.94E-59	Ano3
ENSMUSG00000053825.11	515.7	9.19	7.88E-75	Ppfia2
ENSMUSG00000035493.9	2715.3	9.41	3.85E-77	Tgfbi
ENSMUSG00000029563.13	9722.1	9.49	2.22E-58	Foxp2
ENSMUSG00000039457.3	7164.7	9.53	0	Ppl
ENSMUSG00000041703.7	701.6	9.61	7.81E-85	Zic5
ENSMUSG00000043342.9	712.2	9.63	2.14E-85	Hoxd9
ENSMUSG00000000627.12	736.1	9.68	1.77E-86	Sema4f
ENSMUSG00000020911.11	4034.1	9.69	1.10E-122	Krt19
ENSMUSG00000038903.10	796.7	9.78	5.07E-89	Ccdc68
ENSMUSG00000073125.7	796.1	9.78	4.13E-89	Xlr3b
ENSMUSG00000059336.11	886.4	9.92	1.06E-92	Slc14a1
ENSMUSG00000079350.2	903.0	9.95	2.40E-93	Magea8
ENSMUSG00000074743.4	906.6	9.95	2.05E-93	Thbd
ENSMUSG00000061524.8	961.4	10.02	1.90E-95	Zic2
ENSMUSG00000079349.6	1026.4	10.11	8.77E-98	Magea5
ENSMUSG00000031871.8	5564.0	10.20	2.49E-145	Cdh5

ENSMUSG00000046942.14	1243.0	10.36	1.58E-104	Mageb16
ENSMUSG00000027102.4	1287.4	10.40	8.81E-106	Hoxd8
ENSMUSG00000029108.11	10579.7	10.63	9.87E-148	Pcdh7
ENSMUSG00000021342.10	1636.0	10.70	1.74E-114	Prl
ENSMUSG00000038859.7	1991.8	10.96	1.91E-122	Baiap2l1
ENSMUSG00000051257.3	9972.6	11.25	7.78E-132	Trap1a
ENSMUSG00000086503.3	18585.8	12.12	0	Xist

Appendix II

Reactive Cysteine Profiling Data from HEK293T Cells Treated with Copper

The following pages list the proteins labelled in the reactive cysteine profiling experiment conducted on HEK293T cells in the presence and absence of exogenous copper, as described in Chapter 3. As stated in the legend to Table 3.4, the columns provide the UniProt ID (uniprot.org), number of the cysteine labeled, name of the protein containing that cysteine, ratio of labeling (control sample)/(copper addition sample), standard deviation of ratios from the replicates in which this cysteine was labeled, and number of replicates in which this cysteine was labeled.

UniProt ID	Labeled Cys	Protein	Ratio	Std Dev	Rep No
Q6FI81	C249	CIAPIN1	20	NA	3
P53384	C25	NUBP1	20	NA	2
P53384	C235	NUBP1	20	NA	2
P53384	C277	NUBP1	20	NA	2
P07339	C117	CTSD	20	NA	2
Q6PJ69	C112	TRIM65	20	NA	2
Q7RTV0	C40	PHF5A	20	NA	2
Q9Y3E2	C18	BOLA1	18.0	3.54	4
Q9Y3E2	C20	BOLA1	18.0	3.54	4
P23921	C787	RRM1	16.6	5.93	4
P23921	C790	RRM1	16.6	5.93	4
P23921	C779	RRM1	16.0	7.01	4
O95793	C574	STAU1	12.8	5.29	3
O00244	C12	ATOX1	12.4	5.06	4
O00244	C15	ATOX1	12.4	5.06	4
Q13572	C391	ITPK1	11.5	4.13	2
Q13572	C403	ITPK1	11.5	4.13	2
Q3KQU3	C361	MAP7D1	9.85	7.19	3
P00441	C147	SOD1	8.96	5.30	4
Q9UJY4	C343	GGA2	8.9	3.31	2
Q3KQU3	C373	MAP7D1	6.02	2.14	3
Q9Y5Y2	C54	NUBP2	4.93	1.02	3
Q15005	C17	SPCS2	4.65	1.47	2
Q15005	C26	SPCS2	4.65	1.47	2
P54136	C32	RARS	4.37	0.60	3
P54136	C34	RARS	4.37	0.60	3
Q9UBB4	C354	ATXN10	4.29	1.30	2
Q9UBB4	C356	ATXN10	4.29	1.30	2
P85037	C254	FOXK1	4.09	0.69	2
Q96SK2	C158	TMEM209	3.97	1.46	2
P40763	C712	STAT3	3.85	1.03	3
P40763	C718	STAT3	3.85	1.03	3
Q53EZ4	C159	CEP55	3.79	0.54	2
Q9Y5Y2	C196	NUBP2	3.71	0.42	2
Q9Y5Y2	C199	NUBP2	3.71	0.42	2
Q9Y5Y2	C202	NUBP2	3.71	0.42	2
Q9H7E9	C42	C8orf33	3.54	7.23	3
Q9H7E9	C44	C8orf33	3.54	7.23	3
Q9H7E9	C50	C8orf33	3.54	7.23	3
Q9C0C2	C631	TNKS1BP1	3.51	8.25	2

Q14145	C288	KEAP1	3.51	0.02	2
Q147X3	C74	NAA30	3.51	0.47	2
Q15365	C201	PCBP1	3.46	0.52	4
P17509	C72	HOXB6	3.45	0.01	2
Q6FI81	C285	CIAPIN1	3.44	0.02	2
Q6FI81	C288	CIAPIN1	3.44	0.02	2
Q15365	C194	PCBP1	3.41	0.66	4
O14654	C658	IRS4	3.36	0.84	2
Q9UHQ1	C172	NARF	3.34	8.33	2
O95685	C26	PPP1R3D	3.28	0.44	2
P51610	C1139	HCFC1	3.13	1.17	3
P42166	C341	TMPO	3.13	0.30	2
Q9BRA2	C43	TXNDC17	3.12	1.41	4
P29401	C133	TKT	3.08	0.35	2
H3BVE0	C63	Uncharacteriz	3	0.61	2
P60174	C124	TPI1	3	1.02	2
Q9H3K6	C31	BOLA2B	3	0.61	2
Q9ULW0	C536	TPX2	2.96	0.17	2
Q9Y570	C381	PPME1	2.92	0.09	4
Q9Y570	C386	PPME1	2.92	0.09	4
Q6F5E8	C1323	RLTPR	2.91	0.27	2
Q9UER7	C664	DAXX	2.81	0.21	2
Q15654	C47	TRIP6	2.8	0.52	3
Q15654	C54	TRIP6	2.8	0.52	3
Q9BRP1	C80	PDCD2L	2.77	0.75	4
Q9BRP1	C82	PDCD2L	2.77	0.75	4
Q9NVN8	C213	GNL3L	2.75	0.22	2
Q96HE7	C37	ERO1L	2.72	1.05	3
Q9UKG1	C462	APPL1	2.72	0.84	2
P51610	C1872	HCFC1	2.67	0.74	3
O15287	C392	FANCG	2.67	0.30	2
Q8N5W9	C81	FAM101B	2.63	0.47	3
Q8N8R5	C43	C2orf69	2.63	1.06	3
P04183	C230	TK1	2.59	0.54	3
O60888	C96	CUTA	2.56	0.97	2
O15530	C385	PDPK1	2.55	0.43	2
Q96EK4	C48	THAP11	2.54	0.41	3
Q12948	C529	FOXC1	2.53	0.22	4
Q99497	C46	PARK7	2.5	0.98	2
P10599	C32	TXN	2.48	0.48	3
P10599	C35	TXN	2.48	0.48	3

Q14790	C360	CASP8	2.46	0.11	2
P09017	C117	HOXC4	2.45	0.74	3
Q9ULX6	C128	AKAP8L	2.42	1.15	3
Q99439	C164	CNN2	2.41	0.44	4
Q8TD19	C878	NEK9	2.41	0.03	2
O00178	C662	GTPBP1	2.4	0.79	4
Q9UPT9	C171	USP22	2.4	0.10	3
O94992	C79	HEXIM1	2.38	0.94	4
O94992	C84	HEXIM1	2.38	0.94	4
Q08945	C139	SSRP1	2.38	0.04	2
O75935	C173	DCTN3	2.38	0.54	2
Q99956	C166	DUSP9	2.35	0.02	2
Q99956	C171	DUSP9	2.35	0.02	2
Q9BRJ7	C88	NUDT16L1	2.33	0.52	4
Q7Z4H7	C926	HAUS6	2.33	0.06	2
Q96G74	C434	OTUD5	2.33	0.57	2
Q15365	C293	PCBP1	2.32	0.44	3
P15170	C276	GSPT1	2.3	0.79	2
Q99832	C511	CCT7	2.29	0.88	2
P09936	C47	UCHL1	2.29	0.47	2
Q15834	C198	CCDC85B	2.27	0.50	2
Q9Y6Y8	C604	SEC23IP	2.27	0.38	2
O15304	C6	SIVA1	2.27	0.27	2
Q9NZT2	C417	OGFR	2.25	0.60	2
Q00796	C45	SORD	2.25	0.75	2
P04632	C232	CAPNS1	2.24	0.90	2
P27635	C49	RPL10	2.23	0.44	4
Q99439	C274	CNN2	2.23	0.51	4
Q99439	C290	CNN2	2.23	0.51	4
Q6P1K2	C64	PMF1	2.18	0.11	2
Q99439	C215	CNN2	2.17	0.40	4
Q99439	C175	CNN2	2.15	0.65	4
Q96GY3	C28	LIN37	2.15	0.29	2
P35244	C81	RPA3	2.14	0.73	2
P31260	C200	HOXA10	2.14	0.50	2
Q9BUK6	C411	MSTO1	2.13	0.49	2
Q6PJ69	C421	TRIM65	2.13	0.61	2
Q8WXE0	C1109	CASKIN2	2.13	0.70	2
Q9NVP2	C189	ASF1B	2.12	0.29	4
Q9NVP2	C201	ASF1B	2.12	0.29	4
Q9NVP2	C172	ASF1B	2.12	0.12	3

Q9NVP2	C178	ASF1B	2.12	0.12	3
Q96C92	C371	SDCCAG3	2.11	0.68	2
Q9NYL9	C150	TMOD3	2.1	0.30	4
Q9NUG6	C60	PDRG1	2.1	0.65	2
Q9HD26	C408	GOPC	2.09	0.14	2
P19174	C646	PLCG1	2.08	0.46	2
Q8N3X6	C130	LCORL	2.07	0.21	2
Q9NYL9	C132	TMOD3	2.06	0.26	3
P30040	C157	ERP29	2.06	0.72	2
Q92667	C147	AKAP1	2.06	0.02	2
O14654	C206	IRS4	2.05	8.98	2
Q14012	C354	CAMK1	2.04	0.67	2
Q14012	C355	CAMK1	2.04	0.67	2
Q7L5D6	C205	GET4	2.04	0.30	2
O75400	C39	PRPF40A	2.03	0.15	4
H7BZ11	C99	Uncharacteriz	2.03	0.71	2
Q969Q0	C88	RPL36AL	2.03	0.71	2
Q99439	C240	CNN2	2.02	0.25	3
O75319	C325	DUSP11	2.02	0.03	2
Q9NUQ6	C367	SPATS2L	2.02	0.60	2
Q9NUQ3	C127	TXLNG	2.01	0.74	2
Q01433	C107	AMPD2	2	0.59	4
P27635	C105	RPL10	2	0.75	3
Q7LG56	C279	RRM2B	1.99	0.56	2
P22681	C508	CBL	1.98	0.90	3
Q9Y4P1	C189	ATG4B	1.97	0.37	4
O96017	C231	CHEK2	1.97	0.52	3
Q9Y617	C224	PSAT1	1.97	0.45	2
P27635	C195	RPL10	1.96	0.39	4
Q99497	C106	PARK7	1.96	0.60	2
P13797	C566	PLS3	1.96	0.54	2
P36969	C102	GPX4	1.96	0.78	2
Q7Z3C6	C630	ATG9A	1.95	0.58	3
Q99956	C185	DUSP9	1.94	0.44	2
Q5SQN1	C369	SNAP47	1.94	0.18	2
P00558	C108	PGK1	1.94	0.23	2
P85037	C439	FOXK1	1.93	0.42	4
Q8IWD4	C81	CCDC117	1.93	0.57	3
O14654	C314	IRS4	1.92	0.17	2
Q6ZN17	C201	LIN28B	1.91	0.71	3
Q8IX90	C290	SKA3	1.91	0.28	3

Q92667	C102	AKAP1	1.91	0.41	2
P28161	C174	GSTM2	1.9	0.20	2
Q9UL45	C95	PLDN	1.9	0.73	2
Q96HE7	C241	ERO1L	1.9	0.19	2
Q9NXW9	C159	ALKBH4	1.9	0.75	2
Q9BRX2	C258	PELO	1.9	9.05	2
P09497	C199	CLTB	1.89	0.66	4
Q8IYL3	C215	C1orf174	1.89	0.54	4
Q9NUQ3	C56	TXLNG	1.89	0.36	2
Q9NUQ3	C71	TXLNG	1.89	0.36	2
P48200	C137	IREB2	1.88	0.36	3
I3L420	C311	LSM14A	1.88	0.24	2
Q8ND56	C375	LSM14A	1.88	0.24	2
P68366	C295	TUBA4A	1.87	0.39	4
Q71U36	C295	TUBA1A	1.87	0.39	4
Q9Y4R8	C628	TELO2	1.87	0.26	2
Q13155	C23	AIMP2	1.86	0.29	4
Q9UGP4	C305	LIMD1	1.85	0.31	3
Q6NSH3	C109	CT45A5	1.85	0.20	3
Q9UNW1	C475	MINPP1	1.85	0.31	3
Q92785	C53	DPF2	1.85	0.44	3
Q7Z7L8	C402	C11orf96	1.85	0.45	2
Q9Y4W2	C140	LAS1L	1.84	0.28	3
Q96RN5	C660	MED15	1.84	0.04	2
P31946	C96	YWHAB	1.83	0.59	2
Q9Y4W2	C456	LAS1L	1.83	0.42	2
P68366	C200	TUBA4A	1.83	0.05	2
P68366	C213	TUBA4A	1.83	0.05	2
Q71U36	C200	TUBA1A	1.83	0.05	2
Q71U36	C213	TUBA1A	1.83	0.05	2
Q9NUQ3	C101	TXLNG	1.83	0.18	2
P49721	C46	PSMB2	1.83	0.33	2
P42166	C561	TMPO	1.82	0.21	3
Q7L2J0	C177	MEPCE	1.82	0.51	3
Q9UHQ1	C99	NARF	1.81	0.37	4
O76003	C46	GLRX3	1.81	0.24	2
A9UHW6	C49	MIF4GD	1.8	9.10	2
Q9P2X3	C226	IMPACT	1.8	0.18	2
Q8IYL3	C92	C1orf174	1.8	0.16	2
Q8IYL3	C124	C1orf174	1.8	0.16	2
Q9NR31	C102	SAR1A	1.8	0.66	2

O43439	C111	CBFA2T2	1.79	0.19	4
P45880	C13	VDAC2	1.79	0.61	4
P23921	C352	RRM1	1.79	0.54	4
P23921	C356	RRM1	1.79	0.54	4
P06280	C142	GLA	1.79	0.36	2
Q7L3B6	C35	CDC37L1	1.79	0.18	2
P63279	C138	UBE2I	1.79	0.46	2
P10768	C243	ESD	1.79	0.44	2
O15027	C2159	SEC16A	1.78	0.53	3
Q13569	C233	TDG	1.78	0.27	2
P51617	C608	IRAK1	1.77	0.32	3
Q8IZ69	C243	TRMT2A	1.77	0.17	3
Q16658	C456	FSCN1	1.77	0.63	2
P68104	C234	EEF1A1	1.77	0.43	2
Q16555	C179	DPYSL2	1.77	0.09	2
P48739	C13	PITPNB	1.76	0.54	2
Q53EZ4	C236	CEP55	1.75	0.06	2
Q9UKX7	C151	NUP50	1.75	0.25	2
Q9UBQ7	C216	GRHPR	1.75	0.51	2
Q9UBQ7	C226	GRHPR	1.75	0.51	2
P15927	C49	RPA2	1.75	0.25	2
A6NE09	C163	RPSAP58	1.74	0.83	3
Q9HCJ3	C595	RAVER2	1.74	0.42	3
Q9BUJ2	C391	HNRNPUL1	1.74	0.72	2
Q5T6F2	C208	UBAP2	1.73	0.39	3
Q14694	C94	USP10	1.72	0.30	3
Q16352	C54	INA	1.72	0.78	3
Q13356	C15	PPIL2	1.72	0.33	2
Q9GZU8	C187	FAM192A	1.72	0.35	2
Q8N0X7	C504	SPG20	1.71	0.32	4
O43741	C178	PRKAB2	1.71	0.24	2
Q9HCJ3	C362	RAVER2	1.71	0.22	2
Q8WUX2	C113	CHAC2	1.71	0.14	2
P49368	C279	CCT3	1.71	0.60	2
Q9UN37	C403	VPS4A	1.7	0.42	3
Q8N6N7	C45	ACBD7	1.7	2.58	2
P68366	C315	TUBA4A	1.69	0.53	4
P68366	C316	TUBA4A	1.69	0.53	4
Q71U36	C315	TUBA1A	1.69	0.53	4
Q71U36	C316	TUBA1A	1.69	0.53	4
A6NHL2	C322	TUBAL3	1.69	0.53	4

A6NHL2	C323	TUBAL3	1.69	0.53	4
P13010	C339	XRCC5	1.69	0.09	2
Q96CW6	C156	SLC7A6OS	1.69	0.32	2
Q9HCD5	C137	NCOA5	1.69	0.23	2
Q9UGP4	C374	LIMD1	1.68	0.50	3
Q9UBC1	C304	NFKBIL1	1.68	0.40	3
Q8IZ69	C463	TRMT2A	1.68	0.25	3
P50395	C317	GDI2	1.68	0.61	2
P31150	C317	GDI1	1.68	0.61	2
O76071	C72	CIAO1	1.68	0.41	2
P25789	C34	PSMA4	1.68	0.59	2
Q14974	C436	KPNB1	1.68	0.26	2
Q14974	C455	KPNB1	1.68	0.26	2
Q9BUK6	C46	MSTO1	1.67	0.09	3
Q96I24	C460	FUBP3	1.67	0.30	3
Q8NCE2	C182	MTMR14	1.67	0.54	2
P78332	C1057	RBM6	1.67	0.11	2
Q8NBA8	C220	DTWD2	1.67	0.13	2
O14893	C63	GEMIN2	1.67	0.42	2
Q13371	C35	PDCL	1.66	0.43	4
O00505	C495	KPNA3	1.66	0.04	2
P04183	C206	TK1	1.65	0.37	4
Q9BTE3	C200	MCMBP	1.65	0.19	3
P06132	C59	UROD	1.65	0.50	3
O14893	C154	GEMIN2	1.65	0.20	2
P22061	C95	PCMT1	1.64	0.60	4
Q13643	C272	FHL3	1.64	0.43	2
Q13643	C275	FHL3	1.64	0.43	2
Q9Y4X0	C175	AMMECR1	1.64	0.05	2
Q6ZN17	C107	LIN28B	1.64	0.15	2
Q969E8	C17	TSR2	1.64	0.31	2
Q6DCA0	C153	AMMECR1L	1.64	0.05	2
Q13352	C39	ITGB3BP	1.63	0.29	3
Q13418	C239	ILK	1.63	0.19	2
P30876	C1093	POLR2B	1.63	0.01	2
Q9BQ70	C83	TCF25	1.62	0.61	4
P30041	C47	PRDX6	1.62	0.77	3
A6NDG6	C35	PGP	1.62	0.28	2
P22234	C185	PAICS	1.62	0.40	2
Q9Y3C4	C167	TPRKB	1.62	0.26	2
P37837	C250	TALDO1	1.62	2.04	2

Q9Y696	C234	CLIC4	1.62	0.60	2
Q32MZ4	C644	LRRFIP1	1.62	9.19	2
O76003	C146	GLRX3	1.62	0.65	2
Q8TC07	C197	TBC1D15	1.61	0.41	4
O60664	C39	PLIN3	1.61	0.46	4
P09110	C123	ACAA1	1.61	0.37	3
Q9UL15	C118	BAG5	1.61	0.38	3
Q9BV29	C47	C15orf57	1.61	0.08	2
Q71U36	C4	TUBA1A	1.61	0.49	2
Q71U36	C20	TUBA1A	1.61	0.49	2
Q71U36	C25	TUBA1A	1.61	0.49	2
P55265	C1224	ADAR	1.61	0.23	2
Q96FW1	C212	OTUB1	1.61	0.10	2
Q9NUQ3	C480	TXLNG	1.6	0.51	2
Q9BTX1	C468	TMEM48	1.6	0.27	2
P83731	C6	RPL24	1.59	0.22	4
Q9H814	C51	PHAX	1.59	0.33	3
Q8N5L8	C131	RPP25L	1.59	0.66	3
Q8N5L8	C150	RPP25L	1.59	0.66	3
Q7Z2W4	C645	ZC3HAV1	1.59	0.62	3
Q8IWZ3	C615	ANKHD1	1.59	0.07	2
Q9BSU1	C222	C16orf70	1.59	0.22	2
Q96EB1	C218	ELP4	1.58	0.34	4
Q6PCE3	C303	PGM2L1	1.58	0.20	3
P10398	C597	ARAF	1.58	0.15	3
Q9NZN8	C175	CNOT2	1.58	0.41	3
Q9Y5T5	C205	USP16	1.58	0.12	2
O43159	C451	RRP8	1.58	0.28	2
Q9UBV8	C146	PEF1	1.58	9.21	2
P62829	C28	RPL23	1.57	0.27	4
Q7Z2T5	C239	TRMT1L	1.57	0.13	3
Q15649	C6	ZNHIT3	1.57	0.27	3
P27707	C9	DCK	1.57	0.19	3
P49207	C46	RPL34	1.57	0.46	3
P49207	C49	RPL34	1.57	0.46	3
P49327	C161	FASN	1.57	0.27	2
P49327	C180	FASN	1.57	0.27	2
P07195	C132	LDHB	1.57	0.64	2
Q71U36	C129	TUBA1A	1.57	0.20	2
Q7Z5K2	C160	WAPAL	1.56	0.41	3
Q86X76	C165	NIT1	1.56	0.26	3

Q86X76	C176	NIT1	1.56	0.26	3
Q9UL40	C68	ZNF346	1.56	0.41	3
Q6PJG6	C673	BRAT1	1.56	0.05	3
Q9BU23	C696	LMF2	1.56	0.63	3
Q6ZN17	C187	LIN28B	1.56	0.58	3
Q9Y2X0	C539	MED16	1.56	0.24	3
A0JLT2	C62	MED19	1.56	0.23	2
Q13501	C26	SQSTM1	1.56	0.29	2
Q13501	C27	SQSTM1	1.56	0.29	2
P06400	C853	RB1	1.56	0.51	2
Q9UNI6	C23	DUSP12	1.56	0.24	2
Q7Z5K2	C94	WAPAL	1.55	0.09	3
Q15345	C297	LRRC41	1.55	0.35	3
P04075	C73	ALDOA	1.55	0.57	2
P35268	C25	RPL22	1.55	0.38	2
P62906	C164	RPL10A	1.55	0.64	2
O14777	C449	NDC80	1.54	0.35	4
P51610	C1886	HCFC1	1.54	0.35	4
P51610	C1895	HCFC1	1.54	0.35	4
Q99873	C350	PRMT1	1.54	0.51	4
Q9NS86	C187	LANCL2	1.54	0.70	3
Q7Z2T5	C320	TRMT1L	1.54	0.39	3
P46736	C273	BRCC3	1.54	0.55	3
Q9UPT9	C44	USP22	1.54	0.41	3
Q7Z3C6	C764	ATG9A	1.54	0.24	3
P06280	C52	GLA	1.54	0.24	2
P06280	C56	GLA	1.54	0.24	2
P61970	C80	NUTF2	1.54	0.50	2
P48643	C302	CCT5	1.54	0.21	2
Q13503	C20	MED21	1.54	0.47	2
Q13503	C29	MED21	1.54	0.47	2
Q9NY65	C376	TUBA8	1.53	0.29	4
Q9BV86	C195	NTMT1	1.53	0.43	4
P68366	C376	TUBA4A	1.53	0.29	4
Q71U36	C376	TUBA1A	1.53	0.29	4
Q9Y4P8	C393	WIPI2	1.53	0.42	3
P15531	C145	NME1	1.53	0.67	3
P40227	C406	CCT6A	1.53	0.36	2
Q00587	C161	CDC42EP1	1.53	0.36	2
Q13155	C291	AIMP2	1.53	0.14	2
P34896	C96	SHMT1	1.53	0.14	2

Q53H96	C49	PYCRL	1.53	0.18	2
Q99873	C216	PRMT1	1.53	0.17	2
P40925	C137	MDH1	1.52	0.73	4
Q9NTM9	C248	CUTC	1.52	0.32	4
Q92575	C144	UBXN4	1.52	0.43	3
P37802	C38	TAGLN2	1.52	0.71	3
Q9BVS4	C449	RIOK2	1.52	0.15	3
Q96EB1	C412	ELP4	1.52	0.51	3
P13807	C699	GYS1	1.52	0.26	2
P42166	C518	TMPO	1.52	0.10	2
Q96EV2	C726	RBM33	1.52	0.58	2
P42224	C247	STAT1	1.52	0.41	2
P42224	C255	STAT1	1.52	0.41	2
Q13542	C73	EIF4EBP2	1.52	0.22	2
Q5VSY0	C90	GKAP1	1.52	0.27	2
P51648	C237	ALDH3A2	1.52	0.01	2
P51648	C241	ALDH3A2	1.52	0.01	2
Q6PKG0	C864	LARP1	1.52	0.44	2
O75150	C950	RNF40	1.52	0.54	2
Q9NSV4	C102	DIAPH3	1.52	0.20	2
P31749	C310	AKT1	1.51	0.27	4
Q9Y243	C307	AKT3	1.51	0.27	4
Q71UM5	C77	RPS27L	1.51	0.29	4
P42677	C77	RPS27	1.51	0.29	4
P31751	C311	AKT2	1.51	0.27	4
Q8WW01	C13	TSEN15	1.51	0.38	4
O75179	C210	ANKRD17	1.51	0.37	3
Q8IWZ3	C181	ANKHD1	1.51	0.37	3
Q96F86	C499	EDC3	1.51	0.11	2
Q9NZ32	C388	ACTR10	1.51	0.00	2
Q16543	C336	CDC37	1.5	0.29	4
Q96T76	C819	MMS19	1.5	0.39	3
Q9BXP2	C911	SLC12A9	1.5	0.37	3
Q6ZTU2	C151	EP400NL	1.5	0.33	3
Q96F86	C410	EDC3	1.5	0.35	3
Q96F86	C413	EDC3	1.5	0.35	3
P63244	C240	GNB2L1	1.5	0.69	3
Q9Y314	C8	NOSIP	1.5	0.26	3
Q6NXT1	C23	ANKRD54	1.5	0.22	2
Q9NP61	C241	ARFGAP3	1.5	0.39	2
P68104	C363	EEF1A1	1.5	0.19	2

P68104	C370	EEF1A1	1.5	0.19	2
Q9BXJ9	C817	NAA15	1.5	0.35	2
Q969E8	C114	TSR2	1.49	0.22	4
Q9H7D7	C656	WDR26	1.49	0.35	4
O94885	C1120	SASH1	1.49	0.54	3
Q02790	C396	FKBP4	1.49	0.70	3
Q9C0C9	C910	UBE2O	1.49	1.13	2
Q9C0C9	C913	UBE2O	1.49	1.13	2
Q9Y2X3	C106	NOP58	1.49	0.22	2
P52597	C267	HNRNPF	1.48	0.29	4
Q96CD2	C173	PPCDC	1.48	0.43	3
Q9NUU6	C177	FAM105A	1.48	0.52	2
O00273	C78	DFFA	1.48	0.26	2
E2QRD5	C183	C15orf38-AP3	1.48	0.51	2
P78417	C237	GSTO1	1.48	0.43	2
Q9UBE0	C303	SAE1	1.48	0.49	2
Q96DI7	C52	SNRNP40	1.48	0.39	2
P15104	C53	GLUL	1.48	0.18	2
P50579	C121	METAP2	1.48	0.42	2
Q5T0N5	C69	FNBP1L	1.48	0.12	2
Q8WVJ2	C14	NUDCD2	1.48	0.17	2
Q9Y5N6	C88	ORC6	1.48	0.21	2
P09104	C389	ENO2	1.47	0.65	3
P09110	C177	ACAA1	1.47	0.52	3
Q96N21	C302	ENTHD2	1.47	0.17	3
P06733	C389	ENO1	1.47	0.65	3
P13929	C389	ENO3	1.47	0.65	3
Q96EM0	C139	L3HYPDH	1.47	0.13	2
O60664	C341	PLIN3	1.47	0.12	2
Q9NR33	C84	POLE4	1.47	0.58	2
P54646	C382	PRKAA2	1.46	0.29	4
Q12894	C111	IFRD2	1.46	0.61	3
P00338	C293	LDHA	1.46	0.66	3
Q9BVA1	C127	TUBB2B	1.46	0.49	3
Q9BVA1	C129	TUBB2B	1.46	0.49	3
P06730	C170	EIF4E	1.46	0.31	3
O75150	C890	RNF40	1.46	0.54	3
P36578	C125	RPL4	1.46	0.54	3
Q8TD19	C623	NEK9	1.46	0.60	2
Q9NQ55	C391	PPAN	1.46	1.89	2
Q8NBS9	C217	TXNDC5	1.46	0.30	2

Q9H2M9	C67	RAB3GAP2	1.46	0.46	2
C9J3F9	C391	PPAN-P2RY1	1.46	1.89	2
P49189	C484	ALDH9A1	1.45	0.69	3
Q07020	C134	RPL18	1.45	0.58	3
Q96EB6	C67	SIRT1	1.45	0.66	3
Q9UMS4	C230	PRPF19	1.45	0.25	2
Q9UGP8	C295	SEC63	1.45	0.29	2
P22234	C63	PAICS	1.45	0.39	2
Q9UG63	C411	ABCF2	1.45	0.05	2
Q9NRA8	C767	EIF4ENIF1	1.45	0.11	2
Q9NRZ9	C836	HELLS	1.44	0.30	4
Q5JPI3	C259	C3orf38	1.44	0.34	4
P40222	C523	TXLNA	1.44	0.49	3
Q13547	C100	HDAC1	1.44	0.27	3
Q13547	C110	HDAC1	1.44	0.27	3
Q96N67	C2125	DOCK7	1.44	0.40	2
A5YKK6	C2359	CNOT1	1.44	0.55	2
A5YKK6	C2360	CNOT1	1.44	0.55	2
Q9UK41	C128	VPS28	1.44	0.23	2
Q9HA64	C24	FN3KRP	1.44	0.28	2
Q8N300	C58	CCDC23	1.44	0.50	2
P61081	C47	UBE2M	1.44	0.19	2
O43708	C205	GSTZ1	1.44	0.23	2
P53582	C14	METAP1	1.44	0.30	2
Q9UHI6	C577	DDX20	1.44	0.42	2
P51668	C107	UBE2D1	1.44	0.02	2
P51668	C111	UBE2D1	1.44	0.02	2
Q16527	C33	CSRP2	1.43	0.33	4
P42575	C370	CASP2	1.43	0.44	4
P07741	C140	APRT	1.43	0.32	3
P62917	C114	RPL8	1.43	0.18	3
P62917	C115	RPL8	1.43	0.18	3
Q86UV5	C39	USP48	1.43	0.32	2
O00541	C153	PES1	1.43	0.54	2
Q9NRL3	C17	STRN4	1.43	0.07	2
P53582	C22	METAP1	1.43	0.44	2
P55735	C234	SEC13	1.43	0.56	2
P04818	C180	TYMS	1.43	0.53	2
Q96T76	C848	MMS19	1.42	0.15	3
Q7L5N1	C299	COPS6	1.42	0.46	3
P40763	C259	STAT3	1.42	0.22	2

P10644	C18	PRKAR1A	1.42	0.07	2
Q01081	C67	U2AF1	1.42	0.10	2
Q9UHR5	C127	SAP30BP	1.42	0.21	2
Q5VTL8	C113	PRPF38B	1.42	0.23	2
P13798	C30	APEH	1.42	0.38	2
P28702	C340	RXRB	1.42	0.03	2
Q15392	C91	DHCR24	1.42	0.07	2
P26583	C23	HMGB2	1.41	0.41	4
Q6L8Q7	C108	PDE12	1.41	0.26	4
Q6L8Q7	C119	PDE12	1.41	0.26	4
Q5VSL9	C798	FAM40A	1.41	0.35	4
P04075	C339	ALDOA	1.41	0.73	4
P09429	C23	HMGB1	1.41	0.41	4
O60568	C691	PLOD3	1.41	0.31	4
Q99986	C50	VRK1	1.41	0.24	3
Q8WUA4	C212	GTF3C2	1.41	0.21	3
Q9NYL2	C22	MLTK	1.41	0.19	3
Q08945	C200	SSRP1	1.41	0.44	2
P22314	C278	UBA1	1.41	0.49	2
Q9UH92	C159	MLX	1.41	0.39	2
Q9P0W2	C177	HMG20B	1.41	0.35	2
B0V043	C41	VARS	1.41	0.52	2
Q9NPH2	C235	ISYNA1	1.4	0.39	4
P07195	C294	LDHB	1.4	0.46	3
P36507	C384	MAP2K2	1.4	0.33	3
Q9NYK5	C133	MRPL39	1.4	0.19	2
Q15527	C127	SURF2	1.4	0.08	2
Q9NXW9	C204	ALKBH4	1.4	0.18	2
Q9GZT4	C113	SRR	1.4	0.02	2
Q9BTW9	C850	TBCD	1.4	0.25	2
P55884	C302	EIF3B	1.4	0.42	2
P52657	C68	GTF2A2	1.39	0.40	3
P63146	C88	UBE2B	1.39	0.66	3
P62829	C125	RPL23	1.39	0.22	3
P49459	C88	UBE2A	1.39	0.66	3
Q8N9T8	C673	KRI1	1.39	0.32	3
Q8TBE9	C67	NANP	1.39	0.23	2
Q9GZN8	C156	C20orf27	1.39	0.33	2
Q6WKZ4	C1192	RAB11FIP1	1.39	0.20	2
Q01664	C29	TFAP4	1.39	0.35	2
Q9BSY9	C108	DESI2	1.39	0.34	2

Q96KB5	C70	PBK	1.39	0.45	2
Q92989	C338	CLP1	1.38	0.10	4
P04406	C152	GAPDH	1.38	1.63	4
P04406	C156	GAPDH	1.38	1.63	4
Q96CD2	C7	PPCDC	1.38	0.15	4
Q53ET0	C675	CRTC2	1.38	0.27	3
P04637	C182	TP53	1.38	8.50	3
Q71RC2	C599	LARP4	1.38	8.74	3
P25789	C107	PSMA4	1.38	0.63	3
P25789	C115	PSMA4	1.38	0.63	3
Q14152	C78	EIF3A	1.38	8.56	3
P27707	C59	DCK	1.38	0.06	3
Q9UI30	C100	TRMT112	1.38	0.12	2
P47712	C726	PLA2G4A	1.37	0.36	4
Q14558	C19	PRPSAP1	1.37	0.40	4
Q9NYG5	C7	ANAPC11	1.37	0.15	3
Q9UI10	C69	EIF2B4	1.37	0.67	3
A6NED2	C139	RCCD1	1.37	0.15	3
O00743	C262	PPP6C	1.37	0.30	3
Q99614	C28	TTC1	1.37	0.51	3
Q9UFW8	C92	CGGBP1	1.37	0.43	3
Q9BPY3	C319	FAM118B	1.37	0.36	3
P52294	C529	KPNA1	1.37	0.27	3
P84090	C28	ERH	1.37	1.26	2
P84090	C33	ERH	1.37	1.26	2
Q00839	C562	HNRNPU	1.37	0.45	2
Q9BV38	C384	WDR18	1.37	0.40	2
P51991	C85	HNRNPA3	1.37	0.23	2
P51991	C94	HNRNPA3	1.37	0.23	2
Q9NY65	C347	TUBA8	1.36	0.26	4
P42166	C684	TMPO	1.36	0.21	4
O15355	C241	PPM1G	1.36	0.46	4
Q71U36	C347	TUBA1A	1.36	0.26	4
P46779	C13	RPL28	1.36	0.34	4
Q13200	C779	PSMD2	1.36	0.38	3
Q9NUL3	C491	STAU2	1.36	0.22	3
Q5JPI3	C308	C3orf38	1.36	0.15	3
P00492	C23	HPRT1	1.36	0.50	3
Q6PKG0	C1054	LARP1	1.36	0.54	3
Q16643	C96	DBN1	1.36	0.38	2
P48059	C272	LIMS1	1.36	0.41	2

P48059	C281	LIMS1	1.36	0.41	2
Q92597	C394	NDRG1	1.36	0.18	2
P17987	C76	TCP1	1.36	0.18	2
Q9Y4R8	C644	TELO2	1.36	0.23	2
Q8WV74	C207	NUDT8	1.36	0.30	2
O43791	C361	SPOP	1.35	0.32	4
Q13642	C71	FHL1	1.35	0.29	4
Q96T76	C549	MMS19	1.35	0.29	4
Q9BTE3	C287	MCMBP	1.35	0.20	4
O75477	C310	ERLIN1	1.35	0.50	4
O95671	C333	ASMTL	1.35	0.22	4
Q9BUF5	C201	TUBB6	1.35	0.28	3
Q9BUF5	C211	TUBB6	1.35	0.28	3
P68371	C201	TUBB4B	1.35	0.28	3
P68371	C211	TUBB4B	1.35	0.28	3
P62873	C204	GNB1	1.35	0.11	3
O43847	C1109	NRD1	1.35	0.33	3
Q9UBT2	C30	UBA2	1.35	0.60	3
Q9Y5K6	C540	CD2AP	1.35	0.33	3
Q9BVA1	C201	TUBB2B	1.35	0.28	3
Q9BVA1	C211	TUBB2B	1.35	0.28	3
P07437	C201	TUBB	1.35	0.28	3
P07437	C211	TUBB	1.35	0.28	3
O75607	C79	NPM3	1.35	0.13	3
Q9P253	C22	VPS18	1.35	0.17	3
Q96SZ5	C239	ADO	1.35	0.55	2
O60232	C53	SSSCA1	1.35	0.32	2
O60232	C56	SSSCA1	1.35	0.32	2
Q96F86	C137	EDC3	1.35	9.33	2
Q15813	C141	TBCE	1.35	0.42	2
Q96K58	C126	ZNF668	1.35	0.06	2
Q14145	C319	KEAP1	1.35	2.80	2
O43264	C568	ZW10	1.35	0.11	2
Q9NWA0	C139	MED9	1.34	0.30	4
Q9BTE3	C325	MCMBP	1.34	0.27	4
P35754	C23	GLRX	1.34	0.36	4
P23921	C492	RRM1	1.34	0.34	4
P26641	C339	EEF1G	1.34	0.16	3
P40855	C128	PEX19	1.34	0.20	3
Q96F45	C120	ZNF503	1.34	0.31	3
Q00577	C292	PURA	1.34	0.31	3

Q9NUP9	C47	LIN7C	1.34	0.32	3
Q9Y696	C100	CLIC4	1.34	0.56	3
Q9H7S9	C96	ZNF703	1.34	0.31	3
O43290	C645	SART1	1.34	0.37	3
Q06136	C121	KDSR	1.34	1.64	2
P28482	C65	MAPK1	1.34	0.45	2
P42695	C541	NCAPD3	1.34	0.44	2
P27361	C82	MAPK3	1.34	0.45	2
Q15102	C55	PAFAH1B3	1.34	0.31	2
Q9NQE9	C16	HINT3	1.34	0.05	2
Q9NQE9	C32	HINT3	1.34	0.05	2
P48507	C35	GCLM	1.34	0.40	2
P21964	C238	COMT	1.33	0.39	4
P68366	C347	TUBA4A	1.33	0.24	4
P50552	C334	VASP	1.33	0.64	4
P83731	C36	RPL24	1.33	7.91	4
Q13232	C158	NME3	1.33	0.47	3
P68371	C239	TUBB4B	1.33	0.19	3
Q6PJG6	C539	BRAT1	1.33	0.33	3
Q8N806	C35	UBR7	1.33	0.21	3
Q9BVA1	C239	TUBB2B	1.33	0.19	3
P07437	C239	TUBB	1.33	0.19	3
I3L420	C80	LSM14A	1.33	0.23	3
Q96E39	C338	RBMXL1	1.33	0.30	3
Q8ND56	C85	LSM14A	1.33	0.23	3
Q5T1V6	C414	DDX59	1.33	0.30	2
Q14008	C1946	CKAP5	1.33	1.14	2
P0CB43	C51	FAM203B	1.33	0.16	2
P0CB43	C368	FAM203B	1.33	0.15	2
P49327	C2359	FASN	1.33	0.04	2
Q7L2J0	C324	MEPCE	1.33	0.49	2
Q9UQR0	C559	SCML2	1.33	0.09	2
P04049	C637	RAF1	1.33	0.04	2
Q13185	C69	CBX3	1.33	1.03	2
Q7Z401	C117	DENND4A	1.33	0.33	2
P04818	C195	TYMS	1.33	0.17	2
P04818	C199	TYMS	1.33	0.17	2
Q9BUF5	C303	TUBB6	1.32	0.27	4
Q92688	C123	ANP32B	1.32	0.52	4
P68371	C303	TUBB4B	1.32	0.27	4
P42167	C363	TMPO	1.32	0.29	4

Q9NRW3	C130	APOBEC3C	1.32	0.19	4
I3L2F9	C269	Uncharacteriz	1.32	0.27	4
Q8WUM4	C250	PDCD6IP	1.32	0.15	4
Q13509	C303	TUBB3	1.32	0.27	4
P39687	C123	ANP32A	1.32	0.52	4
Q9BVA1	C303	TUBB2B	1.32	0.27	4
P07437	C303	TUBB	1.32	0.27	4
Q7Z4W1	C138	DCXR	1.32	0.48	4
Q3ZCM7	C303	TUBB8	1.32	0.27	4
Q53H96	C266	PYCRL	1.32	0.30	3
Q16514	C100	TAF12	1.32	0.11	2
Q9BQ39	C603	DDX50	1.32	0.09	2
Q0VGL1	C51	C7orf59	1.32	0.07	2
Q96JN8	C57	NEURL4	1.32	0.34	2
Q53ET0	C515	CRTC2	1.31	0.29	4
Q9BTE6	C209	AARSD1	1.31	0.29	4
Q9BTE6	C210	AARSD1	1.31	0.29	4
Q5T440	C170	IBA57	1.31	0.44	4
P27708	C1889	CAD	1.31	0.18	4
Q15369	C112	TCEB1	1.31	0.14	3
Q8TC07	C24	TBC1D15	1.31	0.19	3
Q8WTW3	C513	COG1	1.31	0.13	3
Q99757	C90	TXN2	1.31	0.31	3
Q99757	C93	TXN2	1.31	0.31	3
P31949	C13	S100A11	1.31	0.07	2
Q9NS91	C64	RAD18	1.31	0.22	2
Q6IS14	C129	EIF5AL1	1.31	0.15	2
Q9P289	C392	MST4	1.31	3.10	2
P60468	C39	SEC61B	1.31	0.45	2
P07741	C83	APRT	1.31	0.03	2
O95071	C2267	UBR5	1.31	0.30	2
P68371	C354	TUBB4B	1.3	0.25	4
I3L2F9	C320	Uncharacteriz	1.3	0.25	4
Q13155	C306	AIMP2	1.3	0.40	4
Q9BVA1	C354	TUBB2B	1.3	0.25	4
P07437	C354	TUBB	1.3	0.25	4
Q3ZCM7	C354	TUBB8	1.3	0.25	4
P38606	C240	ATP6V1A	1.3	0.25	3
P38606	C254	ATP6V1A	1.3	0.25	3
P61970	C38	NUTF2	1.3	0.56	3
Q14258	C70	TRIM25	1.3	0.32	3

P35611	C430	ADD1	1.3	0.21	3
Q9UN36	C321	NDRG2	1.3	0.34	3
P22102	C646	GART	1.3	0.42	3
O60942	C419	RNGTT	1.3	0.38	2
P25786	C148	PSMA1	1.3	0.14	2
P25786	C156	PSMA1	1.3	0.14	2
Q9HAV0	C204	GNB4	1.3	0.08	2
Q96C90	C85	PPP1R14B	1.3	0.23	2
Q12905	C271	ILF2	1.3	0.39	2
Q12905	C291	ILF2	1.3	0.39	2
Q53H96	C235	PYCRL	1.3	0.34	2
Q9BX40	C310	LSM14B	1.29	0.21	4
P78417	C32	GSTO1	1.29	0.22	4
O14733	C131	MAP2K7	1.29	0.28	4
Q9Y448	C296	SKAP	1.29	0.39	4
Q9NZB2	C531	FAM120A	1.29	0.40	4
Q9Y5Y2	C269	NUBP2	1.29	0.15	4
Q6P6C2	C378	ALKBH5	1.29	0.44	3
Q99967	C261	CITED2	1.29	0.54	3
P07814	C1377	EPRS	1.29	0.56	3
Q9C0B1	C397	FTO	1.29	0.59	3
P13861	C101	PRKAR2A	1.29	0.40	3
Q92597	C168	NDRG1	1.29	0.34	3
Q9NPA3	C62	MID1IP1	1.29	0.25	3
P47756	C36	CAPZB	1.29	0.46	3
Q04726	C26	TLE3	1.29	0.18	2
P22234	C374	PAICS	1.29	0.16	2
Q9NUL3	C140	STAU2	1.29	0.26	2
Q9NT62	C182	ATG3	1.29	0.26	2
Q8N8A6	C402	DDX51	1.29	0.25	2
Q9H7B2	C135	RPF2	1.29	0.48	2
O15479	C301	MAGEB2	1.29	0.26	2
Q14C86	C568	GAPVD1	1.29	0.09	2
P30519	C265	HMOX2	1.28	0.27	4
P32929	C229	CTH	1.28	0.29	4
Q8WZA9	C340	IRGQ	1.28	0.33	4
Q9NR45	C287	NANS	1.28	0.29	4
Q9BUL9	C16	RPP25	1.28	0.27	4
P49588	C773	AARS	1.28	0.42	4
Q9NZL4	C22	HSPBP1	1.28	0.40	3
Q09161	C44	NCBP1	1.28	0.19	3

P13639	C466	EEF2	1.28	0.40	3
Q9H3U1	C426	UNC45A	1.28	0.28	3
Q5JTD0	C350	TJAP1	1.28	0.12	3
O75688	C172	PPM1B	1.28	0.29	3
Q96GD4	C234	AURKB	1.28	0.26	3
Q9UQB9	C200	AURKC	1.28	0.26	3
P55072	C535	VCP	1.28	0.13	3
Q9Y6C9	C296	MTCH2	1.28	0.50	3
Q8IU81	C280	IRF2BP1	1.28	0.35	3
P13693	C28	TPT1	1.28	1.08	2
Q9BSJ2	C848	TUBGCP2	1.28	0.36	2
Q9P2R3	C34	ANKFY1	1.28	0.46	2
Q9BQB6	C43	VKORC1	1.28	0.06	2
Q9H9A6	C264	LRRC40	1.28	0.00	2
Q96F86	C47	EDC3	1.28	0.09	2
E9PLN8	C43	Uncharacteriz	1.28	0.06	2
P06744	C404	GPI	1.28	1.76	2
P20338	C165	RAB4A	1.28	9.36	2
P35754	C79	GLRX	1.27	0.32	4
P35754	C83	GLRX	1.27	0.32	4
Q8NFH5	C255	NUP35	1.27	0.25	4
O43865	C272	AHCYL1	1.27	0.30	4
P55884	C384	EIF3B	1.27	0.44	4
Q96HN2	C353	AHCYL2	1.27	0.30	4
Q15366	C217	PCBP2	1.27	0.17	3
Q14671	C234	PUM1	1.27	0.35	3
P21964	C223	COMT	1.27	0.43	3
Q8WVV9	C464	HNRPLL	1.27	0.27	3
Q9NVU0	C70	POLR3E	1.27	0.35	3
Q9NVE7	C537	PANK4	1.27	0.24	3
P18085	C159	ARF4	1.27	0.58	3
Q9UHB9	C562	SRP68	1.27	0.33	3
P49327	C2202	FASN	1.27	0.19	2
P04049	C27	RAF1	1.27	0.02	2
P12532	C396	CKMT1B	1.27	1.15	2
Q16718	C17	NDUFA5	1.27	0.54	2
Q96S90	C32	LYSMD1	1.27	0.21	2
Q12874	C103	SF3A3	1.27	0.21	2
Q9Y3Z3	C522	SAMHD1	1.27	0.27	2
Q13496	C53	MTM1	1.27	0.01	2
Q06124	C567	PTPN11	1.26	0.19	4

Q06124	C573	PTPN11	1.26	0.19	4
Q96P16	C151	RPRD1A	1.26	0.16	4
P12277	C283	CKB	1.26	0.17	3
P43246	C822	MSH2	1.26	0.19	3
P27708	C73	CAD	1.26	0.19	3
P30626	C194	SRI	1.26	0.12	3
Q53EU6	C306	AGPAT9	1.26	0.10	2
P30153	C377	PPP2R1A	1.26	0.14	2
O95273	C300	CCNDBP1	1.26	0.13	2
P67936	C247	TPM4	1.26	0.36	2
P00918	C205	CA2	1.26	1.46	2
Q86UL3	C325	AGPAT6	1.26	0.10	2
Q8N9N8	C89	EIF1AD	1.25	0.43	4
P50570	C27	DNM2	1.25	0.03	4
P14735	C974	IDE	1.25	0.06	3
Q7Z2W4	C38	ZC3HAV1	1.25	0.44	3
Q96RN5	C618	MED15	1.25	0.25	3
Q13547	C261	HDAC1	1.25	0.42	3
Q7L5N1	C283	COPS6	1.25	0.36	3
O75607	C105	NPM3	1.25	0.21	3
Q8IUR0	C139	TRAPPC5	1.25	0.21	3
Q6PCB5	C280	RSBN1L	1.25	0.23	3
P17858	C89	PFKL	1.25	0.35	2
P50416	C96	CPT1A	1.25	0.29	2
P49327	C2468	FASN	1.25	0.28	2
O15355	C164	PPM1G	1.25	0.25	2
P13489	C409	RNH1	1.25	0.03	2
P13639	C591	EEF2	1.25	0.52	2
Q8TCG1	C337	KIAA1524	1.25	0.13	2
P27635	C71	RPL10	1.25	0.39	2
Q14203	C1252	DCTN1	1.24	0.26	4
O15372	C327	EIF3H	1.24	0.38	4
P55795	C267	HNRNPH2	1.24	0.21	4
Q5TFE4	C119	NT5DC1	1.24	0.24	4
P27816	C126	MAP4	1.24	0.23	4
P31943	C267	HNRNPH1	1.24	0.21	4
Q06203	C100	PPAT	1.24	0.29	4
Q06203	C105	PPAT	1.24	0.29	4
P12268	C331	IMPDH2	1.24	0.27	4
Q6ICB0	C108	DESI1	1.24	0.22	3
P13639	C751	EEF2	1.24	0.49	3

P07900	C374	HSP90AA1	1.24	0.41	3
Q9BVP2	C158	GNL3	1.24	0.54	3
Q92688	C27	ANP32B	1.24	0.41	2
O95347	C1174	SMC2	1.24	0.32	2
P35610	C92	SOAT1	1.24	0.41	2
O15541	C15	RNF113A	1.24	0.09	2
Q9NRA8	C125	EIF4ENIF1	1.24	0.23	2
P53041	C77	PPP5C	1.24	0.40	2
Q14232	C169	EIF2B1	1.24	0.18	2
Q9H6Q4	C300	NARFL	1.23	0.21	4
P40616	C80	ARL1	1.23	0.43	4
P39023	C253	RPL3	1.23	0.29	4
O60232	C152	SSSCA1	1.23	0.27	4
P10599	C73	TXN	1.23	0.35	4
Q969H6	C146	POP5	1.23	0.15	4
Q9NPJ6	C162	MED4	1.23	0.16	4
P48643	C253	CCT5	1.23	0.26	4
P61247	C201	RPS3A	1.23	0.43	4
Q92901	C253	RPL3L	1.23	0.29	4
Q96RS6	C376	NUDCD1	1.23	0.26	3
P62837	C107	UBE2D2	1.23	0.17	3
P62837	C111	UBE2D2	1.23	0.17	3
P57678	C210	GEMIN4	1.23	0.29	3
P22307	C307	SCP2	1.23	0.17	3
Q99575	C705	POP1	1.23	0.25	3
P61077	C107	UBE2D3	1.23	0.17	3
P61077	C111	UBE2D3	1.23	0.17	3
Q9UHR5	C172	SAP30BP	1.23	0.06	3
O95671	C441	ASMTL	1.23	0.27	3
Q92530	C185	PSMF1	1.23	0.29	3
Q15004	C99	KIAA0101	1.23	0.41	2
Q86UA6	C122	RPAIN	1.23	0.07	2
Q86X76	C203	NIT1	1.23	0.17	2
Q9NXV6	C516	CDKN2AIP	1.23	0.28	2
Q9Y3B4	C74	SF3B14	1.23	0.21	2
Q9Y3B4	C83	SF3B14	1.23	0.21	2
Q12789	C42	GTF3C1	1.23	0.01	2
Q8NEC7	C140	GSTCD	1.23	0.11	2
Q99598	C202	TSNAX	1.23	0.37	2
P54274	C118	TERF1	1.23	0.12	2
O00429	C361	DNM1L	1.23	0.27	2

Q7L8W6	C88	ATPBD4	1.23	0.04	2
Q9BW61	C25	DDA1	1.23	0.22	2
P38606	C277	ATP6V1A	1.22	0.16	4
Q15021	C596	NCAPD2	1.22	0.39	4
Q9HAV4	C1131	XPO5	1.22	0.32	4
Q06323	C22	PSME1	1.22	0.39	4
O75874	C269	IDH1	1.22	0.21	4
Q9BTA9	C553	WAC	1.22	0.25	4
Q9Y6G9	C51	DYNC1LI1	1.22	0.24	3
O95163	C213	IKBKAP	1.22	0.37	3
P13639	C812	EEF2	1.22	0.33	3
Q9NX38	C74	FAM206A	1.22	0.53	3
Q9H467	C159	CUEDC2	1.22	0.20	3
Q01433	C230	AMPD2	1.22	0.29	3
P27707	C45	DCK	1.22	0.35	3
O14893	C34	GEMIN2	1.22	0.20	3
P28074	C111	PSMB5	1.22	0.43	3
Q00534	C306	CDK6	1.22	0.37	2
Q13428	C1298	TCOF1	1.22	0.02	2
Q9BYV8	C274	CEP41	1.22	0.39	2
P05386	C61	RPLP1	1.21	0.25	4
Q9Y383	C348	LUC7L2	1.21	0.41	4
Q9ULV4	C420	CORO1C	1.21	0.29	4
Q9BUH6	C180	C9orf142	1.21	0.25	4
O75832	C107	PSMD10	1.21	0.24	4
P33316	C222	DUT	1.21	0.36	4
P19447	C342	ERCC3	1.21	0.25	4
O14929	C101	HAT1	1.21	0.14	4
Q96A49	C283	SYAP1	1.21	0.48	4
P12955	C467	PEPD	1.21	0.29	3
P11586	C863	MTHFD1	1.21	0.29	3
Q9NTK5	C55	OLA1	1.21	0.20	3
Q9BWD1	C88	ACAT2	1.21	0.33	3
Q9BWD1	C92	ACAT2	1.21	0.33	3
Q99504	C56	EYA3	1.21	0.20	3
Q8NFP7	C3	NUDT10	1.21	0.32	2
Q9BSD7	C101	NTPCR	1.21	0.28	2
O43252	C360	PAPSS1	1.21	0.26	2
O95619	C210	YEATS4	1.21	0.16	2
P35611	C68	ADD1	1.21	0.01	2
Q9UM19	C187	HPCAL4	1.21	0.20	2

O75175	C600	CNOT3	1.21	0.09	2
Q6NZY4	C393	ZCCHC8	1.21	0.27	2
Q9Y3C1	C36	NOP16	1.21	0.49	2
Q9UBW8	C110	COPS7A	1.21	0.17	2
Q9NVR0	C341	KLHL11	1.21	0.28	2
P53396	C633	ACLY	1.21	0.46	2
Q15170	C88	TCEAL1	1.2	0.41	4
Q9BUK6	C485	MSTO1	1.2	0.27	4
Q9BT78	C378	COPS4	1.2	0.41	4
P57081	C137	WDR4	1.2	0.48	4
O76075	C194	DFFB	1.2	0.19	4
Q9Y265	C141	RUVBL1	1.2	0.26	4
Q9NQR4	C153	NIT2	1.2	0.41	4
Q16576	C97	RBBP7	1.2	0.21	4
Q96KB5	C22	PBK	1.2	0.30	4
P53992	C78	SEC24C	1.2	0.33	3
Q4VCS5	C1047	AMOT	1.2	0.58	3
P49841	C14	GSK3B	1.2	0.22	3
O14972	C219	DSCR3	1.2	0.30	3
O14972	C221	DSCR3	1.2	0.30	3
P34932	C290	HSPA4	1.2	0.26	3
P45973	C160	CBX5	1.2	0.51	3
Q13185	C160	CBX3	1.2	0.51	3
Q5VWQ0	C282	RSBN1	1.2	0.25	3
Q96SW2	C188	CRBN	1.2	0.19	3
P43243	C230	MATR3	1.2	0.21	3
Q9Y617	C291	PSAT1	1.2	1.76	2
Q13371	C95	PDCL	1.2	0.40	2
Q6NXT1	C230	ANKRD54	1.2	0.34	2
Q96EY5	C33	FAM125A	1.2	0.10	2
Q9Y262	C417	EIF3L	1.2	0.32	2
P19623	C25	SRM	1.2	0.13	2
P46777	C144	RPL5	1.2	9.40	2
P18031	C92	PTPN1	1.2	0.27	2
Q9H8M7	C131	FAM188A	1.2	0.14	2
O60563	C630	CCNT1	1.2	1.28	2
P05388	C27	RPLP0	1.19	0.43	4
Q5MNZ6	C63	WDR45L	1.19	0.25	4
Q8NFC6	C74	BOD1L1	1.19	0.41	4
Q96GX2	C75	ATXN7L3B	1.19	0.14	4
Q96IZ6	C171	METTL2A	1.19	0.13	4

Q96IK1	C72	BOD1	1.19	0.41	4
P35611	C525	ADD1	1.19	0.34	4
Q9UNM6	C357	PSMD13	1.19	0.58	4
Q9NQ88	C114	TIGAR	1.19	0.28	4
Q92841	C584	DDX17	1.19	0.29	4
P12277	C254	CKB	1.19	0.52	4
P49589	C27	CARS	1.19	0.12	4
Q96CP2	C64	FLYWCH2	1.19	0.33	4
Q99873	C109	PRMT1	1.19	0.29	4
O95336	C32	PGLS	1.19	0.28	3
Q9UGV2	C359	NDRG3	1.19	0.33	3
O76071	C234	CIAO1	1.19	0.18	3
P42224	C492	STAT1	1.19	0.19	3
Q8N0Z8	C292	PUSL1	1.19	0.28	3
P55210	C186	CASP7	1.19	0.42	3
O15294	C758	OGT	1.19	0.10	3
P52292	C133	KPNA2	1.19	0.29	3
Q9NS18	C77	GLRX2	1.19	0.36	3
Q9H4A4	C304	RNPEP	1.19	0.31	3
Q9H4A4	C311	RNPEP	1.19	0.31	3
O75153	C333	KIAA0664	1.19	0.21	3
P62487	C38	POLR2G	1.19	0.44	3
P61289	C92	PSME3	1.19	0.22	3
Q9Y613	C502	FHOD1	1.19	0.18	2
Q8WVV9	C84	HNRPLL	1.19	0.35	2
P78527	C25	PRKDC	1.19	0.27	2
Q96GG9	C115	DCUN1D1	1.19	0.26	2
P61927	C37	RPL37	1.19	0.44	2
Q15365	C109	PCBP1	1.18	0.22	4
Q69YN2	C141	CWF19L1	1.18	0.30	4
O15067	C1285	PFAS	1.18	0.34	4
O15067	C1287	PFAS	1.18	0.34	4
Q8NBS9	C350	TXNDC5	1.18	0.26	4
Q8NBS9	C353	TXNDC5	1.18	0.26	4
Q99961	C277	SH3GL1	1.18	0.25	4
Q9NR50	C281	EIF2B3	1.18	0.36	4
Q9NR50	C285	EIF2B3	1.18	0.36	4
Q9Y4B6	C1227	VPRBP	1.18	0.32	4
P14618	C358	PKM	1.18	0.51	3
Q9BUK6	C403	MSTO1	1.18	0.25	3
O95372	C213	LYPLA2	1.18	0.19	3

P22234	C350	PAICS	1.18	0.50	3
O43175	C18	PHGDH	1.18	0.27	3
B0V043	C112	VARS	1.18	0.28	3
P52292	C223	KPNA2	1.18	0.24	3
O43242	C483	PSMD3	1.18	0.18	2
Q969T7	C202	NT5C3L	1.18	0.34	2
P31949	C91	S100A11	1.18	0.12	2
Q9NP72	C160	RAB18	1.18	0.31	2
Q9NZD2	C36	GLTP	1.18	0.25	2
Q96EP5	C85	DAZAP1	1.18	0.35	2
P84074	C185	HPCA	1.17	0.21	4
P05388	C119	RPLP0	1.17	0.39	4
H7BZ11	C83	Uncharacteriz	1.17	0.29	4
H7BZ11	C88	Uncharacteriz	1.17	0.29	4
P37235	C185	HPCAL1	1.17	0.21	4
Q9NQC3	C1101	RTN4	1.17	0.44	4
Q9BRP1	C278	PDCD2L	1.17	0.25	4
Q13310	C339	PABPC4	1.17	0.43	4
Q9NQ88	C161	TIGAR	1.17	0.19	4
P30041	C91	PRDX6	1.17	0.58	4
P15121	C299	AKR1B1	1.17	0.30	4
P15121	C304	AKR1B1	1.17	0.30	4
P07900	C597	HSP90AA1	1.17	0.49	4
P07900	C598	HSP90AA1	1.17	0.49	4
P63244	C138	GNB2L1	1.17	0.30	4
Q969Q0	C72	RPL36AL	1.17	0.29	4
Q969Q0	C77	RPL36AL	1.17	0.29	4
Q8NFF5	C496	FLAD1	1.17	0.03	3
Q8NFF5	C499	FLAD1	1.17	0.03	3
P36405	C174	ARL3	1.17	0.33	3
P10768	C45	ESD	1.17	0.32	3
P10768	C56	ESD	1.17	0.32	3
O00743	C192	PPP6C	1.17	0.13	3
Q9BYB4	C175	GNB1L	1.17	0.26	3
Q86Y37	C362	CACUL1	1.17	0.15	3
Q15370	C60	TCEB2	1.17	1.16	2
Q9H668	C8	OBFC1	1.17	0.09	2
P12955	C482	PEPD	1.17	0.17	2
P48643	C181	CCT5	1.17	0.46	2
Q14204	C1977	DYNC1H1	1.17	0.07	2
P07814	C92	EPRS	1.17	0.47	2

Q7KZF4	C560	SND1	1.17	0.22	2
O96017	C385	CHEK2	1.17	0.19	2
A6NDG6	C297	PGP	1.16	0.19	4
P11413	C13	G6PD	1.16	0.23	4
P13639	C651	EEF2	1.16	0.46	4
Q07065	C100	CKAP4	1.16	0.38	4
Q8NBF2	C716	NHLRC2	1.16	0.23	4
Q9H840	C44	GEMIN7	1.16	0.29	4
Q16555	C504	DPYSL2	1.16	0.22	4
Q9H2G2	C1212	SLK	1.16	0.15	4
P49023	C108	PXN	1.16	0.27	4
Q9HBM6	C121	TAF9B	1.16	0.17	3
Q8N999	C294	C12orf29	1.16	0.12	3
Q8N999	C302	C12orf29	1.16	0.18	3
P43487	C132	RANBP1	1.16	0.25	3
Q5VWZ2	C12	LYPLAL1	1.16	0.50	3
Q13158	C98	FADD	1.16	0.16	3
Q13158	C105	FADD	1.16	0.16	3
Q16594	C121	TAF9	1.16	0.17	3
O14733	C260	MAP2K7	1.16	0.15	3
Q96GM5	C460	SMARCD1	1.16	0.21	3
O94788	C319	ALDH1A2	1.16	0.33	3
O94788	C320	ALDH1A2	1.16	0.33	3
Q7Z417	C234	NUFIP2	1.16	0.28	3
Q9BWU1	C349	CDK19	1.16	0.13	2
P25205	C148	MCM3	1.16	0.22	2
Q9Y617	C80	PSAT1	1.16	0.17	2
P18124	C186	RPL7	1.16	0.22	2
P40926	C285	MDH2	1.16	0.13	2
Q15181	C254	PPA1	1.16	0.34	2
P45983	C245	MAPK8	1.16	0.21	2
P53779	C283	MAPK10	1.16	0.21	2
Q13428	C38	TCOF1	1.16	0.26	2
Q96QD9	C242	FYTTD1	1.16	0.28	2
Q0PNE2	C218	ELP6	1.15	0.35	4
Q9NZJ9	C147	NUDT4	1.15	0.28	4
Q99832	C29	CCT7	1.15	0.37	4
P13639	C41	EEF2	1.15	0.30	4
Q9NVG8	C36	TBC1D13	1.15	0.12	4
Q14181	C198	POLA2	1.15	0.21	4
Q15417	C173	CNN3	1.15	0.19	4

Q9Y3F4	C340	STRAP	1.15	0.25	4
Q99614	C149	TTC1	1.15	0.30	4
Q9Y508	C8	RNF114	1.15	0.21	4
P62910	C91	RPL32	1.15	0.31	4
Q96FW1	C23	OTUB1	1.15	0.22	4
O15067	C270	PFAS	1.15	0.22	3
Q96HC4	C213	PDLIM5	1.15	0.40	3
Q9BR61	C267	ACBD6	1.15	0.28	3
Q8N0Z6	C439	TTC5	1.15	0.18	3
Q9HAV4	C44	XPO5	1.15	0.33	3
Q9Y679	C391	AUP1	1.15	0.19	3
O14733	C280	MAP2K7	1.15	0.12	3
P12532	C316	CKMT1B	1.15	0.53	3
P53602	C386	MVD	1.15	0.28	3
O14980	C34	XPO1	1.15	0.19	3
P34949	C286	MPI	1.15	0.35	3
P34949	C289	MPI	1.15	0.35	3
Q9BVP2	C280	GNL3	1.15	0.40	3
Q9Y487	C165	ATP6V0A2	1.15	0.51	3
P17540	C317	CKMT2	1.15	0.53	3
O95229	C54	ZWINT	1.15	0.22	3
Q9NVM9	C349	Asun	1.15	0.20	2
Q5RKV6	C117	EXOSC6	1.15	0.42	2
P27695	C296	APEX1	1.15	1.44	2
Q9HAS0	C288	C17orf75	1.15	0.02	2
O75179	C644	ANKRD17	1.15	0.30	2
Q9UNE7	C199	STUB1	1.15	0.32	2
Q6NXT1	C265	ANKRD54	1.15	0.10	2
Q9C0B1	C326	FTO	1.15	0.22	2
Q9UHR6	C188	ZNHIT2	1.15	0.30	2
Q5VSL9	C769	FAM40A	1.15	0.08	2
Q8NC96	C162	NECAP1	1.15	0.24	2
Q06830	C52	PRDX1	1.15	0.20	2
Q06546	C421	GABPA	1.15	0.28	2
P49591	C438	SARS	1.15	0.02	2
O75934	C106	BCAS2	1.15	0.35	2
Q9NQT5	C215	EXOSC3	1.14	0.23	4
Q96FX7	C209	TRMT61A	1.14	0.28	4
P55795	C122	HNRNPH2	1.14	0.52	4
O95817	C179	BAG3	1.14	0.18	4
P68104	C411	EEF1A1	1.14	0.19	4

P14866	C581	HNRNPL	1.14	0.59	4
O95059	C31	RPP14	1.14	0.52	4
P31943	C22	HNRNPH1	1.14	0.42	4
P31943	C122	HNRNPH1	1.14	0.52	4
Q7Z6M1	C115	RABEPK	1.14	0.39	4
P61978	C132	HNRNPK	1.14	0.22	3
Q9UKF6	C498	CPSF3	1.14	0.17	3
Q9Y224	C19	C14orf166	1.14	0.23	3
Q8IV63	C191	VRK3	1.14	0.14	3
P13010	C235	XRCC5	1.14	0.34	2
P41091	C105	EIF2S3	1.14	0.40	2
P23526	C421	AHCY	1.14	0.26	2
Q9ULA0	C327	DNPEP	1.14	0.10	2
Q96PU8	C35	QKI	1.14	0.07	2
Q9Y2L1	C213	DIS3	1.14	0.34	2
Q9NVR0	C73	KLHL11	1.14	0.39	2
P08236	C644	GUSB	1.14	0.11	2
Q9UI30	C33	TRMT112	1.13	0.41	4
P49189	C288	ALDH9A1	1.13	0.25	4
P49189	C289	ALDH9A1	1.13	0.25	4
Q15181	C270	PPA1	1.13	0.26	4
Q15181	C274	PPA1	1.13	0.26	4
P22234	C81	PAICS	1.13	0.31	4
P22234	C91	PAICS	1.13	0.31	4
P22234	C100	PAICS	1.13	0.31	4
P52789	C517	HK2	1.13	0.15	4
O43175	C369	PHGDH	1.13	0.20	4
P26599	C23	PTBP1	1.13	0.22	4
P62258	C97	YWHAE	1.13	0.55	4
P62258	C98	YWHAE	1.13	0.55	4
O00487	C238	PSMD14	1.13	0.29	4
O75663	C87	TIPRL	1.13	0.20	4
Q01518	C93	CAP1	1.13	0.34	4
P22392	C145	NME2	1.13	0.54	4
O60361	C130	NME2P1	1.13	0.54	4
Q99873	C262	PRMT1	1.13	0.58	4
Q96GM8	C80	TOE1	1.13	0.35	3
P27695	C99	APEX1	1.13	0.39	3
Q96RE7	C416	NACC1	1.13	0.14	3
Q8TBC4	C237	UBA3	1.13	0.25	3
Q7L2J0	C522	MEPCE	1.13	0.31	3

Q8NHU6	C1029	TDRD7	1.13	0.07	3
Q9NVA2	C41	11-Sep	1.13	0.32	3
P37268	C6	FDFT1	1.13	0.17	3
P22314	C23	UBA1	1.13	0.43	3
P61981	C97	YWHAG	1.13	0.34	3
O60921	C200	HUS1	1.13	0.10	3
P50851	C2675	LRBA	1.13	0.15	3
Q6PJT7	C261	ZC3H14	1.13	0.22	3
Q9Y266	C188	NUDC	1.13	0.34	3
Q13148	C39	TARDBP	1.13	0.38	3
Q9BV20	C168	MRI1	1.13	0.27	3
Q13630	C112	TSTA3	1.13	0.26	3
Q13630	C116	TSTA3	1.13	0.26	3
Q9BXJ9	C322	NAA15	1.13	0.19	3
Q9ULE6	C845	PALD1	1.13	0.17	3
Q96BF6	C393	NACC2	1.13	0.14	3
O75131	C506	CPNE3	1.13	0.24	3
P33992	C482	MCM5	1.13	8.79	3
P60981	C163	DSTN	1.13	0.25	3
Q9Y2X3	C439	NOP58	1.13	0.50	3
Q8IU81	C363	IRF2BP1	1.13	0.12	3
Q16514	C143	TAF12	1.13	0.37	2
O95757	C290	HSPA4L	1.13	0.33	2
Q13596	C318	SNX1	1.13	0.12	2
Q7L5D6	C160	GET4	1.13	0.32	2
P17655	C98	CAPN2	1.13	0.29	2
P17655	C105	CAPN2	1.13	0.29	2
Q8N0X7	C562	SPG20	1.13	0.11	2
Q13620	C248	CUL4B	1.13	0.14	2
P60981	C23	DSTN	1.13	0.27	2
Q15398	C129	DLGAP5	1.13	0.26	2
Q9Y4P1	C74	ATG4B	1.12	0.14	4
Q14353	C91	GAMT	1.12	0.41	4
Q06124	C259	PTPN11	1.12	0.28	4
P60842	C131	EIF4A1	1.12	0.24	4
P60842	C134	EIF4A1	1.12	0.24	4
O75569	C106	PRKRA	1.12	0.17	4
O43765	C153	SGTA	1.12	0.19	4
Q13185	C177	CBX3	1.12	0.20	4
Q86W42	C35	THOC6	1.12	0.32	4
O00299	C24	CLIC1	1.12	0.15	4

O00429	C367	DNM1L	1.12	0.26	4
Q96FV9	C49	THOC1	1.12	0.16	4
Q7RTV0	C61	PHF5A	1.12	0.40	4
P49321	C708	NASP	1.12	0.23	4
A0AVT1	C347	UBA6	1.12	0.29	3
Q9Y295	C195	DRG1	1.12	0.47	3
Q8N1F7	C422	NUP93	1.12	0.28	3
Q96EY5	C231	FAM125A	1.12	0.30	3
Q86W42	C314	THOC6	1.12	0.15	3
O95456	C137	PSMG1	1.12	0.30	3
O95456	C139	PSMG1	1.12	0.30	3
Q96DE5	C55	ANAPC16	1.12	0.08	3
Q96MG7	C283	NDNL2	1.12	0.27	2
Q13257	C106	MAD2L1	1.12	0.05	2
Q9BQI3	C494	EIF2AK1	1.12	0.24	2
Q9NVS9	C156	PNPO	1.12	0.21	2
Q5TDH0	C361	DDI2	1.11	0.22	4
Q9NRX1	C64	PNO1	1.11	0.22	4
Q8N5K1	C92	CISD2	1.11	0.53	4
P45984	C177	MAPK9	1.11	0.23	4
Q9UJX3	C259	ANAPC7	1.11	0.23	4
Q9UJW0	C258	DCTN4	1.11	0.23	4
P11802	C78	CDK4	1.11	0.21	4
P35219	C266	CA8	1.11	0.29	4
O95295	C66	SNAPIN	1.11	0.53	3
O15067	C66	PFAS	1.11	0.19	3
Q9UPY8	C182	MAPRE3	1.11	0.17	3
P45974	C195	USP5	1.11	0.29	3
Q9P000	C147	COMMD9	1.11	0.33	3
P11802	C135	CDK4	1.11	0.20	3
Q9BVC5	C10	C2orf49	1.11	0.03	2
Q16186	C88	ADRM1	1.11	0.26	2
P53618	C888	COPB1	1.11	0.23	2
Q4VCS5	C741	AMOT	1.11	0.07	2
Q96GW9	C425	MARS2	1.11	0.11	2
P00338	C35	LDHA	1.11	0.94	2
Q8WWY3	C247	PRPF31	1.11	9.45	2
O96011	C153	PEX11B	1.11	0.15	2
Q86Y37	C166	CACUL1	1.11	0.08	2
Q15370	C89	TCEB2	1.1	0.20	4
O95400	C234	CD2BP2	1.1	0.16	4

Q96EY9	C13	ADAT3	1.1	0.34	4
Q9NUQ9	C10	FAM49B	1.1	0.22	4
P49458	C48	SRP9	1.1	0.42	4
Q9NVG8	C387	TBC1D13	1.1	0.12	4
P62888	C92	RPL30	1.1	0.47	4
Q6QNY0	C168	BLOC1S3	1.1	0.40	4
Q9BQA1	C65	WDR77	1.1	0.22	4
Q9BQA1	C73	WDR77	1.1	0.22	4
P61758	C113	VBP1	1.1	0.23	4
Q13526	C113	PIN1	1.1	0.16	4
O60256	C31	PRPSAP2	1.1	0.30	4
P15927	C219	RPA2	1.1	0.25	4
O15269	C438	SPTLC1	1.1	0.20	4
P00558	C367	PGK1	1.1	0.40	4
P00558	C379	PGK1	1.1	0.40	4
P00558	C380	PGK1	1.1	0.40	4
Q9BQ67	C11	GRWD1	1.1	0.21	4
Q9UMS0	C210	NFU1	1.1	0.16	3
Q9UMS0	C213	NFU1	1.1	0.16	3
Q96GX9	C147	APIP	1.1	0.28	3
Q13561	C240	DCTN2	1.1	0.31	3
Q13561	C256	DCTN2	1.1	0.31	3
P11586	C918	MTHFD1	1.1	0.16	3
P48739	C187	PITPNB	1.1	0.30	3
Q8N0X7	C558	SPG20	1.1	0.25	3
Q86U90	C99	YRDC	1.1	0.23	3
Q96DF8	C263	DGCR14	1.1	0.15	3
J3QR44	C430	CDK11B	1.1	0.12	2
P78368	C54	CSNK1G2	1.1	0.06	2
Q9HCP0	C52	CSNK1G1	1.1	0.06	2
Q99543	C394	DNAJC2	1.1	0.01	2
Q9Y6M4	C51	CSNK1G3	1.1	0.06	2
P21127	C440	CDK11B	1.1	0.12	2
Q9H5V9	C11	CXorf56	1.1	0.25	2
Q06330	C397	RBPJ	1.1	0.28	2
P22061	C102	PCMT1	1.1	0.31	2
P52701	C88	MSH6	1.1	0.11	2
Q15366	C109	PCBP2	1.09	0.25	4
A6NDU8	C179	C5orf51	1.09	0.22	4
Q9BY32	C146	ITPA	1.09	0.21	4
Q9BY32	C154	ITPA	1.09	0.21	4

P30519	C282	HMOX2	1.09	0.32	4
Q92499	C110	DDX1	1.09	0.49	4
Q92499	C111	DDX1	1.09	0.49	4
P27348	C237	YWHAQ	1.09	0.21	4
Q9Y696	C35	CLIC4	1.09	0.18	4
P20073	C363	ANXA7	1.09	0.20	4
P14868	C349	DARS	1.09	0.53	4
P04843	C477	RPN1	1.09	0.40	4
Q9UK45	C85	LSM7	1.09	0.32	4
P53396	C20	ACLY	1.09	0.20	4
Q15185	C58	PTGES3	1.09	0.29	3
P16333	C266	NCK1	1.09	0.18	3
Q14137	C108	BOP1	1.09	0.02	3
P39023	C114	RPL3	1.09	0.49	3
P62837	C85	UBE2D2	1.09	0.39	3
Q9H7X7	C12	RABL5	1.09	0.15	3
Q96B45	C27	C10orf32	1.09	0.24	3
Q96IJ6	C389	GMPPA	1.09	0.41	3
P13639	C131	EEF2	1.09	0.29	3
P13639	C136	EEF2	1.09	0.29	3
Q4VCS5	C254	AMOT	1.09	0.17	3
P63208	C160	SKP1	1.09	0.25	3
Q2TAA2	C137	IAH1	1.09	0.10	3
Q14997	C1840	PSME4	1.09	0.16	3
P61077	C85	UBE2D3	1.09	0.39	3
P52888	C682	THOP1	1.09	0.10	3
P52888	C689	THOP1	1.09	0.10	3
Q7L1Q6	C35	BZW1	1.09	0.18	3
Q13045	C46	FLII	1.09	0.30	3
P41240	C31	CSK	1.09	0.38	3
P51668	C85	UBE2D1	1.09	0.39	3
Q12824	C147	SMARCB1	1.09	0.24	3
P30153	C294	PPP2R1A	1.09	0.31	2
Q9NV35	C23	NUDT15	1.09	0.34	2
Q9NRW3	C97	APOBEC3C	1.09	0.43	2
Q7Z2E3	C161	APTX	1.09	0.27	2
O14579	C212	COPE	1.09	0.22	2
Q6PJG6	C228	BRAT1	1.09	0.22	2
P53396	C764	ACLY	1.09	0.10	2
O75369	C2501	FLNB	1.08	0.34	4
Q16644	C203	MAPKAPK3	1.08	0.30	4

P15531	C109	NME1	1.08	0.25	4
Q8IWX8	C69	CHERP	1.08	0.29	4
P18621	C144	RPL17	1.08	0.27	4
O75822	C207	EIF3J	1.08	0.29	4
J3QL51	C144	RPL17-C18O	1.08	0.27	4
P14625	C645	HSP90B1	1.08	0.50	4
P55072	C522	VCP	1.08	0.26	4
Q9BXJ9	C721	NAA15	1.08	0.20	4
P49721	C91	PSMB2	1.08	0.27	4
Q9NSD9	C195	FARSB	1.08	0.23	4
P22392	C109	NME2	1.08	0.25	4
P13797	C104	PLS3	1.08	0.20	4
Q9NWV8	C222	BABAM1	1.08	0.31	4
O60361	C94	NME2P1	1.08	0.25	4
P40222	C87	TXLNA	1.08	0.13	3
Q14247	C246	CTTN	1.08	0.30	3
Q96C36	C262	PYCR2	1.08	0.18	3
P27348	C134	YWHAQ	1.08	0.28	3
Q9HAV4	C941	XPO5	1.08	0.34	3
P32322	C262	PYCR1	1.08	0.18	3
J3KR12	C188	Uncharacteriz	1.08	0.18	3
Q96JB2	C65	COG3	1.08	0.23	3
Q7Z4W1	C244	DCXR	1.08	0.32	3
P49368	C173	CCT3	1.08	0.28	3
Q6Y7W6	C938	GIGYF2	1.08	0.28	3
P78345	C80	RPP38	1.08	0.11	2
P53992	C1083	SEC24C	1.08	0.30	2
P63220	C17	RPS21	1.08	0.40	2
P51812	C229	RPS6KA3	1.08	0.25	2
O95232	C58	LUC7L3	1.08	0.16	2
Q9ULR5	C60	PAIP2B	1.08	0.16	2
O95674	C286	CDS2	1.08	0.38	2
O95674	C289	CDS2	1.08	0.38	2
Q12800	C453	TFCP2	1.08	0.31	2
O15294	C620	OGT	1.08	0.15	2
Q15554	C118	TERF2	1.08	0.30	2
Q15418	C223	RPS6KA1	1.08	0.25	2
Q9HBM1	C27	SPC25	1.07	0.30	4
Q15366	C54	PCBP2	1.07	0.22	4
Q15365	C54	PCBP1	1.07	0.22	4
Q969T9	C80	WBP2	1.07	0.50	4

P45880	C76	VDAC2	1.07	0.36	4
P07195	C164	LDHB	1.07	0.37	4
Q8WU79	C196	SMAP2	1.07	0.22	4
Q13573	C250	SNW1	1.07	0.17	4
P45973	C133	CBX5	1.07	0.25	4
Q9UJX3	C131	ANAPC7	1.07	0.27	4
Q9UBB4	C283	ATXN10	1.07	0.24	4
P00338	C163	LDHA	1.07	0.37	4
P54819	C40	AK2	1.07	0.55	4
P61247	C96	RPS3A	1.07	0.34	4
O75874	C379	IDH1	1.07	0.29	4
P00492	C106	HPRT1	1.07	0.38	4
Q8NCF5	C232	NFATC2IP	1.07	0.20	4
P26641	C68	EEF1G	1.07	0.35	3
P60709	C257	ACTB	1.07	0.39	3
P60709	C272	ACTB	1.07	0.39	3
P11216	C326	PYGB	1.07	0.22	3
Q86YR5	C670	GPSM1	1.07	0.29	3
Q7L4I2	C382	RSRC2	1.07	0.23	3
Q9NPH2	C541	ISYNA1	1.07	0.21	3
Q9BZX2	C241	UCK2	1.07	0.27	3
Q99829	C53	CPNE1	1.07	0.27	3
Q5VTR2	C924	RNF20	1.07	0.38	3
O00541	C272	PES1	1.07	0.22	3
P36405	C118	ARL3	1.07	0.45	3
P51956	C504	NEK3	1.07	0.28	3
O95801	C63	TTC4	1.07	0.21	3
P12004	C81	PCNA	1.07	0.38	3
P53602	C108	MVD	1.07	0.36	3
Q9UBU9	C252	NXF1	1.07	0.41	3
Q53EL6	C288	PDCD4	1.07	0.41	3
O60502	C596	MGEA5	1.07	0.30	3
P36969	C93	GPX4	1.07	0.33	3
Q9BYG3	C269	MKI67IP	1.07	0.24	2
P14618	C326	PKM	1.07	0.31	2
Q15417	C273	CNN3	1.07	0.10	2
Q9NR50	C106	EIF2B3	1.07	0.05	2
Q13042	C194	CDC16	1.07	0.01	2
Q7L5Y1	C307	ENOSF1	1.07	0.15	2
O60610	C1227	DIAPH1	1.06	0.31	4
P22314	C632	UBA1	1.06	0.20	4

O00233	C59	PSMD9	1.06	0.20	4
Q9NVG8	C145	TBC1D13	1.06	0.28	4
O15371	C19	EIF3D	1.06	0.27	4
Q13325	C137	IFIT5	1.06	0.34	4
O95801	C238	TTC4	1.06	0.18	4
P54105	C73	CLNS1A	1.06	0.25	4
Q9Y3F4	C305	STRAP	1.06	0.19	4
P12268	C140	IMPDH2	1.06	0.14	4
P51665	C116	PSMD7	1.06	0.32	4
Q8WVJ2	C99	NUDCD2	1.06	0.16	4
P42772	C74	CDKN2B	1.06	0.39	3
P42771	C72	CDKN2A	1.06	0.39	3
Q9BQ15	C99	NABP2	1.06	0.34	3
Q6P4I2	C106	WDR73	1.06	0.10	3
P37802	C124	TAGLN2	1.06	0.24	3
Q53EL6	C275	PDCD4	1.06	0.22	3
Q13057	C140	COASY	1.06	0.22	3
Q13057	C143	COASY	1.06	0.22	3
Q13057	C144	COASY	1.06	0.22	3
Q6P4I2	C259	WDR73	1.06	0.11	2
P05455	C245	SSB	1.06	0.35	2
Q6P2E9	C838	EDC4	1.06	0.26	2
P26641	C266	EEF1G	1.05	0.20	4
P30566	C27	ADSL	1.05	0.16	4
Q9UL25	C29	RAB21	1.05	0.34	4
O75821	C139	EIF3G	1.05	0.34	4
P47897	C657	QARS	1.05	0.32	4
Q9P2X3	C195	IMPACT	1.05	0.29	4
Q1KMD3	C308	HNRNPUL2	1.05	0.31	4
H3BQZ7	C308	Uncharacteriz	1.05	0.31	4
P63244	C182	GNB2L1	1.05	0.28	4
Q9BRJ6	C107	C7orf50	1.05	0.24	4
P55735	C187	SEC13	1.05	0.14	4
P55735	C245	SEC13	1.05	0.23	4
Q9UNH7	C264	SNX6	1.05	0.37	4
P48147	C25	PREP	1.05	0.20	3
O43684	C129	BUB3	1.05	0.26	3
Q13148	C244	TARDBP	1.05	0.26	3
P17987	C385	TCP1	1.05	0.44	3
O14980	C1070	XPO1	1.05	0.26	3
O75600	C218	GCAT	1.05	0.35	3

O75600	C219	GCAT	1.05	0.35	3
Q9P258	C280	RCC2	1.05	0.27	3
P62910	C96	RPL32	1.05	0.39	3
Q9BT25	C354	HAUS8	1.05	0.16	3
H3BN98	C109	Uncharacteriz	1.05	0.23	2
P35658	C728	NUP214	1.05	0.16	2
Q9NRX1	C226	PNO1	1.05	0.33	2
O15344	C42	MID1	1.05	0.44	2
O43504	C66	HBXIP	1.05	0.15	2
Q15796	C81	SMAD2	1.05	0.28	2
Q9UBR2	C89	CTSZ	1.05	0.33	2
Q9UBR2	C92	CTSZ	1.05	0.33	2
Q15041	C109	ARL6IP1	1.05	0.23	2
Q16643	C632	DBN1	1.04	0.42	4
P45880	C47	VDAC2	1.04	0.36	4
P49327	C1448	FASN	1.04	0.22	4
P60763	C178	RAC3	1.04	0.24	4
P63000	C178	RAC1	1.04	0.24	4
P49915	C456	GMPS	1.04	0.17	4
P24941	C177	CDK2	1.04	0.19	4
Q9H3R5	C35	CENPH	1.04	0.49	4
Q9NPF4	C265	OSGEP	1.04	0.22	3
Q8TBC4	C28	UBA3	1.04	0.09	3
P53365	C106	ARFIP2	1.04	0.23	3
P50991	C252	CCT4	1.04	0.19	3
Q9NP73	C86	ALG13	1.04	8.89	3
Q04917	C97	YWHAH	1.04	0.18	3
Q14141	C432	6-Sep	1.04	0.29	3
Q9NUY8	C283	TBC1D23	1.04	0.17	3
Q99638	C114	RAD9A	1.04	0.29	3
Q9H6S0	C1265	YTHDC2	1.04	0.08	2
Q8NFP7	C131	NUDT10	1.04	0.29	2
Q9NZJ9	C131	NUDT4	1.04	0.29	2
Q8NG68	C91	TTL	1.04	0.13	2
Q96EY5	C90	FAM125A	1.04	0.27	2
P09661	C89	SNRPA1	1.04	0.84	2
Q9BQA1	C26	WDR77	1.04	0.05	2
Q00839	C607	HNRNPU	1.04	0.41	2
Q9Y520	C177	PRRC2C	1.04	0.78	2
Q9H7Z6	C416	KAT8	1.04	0.32	2
Q15024	C85	EXOSC7	1.04	0.25	2

P62917	C90	RPL8	1.04	1.01	2
Q9Y2Z0	C62	SUGT1	1.03	0.11	4
Q15645	C14	TRIP13	1.03	0.22	4
Q04917	C112	YWHAH	1.03	0.30	4
Q12906	C203	ILF3	1.03	0.45	4
Q99460	C806	PSMD1	1.03	0.32	3
P62979	C144	RPS27A	1.03	0.37	3
P62979	C145	RPS27A	1.03	0.37	3
P62979	C149	RPS27A	1.03	0.37	3
O75391	C191	SPAG7	1.03	0.49	3
Q12765	C324	SCRN1	1.03	0.37	3
O60831	C28	PRAF2	1.03	0.41	3
Q9NVG8	C282	TBC1D13	1.03	0.23	3
Q13148	C50	TARDBP	1.03	0.28	3
O00571	C128	DDX3X	1.03	0.11	3
Q5JS54	C55	PSMG4	1.03	0.16	3
Q9C0B1	C171	FTO	1.03	0.29	3
Q8WXD5	C91	GEMIN6	1.03	0.33	3
Q9BUM1	C269	G6PC3	1.03	0.36	3
Q9BQ61	C165	C19orf43	1.03	0.35	2
P61204	C159	ARF3	1.03	0.94	2
H0YGG7	C34	Uncharacteriz	1.03	0.94	2
O75940	C214	SMNDC1	1.02	0.18	4
Q9Y296	C195	TRAPPC4	1.02	0.19	4
Q9Y5P6	C245	GMPPB	1.02	0.22	4
Q16643	C613	DBN1	1.02	0.38	4
Q9NX24	C18	NHP2	1.02	0.14	4
Q6IBS0	C141	TWF2	1.02	0.25	4
O00541	C361	PES1	1.02	0.28	4
Q9Y277	C65	VDAC3	1.02	0.47	4
Q8TDN6	C52	BRIX1	1.02	0.27	4
P14866	C472	HNRNPL	1.02	0.18	4
P09936	C152	UCHL1	1.02	0.18	4
P78346	C87	RPP30	1.02	0.19	3
Q13126	C136	MTAP	1.02	0.09	3
Q13642	C150	FHL1	1.02	0.26	3
Q9UL46	C91	PSME2	1.02	0.35	3
P15735	C294	PHKG2	1.02	0.10	3
O60825	C158	PFKFB2	1.02	0.34	3
O15371	C195	EIF3D	1.02	0.31	3
O15371	C196	EIF3D	1.02	0.31	3

P17812	C362	CTPS1	1.02	0.33	3
P61221	C88	ABCE1	1.02	0.28	3
Q08J23	C221	NSUN2	1.02	0.41	3
P10398	C192	ARAF	1.02	0.17	3
Q15631	C225	TSN	1.02	0.27	3
O95861	C42	BPNT1	1.02	0.23	3
P35658	C186	NUP214	1.02	0.34	2
P31153	C56	MAT2A	1.02	0.32	2
P13667	C206	PDIA4	1.02	0.05	2
P13667	C209	PDIA4	1.02	0.05	2
P14649	C89	MYL6B	1.02	0.22	2
P60660	C32	MYL6	1.02	0.22	2
P50749	C251	RASSF2	1.02	0.01	2
Q96ER3	C366	SAAL1	1.02	0.20	2
Q00765	C18	REEP5	1.01	0.41	4
Q9H0C8	C301	ILKAP	1.01	0.19	4
Q8N6M0	C292	OTUD6B	1.01	0.33	4
P50990	C244	CCT8	1.01	0.21	4
P49841	C199	GSK3B	1.01	0.25	4
P49840	C262	GSK3A	1.01	0.25	4
P18085	C62	ARF4	1.01	0.24	4
P68036	C86	UBE2L3	1.01	0.36	4
Q9Y3A3	C134	MOB4	1.01	0.26	4
P13797	C33	PLS3	1.01	0.23	4
Q96LB3	C53	IFT74	1.01	0.32	4
O75131	C54	CPNE3	1.01	0.18	4
P25398	C92	RPS12	1.01	0.29	4
Q9NPD3	C97	EXOSC4	1.01	0.25	4
P05412	C99	JUN	1.01	0.41	4
Q9Y2Y0	C149	ARL2BP	1.01	0.34	3
Q8IY67	C255	RAVER1	1.01	0.16	3
P62993	C32	GRB2	1.01	0.28	3
P31943	C290	HNRNPH1	1.01	0.46	3
P84243	C111	H3F3B	1.01	0.16	3
Q8TAF3	C342	WDR48	1.01	0.38	3
Q15369	C11	TCEB1	1.01	0.40	2
Q99543	C240	DNAJC2	1.01	0.33	2
P13667	C555	PDIA4	1.01	0.41	2
P13667	C558	PDIA4	1.01	0.41	2
Q5VZE5	C409	NAA35	1.01	0.39	2
P30101	C406	PDIA3	1.01	0.41	2

P30101	C409	PDIA3	1.01	0.41	2
P28838	C376	LAP3	1.01	0.13	2
P00491	C206	PNP	1.01	0.17	2
Q96BN8	C347	FAM105B	1	0.20	4
Q15233	C208	NONO	1	0.31	4
P26358	C62	DNMT1	1	0.39	4
P23528	C139	CFL1	1	0.23	4
B5ME19	C444	EIF3CL	1	0.29	3
O00264	C129	PGRMC1	1	0.28	3
O60828	C60	PQBP1	1	0.10	3
Q9UJX3	C329	ANAPC7	1	0.11	3
P63244	C153	GNB2L1	1	1.08	3
P84103	C6	SRSF3	1	0.25	3
P84103	C10	SRSF3	1	0.25	3
Q9Y285	C493	FARSA	1	0.10	2
P31153	C214	MAT2A	1	0.25	2
Q9BTE3	C636	MCMBP	1	0.07	2
P60866	C70	RPS20	1	0.37	2
Q9Y2L1	C533	DIS3	1	9.50	2
Q17RN3	C36	FAM98C	1	0.08	2
P83436	C505	COG7	1	9.50	2
Q9BQ52	C670	ELAC2	0.99	0.23	4
Q52LJ0	C63	FAM98B	0.99	0.30	4
P51812	C579	RPS6KA3	0.99	0.17	4
Q00839	C594	HNRNPU	0.99	0.21	4
P08238	C589	HSP90AB1	0.99	0.29	4
P08238	C590	HSP90AB1	0.99	0.29	4
Q9P258	C428	RCC2	0.99	0.16	4
P09936	C90	UCHL1	0.99	0.27	4
Q15418	C575	RPS6KA1	0.99	0.17	4
Q7RTV0	C49	PHF5A	0.99	0.25	4
O75934	C132	BCAS2	0.99	0.13	4
Q5TA50	C163	GLTPD1	0.99	0.32	3
P25205	C360	MCM3	0.99	0.28	3
O14776	C1062	TCERG1	0.99	0.06	3
P22234	C288	PAICS	0.99	0.13	3
P22234	C295	PAICS	0.99	0.13	3
P62879	C204	GNB2	0.99	0.13	3
Q9H3U1	C663	UNC45A	0.99	0.07	2
Q9Y3D2	C105	MSRB2	0.99	0.25	2
O15144	C120	ARPC2	0.99	0.12	2

Q15648	C135	MED1	0.99	0.12	2
Q12857	C404	NFIA	0.99	0.14	2
Q9NRG0	C55	CHRAC1	0.98	0.45	4
Q15233	C145	NONO	0.98	0.23	4
P50990	C148	CCT8	0.98	0.41	4
P50990	C149	CCT8	0.98	0.41	4
Q15019	C111	2-Sep	0.98	0.28	4
Q01469	C120	FABP5	0.98	0.99	4
Q16763	C118	UBE2S	0.98	0.23	4
Q7Z4G1	C35	COMMD6	0.98	0.25	4
P19784	C336	CSNK2A2	0.98	0.31	4
P49336	C349	CDK8	0.98	0.29	3
Q9P1F3	C39	ABRACL	0.98	0.20	3
Q96Q11	C373	TRNT1	0.98	0.26	3
Q9NZ63	C145	C9orf78	0.98	0.34	3
P35080	C84	PFN2	0.98	0.29	3
Q9BXK1	C233	KLF16	0.98	0.12	3
Q16630	C159	CPSF6	0.98	0.29	3
Q00537	C233	CDK17	0.98	0.18	2
Q00536	C206	CDK16	0.98	0.18	2
Q9NQZ6	C124	ZC4H2	0.98	0.07	2
P22307	C94	SCP2	0.98	0.17	2
O60784	C415	TOM1	0.98	0.16	2
Q9GZT9	C127	EGLN1	0.98	0.79	2
Q07002	C183	CDK18	0.98	0.18	2
Q9H3H3	C222	C11orf68	0.98	0.23	2
Q8N2G8	C502	GHDC	0.98	0.12	2
P63208	C120	SKP1	0.97	0.24	4
P22102	C41	GART	0.97	0.13	4
P62306	C66	SNRPF	0.97	0.21	4
Q9H4A6	C84	GOLPH3	0.97	0.22	4
Q9H4A5	C70	GOLPH3L	0.97	0.22	4
Q13838	C165	DDX39B	0.97	0.44	3
O15067	C1338	PFAS	0.97	0.26	3
P13489	C75	RNH1	0.97	0.26	3
Q9BV79	C263	MECR	0.97	0.14	3
Q04724	C526	TLE1	0.97	0.31	3
Q04727	C529	TLE4	0.97	0.31	3
Q9P289	C77	MST4	0.97	0.24	3
P61513	C57	RPL37A	0.97	0.31	3
P61513	C60	RPL37A	0.97	0.31	3

Q9UBQ5	C190	EIF3K	0.97	0.25	3
P55060	C842	CSE1L	0.97	0.24	3
Q9NRP0	C14	OSTC	0.97	0.25	3
P31939	C241	ATIC	0.97	0.26	3
P51570	C182	GALK1	0.97	0.32	3
P62753	C100	RPS6	0.97	0.27	3
P36551	C198	CPOX	0.97	0.36	3
P15374	C95	UCHL3	0.97	0.23	3
Q9NZL4	C204	HSPBP1	0.97	0.01	2
Q96EX3	C65	WDR34	0.97	0.03	2
O43815	C765	STRN	0.97	0.09	2
Q13542	C35	EIF4EBP2	0.97	0.07	2
O15228	C54	GNPAT	0.97	0.16	2
Q14149	C15	MORC3	0.97	0.08	2
Q15084	C55	PDIA6	0.97	0.31	2
Q15084	C58	PDIA6	0.97	0.31	2
P53396	C845	ACLY	0.97	0.33	2
P17844	C234	DDX5	0.96	0.25	4
Q9NVC6	C649	MED17	0.96	0.08	4
P53611	C40	RABGGTB	0.96	0.11	4
Q15022	C46	SUZ12	0.96	0.35	4
Q14671	C1179	PUM1	0.96	0.14	3
Q7L2J0	C419	MEPCE	0.96	0.30	3
O95373	C757	IPO7	0.96	0.23	3
O95340	C350	PAPSS2	0.96	0.07	2
P49327	C212	FASN	0.96	0.16	2
Q9BQG2	C117	NUDT12	0.96	0.01	2
Q13155	C143	AIMP2	0.96	0.12	2
P55769	C30	NHP2L1	0.95	0.17	4
Q13162	C245	PRDX4	0.95	0.39	4
Q06830	C173	PRDX1	0.95	0.39	4
Q04637	C662	EIF4G1	0.95	0.31	4
Q13126	C131	MTAP	0.95	0.24	3
Q15004	C54	KIAA0101	0.95	0.33	3
P45880	C210	VDAC2	0.95	0.42	3
P45880	C227	VDAC2	0.95	0.42	3
Q53GQ0	C166	HSD17B12	0.95	0.82	3
Q52LJ0	C216	FAM98B	0.95	0.26	3
Q08J23	C93	NSUN2	0.95	0.24	3
Q06830	C83	PRDX1	0.95	0.15	3
Q9H8M7	C27	FAM188A	0.95	0.13	3

Q9NRZ9	C169	HELLS	0.95	0.06	2
Q8TB03	C12	CXorf38	0.95	0.19	2
Q9UBL3	C581	ASH2L	0.95	0.34	2
Q14247	C112	CTTN	0.95	0.40	2
O00541	C391	PES1	0.95	0.26	2
Q96SB4	C356	SRPK1	0.95	0.33	2
O95487	C87	SEC24B	0.95	0.09	2
Q9Y230	C227	RUVBL2	0.95	0.23	2
Q13242	C138	SRSF9	0.95	0.05	2
P63220	C56	RPS21	0.94	0.40	4
P37268	C374	FDFT1	0.94	0.20	4
P23396	C97	RPS3	0.94	0.22	4
P15880	C229	RPS2	0.94	0.26	4
O43390	C99	HNRNPR	0.94	0.36	4
P84085	C62	ARF5	0.94	0.27	4
O60506	C96	SYNCRIP	0.94	0.36	4
Q9BWJ5	C76	SF3B5	0.94	0.40	3
Q9Y5S9	C149	RBM8A	0.94	0.35	3
Q9Y570	C238	PPME1	0.94	0.18	3
Q5XKP0	C60	QIL1	0.94	0.22	3
Q96F63	C78	CCDC97	0.94	0.01	2
Q9HAD4	C131	WDR41	0.94	0.02	2
Q9UPT9	C494	USP22	0.94	0.19	2
Q9H840	C121	GEMIN7	0.94	0.09	2
Q15437	C767	SEC23B	0.94	0.14	2
Q8WWH5	C331	TRUB1	0.94	0.01	2
Q6YN16	C218	HSDL2	0.93	0.15	4
P78371	C395	CCT2	0.93	0.22	4
P28838	C462	LAP3	0.93	0.16	4
P49419	C478	ALDH7A1	0.93	0.19	3
P30153	C390	PPP2R1A	0.93	0.21	3
Q92796	C519	DLG3	0.93	0.32	3
O00244	C41	ATOX1	0.93	0.17	2
Q7Z6Z7	C3239	HUWE1	0.93	0.75	2
Q9H2U1	C135	DHX36	0.93	0.04	2
O75935	C140	DCTN3	0.93	0.07	2
Q14137	C404	BOP1	0.92	0.26	4
Q7L2H7	C134	EIF3M	0.92	0.20	4
P30048	C229	PRDX3	0.92	0.13	4
P46776	C70	RPL27A	0.92	0.27	4
A1KXE4	C63	FAM168B	0.92	0.06	4

P22314	C1039	UBA1	0.92	0.21	3
P22314	C1040	UBA1	0.92	0.21	3
Q9ULV4	C456	CORO1C	0.92	0.41	3
O00148	C164	DDX39A	0.92	0.31	3
Q9H3P7	C129	ACBD3	0.92	0.12	3
P22087	C99	FBL	0.92	9.54	2
Q8NFF5	C236	FLAD1	0.92	0.23	2
Q9UJX4	C86	ANAPC5	0.92	0.30	2
O75348	C69	ATP6V1G1	0.92	0.10	2
Q6DKI1	C184	RPL7L1	0.92	0.16	2
Q9NVN8	C278	GNL3L	0.92	0.16	2
Q9BRX5	C188	GINS3	0.92	0.02	2
Q9H832	C100	UBE2Z	0.92	0.01	2
Q7RTV0	C11	PHF5A	0.92	0.10	2
O14950	C109	MYL12B	0.91	0.30	4
Q9Y295	C243	DRG1	0.91	0.21	3
Q9BRR6	C40	ADPGK	0.91	0.02	3
F8VZW7	C74	Uncharacteriz	0.91	0.31	3
F8VZW7	C77	Uncharacteriz	0.91	0.31	3
P22307	C71	SCP2	0.91	0.35	3
P55263	C353	ADK	0.91	0.27	3
Q00839	C648	HNRNPU	0.91	0.28	3
P08238	C366	HSP90AB1	0.91	0.16	3
Q9Y5J1	C90	UTP18	0.91	0.14	3
Q9NXF7	C173	DCAF16	0.91	0.12	2
Q00839	C497	HNRNPU	0.91	0.34	2
Q96AT9	C23	RPE	0.91	0.29	2
P49915	C523	GMPS	0.91	0.05	2
P49753	C401	ACOT2	0.91	0.06	2
Q12824	C350	SMARCB1	0.91	0.37	2
P53004	C204	BLVRA	0.9	0.29	4
Q8N1F7	C522	NUP93	0.9	8.99	3
Q00013	C242	MPP1	0.9	0.17	3
Q99496	C72	RNF2	0.9	0.24	3
P62316	C46	SNRPD2	0.9	0.78	3
P28838	C335	LAP3	0.9	0.20	3
Q96EY4	C162	TMA16	0.9	0.29	3
P41240	C290	CSK	0.9	0.10	3
Q7L5Y9	C195	MAEA	0.9	0.16	3
P21266	C39	GSTM3	0.9	0.09	3
Q9Y4W2	C306	LAS1L	0.9	0.21	2

Q99538	C219	LGMN	0.9	0.06	2
Q9UNS2	C383	COPS3	0.9	0.14	2
O95571	C170	ETHE1	0.9	0.11	2
O95881	C66	TXNDC12	0.9	0.22	2
Q53EL6	C150	PDCD4	0.89	0.32	4
Q92878	C1302	RAD50	0.89	0.30	4
Q9Y5A9	C482	YTHDF2	0.89	0.05	3
P60604	C89	UBE2G2	0.89	0.22	3
P40337	C77	VHL	0.89	0.11	3
P61978	C184	HNRNPK	0.89	0.35	3
P61978	C185	HNRNPK	0.89	0.35	3
P52597	C290	HNRNPF	0.89	0.14	3
P35998	C377	PSMC2	0.89	0.24	3
Q6P1J9	C145	CDC73	0.89	0.11	3
Q9BSD7	C110	NTPCR	0.89	0.28	2
P62826	C85	RAN	0.89	1.48	2
Q9BRP1	C100	PDCD2L	0.89	0.07	2
Q96I15	C22	SCLY	0.89	0.19	2
P61247	C111	RPS3A	0.89	0.24	2
Q9BQ69	C186	MACROD1	0.89	0.27	2
Q14566	C301	MCM6	0.88	0.29	4
P51610	C1187	HCFC1	0.88	1.18	4
O75153	C1196	KIAA0664	0.88	0.29	4
P36578	C96	RPL4	0.88	8.13	4
Q7L2E3	C346	DHX30	0.88	0.27	3
P24752	C142	ACAT1	0.88	0.39	3
P41214	C489	EIF2D	0.88	0.10	2
O15155	C28	BET1	0.88	0.04	2
P49189	C267	ALDH9A1	0.88	0.25	2
P17812	C218	CTPS1	0.88	0.26	2
P48739	C94	PITPNB	0.88	0.32	2
Q96DT6	C107	ATG4C	0.88	0.32	2
Q96DT6	C111	ATG4C	0.88	0.32	2
Q92598	C34	HSPH1	0.88	0.01	2
P15311	C117	EZR	0.88	1.29	2
P10599	C62	TXN	0.87	0.34	3
P10599	C69	TXN	0.87	0.34	3
P62266	C90	RPS23	0.87	0.23	3
Q13418	C346	ILK	0.87	0.18	3
O00273	C38	DFFA	0.87	0.04	2
Q9UFC0	C249	LRWD1	0.87	9.57	2

P22314	C234	UBA1	0.87	0.87	2
O60701	C276	UGDH	0.86	0.19	4
Q9Y3T9	C585	NOC2L	0.86	0.26	4
P46776	C144	RPL27A	0.86	0.30	4
P50914	C42	RPL14	0.86	0.84	4
P41250	C466	GARS	0.86	0.24	3
P41250	C471	GARS	0.86	0.24	3
Q15459	C244	SF3A1	0.86	0.15	3
P50395	C202	GDI2	0.86	0.67	2
Q96T76	C747	MMS19	0.86	0.09	2
Q96T76	C750	MMS19	0.86	0.09	2
Q8N6M0	C172	OTUD6B	0.86	9.57	2
Q96JM7	C169	L3MBTL3	0.86	0.04	2
Q13363	C134	CTBP1	0.86	0.16	2
O15379	C94	HDAC3	0.86	0.04	2
O14497	C336	ARID1A	0.86	0.08	2
Q9Y512	C457	SAMM50	0.86	0.34	2
Q9NR30	C682	DDX21	0.86	0.28	2
Q9P2T1	C348	GMPR2	0.85	0.91	4
Q96FZ5	C12	CMTM7	0.85	8.23	4
P38606	C138	ATP6V1A	0.85	1.27	4
P09211	C48	GSTP1	0.85	0.24	4
P08670	C328	VIM	0.85	0.24	4
Q9UNF1	C516	MAGED2	0.85	0.22	3
Q9Y3D0	C158	FAM96B	0.85	0.16	3
P33991	C605	MCM4	0.85	0.35	3
Q15418	C432	RPS6KA1	0.85	0.18	3
Q07866	C114	KLC1	0.85	0.78	2
Q96B54	C114	ZNF428	0.85	0.06	2
Q96B54	C115	ZNF428	0.85	0.06	2
Q14683	C987	SMC1A	0.85	0.15	2
P67775	C20	PPP2CA	0.85	0.81	2
E7EVH7	C286	KLC1	0.85	0.78	2
P33240	C150	CSTF2	0.84	0.11	3
P51610	C227	HCFC1	0.84	0.08	3
O15235	C64	MRPS12	0.84	0.17	3
Q9Y312	C370	AAR2	0.84	0.02	3
P52272	C114	HNRNPM	0.84	0.17	2
Q6P1X6	C98	C8orf82	0.84	0.02	2
P45985	C379	MAP2K4	0.84	1.82	2
Q14690	C361	PDCD11	0.84	0.04	2

Q9HB71	C173	CACYBP	0.84	0.12	2
Q9H1K1	C69	ISCU	0.84	0.02	2
P27816	C635	MAP4	0.84	1.85	2
Q96IZ0	C173	PAWR	0.84	0.85	2
Q9H0C8	C325	ILKAP	0.83	0.21	4
Q9GZR2	C382	REXO4	0.83	0.15	4
P62280	C116	RPS11	0.83	0.19	4
Q96AB3	C114	ISOC2	0.83	0.21	3
Q9UJU6	C127	DBNL	0.83	0.10	3
Q05639	C111	EEF1A2	0.83	0.81	3
O75521	C380	ECI2	0.83	0.24	3
P68104	C111	EEF1A1	0.83	0.81	3
Q9HCC0	C216	MCCC2	0.83	0.21	3
P55884	C420	EIF3B	0.83	0.33	3
H3BN98	C196	Uncharacteriz	0.83	0.35	2
P62633	C171	CNBP	0.83	0.26	2
Q99536	C86	VAT1	0.83	0.79	2
Q8IXH7	C195	TH1L	0.83	0.08	2
P62244	C30	RPS15A	0.83	0.35	2
O43310	C556	CTIF	0.83	0.04	2
Q7L2E3	C1183	DHX30	0.82	0.16	3
P14868	C203	DARS	0.82	0.22	3
O95630	C264	STAMBP	0.82	0.26	2
Q9UNE7	C232	STUB1	0.82	0.13	2
P17812	C491	CTPS1	0.82	0.03	2
P53041	C11	PPP5C	0.82	0.06	2
P51649	C340	ALDH5A1	0.81	0.21	4
Q9UHB9	C525	SRP68	0.81	9.04	3
P49207	C83	RPL34	0.81	0.27	3
Q6YN16	C166	HSDL2	0.81	0.14	2
Q8WVV9	C405	HNRPLL	0.81	0.71	2
Q68D10	C535	SPTY2D1	0.81	0.11	2
P00519	C1100	ABL1	0.81	0.15	2
P14866	C452	HNRNPL	0.81	0.71	2
Q14980	C160	NUMA1	0.81	0.14	2
P49757	C611	NUMB	0.81	0.04	2
P78347	C215	GTF2I	0.8	0.21	4
P26599	C250	PTBP1	0.8	0.35	4
P26599	C251	PTBP1	0.8	0.35	4
O75446	C184	SAP30	0.8	0.15	4
P13639	C728	EEF2	0.8	0.87	3

Q9NXH9	C639	TRMT1	0.8	0.15	3
Q3SXM5	C265	HSDL1	0.8	0.59	2
P25789	C74	PSMA4	0.8	0.77	2
P31930	C453	UQCRC1	0.8	0.02	2
Q9BYB4	C109	GNB1L	0.8	0.08	2
O00116	C226	AGPS	0.8	0.02	2
P24752	C126	ACAT1	0.8	0.06	2
P36578	C250	RPL4	0.8	0.32	2
Q7Z6Z7	C4341	HUWE1	0.79	0.19	3
P47756	C147	CAPZB	0.79	0.22	3
Q06587	C332	RING1	0.79	0.59	2
Q15022	C325	SUZ12	0.79	0.12	2
O75821	C169	EIF3G	0.79	0.26	2
P55210	C290	CASP7	0.79	0.07	2
P09001	C338	MRPL3	0.78	0.17	3
P30086	C168	PEBP1	0.78	0.95	3
Q14103	C226	HNRNPD	0.78	0.89	2
Q16181	C126	7-Sep	0.78	1.57	2
P13639	C369	EEF2	0.78	0.67	2
O00567	C211	NOP56	0.78	0.10	2
Q32NC0	C175	C18orf21	0.78	0.04	2
P54886	C612	ALDH18A1	0.78	0.31	2
P52789	C794	HK2	0.77	0.21	4
Q96C19	C53	EFHD2	0.77	1.00	3
Q6P1L8	C90	MRPL14	0.77	0.17	3
Q09028	C138	RBBP4	0.77	0.08	2
Q96DM3	C333	C18orf8	0.77	0.11	2
Q15024	C34	EXOSC7	0.77	0.66	2
Q15050	C52	RRS1	0.77	0.18	2
P83916	C156	CBX1	0.77	1.21	2
P62280	C60	RPS11	0.76	0.14	4
P54886	C88	ALDH18A1	0.76	0.19	4
P61158	C12	ACTR3	0.76	0.07	3
Q9H9A6	C23	LRRC40	0.76	9.00	3
P13995	C166	MTHFD2	0.76	0.12	3
Q15024	C238	EXOSC7	0.76	0.18	3
Q13619	C633	CUL4A	0.76	0.82	3
P55084	C458	HADHB	0.76	0.15	3
Q13620	C787	CUL4B	0.76	0.82	3
O75439	C265	PMPCB	0.76	0.12	2
Q9P0J1	C149	PDP1	0.76	0.12	2

Q9P0J1	C151	PDP1	0.76	0.12	2
P61163	C222	ACTR1A	0.76	0.07	2
Q9ULC4	C14	MCTS1	0.76	0.23	2
Q16763	C95	UBE2S	0.76	0.73	2
Q8IXW5	C358	RPAP2	0.76	0.74	2
P46782	C66	RPS5	0.75	0.22	4
P04406	C247	GAPDH	0.75	2.36	4
P24752	C413	ACAT1	0.75	0.09	4
P33993	C482	MCM7	0.75	0.15	3
Q9BXW7	C392	CECR5	0.75	0.07	2
Q15417	C59	CNN3	0.75	0.74	2
P08107	C306	HSPA1B	0.75	1.62	2
Q14160	C1612	SCRIB	0.75	0.69	2
P24752	C119	ACAT1	0.74	0.13	4
P36542	C103	ATP5C1	0.74	0.19	3
Q8N6Q8	C96	METTL25	0.74	0.06	2
P51812	C436	RPS6KA3	0.74	0.61	2
Q9Y3C7	C93	MED31	0.74	0.08	2
P24752	C196	ACAT1	0.74	0.15	2
Q9H307	C249	PNN	0.74	0.69	2
P61927	C19	RPL37	0.74	0.27	2
P42765	C92	ACAA2	0.73	0.07	4
O43175	C295	PHGDH	0.73	0.19	4
Q9NRF9	C51	POLE3	0.73	0.13	3
Q9HAV7	C124	GRPEL1	0.73	0.16	3
Q92879	C150	CELF1	0.73	0.14	3
P27816	C1098	MAP4	0.73	5.41	3
P31153	C104	MAT2A	0.73	0.09	2
Q6PJG6	C326	BRAT1	0.73	0.02	2
P46734	C227	MAP2K3	0.73	0.30	2
Q9ULW3	C37	ABT1	0.72	0.60	3
P36507	C211	MAP2K2	0.72	0.27	3
Q02750	C207	MAP2K1	0.72	0.27	3
P37802	C63	TAGLN2	0.72	0.70	3
Q1KMD3	C57	HNRNPUL2	0.72	1.44	3
H3BQZ7	C57	Uncharacteriz	0.72	1.44	3
O76003	C229	GLRX3	0.72	0.73	3
P62308	C45	SNRPG	0.72	0.86	2
O00299	C191	CLIC1	0.72	0.66	2
P30044	C100	PRDX5	0.71	0.24	4
P62913	C21	RPL11	0.71	0.33	4

P62913	C25	RPL11	0.71	0.33	4
P62701	C41	RPS4X	0.71	0.22	3
Q9Y3D0	C93	FAM96B	0.71	0.13	3
P23588	C457	EIF4B	0.71	0.77	2
P61218	C76	POLR2F	0.71	0.21	2
O43823	C631	AKAP8	0.71	1.32	2
P47756	C206	CAPZB	0.71	0.78	2
P52272	C653	HNRNPM	0.7	0.21	4
P14618	C423	PKM	0.7	9.03	3
P14618	C424	PKM	0.7	9.03	3
P50914	C54	RPL14	0.7	0.57	3
P13489	C95	RNH1	0.7	0.20	2
P13489	C96	RNH1	0.7	0.20	2
P11142	C603	HSPA8	0.7	0.07	2
O75643	C1580	SNRNP200	0.7	0.05	2
Q14697	C502	GANAB	0.7	0.07	2
Q12931	C573	TRAP1	0.69	0.13	3
P24468	C326	NR2F2	0.69	0.12	2
P32969	C134	RPL9P9	0.69	1.25	2
Q9NR50	C334	EIF2B3	0.69	0.09	2
Q9UKS6	C421	PACSIN3	0.69	0.20	2
P62333	C193	PSMC6	0.69	0.12	2
O96017	C539	CHEK2	0.69	0.13	2
Q86SX6	C67	GLRX5	0.68	0.13	4
Q99576	C112	TSC22D3	0.68	0.69	4
P61513	C39	RPL37A	0.68	0.28	3
P61513	C42	RPL37A	0.68	0.28	3
P12004	C135	PCNA	0.68	0.96	3
P63244	C286	GNB2L1	0.68	0.85	3
Q06330	C313	RBPJ	0.68	0.73	3
P46109	C249	CRKL	0.68	0.69	3
P78549	C118	NTHL1	0.68	0.01	2
Q8TEX9	C708	IPO4	0.68	0.05	2
Q6IS14	C73	EIF5AL1	0.68	1.03	2
Q9GZV4	C73	EIF5A2	0.68	1.03	2
O60671	C239	RAD1	0.68	0.05	2
O95571	C34	ETHE1	0.68	0.27	2
P62280	C131	RPS11	0.67	0.25	4
P62753	C12	RPS6	0.67	0.18	4
Q99714	C214	HSD17B10	0.67	0.16	4
P48735	C308	IDH2	0.67	0.11	4

Q15366	C158	PCBP2	0.67	0.27	3
P35219	C200	CA8	0.67	0.88	3
O75419	C267	CDC45	0.67	0.54	2
P23396	C134	RPS3	0.67	1.01	2
Q9Y277	C36	VDAC3	0.67	0.05	2
P09884	C141	POLA1	0.67	0.90	2
Q96HE7	C166	ERO1L	0.66	0.86	4
P61106	C40	RAB14	0.66	0.63	4
P18669	C153	PGAM1	0.66	5.87	3
O95563	C54	MPC2	0.66	0.12	3
Q15020	C670	SART3	0.66	0.73	3
Q9UHD1	C86	CHORDC1	0.66	0.19	2
Q02252	C317	ALDH6A1	0.66	0.10	2
P78371	C289	CCT2	0.66	0.75	2
P51148	C64	RAB5C	0.66	0.62	2
Q9BSC4	C16	NOL10	0.66	0.11	2
P49756	C83	RBM25	0.66	0.17	2
P60228	C141	EIF3E	0.66	0.77	2
O00483	C44	NDUFA4	0.65	0.23	4
P30084	C62	ECHS1	0.65	0.16	3
Q6UB35	C961	MTHFD1L	0.65	0.01	2
Q9H0U9	C160	TSPYL1	0.65	0.59	2
P41227	C194	NAA10	0.65	0.64	2
P30050	C17	RPL12	0.64	0.94	4
P19367	C834	HK1	0.64	0.13	4
P63244	C249	GNB2L1	0.64	0.67	4
Q9BQP7	C79	C20orf72	0.64	0.09	3
P43487	C99	RANBP1	0.64	0.73	3
P62241	C182	RPS8	0.64	0.21	3
P17987	C397	TCP1	0.64	0.50	3
P46777	C100	RPL5	0.64	1.01	3
P09651	C43	HNRNPA1	0.64	1.11	2
Q08J23	C321	NSUN2	0.64	0.00	2
Q32P51	C43	HNRNPA1L2	0.64	1.11	2
Q99832	C158	CCT7	0.63	0.57	4
Q96EY8	C132	MMAB	0.63	0.16	4
P25789	C163	PSMA4	0.63	0.64	4
P63244	C207	GNB2L1	0.63	0.77	4
P10809	C442	HSPD1	0.63	0.06	4
Q9NY27	C22	PPP4R2	0.63	0.68	4
Q15424	C225	SAFB	0.63	0.51	3

P60763	C157	RAC3	0.63	0.58	3
P63000	C157	RAC1	0.63	0.58	3
Q14151	C224	SAFB2	0.63	0.51	3
P39687	C87	ANP32A	0.63	0.83	3
O60763	C678	USO1	0.63	0.15	2
P31948	C461	STIP1	0.63	0.05	2
O95983	C215	MBD3	0.63	0.55	2
P51149	C143	RAB7A	0.63	9.69	2
P55795	C290	HNRNPH2	0.63	0.52	2
Q9NUJ3	C495	TCP11L1	0.63	0.07	2
P21266	C208	GSTM3	0.63	0.12	2
P63104	C94	YWHAZ	0.62	1.32	4
P50995	C384	ANXA11	0.62	1.04	3
Q86YH6	C71	PDSS2	0.62	0.12	3
P60709	C285	ACTB	0.62	1.15	2
Q8IYS1	C14	PM20D2	0.62	0.58	2
P04075	C178	ALDOA	0.62	1.30	2
Q96FW1	C91	OTUB1	0.62	0.47	2
Q15185	C40	PTGES3	0.61	0.69	4
O00299	C223	CLIC1	0.61	0.74	4
P08107	C603	HSPA1B	0.61	0.87	4
P61163	C34	ACTR1A	0.61	0.50	3
P09104	C119	ENO2	0.61	0.99	3
P30042	C177	C21orf33	0.61	0.14	3
P62304	C46	SNRPE	0.61	0.69	3
P06733	C119	ENO1	0.61	0.99	3
P36969	C134	GPX4	0.61	0.51	3
P42025	C34	ACTR1B	0.61	0.50	3
H7C455	C156	Uncharacteriz	0.61	0.14	3
P13929	C119	ENO3	0.61	0.99	3
P45880	C103	VDAC2	0.61	0.01	2
P00491	C31	PNP	0.61	0.63	2
Q9H773	C162	DCTPP1	0.6	0.87	4
P07737	C128	PFN1	0.6	0.79	4
P35637	C428	FUS	0.6	0.12	3
P07195	C36	LDHB	0.6	0.94	3
P52565	C79	ARHGDIA	0.6	0.97	3
Q99460	C898	PSMD1	0.6	0.08	2
Q00013	C454	MPP1	0.6	0.03	2
Q9Y277	C229	VDAC3	0.6	1.04	2
P14618	C49	PKM	0.59	0.63	4

P46734	C207	MAP2K3	0.59	0.18	4
Q04760	C139	GLO1	0.59	0.78	4
P52564	C196	MAP2K6	0.59	0.18	4
P62937	C161	PPIA	0.59	1.00	4
P23919	C31	DTYMK	0.59	9.12	3
O00154	C288	ACOT7	0.59	0.57	3
P09936	C220	UCHL1	0.59	1.00	3
Q96CP2	C132	FLYWCH2	0.59	0.78	3
P09234	C25	SNRPC	0.59	0.58	2
P61758	C8	VBP1	0.59	0.62	2
P52564	C216	MAP2K6	0.59	0.06	2
P14174	C81	MIF	0.58	0.75	4
P62826	C112	RAN	0.58	0.75	4
P62826	C120	RAN	0.58	0.75	4
P61970	C114	NUTF2	0.58	0.73	4
Q00325	C237	SLC25A3	0.58	0.26	3
Q9H9P8	C376	L2HGDH	0.58	0.04	2
Q12959	C378	DLG1	0.58	0.22	2
Q08J23	C673	NSUN2	0.58	0.49	2
Q08J23	C678	NSUN2	0.58	0.49	2
O60568	C494	PLOD3	0.58	0.09	2
P46782	C172	RPS5	0.57	0.72	4
Q8TAQ2	C145	SMARCC2	0.57	0.76	4
P62937	C62	PPIA	0.57	0.95	4
P46063	C606	RECQL	0.57	0.47	2
P46782	C155	RPS5	0.56	0.73	4
P27348	C94	YWHAQ	0.56	1.12	4
Q2NL82	C126	TSR1	0.56	0.88	4
P10809	C237	HSPD1	0.56	0.13	4
A6NHG4	C24	DDTL	0.56	1.51	3
P13639	C693	EEF2	0.56	0.74	3
P30046	C24	DDT	0.56	1.51	3
P27816	C535	MAP4	0.56	1.27	3
P62140	C126	PPP1CB	0.56	0.22	2
P36873	C127	PPP1CC	0.56	0.22	2
P62136	C127	PPP1CA	0.56	0.22	2
P04075	C202	ALDOA	0.56	0.49	2
Q9H1E5	C326	TMX4	0.56	0.15	2
P28288	C477	ABCD3	0.56	0.46	2
Q9NZZ3	C20	CHMP5	0.55	0.77	4
H0Y2S0	C31	Uncharacteriz	0.55	0.10	4

Q9H910	C118	HN1L	0.55	0.62	4
Q6UB35	C906	MTHFD1L	0.55	0.10	4
P00390	C102	GSR	0.55	0.09	4
Q15365	C158	PCBP1	0.55	0.20	3
P60709	C217	ACTB	0.55	0.68	3
Q9UHX1	C129	PUF60	0.55	0.64	3
Q6S8J3	C917	POTEE	0.55	0.68	3
Q5U5X0	C97	LYRM7	0.55	0.04	2
Q9NYK5	C335	MRPL39	0.55	0.21	2
Q96C19	C172	EFHD2	0.54	1.28	4
P07203	C202	GPX1	0.54	0.63	4
P62937	C115	PPIA	0.54	0.99	4
P61978	C145	HNRNPK	0.54	0.56	3
P08107	C17	HSPA1B	0.54	0.92	3
P49458	C39	SRP9	0.54	0.74	2
P55795	C34	HNRNPH2	0.54	0.57	2
P61247	C139	RPS3A	0.54	0.56	2
Q12874	C274	SF3A3	0.54	0.47	2
P31943	C34	HNRNPH1	0.54	0.57	2
Q9UBF6	C61	RNF7	0.54	0.09	2
P60174	C79	TPI1	0.53	1.17	4
P32969	C74	RPL9P9	0.53	0.78	4
P62241	C71	RPS8	0.53	0.16	4
P62241	C72	RPS8	0.53	0.16	4
P82912	C112	MRPS11	0.53	0.08	2
P22087	C268	FBL	0.53	0.02	2
P23396	C119	RPS3	0.53	0.91	2
Q8NBZ0	C179	INO80E	0.53	0.03	2
P22626	C50	HNRNPA2B1	0.53	1.06	2
P08238	C521	HSP90AB1	0.52	1.35	4
P20290	C22	BTF3	0.52	1.21	4
Q9UHD8	C248	9-Sep	0.52	0.53	3
Q9UKK9	C76	NUDT5	0.52	0.57	3
Q12849	C476	GRSF1	0.52	0.18	3
P24534	C50	EEF1B2	0.52	1.11	3
O75663	C75	TIPRL	0.52	0.51	3
P63167	C24	DYNLL1	0.52	1.05	3
P30084	C213	ECHS1	0.52	0.17	2
P30084	C225	ECHS1	0.52	0.17	2
P62241	C100	RPS8	0.51	0.26	4
P84077	C159	ARF1	0.51	0.59	3

O75531	C85	BANF1	0.51	0.83	3
Q9Y2H1	C235	STK38L	0.51	0.44	2
Q15208	C234	STK38	0.51	0.44	2
P08047	C68	SP1	0.5	0.52	4
P45985	C246	MAP2K4	0.5	0.22	4
P08621	C39	SNRNP70	0.5	1.26	3
Q15181	C113	PPA1	0.5	0.41	3
Q15181	C114	PPA1	0.5	0.41	3
Q9UMS4	C298	PRPF19	0.5	0.93	2
P60174	C255	TPI1	0.49	0.92	4
Q16881	C209	TXNRD1	0.49	0.06	2
H0YBQ0	C258	TXNRD3	0.49	0.06	2
Q9NNW7	C86	TXNRD2	0.49	0.06	2
P41252	C526	IARS	0.49	0.15	2
P62913	C72	RPL11	0.49	1.11	2
P17987	C147	TCP1	0.48	0.71	4
Q8TEX9	C42	IPO4	0.48	0.49	3
P14618	C474	PKM	0.48	0.73	3
O00267	C626	SUPT5H	0.48	0.57	2
Q9BVP2	C234	GNL3	0.48	0.04	2
P21964	C119	COMT	0.47	0.19	2
P55809	C67	OXCT1	0.47	0.38	2
P19367	C813	HK1	0.47	0.11	2
P07355	C133	ANXA2	0.47	0.45	2
Q8WUY1	C104	THEM6	0.47	0.47	2
P30044	C204	PRDX5	0.46	0.63	4
Q96CX2	C50	KCTD12	0.46	1.01	4
Q9BQG0	C1031	MYBBP1A	0.46	9.19	3
Q9BTT0	C87	ANP32E	0.46	0.59	3
Q9BRT3	C30	MIEN1	0.46	0.81	3
Q9BRT3	C33	MIEN1	0.46	0.81	3
P31350	C317	RRM2	0.46	0.78	3
P61160	C221	ACTR2	0.46	0.10	2
P40926	C212	MDH2	0.45	0.58	4
P0CW22	C35	RPS17L	0.45	0.71	4
P00558	C316	PGK1	0.45	0.73	4
P18754	C352	RCC1	0.45	0.66	3
P51858	C108	HDGF	0.44	1.07	4
Q9NUU7	C392	DDX19A	0.44	0.71	3
P62263	C85	RPS14	0.44	0.54	3
P49588	C947	AARS	0.44	0.46	3

P25398	C50	RPS12	0.44	0.55	3
P25398	C56	RPS12	0.44	0.55	3
Q9UMR2	C393	DDX19B	0.44	0.71	3
P60174	C164	TPI1	0.43	0.92	4
Q9HCC0	C431	MCCC2	0.43	0.03	2
P08758	C316	ANXA5	0.42	1.69	4
P60891	C91	PRPS1	0.42	0.56	3
P21108	C91	PRPS1L1	0.42	0.56	3
P11908	C91	PRPS2	0.42	0.56	3
P00558	C50	PGK1	0.42	1.20	3
P23528	C39	CFL1	0.41	1.00	4
Q96AG4	C48	LRRC59	0.41	0.07	3
P02545	C522	LMNA	0.41	0.16	2
Q8WUZ0	C211	BCL7C	0.41	0.52	2
O43242	C210	PSMD3	0.4	0.75	2
P62857	C27	RPS28	0.4	1.59	2
Q02543	C22	RPL18A	0.39	0.93	3
P36578	C208	RPL4	0.39	0.60	3
P62714	C266	PPP2CB	0.39	0.44	2
Q96S66	C550	CLCC1	0.39	0.37	2
P67775	C266	PPP2CA	0.39	0.44	2
P25398	C69	RPS12	0.38	0.55	4
P62249	C25	RPS16	0.38	0.85	2
P62241	C174	RPS8	0.37	0.12	3
Q92747	C279	ARPC1A	0.37	0.49	3
H0YIN7	C130	Uncharacteriz	0.37	0.78	2
Q9UQ80	C149	PA2G4	0.37	0.78	2
O43175	C281	PHGDH	0.36	0.42	3
P50991	C221	CCT4	0.36	0.06	2
Q15365	C163	PCBP1	0.35	0.42	3
P41250	C616	GARS	0.35	0.68	3
Q9BSD7	C184	NTPCR	0.32	0.34	3
P61158	C235	ACTR3	0.31	0.25	3
P25398	C106	RPS12	0.31	9.85	2
P25398	C108	RPS12	0.31	9.85	2
P49368	C455	CCT3	0.3	9.21	3
P49591	C300	SARS	0.24	0.30	3
P10768	C176	ESD	0.23	0.64	2
P10768	C181	ESD	0.23	0.64	2
O43502	C355	RAD51C	0.23	0.78	2
P60174	C104	TPI1	0.22	1.21	4

Q8WXI9	C308	GATAD2B	0.22	0.39	3
P49006	C134	MARCKSL1	0.21	2.06	4
P04637	C124	TP53	0.2	0.22	3
Q13263	C83	TRIM28	0.19	0.21	2
Q13263	C88	TRIM28	0.19	0.21	2
Q13263	C91	TRIM28	0.19	0.21	2
Q13263	C117	TRIM28	0.19	0.21	2
P23919	C163	DTYMK	0.15	0.27	3
Q9Y314	C185	NOSIP	0.15	0.04	2

Appendix III

ICP-MS Manager Guide for Liquid and Laser Samples

Our laser ICP
Helped us map biology
From the sets of metal data
It recorded.

And when it was good
it was very, very good
And when it was bad
it was horrid.

Index

Quick Guide for Starting and Finishing Liquid Samples

1. Check the argon level, chiller, and vacuum. Change tanks if needed.
2. If the instrument is not in liquid mode, change to liquid mode.
    a. Change the cones to the High Matrix cones (both skimmer and samples).
    b. Unhook the laser sample-introduction system.
    c. Change the injector from the gas injector to the liquid injector.
        i. DO NOT let the glass of the torch or the injector touch the counter!
    d. Hook up the nebulizer, spray chamber, and sample introduction tubing.
        i. Make sure the outlet tubing and inlet tubing are threaded in opposite directions!
3. Check the autosampler waste line, and set up the sample waste beaker.
4. Place the inlet line into the Tune B solution.
5. Turn on the instrument in the Instrument Control software.
    a. Keep your hand on the door latch so you can quickly twist it if a fireball forms!
6. Set the Configuration to “Installer with ASX 520” to run with the autosampler or “Manual sampling” to run manual samples.
7. Set the mode to “STD.”
8. Press “Run,” and warm up the instrument for 10 minutes, monitoring the ion counts in Data Display.
9. Run the Autotune sequence “SourceTune High Matrix” from the Tune B solution.
10. Run the Performance Report.
11. Change the mode to “KED” and check that the 10 ppm phosphorous standard is 100,000-150,000 cps.
12. For manual samples, you’re ready to go. Run your samples.
13. For autosampler samples, set up the autosampler.
    a. Hook up the autosampler line.
    b. Put the wash line in the rinse acid (2% nitric).
    c. Press “Run” to monitor zinc levels during the washes.
    d. Flush the autosampler line with 10% nitric acid for >2 but <10 minutes.
    e. Flush the autosampler line with the rinse/wash acid for >2 minutes.
    f. Flush the autosampler line with fresh 2% acid in a 50 mL tube for >2 minutes. Keep the autosampler probe in this tube until you are ready to start your samples.
    g. Measure the uptake time with the pump running on High. If it is longer than 1 minute, keep cleaning the line or change the line.
14. To run samples in manual mode, create a Qtegra LabBook using an existing LabBook that was run in manual mode.
15. To run samples in autosampler mode, create a Qtegra LabBook using an existing LabBook that was run in autosampler mode.
16. See “Creating Methods in Qtegra” for more information.

17. To shut the instrument off:
    a. Rinse the line for at least 12 hours with 2% nitric acid using an “Auto cleaning” method. Put the sample intake directly into >300 mL of clean 2% nitric acid, and BE SURE the nitric acid waste beaker is big enough, empty, and covered with aluminum foil.
    b. Set up the shutdown options in Qtegra that you want by selecting the “Options” button in the Scheduler panel and changing “Closedown” to “Closedown on an empty queue or LabBook error” if you want the instrument to turn itself off manually when it finishes rinsing the lines.
    c. You can also turn the instrument off manually by pressing the “Off” button in Instrument Control.
    d. The argon valve should be left open to maintain pressure in the lines.
18. BE SURE to come back within 48 hours to:
    a. Remove the inlet line from the acid bottle. Cap the bottle and move it away from the laser.
    b. Run the peristaltic pump for 5 minutes on high clear the line of nitric acid.
    c. Unscrew the nebulizer from the spray chamber and dry the outside of the nebulizer.
    d. Unhook the tubing from the peristaltic pump.
    e. Empty the waste beaker and store it in the secondary waste container in the cabinet.
19. DO NOT LET ACID SIT NEXT TO THE LASER STAGE for longer that 24-48 hours!!!! The acid will evaporate, corrode the stage and ruin the laser setup!!!!!

Quick Guide for Starting and Finishing Laser Samples

1. Check the argon and helium levels, chiller, and vacuum. Change tanks if needed.
2. Check that the laser base is only touching the table with its feet.
3. If the instrument is not in laser mode, change to laser mode.
    a. Change the cones to the High Sensitivity cones (both skimmer and samples).
    b. Drain the liquid sample-introduction system of excess liquid.
    c. Unhook the liquid sample-introduction system.
    d. Change the injector from the liquid injector to the gas injector.
    e. Hook up the nebulizer gas to the injector.
    f. Hook up the laser sample outlet line to the injector.
    g. Place two tube racks under the plastic tubing to keep the tubing level.
4. Prepare the sample chamber.
    a. Unhook the “EXT INTLK” connection on the back on the laser.
    b. Cap the “EXT INTLK” with the metal cap.
    c. Open the NWR laser software and/or click the “Remote” button to clear the interlock error.
    d. Position the stage so that the sample chamber can be removed (drag the scroll bars down and to the left).
    e. Unscrew the fasteners for the sample chamber and slide the chamber out.
    f. Put your samples in. Be sure the homemade and NIST 612 standards are in the chamber.
    g. Insert the sample chamber gently and secure the screws.
5. Clear oxygen from the Bypass and Online gas lines.
    a. In the NWR software, click the “Bypass” button if it is not already green.
    b. Set the Mass Flow to 800 mL/min for 20 seconds. **Move the Mass Flow Controller window out of the center of the screen**
    c. Go to “Online” mode and override the error that pops up.
    d. Flush in Online mode for 20 seconds.
    e. Set the Mass Flow to 50 mL/min.
    f. Switch back to Bypass mode.
6. Purge the sample chamber.
7. While purging, turn on the iCAP-Q in the Instrument Control software.
    a. Keep your hand on the door latch so you can quickly twist it if a fireball forms!
8. Set the Configuration to “ICAP Q Laser with sync cable.”
9. Set the mode to “Laser-STDS.”
10. Press “Run,” and warm up the instrument for 10 minutes, monitoring the ion counts in Data Display.
11. Warm up the laser.
    a. Set the laser fluence to 7.0 J/cm2 and the firing rate to 20 Hz.
    b. Click the “Fire” button and let the laser run for at least 15 minutes.
12. After the purge, confirm that the laser is in Online mode.

13. Reattach the EXT INTLK cable and restart the laser and gas flow.
    a. Remove the cap and connect the cable.
    b. Override the interlock error by clicking “Remote” on the popup box.
    c. Restart the laser by changing the fluence to 0, pressing fire, pressing fire again to turn it off, changing the fluence back to 7, and pressing fire.
    d. Ramp the Mass Flow to 200 mL/min and then 800 mL/min.
14. Tune the instrument.
    a. Open the “999999-Tune” experiment.
    b. Position the “Tune” line on the NIST 612 standard, in focus, parallel to the scars from previous tunes by using the “Move Scan to Crosshairs,” “Move Scan to Focus” and “Edit Endpoints” functions.
    c. Open the Autotune program “SourceTune Laser” in Instrument Control.
    d. In the NWR software, select the “Tune” pattern and click “Run.”
    e. Check the “Trig In/Sync Out Options” to be sure that “Don’t wait for trigger” is checked under the “Trigger In” tab.
    f. Press “Run”
    g. Let the laser run for 10-15 seconds.
    h. Start the Autotune sequence in Instrument Control by pressing “Next”
15. Set up your samples.
    a. Open an old experiment. Delete all old patterns except “ExtraStds” and “ExtraLine.”
    b. Move the “ExtraStds” pattern to a good starting location and focal plane on Standard G.
    c. Explode “ExtraStds” and position each set of lines for Standards F, E, D, and C in a good position and focal plane.
    d. Use “Merge Line Scans” to merge the standard scans into one scan.
    e. Duplicate the standards to make the same number of standards as samples you plan to run with one extra. Use a Y offset = (line width) x (number of lines per std).
    f. Name your standards “Stds1….StdsN, ExtraStds”
    g. Navigate to your first sample.
    h. Position the “ExtraLine” so that it starts above and off to the left of your first sample and is in focus.
    i. Use “Edit Endpoints” to adjust the endpoint of the line so that it finishes slightly to the right of your samples right edge.
    j. Duplicate the line so that there are enough patterns to cover the entire sample and have one left over. Use a Y offset equal to the line width.
    k. Record the number of patterns used to cover the sample.
    l. Record the Estimated Time for the line.
    m. Merge the patterns used to cover the sample into a single scan and rename it “Sample1.”
    n. Navigate to the next sample, and create patterns for all remaining samples (Sample2….SampleN). ***BE SURE that the Estimated Time for the lines of each sample are at least 2 seconds different from each other.***
    o. Name the leftover line “ExtraLine.”

p. In the Scan Patterns panel, drag the “Sample1” pattern so it is directly below the “Stds1” pattern, and merge them.
q. Merge “StdsX” and “SampleX” for all standards and samples 2 through N.
r. Save the experiment.
s. Click on each “StdsX” and record the Estimated Time.
t. Navigate to the start of “Stds1”
u. Adjust the stage speed in “X” so that the return time from the end of any line to the beginning of the next line is as long as possible without being more than 8 seconds.
v. Calculate the scan times required for each sample using the LA-ICP-MS Time Calculator Google Sheet.
w. Create a LabBook for each sample by building from an existing LabBook run using the settings you want.
x. Schedule the LabBooks for the samples in the Scheduler in the order you want to run the samples.

16. Run your samples.
    a. Check that the Mass Flow is running at 800 mL/min. Leave the window open.
    b. In the NWR software, select all the patterns for the samples you want to run.
    c. Press “Run.”
    d. Check the following settings:
        i. “Selected Patterns Only”
        ii. Trig In/Syn Out Options -> Trigger In -> select “Wait for Trigger”
        iii. “Enable Laser”
        iv. “Log Scan Event Timestamps”
    e. Press “Run” at the bottom of the popup box.
    f. In the Qtegra software, press the green “Play” button on the scheduler.
17. Set up the shutdown options in Qtegra that you want by selecting the “Options” button in the Scheduler panel and changing “Closedown” to “Closedown on an empty queue or LabBook error” if you want the instrument to turn itself off.
18. BE SURE TO COME BACK AS SOON AS POSSIBLE to turn off the helium tank valve. The helium will continue to run (it’s tiny and leaks out of the tubing), and the tank will run to empty if you don’t close the valve.
19. The argon valve should be left open to maintain pressure in the lines.

Complete Guide for Starting and Finishing Liquid Samples

Setting up the instrument

Check that there is sufficient argon and that the chiller and vacuum are working well:

- *Check the pressure and gas level on the argon dewar.* The pressure output should be set to 90-95 psi. The pressure displayed on the Starwatch unit must remain above 95 psi or there will not be enough Cool Gas Flow, and the ICP will shut down. Generally, each percent of argon will last about 1 hour, so if you have >24%, you will be able to use the instrument for about 20 hours (DON'T use the last 5% because the pressure typically drops as you reach the end of the tank!). Change the tank if necessary (***Refer to the section on changing tanks for ICP-MS. There are specific considerations for ICP-MS!!). Open the pressure builder valve if necessary.

- *Check that the chiller and vacuum are running well.* The chiller and vacuum are on the balcony outside. The chiller should read ~20C +/- 1C. Check the vacuum light on the front of the instrument to ensure that the internal vacuum is correct. If anything doesn't look good, note it. If the problem persists, call for tech support.


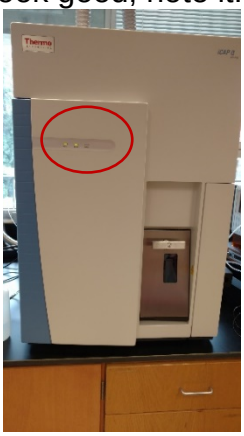

If the instrument has been running in laser mode, change to liquid mode:

- *Change the cones to the High Matrix cones.*
    - Refer to iCAP-Q Operating Manual, pages 8-20 through 8-26. See the section of this guide about changing cones (in the section about setting up the laser) for pictures of how to switch the cones.

    - Be sure the graphene seal is present and not damaged.
    - If you need to clean graphene off of the cone holder, use a plastic or wooden scraper. NEVER touch metal to the cone holders or cones.
    - Be sure the small metal insert in the small cone (skimmer cone) is securely in place.
    - Do not damage the cone tips or overtighten the cones when screwing them in.
    - Check that the cones are clean. This is a visual inspection; if the outside cone looks clean, the inside cone is fine. Also, if you see a significant increase in the random shot noise of the instrument or a gradually increasing Li signal, it is time to clean the cones. To clean the cones, see the section on cone cleaning under Maintenance.

- *Unhook the laser sample-introduction system:*
  - Unhook the metal clamps that hold the glass adapters for the gas introduction lines in place.
  - Place the glass adapter that is connected to the laser itself in the laser stage area, along with its metal clip.

  - Fully remove the tubing for the nebulizer gas introduction by pushing up on the black ring on the valve while pulling down on the tubing.

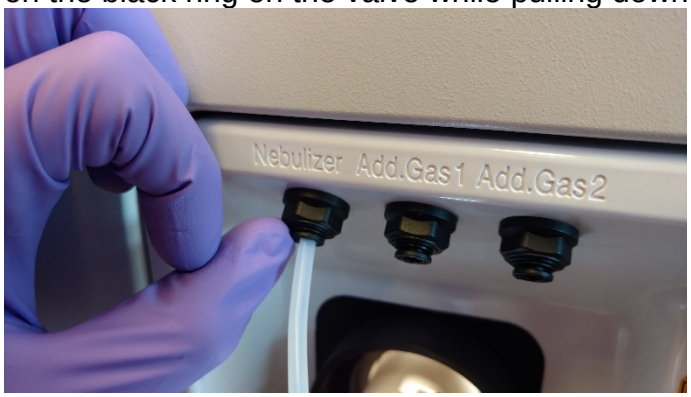

  - Put the tubing in the drawer in the spare parts box, along with its metal clip.

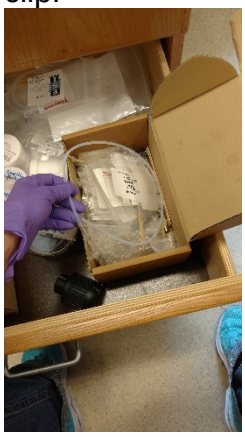

- *Change the injector from the gas injector to the liquid injector.*
    - Refer to the iCAP-Q Operation Manual, pages 8-16 through 8-18. See the instructions in the Setting up Laser ICP-MS section for pictures of how to do this.
    - DO NOT LET THE GLASS OF THE TORCH OR EITHER INEJCETOR TOUCH THE COUNTER; IT CAN CHIP.
    - Visually inspect the injector, torch, nebulizer and spray chamber as you handle them. Brown stains are normal. Cracks are not. If the torch or injector is cracked, order a new one. You can still use a torch or injector that has a line crack, but if the crack causes the glass to separate, do not use it.
    - Before removing the torch from the instrument, get the liquid injector out of its box (in the third drawer, in the cardboard box on the left) and place it plastic-base-down on the bench so that the box that holds the injectors is empty.

    - Press the red knob on the side of the torch housing, and gently twist to the left until the silver knob is able to slide out.
    - Pull out the torch and gas injector (torch = outer glass piece; injector = inner glass piece).
    - Unscrew the gas injector using the white knobs and carefully remove the injector from the torch.
    - Place the torch flat-side-down on the counter. DO NOT let the glass touch the counter; it can chip.
    - Place the gas injector into the empty box, and set it aside.
    - Screw the liquid injector into the torch.
    - Insert the torch+injector back into the instrument so that the silver knob slides in cleanly. Twist it to the right to lock it in place.
    - Place the cover on the injector storage box, and put it back in the drawer.

- *Hook up the nebulizer and sample-introduction tubing.*
    - Open the spray chamber insulator: unscrew the knob on the outer door and open the inner door.
    - Get the spray chamber & its inlet/outlet tubing out of the spare parts box.
    - Feel the tubing to make sure it is smooth & round. Dents cause variation in the sample introduction speed, introducing error into the analysis. Move to another section of the tubing or change the tubing if necessary.
        - Pump inlet tubing catalog number and description: 1320050, “Tubing orange/yellow 12 pieces, PVC-flared end, 3 bridges – 95mm, ID=0,508mm, 0,020inch, L=406mm”
        - Pump outlet tubing catalog number and description: 1320110, “Tubing grey/grey 12 pieces, Santoprene, 3 bridges – 95mm, ID=1,295mm, 0,05inch, L=406mm”
    - Unscrew the inlet tube from the nebulizer, and use the fine silicon-coated wire to check whether the inside of the nebulizer is free of obstructions. If the wire gets stuck on anything (or is hard to move in and out), clean the nebulizer (see the section on nebulizer cleaning.

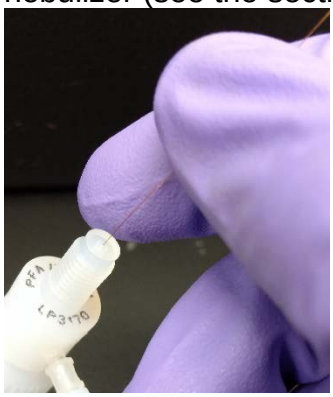
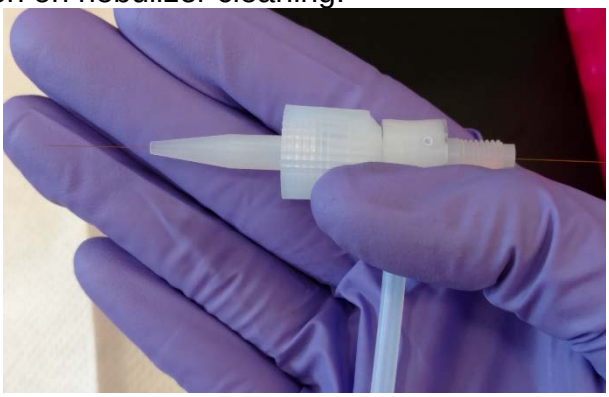

    - Connect the inlet tubing and outlet tubing to the spray chamber by screwing on the adapters.

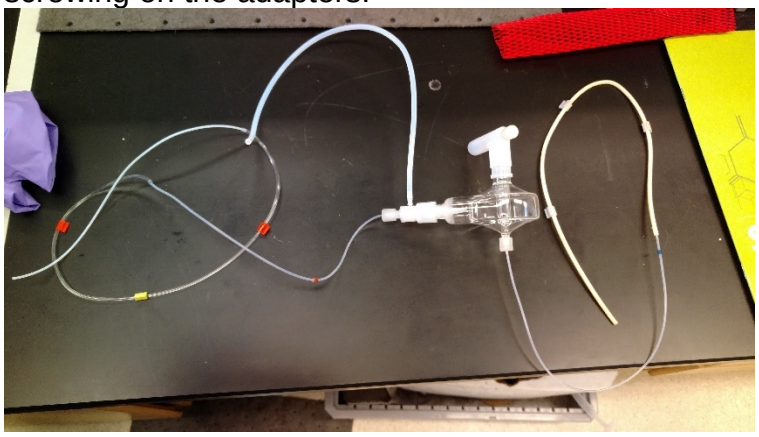

- Applying pressure to the plastic L-shaped head of the spray chamber ONLY (DO NOT push on the spray chamber gass!), insert the plastic head of the spray chamber into the injector until you hear a click. When you stop applying pressure, you will hear another click.

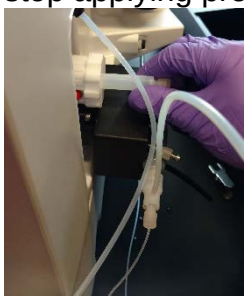

- Connect the nebulizer gas tubing to the Nebulizer Gas outlet by pressing the tubing gently into the black valve.

- Close the spray chamber insulator.

- Connect the outlet tubing to the second tube spot on the peristaltic pump by stretching the tubing around the pump, lowering the grip/lever, and clicking the clamp into place. Be sure the tubing is aligned with the grip/lever so that it is pressed down smoothly underneath the grip/lever and not poking out on either side.

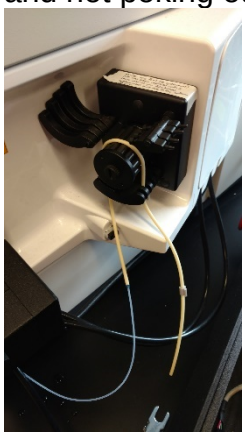
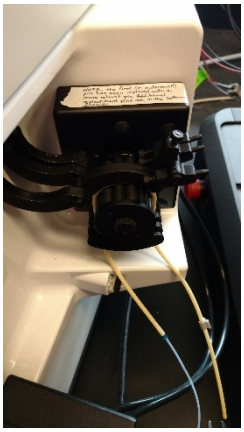

- Do the same for the inlet tubing. TAKE CARE that the inlet tubing is threaded in the opposite direction as the outlet tubing! You want the pump to pump liquid IN to the inlet tubing and OUT of the outlet tubing. Be sure the tubing is aligned with the grip/lever so that it is pressed down smoothly underneath the grip/lever and not poking out on either side.

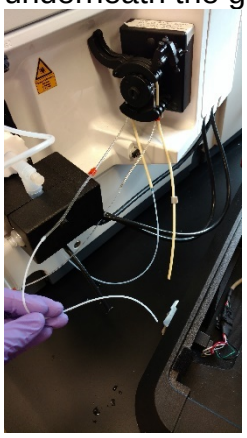

- *Check the waste bottle.* Be sure that the waste tubes from the autosampler is in the top of the waste container.

- *Set up the waste beaker.* Put the outlet line from the ICP-MS into the beaker, and cover the beaker with aluminum foil to shield the laser stage as much as possible from nitric acid fumes.
- *Place the sample introduction tube into Tune B solution (THERMO-4A-REV from Inorganic Ventures).* The final set-up looks like this:

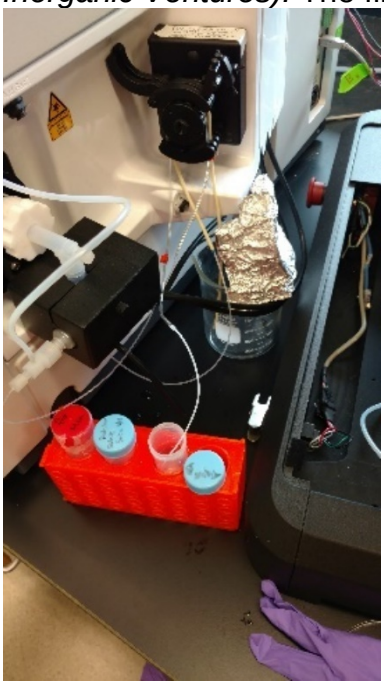

Start and tune the instrument:

- *Click the "On" button on the Instrument Control Panel; click "yes" in the warning box.*
- *While the instrument is turning on, keep your hand on the door latch. Twist the latch if the plasma forms as an orange ball.* If the plasma forms as a green flame, do not twist the latch. The latch serves as an emergency shut-off for the plasma (see page 4-13 of the iCAP-Q Operation Manual). If the instrument fails to light, see the troubleshooting section.

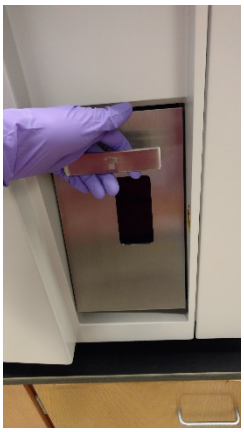

Normal plasma:

- *Check the drain line to make sure that it is actually draining.* You should be able to see liquid flowing through the line and dripping into the waste beaker. If not, press down firmly with your fingers on the top of the grip/lever that holds the brown outlet tubing to the peristaltic pump. This should increase the pressure in the tubing and draw the liquid out. Once the drain line is flowing, lift the pressure, and the liquid should continue to flow. If it does not, try tightening the screw on the top of the pump clamp slightly. If that doesn't help, check for a clog in the outlet tubing and/or change the outlet tubing.

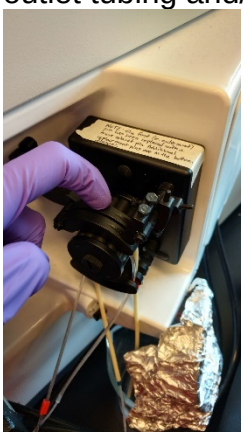

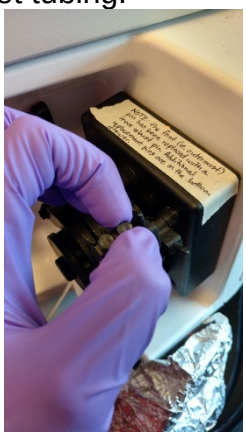

- *Set the instrument is to the Configuration and Mode that you desire.*
    - Configuration is set in the Experiment Configuration tab in Instrument Control, using the drop-down menu at the top of the screen. Select “Manual Sampling” for manual sampling. Select “Installer with ASX 520” for use with the autosampler.

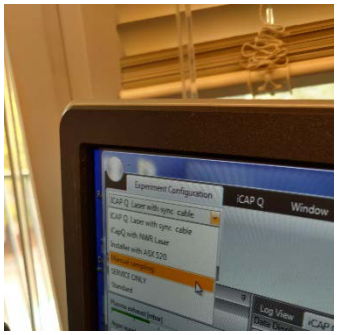

    - Mode is set in the iCAP-Q tab in Instrument Control, using the drop-down menu at the top of the screen. Select “STD” for setup and analysis without KED. Select “KED” for analysis with KED. DO NOT TUNE OR SETUP THE DETECTOR IN KED MODE. The signal won’t be high enough, and it will error out.

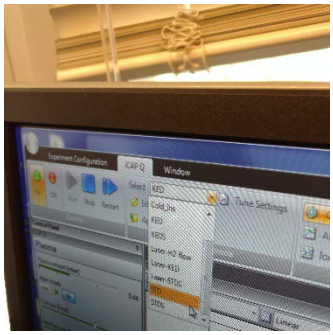

- *Press “Run,” and allow the instrument to warm up for at least 10 minutes.* Monitor the warm-up by watching the real-real-time signal in the Data Display window. Allow the signal to stabilize before proceeding.

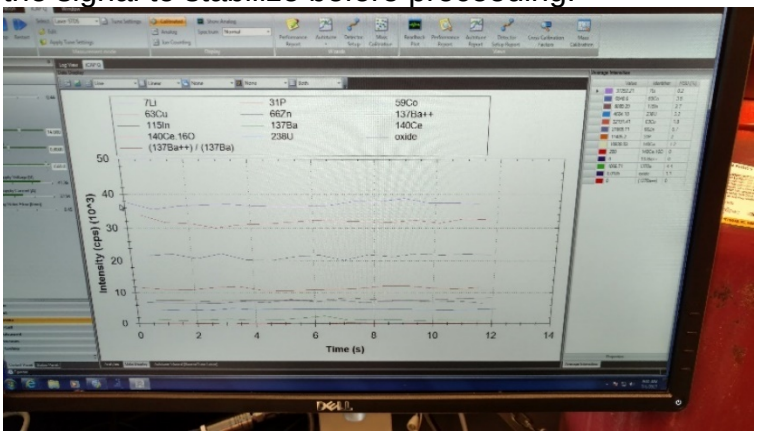

- If the signal is varies in regular oscillations, try adjusting the peristaltic pump screws to change the pressure on the tubing or try changing the peristaltic pump tubing in case it is flattened in some areas.
- If the signal is highly variable or takes longer than 20 minutes to stabilize, try changing the sample introduction tubing (if the tubing is old, it may have particles caked on the inside of the tube which randomly break loose and contribute to variable background signal). Also, visually inspect the spray chamber (remove the insulator/cooling housing) to ensure that the nebulizer spray is uniform. If it is not, shut down the instrument down and clean the nebulizer with a the cleaning tool (a very fine, plastic-coated wire). Check the joint where the tubing connects to the nebulizer; particulates tend to build up in this area and then break loose, causing random spikes in signal. If the nebulizer is dirty, clean it using the procedures described under “Nebulizer Cleaning” in “Maintenance.” If the problem persists, call Customer Support.

- *Run Autotune High Matrix.* If the instrument was already in liquid mode and was tuned in the last 48 hours, skip to running the Performance Report.
  - Place the sample introduction tubing in Tune B solution (if not already there).
  - In the Instrument Control software, click the “Autotune” icon in the “Wizards” section of the screen (upper middle). If you click the dropdown arrow instead of the directly clicking the icon, just select “Source Autotune.”

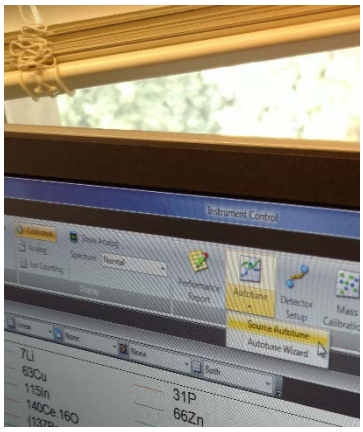

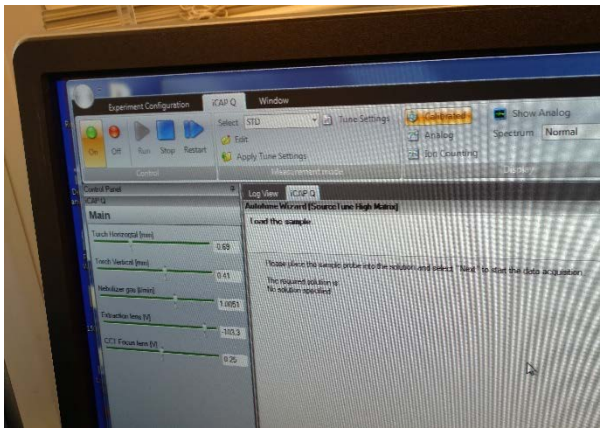

  - Click “Next”

- When the autotuned is finished, click “Next” to view the result log.

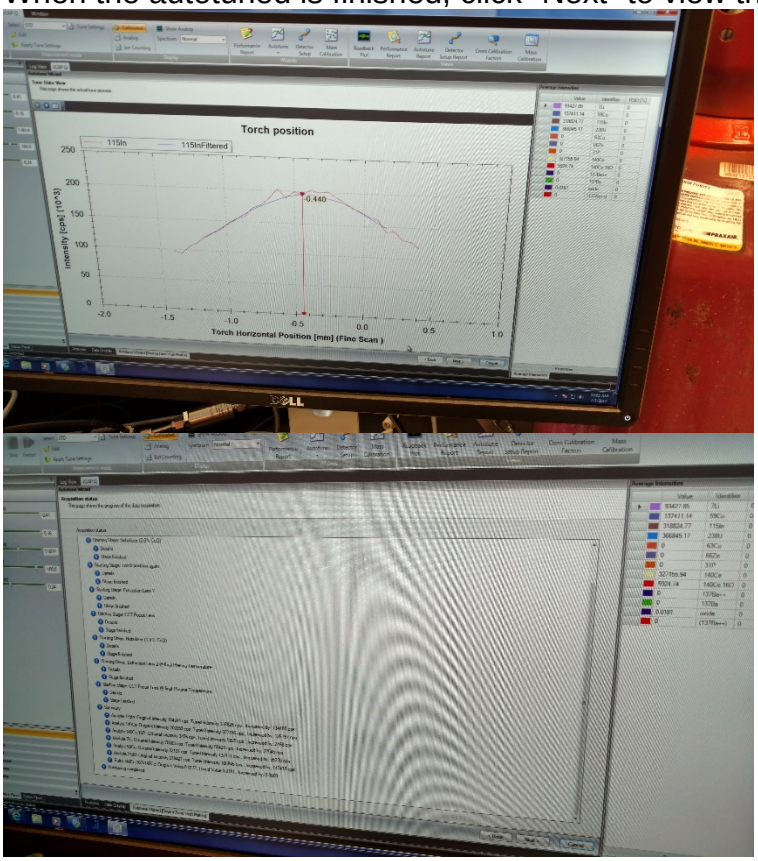

- Click “Next” again, and on the final screen, make sure “Yes” and “Open Report” are checked before clicking “Finish.” If you click “Finish” without clicking “Yes,” the tune settings will not save, and you’ll need to rerun the Autotune. If you click “Finish” without clicking “Open Report,” you can always open the Autotune Report using the “Autotune Report” icon in the “Views” panel on the upper right of the Instrument Control software.

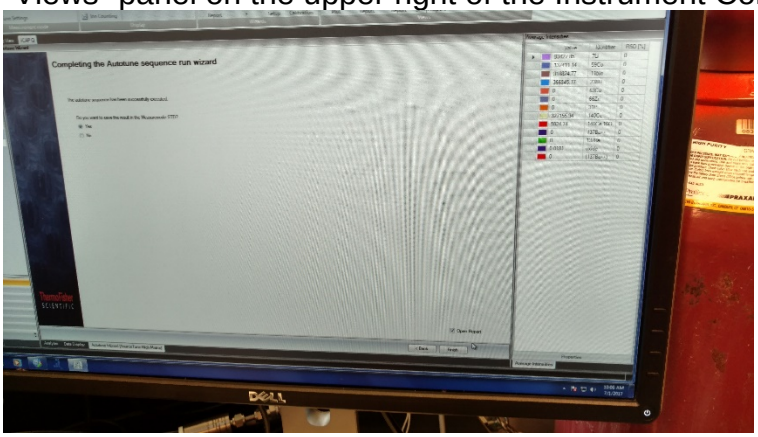

- Check that the new autotune settings look normal (ie. not that different from the last time the instrument was tuned). Scroll down to look through the tune curves as well. All the tune curves should be smooth.

Example settings: 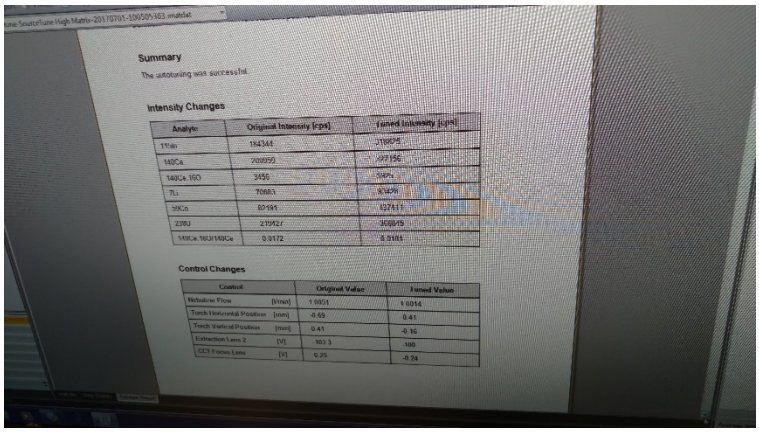

Eg. good curve: 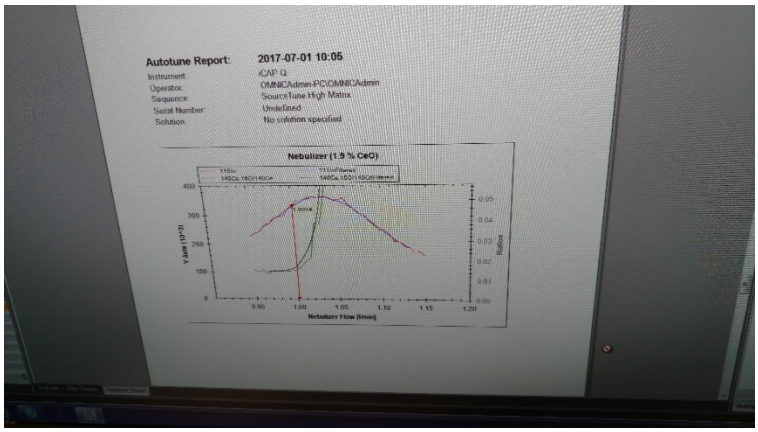

- SIDE NOTE: If you click the “Autotune” the dropdown box, you can select the “Autotune Wizard”. This will display all of the possible tune sequences you can run, including an option to tune KED mode (KED Autotune Line 1). From this window, you can edit and create tune sequences. You can also choose to run an existing Autotune sequence. Only create and edit Autotune sequences if you manage the instrument.

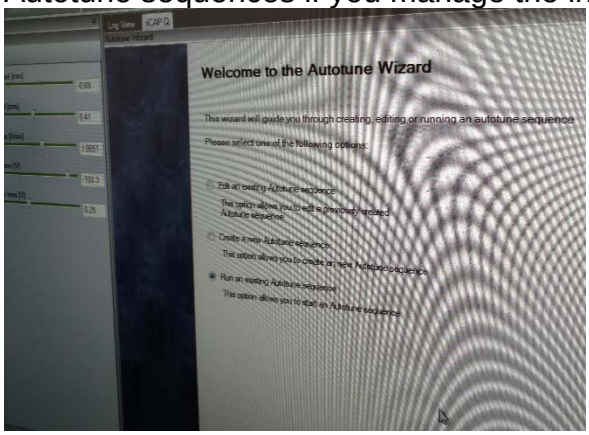

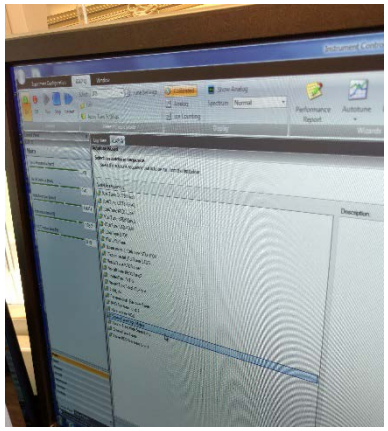

- *Run a Performance Report.*
    - Place the sample introduction tubing in Tune B solution (if not already there).
    - In the Instrument Control software, click the “Performance Report” icon in the “Wizards” section of the screen (upper middle).

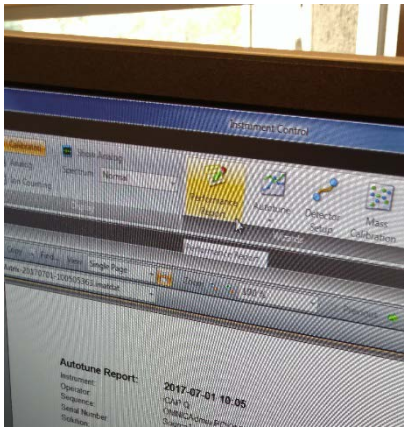

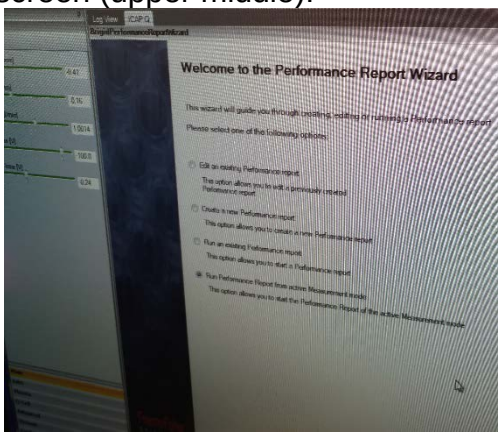

    - Click “Next”
    - If the instrument passes the performance report, begin collecting data. If the instrument fails the performance report, run the Autotune High Matrix sequence using the Tune B solution (THERMO-4A-REV from Inorganic Ventures).

- *If the instrument continues to fail the performance report, try Mass Calibration and Detector Setup using the Detector Setup Solution (THERMO-5A from Inorganic Ventures).*
    - Both of these programs can be run using the icons found in the “Wizards” section of the screen.

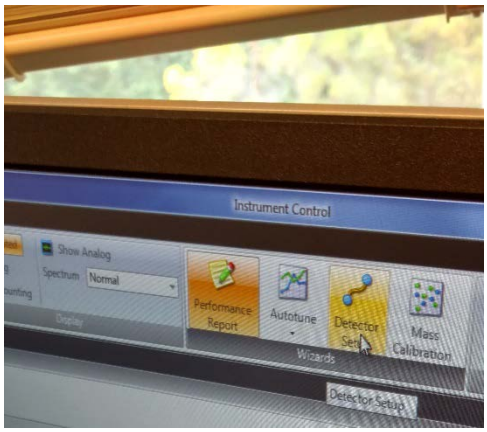

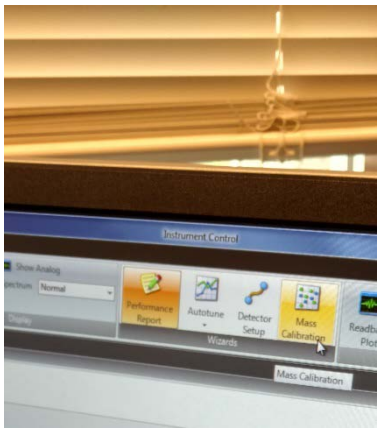

- For Detector Setup, run “Detector HV + Cross Calibration”

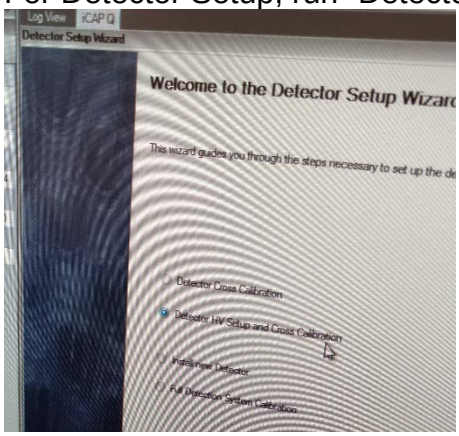

  - If the detector continues having trouble, try “Full Detection System Calibration.”
  - Contact Customer Support if the problem persists.
- *Change the Mode to “KED” and briefly put the sample inlet into the 10,000 ppb phosphorous standard to check that the phosphorous signal is 100,000-150,000 cps in KED mode.* For some reason, this element is particularly sensitive to issues with the detector. If it is significantly higher than 150,000 (say, 500,000 or a million), run the Detector Setup.

Running samples:

With the autosampler:

- *Rinse the autosampler lines:*
  - *Place the wash line into a bottle or beaker of clean 2% nitric acid. If you use a beaker, cover it with foil.*

  - *Attach the sample intake line to the autosampler line.*

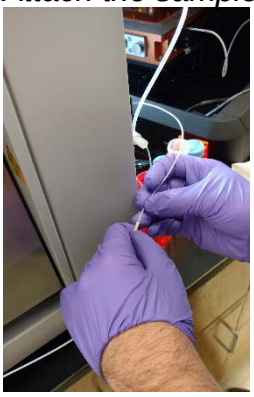

  - *Place a 50 mL conical of clean 2% nitric acid in Standard Rack 1 of the autosampler, and place a 50 mL conical of clean 10% nitric acid in Standard Rack 2 of the autosampler.*

- *If the Data Display is running, click the Run button to turn it off. DO NOT collect ions while running 10% nitric acid.*
- *In the CetaASX520 window of the Instrument Control software, click on position 2 of the Standard Rack to move the autosampler probe into the 10% nitric acid.* ***If the autosampler does not respond, flip the on/off switch on the back of the autosampler. Wait a few seconds, and try again.

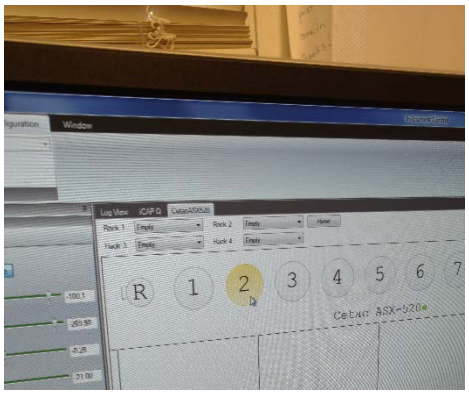

If needed:

- *In the Inlet System tab of Instrument Control (bottom of left-hand panel), change the Peristaltic Pump Turbo to "High"*

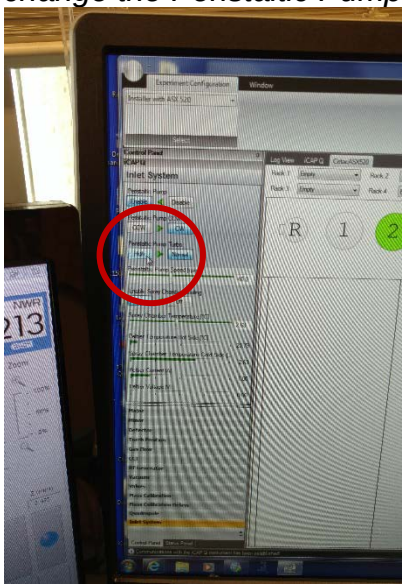

- *Flush the autosampler line with 10% nitric acid for 2 minutes.*
- *In the CetacASX520 window of the Instrument Control software, click on the "R" button to send the autosampler probe to the Rinse position.*
- *Click the "Run" button and watch the Zn signal.*
- *Flush the autosampler with rinse acid until the zinc signal has fallen and stabilized (usually ~5 minutes).*
- *In the CetacAX520 window of the Instrument Control software, click on the "1" position in the Standards Rack to move the autosampler to the clean 2% nitric acid.*

    - *Run 2% nitric acid until the zinc signal has fallen further and stabilized again. Usually ~5 minutes.*
    - *Measure the uptake time from the time the probe enters a tube of liquid to the time the liquid reaches the spray chamber:*
        - With the pump running on “High” (it probably already is), send the autosampler probe to the “Home” position for a few seconds.
        - Send the autosampler probe to position “1” in the Standard Rack, and simultaneously start a stopwatch.
        - Watch the leading edge travel along the autosampler line until it gets to the spray chamber, and note the number of seconds it takes.
        - The uptake time is typically ~45-55 seconds.
        - In the Qtegra software, you enter the Uptake time manually, under the “Cetac ASX520” tab. The time you enter into the program should be the real uptake time + 15-20 seconds (typically 65-75 seconds).
        - During rinsing and measuring the uptake time, if you get any sense that the line is clogged or not behaving normally or the signal is oscillating/variable, try flushing the tube longer with 10% nitric acid. If that doesn’t help, change the autosampler introduction tubing. Typically, the installed tubing is 40002402160, 1600061, Tube Teflon 1/16OD .02/D10ft.
    - *Keep the autosampler probe in this tube until you start running your samples.*
- *Create your method in the Qtegra software.* See the section on making Qtegra methods if needed.
- *Line up your samples in the autosampler.* Each sample must be >1.8 mL in order to have enough sample to get from the autosampler to the detector.
- *Fill the bottle or beaker of wash acid with 2% nitric acid.* The autosampler needs ~15 mL of rinse acid per sample (for a 30 second rinse). Be sure that there will be enough acid for all the samples. If there will not be, refill the rinse during the run.
- *Place the autosampler rinse drain line into the waste bottle in the cabinet.* Be sure there is enough space for all the rinse acid that the autosampler will use.
- *Schedule and Run the method in Qtegra.*

With Manual Sampling:

- *Switch the Experiment Configuration to "Manual Sampling"*
- *Create your method in the Qtegra software.* See the section on making Qtegra methods if needed.
- *Schedule and Run the method in Qtegra.*
- *Begin with the intake tubing in a 50 mL conical of 2% nitric acid in a tube rack.*
- *When the instrument prompts you, pull the probe out of the 2% nitric acid, and wipe it clean with a Kimwipe.*
- *Press "OK" on the software, and immediately insert the inlet tubing into the sample.* Typically, an uptake time of 14 seconds will fully (or almost fully) take up a sample of 220 uL.
- *Watch to make sure that the sample reaches the spray chamber during the uptake time (Rabbiting time) ie. before the pump slows back down.* If it does not, you need to turn the instrument off and clean the nebulizer. See the section on cleaning the nebulizer.
- *As soon as the pump changes back to its slower speed, wipe the intake tubing with a Kimwipe and place it back in the wash acid (the 50 mL conical of 2% nitric acid).*
- *When the instrument prompts you to "Wash," press OK. The pump will turn up to high speed for three seconds. When it slows back down, pull the tubing out of the wash acid, wipe it with a Kimwipe, and get ready to run the next sample.*
- *When the popup window for the next sample appears, click OK, and immediately insert the intake tubing into the sample.*
- *Continue in this manner, alternating between samples and short washes, until you finish the LabBook.*

Shutting down the instrument:

- *If the next person to use the instrument will be running in laser mode, set up an auto-cleaning run to remove contaminants from the line.*
    - Create a new “Auto cleaning” method from an existing method.
    - If the instrument was running in autosampler mode, disconnect the autosampler line from the inlet tubing, leaving the brown connector tubing connected to the autosampler line.
    - Place the inlet tubing into a bottle of fresh 2% nitric acid (at least 300 mL).
    - Empty the waste beaker and BE SURE that it is big enough to collect all of the acid in the bottle.
    - Cover the waste beaker with foil.

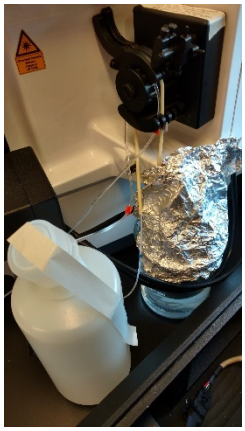

    - Run the autocleaning method.
- Set up the shutdown options in Qtegra that you want by selecting the “Options” button in the Scheduler panel and changing “Closedown” to “Closedown on an empty queue or LabBook error” if you want the instrument to turn itself off manually when it finishes rinsing the lines.
- You can also turn the instrument off manually by pressing the “Off” button in Instrument Control.
- *Leave the argon tank open so that pressure remains in the line.* Continuous argon bleed stabilizes the system by preventing oxygen or nitrogen from seeping into the plastic gas lines.
- BE SURE to come back within 48 hours to:
    - Remove the inlet line from the acid bottle. Cap the bottle and move it away from the laser.
    - Run the peristaltic pump for 5 minutes on high clear the line of nitric acid.
    - Unscrew the nebulizer from the spray chamber and dry the outside of the nebulizer.
    - Unhook the tubing from the peristaltic pump.
    - Empty the waste beaker and store it in the secondary waste container in the cabinet.
- DO NOT LET ACID SIT NEXT TO THE LASER STAGE for longer that 24-48 hours!!!! The acid will evaporate, corrode the stage and ruin the laser setup!!!!!

Laser Analysis:

Setting up the instrument

Check that there is sufficient argon and helium and that the chiller and vacuum are working well:

- *Check the pressure and gas level on the argon dewar.* The pressure output should be set to 90-95 psi. The pressure displayed on the Starwatch unit must remain above 95 psi or there will not be enough Cool Gas Flow, and the ICP will shut down. The pressure must remain above 110 psi to maintain a good signal without detector noise. Generally, each percent of argon will last about 1 hour, so if you have >24%, you will be able to use the instrument for about 20 hours (DON'T use the last 5% because the pressure typically drops as you reach the end of the tank!). Change the tank if necessary (***Refer to the section on changing tanks for ICP-MS. There are specific considerations for ICP-MS!!). Open the pressure builder valve if necessary

- *Open the helium tank valve.* The pressure output should be 10 psi to protect the mass flow controllers in the laser from damage. The total pressure in a full tank is ~2100 psi, and the tanks are good all the way down to 50 psi. For helium, 100 psi gets you ~3 hours of run time, so a full tank is 63 hours.

- *Check that the chiller and vacuum are running well.* The chiller and vacuum are on the balcony outside. The chiller should read ~20C +/- 1C. Check the vacuum light on the front of the instrument to ensure that the internal vacuum is correct. If anything doesn't look good, note it. If the problem persists, call for tech support.


- *Check that the laser housing is only touching the table with its feet* (not the edge of the housing); you should be able to run a piece of paper underneath the edge of the housing, all the way around. If this housing is touching, it causes building vibrations to mess up the stage and laser alignment. By pushing *on the black base*, move the laser housing until it touches the counter only with its feet. ***DO NOT PUSH on the blue casing on the top!!!!***

If the instrument has been running in liquid mode, change to laser mode:

- *Change the cones to the High Sensitivity cones.*
  - Refer to iCAP-Q Operating Manual, pages 8-20 through 8-26.

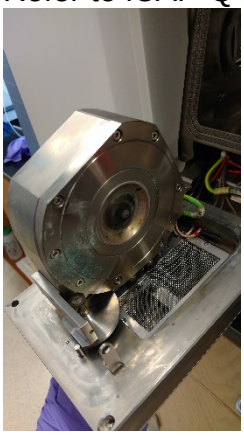


go to next page for more pics

- Be sure the graphene seal is present and not damaged.
- If you need to clean graphene off of the cone holder, use a plastic or wooden scraper. NEVER touch metal to the cone holders or cones.
- Be sure the small metal insert in the small cone (skimmer cone) is securely in place.
- Do not damage the cone tips or overtighten the cones when screwing them in.
- Check that the cones are clean. Refer to Liquid Analysis setup for more information. I have never cleaned the laser cones. They have always worked well.

- *Clear the liquid intake system of liquid, and remove the liquid intake system.*
    - If there is liquid in the system, remove the intake tubing from the tube/bottle of 2% acid and dry it with a paper towel.

    - In the Instrument Control software, navigate to the “Inlet” tab on the left side panel.
    - Under the Peristaltic Pump, click “On” or “Enable.”

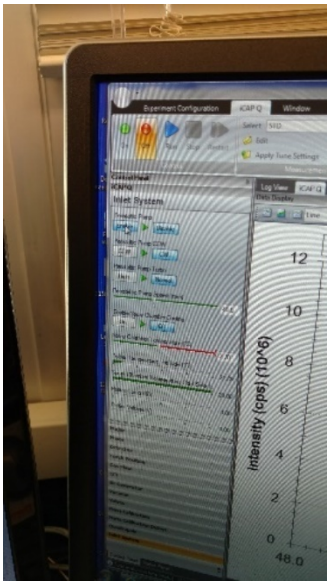

    - Let the pump run until all liquid has drained from the intake line.
    - Click “Off” or “Disable” to stop the pump.

- Disconnect the tubing from the pump by popping open the clamps on the top of the pump and unhooking the tubing.

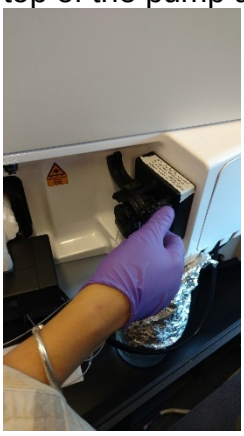
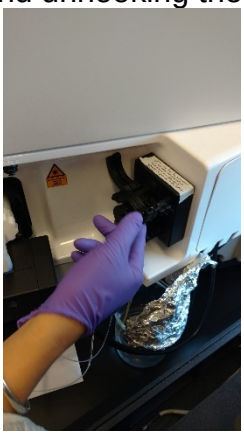
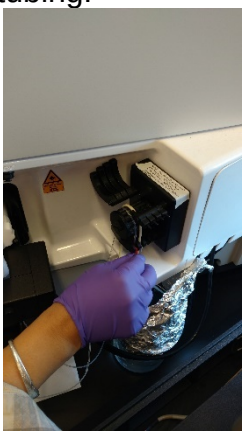

- Open the spray chamber insulator: unscrew the knob on the outer door and open the inner door.

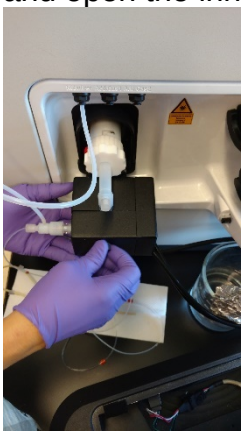

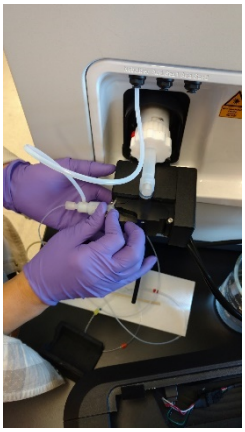
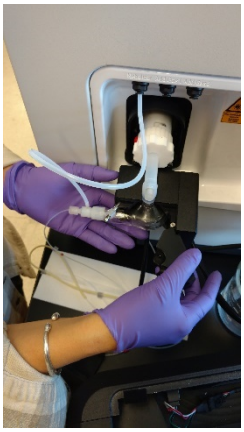

- Unhook the nebulizer gas tubing (press up on the black ring and then pull the tubing out).

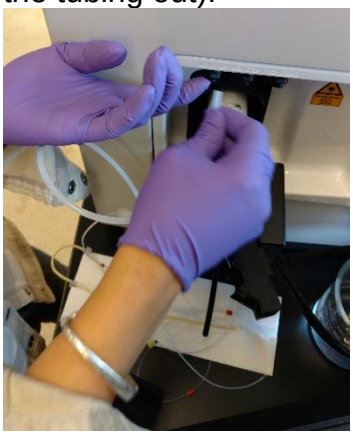

- Gently but firmly pull the spray chamber out of the insulator by pulling on the plastic L-shaped connector. DO NOT pull on the glass.


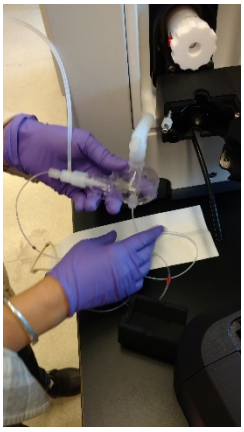

- Once the spray chamber is disconnected, unscrew the exit line connector and dab an extra nitric acid with a paper towel.

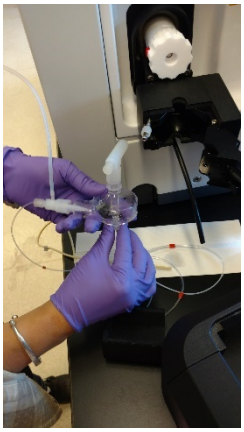

- Unscrew the nebulizer connection (large plastic connector) and pull the nebulizer out. Dab it dry with a paper towel.

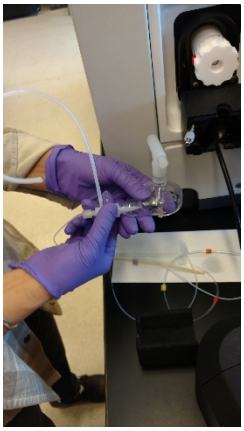
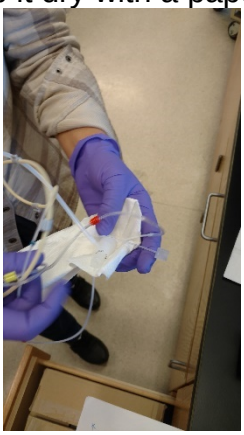

- Store the liquid inlet system in the cardboard box in the third drawer.

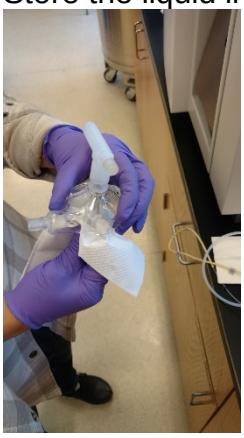


- *Change the injector from the liquid injector to the gas injector.*
  - Visually inspect the injector, torch, nebulizer and spray chamber as you handle them. Brown stains are normal. Cracks are not. If the torch or injector is cracked, order a new one. You can still use a torch or injector that has a line crack, but if the crack causes the glass to separate, do not use it.
  - Press the red knob on the side of the torch housing, and gently twist to the left until the silver knob is able to slide out.


- Pull out the torch and injector (torch = outer glass piece; injector = inner glass piece).
- Unscrew the injector using the white knobs and carefully remove the injector from the torch.


- Place the torch and injector flat-side-down on the counter. DO NOT let the glass touch the counter; it can chip.

- Open the box containing the gas injector, and take it out.


- Screw the gas injector into the torch.


- Insert the torch+injector back into the instrument so that the silver knob slides in cleanly. Twist it to the right to lock it in place.


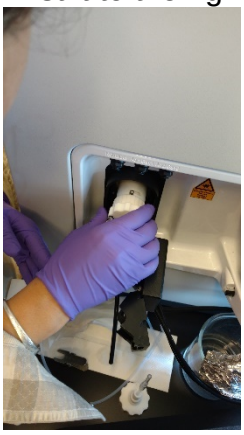
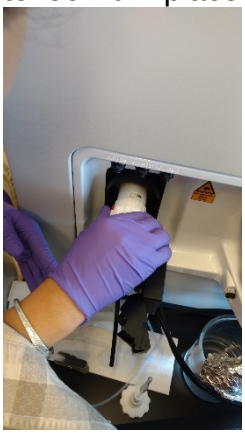

- Put the liquid injector in the injector storage box, and put it back in the drawer.

- *Connect the nebulizer gas to the injector.*
  - Insert the tubing into the black inlet valve.

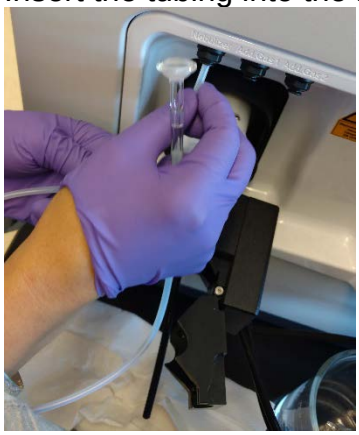

- Clip the glass adapter onto the top inlet on the injector. Be sure it forms a nice seal with the black o-ring on the injector.

- *Connect the laser sample outlet line to the injector.*
  - Clip the glass adapter onto the top inlet on the injector. Be sure it forms a nice seal with the black o-ring on the injector.

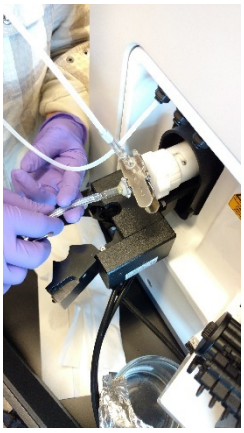

- *Close the insulation chamber.*

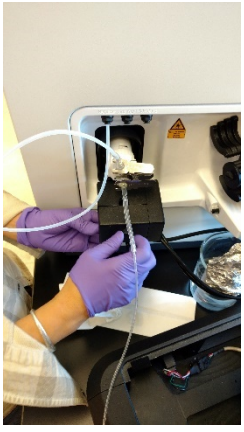

- *Place two tube racks under the plastic tubing to keep the tubing as flat as possible.* Any curves in the tubing should be as gentle and smooth as possible.

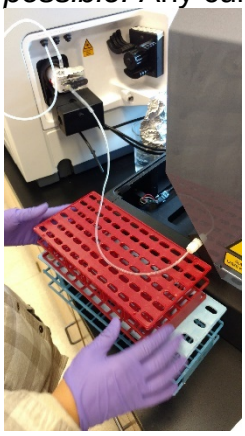

Prepare the sample chamber and software:

- *Unhook the sync cable from the "EXT INTLK" connection on the back of the instrument.*

- *Place the metal cap on the "EXT INTLK" port.*

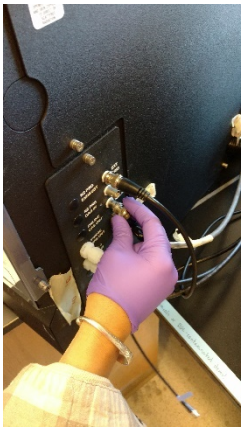

- *If the software is already open, the “Laser” and “Remote” interlocks will be tripped (because the iCAP-Q is off). Click the “Remote” button, and the laser should power up again.*

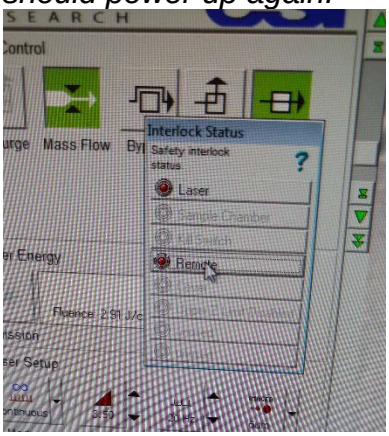

- *If the NWR software is not open, open it from the desktop.*
- *Place the sample into the laser chamber.*
    - Move the sample chamber to the correct position to get the sample holder out (drag the stage control scroll buttons to the bottom and far left of the screen).

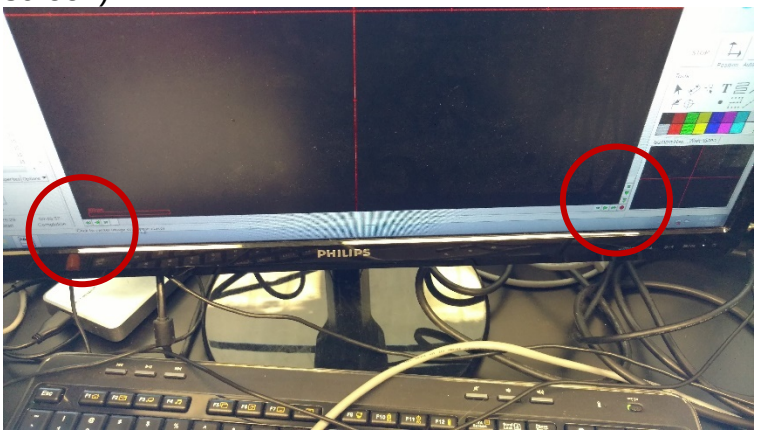

- Unscrew the two silver screws on the front of the chamber.

- Gently slide the holder out.

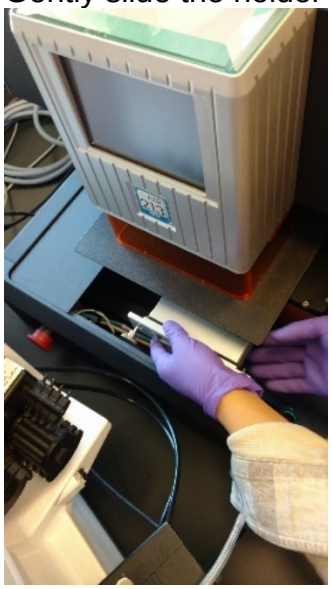

- Remove old sample slides and place fresh sample slides in the chamber. Don't move the support slides below (there are two layers of blank slides already in the sample chamber that keep the sample slide (the third layer) at the correct height to be in the laser focal range). The chamber can hold up to four slides in addition to the standard slide.
- Put the standard slide in the second position becuase that is where we've been putting it for years. This will make it easier to build your new method from an old method because the standard laser patterns will be basically in the right place.

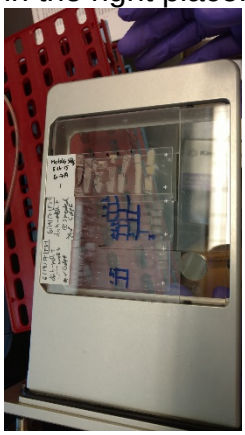

- If you're only putting in one or two slides, put them below the standard slide because the navigation camera doesn't have a good angle on the top ~1 cm of the sample chamber.
- NOTE that the laser cannot access ~3-5 mm around the edges of the sample chamber, so it's best for the slides not to touch the edges of the chamber if possible.
- Slide the holder back into the laser chamber, gently pushing it so that it seals,
- Tighten the silver screws.

Clear oxygen from the laser gas lines/chamber, and turn on the ICP-MS:

- *The following steps remove oxygen from the Bypass and Online gas lines before the purge to prevent residual oxygen from extinguishing the torch after the purge is finished:*
  - *In the NWR software, be sure that the "Bypass" button is green.*

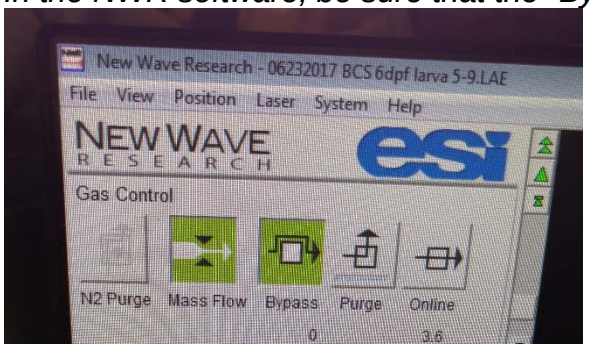

  - *Click the "Mass Flow" button in the top left to open the Mass Flow Control window.* Move the window out of the center of the screen so that it doesn't overlay any of the popup windows. The Channel 1 "Enable flow controller" should be checked, and the "Ramp up rate (ml/minute/second)" should be 50. Do NOT check the "Stop gass on experiment end" box or the gas will shut off in the middle of your scans. It thinks that an "experiment" is one scan, not all of your scans. You will have to manually turn the gas off when you are done.

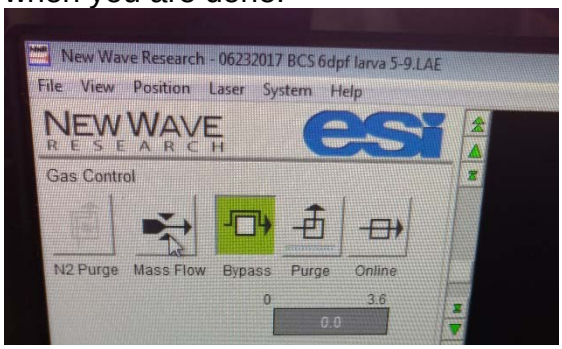

  - *Change the "Select the desired flow rate in ml/minute" to 800, and flush for 20 seconds.* This flows He through the bypass lines, removing most of the oxygen.

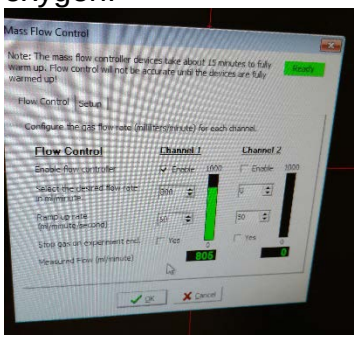

- *Press the “Online” button.* Because you haven’t purged the chamber yet, an error window will appear.

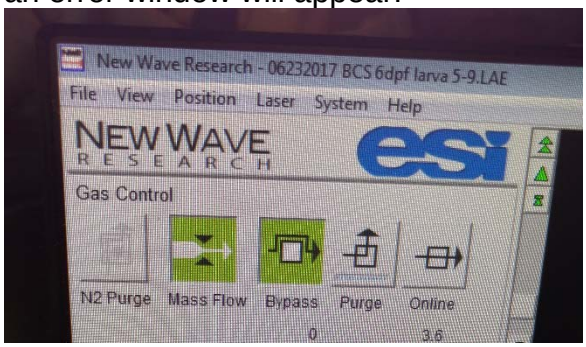

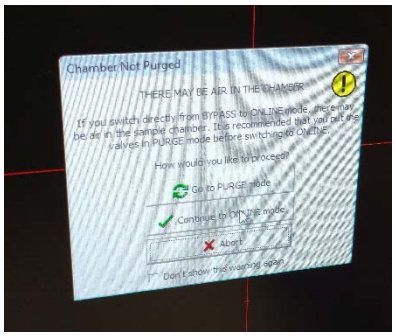

- *Click “Go to Online mode” to override the error, and flush for 20 seconds.*
- *While in Online mode, set the flow rate back to 50.* Allow the green bar to lower to 50.

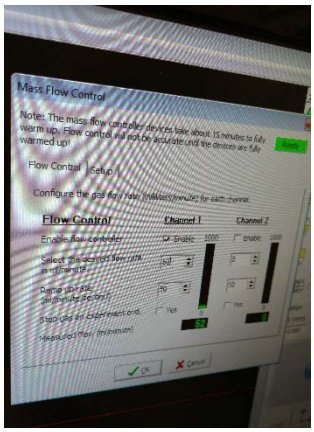

- *Switch back to Bypass mode by clicking the “Bypass” button.*

- *Hit the "Purge" button.* A loud rushing noise should start because He is being pumped through the sample chamber at 4 L/min.

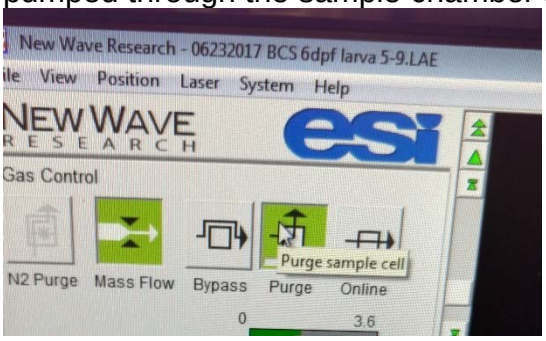

- *While the purge is running, turn the iCAP-Q on by clicking the "On" button on the Instrument Control Panel; click "yes" in the warning box.*

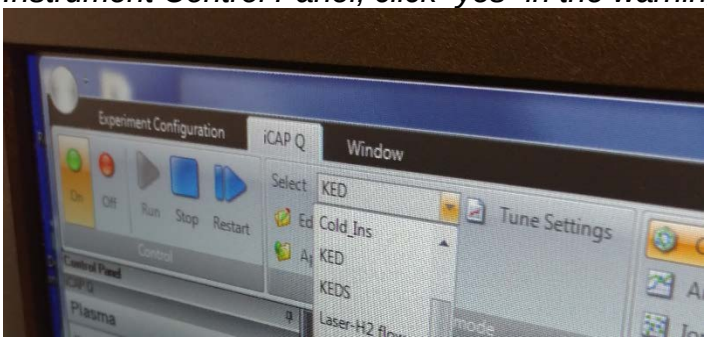

- *While the instrument is turning on, keep your hand on the door latch. Twist the latch if the plasma forms as a ball.* If the plasma forms as a flame, do not twist the latch. The latch serves as an emergency shut-off for the plasma.

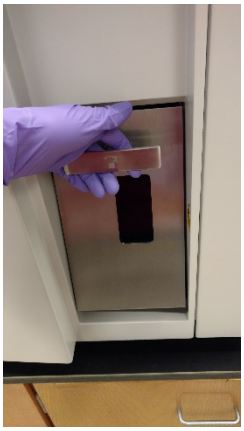

Normal plasma:

- *Set the instrument is to the Configuration and Mode that you desire.*
    - Configuration is set in the Experiment Configuration tab in Instrument Control, using the drop-down menu at the top of the screen. Select “ICAP Q Laser with sync cable.”

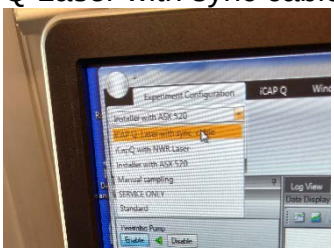

    - Mode is set in the iCAP-Q tab in Instrument Control, using the drop-down menu at the top of the screen. Select “Laser-STDS” for setup and analysis without KED. Select “Laser-KED” or “Laser-H2” for analysis with KED He or H2. DO NOT TUNE OR SETUP THE DETECTOR IN Laser-KED MODE. The signal won’t be high enough, and it will error out.

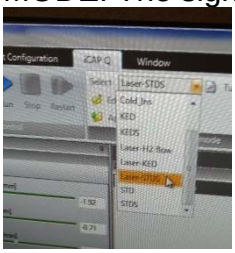

- *Allow the ICP-MS to warm up for at least 10 minutes.* Monitor the warm-up by clicking the “Run” button and watching the real-time signal in the Data Display window. Background copper counts should be around 500 cps in Laser-STDS mode.

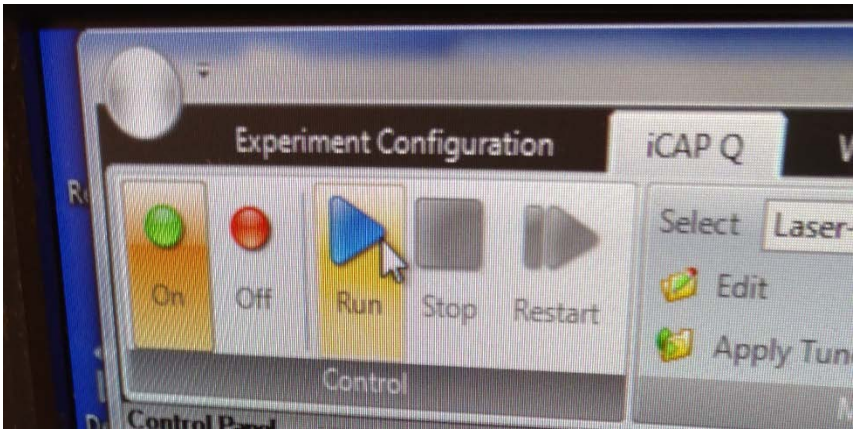

- *Warm up the laser:*
  - *Set the laser fluence to 7.0 J/cm2*

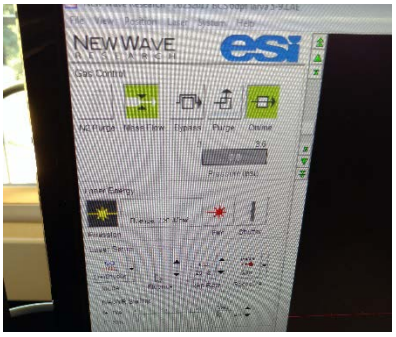

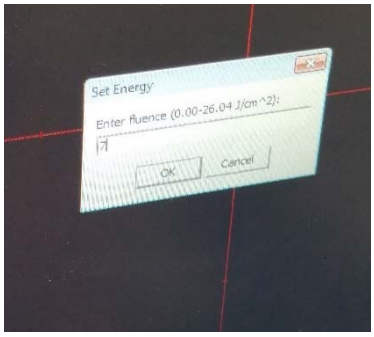

  - *Set the firing rate to 20 Hz*
  - *Turn on the laser by clicking the "Fire" button in the middle of the left-side panel*

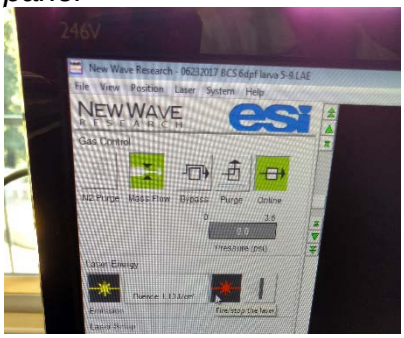

  - *Let the laser warm up for at least 15 minutes before starting*

Finalize the setup for scanning and tune the instrument:

- *Once the purge is finished, the laser automatically switches to Online mode. Check that it is Online before continuing.*
- *Reattach the EXT INTLK cable by removing the metal cap (it goes in the small box in the top drawer) and attaching the cable.*

- *Press the “Remote” option on the interlock error box that popped up when the metal cap was removed.*
- *Restart the laser:*
    - *Set the laser fluence to 0.0 J/cm2. Press OK.*
    - *Click the “Fire” button on and off.*
        - Not sure why, but the fluence sensor gets screwed up by the interlock being tripped, so you have to reset it after attaching the cable.
    - *Set the laser fluence to 7.0 J/cm2. Press OK.*
    - *Click the “Fire” button to turn the laser back on.*
- *In the Mass Flow Control window, type “200” into the “Select the desired flow rate in ml/minute” box.* You don’t need to press OK. Just wait. Watch the green bar ramp up to ~200. Keep an eye on the ICP-MS plasma. If it flickers, wait until it stops flickering to continue.
- *In the Mass Flow Control window, type “800” into the “Select the desired flow rate in ml/minute” box.* You don’t need to press OK. Just wait. Watch the green bar ramp up to ~800. If the plasma flickers, wait until it is steady.
- *Press “OK” in the Mass Flow Control window.* It will close.

- *Tune the instrument by running SourceTune Laser.*
    - You need to draw a pattern that lasts at least 10 minutes, using an 85 um spot at 20 Hz on >7 J/cm2 power, that runs across the glass NIST 612 standard. The easiest way to do this is to use the “999999-Tune” experiment and modify it. The standard is not flat; be sure that both the beginning and ending points are at the correct height. Follow the steps below to do this.
        - *Click File -> Open Experiment*
        - *Select 999999-Tune*
        - *Right-click on the “Tune” pattern and select “Move to Scan.”* This is to easily navigate to the NIST 612 standard location.

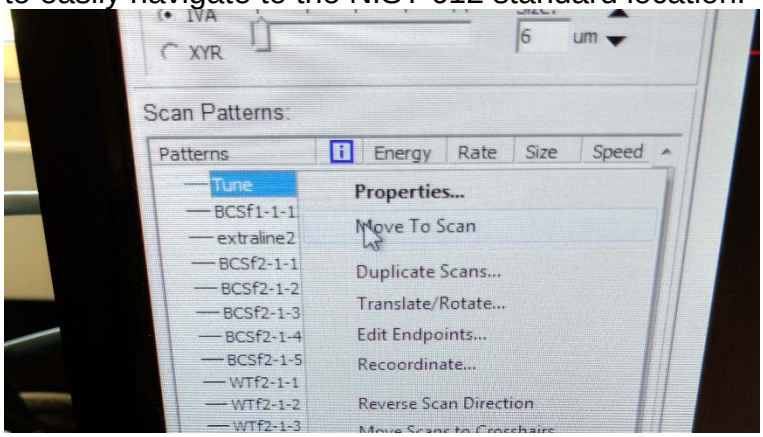

- *If the screen is dark when the stage arrives, turn up the Transmitted Light using the slider on the top of the right panel.* The NIST 612 standard is quite thick. You can also adjust the Polarizer to improve the contrast if necessary.

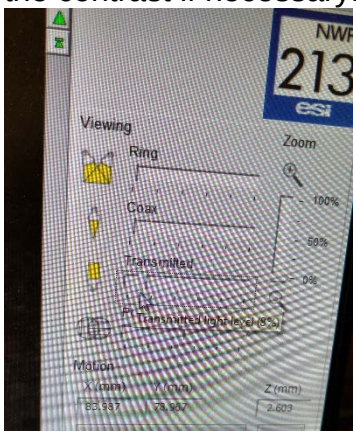

- *Move the TV2 cup out of the way by right clicking on the screen and selecting "Offset TV2 cup."* The NIST 612 glass piece should now be visible in the wide-view camera in the lower right corner of the screen.
- *Find the scars on the NIST 612 glass left over from previous tune scans.*
- *Place the crosshairs in the center of the screen at the location where you want the tune scan to start.* ***Align with previous scans to get the most out of each NIST 612 standard.

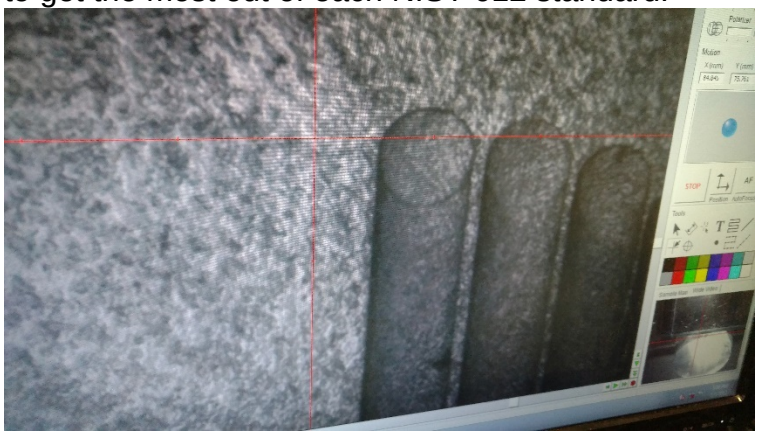

- *Adjust the focus using the Z scroll bar on the upper left.*

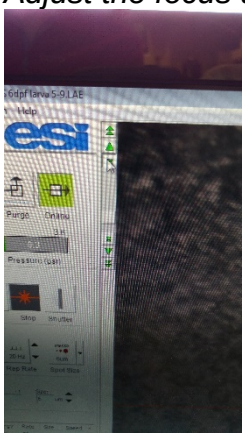

- *Right click on the “Tune” pattern and select “Move Scan to Crosshairs”*
- *Click OK on the dialog box*

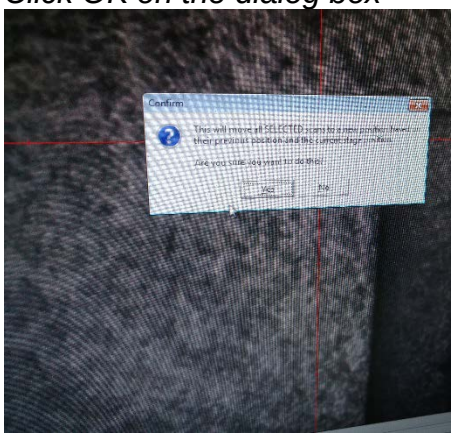

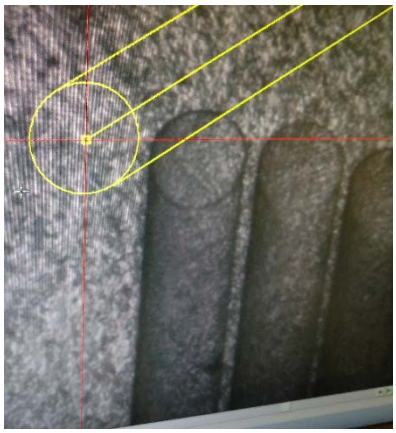

- *Navigate to the location where you want the tune scan to end (line up with previous tune scan scars).*
- *Adjust the focus.*

- *Right-click on the “Tune” pattern and select “Edit Endpoints”*
- *Type the current coordinates (found in the middle of the right-hand panel) into the lower row of the endpoints window that pops up.* Leave the upper row of values alone (those are the starting point values).

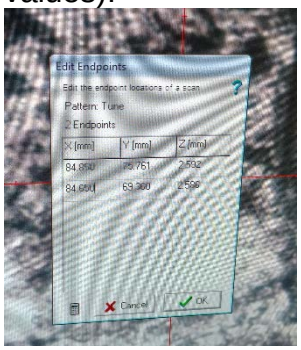

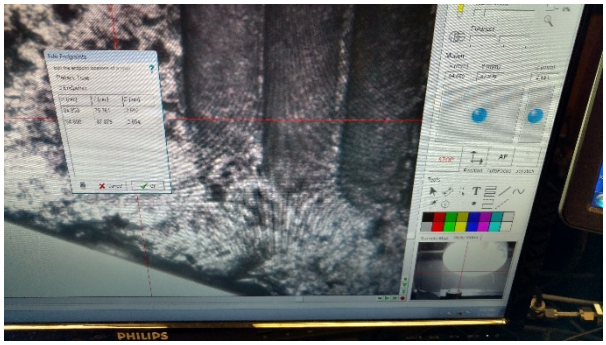

- *You should now see the end of the scan at the correct location.*

- *Navigate to the start of the scan by right clicking on the “Tune” pattern and selecting “Move to Scan.”*

- Now set up the Autotune program on the ICP-MS computer:
  - *In the Instrument Control software, click on the “Autotune” icon.*

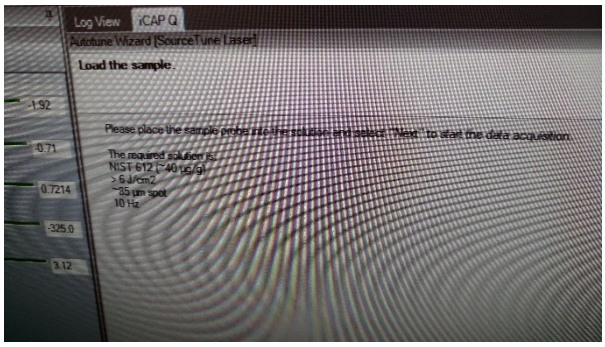

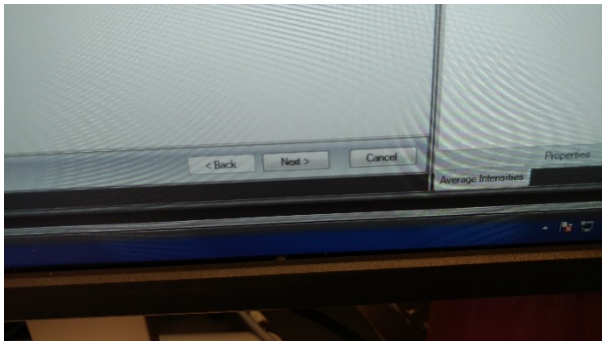

  - SIDE NOTE: If you click the icon directly, the SourceTune Laser sequence will open; you’ll see a prompt to start the scan. If you click the dropdown box, you’ll see “SourceTune” and “Autotune Wizard”. If you click “SourceTune”, once again, SourceTune Laser will start. If you click the wizard, you’ll see all of the possible tune sequences you can run. From this window, you can modify and create tune sequences. Do this only if you manage the instrument.

- *In the NWR Software, select the “Tune” pattern and click “Run”*

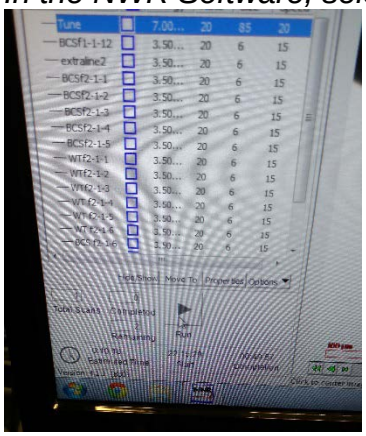

- *In the control panel that appears, check the following settings and adjust if necessary*
  - *“Selected Patterns Only” should be checked*
  - *Washout time: 5 seconds*
  - *Warm-up time: 12 seconds*
  - *Click “Trig In/Sync Out Options”*
  - *In the new window, select the “Trigger In” tab*
  - *Check “Don’t wait for trigger” and click OK*

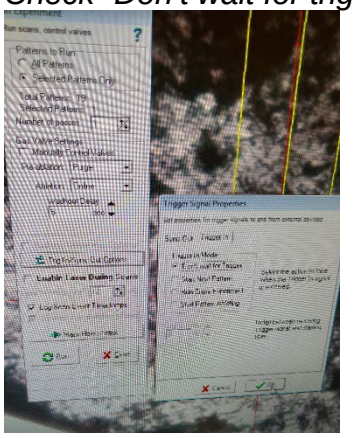

  - *“Enable Laser” should be checked.*
  - *Finally, press “Run” on box (not the original “Run” button*

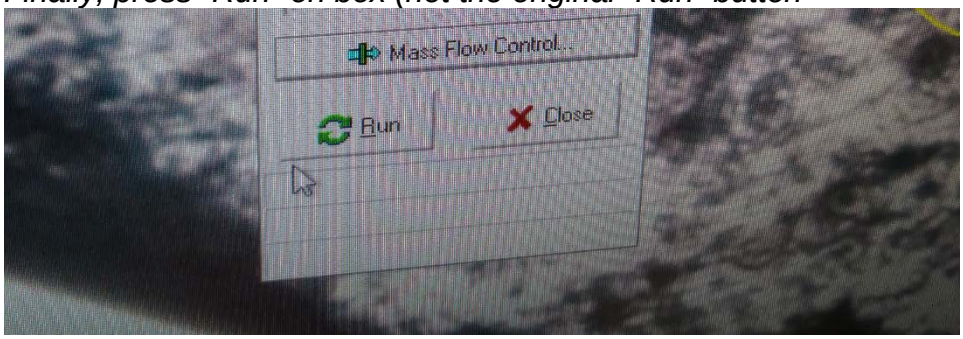

- *Let the laser run for 10-15 seconds.*

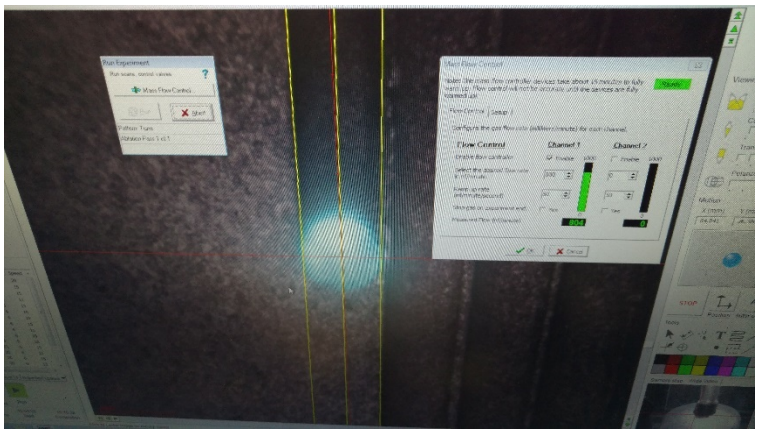

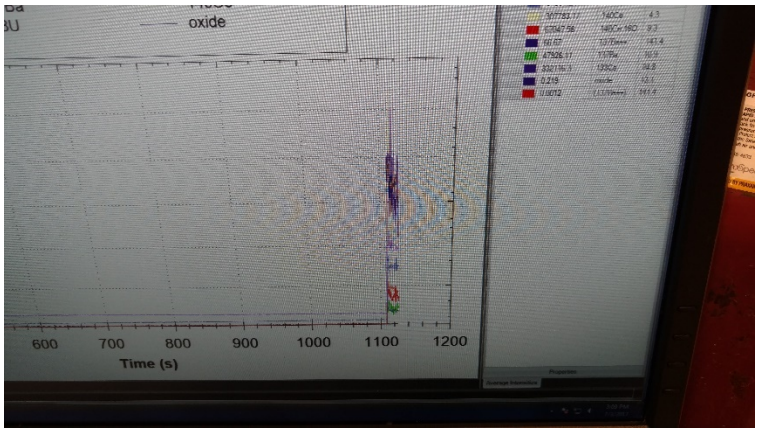

- *If all looks good, click "Next" on the Autotune program in the ICP-MS software.* The autotune sequence will being. It takes about 9.5 minutes.
- *When the autotune is done click "Next"*

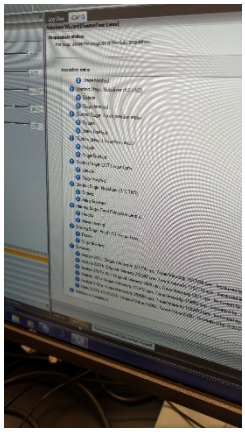

- *Be sure the "Yes" option is checked under "Save new settings…"*

- *Check “Open Report”*

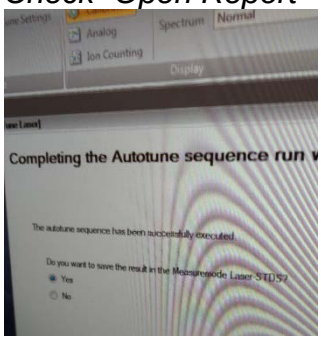

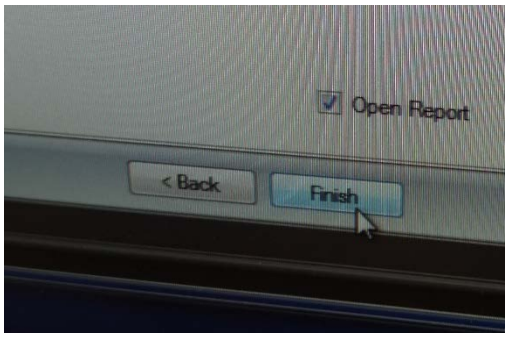

- *Press Finish*
- *Check that the new autotune settings look reasonable.* All the tune curves should be smooth, and the new settings should not be drastically different from the old settings.

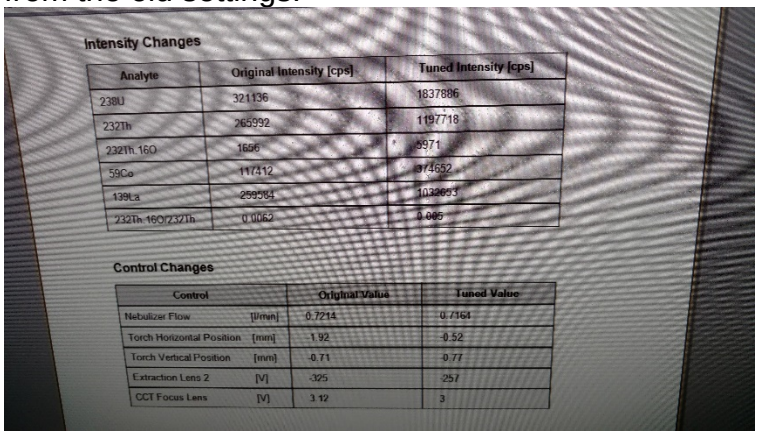

- *If the instrument does not tune well, it needs to be switched back to liquid mode in order to do full troubleshooting.* Contact Customer Support if the problem persists.
- *From here, you’re ready to run samples.*

Running Samples:

- These directions assume a basic knowledge of the NWR software and Qtegra software. If you need additional help with these, please see the sections on operating these software packages.
- These directions also assume that an experiment file already exists that uses the settings you want to use. If you're starting from scratch, see the "Optimizing Laser Settings for New Samples" section below.

- *Keep the laser warm by clicking the "Fire" button. Be sure the shutter is closed!* You want to keep the laser firing during the setup period.
- *Double check that the Mass Flow is running at 800 ml/min.* The sample chamber expands slightly when it pressurizes (when the gas flow is at 800 ml/min), and the focal plane moves. If you draw patterns before ramping up the flow rate, they will be out of focus.
- *Double check that the EXT INTLK cables are connected before beginning.*
- *Double check that the laser housing is only touching the table with its feet* (not the edge of the housing); you should be able to run a piece of paper underneath the edge of the housing, all the way around. If this housing is touching, it causes building vibrations to mess up the stage and laser alignment. If necessary, move the laser by pushing on the black base. ***DO NOT PUSH on the blue upper casing!!***

- *Create patterns for one set of standards, and name it Stds1.* Generally, you need to draw patterns for your standards and merge one set of standards into a single scan. Include at least 3 lines/standard (for 6 um lines, I usually do 5 lines/standards; for larger lines, I usually do 3 lines/standard). The first line will ablate more material than the rest of the lines because it is firing on fresh material, so this line cannot be used in the standard calculation. The rest of the lines can be averaged, or one of the other lines can be used individually to calculate the value for that standard. Make sure that the properties of the line you are using to run your standards matches the properties of the line you will use for your analysis. To do this, follow these steps:
    - *Open an existing experiment that has lines that have the properties you want for your experiment.*
    - *Delete old patterns (usually have names like Stds1, etc.). Keep "ExtraStds" and ExtraLine".*

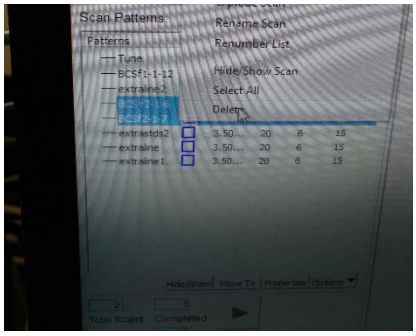

- *Right click on “ExtraStds” and select “Move to Scan.”* This should put the stage more-or-less on top of the first standard.

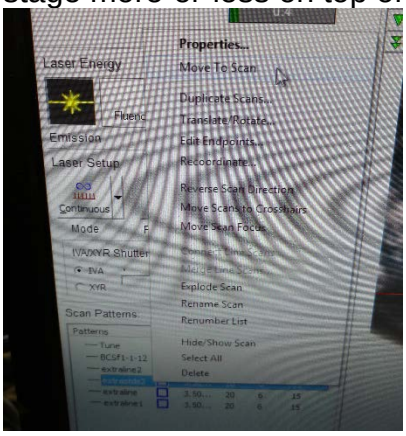

- *Read this:* The standards slides have 7 standards on them, arranged from left to right: G to A (low to high). G is farthest to the left and is the lowest standard. We only use G, F, E, D, and C. B and A hardened and cracked (and are also much higher than the physiological range).
- *Find a location on Standard G that has enough space to run the number of standard patterns x the number of samples that you want to run.*
- *Place the crosshairs of the screen at the location where you want the standard scans to start.*
- *Adjust the focus.*
- *Right click on “ExtraStds” and select “Move Scan to Crosshairs.”*
- *Click OK in the warning window.* The first standard patterns should now be located at the center of your current screen, in the location where you want them to run.

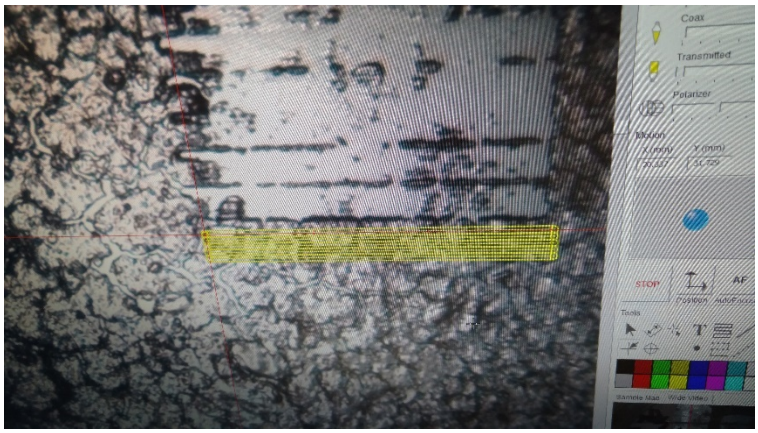

- *Separate the standard patterns by right clicking on "ExtraStds" and selecting "Explode Scan."* The "ExtraStds" pattern will disappear and be replaced by 15-25 individual scan patterns. The first 3-5 patterns are the lines on your current screen. Click on the patterns (eg. Line #3, Line #4, Line #5, etc.), and watch the lines on your screen. When you click on a scan, it turns yellow.

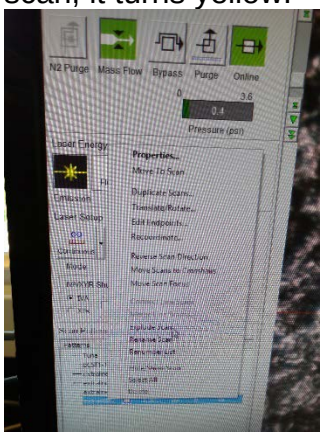

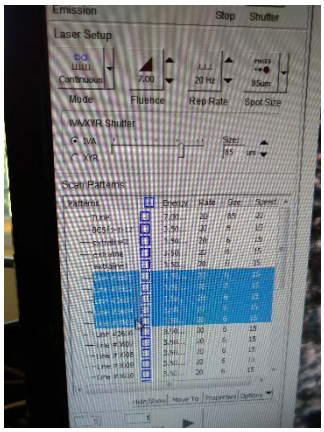

- *Select the first line that is NOT one of the lines for Standard G.*
- *Right click on that line, and select "Move to Scan"*
- *Find a location on Standard F that has enough space to run the number of standard patterns x the number of samples that you want to run.*
- *Place the crosshairs of the screen at the location where you want the next standard scans to start.*
- *Adjust the focus.*
- *Select the 3-5 line patterns that belong to Standard F.*
- *Right click on the selected lines, and select "Move Scan to Crosshairs."*
- *Click OK in the warning window.* The second set of standard patterns should now be located at the center of your current screen, in the location where you want them to run (on Standard F).
- *Follow the above steps to move the line patterns for Standards E, D, and C to appropriate locations on Standards E, D, and C.*
- *Select all the lines for Standards G, F, E, D, and C (typically 15-25 lines).* This is easiest to do by right clicking on any pattern, selecting "Select All" and then deselecting the patterns that are NOT for the standards by holding the Ctl button while clicking on the unwanted patterns.
- *Right click on the selection, and select "Merge Line Scans."* DO NOT select "Connect Line Scans;" this function will connect the line scans with other lines, so the laser will stay on while moving to the start of the next scan, drawing random ablation lines across your standards and samples. Bad news.
- *Right click on the newly merged line and select "Rename."*
- *Name the merged standard "Stds1."*

- *Right click on Stds1 and select "Duplicate;" duplicate Stds1 enough times to have 1 standard set for each sample + 1 extra standard set.* When you duplicate the pattern, the offset in Y should be the total height of all the lines for one standard (eg. for standards that are 5 lines of 6 um scans, offset by 30 um).

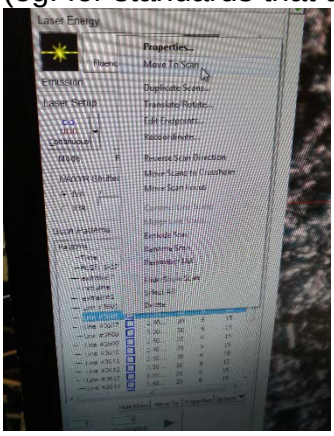

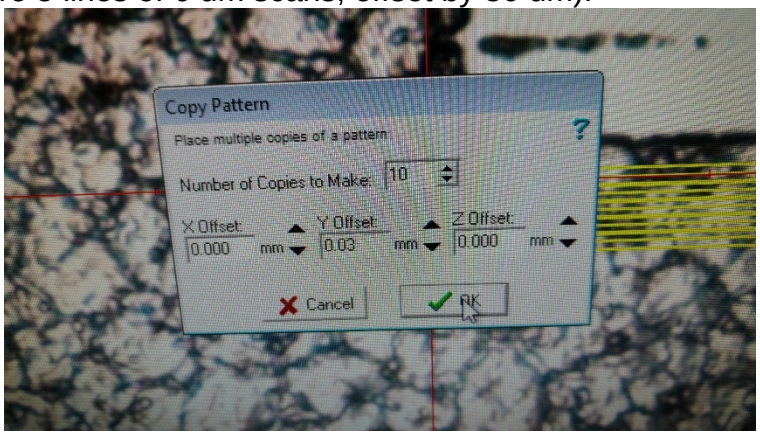

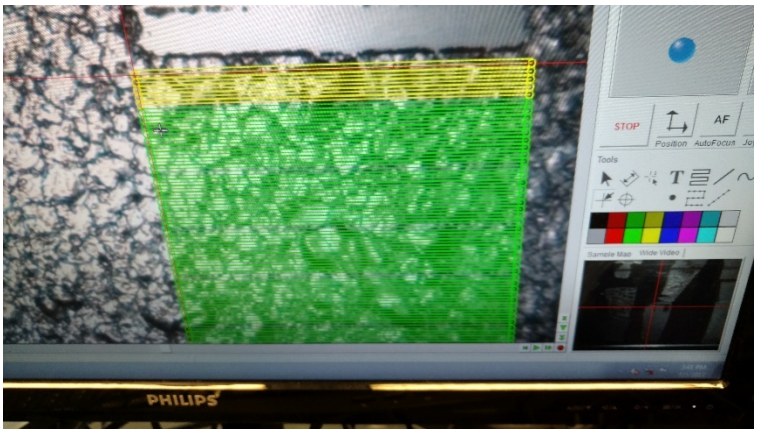

- *Rename the duplicated standards "Stds2, … StdsN, ExtraStds."*

- *Navigate to your first sample.*
- *Adjust the focus.*
- *Draw enough lines to cover your first sample. Merge them and rename them Sample1.* To do this, follow these steps:
    - *Navigate to a location that is both above and off to the left of the sample.* The crosshairs on the screen should be ~1-2 line-widths (eg. for 6 um line: 6-12 um) above the top of the sample. The crosshairs on the screen have tick marks on them. The crosshairs should be about one tick mark away from the left edge of the sample (~2-3 cm on the screen).

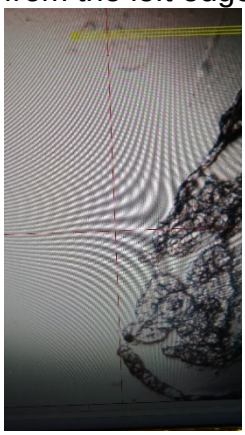

    - *Right click on "ExtraLine" and select "Move Scan to Crosshairs"*
    - *Click OK on the warning box.* The line should now be positioned at the center of your screen. Scroll down to check that the line does start ~1 tick mark away from the left edge of the sample. Move back to the scan and scroll to the right to make sure the scan is ~1-2 line widths above the sample.
    - *Navigate to the right edge of the sample. Move slightly off the sample to the right.*
    - *Right click on "ExtraLine" and select "Edit Endpoints"*
    - *Type the current Y coordinate into the bottom box under "Y" and press OK.* The line should now end just after the right edge of the sample. Navigate to the line to double check this.

    - *Click on "ExtraLine" and record the "Estimated Time" for the line (in the lower left corner).* NOTE: you have to click on the ExtraLine for the time to be correct!!
    - *Right click on "ExtraLine" and select "Duplicate."* Duplicate that line enough times to cover the length of your sample and have one line left over. When you duplicate the line, the offset in Y should be the width of the line (eg. a 6 um line should have a 6 um offset).
    - *Record the number of lines used to cover the sample.*
    - *Right click on any pattern, and select "Select All."*
    - *Deselect any lines that are not for the sample by clicking on them while holding the Ctl button.* ***Be sure to deselect all of the Standards AND the last line at the end of the sample - you want to have a line left over to use to draw your next sample.***
    - *Right click on the selected scans and select "Merge Scans."*
    - *Right click on the newly merged scan and select "Rename"*
    - *Rename the scan "Sample1".*
- *Navigate to sample 2.*
- *Adjust the focus.*
- *Select the line left over from making "Sample1," and move it to a location that is above and to the left of Sample2 (as you did for Sample1).*
- *IMPORTANT:* When picking the endpoint for this line, pay attention to the "Estimated Time" for the line (in the lower left corner of the left panel). **For samples that will be run back-to-back, the length of the lines used for each sample should be different by at least 2 seconds!** So if you used a 59 second line for the first sample, the next sample could have line lengths of 55, 57, 61, 63, etc. but NOT 59. Let's say you use a 61-second line for the second sample; then the third sample can have line lengths of 55, 57, 63, 65, etc., but NOT 59 or 61. This will make data analysis a LOT easier.
- *Following the steps used for Sample1, draw patterns for any remaining samples, and name these "Sample2, … SampleN".*
- *Name the line that you don't use "ExtraLine".* You'll use this line next time to build your sample patterns.
- *Click and drag Sample1 so that it is underneath Stds1.*
- *Select Stds1 and Sample1.*
- *Right click on the selection, and select "Merge Scans."*
- *For each "StdsX" and "SampleX", merge the two standard and sample scans into a single scan.* The list of patterns should now read "Stds1, Stds2, ...StdsN, StdsExtra, ExtraLine".
- *Save your experiment.*

- *Click on each scan, and record the time required to scan each sample,* displayed in the lower left corner.

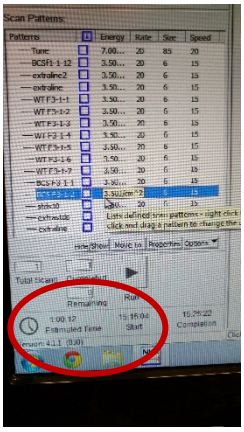

- *Navigate to the start of the first pattern (Stds1).*
- *Adjust the stage speed to that the return time from the end of any line to the beginning of the next is <8 seconds.* To do this, follow these steps:
    - *Right click on the pattern that has the longest lines (based on the line times that you recorded earlier ie. 59 seconds), and select "Edit Endpoints"*
    - *In the popup box, scroll to the last line.*
    - *Record the X positions for the last line.*

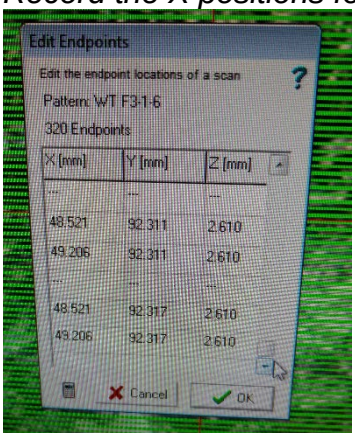

    - *Find the difference between the two X positions you recorded.*
    - *Divide this number by 8.*
    - *Round the answer up to the nearest tenth (eg. 0.014 becomes 0.02), and record this number.* This is the stage speed you should use. For zebrafish embryos, it's probably around 0.02. For adult zebrafish tissue, it's probably around 0.3. For mouse tissue, it's probably around 1.4.
    - *Close the "Edit Endpoints" box by clicking "Cancel"*

- *Right click on the scroll bar for the X direction (the bottom of the screen) and select “Properties”*

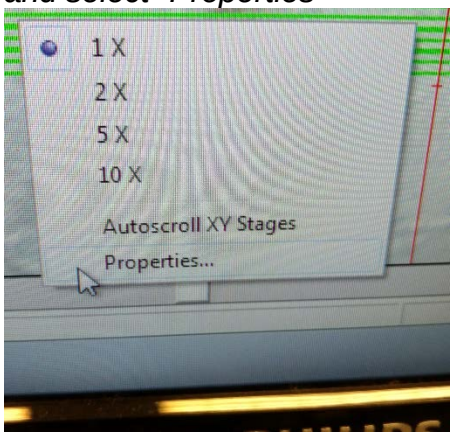

- *Under the “X” tab, type the number you calculated into the “Max Speed” box.*

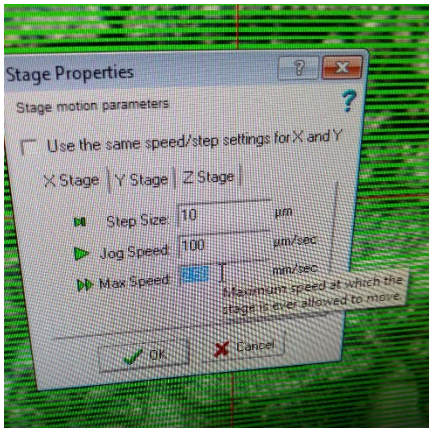

- *Press OK*
- NOTE: When you adjust the stage speed, the estimated times for each scan will change (because the travel time between scans has changed). DO NOT use these modified values. Use the ones that you recorded earlier.

- The laser experiment is now set up.

- *Calculate the scan times required for each sample using the following steps:*
  - *Open the "LA-ICP-MS Time Calculator" Google Sheet.*

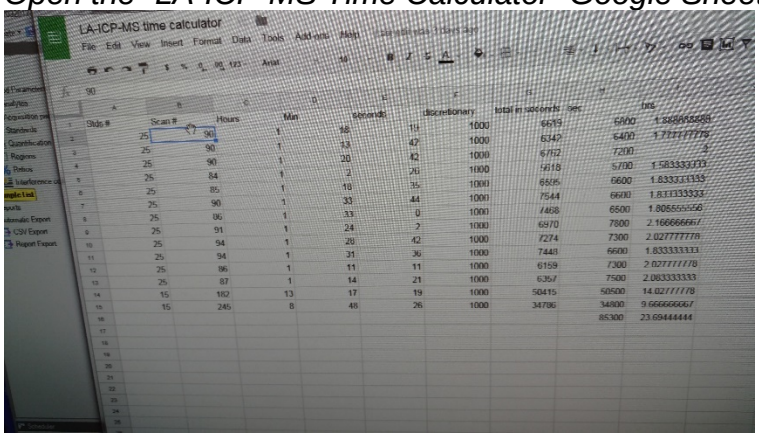

  - *For each sample, enter the number of lines used for the standards in the Stds # column*
  - *For each sample, enter the number of lines used to cover the sample in the Sample # column*
  - *For each sample, enter the hours, minutes, and seconds that you recorded for the estimated time for that sample.*
  - The calculator multiplies the number of lines by 8 seconds, which assumes that the time it will take to return from the end of each line to the beginning of the next one is 8 seconds. It also includes a 1000 second buffer to allow navigation between the standards and the sample. The resulting value is the number of seconds required to scan the standards+sample for each sample.
  - *Round the calculated value up to the nearest hundred (eg. 6894 becomes 6900).* ***This is the value you'll type into the Qtegra software.***
  - *Type that value into the next column, and the following column will contain the number of hours necessary for that scan.*

- *Create a LabBook for the first sample by following these steps:*
  - *If the Qtegra software is not open, open it.*
  - *Click on the LabBooks tab on the left.*

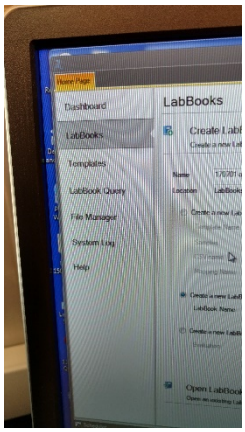

  - *In the first dialog box, enter the name you want for your new LabBook.*
  - *Underneath the name, select the correct path to your folder.* Click on the small box with three dots on it to open the navigation window. Select your folder, and click OK.

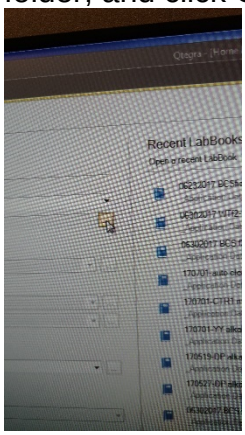

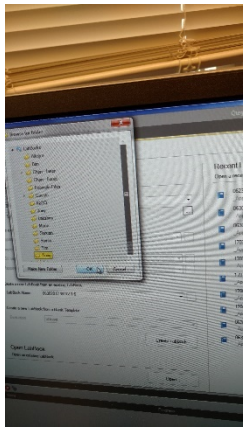

  - *Select the option to "Create a new LabBook from an existing LabBook"*
  - *Select the correct path to the LabBook you want to build from.* If a LabBook does not exist in the format you want, read the Qtegra software manual. That is beyond the scope of this guide.
  - *Click the "Create LabBook" box.* A new LabBook will open.

- *If the sample list does not appear automatically, select "Sample List" from the menu on the left.*
- *Rename the sample by clicking on the name and typing in the box.*
- *Enter the number of seconds for that sample into the "Duration" column.*

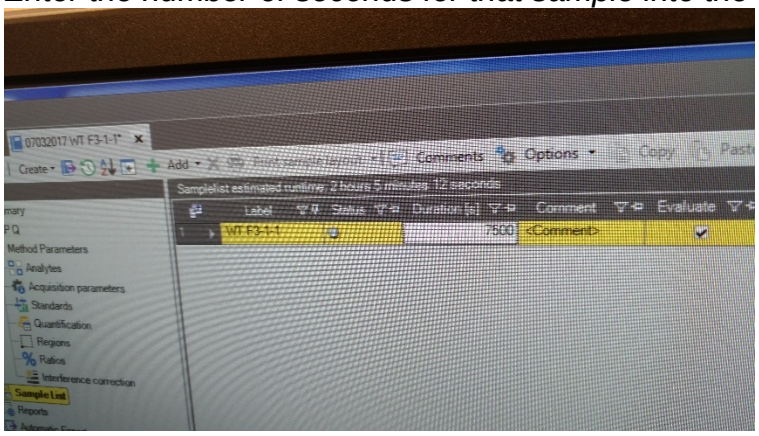

- *Click the green "Play" button at the top of the Qtegra window.*

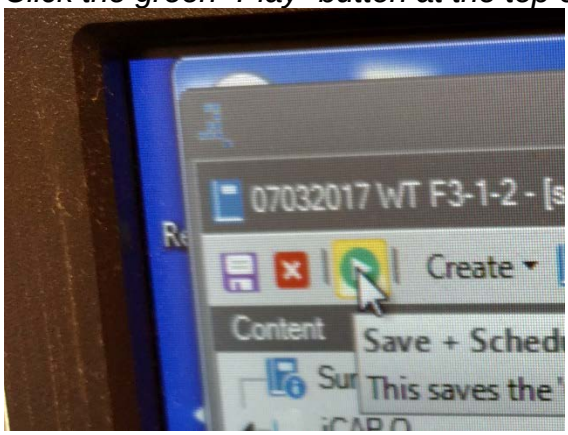

- *Click OK on the popup box to save the LabBook*
- *Click OK on the comments box (you don't need to leave any comment)*
- The LabBook is now saved and should appear in the scheduler below.

- *Create a LabBook for all subsequent samples by clicking on the "Create" button at the top of the current LabBook window and selecting "New LabBook."* This will take you back to the LabBooks tab. You can create a new name in the dialog box and press the "Create LabBook" button. Enter a name and the number of seconds for each sample under the Sample List, as for the first sample.
- *Save and schedule each LabBook by pressing the green "Play" button at the top of the Qtegra window.* At the end of this step, you should have as many LabBooks in your scheduler list (at the bottom of the Qtegra window) as you have samples.

- Once the patterns are ready in the NWR software and the LabBooks are scheduled in the Qtegra software, you're ready to start. YAY!
- *In the NWR software, right click on the screen and select "Center TV2 Cup."*

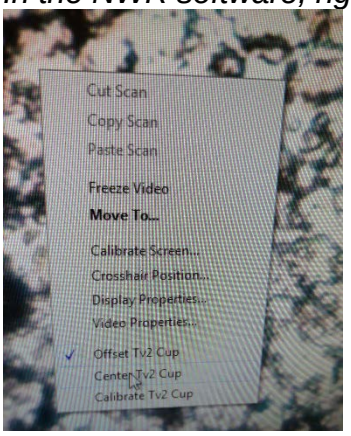

- *Open the Mass Flow Controller to ensure gas is flowing at 800 ml/min.* Leave it open, and drag it off to the upper right corner.
- *Select the patterns that you want to run.*

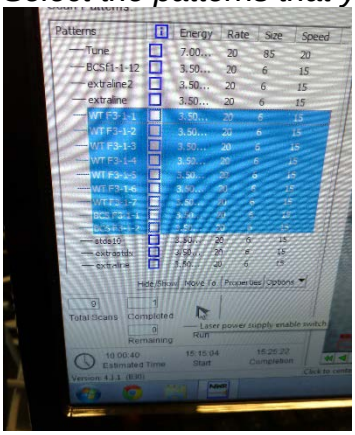

- *Press the "Run" button.* A dialog box pops up. Be sure the following settings are selected:
  - *"Selected Patterns Only" should be checked*
  - *Washout time: 5 seconds*
  - *Warm-up time: 12 seconds*
  - *Click "Trig In/Sync Out Options"*
  - *In the new window, select the "Trigger In" tab*

- *Check “Wait for Trigger” and click OK*

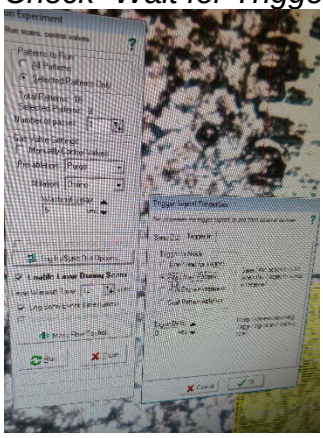

- *“Enable Laser” should be checked.*
- *Finally, press “Run” on the popup box (not the original “Run” button.* A new dialog box pops up that says “Waiting for trigger…”

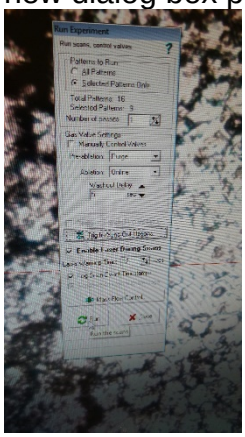

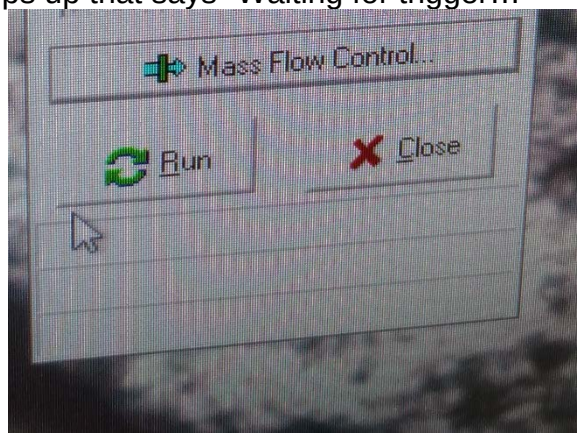

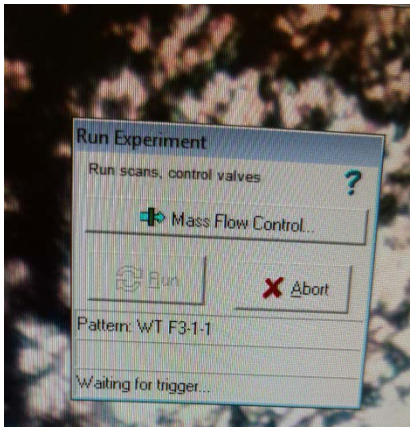

- *In the Qtegra software, press the green "Play" button in the scheduler* (different from the one that is at the top of the screen).

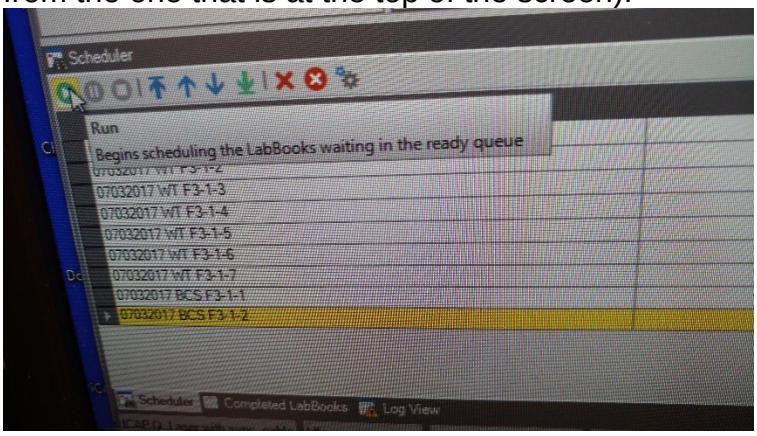

- The first LabBook should initialize, causing the laser to initialize.

Shutting Down the Instrument:

- When the last LabBook has finished, the instrument will idle unless you tell it otherwise. As soon as it the last laser pattern is done, the laser/ICP-MS is immediately ready to be programmed again or turned off and converted to liquid mode. No cleaning is necessary when switching from laser to liquid mode.
- *To turn the instrument off manually:*
    - Press the red “Off” button in the Instrument Control software.
    - In the warning box that pops up, click “yes”.
    - As soon as the plasma goes out, an interlock will trip in the laser, causing it to shut off. You don’t need to do anything to the laser.
    - Close the valve on the helium tank if there is helium remaining.
    - Leave the argon tank ON to keep pressure in the line.
- *If you want the instrument to turn itself off (eg. if the run will end at 3 am):*
    - In the Qtegra software, under the scheduler, click on the “Options” icon, which is the right-most icon under the Scheduler area, with little cogs drawn on it.

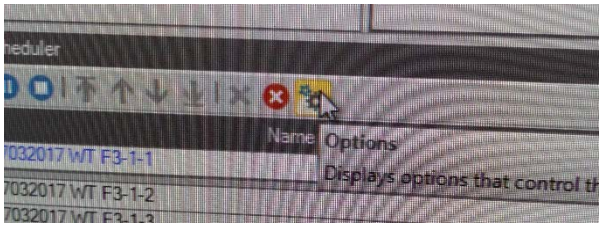

    - Under the Closedown menu, select “Close down upon empty queue or LabBook error.”

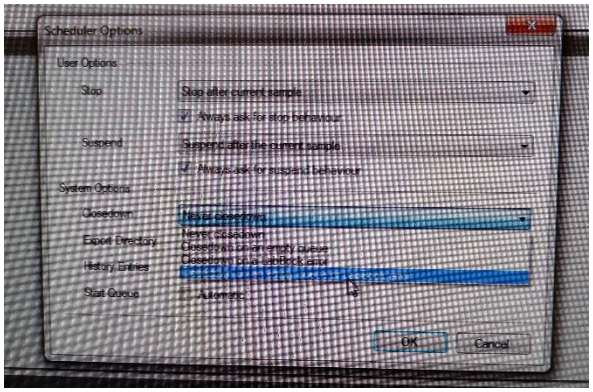

    - When the last LabBook finishes, the ICP-MS will turn off, which will trip an interlock in the laser, turning it off.
    - YOU STILL NEED TO TURN THE HELIUM OFF. So make sure that you come back as soon as possible to close the valve on the helium tank if there is a significant amount of helium left that you want to use for the next run.
    - Leave the argon tank ON to keep pressure in the line.

Optimizing Laser Settings for New Samples:

- These directions assume both a basic knowledge of the NWR and Qtegra software, as well as knowledge of how a basic experiment is set up. If you are not proficient in these areas, please refer to the relevant sections.
- See notebook CMA-XRF pg. 137 for an example of optimizing for a biological sample (adult zebrafish tissue). See notebook CMA-XRF pg. 115 for an example of optimizing for an inorganic sample (Co film on ITO).

- *Determine the spot size and shape:*
    - Our laser can run round spots (4-110 um diameter, using the Infinitely Variable Aperture, IVA) or square/rectangular spots (5x5 um to 200x200 um) using the XYR aperture (XYR allows you to set the length in X and Y, as well as the rectangle rotation, R). Note that the beam is only ~105 um across, so functionally, 80x80 um is about as big of a square as the beam can actually cover.
    - Start by assessing the spatial resolution necessary to see the structures you are looking for: How big are the features you want to resolve? You need a spot size that is <50% of the size of those features. If you're scanning something more-or-less featureless (eg. a coated electrode), use the largest spot size you can in order to get the highest signal above background. Note that our instrument cannot resolve features that are smaller than ~10 um (eg. a few cells).
    - Now balance that desired spatial resolution with (1) the time you want to spend on data acquisition, (2) the sensitivity you need above background, and (3) the number of elements you need to be able to analyze during each scan.
        - How much time do you want to spend per sample? A typical dwell time/pixel is ~0.5-1 second, so do the math. A 500x500 um sample, analyzed with a 10 um spot = 50x50 pixels = 2500 pixels*1 second/pixel = 2500 seconds = 40 minutes. But the same sample analyzed with a 5 um spot = 100x100 pixels = 10,000 pixels = 2.8 hours. The scan time scales with the square of the linear resolution.
        - You'll also need to think about sensitivity over background. Each laser shot releases a certain volume of material, and the signal from this volume of material needs to be above the background signal (ideally >2x the background). Larger spot sizes will release larger volumes, giving you better signal:noise.
        - The size of the spot will also influence the number of elements you can analyze at one time. If you have an element that only has a signal that is 2x higher than the noise, then you will likely need a longer dwell time to accurately determine the value of that element at each pixel. There are only so many shots that can be fired in a given location before the sample is gone, so the longer the dwell time, the fewer elements you can analyze.

        - ***NOTE: this is the case because we have a quadrupole mass spec that cycles between different masses during collection. There are instruments that can collect many masses at once because they have TOF or sector field detectors.
    - Next consider the shape of the spot you'll use. The smallest spot sizes can only be achieved using round spots (with the IVA). For larger spot sizes, a square or rectangular spot is recommended because a straight edge gives a cleaner distinction between two pixel areas than a curved edge.
        - For samples where you want to collect a lot of elements, one trick is to use a rectangular spot that is longer in Y than in X (eg. 40 um tall and 20 um wide). As the laser scans left to right, it will now take 2 seconds to cover a "pixel" ie. 40x40 um, which gives more time to collect multiple elements.
    - For zebrafish embryos, we use a 6 um spot for Cu. Analysis of Zn and Fe can go down to 4 um spots, but since we usually want to show all three elements in a publication, we typically use 6 um spots for all three.
    - For zebrafish adult tissue, we usually use 6 um as well, although we've also used 10x20 um to cover area faster.
    - For mouse adult tissue, we use 20x40 um.

- For your spot size/shape, optimize the laser power and calculate scan speed.

- *Optimize the laser power:*
    - The ideal laser power ablates the entire sample but does not ablate the glass. It should also be gentle enough to ablate only the area you are trying to ablate (eg. 6 um diameter). If too much energy is delivered, it will ablate a larger spot even though it is being fired in a very precise location because the excess energy diffuses out into the surrounding tissue, causing ablation. For 20 um tissue samples, this is typically 2-3 J/cm2 for a 6 um spot and 3-4 J/cm2 for larger spots. Typically, at these values, it takes 8-10 shots to ablate the entire sample thickness.
    - To optimize the laser power for a given sample type, load a sacrificial sample to fire on.
    - In the NWR software, slow the firing rate down to 1 Hz.
    - In Instrument Control, under "Analytes," select one of the elements you're interested in analyzing, and select Si (a proxy for glass). Adjust the dwell times for these elements to 0.1 seconds.
    - Press Run to start the Data Display. Two lines should appear.
    - In the NWR software, move to a location on your sacrificial sample.
    - Begin the laser firing with the shutter closed.
    - Open and close the shutter quickly by clicking on the Shutter button (next to the Fire button), allowing one shot to fire on the sample.
    - Watch the Data Display in the Instrument Control software to see which elements are detected.

- Visually inspect the crater. You can use the measuring tool (on the right panel of the NWR software control) to measure the diameter or length/width of the crater. If it is significantly larger than expected, lower the laser power. If it is smaller, keep going.

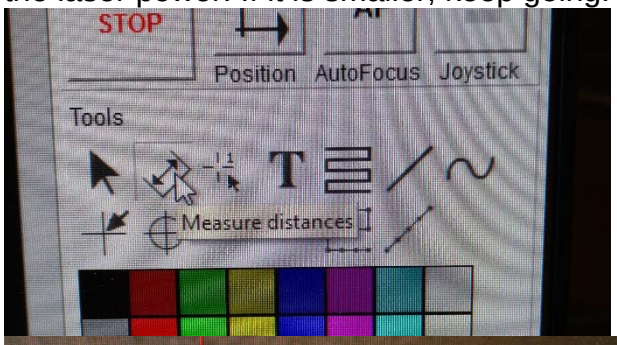

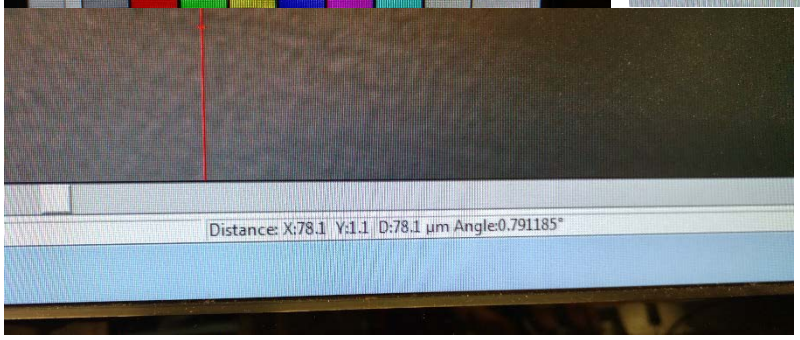

- Open the shutter and count the number of shots that are fired until the crater fully forms and the sample is fully ablated. Watch the data display. Count the number of peaks containing your analyte of interest (the number of these peaks should agree +/- 1 with the number of shots you counted). Note whether or not a silicon peak appeared at any time. If so, lower the power.
- Measure the width of the crater using the measuring tool and be sure that you are actually getting the spatial resolution you desire. If the crater is significantly larger than expected, lower the laser power.
- For flash-frozen tissue, the highest power that can be used without creating craters that are too big usually requires 8-10 shots to fully ablate the tissue. You want to use the highest power that you can in order to improve signal-to-noise and speed the analysis time. Don't go too high or you'll start blurring the edges between lines by ablating outside of the desired crater diameter.

- *Set the firing rate:* The firing rate should always be 20 Hz (max firing rate) on our instrument. Each time the laser fires, it releases a packet of particles that are caught by the carrier gas and carried into the instrument. With a firing rate of 20 Hz, 20 of these particle packets are generated per second, and a new packet arrives to the ICP-MS every 0.05 seconds. In the TV2 cell, the washout time (the time from when the packet is generated to when the majority of it exits the sample chamber is ~0.25 seconds). By firing very quickly, packets are generated

very close together so that there are no spaces between the packets, and in fact, they overlap/average a little. This is a good thing because the ICP-MS is using an analysis dwell time that is not coordinated with the laser firing at all. If there are spaces between the particle packets, sometimes the ICP-MS will record while a packet is arriving, and sometimes it will record during a gap between packets. The result is an ICP-MS signal that is highly variable and looks like it is oscillating. If you want to see this in real time, use the Data Display in the Instrument Control window to watch Cu and Zn (use 0.1 and 0.1 second dwell times) and slow the firing rate down to 1 Hz. The signals will be very choppy. Gradually ramp up the firing rate, and you can watch the signals become steady.

- *Calculate scan speed:* Using the spot size, optimized laser power (which determines the number of shots necessary to fully ablate an area) and a 20 Hz firing rate, you can calculate the scan speed necessary to fully ablate one area and move on without firing on empty glass.
    - Spot size = um
    - Shots to full ablation = shots
    - Firing rate = shots/second
    - So: spot size / shots x firing rate = um/second scan speed. DO NOT ROUND.
    - Using this scan speed, run a line on your sacrificial sample. It should ablate >90% of the material (there may be a few particularly hard spots left), and maintain the desired spot size throughout the analysis.

- *Optimize KED mode:*
    - Kinetic Energy Discrimination is a capability of our ICP-MS that allows you to remove polyatomic interferences. For a better explanation see the section on Acquisition Parameters in the section on Creating LabBooks in Qtegra.
    - When KED mode is optimal, the background is as low as possible while still keeping the signal above background as high as possible. A gas flow that is too low won't knock down the background. A gas flow that is too high will destroy the signal.
    - We have a helium gas hookup that goes to Collision Cell 1 and a hydrogen gas hookup that goes to Collision Cell 2. Helium is used for normal KED mode. Hydrogen is used specifically for analyzing 56Fe in "Laser-H2 flow" mode. We used hydrogen based on Lear *et al.* 2012.[1] Note that this is different from adding hydrogen to the carrier gas (which makes the plasma hotter), since the hydrogen only gets to the sample post-ionization, once it is inside the vacuum chamber.

- BEFORE OPTIMIZING “LASER-KED” or “LASER-H2 FLOW” modes, make sure that the laser ICP-MS setup is fully tuned using Laser-STDS mode!!!! If it is not fully tuned, you’ll have to re-optimize after tuning!
- **The following steps are written for optimizing helium flow in Laser-KED mode. If you are optimizing hydrogen flow, use the “Laser-H2 flow” mode, and adjust the “Collision gas 2” flow.**
- Find a uniform section of Standard G (the matrix-matched standard with the lowest metal concentrations) to work with. Set up a line with the properties you plan to use for your analysis.
- In Instrument Control, set the instrument mode to “Laser-KED” in the dropdown menu at the top of the window. Select the isotope you want to optimize for in the Analytes section. Click “Run” so that you can monitor the analyte signal in real time.
- Create a spreadsheet that you can easily type values into (there’s a tab in the LA-ICP-MS Calculator spreadsheet that is set up already). Have the spreadsheet calculate the ratio of the signal/background as you go.
- In the “Q-Cell” tab (along the left-hand side), set the Collision gas 1 to 1 mL/min to start. Let the instrument settle into this mode for a few seconds, and record the average background signal (either using the scale bar on the left or reading the values in the “Average Intensities” display chart on the right.

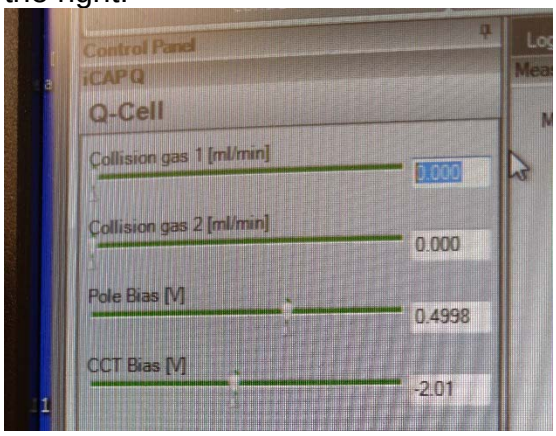

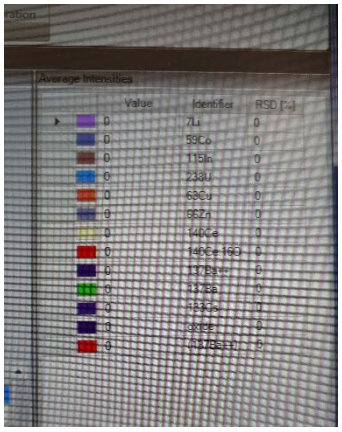

- Now run the line scan on the laser, and record the average signal while the laser is running. The spreadsheet should then calculate the signal:background ratio.
- Modify the Collision gas 1 flow by decreasing it in 0.1 mL/min increments, recording the background signal and recording the signal from running a fresh line scan on the same standard. Continue decreasing the gas flow rate until the signal:background ratio falls enough that you know that you are outside the optimal range.
- Reset the Collision gas 1 flow to 1 mL/min and increase it by 0.1 mL/min increments, recording the background signal and the signal from running a fresh line scan.

- Plot the signal:background for each flow rate, and you should get a plot that is shaped like a mountain, where the peak is centered on the optimal flow rate. Because there is error in all of these measurements, you might need to test each flow rate a couple times. An example result is shown below. See CMA-XRF pg. 113 and pg. 133 for examples of this.

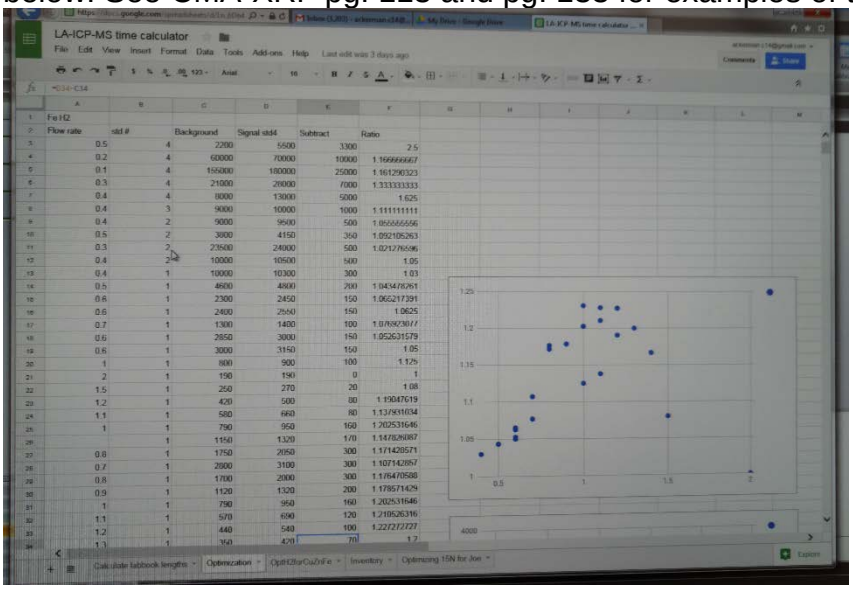

- Once you have found the optimal flow rate, set the Collision gas 1 to that flow rate click “Apply Tune Settings” in the Measurement Mode panel along the top of the Instrument Control software. The gray triangle that is underneath the Collision gas 1 green bar should now match the gray triangle that is above the green bar (the top triangle tells you what the instrument is doing in real time; the bottom triangle tells you what the settings for that mode are).

- If you want to see the settings used for previous optimizations, select either Laser-KED or Laser-H2 flow mode, and click “Edit” underneath the mode dropdown box. A new tab will open called “Measurement Modes.” In “Measurement Modes,” you can see all of the times that mode was tuned, and each of the settings after those tunes.

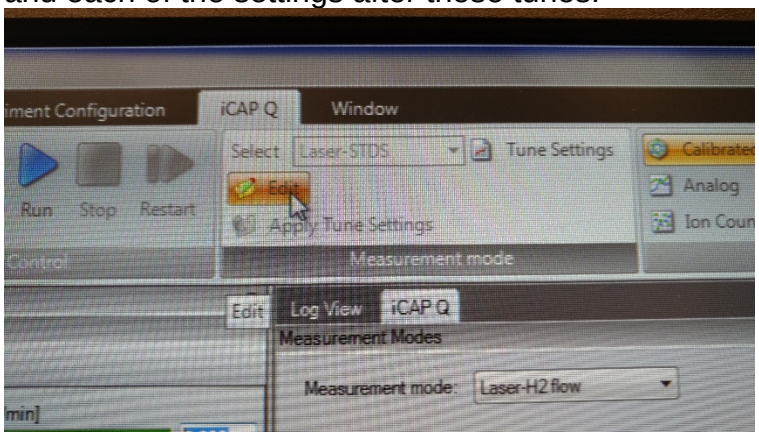

- You can also set the “Added stabilization time” in this window. This is the amount of time that the instrument waits after switching to that mode before it begins collecting data. The auto setting is 10 seconds, which is definitely NOT long enough, but I’ve never worked on figuring out how much time is actually needed.

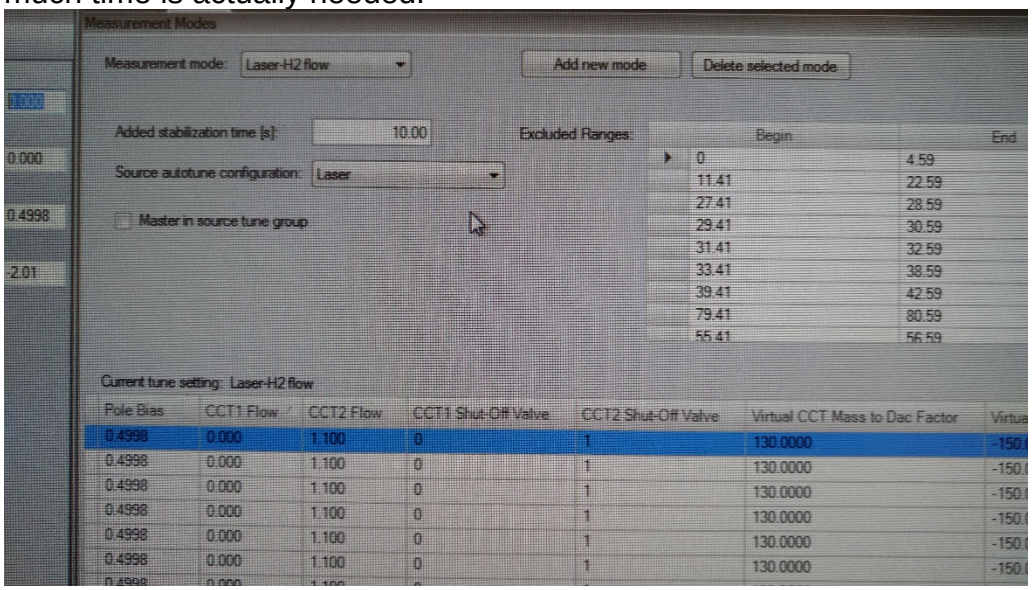

- See the attachment on How to Make a New Mode for more information on making and editing modes.

Using Qtegra

Creating new LabBooks:

- There are many types of LabBooks that allow you to analyze counts in different ways. You can see all the options in the “Create a new LabBook from a blank Template” option in the LabBooks tab of the Qtegra software.
    - We use eQuant for liquid analysis. It collects data over some time period and provides an average value at the end (one value/sample with a standard deviation).
    - We use trQuant for laser analysis. It continuously takes data points over time and displays them in a time-resolved manner, allowing us to make maps.
- Each of these types of LabBooks can be made while the instrument is in a different configuration, and the configuration cannot be changed later (as far as I know). If the configuration of the LabBook does not match the configuration of the instrument, the LabBook won’t run.
- The easiest way to get the right LabBook is to make one from an old LabBook that has a similar method to the one you want to run. In the LabBooks tab of Qtegra, type the name of your new LabBook in the dialog box and select your folder in the path below the dialog box. Select “Create new LabBook from existing LabBook” and navigate to the LabBook you want to build from. Click “Create LabBook.”

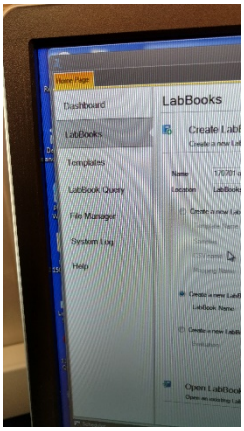

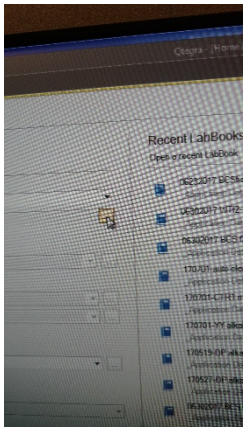

- Once you make a LabBook, a “Content” panel appears along the left-hand side of the screen.
    - **Summary:** Information about the LabBook (when it was made, when it started and finished, etc.).
    - **Method Parameters:** Contains all the settings that the iCAP-Q will follow to do the analysis:
        - **Analytes**
            - Select the analytes you want to analyze by clicking on the elements in the periodic table.
            - The software automatically selects the isotope that is most favorable to analyze in the mode the instrument is running in at the time. It is trying to balance isotope abundance and potential problems with interferences. Interferences are polyatomic ions that have the same mass as the isotope you are trying to analyze (eg. 40Ar16O has the same mass as 56Fe, so the instrument can’t tell ArO apart from 56Fe, creating a really high background when 56Fe is collected in standard mode).
            - To check which isotope the instrument selected, right click on the element, and a window that shows the isotopes of that element will appear. The abundances are also listed in that window. To see the interferences for each isotope, click on the list of polyatomic ions in the “Interferences” column. A popup box with the list of possible interferences will pop up. You only need to worry about the ones that are significantly abundant. Also, typically, interferences that require three atoms to come together (eg. ArOH) are pretty rare, so we don’t usually worry about those either.

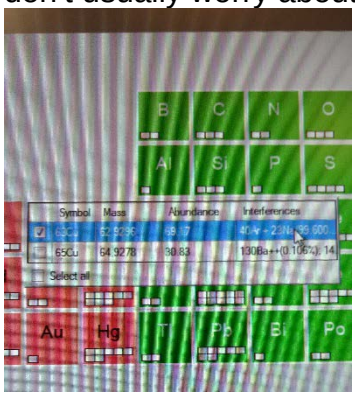

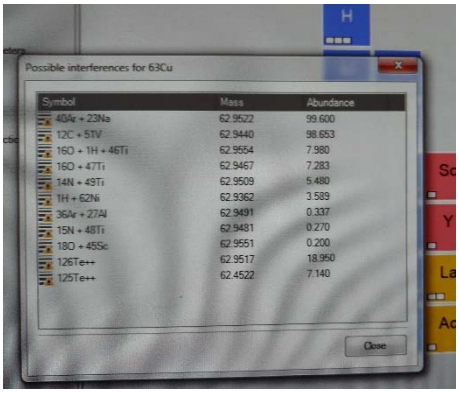

            - If possible, you want to use the most abundant isotope to get the highest signal:noise. However, if one of the isotopes has a very high interference (eg. 56Fe), you’ll actually get better signal:noise with a less abundant isotope that has lower background noise (eg. 57Fe in standard mode).

        - For iron, 56Fe is better in KED mode than 57Fe, though, because 57Fe is not abundant enough to give a good signal when KED mode is being used (more on that under Acquisition Parameters, below).
        - You can also select multiple isotopes if you don't know which one will be best for your sample.
- **Acquisition Parameters**
    - Each isotope that you selected under analytes will have a row in the Acquisition Parameters table.
    - For liquid ICP-MS:
        - Dwell time: 0.1 seconds
        - Channels: 1
        - Spacing 0.1
        - Measurement Mode: select either STD or KED. Use STD mode for most isotopes. Use KED mode for isotopes that have high polyatomic interferences. In KED mode, He flows through the collision cell and preferentially removes polyatomic over monoatomic species. The overall signal is lower (because some monoatomic species are removed too), but the signal:noise is a lot better for isotopes with high background due to interferences. We've typically run all transition metal analysis in this mode, since it is required for 56Fe.
        - NOTE: I do NOT recommend switching back and forth between different modes in one analysis. The instrument doesn't give itself enough time to stabilize after switching, and the values you get when you switch back and forth during one analysis are different from the values you get when you run a full LabBook in KED and then a full LabBook in STD on the same samples. If you want to change this stabilization time, click on "Edit" in the "Measurement Modes" panel on the top of the Instrument Control software. This opens a new tab called "Measurement Modes." The "Added stabilization time" is the amount of time that the instrument waits after switching to that mode before it begins collecting data. The auto setting is 10 seconds, which is definitely NOT long enough, but I've never worked on figuring out how much time is actually needed. To optimize this, you probably just need to run Tune B and watch the Data Display while you switch back and forth between the modes, and see how long it takes for the signal to stabilize in the new mode.

        - Number of sweeps: 10. This is the number of times the instrument will cycle through the elements listed in the table. Note that it is better to have a short dwell time and more sweeps than a long dwell time and one sweep because more cycles means that it is averaging over a longer time in real life (ie. it samples for 0.1 seconds ten times over the course of 3 or 4 seconds, rather than sampling one element for 1 second and then the next element for 1 second etc.). This way, if the signal is fluctuating up and down slightly over the course of a few seconds, that fluctuation will average out over the 10 measurements.
        - Measurement order: We only use one mode at a time, but if you used two modes, this would allow you to say whether you want the instrument to analyze STD and then KED or KED and then STD.
- **Monitor Analytes** (for liquid analysis only): This allows you to collect data until you reach a threshold of counts for a particular analyte. We don't use this.
- **Survey Scan Settings** (for liquid analysis only): Use the defaults. This records a very quick measurement (dwell time: 0.001 seconds) at each mass from 4.6 amu to 245 amu and allows you to go back later and check the level of an isotope that you didn't actually analyze. The numbers won't be super accurate, but if there are significant differences between samples (>10%), you'll be able to see it.
- **Interferences correction** (for liquid analysis only): If there is a simple mathematical interference correction possible for one of your isotopes, you can check the "Measure and Apply" next to the correction. Most of the isotopes we analyze don't have this.
- **Standards:** For liquid samples, program in the standards you use. Don't use this for laser samples.
    - Click the "New" button.
    - Select "Elemental Standard"
    - Type the name into the "Standard Name" box
    - Check the "Create standard using analyte list" if the elements in your standard are the same as the analytes you selected earlier.
    - Click "OK"

        - If you checked the “Create standard using analyte list” box, the new standard will appear with your analyte elements already selected. Type the correct concentration next to each element in the “Selected Elements” table.
        - If you didn’t check the “Create standard using analyte list” box, click on each element you want in the periodic table to add them to your standard. Type the correct concentration next to each element in the “Selected Elements” table.
        - Continue adding standards until all your standards are listed.
        - Save your method by clicking the Save icon in the very top left corner of the Qtegra screen.
- **Quantification:**
    - Don’t use this for laser analysis.
    - For liquid analysis, if you are using an internal standard, set that element as the internal standard by selecting “Use as Internal Standard” from the dropdown menu in the “Internal Standard” column. Under the “Internal Standard” column for each other element, select the internal standard element so that the program knows to normalize that analyte to the internal standard (ie. select Ga(KED) in the Cu(KED) row so that the program normalizes copper levels to gallium levels).
    - Other settings:
        - Quantify: Yes
        - Fit Type: Linear
        - Weighting: None
        - Forcing: Blank (or none, depending on what you want)
        - Use for SemiQuant: Yes
        - IS Recovery Settings (we don’t actually use these):
            - Low warning limit: 80
            - High warning limit: 120
            - Low failure limit: 75
            - High failure limit: 125
- **Regions** (laser only): don’t use.
- **Ratios:**
    - Laser analysis: don’t use.
    - Liquid analysis: If you want to see a ratio of two elements in real time, you can ask it to calculate the ratio for you. Select the numerator (eg. 63Cu(KED)) under Analyte 1 and the denominator (eg. 31P(KED)) under Analyte 2.

- **Manual Sample Control** (for manual samples only):
  - Uptake time: the amount of time the instrument will run the pump on “High” speed to get the sample from the start of the sample introduction tube to the spray chamber. We usually use 14 seconds.
  - Wash time: the amount of time the instrument will run the pump on “High” speed while the probe is in the 2% nitric acid wash. We usually use 3 seconds.
- **Cetac ASX-520** (for autosampler samples only):
  - Wash time: the amount of time the autosampler will be in the rinse position and the sample pump will run on “High” speed to wash the line between samples. We usually use 30 seconds, which requires ~15 mL of acid/wash. If you lengthen this time, be sure to increase the amount of rinse acid you use so that there will be enough to wash between all the samples.
  - Uptake time: the amount of time the pump runs on “High” speed to get the sample from the probe to the spray chamber. You typically measure this during setup. The value you type in here should be your measured value + 15-20 seconds. We usually have uptake times of 65-75 seconds.
  - The layout of the autosampler is shown. If we ever bought different racks, you could change the rack layout using the dropdown boxes under “Rack settings,” but as of right now, we only have one kind of rack.
- **Sample List:**
  - Tips and tricks for navigating the Sample List:
    - If you highlight down a column and right click, you have the option of “Fill Down,” which applies the value in the top box of the selected column to each box in the selection (eg. if the top box is “3,” then all the values in the column would become “3”). You can also “Fill Up,” which works like Fill Down, but goes the other way. You can also “Increment Fill,” which works like Fill Down, but adds 1 to each row as it goes down (eg. if the top box is “3,” then the values in the column would become “4” “5” “6” etc.).
    - You can cut, copy, and paste rows by highlighting and right-clicking. Be sure to note if you are highlighting entire rows when doing this or just cells in a row.
    - You can paste cells from Google Sheets (the computer doesn’t have Excel), so you can make your list of sample names ahead of time, and paste it all at once.
  - For Laser Samples: fill in the sample name and the scan duration (as explained in the section on setting up laser samples.

- For Liquid Samples, the sample order should begin with a rinse (2% nitric acid) to see the background/baseline signal from the acid that you used to dilute the signal. Next run the blank (2% nitric acid with 20 ppm Ga). Next run your standards in the order of increasing concentration. Run another rinse before beginning the samples (to ensure that the highest standard has been thoroughly washed away). Run samples. If you have more than 20-30 samples, rerun the standards every 20-30 samples to ensure that the instrument remains stable throughout the analysis. At the end of the analysis, run another rinse and rerun the blank to ensure that the background signal has not changed significantly.
    - For Manual Samples:
        - Add samples by clicking the “+ Add” box at the top of the screen. You can click the box directly to add a single line, or use the arrow next to “Add” to add multiple rows at once.
        - Set the sample names under “Label”
        - The “Status” bubble will be gray if the sample has not been run, green if the sample ran successfully, and red if the instrument had an error while that sample was running.
        - “Survey Runs” should be 0 (if your samples are only 220 uL, you don’t have time for a survey run).
        - Main Runs should be 3. This is the number of times the instrument will take a measurement for that sample. This value should always be more than 3 so that you have multiple measurements to average over.
        - Be sure the “Evaluate” box is checked, or the instrument won’t run that sample.
        - “Sample Type” should be set to ‘UNKNOWN” for your samples, “BLK” for your blank(s), and “STD” for each standard. Once you select “STD,” a red error icon will appear in the next column, reminding you to select which standard you are running. Select the name of the standard you plan to run in the dropdown menu.
        - Dilution factor should be 1.

- For Autosampler Samples:
    - Add samples by clicking the “+ Add” box at the top of the screen. You can click the box directly to add a single line, or use the arrow next to “Add” to add multiple rows at once.
    - Set the sample names under “Label”
    - The “Status” bubble will be gray if the sample has not been run, green if the sample ran successfully, and red if the instrument had an error while that sample was running.
    - “Survey Runs” should be 1.
    - Main Runs should be 5. This is the number of times the instrument will take a measurement for that sample. This value should always be more than 3 so that you have multiple measurements to average over.
    - Be sure the “Evaluate” box is checked, or the instrument won’t run that sample.
    - “Sample Type” should be set to ‘UNKNOWN” for your samples, “BLK” for your blank(s), and “STD” for each standard. Once you select “STD,” a red error icon will appear in the next column, reminding you to select which standard you are running. Select the name of the standard you plan to run in the dropdown menu.
    - Dilution factor should be 1.
    - The “Rack” and “Vial” columns should direct the autosampler to the location of each sample. Be careful that the location you program in matches the location of the samples. Deconvoluting incorrect locations later is pretty confusing.

During and After Analysis:

- Once the method is running, a new set of options will appear in the Content Menu (left-hand panel) called “Evaluation Results”
    - Liquid analysis:
        - Concentrations and Concentration Ratios give you the calibrated concentrations of each element in each sample.
        - To see the standard curve, click the “+” sign on the right side of the STD row.

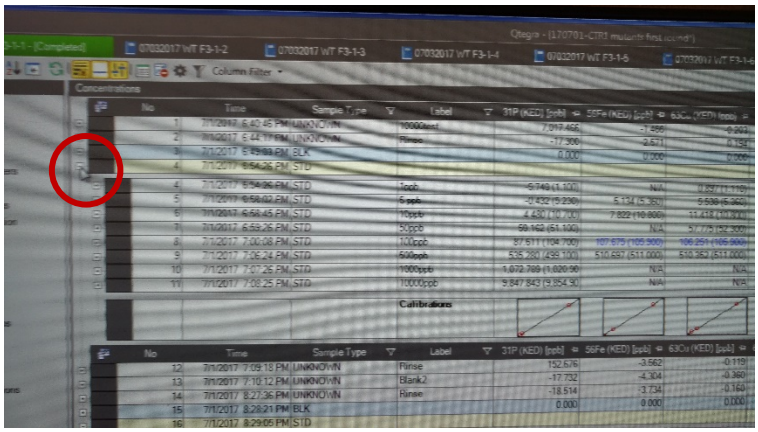

        - To see the replicates of each standard, click the “+” sign on the right side of each standard in the curve. This is especially helpful if you know that the sample didn’t quite reach the spray chamber or the sample ran out before the analysis ended. You can omit values by right clicking on the value and selecting “Exclude entry” if needed. If you do this, the entry turns blue.

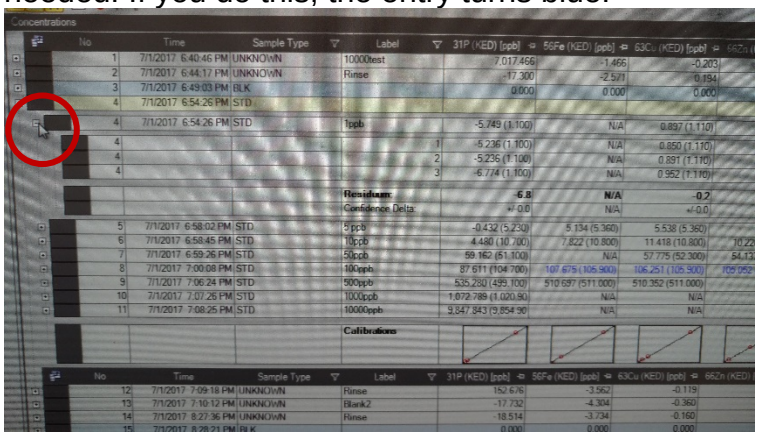

- To see the standard curve with its slope and R^2 value, double click on the standard curve.

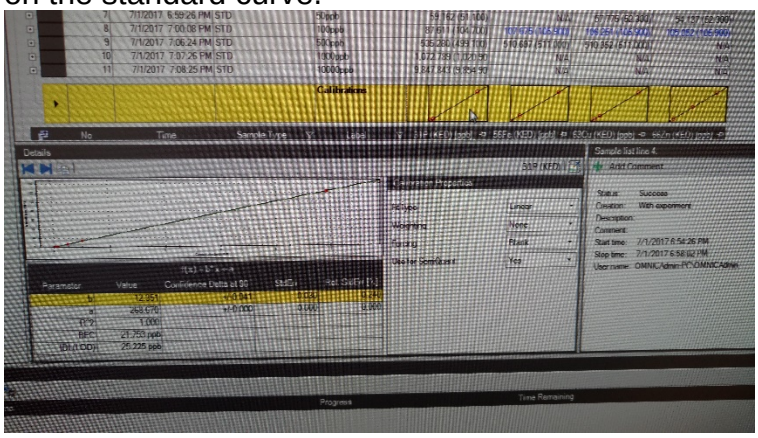

- You can zoom in on regions of the standard curve by clicking and dragging over that region. Double clicking anywhere on the graph resets the zoom to fully zoomed out.

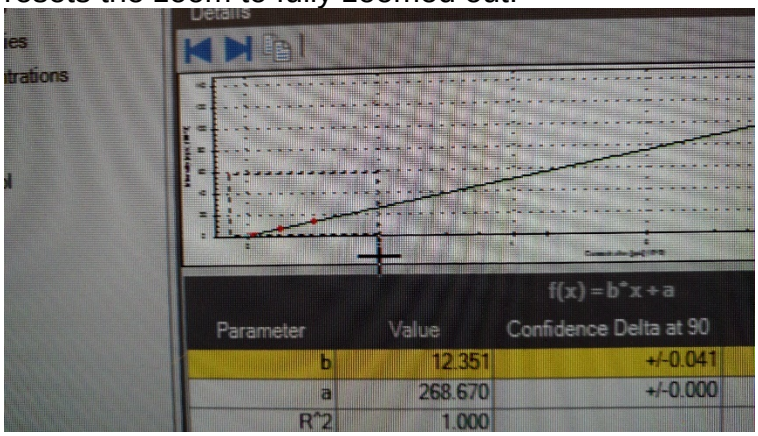

  - Intensities and Intensity Ratios give you the raw counts-per-second values for each element. These can be helpful for troubleshooting. You can click on the "+" signs to see the raw replicates.
  - Survey Intensities and Survey Concentrations give you the results of the Survey Scan.
  - I've never used "Spectra View"
  - Instrument State is a record of the readback settings during the analysis. If you are concerned that one of the settings wasn't correct (for example, that the nebulizer flow wasn't as high as it should have been during the analysis), you can check that here.
- Export the data by clicking on the "Export" button at the top of the Qtegra screen. Select "CSV Export" and click on the "Data" box under "Available data." Select your folder in the "Path." Make the column separator "Custom" and make sure a comma symbol is in the box. Check the "Export sample lines as rows" and "Export complete LabBook" boxes. Click "Export."

- Laser analysis:
    - “Average Intensity Data” displays your data in real time. If you’re analyzing multiple elements, you can click on each element in the top left of the window to see the traces individually, and you can zoom in by clicking and dragging on the screen. Double click anywhere on the graph to zoom out and go back to seeing all the elements.
    - Export the data by clicking on the “Export” button at the top of the screen.
        - In the dropdown menu, select “Laser Data Reduction Export.”
        - Click “Select All” to move all of the analytes into the “Exported Analytes” column.
        - Select your folder in the “Path”
        - Click “Export”

Operating the NWR Laser Software:

Navigating:

- You can move the stage multiple ways:
    - Use the scroll bars along the edges of the central camera display. The lower bar is “X”. The bar on the right side is “Y”. The small bar on the upper left is “Z” (focal plane).
    - Select the “Crosshairs” icon from the right hand panel, and click anywhere on the screen to move to that location. You can make larger movements by clicking on the wide-view camera image on the lower right side of the software window.

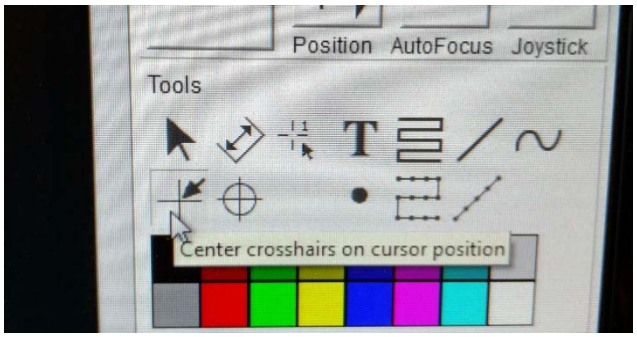

    - Use the joystick cartoon (the blue ball) in the right hand panel.
    - Right click on any pattern that you want to move to and click “Move to Scan”
- The coordinates of the stage are displayed on the right hand panel at all times.
- To adjust the speed of any of the motors, right click on the scroll bars and select “Properties”

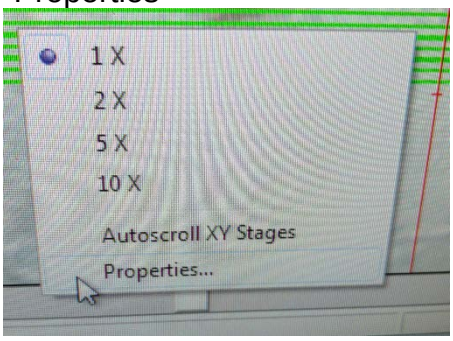

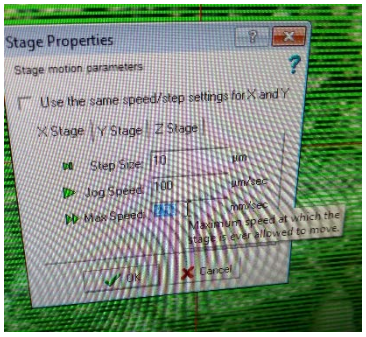

    - Step speed: the speed of the tiny arrow with a line in front of it
    - Jog speed: the speed of the medium arrow (middle button)
    - Max speed: the speed of the double arrow; highest possible value = 2.5 mm/sec. Lowest possible value = 0.1 mm/sec. This is the fastest that the stage can move, even during your experiments. Adjust this speed to prevent the intervals between scans from being too short or too long.

Drawing a pattern:

- On the right hand panel of the software, toward the bottom of the screen, click on the line icon.

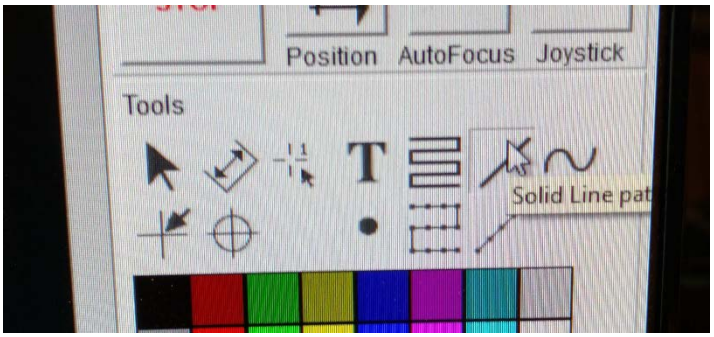

- Start the line by left clicking at the desired starting place.
- End the line by left clicking AND THEN right clicking at the ending place.
    - NOTE: A left click just puts an anchor in the line. The right click ends the line at the last anchor point. If you just right click (without placing an ending anchor), the line will not form because you did not place two anchors (start and end).

Selecting multiple scan patterns:

- “Shift+Click” doesn’t work on the Scan Patterns list. Instead, click on the space in between the line name and the blue box and drag down. You can also hold the “Ctl” key and select individual scans by clicking on them (but don’t click too fast or it will register as a double click and open the Properities window).

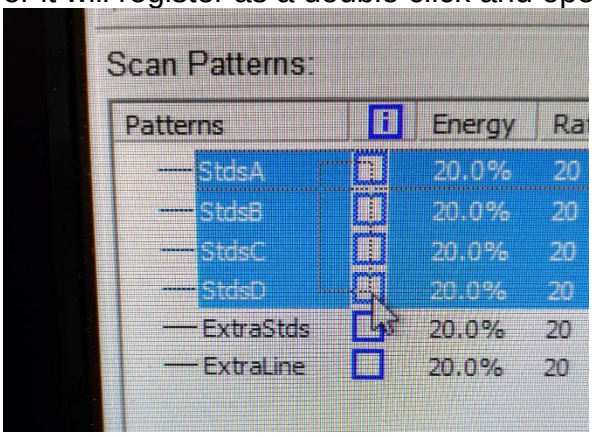

A Brief Introduction to the Configurator

The Configurator software holds the settings for each Experiment Configuration. Each configuration shows the instruments involved in that configuration. If you right click on the instrument and click “Edit settings…”, you can change some of the startup settings. This piece of software was very important during setup, but hopefully will be basically obsolete now that things are running.

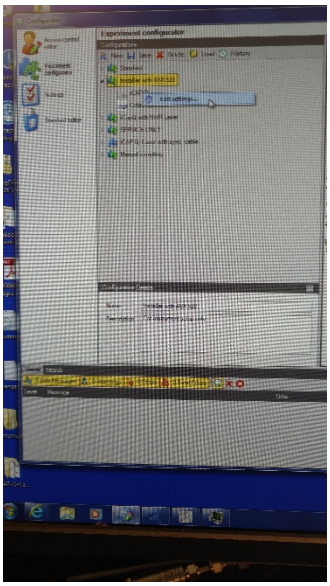

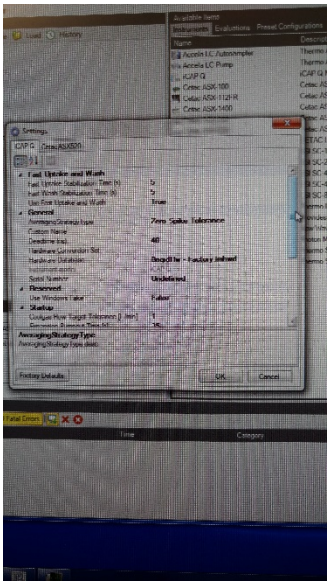

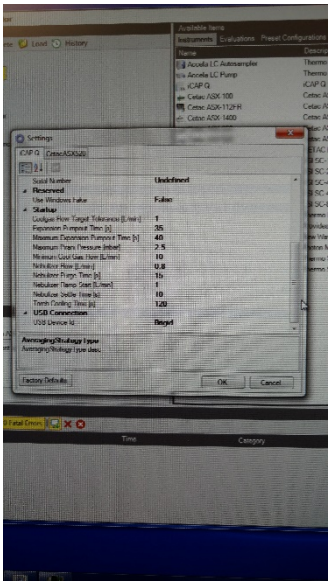

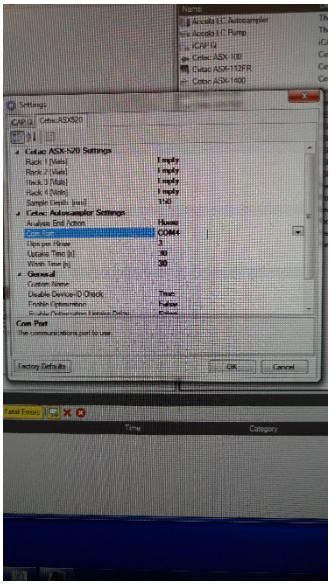

General Information

Tubing Part Numbers:

- Pump inlet tubing catalog number: 1320050
  - Pump inlet tubing description: “Tubing orange/yellow 12 pieces, PVC-flared end, 3 bridges – 95mm, ID=0,508mm, 0,020inch, L=406mm”
- Pump outlet tubing catalog number: 1320110
  - Pump outlet tubing description: “Tubing grey/grey 12 pieces, Santoprene, 3 bridges – 95mm, ID=1,295mm, 0,05inch, L=406mm”
- Autosampler line that runs from the autosampler to the sample intake tubing: 1600061, Tube Teflon 1/16OD .02/D10ft.

Changing Gas Tanks:

- *We order tanks from Praxair:*
  - *Argon:* AR 4.8IC23035SW
    - *Note that this is specifically ICP-MS-grade argon.* If you switch suppliers or tanks, be sure to ask about getting ICP-MS-grade to avoid contaminants in the gas.
  - *Helium:* HE 5.0UH-K
  - *Lead time is ~3 days.*
- *For argon:* The pressure gauge on the first stage of the regulator will always read very low because the tank pressure is below the range of that gauge. Use the “Starwatch” gauge on the top of the instrument to tell how much gas is left (1% ~1 hour of instrument time). The pressure gauge on the second stage should read 90 psi.
- *For helium:* The pressure gauge on the first stage of the regulator tells you how much gas is left (100 psi ~3 hours of run time). The second stage should supply 10 psi. Do not exceed 15 psi or you will damage the ablation unit’s mass flow controllers.
- ***Do not adjust the regulator settings or close the valves on the regulators themselves.***
- ***To change a tank:***
  - *Close the tank valve by screwing it to the right as much as possible.*
  - *Loosen the regulator using a wrench.*
  - *While supporting the regulator with one hand, finger-loosen the regulator fitting until the regulator comes out of the tank.*
  - *If it’s a cylinder: Cap the empty cylinder. Place an “Empty” sign on it for pickup. Uncap a new cylinder. Remove the plastic cover and discard it.*
  - *For tanks and cylinders:* ***clear the valve*** *on the full tank by releasing a small amount of gas before hooking up the regulator (without hooking up the regulator, open the valve slightly and close it again).* This decreases the amount of contamination from dirt in the valve that can get into the gas lines.
  - *Place the regulator in the tank fitting, and finger-tighten the regulator fitting until you can’t twist it anymore.*

- *Use a wrench to tighten the fitting securely.*
- *Open the tank valve.* If there is a hissing sound, close the tank valve and further tighten the fittings until the hissing sound is gone. If you cannot create a secure connection, report the bad tank to Praxair.

Water:
Ultrapure water = milliQ water = 18 mega-ohm water
DI water = the water that comes out of the DI tap. Do not substitute milliQ.

Troubleshooting:

ICP-MS Problems:

- *If the plasma won't light:*
    - Let the instrument return to standby mode (you can monitor this in the LogView window), and try starting it again.

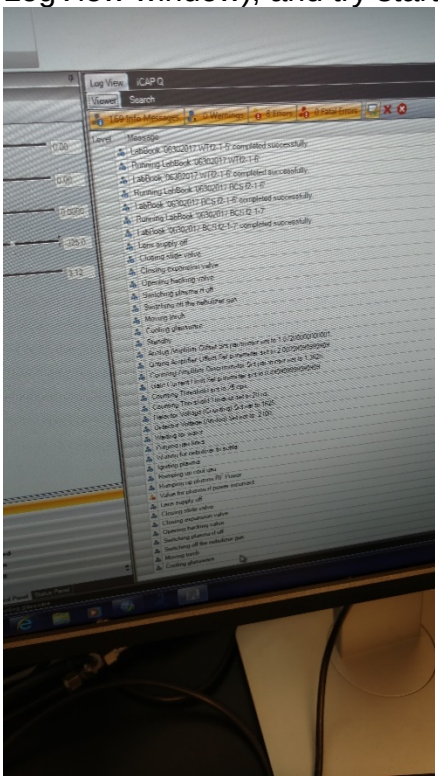

    - If it still won't start, read the error log in the Instrument Control "Log View" window to see if the instrument has diagnosed its own problem.
    - Check that the argon pressure is >110 psi
    - Check that the vacuum light on the side of the ICP-MS is green and that the vacuum is running well (on the balcony)
    - Check that the water cooler is running well (on the balcony)
    - Check that the drain line is working and that there is no built up acid in the torch, nebulizer or spray chamber.
    - Check the nebulizer flow rate at startup. In my experience, it works best below 1 L/min. If it's ramping to something faster than that, go into the Experiment Configurator and change "Nebulizer Ramp Start" to 1. Click "OK" and click the "Save" button to save the changes to the configuration.
    - Check that the plasma exhaust is correct. It should be 0.4-0.5 mbar. If it's too high, it will blow the plasma out before it can light. Lower it be adjusting the damper on the exhaust duct (see "If the signal is lower than you expect" below).
    - Turn the instrument fully off (see "All Problems" section below).

- *If the plasma randomly shuts off:*
    - Check that the argon pressure is >110 psi
    - Check that the drain line is working and that there is no built up acid in the torch, nebulizer or spray chamber. If there is, dry everything off and try again. See the section on setting up the peristaltic pump for how to preven this from happening.

- *If vacuum chambers come to room pressure (typically this happens because the power goes out or because the argon runs out):*
    - If the argon runs so low that the instrument has to turn itself off, sometimes the slide valve that maintains the internal vacuum doesn't close well enough (it needs sufficient argon pressure to slam shut). This can cause the vacuum chamber to come to room pressure, and the computer shuts off the vacuum pump in order to keep it from burning out.
    - If the power goes out, the slide valve won't be able to shut, and the same things can happen.
    - Open the ICP-MS door (twist and pull), and see if it looks like the door behind the cones isn't shut correctly. If it is slightly ajar, you'll need to call tech support.
    - If the door looks fine, try turning the instrument off and on. If the vacuum isn't starting, follow the directions below for "If the vacuum won't turn on."

- *If the vacuum won't turn on:*
    - This can be because the vacuum has been switched off in the Instrument Control software. Under the "Vacuum" tab in the Control Panel of the Instrument Control software (along the left-hand side of the screen), make sure the Vacuum System is switched to "On." If it is "Off," an interlock likely caused it to switch off. Try clicking "On" and seeing if the vacuum works. If it keeps flipping to "Off," it's probably time to call tech support.

- *If the signal is lower than you expect:*
    - Check that the nebulizer is creating a good spray in the spray chamber. Open the spray chamber insulator door. Send an air bubble through the line. You should see the spray cloud disappear when the air bubble arrives and reappear when the liquid reaches the spray chamber again. If you don't there's likely a clog in the line.
    - The plasma works best when the exhaust speed is 0.4-0.5 mbar. Check the exhaust speed by clicking on the "Plasma" tab in the Control Panel of the Instrument Control Software (on the left-hand side of the screen). The Plasma exhaust is displayed at the top. To adjust the flow rate, open or close the damper on the exhaust duct, shown below.

- *If the detector says that it can't be calibrated:*
    - Try running the "Full Detector System Calibration"
    - Try turning the instrument off and on again.
    - Call tech support.
    - We have a spare detector because the time in June 2017 when it said that it needed to have the detector replaced, we ordered a new one and then it randomly started working again.

Laser Problems:

- *TeamViewer:*
    - ESI likes to use TeamViewer to look remotely troubleshoot.
    - Our username is NWR101107.
    - Our password is Nwr$upport

- *If the laser asks you to home the stages:*
    - Sometimes the laser stage gets lost and will ask you to home the stages.
    - Make sure that the stage speed is set to Max Speed = 2.5 mm/sec for X and Y
    - Go to Position -> Home Stages and let it do it's thing.

- *If the ablation is not occurring efficiently (especially for smaller spots), even though the laser fluence appears to be fine:*
    - The fluence reader is positioned before the aperture, so it reads the raw value coming out of the laser, not the fluence that is actually hitting the sample.
    - Check to see if the laser beam is still centered: Use a 110 um spot to fire on glass (usually NIST 612 is good), using the lowest power that still creates a scar. Fire on the glass at 1 Hz and watch whether the whole circle ablates at about the same rate. The Tempest laser (which we have) does not ever have a perfectly flat intensity surface, but if half of the spot ablates before the other half does, this is because the laser beam has gone off center. When the beam goes off center, the highest intensity part of the laser is no longer in the middle of the aperture, so smaller spots will ablate less and less efficiently because the aperture is masking the most intense part of the beam when it creates the smaller spot.

All Problems:

- *When all else fails:*
    - Turn everything off and back on again. No kidding. When you call tech support, this is the first thing they're going to tell you to try anyway.
    - First turn off the computers by shutting them down.
    - If you're using the laser, there's an on-off switch in the back right corner of the instrument. Flip it off.

    - There is a master switch on the back of the ICP-MS. Flip it off.

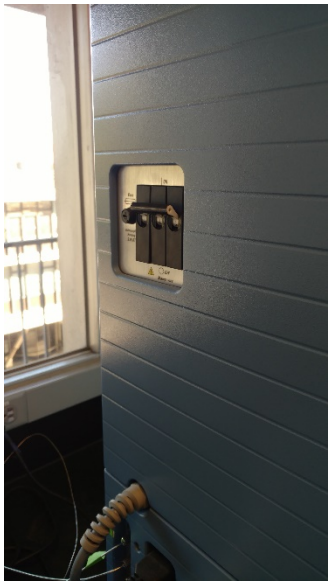

- There is a switch on the back of the autosampler. Flip it off.

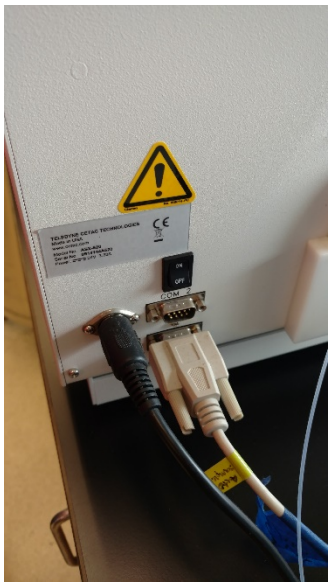

- Let everything sit for ~15 seconds.
- Switch on the ICP-MS.
- Switch on the autosampler.
- Switch on the laser.
- Turn on the ICP-MS computer (note that the laser computer is actually inside the laser, so when you turn the laser on, it's computer will automatically boot).

Maintenance:

As-Needed:

- *Nebulizer cleaning:* Nebulizer cleaning can be done by removing the nebulizer from the spray chamber and using the peristaltic pump (which can still be controlled when the instrument is off) to pump a small amount of <50% nitric acid through the nebulizer. Collect the acid that flows through the nebulizer in a small beaker. Immediately, flush the nebulizer with 2% nitric acid, collecting the acid in a beaker. With acid still inside the nebulizer, place the nebulizer in a clean glass beaker containing milliQ water. Place the beaker inside the bath sonicator (do NOT allow water from the sonicator bath to enter the beaker). Sonicate the nebulizer for ~2 minutes. Use the peristaltic pump to pump more 2% nitric acid through the nebulizer. Use the silicon-coated nebulizer cleaning wire to push any debris through the nebulizer. It's a good idea to run the wire through the nebulizer only in the forward direction (the same direction as the liquid flows) to avoid drawing any gunk back into the nebulizer. Flow more 2% nitric acid through the nebulizer. Repeat the sonication process and wire cleaning once more. In extreme cases, the nebulizer can be flushed with <50% nitric acid for <10 minutes.

- *Cone cleaning:* submerge the cones in ultrapure water on a plastic stand in a clean glass beaker. Lower the beaker into the bath sonicator so that the water level in the beaker is even with the water level in the sonicator. Sonicate for a few minutes (you should be able to see pieces of caked-on dirt breaking off). If needed, lower ONLY THE TIP of the cone (NOT the part that forms the seal with the instrument) into a solution of 10% nitric acid for <1 minute. Swirl gently; you may see significant color change in the liquid. Rinse the cone with ultrapure water; place it back in the beaker with the plastic stand and ultrapure water bath and sonicate again. Repeat this cycle until nothing else comes off of the cone. Dry the cones thoroughly with a KimWipe and nitrogen gas flow before putting them back into the instrument.

Regular Maintenance

- Once a week:
    - If there is ever a time when the laser is not being used frequently, at least turn the laser on once/week to let the water circulate and prevent corrosion and pitting within the laser.
- Once every three months:
    - Change the water in the laser power supply by removing the cover on the power supply (three screws along each side, six screws in the back, and you have to take the black DI water cap off to get the lid to slide off), emptying the water in the plastic container in the front, and refilling it.
- Once every six months:
    - Change the water filter in the chiller.

- Clean the air filter on the chiller. This can be removed from the front of the chiller by gently pulling. Clean the filter by running DI water through the screen in the opposite direction of the air flow (ie. pour the water on the inside of the screen so that it flows to the outside and washes the dirt away).
- Change the DI cartridge in the laser power supply.
- Last performed: Feb 2016

Maintenance Log:

Update from 16-18 Aug 2016 maintenance:

- Chiller now uses DI water with a little bit of tap water 10-1000 micro-Seimens. It is currently at 50 uS (measured with a conductivity meter). DO NOT USE the anti-corrosion solution anymore.
- RF generator board was the problem. It wasn't keeping up with changes in load.
- Plasma exhaust should be ~0.4-0.42. Our was at 0.5-0.6, so we closed the damper a bit to lower it. This should be checked each time the instrument is run.
- We need a service contract because our warranty runs out in October. There are two available: one is a 1x/year (preventative maintenance and emergency service). The other is unlimited with 1x/year preventative maintenance.
- Overall, the instrument is running well. Pump oil is clean. O-rings and seals look good.
- We might consider cleaning the extraction lens in between the liquid and laser runs (sonicate in 2% HNO3) because that might clean up the background signal without having to run 2% HNO3 for 18 hours in between liquid and laser.
- The old RF generator parts can be disposed of as electrical waste.
- The old RF generator board needs to be shipped back to Thermo. Javier will send a FedEx label and declaration of non-hazardous content for us to ship it.
- Say hello to Marshall next time :)

Update from May 2017 maintenance:

- The power supply for the laser should have its water changed every 3-6 months. The DI cartridge should be changed every year.
- The power for the laser is under spec, but only a little bit.
- When Myron took the cover off of the laser, it jumped from its super low levels to almost normal.

Update from June 2017 maintenance:

- The detector said that it couldn't be calibrated, but when Minna came to work on it, it was fine. We ran the "Full Detector System Calibration," and everything worked well.

Continuing Maintenance Log:

Date:
Maintenance Performed:

Date:
Maintenance Performed:

Date:
Maintenance Performed:

Contact Information for Service

- *To get help with the laser:*
  - Email americasupport@esi.com.
  - Our serial number is NW101107.
  - ESI likes to use TeamViewer to look remotely troubleshoot. Our username is NWR101107, and the password is Nwr$upport
  - Myron Peskar installed the instrument and has done maintenance on it since the beginning.

- *To get help with the ICP-MS:*
  - Call (800) 532-4752.
  - Our serial number is SN03056R.
  - The company that Thermo Fisher contracts through is Unity Lab Services. Henry Lu installed the instrument and serviced it for the first year or so. Marshall Allin serviced it for a while. Our current contact is Minna Jyrala.

References

1 Lear, J. *et al.* High-Resolution Elemental Bioimaging of Ca, Mn, Fe, Co, Cu, and Zn Employing LA-ICP-MS and Hydrogen Reaction Gas. *Analytical Chemistry* **84**, 6707-6714, doi:10.1021/ac301156f (2012).